AdriaClim

Climate change information, monitoring and management tools for adaptation strategies in Adriatic coastal areas

Project ID: 10252001

D.5.8.2. Guidance for local adaptation and mitigation strategies.

PP6 – PP RERA SD

Final version

Public document

May 2023

GUIDELINESS

for improving the management plan of the marine environment and coastal areas of the Split-Dalmatia County regarding beach erosion

Made by:

OBALA d.o.o. SPLIT

European Regional Development Fund

GUIDELINES FOR IMPROVING THE MANAGEMENT OF THE MARINE ENVIRONMENT AND COASTAL AREA OF SPLIT-DALMATIA COUNTY IN THE PART OF BEACH EROSION

Abbreviated:
GUIDELINES FOR IMPROVING MANAGEMENT IN THE PART OF BEACH EROSIONS SDŽ

This document was developed within the cross-border cooperation program INTERREG V-A Italy-Croatia 2014-2020, a strategic project Climate change information, monitoring and management tools for adaptation strategies in Adriatic coastal areas – AdriaClim, identification number 10252001.

The strategic project was approved as part of the first strategic call for proposals under Priority Axis 2: Safety and Resilience; Specific objective 2.1: Improving the monitoring, forecasting, and planning of climate change adaptation measures.

Customer:	**RERA** – Public Institution for Coordination and Development of Split-Dalmatia County
Made by:	**Obala** d.o.o., Split
Document label:	1266/23 (1266-23_ST_Guideliness beach erosion SDŽ)
Contract:	KLASA: 432-02/22-01/0016; URBROJ: 2181-223-01-22-00008
Team: (Alphabetical ord.)	mr.sc. **Željan Pernat**, dipl.ing.građ. dr.sc. **Goran Vego**, dipl.ing.građ. **Josip Zekan**, mag.ing.aedif.
Associates:	**Goran Maričić**, dipl.ing.građ., Institut IGH d.d. (granulometry testing)
Coordination council:	**Matea Dorčić**, Administrative Department for Tourism and Maritime Affairs SDŽ **Ivan Samardžija** Public institution RERA S.D. for coordination and development SDŽ **Katarina Šuta**, Administrative Department of Economy, EU Funds and agriculture **Marija Vuković**,Administrative Department for Municipal Affairs, Municipal Infrastructure and Environmental Protection **Jelena Kurtović**, Public Institution Sea and Karst **Joško Stella**, Split-Dalmatia County Tourist Board
Advisory council:	**Gorana Jelić Mrčelić**, Faculty of Maritime Studies, University of Split **Gojko Berlengi**, Cooperative Granum Salis **Vinka Kolić**, Hydrographic Institute of the Republic of Croatia **Živana Ninčević Gladan**, Institute of Oceanography and Fisheries **Ana Mikačić**, Ministry of the Interior, Directorate of Civil Protection, Regional Teaching Centre Split **Martina Baučić**, Faculty of Civil Engineering, Architecture and Geodesy, University of Split **Željka Škaričić**, PAP/RAC **Daša Dragnić**, City Hall of the Split-Dalmatia County Assembly **Ivana Krstulović Baković**, Association for Nature, Environment and Sustainable Development „Sun“
Partner council:	**Ivana Mrković Kusanović**, Municipality of Nerežišća; **Marin Perčić**, Association of underwater activities Rostrum Split; **Dijana Miše**, Municipality of Okrug; **Josko Roščić**, Municipality of Baška Voda; **Stipe Žuljević-Mikas**, Town of Omiš; **Ana Sviličić**, Town of Vis; **Jozo Tomaš**, HGK-County Chamber Split; **Zoran Paunović**, City of Makarska; **Dujo Odžak**, , City of Makarska; **Ivan Krželj**, Općina Zadvarje; **Ante Čobrnić**, Općina Tučepi; **Siniša Marović**, Općina Postira; **Marino Kaštelan**, Municipality of Pučišća; **Frane Lozić**, Municipality of Milna; **Ante Jurić**, City of Komiža; **Nikola Cvitanić**, Municipality of Bol; **Zlata**

Seferović, City of Split; **Ivan Slavić**, Municipality of Sućuraj; **Tanja Antunović**, Municipality of Podgora; **Stipe Ursić**, Municipality of Brela; **Božen Živaljić**, Municipality of Podstrana; **Marija Vučica**, City of Kaštela; **Ante Ljubičić**, City of Solin; **Danijela Kirigin**, City of Supetar; **Tonko Faldić**, Grad Stari Grad; **Pavao Tomić**, Municipality of Dugi Rat; **Ivica Keršić**, Municipality of Jelsa; **Darija Najev Jurač**, Municipality of Marina; **Ivo Sorić**, Municipality of Seget; **Petar Bezmalinović**, Municipality of Selca; **Petar Anibalović**, Municipality of Sutivan; **Nikola Cecić-Karuzić**, Municipality of Šolta; **Nino Pijanović**, City of Hvar; **Maja Jurišić**, island movement

CONTENT

1. INTRODUCTION

1.1. Goal and purpose

Split-Dalmatia County (SDŽ) has initiated the process of drafting the Marine Environment and Coastal Management Plan of Split-Dalmatia County (Cooperative Granum Salis, 2021), as an additional study and planning document whose declared goal is to improve management and achieve sustainability in its coastal area.

One of the reasons for the adoption of this document is to respect the first-class importance of the coastal area of Split-Dalmatia County for its development on the one hand, as well as the vulnerabilities and development constraints in this area on the other, and following the recommendations of the Protocol on Integrated Coastal Zone Management in the Mediterranean and good coastal zone management practices, with the aim of its preservation, sustainable and resilient development.

In the SDŽ area, 1,098 beaches have been identified, with the term beach referring to the sedimentary body of beaches made of granular materials. The current practice of managing beaches in SDŽ, related to ensuring their physical viability, has several weaknesses. Most of the beaches are maintained annually without a professionally made project basis that should include:

- analysis of geomorphological characteristics of the area and wave conditions;
- assessment of the amenities of the location for construction (in case of artificial beach);
- the design of the beach, including groynes for its protection, in accordance with existing terrain and wave conditions;
- defining the slope of the beach in a way that makes it suitable for use, but also relatively stable and resistant to the influence of waves;
- the design of the undersea embankment / sill that retains the beach material and causing the wave to break reduces its destructive effect on the beach;
- defining the granulation range of the backfilling material (crushed rock material) in accordance with the energy of the waves to which it is exposed, because the amount of beach material transport directly depends to its size, and to the size and intensity of the waves.

For the purposes of the SDŽ Coastal Plan, a preliminary analysis and categorization of the vulnerability of beaches to erosion was made, given exposure to waves, according to a simple model in which vulnerability depends on the maximum of significant wave height for characteristic winds in the area of SDŽ and the openness of the beach to different wind blowing directions (chapter 2.4).

Analysis based on a more complete model, supplemented with field research, is the subject of this study.

1.2. Methodology

Based on the defined objectives of the previous chapter, with an emphasis on improving the practice of coastal zone management through its conservation, sustainable and resilient development, it is completely clear that the conclusions of this study must contribute to **raising the level of understanding of the primary** impacts affecting beaches made of granular materials, and **the determination of the basic**

concepts of construction coastal interventions in order to ensure the long-term sustainability of such beaches on primary impacts, taking into account and intensifying impacts due to climate changes, and certainly respecting the ecological aspect to the maximum. The conclusions clearly and unambiguously define guidelines for the analysis, planning, dimensioning and design of sustainable beaches.

In order to adopt quality guidelines that will try to solve the problems of beach erosion made of granular materials and ensure their long-term sustainability, a series of procedures have been carried out that basically represent a methodology summarized through the diagram given in Figure 1.1.

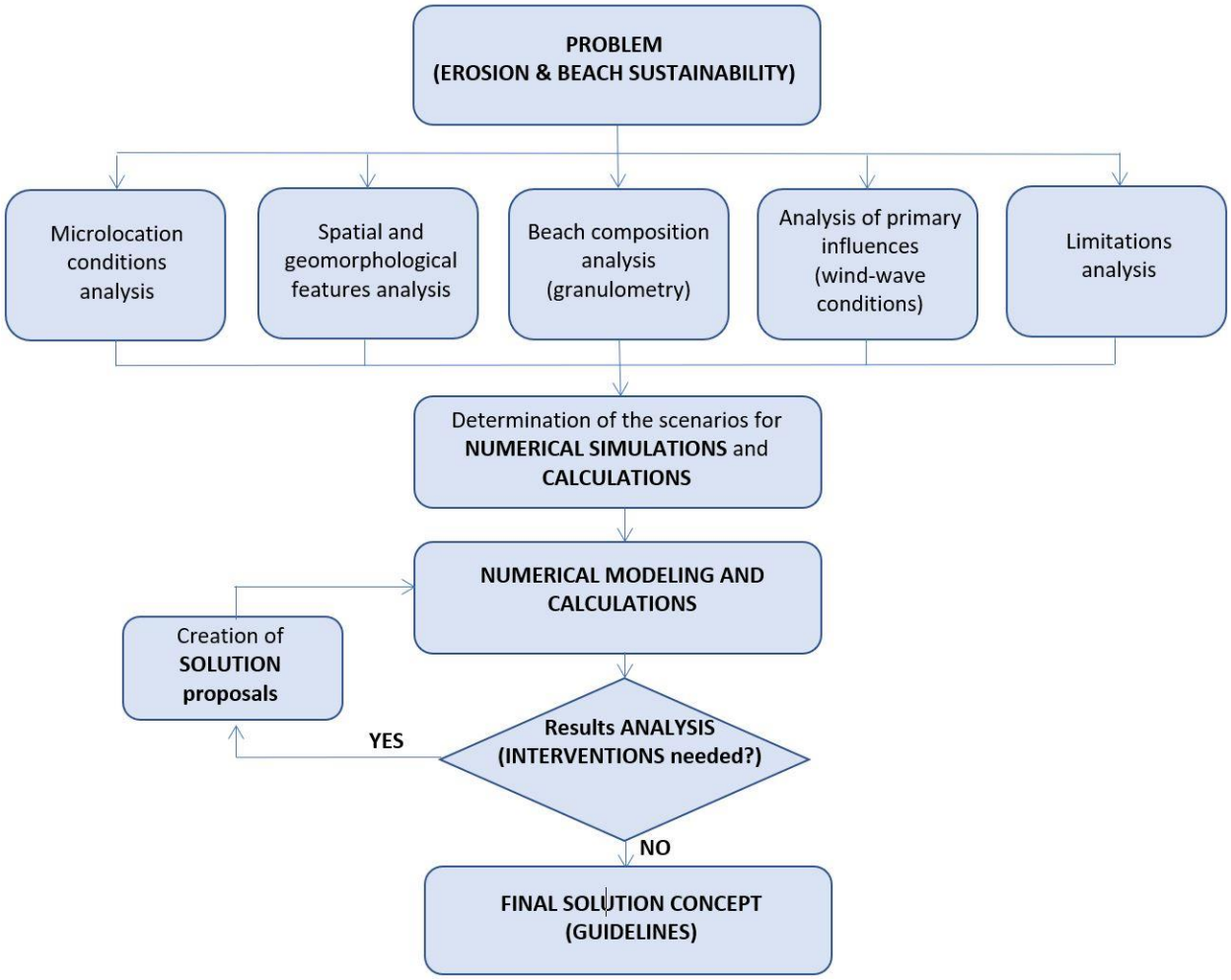

Figure 1.1 – Sequence of procedures (methodologies) for tackling erosion and beach sustainability

In the framework of the proposed methodology, previous analyses have been carried out, which include:

A) Previous analyses determining the characteristics of the microlocation (for each of the 5 selected beach locations separately)

A.1) Analysis of the conditions of the microlocation of the beach – processing of the properties of depths, geomorphological properties of the coastline, catchment area, state of construction of the area, processing of available data and basic surveys, records of interventions regarding previously performed interventions and nourishment procedures;

A.2) Preparation of prior analysis of wind characteristics from the relevant station – analysis of wind measurement data (DHMZ data);

A.3) Creating a wind climate of a deepwater wave at a location of interest – processing and determination of significant wave height, period and wave length for the relevant incident directions for each of the locations;

A.4) Making a granulometric curve of beach sediment samples excluded from the site for each location for a representative sample.

After the previous analysis, which determines the settings of the existing state of each location, and the primary impacts and their intensities, a list of relevant scenarios was made with which numerical modeling was carried out, and the determination of the framework for the implementation of other relevant calculations.

As part of this step, the following was performed:

B) Preparation of scenarios for the implementation of numerical simulations and frameworks for calculations (for each of the 5 selected beach locations separately)

B.1) Creating a list of numerical simulations, with labels and parameters of each simulation;

B.2) Determination of the framework for the calculation of beach material transport.

C) Conducting numerical modeling and calculating (for each of the 5 selected beach locations separately)

C.1) Creation of numerical models and implementation of numerical simulations of waves;

C.2) Calculations of the beach material transport based on the results of conducted numerical simulations of waves and granulometric composition of beaches.

After numerical modeling and control calculations of material transport were made, a critical analysis of the results was carried out:

D) Analysis of the result of the numerical modelling and calculation:

D.1) Model wave field analysis – the relevant values of wave parameters for beach dimensioning have been established, by implementing wave field transformation mechanisms (refraction, diffraction, reflection, and wave breaking) in the zone of influence of the seabed;

D.2) The degree of sustainable composition of the beach is determined based on the executed calculations of the material transport.

The basic principle used in the analysis of the results of numerical modeling of waves and the control calculation of material transport, given by the proposed methodology, included checking the satisfaction of sustainability requirements for the existing state and the assessment of the threat of rising sea levels as a result of climate change in the future. Based on this, the need for construction interventions in the area of the beach in question was determined.

In this case, the necessity of construction interventions in the area of the analyzed beaches was demonstrated in the case of all beaches except Stiniva beach on the island of Vis, for which no significant potential problems were identified due to primary impacts, such as waves and rising sea levels due to the consequences of climate change.

Therefore, for all other beaches, namely Zlatni rat beach on Brač, Podgora beach on the Makarska Riviera,

beaches on the Podgora-Duće stretch, and Kašjuni beach in Split, the analysis of the results of modeling and control calculations of material transport pointed to the need for construction interventions in order to raise the level of their sustainability for existing and future external influences.

For the beaches of Podgora on the Makarska Riviera, the beaches on the Podstrana-Duće area and Kašjuni beach in Split, proposals for solutions with construction interventions for smaller control areas (zones) were given in order to eliminate the observed deficiencies in accordance with the basic technical principles set. No proposal has been made for Zlatni rat beach because it is a protected natural landscape, where any intervention would disrupt the natural processes that make this beach a natural phenomenon. Only guidelines have been given for Zlatni rat beach that should help if sea level rises due to climate changes. For the other three beach locations, for which the need to raise the level of sustainability was determined, the procedures of conducting numerical simulations with proposed solutions in control zones were repeated. Repeated analysis of the results indicates that the proposed solutions have yielded satisfactory results in terms of the achieved degree of sustainability of the beaches concerned, and consequently they represent a good basis for establishing guidelines for ensuring the sustainability of beaches from erosion.

After all, conclusions were reached and guidelines established:

E) Measures to ensure beach sustainability and adaptation to climate changes

E.1) General measures of nourishment and stabilization of beaches;

E.2) Analysis of the effects of climate changes on variables relevant to the beach, such as sea levels and precipitation;

E.3) Analysis of the impact of sea level variability and precipitation on the surface of the face of the beach;

E.4) Guidelines for beach sizing and design - includes a spatial-temporal definition of interventions in space with the aim of preserving the sustainability of selected beaches and adaptation to climate changes.

This methodological approach provides the basic prerequisites for making quality and consistent conclusions, as a necessary and stable basis for the development of general, but also detailed guidelines for the dimensioning and design of beaches made of granular materials, with the goal of conservation and sustainable and resilient development of the coastal area of Split-Dalmatia County.

2. BASIC SURVEYS AND PREVIOUS ANALYSES

In order to draw high-quality and consistent conclusions, as a necessary and high-quality basis for the development of general, but also detailed guidelines for the dimensioning and design of beaches made of granular materials, with the ultimate goal of conservation and sustainable and resilient development of the coastal area of Split-Dalmatia County, the first and basic step is to obtain and analyze the basic necessary bases, review the existing previous analyses, and analyze the conditions of microlocation at each of the five locations (beaches). It is geodetic data, i.e., the geometry of the bottom and coastal land of each of the sites that need to be adequately processed for further analysis. Furthermore, it is necessary to provide an analysis of the conditions of microlocation in terms of depth properties, geomorphological properties of the coastline, analysis of the catchment area, the state of construction of the area, and possibly previously performed interventions and procedures for beach nourishment. Also, it is necessary to give accents from previously conducted analyses, and here it primarily refers to the Marine Environment Management Plan and coastal area of Split-Dalmatia County (Cooperative Granum Salis, 2021).

2.1. Geodetic data with analysis of microlocation conditions

In order to be able to carry out an appropriate model analysis of the beaches concerned regarding hydrodynamic impacts, given as part of Chapter 6 of this study, it is necessary to have relevant geodetic data on the position of the coastline and bathymetry of the waters considered. These are basic surveys that give three-dimensional geometry of the considered area, necessary for a quality numerical interpretation of hydrodynamic physical processes that occur in the coastal area and which dominantly affect the morphology of beaches made of granular materials and their sustainability in time.

For this purpose, the Croatian Hydrographic Institute (HHI) has provided bathymetric data (sea depths) for selected five beaches in Split-Dalmatia County at locations including Zlatni rat (Brač), Stiniva (Vis), Podgora (Makarska Riviera), Podstrana-Duće and Kašjuni (Split).

Below, for each of the locations, i.e., beaches, an overview of these bathymetric data is given, as well as a description and analysis of the microlocation conditions.

2.1.1. Brač (Zlatni rat)

Figure 2.1 shows bathymetric surveys provided by Croatian Hydrographic Institute (HHI) for Zlatni rat beach aquatory on the island of Brač. These are georeferenced images with a display of depths and different survey densities.

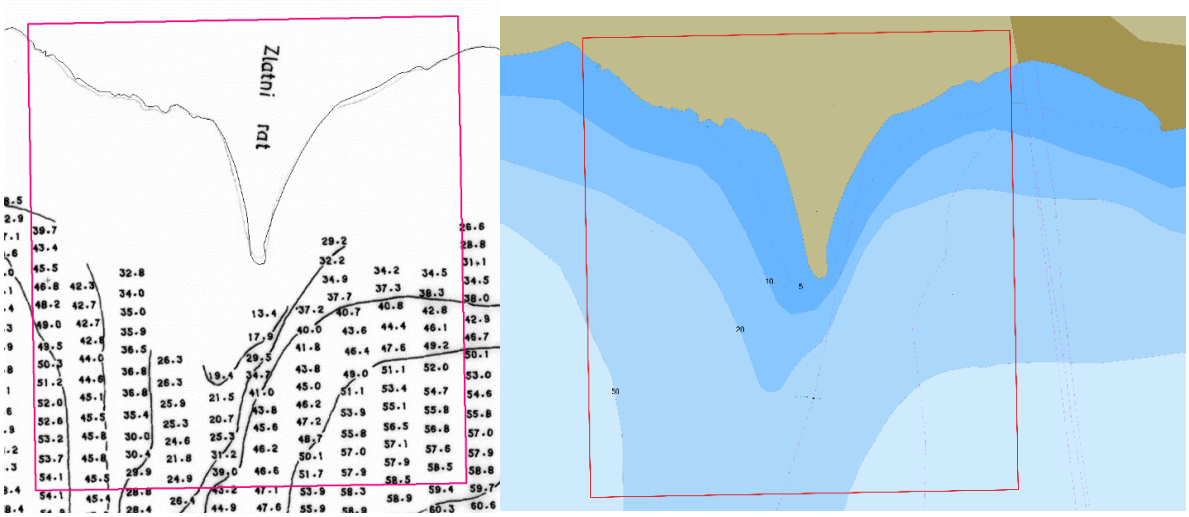

Figure 2.1 – Bathymetric data for the location of the beach Zlatni rat (Brač), *copyright* © HHI

After the digitization of the submitted bathymetric surveys, the data were entered into the computer numerical model (CGWAVE – more in chapter 6), which has the possibility of automatically generating a three-dimensional spatial domain for the purpose of conducting numerical wave simulations.

The domain of numerical model with bathymetry for the location of Zlatni rat beach on the island of Brač, is shown in Figure 2.2.

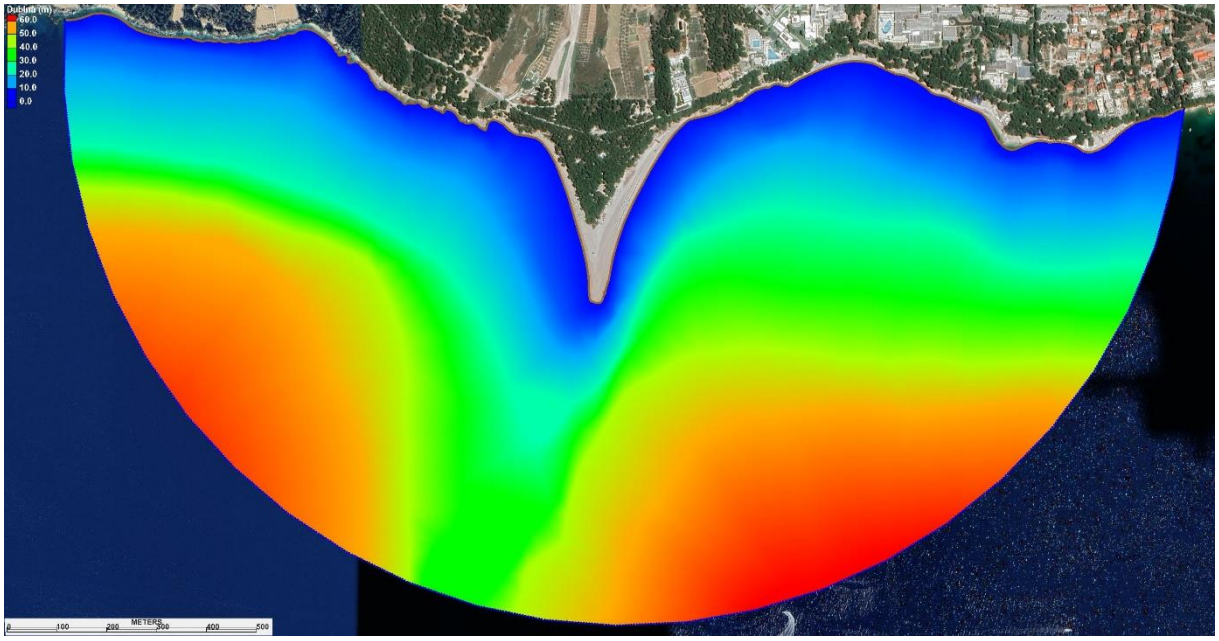

Figure 2.2 – Numerical model domain with bathymetry for Zlatni rat beach (Brač)

As can be seen in Figures 2.1 and 2.2, the aquatory of Zlatni rat beach on the island of Brač, is primarily characterized by a very recognizable outline of the cape of the beach itself, which stands out from the surrounding mainland and "plunges" into the immediate aquatory. The beach is naturally formed and is made of grainy, pebble stone material, with granulometric composition given as part of chapter 4 in this

study.

The depths in the immediate vicinity of the coastline are relatively shallow, and the characteristic transverse profiles of the beach, are given in Figure 2.3, reveal that the slope of the bottom of the beach on the cape, facing east is approximately 1:8 in the shallower part, and somewhat steeper in the deeper part of the beach, while at the western beach it has an approximate slope of 1:20 in the shallower part, and somewhat steeper in the deeper part of the beach.

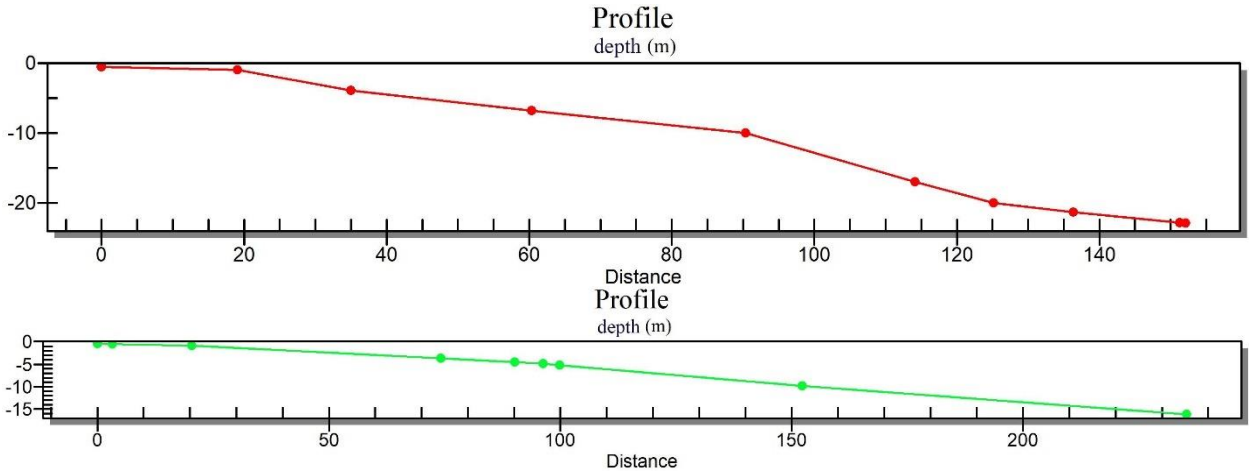

Figure 2.3 – Characteristic profiles of Zlatni rat beach (Brač) – east beach (top), west beach (below)

The specific disposition of the beach in question, which forms a characteristic cape, makes it exposed to waves from second and third quadrants. Namely, it is from these directions that the dominant wind waves come that perform its morphological formation. It is known that the very top of Zlatni rat beach at different period of year can be oriented towards east or west, depending on the direction from which the waves that were more dominant during that period. For example, it is common that during the winter months, the waves of the south and levant coming from the east and southeast, point the top of the beach to the west, while in the summer, due to more frequent wind waves from the western directions, such as mistral, the top of the beach is again restored with orientation towards the east.

This dynamic of the shape of Zlatni rat beach makes it quite stable in terms of maritime degradation and erosion of beach material, because there is a systematic dynamic balance of transport of beach material. Namely, the balancing of the beach material transport occurs when wind waves from one direction seemingly degrade the beach, temporarily taking the material into the depth or pushing it to the shore, while in the next wave situation and the appearance of waves from the opposite direction, the material returns to its original state. This is an extremely important process that ensures relatively good stability of the existing embankment material of Zlatni rat beach over time.

Zlatni rat beach is a natural phenomenon that arose over a long period of time in the past, when stone material from the steep slopes of Vidova Gora was gradually brought towards the sea by torrents, where the dynamic action of waves formed it into the shape as it is known today. With human activity, and primarily with the construction of roads and facilities in the hinterland of the beach, these natural inflows of new stone material have been cut and today there is no longer a possibility of natural nourishment of the Zlatni rat beach with new material. The same applies to the entire coastal area in the immediate vicinity of Zlatni rat beach and the village of Bol. Therefore, it is necessary to carry out artificial periodic

nourishment of the beaches in the coastal zone in question by appropriate granulation of stone material. Which material exactly is in question in terms of granulometric composition, and which will guarantee the stability of the beach in relevant wind conditions and conditions due to climate changes, primarily raising the sea level, more in chapter 7 of this study.

Due to the above-mentioned hydrodynamic phenomena, but also because it is a protected landscape, any construction intervention in the underwater and other part of the beach and the entire coastal zone in question, including the nourishment with new beach material, should be thoroughly and carefully studied,

and analyzed, in order to avoid causing lasting consequences for this unique natural morphological phenomenon.

2.1.2. Vis (Stiniva)

Figure 2.4 shows bathymetric surveys provided by the Croatian Hydrographic Institute (HHI) for Stiniva beach aquatory on the island of Vis. These are georeferenced images with a display of depths and different survey densities.

After the digitization of the submitted bathymetric surveys, the data were entered into the computer numerical model (CGWAVE – more in chapter 6), which has the possibility of automatically generating a three-dimensional spatial domain for the purpose of conducting numerical simulations of waves.

The domain of the numerical model with bathymetry for the location of the beach Stiniva on the island of Vis, is shown in Figure 2.5.

As can be seen in Figures 2.4 and 2.5, the aquatory of the natural beach Stiniva on the island of Vis, is located at the bottom of a relatively deep rocky bay on the south side of the island. The beach itself is very small, only forty meters in length and is sheltered by a high, recognizable, and unique, rock wall with a narrow opening, which separates it from the remaining waters of the entire bay. The beach is made of grainy, pebble stone material, with granulometric composition given as part of chapter 4 of this study.

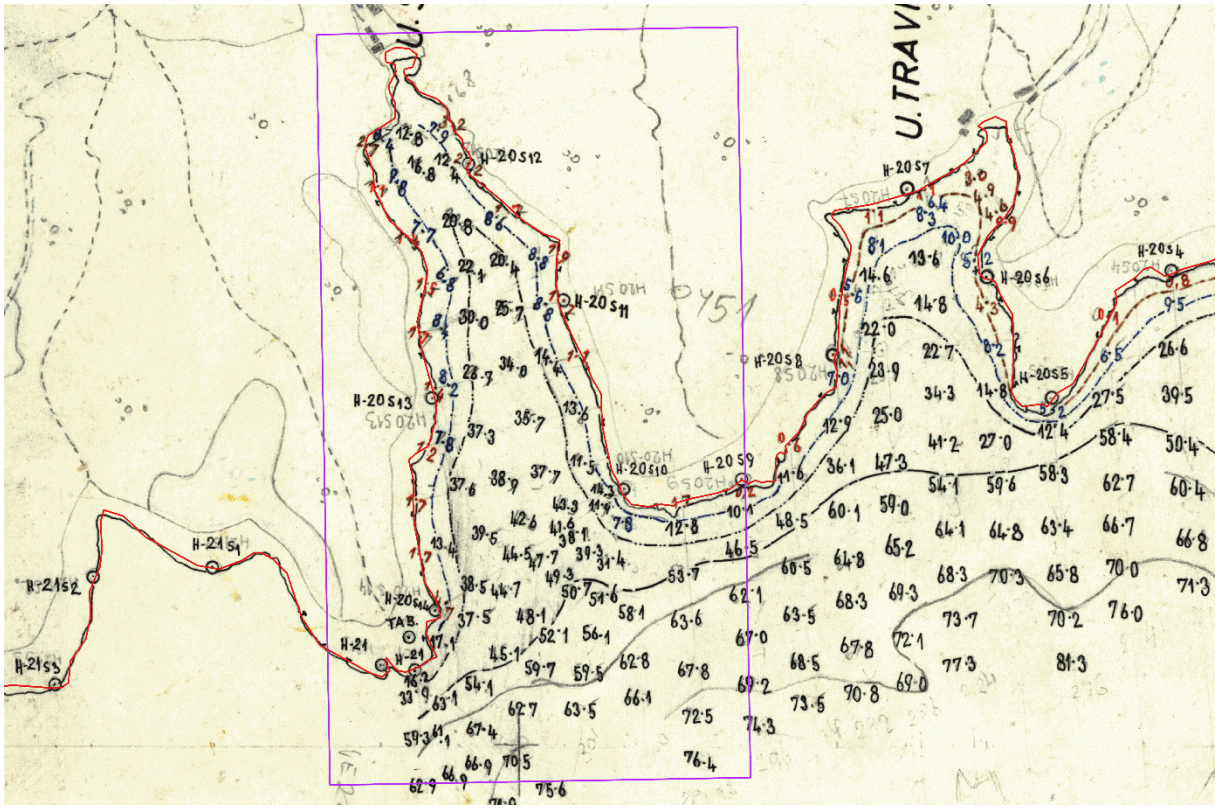

Figure 2.4 – Bathymetric data for the location of the beach Stiniva (Vis), *copyright* © HHI

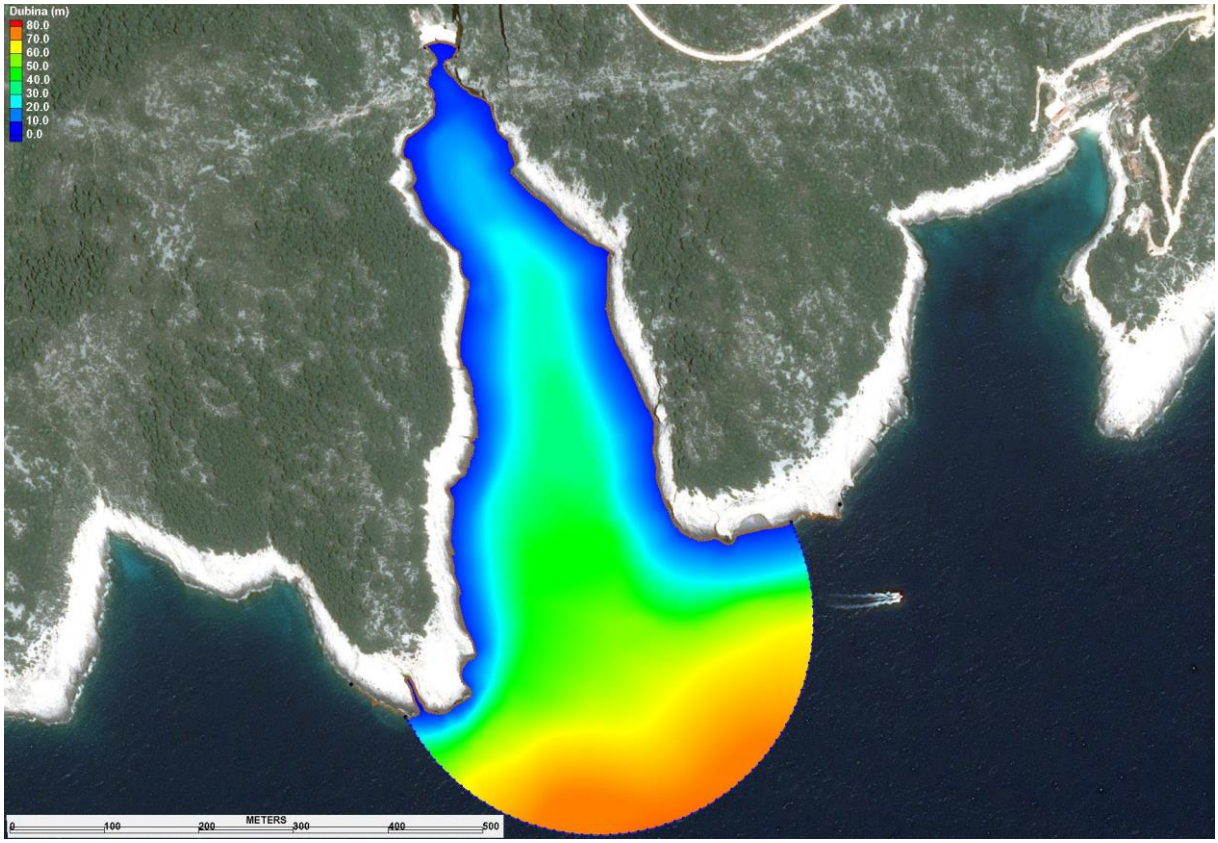

Figure 2.5 – Numerical model domain with bathymetry for Stiniva beach (Vis)

The depths in the immediate vicinity of the coastline are extremely shallow, and the characteristic transverse profile of the beach, is given in Figure 2.6, reveals the transverse slope of the bottom of the beach, which is approximately 1:6.

The specific spatial disposition of the beach in question, which is located within a larger bay and sheltered by a natural rock wall, and the small depth, contribute to a relatively good shelter from all wave influences. As primary wave influences, the most important for the beach are wind waves from the second and third quadrants. However, regardless of their exact direction from which they come, the configuration of the coast and the bottom is such that all incident waves due to physical processes of wave transformations, primarily refraction and diffraction, take on approximately the same direction, so as the only relevant parameter of impact on the beach can be taken into consideration is their intensity, i.e., wave height and wave period.

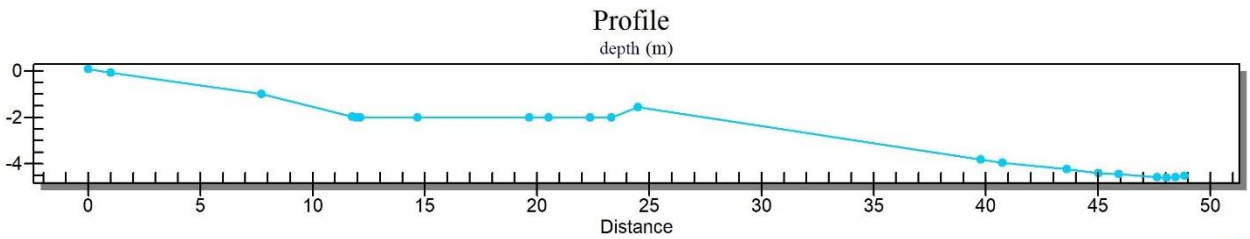

Figure 2.6 – Characteristic profile of Stiniva beach (Vis)

When we add to this spatial specificity of the beach in question the fact that the immediate aquatory is extremely shallow, it can be concluded that Stiniva beach is quite stable in terms of maritime degradation of beach material, because most of the energy of the incident waves is lost well before they reach the very face of the beach. This is shown in more detail in chapters 6 and 8 of this study. In such an environment, the embankment rock material of the beach remains in stable natural dynamic balance, without greater threat from its degradation and erosion due to hydrodynamic action of the sea. The only danger for beach erosion is the possibility of torrential flows from relatively steep slopes in its hinterland, and human activity.

Stiniva beach is a natural phenomenon that arose over a long period of time in the past, when stone material from steep slopes in its hinterland torrents was gradually brought towards the sea, where the dynamic action of waves formed it into the shape as it is known today. Fortunately, the beach avoided significant human intervention. Although there is a smaller catering facility on the site, it seems that there is still the possibility of its natural nourishment with stone material from the slopes in the hinterland via torrential flows, which is why, at least for the time being, it is not necessary to artificially nourish it with beach material. If future trends due to climate changes, primarily raising the sea level, indicate the need for artificial nourishment of the Stiniva beach, it is necessary to do so with a material of a specific granulometric composition, and more about this in chapter 7 of this study.

Due to all the above, and primarily because it is a protected natural landscape, any construction intervention in the underwater and other part of the beach, and in the immediate vicinity of the beach itself, including nourishment with new beach material, should be thoroughly and carefully analyzed, and studied, in order to avoid causing lasting consequences for this natural morphological phenomenon.

2.1.3. Makarska Riviera (Podgora)

Figure 2.7 shows a bathymetric survey provided by the Croatian Hydrographic Institute (HHI) for Podgora beach aquatory on the Makarska Riviera. It is a georeferenced image with a display of depths.

After the digitization of the submitted bathymetric surveys, the data were entered into the computer numerical model (CGWAVE – more in chapter 6), which has the possibility of automatically generating a three-dimensional spatial domain for the purpose of conducting numerical simulations of waves.

The domain of a numerical model with bathymetry for the location of Podgora beach on the Makarska Riviera, is shown in Figure 2.8.

As can be seen in Figures 2.7 and 2.8, the beach areas of Podgora are located along the entire coastal stretch of the settlement itself. These are approximately two kilometers of beaches, which were formed in different periods of time, by filling some beach zones and building stone groynes for stabilization. So, it can be said that the beaches in this area were originally naturally formed, but today they are predominantly artificially nourished and expanded by artificial backfilling. The beaches are made of granular, primarily gravel stone material, with granulometric composition given as part of chapter 4 of this study.

Figure 2.7 – Bathymetric data for the location of Podgora beach (Makarska Riviera), *copyright* © HHI

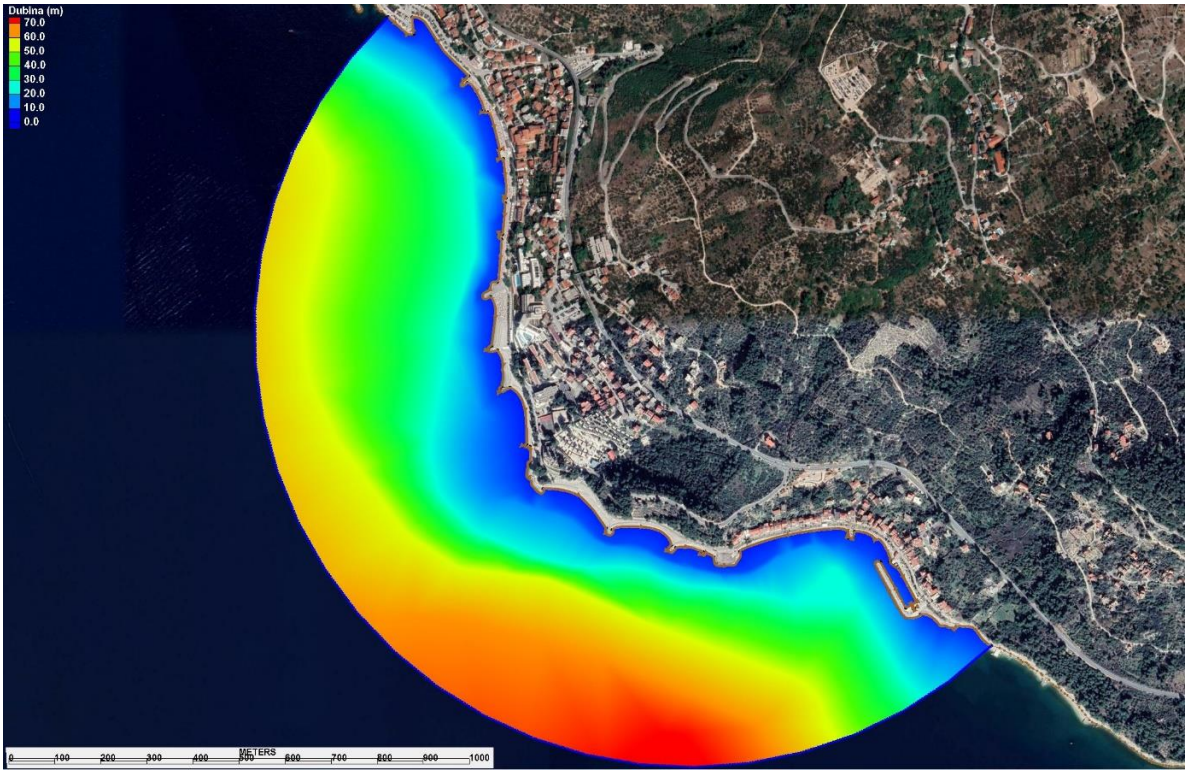

Figure 2.8 – Numerical model domain with bathymetry for Podgora beach (Makarska Riviera)

Interventions of such beach backfilling have shown certain shortcomings, primarily in terms of the sustainability of beach material and its gradual erosion, contributing to the need for their annual nourishment. The reasons for this problem need to be sought primarily in the inadequate spatial placement of protective coastal buildings and/or inadequate embankment material from which the beaches are formed, where part of the material is carried away to the deeper sea during the year, and part of it accumulates towards the land, so it is periodically necessary to align it and return it back to the sea.

The main cause of this practice, which relates significant financial resources and causes permanent damage to the underwater environment, lies in the insufficiently researched physical characteristics of the relevant hydrodynamic influences that affect the immediate waters of the beaches in question.

The depths in the immediate vicinity of the coastline of the beaches in the area of Podgora on the Makarska Riviera are relatively shallow, with the characteristic transverse profile of the beach given in Figure 2.9. The characteristic transverse slope of the bottom of the beach in the shallower part is approximately 1:5, and in the deeper part somewhat milder.

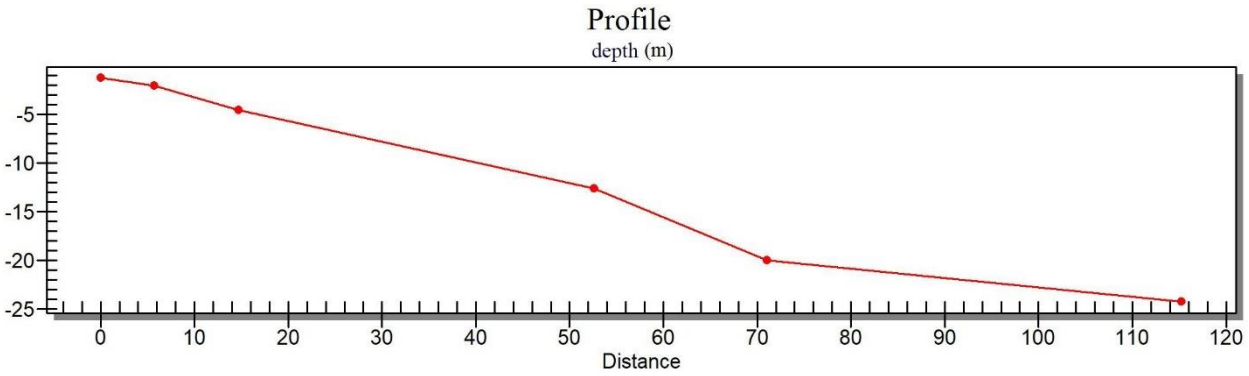

Figure 2.9 – Characteristic profile of Podgora beach (Makarska Riviera)

Given the relatively long stretch of beaches, which are partly oriented in the north-south direction and partly in the north-southeast direction, it can be concluded that the beaches are exposed to a wide range of incident waves. As the primary wave influences, the most important for the beach are wind waves from the second and third, and even the fourth quadrant.

This spatial disposition of the beaches in question makes them extremely unstable in terms of the degradation of beach material, because the relaxation of wave energy waves in the form of wave breaking processes, primarily takes place on the coastal line itself or in its immediate vicinity. Such a hydrodynamic situation is the most unfavorable for beaches from granular materials in terms of their sustainability, because in such situations part of the beach material is pushed towards the mainland, creating relatively steep beach formations, while part of the material is permanently transferred to the deeper parts of the waters, contributing to the gradual erosion of the beach.

As already stated, the beaches in the area of Podgora were originally naturally formed by torrential inflows of material from nearby elevations in the hinterland, over a long period of time in the past, towards the sea where the dynamic action of waves formed it into natural beaches. With the construction of the main road and facilities in the hinterland of the beach, these natural inflows of new stone material have been cut and today there is no longer a possibility of natural replenishment of beaches in the area of Podgora. The same can be said about the entire coastal belt on the Makarska Riviera, but also generally for the entire coastal belt along the Adriatic highway. Therefore, it is necessary to carry out artificial periodic nourishment of the beaches in the coastal zone in question by appropriate granulation of stone material. Which material exactly is in question in terms of granulometric composition, and which will guarantee the stability of the beach in relevant wind conditions and conditions due to climate change, primarily raising the sea level, more in chapter 7 of this study.

If we add to all the above a relatively significant risk of beach erosion due to the possibility of torrential flows from relatively steep slopes in its hinterland, the situation requires a very detailed consideration in order to solve the detected problem.

2.1.4. Podstrana-Duće area

Figure 2.10 shows bathymetric surveys provided by the Croatian Hydrographic Institute (HHI) for aquatory of the beaches on the Podstrana-Duće area. These are georeferenced images with a display of depths and different survey densities.

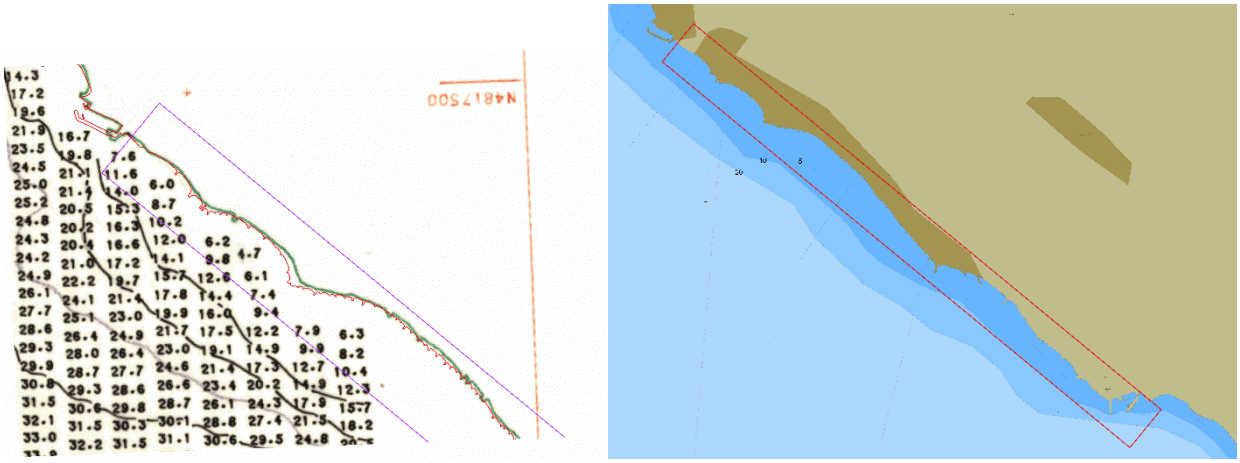

Figure 2.10 – Bathymetric data for the location of the beach on the Podstrana-Duće area, *copyright* © HHI

After the digitization of the submitted bathymetric surveys, the data were entered into the computer numerical model (CGWAVE – more in chapter 6), which has the possibility of automatically generating a three-dimensional spatial domain for the purpose of conducting numerical simulations of waves.

The domain of numerical model with bathymetry for the location of beaches on the Podstrana-Duće area, is shown in Figure 2.11.

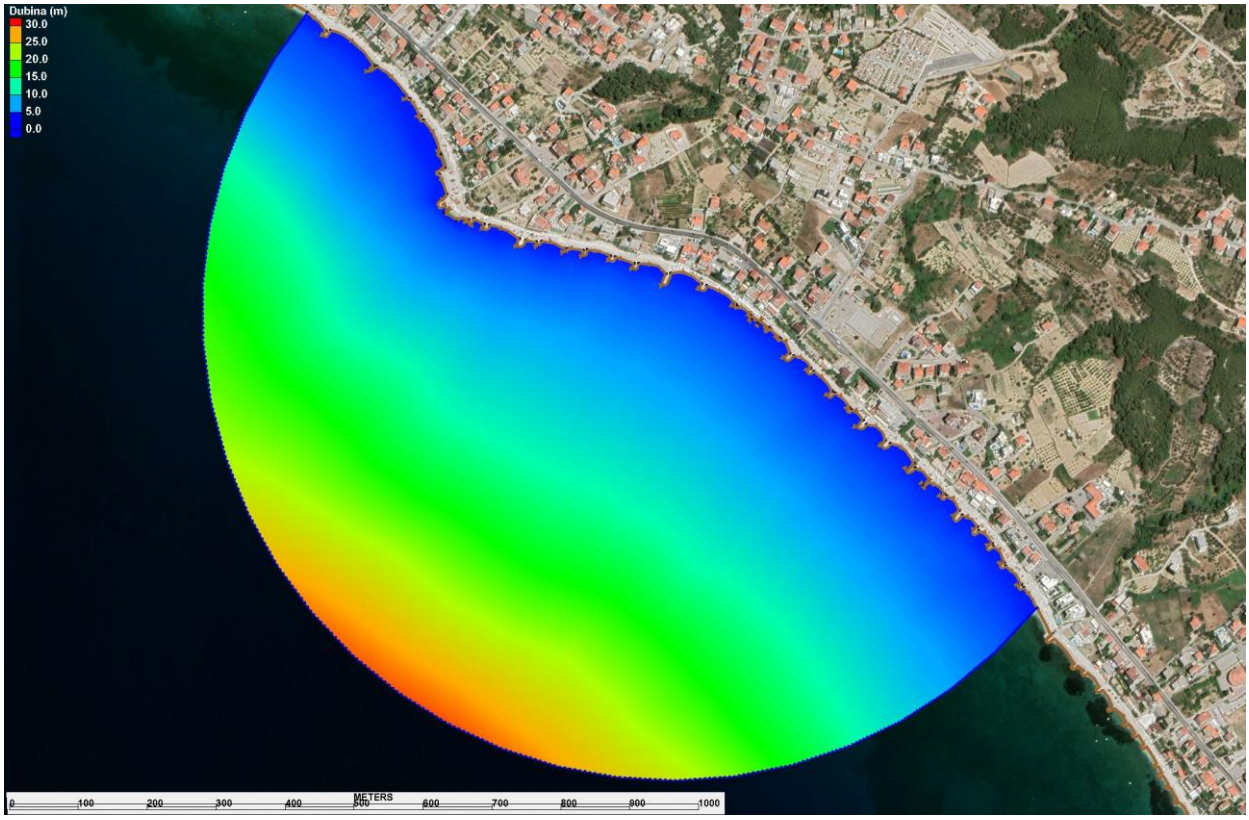

Figure 2.11 – Numerical model domain with bathymetry for beaches on the Podstrana-Duće area

As can be seen in figures 2.10 and 2.11, the multi-kilometer beaches on the Podstrana-Duće area were built of granular, predominantly gravel material, which were formed in different periods of time, by filling individual beach zones and building stone groynes for stabilization. So, it can be said that the beaches in this area were originally naturally formed, but today they are predominantly artificially nourished and expanded by backfilling. The beaches are made of granular, gravel stone material, with granulometric composition given as part of chapter 4 of this study.

Backfilling interventions in space have shown certain shortcomings, primarily in terms of the viability of beach material and its erosion, contributing to the need for annual nourishment with beach material. The reasons for this problem need to be sought primarily in the inadequate spatial placement of protective coastal buildings and / or inadequate embankment material from which the beaches are formed, where part of the material is carried away to the deeper sea during the year, and part of it accumulates towards the land, so it is periodically necessary to align it and return it back to the sea.

The main cause of this practice, which relates significant financial resources and causes permanent damage to the underwater environment, lies in the insufficiently researched physical characteristics of the relevant hydrodynamic influences that affect the immediate waters of the beaches in question.

The depths in the immediate vicinity of the coastline of the beaches on the Podstrana-Duće area are relatively shallow, with a characteristic transverse profile of the beach given in Figure 2.12. The characteristic transverse slope of the bottom of the beach is approximately 1:15.

Given the relatively long stretch of the beach, which is largely oriented in the northwest-southeast direction, it can be concluded that the beach is exposed to a wide range of incident waves. As the primary wave influences, the most important for the beach are wind waves from the second and third, and even the fourth quadrant.

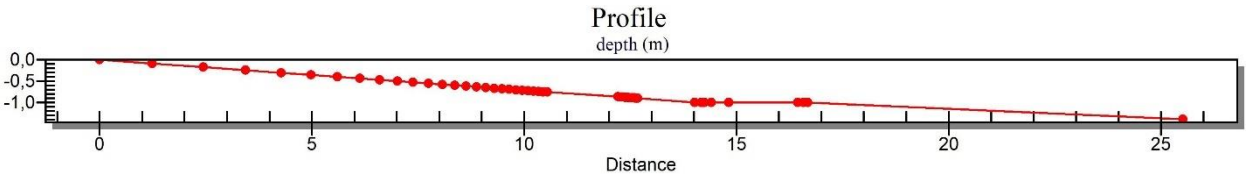

Figure 2.12 – Characteristic profile of the beach on the Podstrana-Duće area

This spatial disposition of the beaches in question makes them extremely unstable in terms of degradation of beach material, because the relaxation of wave energy of the incident waves in the form of wave breaking processes primarily takes place on the coastal line itself or in its immediate vicinity. Such a hydrodynamic situation is the most unfavorable for beaches from granular materials in terms of their sustainability, because in such situations part of the beach material is pushed towards the mainland, creating relatively steep beach formations, while part of the material is permanently transferred to the deeper parts of the waters, contributing to the gradual erosion of the beach.

As already stated, the beaches on the Podstrana-Duće area were originally naturally formed by the flow of material from the nearby elevations in the hinterland, over a long period of time in the past, towards the sea where the dynamic action of the waves formed it into natural beaches. With the construction of the main road and facilities in the hinterland of the beach, these natural inflows of new stone material have been cut and today there is no possibility of natural nourishment of beaches in this area. The same applies, in general, to the entire coastal area along the Adriatic highway, which is why it is necessary to

carry out artificial periodic nourishment of the beaches in the coastal zone in question with appropriate granulation of stone material. Which material exactly is in question in terms of granulometric composition, and which will guarantee the stability of the beach in relevant wind conditions and conditions due to climate change, primarily raising the sea level, more in chapter 7 of this study.

If we add to all the above a relatively significant risk of beach erosion due to the possibility of torrential flows from relatively steep slopes in its hinterland, the situation requires a very detailed consideration in order to solve the detected problem.

2.1.5. Split (Kašjuni)

Figure 2.13 shows bathymetric surveys provided by the Croatian Hydrographic Institute (HHI) for Kašjuni beach aquatory in Split. It is a georeferenced image with a display of depths.

After the digitization of the submitted bathymetric surveys, the data were entered into the computer numerical model (CGWAVE – more in chapter 6), which has the possibility of automatically generating a three-dimensional spatial domain for the purpose of conducting numerical simulations of waves.

The domain of the numerical model with bathymetry for the location of Kašjuni beach in Split, is shown in Figure 2.14.

Figure 2.13 – Bathymetric data for the location of Kašjuni beach (Split), *copyright* © HHI

As can be seen in figures 2.13 and 2.14, Kašjuni beach in Split was formed on the south side of Marjan hill, by gradually artificial lynching of stone material in a naturally formed bay. So, it can be said that Kašjuni beach was originally naturally formed, but today's shape and size was obtained by artificially backfilling the material. In the past, the existing southern protective groyne/breakwater has been upgraded on several occasions, as it has a key function for the sustainability of the beach in question. Namely, as it happened that beach material was carried away from the site due to the action of incident waves, the groyne / breakwater experienced spatial changes, up to the present form.

The main cause of this iterative process of upgrading protective beach construction is insufficiently detailed research of the physical characteristics of the authoritative hydrodynamic influences that affect the immediate waters of the beach in question. The beach is made of grainy, pebble stone material, with granulometric composition given as part of chapter 4 of this study.

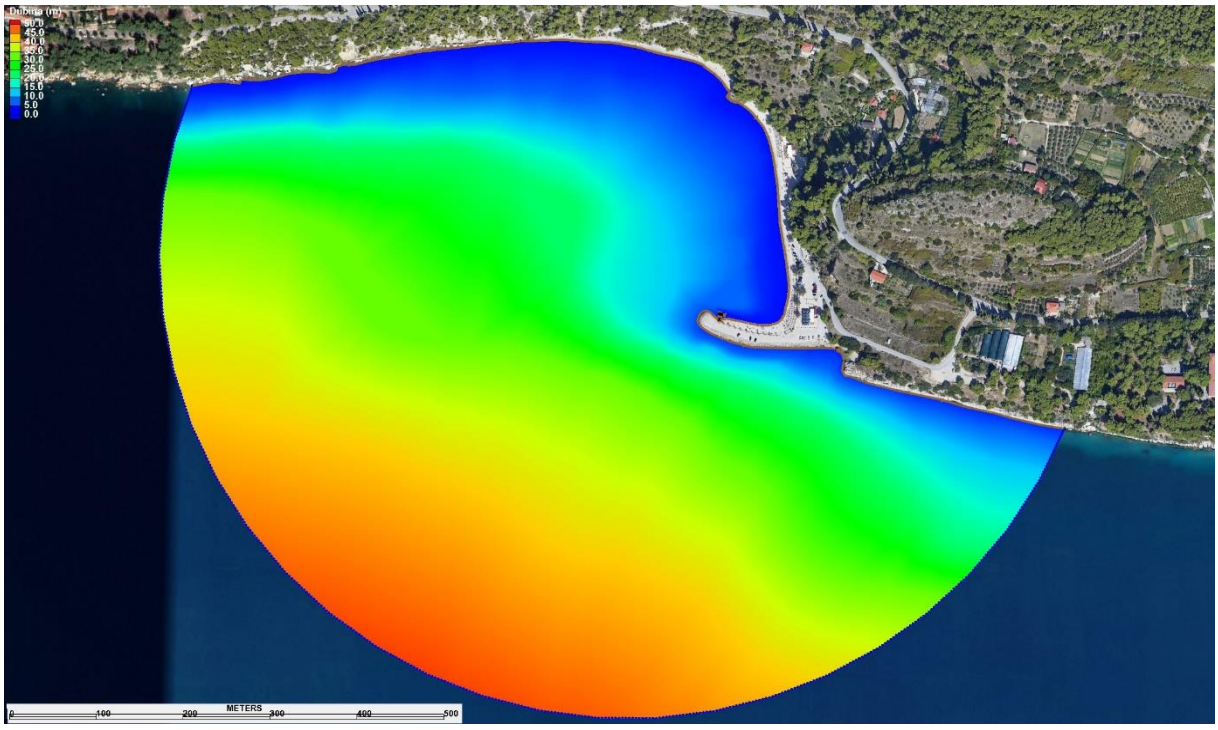

Figure 2.14 – Numerical model domain with bathymetry for Kašjuni beach in Split

The depths in the immediate vicinity of the coastline of Kašjuni beach in Split are relatively small, with the characteristic transverse profile of the beach given in Figure 2.15. The characteristic transverse slope of the bottom of the beach is approximately 1:12.

Given the wider spatial disposition, which makes it open to waves from the third and fourth quadrants, but within the relatively well protected waters, the beach in question in its existing state has relatively good opportunities to ensure stability and sustainability, with only minimally necessary interventions in space.

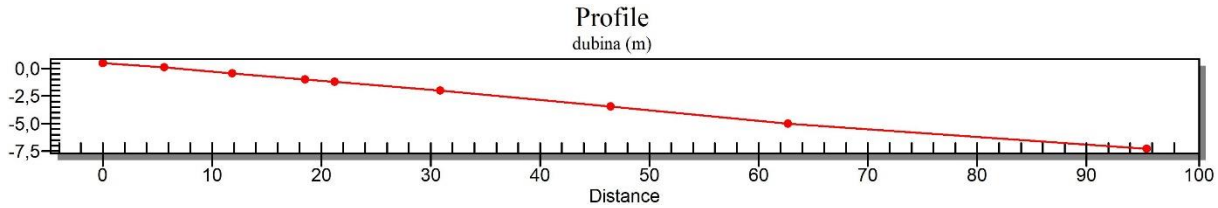

Figure 2.15 – Characteristic profile of Kašjuni beach (Split)

This spatial disposition of the beach in question makes it quite stable in terms of maritime degradation of beach material, because the relaxation of a significant part of the wave energy of the dominant incident waves takes place on the protective groyne / breakwater, before it reaches the beach itself. In such an environment, the appropriate rock material of the beach, with only minor interventions, could remain in relatively good natural dynamic balance, without greater threat of its degradation and erosion due to hydrodynamic action of the sea. However, tests of the granulometric composition of the existing material (Chapter 4 of this study) indicate that beach backfilling is not carried out with adequate material to ensure its stability in relevant wind conditions and conditions due to climate changes, primarily rising sea levels.

The danger of erosion of the beach in question should not be ignored due to the possibility of torrential flows from relatively steep slopes in its hinterland, although in the existing state it is difficult to notice evident evidence of this process due to frequent filling of beach material. Namely, the very configuration of the terrain and the location of the beach at the foot of the hill, suggest caution on this issue.

As already said, Kašjuni beach was originally naturally formed by a stream of material from the nearby hills of Marjan hill in its hinterland, over a long period of time in the past, towards the sea where the dynamic action of waves formed it into a natural beach. With the construction of roads and facilities in the hinterland of the beach, these natural inflows of new stone material have been partially cut and today there is no possibility of significant natural nourishment of the beach, which is why it is necessary to perform artificial periodic nourishment with appropriate granulation of stone material. Which material exactly is in question in terms of granulometric composition, and which will guarantee the stability of the beach in relevant wind conditions and conditions due to climate change, primarily raising the sea level, more in chapter 7 of this study.

If we add to all the above a relatively significant danger of beach erosion due to the possibility of torrential flows from relatively steep slopes in its hinterland, the situation requires a very detailed consideration in order to solve the detected problem.

2.2. Wind data

In order to conduct a quality model analysis of the beaches in question regarding hydrodynamic impacts, given as part of chapter 6 of this study, in addition to geodetic data, it is necessary to have relevant wind data. Namely, the adopted methodology (Chapter 1 of this study) implies the creation of a wind climate of deepwater waves at locations of interest, based on data on wind measurement, i.e., the parameters of waves with which numerical wave simulations were performed were obtained by standardized conversion procedures from wind data (explained in detail in chapter 3 of this study).

For this purpose, the State Hydrometeorological Institute of Croatia (DHMZ) has provided wind data that are relevant for all five selected pilot beach locations in Split-Dalmatia County, i.e., for the locations of beaches Zlatni rat (Brač), Stiniva (Vis), Podgora (Makarska Riviera), Podstrana-Duće and Kašjuni (Split).

2.2.1. Authoritative stations

The main meteorological stations are meteorological stations with 2 to 5 professional meteorological observers that have a fenced observation area and workspace (usually an independent facility) and perform observations or registration of all meteorological elements for 24 hours, according to the regulations of the World Meteorological Organization and the National Meteorological and Hydrological Service.

The data is forwarded by meteorological messages to the WMO's global telecommunications system.

Automatic weather stations have also been introduced at most stations, which perform measurements of one or more meteorological elements over 24 hours and are part of the DHMZ information system. For these stations, operational data control is performed, which includes completeness control, consistency control and spatial control. All data, including data from automatic stations, are archived on computer processing media. Through user programs, data for various purposes can be delivered. The spatial distribution is satisfactory in line with the Recommendations of the WMO.

Climatological (ordinary meteorological) stations perform observations at 07, 14 and 21h mean local time and monitor meteorological phenomena during the day. Observations are carried out by non-professional observers, and the stations are most often located within private estates. Some submit data to inform the public, by phone, one to two times a day. Completed monitoring logs are delivered by mail at the end of the month to the State Hydrometeorological Institute, where data is entered into the computer, controlled, and archived. The data is used directly or through user programs. The spatial distribution is in accordance with WMO regulations.

For the purpose of the study in question, and regarding the selected locations of the beaches in question, the following meteorological stations were selected where wind measurements were made in the thirty-year period 1990-2019:

1. Split Marjan (main meteorological station representative of the locations of beaches Split-Kašjuni and Podstrana-Duće);
2. Bol (climatological – ordinary meteorological station representative of the location of the beach Brač-Zlatni rat);
3. Komiža (the main meteorological station representative of the location of Vis-Stiniva beach);
4. Makarska (main meteorological station representative of the location of the beach Makarska Riviera-Podgora)

Figure 2.1 – DHMZ Meteorological Stations in Split-Dalmatia County
(*https://klima.hr/k4/mreza_postaja31122021.jpg*)

Measurement of wind velocities and associated wind directions at meteorological stations is carried out by automated devices that create records in certain weather increments, recording wind velocity and associated directions. Based on continuous records, statistics of wind data are produced over longer periods of time.

In order to complete the picture of the wind regime, data from climatological stations are used, where there is no anemograph, but observers observe the direction and strength of the wind. Wind strength is estimated visually by the effects of wind on objects in nature in three climatological terms (7, 14 and 21 h) and is expressed in degrees of the Beaufort scale. This scale contains 0–12 degrees, to which corresponding mean wind velocities are associated.

The Beaufort scale was introduced for the needs of maritime affairs back in the time of the sailing ship, so the strength of the wind was then estimated by the number of sails that the standard sailing ship was allowed to keep crucified at a given moment.

Later, the scale is adapted to the phenomena caused by wind on land:

- if the leaves do not move, and the smoke rises vertically in the air, then there is silence,
- light breeze man does not yet feel, but the smoke does not rise vertically,
- a man just feels a breeze on his face and the wind begins to turn,
- a weak wind constantly swaying the leaves, and smaller branches,
- moderately strong wind becomes uncomfortable to man, sways smaller branches and small trees,
- strong wind sways large branches and it is difficult to carry an open umbrella,

- in a very strong wind it is difficult to walk, the wind sways larger leafy trees, on the lake or the sea raises waves and creates crests,
- stormy wind prevents any walking against the wind, whole trunks sway and break branches,
- the storm throws tiles and causes less damage to objects,
- while a severe storm pulls up trees and causes damage to buildings,
- hurricane wind acts devastatingly over a larger area,
- and the hurricane wreaks havoc on the whole area.

Table 2.1 – Beaufort wind scale

Beaufort (Bf)	Description	speed		
		m/s	knot	km/h
0	Calm	0-0.2	< 1	<1
1	Light air	0.3-1.5	1-3	1-5
2	Light breeze	1.6-3.3	4-6	6-11
3	Gentle breeze	3.4-5.4	7-10	12-19
4	Moderate breeze	5.5-7.9	11-16	20-28
5	Fresh breeze	8.0-10.7	17-21	29-38
6	Strong breeze	10.8-13.8	22-27	39-49
7	High wind	13.9-17.1	28-33	50-61
8	Gale	17.2-20.7	34-40	62-74
9	Strong gale	20.8-24.4	41-47	75-88
10	Storm	24.5-28.4	48-55	89-102
11	Violent storm	28.5-32.6	56-63	103-117
12	Hurricane	32.7 >	64 >	118 >

2.2.2. Wind data

Wind data (DHMZ) for the purposes of this study were given in the form of wind contingency tables for the period 1990-2019. The contingency table presents a tabular presentation of the probability of the occurrence of different wind directions, sorted by strength (Bf) and velocity (m/s) classes for the year, in the period 1990-2019.

Contingency tables can be shown as relative frequencies in promiles (‰) or as absolute particles.

Below are the contingency tables for wind measurement from the following meteorological stations:

1. Split Marjan (main meteorological station representative of the locations of beaches Split-Kašjuni and Podstrana-Duće);
2. Bol (climatological – ordinary meteorological station representative of the location of the beach Brač-Zlatni rat);
3. Komiža (the main meteorological station representative of the location of Vis-Stiniva beach);

4. Makarska (the main meteorological station representative of the location of the beach Makarska riviera-Podgora).

2.2.2.1. Split Marjan

Table 2.2a – Probability of simultaneous occurrence of different wind directions (absolute frequency), by strength (Bf) and velocity (m/s) classes for Split Marjan, for the year, in the period 1990.-2019.

Bf	0	1	2	3	4	5	6	7	8	9	10	11	12	sum
speed (m/s)	0,0-0,2	0,3-1,5	1,6-3,3	3,4-5,4	5,5-7,9	8,0-10,7	10,8-13,8	13,9-17,1	17,2-20,7	20,8-24,4	24,5-28,4	28,5-32,6	32,7-36,9	
N	0	394	436	127	39	27	13	0	0	0	0	0	0	1036
NNE	0	511	1347	967	987	900	325	89	26	5	3	0	0	5160
NE	0	383	1105	603	272	224	84	20	2	3	1	0	0	2697
ENE	0	616	1609	1082	599	550	188	45	6	3	0	0	0	4698
E	0	406	627	260	125	54	12	1	0	0	0	0	0	1485
ESE	0	332	514	557	652	694	274	57	7	1	0	0	0	3088
SE	0	218	267	239	332	434	219	64	13	2	0	0	0	1788
SSE	0	440	540	249	259	362	207	85	11	1	0	0	0	2154
S	0	310	262	63	42	48	29	10	4	0	0	0	0	768
SSW	0	493	1174	533	74	36	23	10	2	0	0	0	0	2345
SW	0	331	686	529	115	12	6	0	0	0	0	0	0	1679
WSW	0	477	1080	779	127	10	1	0	0	0	0	0	0	2474
W	0	154	183	60	12	0	0	0	0	0	0	0	0	409
WNW	0	190	392	88	4	0	0	0	0	0	0	0	0	674
NW	0	185	296	94	13	2	1	0	0	0	0	0	0	591
NNW	0	443	579	171	40	13	3	0	0	0	0	0	0	1249
C	576	0	0	0	0	0	0	0	0	0	0	0	0	576
sum	576	5883	11097	6401	3692	3366	1385	381	71	15	4	0	0	32871

Table 2.2b – Probability of simultaneous occurrence of different wind directions (relative frequencies, ‰), by strength (Bf) and velocity (m/s) classes for Split Marjan, for the year, in the period 1990.-2019.

Bf	0	1	2	3	4	5	6	7	8	9	10	11	12	sum
speed (m/s)	0,0-0,2	0,3-1,5	1,6-3,3	3,4-5,4	5,5-7,9	8,0-10,7	10,8-13,8	13,9-17,1	17,2-20,7	20,8-24,4	24,5-28,4	28,5-32,6	32,7-36,9	
N		12,0	13,3	3,9	1,2	0,8	0,4	0,0	0,0	0,0	0,0	0,0	0,0	31,5
NNE		15,5	41,0	29,4	30,0	27,4	9,9	2,7	0,8	0,2	0,1	0,0	0,0	157,0
NE		11,7	33,6	18,3	8,3	6,8	2,6	0,6	0,1	0,1	0,0	0,0	0,0	82,0
ENE		18,7	48,9	32,9	18,2	16,7	5,7	1,4	0,2	0,1	0,0	0,0	0,0	142,9
E		12,4	19,1	7,9	3,8	1,6	0,4	0,0	0,0	0,0	0,0	0,0	0,0	45,2
ESE		10,1	15,6	16,9	19,8	21,1	8,3	1,7	0,2	0,0	0,0	0,0	0,0	93,9
SE		6,6	8,1	7,3	10,1	13,2	6,7	1,9	0,4	0,1	0,0	0,0	0,0	54,4
SSE		13,4	16,4	7,6	7,9	11,0	6,3	2,6	0,3	0,0	0,0	0,0	0,0	65,5
S		9,4	8,0	1,9	1,3	1,5	0,9	0,3	0,1	0,0	0,0	0,0	0,0	23,4
SSW		15,0	35,7	16,2	2,3	1,1	0,7	0,3	0,1	0,0	0,0	0,0	0,0	71,3
SW		10,1	20,9	16,1	3,5	0,4	0,2	0,0	0,0	0,0	0,0	0,0	0,0	51,1
WSW		14,5	32,9	23,7	3,9	0,3	0,0	0,0	0,0	0,0	0,0	0,0	0,0	75,3
W		4,7	5,6	1,8	0,4	0,0	0,0	0,0	0,0	0,0	0,0	0,0	0,0	12,4
WNW		5,8	11,9	2,7	0,1	0,0	0,0	0,0	0,0	0,0	0,0	0,0	0,0	20,5
NW		5,6	9,0	2,9	0,4	0,1	0,0	0,0	0,0	0,0	0,0	0,0	0,0	18,0
NNW		13,5	17,6	5,2	1,2	0,4	0,1	0,0	0,0	0,0	0,0	0,0	0,0	38,0
C	17,5	0,0	0,0	0,0	0,0	0,0	0,0	0,0	0,0	0,0	0,0	0,0	0,0	17,5
sum	17,5	179,0	337,6	194,7	112,3	102,4	42,1	11,6	2,2	0,5	0,1	0,0	0,0	1000,0

2.2.2.2. Makarska

Table 2.3a – Probability of simultaneous occurrence of different wind directions (absolute frequency), by strength (Bf) and velocity (m/s) classes for Makarska, for the year, in the period 1990.-2019.

Bf	0	1	2	3	4	5	6	7	8	9	10	11	12	sum
speed (m/s)	0,0-0,2	0,3-1,5	1,6-3,3	3,4-5,4	5,5-7,9	8,0-10,7	10,8-13,8	13,9-17,1	17,2-20,7	20,8-24,4	24,5-28,4	28,5-32,6	32,7-36,9	
N	0	773	742	156	111	77	66	24	14	4	1	0	0	1968
NNE	0	710	458	209	223	195	185	117	60	19	6	0	0	2182
NE	0	626	349	138	158	141	145	88	55	22	3	0	0	1725
ENE	0	663	361	139	95	81	82	37	25	8	0	0	0	1491
E	0	852	866	308	149	62	23	4	0	0	0	0	0	2264
ESE	0	698	1312	957	538	206	44	6	0	0	0	0	0	3761
SE	0	559	1137	682	494	189	65	3	1	0	0	0	0	3130
SSE	0	923	1444	759	416	176	73	13	1	0	0	0	0	3805
S	0	710	954	86	22	2	0	1	0	0	0	0	0	1775
SSW	0	520	641	72	15	5	1	0	0	0	0	0	0	1254
SW	0	435	688	105	12	1	2	0	0	0	0	0	0	1243
WSW	0	532	964	124	22	2	1	1	0	1	0	0	0	1647
W	0	297	486	106	30	13	2	0	0	0	0	0	0	934
WNW	0	360	450	153	51	12	3	0	0	0	0	0	0	1029
NW	0	440	451	123	55	12	1	0	0	0	0	0	0	1082
NNW	0	706	1055	265	53	23	5	0	0	0	0	0	0	2107
C	1024	0	0	0	0	0	0	0	0	0	0	0	0	1024
sum	1024	9804	12358	4382	2444	1197	698	294	156	54	10	0	0	32421

Table 2.3b – Probability of simultaneous occurrence of different wind directions (relative frequencies, ‰), by strength (Bf) and velocity (m/s) classes for Makarska, for the year, in the period 1990.-2019.

Bf	0	1	2	3	4	5	6	7	8	9	10	11	12	sum
speed (m/s)	0,0-0,2	0,3-1,5	1,6-3,3	3,4-5,4	5,5-7,9	8,0-10,7	10,8-13,8	13,9-17,1	17,2-20,7	20,8-24,4	24,5-28,4	28,5-32,6	32,7-36,9	
N		23,8	22,9	4,8	3,4	2,4	2,0	0,7	0,4	0,1	0,0	0,0	0,0	60,7
NNE		21,9	14,1	6,4	6,9	6,0	5,7	3,6	1,9	0,6	0,2	0,0	0,0	67,3
NE		19,3	10,8	4,3	4,9	4,3	4,5	2,7	1,7	0,7	0,1	0,0	0,0	53,2
ENE		20,4	11,1	4,3	2,9	2,5	2,5	1,1	0,8	0,2	0,0	0,0	0,0	46,0
E		26,3	26,7	9,5	4,6	1,9	0,7	0,1	0,0	0,0	0,0	0,0	0,0	69,8
ESE		21,5	40,5	29,5	16,6	6,4	1,4	0,2	0,0	0,0	0,0	0,0	0,0	116,0
SE		17,2	35,1	21,0	15,2	5,8	2,0	0,1	0,0	0,0	0,0	0,0	0,0	96,5
SSE		28,5	44,5	23,4	12,8	5,4	2,3	0,4	0,0	0,0	0,0	0,0	0,0	117,4
S		21,9	29,4	2,7	0,7	0,1	0,0	0,0	0,0	0,0	0,0	0,0	0,0	54,7
SSW		16,0	19,8	2,2	0,5	0,2	0,0	0,0	0,0	0,0	0,0	0,0	0,0	38,7
SW		13,4	21,2	3,2	0,4	0,0	0,1	0,0	0,0	0,0	0,0	0,0	0,0	38,3
WSW		16,4	29,7	3,8	0,7	0,1	0,0	0,0	0,0	0,0	0,0	0,0	0,0	50,8
W		9,2	15,0	3,3	0,9	0,4	0,1	0,0	0,0	0,0	0,0	0,0	0,0	28,8
WNW		11,1	13,9	4,7	1,6	0,4	0,1	0,0	0,0	0,0	0,0	0,0	0,0	31,7
NW		13,6	13,9	3,8	1,7	0,4	0,0	0,0	0,0	0,0	0,0	0,0	0,0	33,4
NNW		21,8	32,5	8,2	1,6	0,7	0,2	0,0	0,0	0,0	0,0	0,0	0,0	65,0
C	31,6	0,0	0,0	0,0	0,0	0,0	0,0	0,0	0,0	0,0	0,0	0,0	0,0	31,6
sum	31,6	302,4	381,2	135,2	75,4	36,9	21,5	9,1	4,8	1,7	0,3	0,0	0,0	1000,0

2.2.2.3. Bol

Table 2.4a – the probability of simultaneous occurrence of different wind directions (absolute frequencies), by strength (Bf) and velocity (m/s) classes for Bol, for the year, in the period 1990.-2019.

Bf	0	1	2	3	4	5	6	7	8	9	10	11	12	sum
speed (m/s)	0,0-0,2	0,3-1,5	1,6-3,3	3,4-5,4	5,5-7,9	8,0-10,7	10,8-13,8	13,9-17,1	17,2-20,7	20,8-24,4	24,5-28,4	28,5-32,6	32,7-36,9	
N	0	1875	607	768	307	62	3	0	1	0	0	0	0	3623
NNE	0	628	340	682	682	543	290	186	96	24	15	1	2	3489
NE	0	272	157	217	215	66	16	0	1	0	0	0	0	944
ENE	0	753	653	950	607	66	3	1	1	0	0	0	0	3034
E	0	433	219	94	10	0	1	0	0	0	0	0	0	757
ESE	0	877	1605	2158	583	44	2	2	1	0	0	0	0	5272
SE	0	831	1079	1011	526	155	45	10	0	0	0	0	0	3657
SSE	0	703	1018	974	440	199	70	22	12	3	0	0	0	3441
S	0	137	24	7	2	0	0	0	0	0	0	0	0	170
SSW	0	217	752	830	105	7	2	0	0	0	0	0	0	1913
SW	0	138	170	159	66	2	0	0	0	0	0	0	0	535
WSW	0	159	583	890	397	29	1	0	0	0	0	0	0	2059
W	0	91	159	416	40	0	0	0	0	0	0	0	0	706
WNW	0	199	186	255	240	57	3	3	0	0	0	0	0	943
NW	0	168	74	52	22	1	2	0	0	0	0	0	0	319
NNW	0	509	233	195	100	22	6	2	0	0	0	0	0	1067
C	37	0	0	0	0	0	0	0	0	0	0	0	0	37
sum	37	7990	7859	9658	4342	1253	444	226	112	27	15	1	2	31966

Table 2.4b – Probability of simultaneous occurrence of different wind directions (relative frequencies, ‰), by strength (Bf) and velocity (m/s) classes for Bol, for the year, in the period 1990.-2019.

Bf	0	1	2	3	4	5	6	7	8	9	10	11	12	sum
speed (m/s)	0,0-0,2	0,3-1,5	1,6-3,3	3,4-5,4	5,5-7,9	8,0-10,7	10,8-13,8	13,9-17,1	17,2-20,7	20,8-24,4	24,5-28,4	28,5-32,6	32,7-36,9	
N		58,7	19,0	24,0	9,6	1,9	0,1	0,0	0,0	0,0	0,0	0,0	0,0	113,3
NNE		19,6	10,6	21,3	21,3	17,0	9,1	5,8	3,0	0,8	0,5	0,0	0,1	109,1
NE		8,5	4,9	6,8	6,7	2,1	0,5	0,0	0,0	0,0	0,0	0,0	0,0	29,5
ENE		23,6	20,4	29,7	19,0	2,1	0,1	0,0	0,0	0,0	0,0	0,0	0,0	94,9
E		13,5	6,9	2,9	0,3	0,0	0,0	0,0	0,0	0,0	0,0	0,0	0,0	23,7
ESE		27,4	50,2	67,5	18,2	1,4	0,1	0,1	0,0	0,0	0,0	0,0	0,0	164,9
SE		26,0	33,8	31,6	16,5	4,8	1,4	0,3	0,0	0,0	0,0	0,0	0,0	114,4
SSE		22,0	31,8	30,5	13,8	6,2	2,2	0,7	0,4	0,1	0,0	0,0	0,0	107,6
S		4,3	0,8	0,2	0,1	0,0	0,0	0,0	0,0	0,0	0,0	0,0	0,0	5,3
SSW		6,8	23,5	26,0	3,3	0,2	0,1	0,0	0,0	0,0	0,0	0,0	0,0	59,8
SW		4,3	5,3	5,0	2,1	0,1	0,0	0,0	0,0	0,0	0,0	0,0	0,0	16,7
WSW		5,0	18,2	27,8	12,4	0,9	0,0	0,0	0,0	0,0	0,0	0,0	0,0	64,4
W		2,8	5,0	13,0	1,3	0,0	0,0	0,0	0,0	0,0	0,0	0,0	0,0	22,1
WNW		6,2	5,8	8,0	7,5	1,8	0,1	0,1	0,0	0,0	0,0	0,0	0,0	29,5
NW		5,3	2,3	1,6	0,7	0,0	0,1	0,0	0,0	0,0	0,0	0,0	0,0	10,0
NNW		15,9	7,3	6,1	3,1	0,7	0,2	0,1	0,0	0,0	0,0	0,0	0,0	33,4
C	1,2	0,0	0,0	0,0	0,0	0,0	0,0	0,0	0,0	0,0	0,0	0,0	0,0	1,2
sum	1,2	250,0	245,9	302,1	135,8	39,2	13,9	7,1	3,5	0,8	0,5	0,0	0,1	1000,0

2.2.2.4. Komiža

Table 2.5a – Probability of simultaneous occurrence of different wind directions (absolute frequency), by strength (Bf) and velocity (m/s) classes for Komiža, for the year, in the period 1990.-2019.

Bf	0	1	2	3	4	5	6	7	8	9	10	11	12	
speed (m/s)	0,0-0,2	0,3-1,5	1,6-3,3	3,4-5,4	5,5-7,9	8,0-10,7	10,8-13,8	13,9-17,1	17,2-20,7	20,8-24,4	24,5-28,4	28,5-32,6	32,7-36,9	sum
N	0	2230	2785	398	66	8	1	0	0	0	0	0	0	5488
NNE	0	947	3174	621	155	44	2	0	0	0	0	0	0	4943
NE	0	1022	2154	583	184	92	11	2	0	0	0	0	0	4048
ENE	0	87	570	317	158	59	15	0	0	0	0	0	0	1206
E	0	187	892	495	325	258	94	5	0	0	0	0	0	2256
ESE	0	31	307	311	250	148	27	0	0	0	0	0	0	1074
SE	0	114	1134	792	408	153	14	0	0	0	0	0	0	2615
SSE	0	57	570	382	181	63	3	0	0	0	0	0	0	1256
S	0	244	1234	434	190	69	2	0	0	0	0	0	0	2173
SSW	0	325	1303	326	82	31	2	0	0	0	0	0	0	2069
SW	0	215	1454	244	42	7	2	0	0	0	0	0	0	1964
WSW	0	30	259	87	7	2	0	0	0	0	0	0	0	385
W	0	51	319	69	7	0	0	0	0	0	0	0	0	446
WNW	0	14	143	48	3	1	0	0	0	0	0	0	0	209
NW	0	152	676	173	15	0	0	0	0	0	0	0	0	1016
NNW	0	461	880	248	38	6	1	0	0	0	0	0	0	1634
C	86	0	0	0	0	0	0	0	0	0	0	0	0	86
sum	86	6167	17854	5528	2111	941	174	7	0	0	0	0	0	32868

Table 2.5b – Probability of simultaneous occurrence of different wind directions (relative frequencies, ‰), by strength (Bf) and velocity (m/s) classes for Komiža, for the year, in the period 1990.-2019.

Bf	0	1	2	3	4	5	6	7	8	9	10	11	12	sum
speed (m/s)	0,0-0,2	0,3-1,5	1,6-3,3	3,4-5,4	5,5-7,9	8,0-10,7	10,8-13,8	13,9-17,1	17,2-20,7	20,8-24,4	24,5-28,4	28,5-32,6	32,7-36,9	
N		67,8	84,7	12,1	2,0	0,2	0,0	0,0	0,0	0,0	0,0	0,0	0,0	167,0
NNE		28,8	96,6	18,9	4,7	1,3	0,1	0,0	0,0	0,0	0,0	0,0	0,0	150,4
NE		31,1	65,5	17,7	5,6	2,8	0,3	0,1	0,0	0,0	0,0	0,0	0,0	123,2
ENE		2,6	17,3	9,6	4,8	1,8	0,5	0,0	0,0	0,0	0,0	0,0	0,0	36,7
E		5,7	27,1	15,1	9,9	7,8	2,9	0,2	0,0	0,0	0,0	0,0	0,0	68,6
ESE		0,9	9,3	9,5	7,6	4,5	0,8	0,0	0,0	0,0	0,0	0,0	0,0	32,7
SE		3,5	34,5	24,1	12,4	4,7	0,4	0,0	0,0	0,0	0,0	0,0	0,0	79,6
SSE		1,7	17,3	11,6	5,5	1,9	0,1	0,0	0,0	0,0	0,0	0,0	0,0	38,2
S		7,4	37,5	13,2	5,8	2,1	0,1	0,0	0,0	0,0	0,0	0,0	0,0	66,1
SSW		9,9	39,6	9,9	2,5	0,9	0,1	0,0	0,0	0,0	0,0	0,0	0,0	62,9
SW		6,5	44,2	7,4	1,3	0,2	0,1	0,0	0,0	0,0	0,0	0,0	0,0	59,8
WSW		0,9	7,9	2,6	0,2	0,1	0,0	0,0	0,0	0,0	0,0	0,0	0,0	11,7
W		1,6	9,7	2,1	0,2	0,0	0,0	0,0	0,0	0,0	0,0	0,0	0,0	13,6
WNW		0,4	4,4	1,5	0,1	0,0	0,0	0,0	0,0	0,0	0,0	0,0	0,0	6,4
NW		4,6	20,6	5,3	0,5	0,0	0,0	0,0	0,0	0,0	0,0	0,0	0,0	30,9
NNW		14,0	26,8	7,5	1,2	0,2	0,0	0,0	0,0	0,0	0,0	0,0	0,0	49,7
C	2,6	0,0	0,0	0,0	0,0	0,0	0,0	0,0	0,0	0,0	0,0	0,0	0,0	2,6
sum	2,6	187,6	543,2	168,2	64,2	28,6	5,3	0,2	0,0	0,0	0,0	0,0	0,0	1000,0

2.2.3. Winds of interest to individual locations

In the coastal areas of the Croatian Adriatic Sea, the primary force that affects the morphology of beaches made of granular materials are wind waves. These waves in their encounter from the open sea towards the mainland bring significant wave energy to the coastal area. And while part of this energy is lost due to transformational and deformation wave processes, a significant part of the energy is brought to the coastal line itself and to its immediate vicinity, which contributes to the dynamic and continuous process of forming and shaping beaches and their granulometric composition of the granular material from which they are made.

Observing this process over a longer period, along with some other influences of lower intensity and importance, such as coastal sea currents and tides, it is concluded that without a good knowledge of the wind conditions at the location of a particular beach, it is not possible to adequately observe the morphological and hydrodynamic behavior of a particular beach.

Also, without a detailed analysis of these main driving processes of morphological changes, it is not possible to predict the need for certain interventions in the area, with the aim of improving the existing state of beach erosion and ensuring their long-term sustainability, and adapting to the potential consequences of the impact of climate changes.

The effect of waves on the beach brings a whole range of complex physical processes that intertwine and superimpose each other (explained in more detail in chapter 5 of this study), which in most cases

contributes that it cannot be intuitively fully understood, without the use of sophisticated numerical models, especially their impacts on the beach due to their synergistic interaction. Therefore, it is necessary to carry out detailed numerical modeling, which consider the above processes that occur in the encounter of waves towards the beach, in order to ultimately understand the processes and make quality conclusions and decisions based on their results.

Given the lack of systematic wave measurements over a long period of time at the locations of the beaches in question, the selected methodology used in this study includes the calculation of wave parameters, with which numerical modeling will be carried out, indirectly through developed standard methods for forecasting waves from wind data. Such a procedure was carried out for all five locations of the beaches in question.

In order to determine the directions and parameters of waves that contribute to the morphological-hydrodynamic influences of each of the beaches considered, it is necessary to make an analysis of the winds that cause these waves for each beach in question separately. With these wave parameters, numerical simulations were performed, the results of which were given as part of chapter 6 of this study.

2.2.3.1. Brač (Zlatni rat)

Zlatni rat beach on the island of Brač (Figure 2.2) is located on the south side of the island, approximately in its middle looking east-west. The beach is located on a cape that was thrown out south wards approximately 300 meters in relation to the surrounding line of the coast.

Such a disposition of the beach in question makes it exposed to the influences of wind waves from the second and third quadrants, i.e., from wave directions from E (90°) to W (270°) clockwise (Figure 2.3). Accordingly, the total angle of exposure of Zlatni rat beach is 180°.

Realistically, these are waves that can be generated by the following winds:

- Levanat
- Jugo
- Oštro
- Lebić
- Punenat
- Maestral.

Figure 2.2 – Zlatni rat beach (Brač)

By analyzing the contingent tables for the beach Zlatni rat in question (tables 2.4a and 2.4b), it is possible to notice the frequency of occurrences of certain wind directions at the location. The most common directions of winds are levant (ESE) and jugo (SE, SSE), followed by bura (N, NNE), and mistral (WSW). According to the wind strength, i.e., according to wind velocity, the bora (NNE) leads with a measured wind strength of 12 Bf, followed by the sirocco (SSE) with a measured 9 Bf. The frequency and strength of winds and consequent waves at the location are of crucial importance for the morphology of the beach and its shaping over a longer period, and thus for its sustainability.

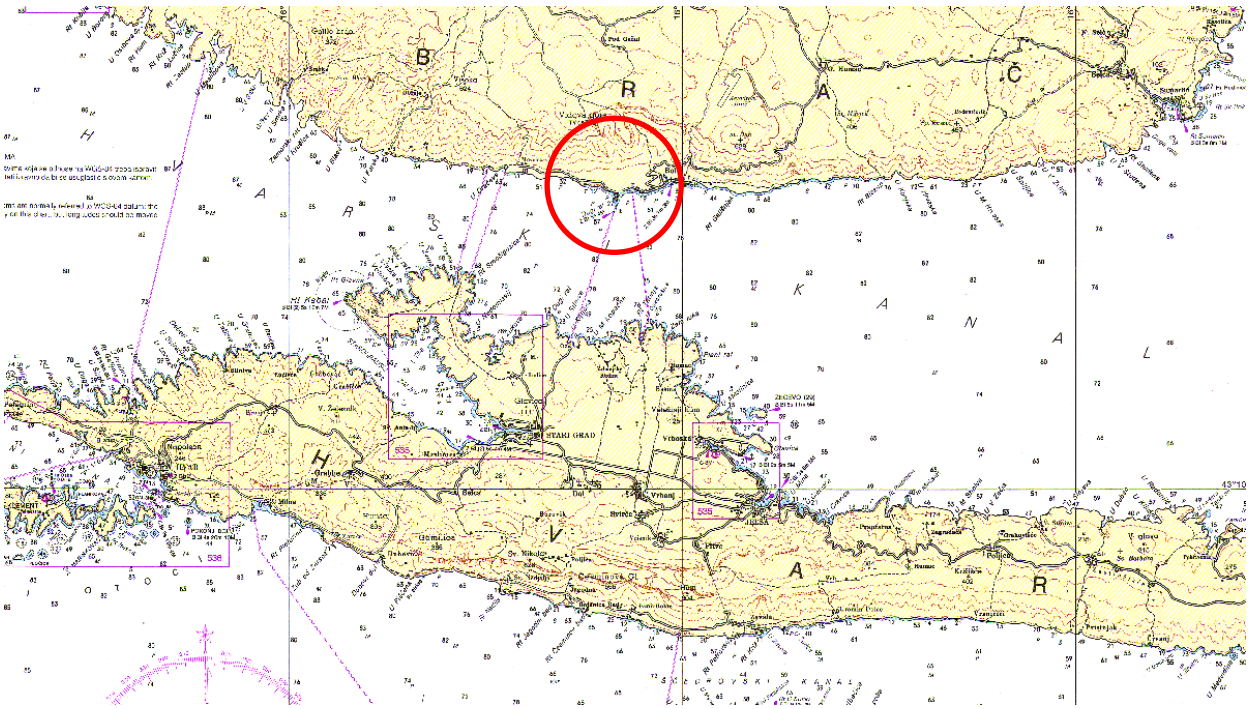

Figure 2.3 – Location of Zlatni rat beach (Brač) in the wider waters

2.2.3.2. Vis (Stiniva)

Stiniva beach on the island of Vis (Figure 2.4) is located on the south side of the island, approximately in its middle looking east-west. The beach is located at the bottom of a relatively deep natural rocky bay and is additionally protected by a natural rocky "wall", which contributes to its visual specificity and recognition.

Figure 2.4 – Stiniva beach (Vis)

This disposition of the beach in question makes it exposed to the influences of wind waves from the second and third quadrants, i.e., from wave directions from SE (135°) to SW (225°), clockwise (Figure 2.5). Accordingly, the total angle of exposure of Stiniva beach is 90°.

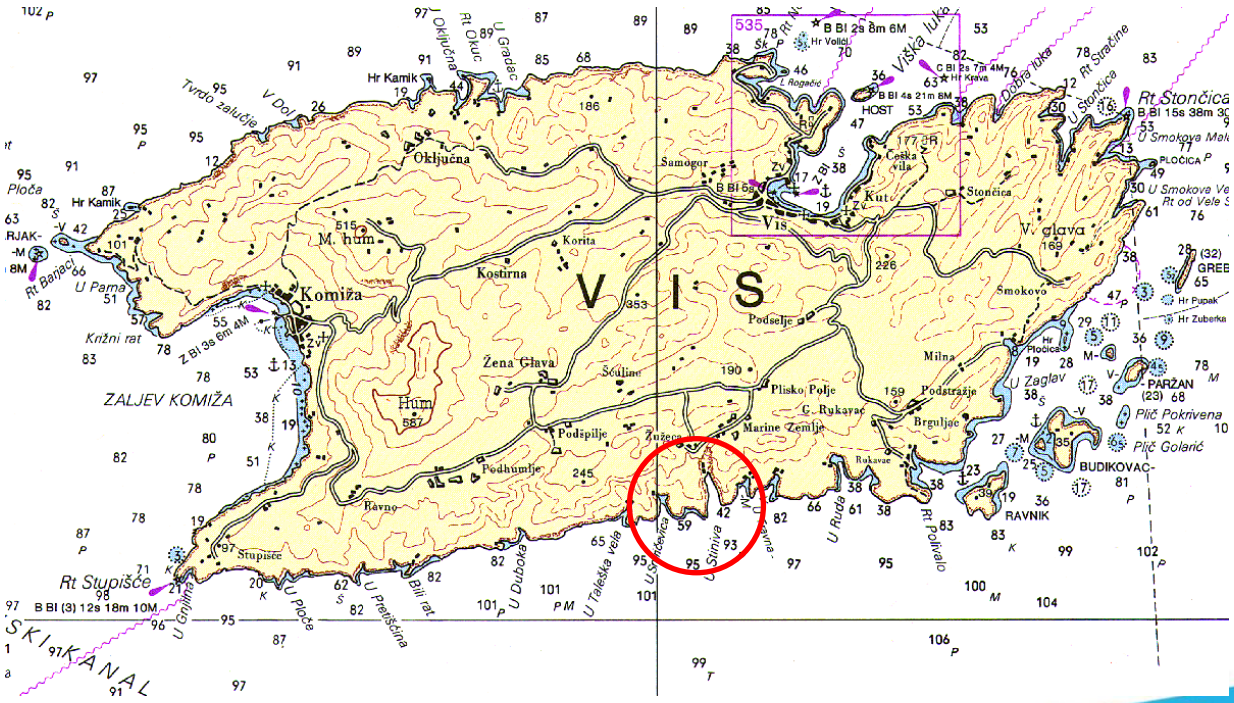

Figure 2.5 – Location of Stiniva beach (Vis) in the wider waters

Realistically, these are waves that can be generated by the following winds:

- Jugo
- Oštro
- Lebić.

By analyzing the contingent tables for the Stiniva beach in question (tables 2.5a and 2.5b), the frequency of occurrence of certain wind directions at the site can be observed. The most common directions of winds are bura (N, NNE and NE), and jugo (SE) and lebić (SSW, SW). According to wind strength, i.e., according to wind velocity, bura (NE) and levant (E) are leading the way with measured wind strengths of 7 Bf, while all other directions are less erratic. The frequency and strength of winds and consequential waves at the site are crucial for the morphology of the beach and its shaping over a longer period, and thus for its sustainability.

2.2.3.3. Makarska Riviera (Podgora)

The beach in Podgora (Figure 2.6) is located near the village and is oriented primarily in the north-south direction, and a smaller part east-west. It is about a kilometer long.

Figure 2.6 – Podgora Beach (Makarska Riviera)

Such a disposition of the beach in question makes it exposed to the influences of wind waves from the second, third and fourth quadrants, i.e., from wave directions from SE (135°) to WNW (292.50°) clockwise (Figure 2.7). Accordingly, the total angle of exposure of Podgora beach is 157.50°.

Realistically, these are waves that can be generated by the following winds:

- Jugo
- Oštro
- Lebić
- Punenat
- Maestral
- Tramuntana.

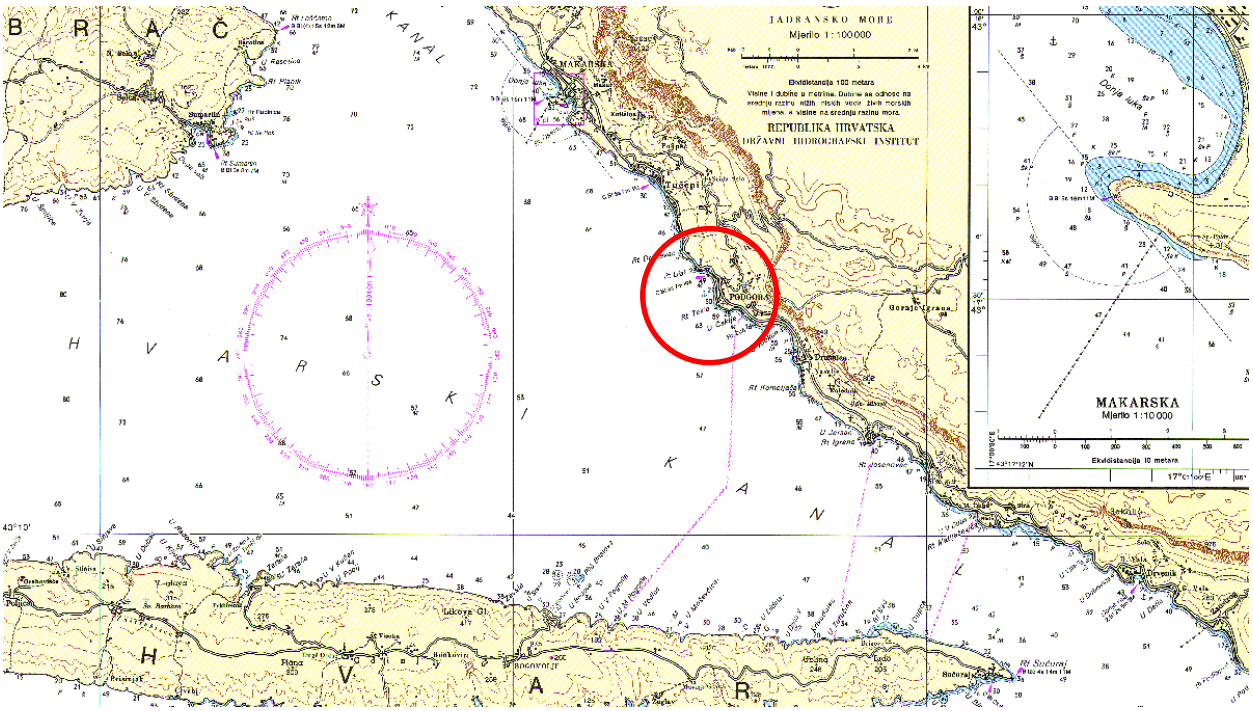

Figure 2.7 – Location of Podgora beach (Makarska Riviera) in the wider waters

By analyzing the contingent tables for the Podgora beach in question (tables 2.3a and 2.3b), it is possible to notice the frequency of occurrences of certain wind directions at the location. The most common directions of winds are sirocco (SSE, ESE, SE), followed by punenat (E), bura (NNE), and lebić (SW, SSW). According to the wind strength, i.e., according to the wind velocity, the bora (N, NNE) leads with a measured wind strength of 8 Bf, followed by the sirocco (SE, SSE) with a measured 8 Bf. The frequency and strength of winds and consequent waves at the location are of crucial importance for the morphology of the beach and its shaping over a longer period, and thus for its sustainability.

2.2.3.4. Podstrana-Duće area

The beaches on the Podstrana-Duće area (Figure 2.8) are mostly pebble beaches with stone groynes, and the entire stretch of the coast of approximately 12 kilometers is mostly oriented in the northwest - southeast direction.

Such a disposition of the beach in question makes them exposed to the influences of wind waves from the second, third and fourth quadrants, i.e., from wave directions from SE (135°) to WNW (292.50°) clockwise. Accordingly, the total angle of exposure of beaches on the Podstrana-Duće area is 157.50°.

Realistically, these are waves that can be generated by the following winds:

- Jugo
- Oštro
- Lebić
- Punenat
- Maestral
- Tramunatana.

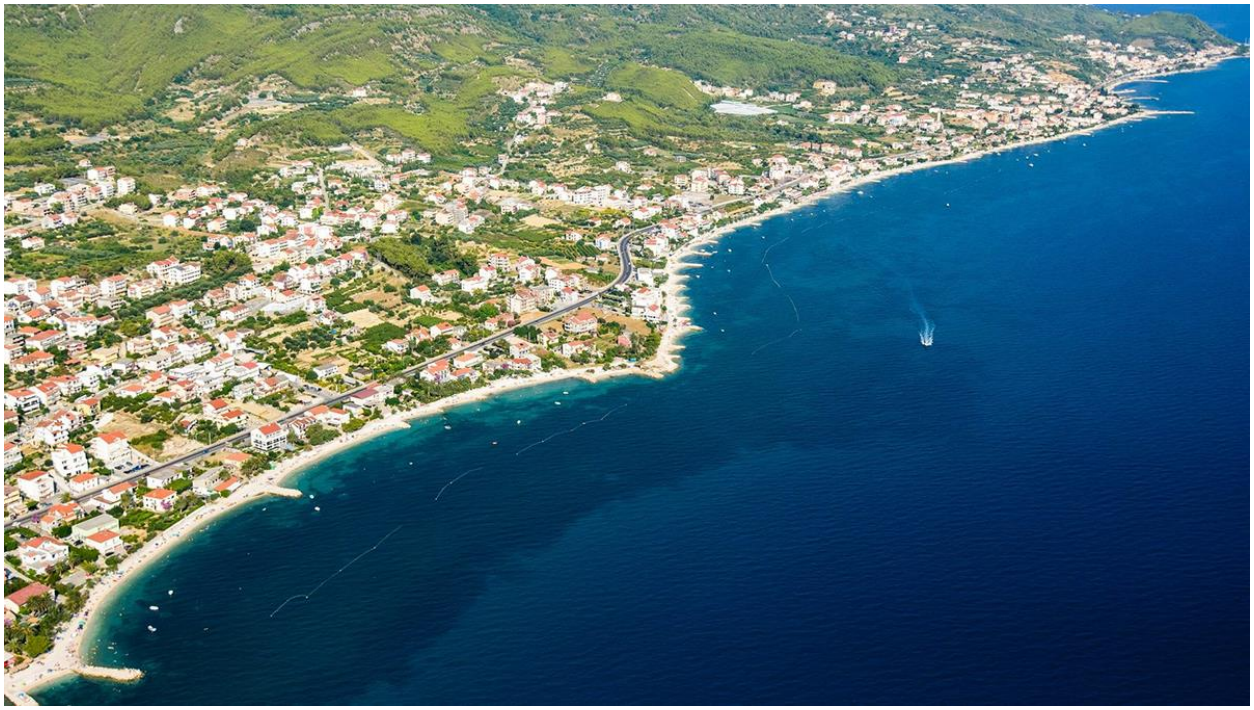

Figure 2.8 – Beaches on the Podstrana – Duće area

By analyzing the contingency tables for the beaches in question on the Podstrana-Duće area (tables 2.2a and 2.2b), the frequency of occurrence of certain wind directions at the location can be observed. The most common directions of winds are bura (NNE), jugo (ESE), followed by mistral (WSW), and lebić (SSW). According to the wind strength, i.e., according to wind velocity, the bora (NE, NNE) leads with a measured wind strength of 10 Bf, followed by the sirocco (SE, SSE) with a measured 9 Bf. The frequency and strength of winds and consequent waves at the location are of crucial importance for the morphology of the beach and its shaping over a longer period, and thus for its sustainability.

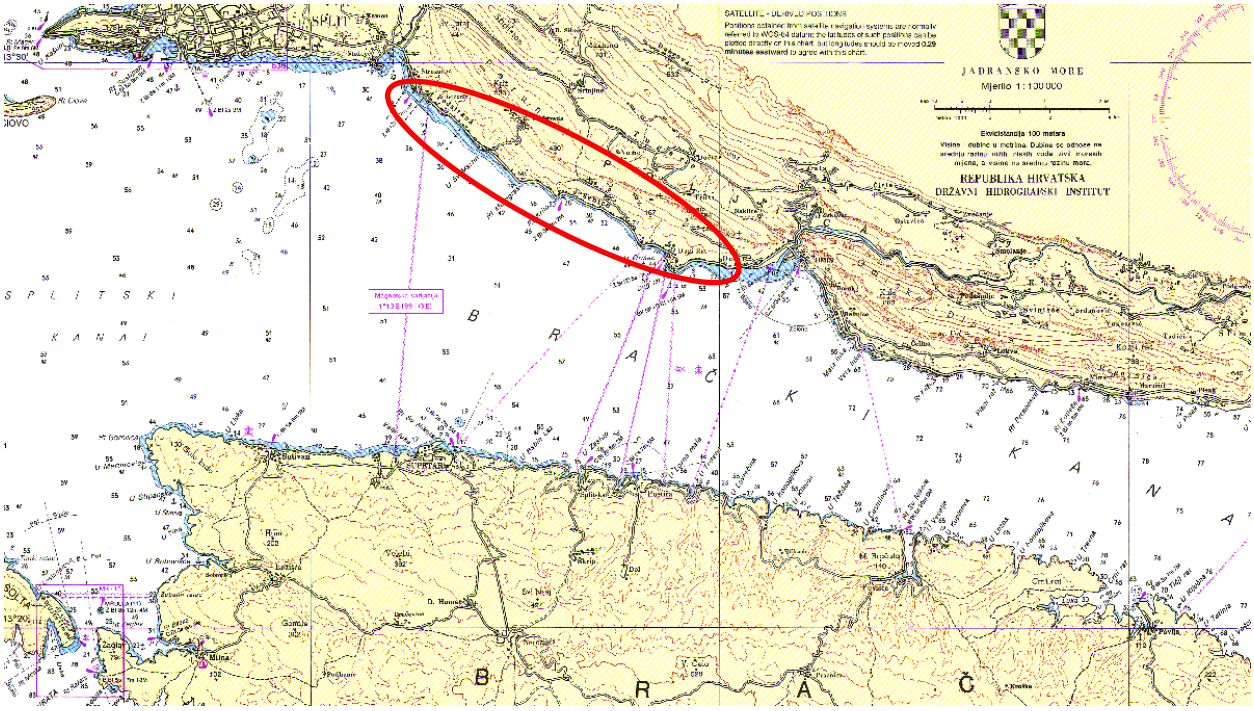

Figure 2.9 – Location of Podstrana-Duće beaches in the wider waters

2.2.3.5. Split (Kašjuni)

Kašjuni beach (figure 2.10) is located under the southern slopes of Marjan forest park in the city of Split. The beach is protected by an artificially embanked groyne /breakwater located in the east-west direction, while the beach itself is oriented in the north-south direction.

Figure 2.10 – Kašjuni Beach (Split)

This disposition of the beach in question makes it exposed to the influences of wind waves from the second, third and fourth quadrants, i.e., from wave directions from SE (135°) to WNW (292.50°) clockwise (Figure 2.11). Accordingly, the total angle of exposure of Kašjuni beach is 157.50°.

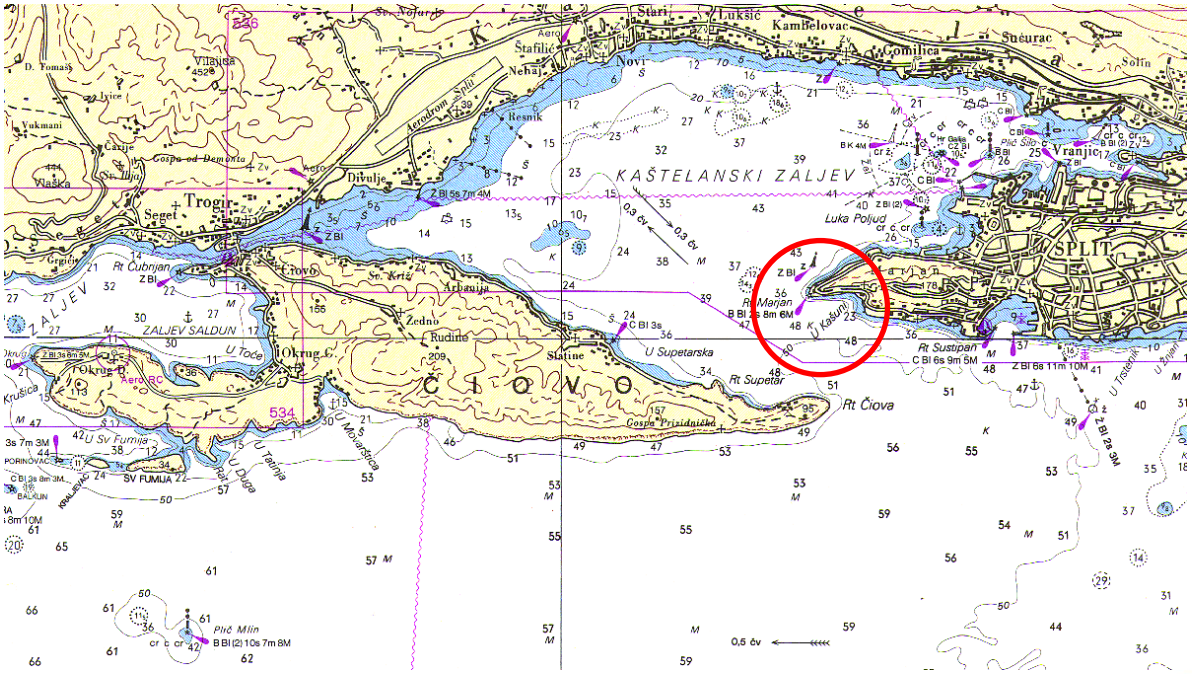

Figure 2.11 – Location of Kašjuni Beach (Split) in the wider waters

Realistically, these are waves that can be generated by the following winds:

- Jugo
- Oštro
- Lebić
- Punenat
- Maestral
- Tramuntana.

By analyzing the contingency tables for Kašjuni beach in question (tables 2.2a and 2.2b), it is possible to notice the frequency of occurrences of certain wind directions at the location. The most common directions of winds are bura (NNE), jugo (ESE), followed by mistral (WSW), and lebić (SSW). According to the wind strength, i.e., according to wind velocity, the bora (NE, NNE) leads with a measured wind strength of 10 Bf, followed by the sirocco (SE, SSE) with a measured 9 Bf. The frequency and strength of winds and consequent waves at the location are of crucial importance for the morphology of the beach and its shaping over a longer period, and thus for its sustainability.

2.3. Hydrographic data on relevant sea levels

For the aquatory of the Split-Dalmatia County, relevant data on sea levels were obtained based on statistical processing of continuous measurement of daily oscillations of sea levels over a longer period on a tide set in the City Port of Split. The official data on sea levels, for the purpose of this study, was provided by the Croatian Hydrographic Institute (HHI).

Data on sea levels are given in relation to the altitude date HVRS71. The "+" mark indicates that the required value is above HVRS71, and the "–" mark indicates that the required value is below HVRS71.

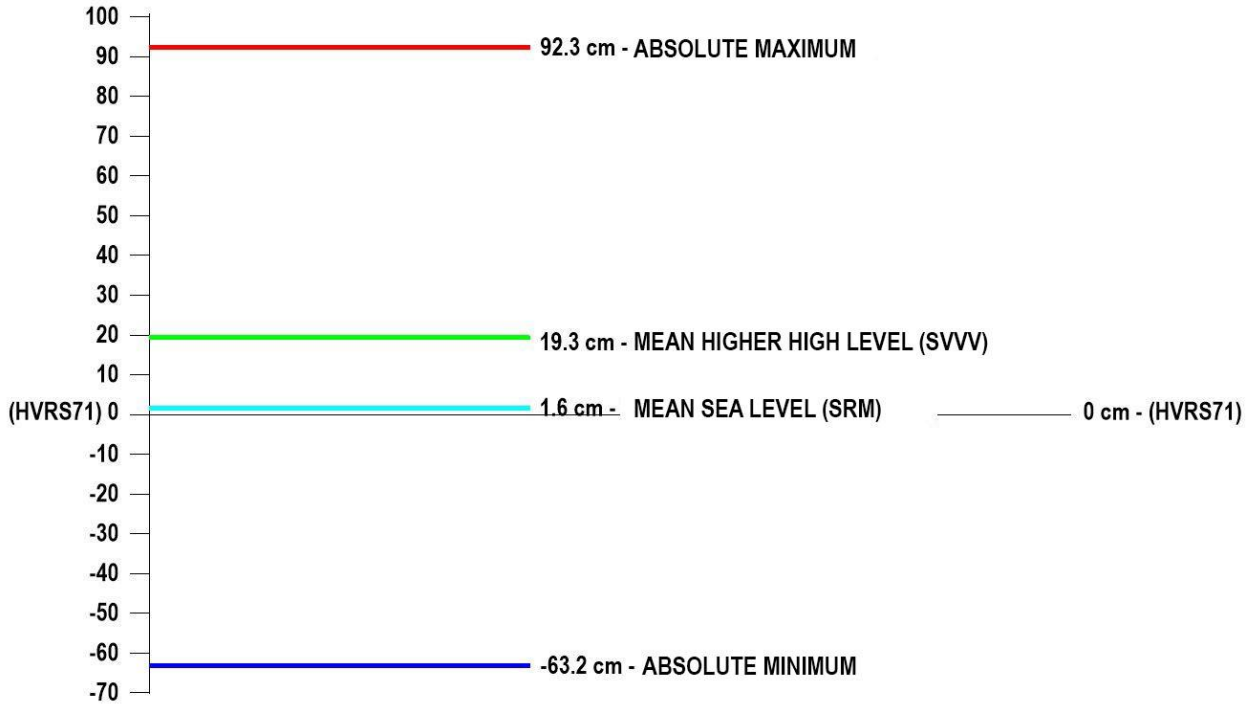

Figure 2.12 – Relevant Sea levels for the Split-Dalmatia County, *copyright* © HHI

For the analysis that is the basis of the development of guidelines, in addition to geodetic data and wind data, data on sea levels is one of the most important data. Namely, apart from the fact that these data are directly related to the geometry of the beach, because the horizontal surface of the sea level defines the intersection with the mainland, i.e., the coastline, they speak of the potential of beach erosion due to measured daily oscillations of the sea levels.

Given that one of the goals of developing these guidelines and analyzing the impact of climate changes, primarily rising sea levels, on beaches made of granular materials, these data can serve to reasonably assess with which elevated sea level a model wave analysis should be carried out, and for the results to be coherent and applicable.

Therefore, for the purpose of further analysis, in addition to the sea level corresponding to the middle sea level (SRM), the hydrodynamic impact on beaches when raising sea level by 1 meter was analyzed, which approximately corresponds to the officially measured absolute maximum (92.3 cm) on the tide set in the City Port of Split, whose data are relevant for the area of Split-Dalmatia County. This can be considered a reasonable assessment of the elevation of the sea level for the purpose of simulating the potential rise of the sea level as a result of climate changes, because it represents an approximate level that has already been detected in the past and on the basis of which it will be possible to draw coherent conclusions about the potential dangers of beach erosion caused by sea level rising, and even in the event that these values of sea levels are exceeded in the future, but also if the "black scenarios" of rising sea levels are realized on a smaller scale.

2.4. Management plan for the marine environment and coastal area of Split-Dalmatia County – Beach erosion

In accordance with the Marine Environment and Coastal Management Plan of Split-Dalmatia County (Coastal Plan SDŽ), 1,098 beaches with a total coastal length of 99.3 km were identified in the Area of SDZ, which makes about 8.5% of the length of the Coastline SDŽ, where the term beach refers to the sedimentary body of beaches made of granular materials.

The current practice of managing beaches in SDŽ, related to ensuring their physical viability, has several weaknesses. Covered beaches regardless of whether they are natural beaches, where construction in its hinterland interrupted the natural supply of material that builds the beach, whether it is an artificially established beach, in a place where there was never any material.

Most of the beaches are maintained annually without foundation in a professionally crafted project that should include:

1. analysis of geomorphological characteristics of the area and wave conditions;
2. assessment of the amenities of the location for construction (if it is an artificial beach);
3. the design of the beach, including groynes for its protection, in accordance with existing terrain and wave conditions;
4. defining the slope of the beach in a way that makes it suitable for use, but also relatively stable and resistant to the influence of waves;
5. the design of the undersea embankment / sill that retains the beach material and causing wave breaking reduces its destructive effect on the beach;
6. defining the granulation range of the backfilling material (crushed rock material) in accordance with the energy of the waves to which it is exposed, because the transfer size of the beach material directly depends on its granulation, and on the size and intensity of the waves.

In conditions where the local self-government unit (JLS) does not find the financial resources for the preparation and execution of such a complete project, initially the cheaper practice of forming beaches *by ad hoc* embankment of materials along the coastline, in places where it would like to have it, and which are not necessarily suitable, without elements in design and design that ensure their stability and resistance to the impact of waves, so the formed beaches last at best one summer season, and then winter storms for the most part simply "sweep away". **In doing so, it is overlooked that the initially more expensive solution, due to its durability, is longer-term and more cost-effective, and during the entire period of use is of higher quality**. In addition, the **negative impact of supplemented material on the surrounding benthic habitats** has been greatly reduced, because the amount of eroded supplementary material is significantly lower in a well-designed and constructed beach.

For the purposes of the SDZ Coastal Plan, a preliminary analysis and categorization of the vulnerability of beaches to erosion, given the exposure to waves, was made, according to a simple model in which vulnerability depends on the maximum of significant wave height for characteristic winds in the Area of SDZ and the openness of the beach to different wind blowing directions.

Based on the wind analysis in the SDZ area, within the Coastal Plan SDŽ, the model analyzed waves for the strongest and most common wind directions for: bura (NNE-NE-ENE directions), jugo (ESE, SE, SSE), southwesterly (SSW-SW), and northwesterly (NW-NNW).

Based on the wind-wave model, an analysis of the stationary state of the waves (the wind blows long enough for the full development of waves) for homogeneous wind directions from 4 quadrants, 2) analysis of several situations with realistic strong to stormy winds for 4 characteristic winds (bura, jugo, SW and mistral), using the results of the weather model WRF (Weather Research and Forecast) which provides spatial distribution of direction and wind velocity over the Adriatic area. When interpreting the results, the following two main expected deviations of the model results from the actual situation should be borne in mind. First, in models for stationary condition and homogeneous wind, the wind blowing time from one direction is usually overestimated, making the estimated wave height higher than the actual one. Secondly, the wind is never spatially homogeneous, unless it is a strong wind due to a large pressure gradient, whose impact then exceeds the influence of local relief, so over the waters of the County can be approximately homogeneous wind direction.

Table 2.6 - Length and proportion of beaches of different vulnerability categories, given their exposure to maximum significant wave height (for oxen induced by real episodes of strong to stormy winds from the 4 most common directions and stationary waves induced by homogeneous storm winds from 16 directions) – Coastal Plan SDŽ (Table 26)

Beach vulnerability category	The length of beaches of a certain category for a realistic situation (m)	Share of beaches of a certain category for a realistic situation (%)	The length of beaches of a certain category with maximum expected wave heights (m)	Share of beaches of a certain category with maximum expected wave heights (%)
0 (protected by the natural coast)	5111.73	5.17	5111.73	5.17
1 (wave height < 0,5m)	26701.20	27.00	733.02	0.74
2 (0,5<h<1m)	53287.42	53.89	4728.26	4.78
3 (1<h<1,5m)	10997.40	11.12	6877.63	6.96
4 (1,5<h<2m)	2324.26	2.35	38435.75	38.87
5 (2<h<2,5m)	333.66	0.34	33213.58	33.59
6 (2,5<h<3)	128.28	0.13	3267.73	3.30
7 (h>3m)	0.00	0.00	6516.26	6.59
Altogether	98883.96	100	98883.96	100

Depending on the maximum significant wave height to which they are exposed, beaches are categorized into **8 vulnerability categories**, ranging from 0 (not endangered) to 7 (most endangered), as follows:

0 – beaches protected by the natural coast;

1 - beaches exposed to waves with a significant wave height of less than 0.5 m;

2 - beaches exposed to waves with a significant wave height of 0.5 to 1 m;

3 - beaches exposed to waves with a significant wave height of 1 to 1.5 m;

4 - beaches exposed to waves with a significant wave height of 1.5 to 2 m;

5 - beaches exposed to waves with a significant wave height of 2 to 2.5 m;

6 - beaches exposed to waves with a significant wave height of 2.5 to 3 m;

7 - beaches exposed to waves with a significant wave height of more than 3 m.

Table 2.6 and Figure 2.13 show the results of the vulnerability analysis for real wind situations from the 4 most common directions in SDŽ, as well as for the homogeneous situation of waves induced by stationary wind from 16 directions. The obtained distribution of beaches by vulnerability categories suggests that in the Area of SDZ there are enough beaches less exposed to waves, i.e., that as a rule, there is no need to create beaches in locations exposed to waves of extreme height and destructive power.

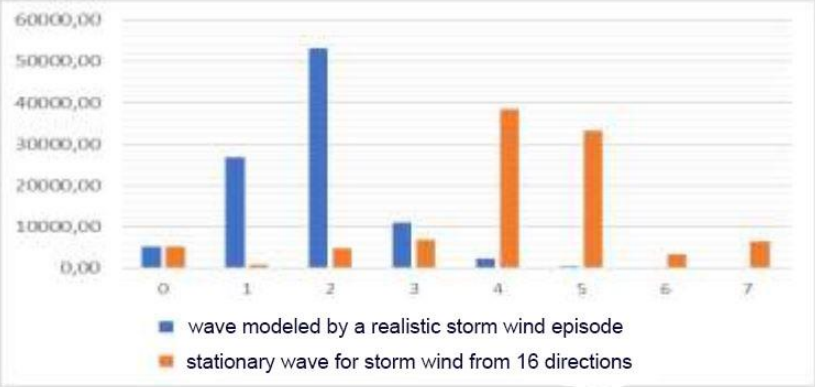

Figure 2.13 - Length [m] of beaches of different categories exposed to maximum significant wave heights for waves induced by realistic 4-way wind episodes and stationary waves induced by homogeneous 16-way wind – Coastal Plan SDŽ (Figure 137)

Figure 2.14 shows the spatial distribution of beaches of different categories of vulnerability, given the spatial maximum of significant wave height for 4 characteristic wind directions in real situations with strong wind in the Area of SDŽ (bura, jugo, SW, mistral), and Figure 2.15 for waves generated by a homogeneous fetch from 16 directions in the SDZ area.

The following are also spatial distributions of beaches of different vulnerability categories, given their exposure to winds and waves separately from each quadrant:

1. **I quadrant:** N - E (directions NNW, N, NNE, NE, ENE) (Figure 2.16);
2. **II quadrant:** E - S (directions ESE, SE, SSE) (Figure 2.17);
3. **III quadrant:** S - W (directions SSW-SW-WSW) (Figure 2.18);
4. **IV quadrant:** W - N (directions WNW-NW-NNW) (Figure 2.19).

The pictures clearly show that within the waters of Split-Dalmatia County there are three areas distinguished, according to the criterion of maximum wave height: coastal areas of more closed bays (Kaštela and Marin Bays); the area of coastal channels (Drvenik, Šolta, Split, Brač, Hvar channel); and the outer area of the SDŽ aquatorium (Vis Channel and the open sea). Accordingly, and the vulnerability of

beaches varies significantly within these three areas.

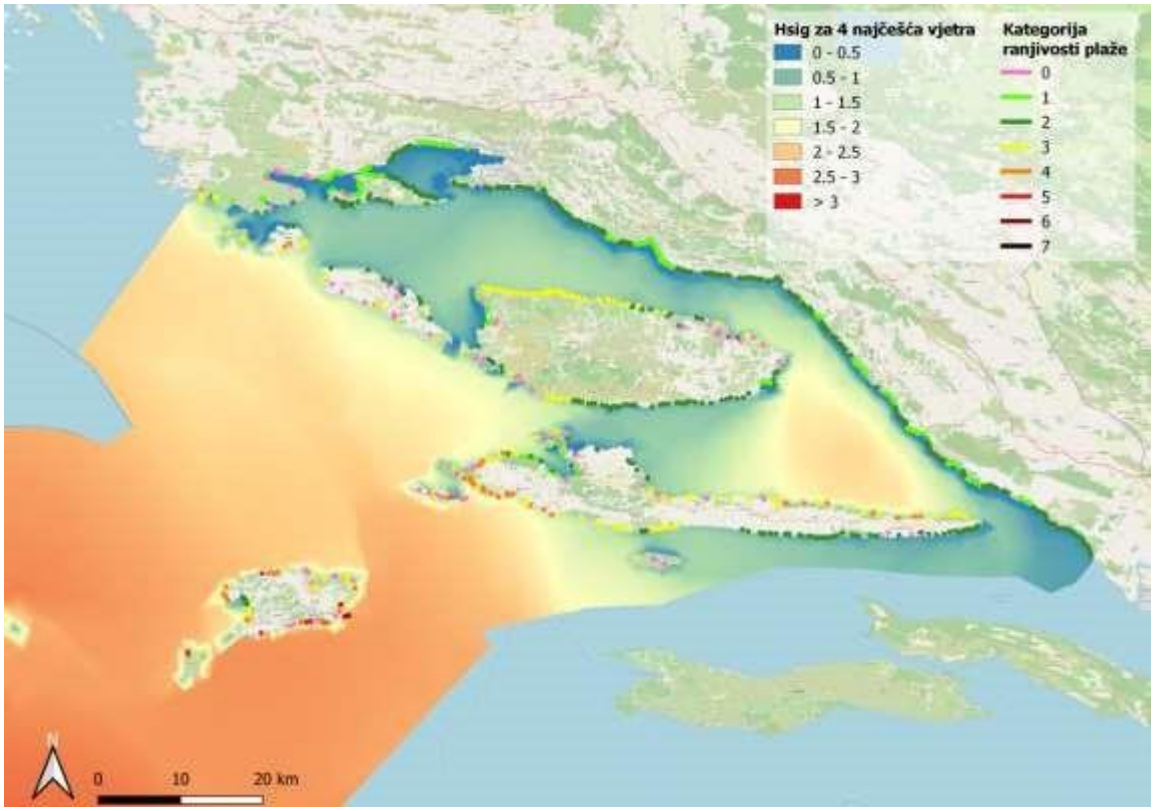

Figure 2.14 - Categorization of beaches with respect to the spatial maximum of significant wave height for 4 characteristic wind directions in real situations with strong wind in the area of SDZ (bura, jugo, SW, mistral) – Coastal plan SDŽ (fig. 138)

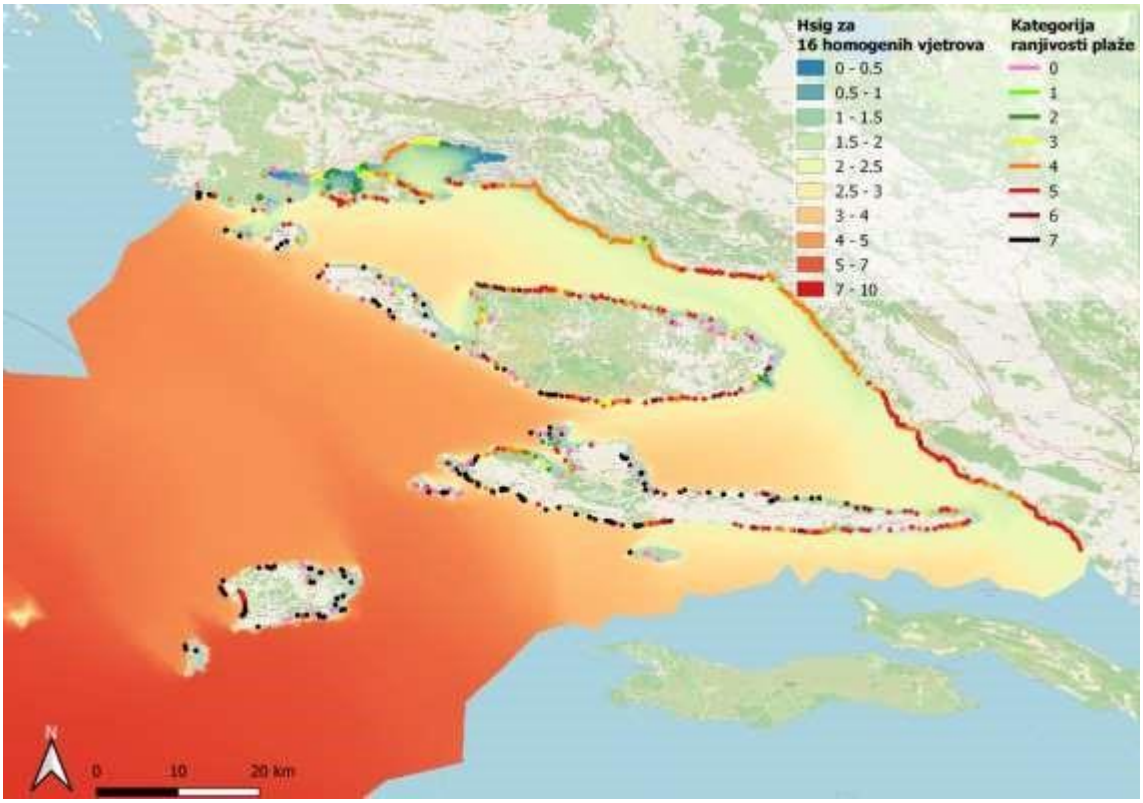

Figure 2.15 - Categorization of beaches with respect to the spatial maximum of a significant wave height for waves generated by a homogeneous fetch from 16 directions in the SDZ area – Coastal Plan SDŽ (Fig. 139)

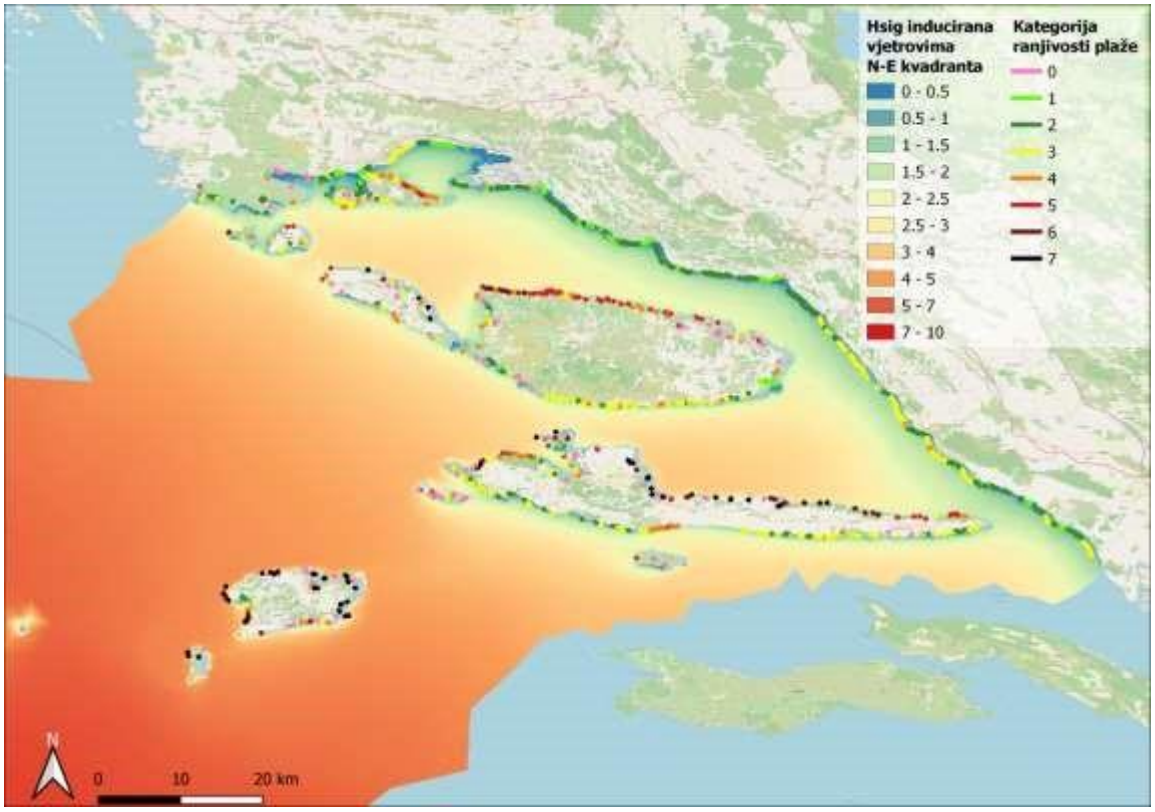

Figure 2.16 - Categorization of beaches with respect to the spatial maximum of a significant wave height for a homogeneous fetch from the I quadrant: N-E – Coastal plan SDŽ (Figure 140)

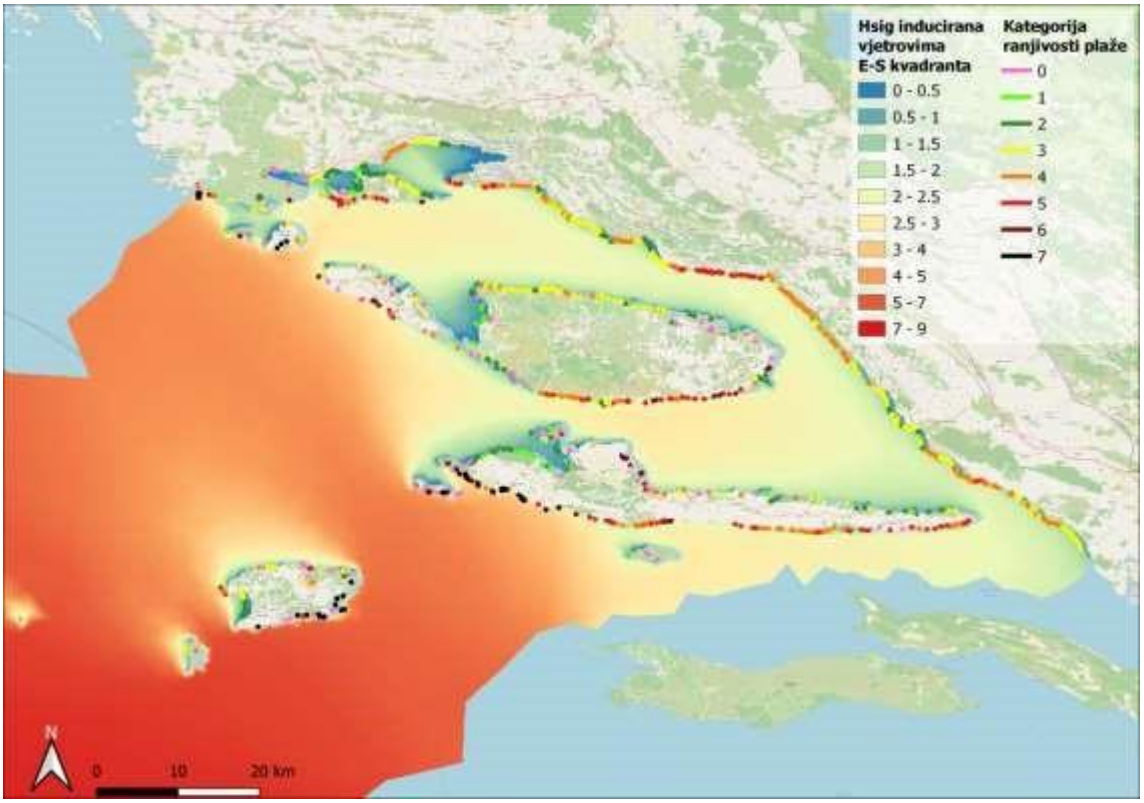

Figure 2.17 - Categorization of beaches with respect to the spatial maximum of a significant wave height for a homogeneous fetch from the II quadrant: E-S – Coastal Plan SDŽ (Figure 141)

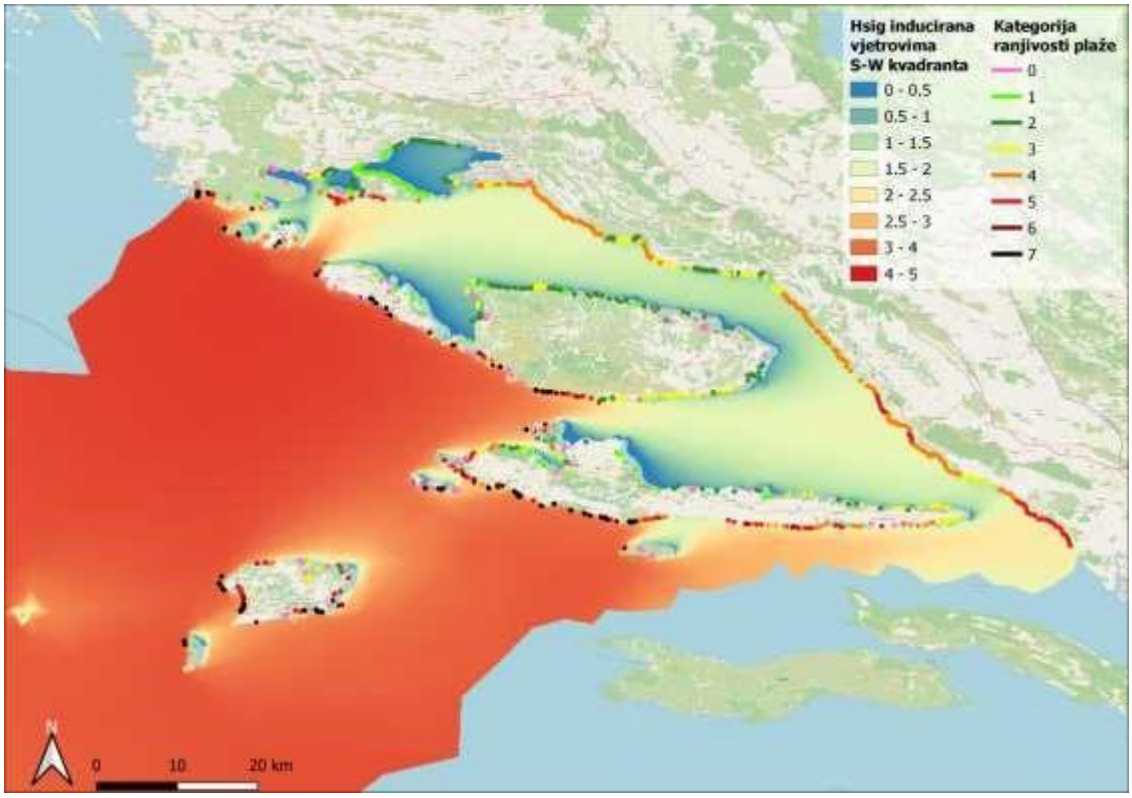

Figure 2.18 - Categorization of beaches with respect to the spatial maximum of a significant wave height for a homogeneous fetch from the III quadrant: S-W – Coastal Plan SDŽ (Figure 142)

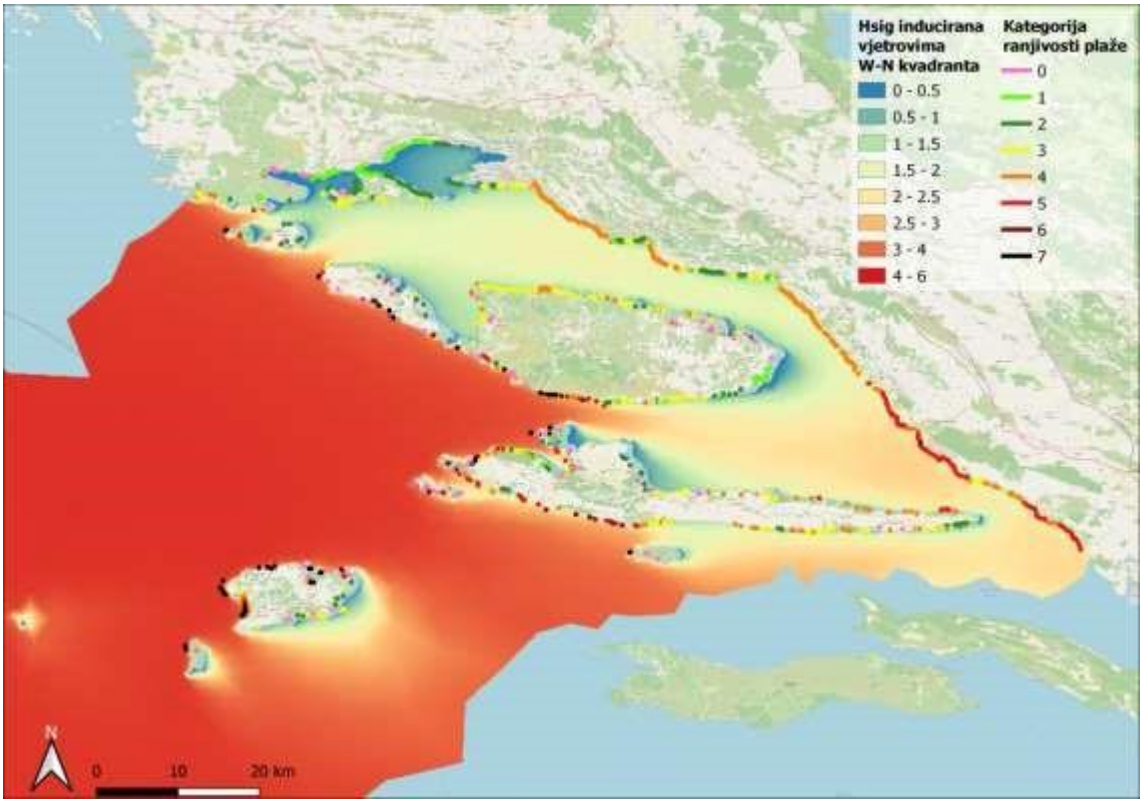

Figure 2.19 - Categorization of beaches with respect to the spatial maximum of a significant wave height for a homogeneous fetch from the IV quadrant: W- N – Coastal Plan SDŽ (Figure 143)

The following two images **show the lengths of beaches of different vulnerability categories in each coastal municipality, for the described two scenarios of modeled maximum significant wave heights.**

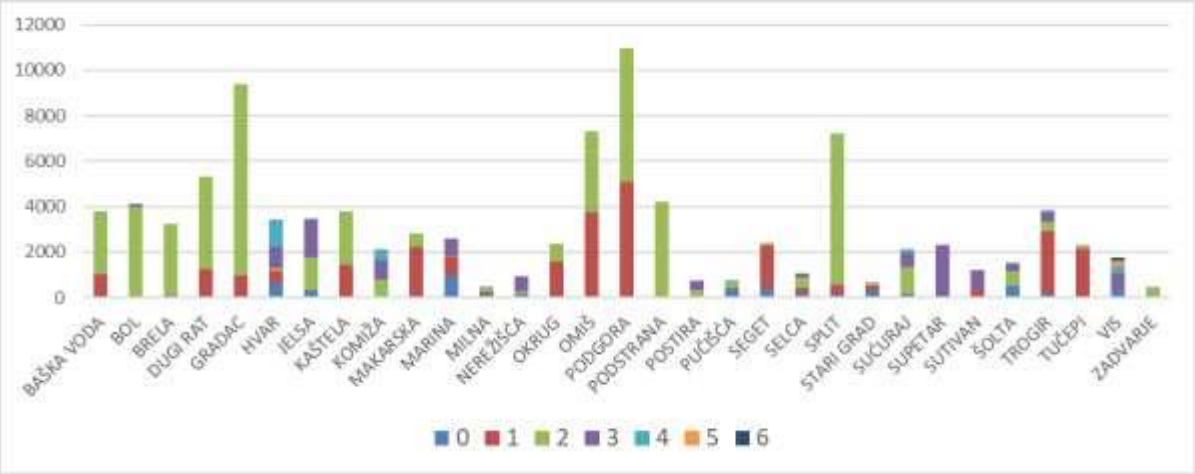

Figure 2.20 - Lengths of beaches [m] by local self-government units of the coastal zone SDŽ different vulnerabilities to erosion from wave action (result of a simple model – see description in the text) – scenario with waves in real wind episodes – Coastal plan SDŽ (Figure 144)

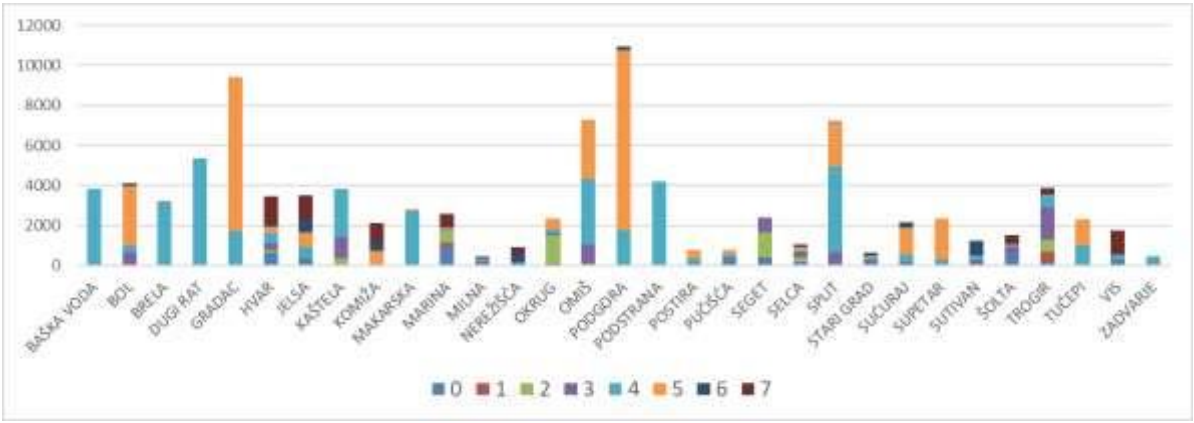

Figure 2.21 - Lengths of beaches [m] by coastal area local self-government units SDZ different vulnerabilities to erosion from wave action (result of a simple model – see description in the text) – scenario with stationary maximum wave generated homogeneous wind from 16 directions - Coastal Plan SDŽ (Figure 145)

3. PARAMETERS OF RELEVANT WAVES – LONG-TERM WAVE FORECAST

In accordance with the adopted methodology (Chapter 1 of this study), after the analysis of spatial and geomorphological features, and the analysis of microlocation conditions and the analysis of wind surveys, as well as the assessment of the degree of vulnerability of the beaches in question according to the Plan of Management of the Marine Environment and coastal area of Split-Dalmatia County (Cooperative Granum Solis, 2021), it is necessary to determine the parameters of the relevant waves. With these wave parameters, numerical wave modeling was carried out (chapter 6 of this study), and calculations of the potential material transport and stable composition of beach material (chapter 7 of this study), all with the aim of making consistent conclusions with the aim of developing quality guidelines that will try to solve the problems of beach erosion made of granular materials and ensure their long-term sustainability.

Long-term wave forecast is made from samples obtained by measuring waves for short-term stationary states of the sea. Since these measurements are not available, a wave sample will be made based on wind measurement data (wind sample for short-term situations from a long observation period).

From the measurement of the wave outline in time η^(t) at a point for a period of one year, it is possible to obtain different wave profile parameters by statistical processing, which indicate annual extremes. These can be random variables such as significant wave height (*Hs*), maximum wave height (H_{max}) and others.

The selected variable has an initial probability distribution assumed to be Fisher-Tippett type, which results in the corresponding probability distribution of extremes of the same type. The same applies to the extreme of a slightly shorter period of 1 year. Accordingly, depending on the time period of consideration of the extreme wave parameter, the following models are distinguished:

1. model of annual extreme values with associated probability distribution (*Annual extreme value probability distribution*) and
2. a model of extreme values exceeding some "threshold" with the associated probability distribution (*Extreme Value Probability distribution*).

For both models, the most used are Weibull (F-T type III) and Gumbel (F-T type I) distribution (Gumbel E.J., 1958; Isacson M. de St. Q., 1986; Chakrabarti S.K., 1987). The Frechet distribution (F-T type II) is the weakest adjustable and therefore practically not used. Log-normal distribution is also commonly used, the use of which is based on empirical knowledge of good adaptation.

The first model is used if it has a sample of approximately 30 years, and the second if it has a sample usually less than 30 years. The sample then encompasses all data that exceeds the set threshold, characterized by a typical large storm, so there may also be more data in 1 year.

A second model will be used here because wind contingency tables are available from which wind samples can be made according to the threshold exceeding criterion.

Since the Hs sample for the long-term forecast should represent individual short-term wave situations with larger waves (i.e., the wind that generates them), a wind velocity threshold of 3 Bf (3.4 – 5.4 m/s) will be selected.

3.1. Fetch

The length of the wave development (or fetch) over the surface of which wind waves of interest are generated is determined by considering the effective distances of the considered location and the land from which the waves come. It is an area or waters in which wave generation occurs due to wind blowing in a certain period. Since wave generation occurs in two-dimensional space, the effective fetch is defined by its width, which generally reduces the greatest potential length of the fetch. In other words, the smaller the ratio of the width and length of the fetch, the shorter the effective length of the fetch.

For determining the effective length of the fetch, it is used Saville method (The Shore Protection Manual, 1984), which assumes that wind blows effectively in the main direction over the surface of the sea, which is divided into two sectors 42° on each side of the main direction. The calculation of the effective length of the fetch is carried out in such a way that a central beam is placed in each of the selected directions, which has a point in front of the location in question as a starting point. After that, with a rotation of 6° clockwise (up to +42°) and counterclockwise (up to -42°), directions are placed through the same starting point. The lengths of each beam from the starting point to the first point of the coast are determined and the sum of their projections on the central air is calculated. This sum is divided by the sum of the sinuses of the corners of the central beam and other rotated rays, which gives the value of the length of the effective fetch.

3.1.1. Brač (Zlatni rat)

As already mentioned in point 2.2.3.1, the Zlatni rat beach aquatory on the island of Brač is exposed to winds from the second and third quadrants and consequent wind waves with different lengths of the fetch. In view of this, according to the criterion of fetch length and similarity of frequency of wind occurrence for a particular direction, certain sectors that are defined by the action of winds from the directions E, ESE, SE, SSE, SSW, SW, WSW and W will be defined.

Sector I is defined by the action of winds and consequent surface wind waves from the directions ESE and SE, sector II by wind action and consequent surface wind waves from SSE and SSE directions, sector III by the action of winds and consequent surface wind waves from the directions SSW and SW, while sector IV is defined by the action of winds and consequent surface wind waves from WSW and W directions.

The longest effective fetch of sector I was calculated for the direction of the ESE and is 28.3 km (Table 3.1). For sector II, the longer effective fetch is calculated for the direction of the SSE and is 10.4 km (Tables 3.2 and 3.3). For sector III, the longer effective fetch was calculated for the direction SW and is 39.8 km (Tables 3.3 and 3.4). For sector IV, the longer effective fetch was calculated for direction W and is 117.4 km (Tables 3.4 and 3.5).

In Figures 3.1 to 3.9, graphical representations of the central beam placement through the analyzed directions and beams with rotation ±6° from the central beam are given. The calculated values of the procedure for determining the effective length of the fetch for all individual directions are given in Tables 3.1 to 3.5.

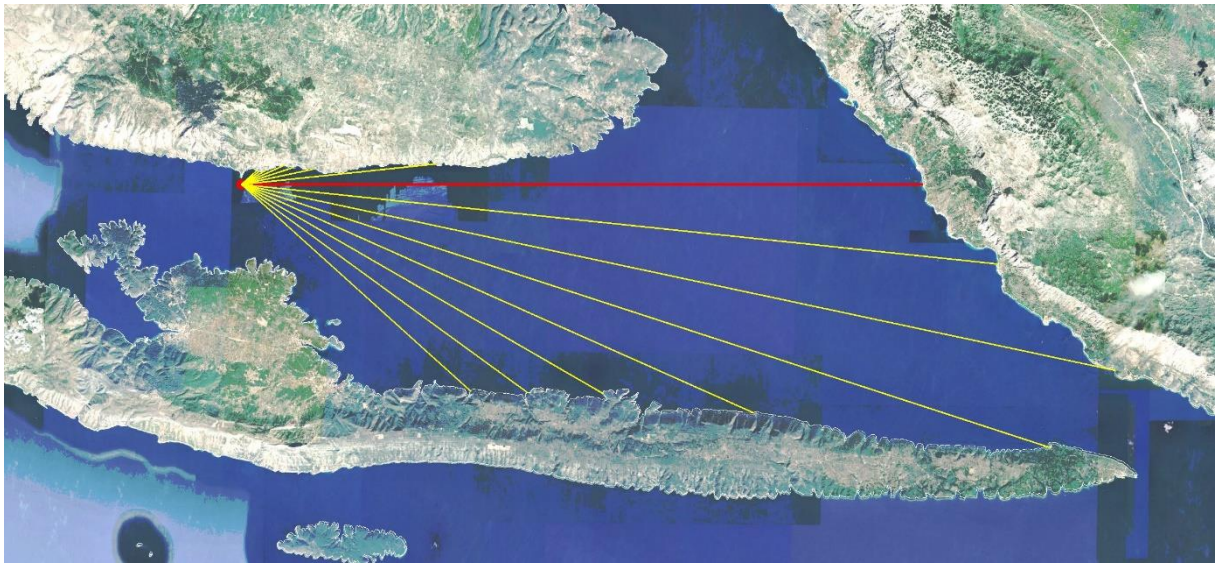

Figure 3.1 – Display of the central beam through direction E (90°), and beams with step ±6°

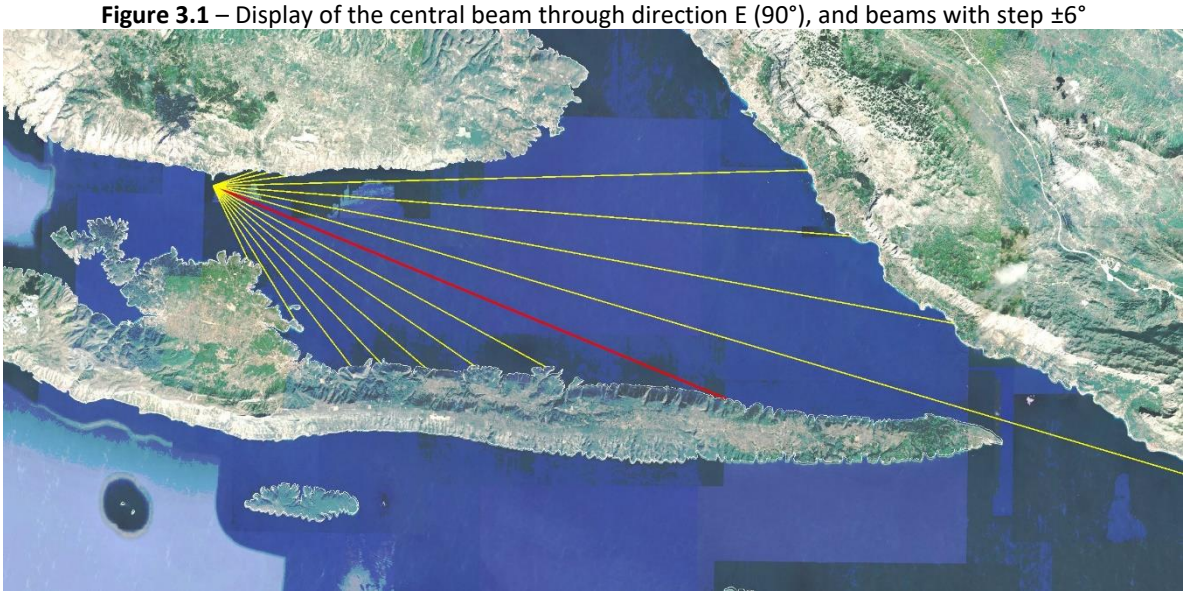

Figure 3.2 – Display of the central beam through the direction of ESE (112.5°), and the beam with step ±6°

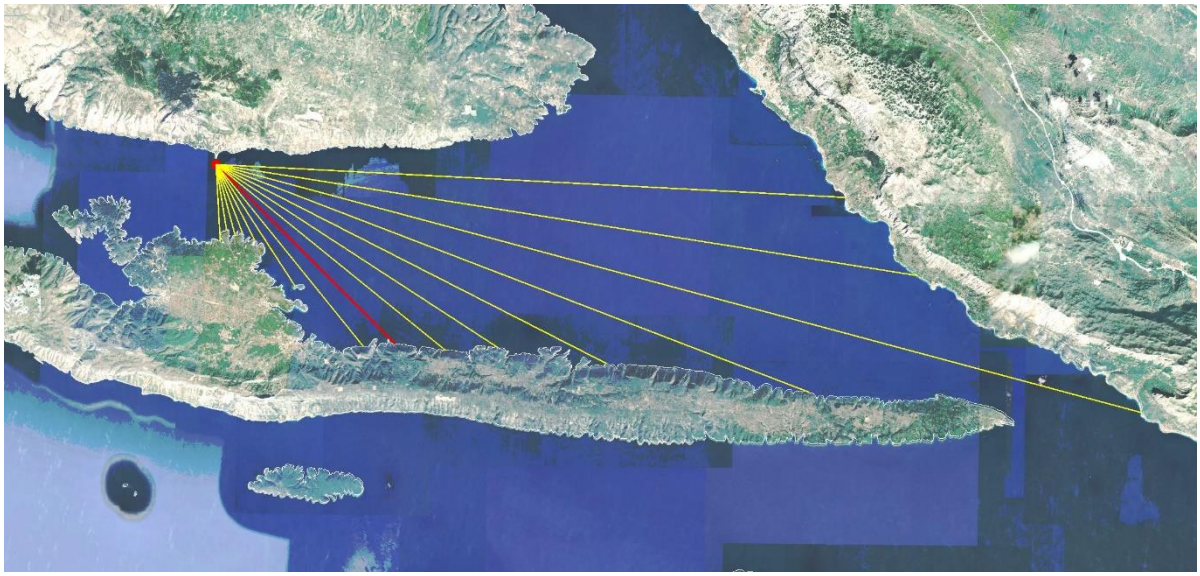

Figure 3.3 – Display of the central beam through the direction of SE (135°), and the beam with the step ±6°

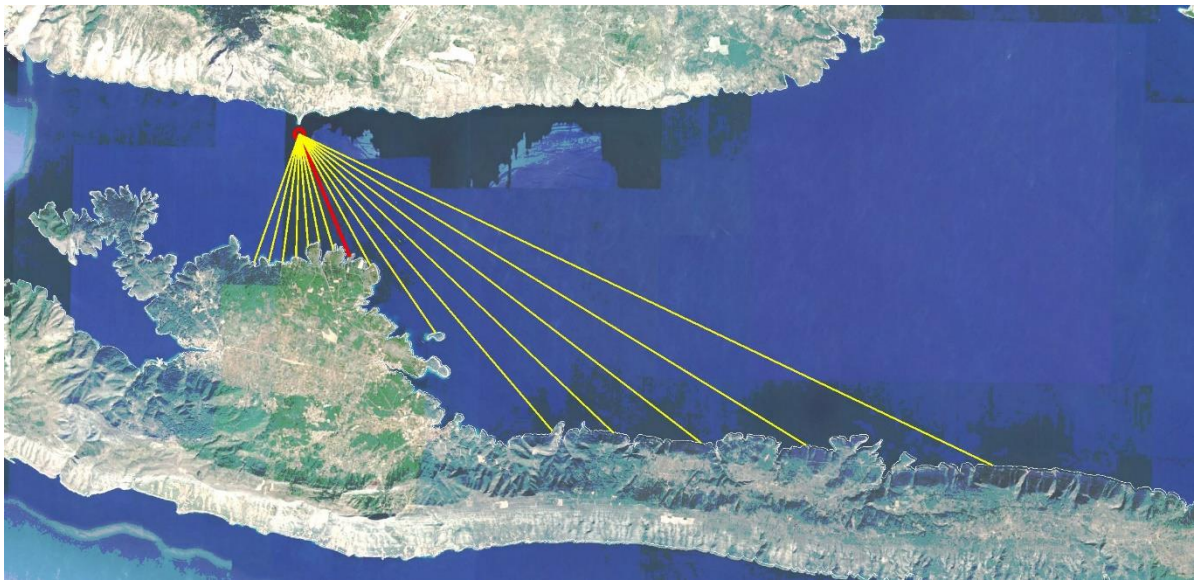

Figure 3.4 – Display of the central beam through the direction of SSE (157.5°), and the beam with a step ±6°

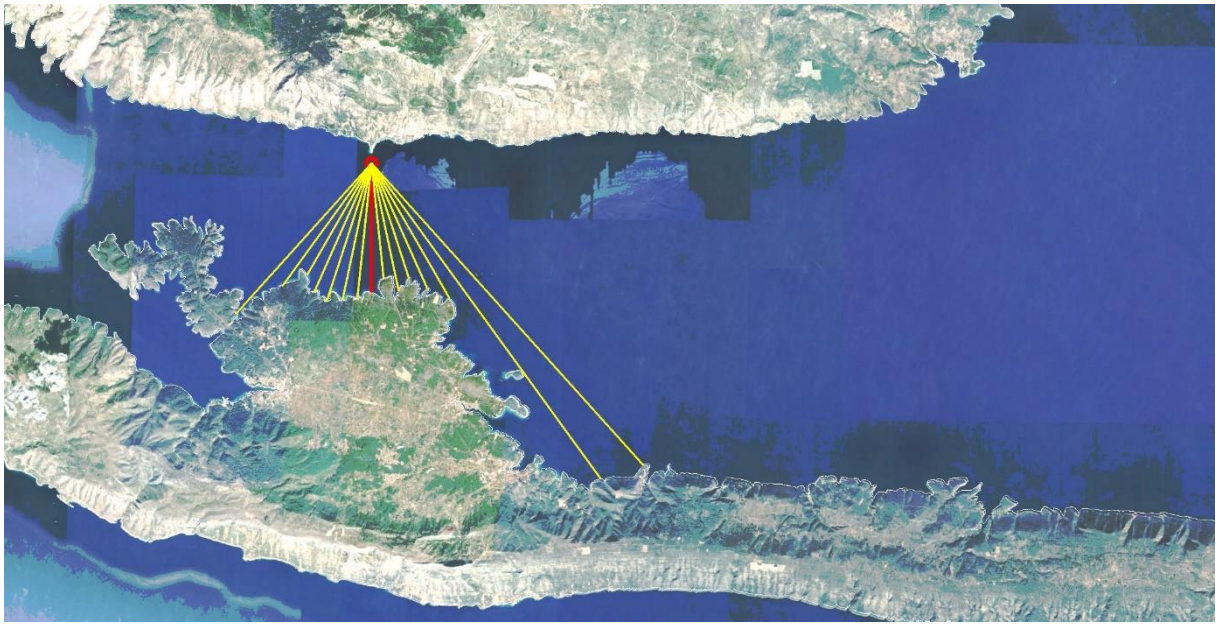

Figure 3.5 – Display of a central beam through direction S (180°), and a beam with a step ±6°

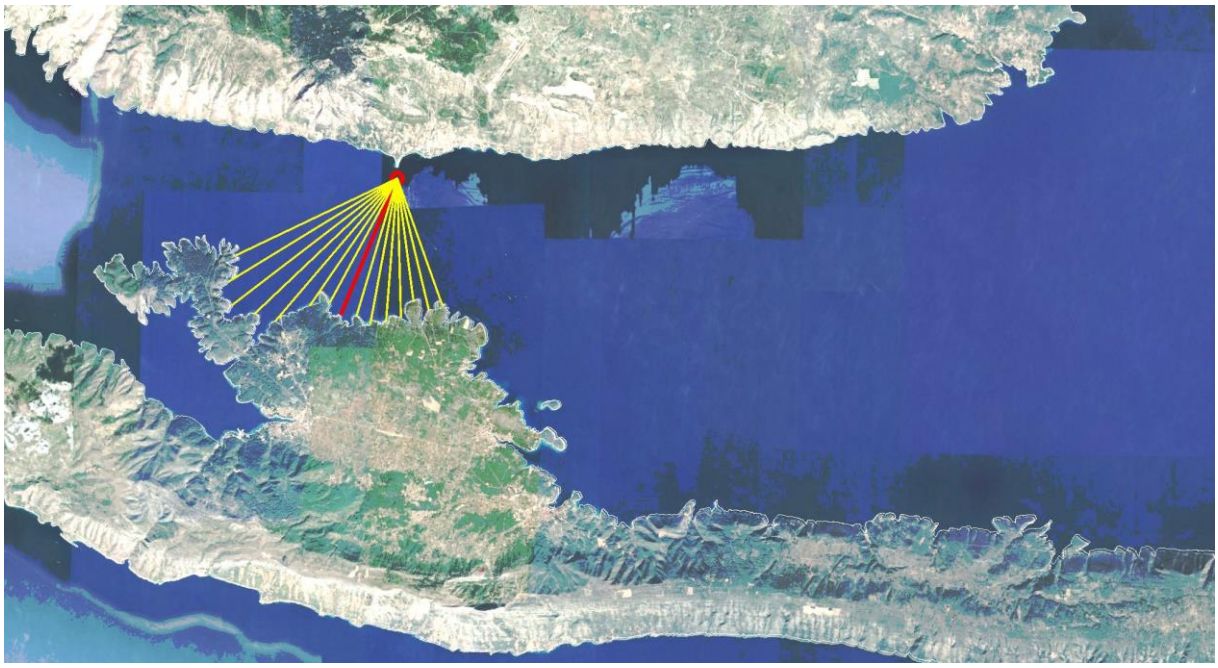

Figure 3.6 – Display of the central beam through the direction of SSW (202.5°), and the beam with step ±6°

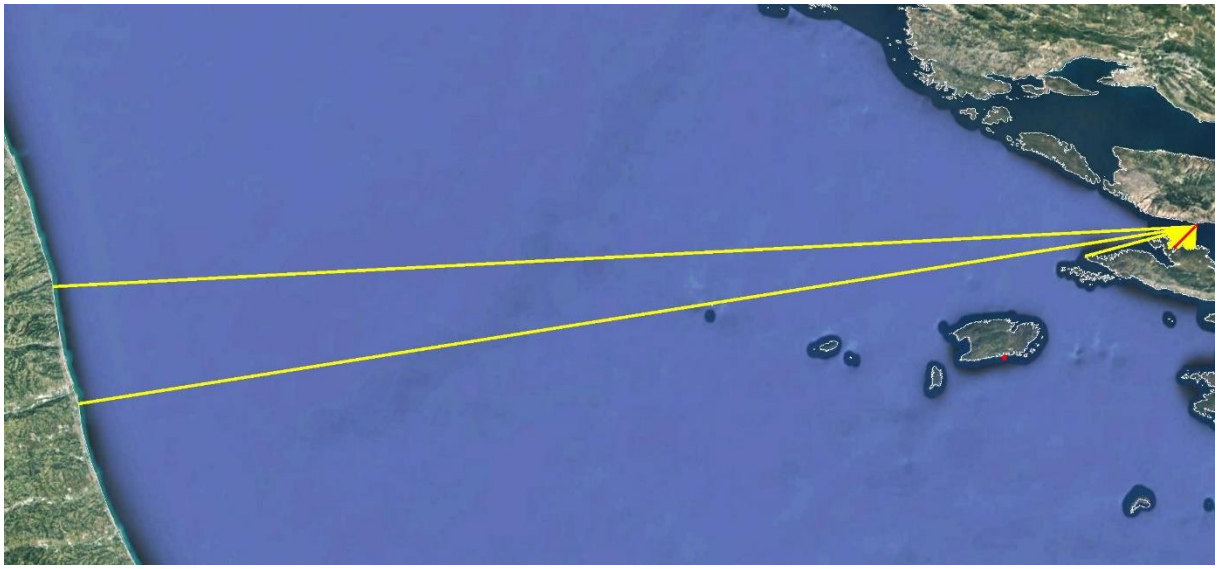

Figure 3.7 – Display of the central beam through the direction SW (225°), and the beam with step ±6°

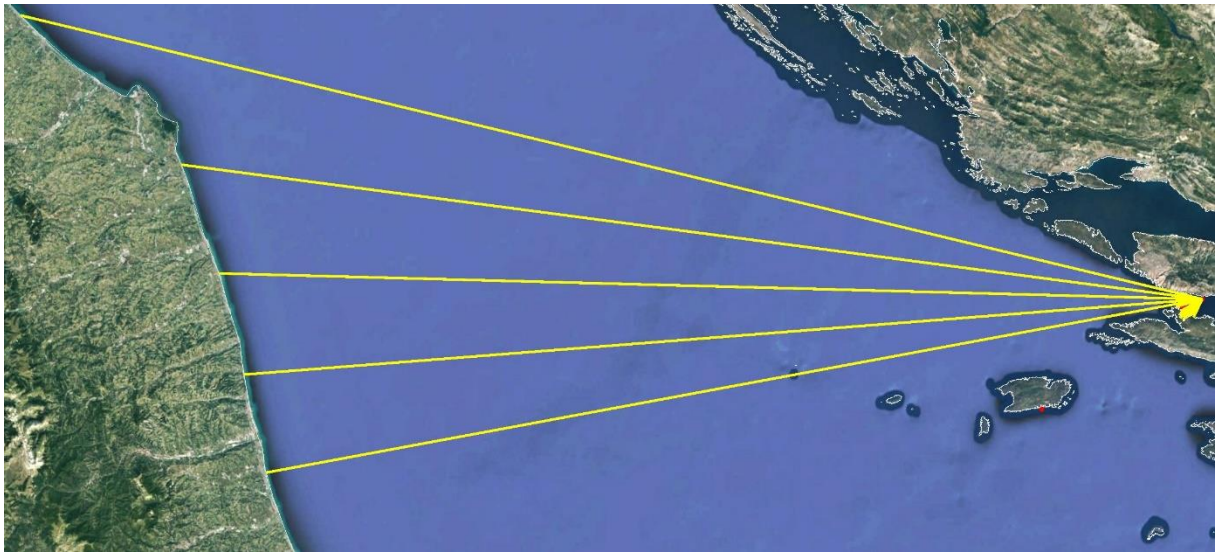

Figure 3.8 – Display of the central beam through the WSW direction (247.5°), and the beam with step ±6°

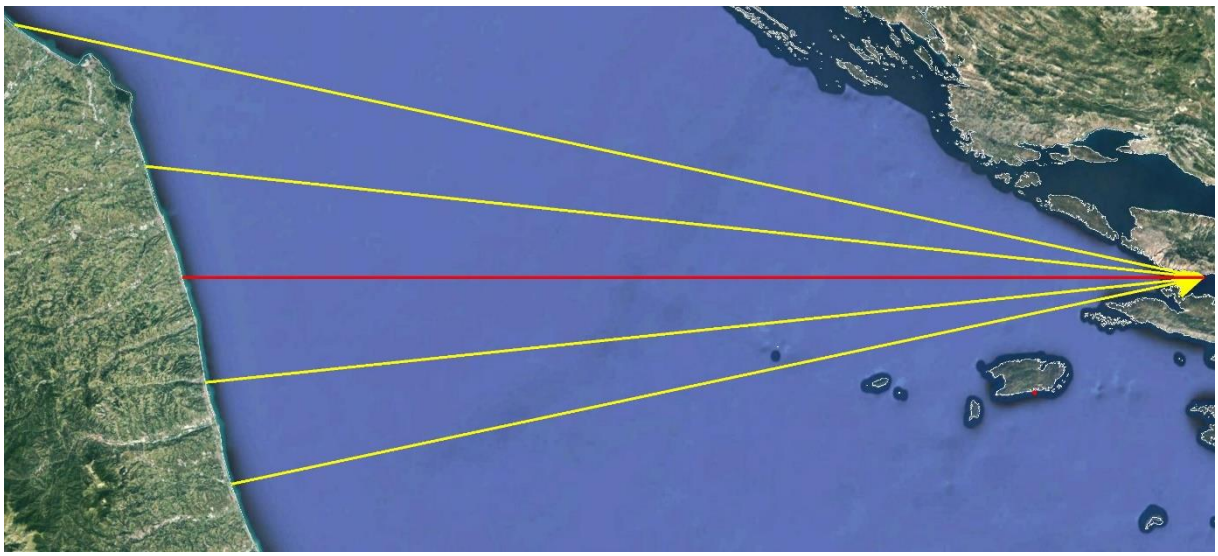

Figure 3.9 – Display of the central beam through direction W (270°), and beams with step ±6°

Table 3.1 - Determination of the effective fetch length for directions E (left) and ESE (right)

E (90°)

Kut α (°)	cosα	cos²α	d (km)	Σd		d·cos²α
42	0,743	0,552	1,06			0,59
36	0,809	0,655	1,07			0,70
30	0,866	0,750	1,41			1,06
24	0,914	0,835	2,4			2,00
18	0,951	0,905	2,76			2,50
12	0,978	0,957	3,77			3,61
6	0,995	0,989	9,92	232,13	267,97	9,81
0	1,000	1,000	34,66			34,66
-6	0,995	0,989	38,71			38,29
-12	0,978	0,957	45,45			43,49
-18	0,951	0,905	43,26			39,13
-24	0,914	0,835	28,52			23,80
-30	0,866	0,750	21,27			15,95
-36	0,809	0,655	18,01			11,79
-42	0,743	0,552	15,7			8,67
Σ(30)	10,407					
Σ(42)	13,511					236,04

L(30)= 22,3 km
L(42)= 19,8 km
Lef.= 22,3 km

ESE (112,5°)

Kut α (°)	cosα	cos²α	d (km)	Σd		d·cos²α
42	0,743	0,552	2,74			1,51
36	0,809	0,655	3,27			2,14
30	0,866	0,750	4,28			3,21
24	0,914	0,835	34,4			28,71
18	0,951	0,905	36,98			33,45
12	0,978	0,957	43,52			41,64
6	0,995	0,989	59,62	294,32	314,13	58,97
0	1,000	1,000	32,08			32,08
-6	0,995	0,989	21,84			21,60
-12	0,978	0,957	18,3			17,51
-18	0,951	0,905	16,11			14,57
-24	0,914	0,835	14,13			11,79
-30	0,866	0,750	13,06			9,80
-36	0,809	0,655	9,03			5,91
-42	0,743	0,552	4,77			2,63
Σ(30)	10,407					
Σ(42)	13,511					285,52

L(30)= 28,3 km
L(42)= 23,3 km
Lef.= 28,3 km

Table 3.2 - Determination of the effective fetch length for the directions SE (left) and SSE (right)

SE (135°)

Kut α (°)	cosα	cos²α	d (km)	Σd		d·cos²α
42	0,743	0,552	35,99		285,92	19,88
36	0,809	0,655	40,57			26,55
30	0,866	0,750	54,68	201,18		41,01
24	0,914	0,835	36,25			30,25
18	0,951	0,905	25			22,61
12	0,978	0,957	19,13			18,30
6	0,995	0,989	16,85			16,67
0	1,000	1,000	14,47			14,47
-6	0,995	0,989	13,36			13,21
-12	0,978	0,957	8,29			7,93
-18	0,951	0,905	4,8			4,34
-24	0,914	0,835	4,15			3,46
-30	0,866	0,750	4,2			3,15
-36	0,809	0,655	3,79			2,48
-42	0,743	0,552	4,39			2,42
Σ(30)	10,407					
Σ(42)	13,511					226,75

L(30)= 19,3 km
L(42)= 21,2 km
Lef.= 21,2 km

SSE (157,5°)

Kut α (°)	cosα	cos²α	d (km)	Σd		d·cos²α
42	0,743	0,552	26,61		141,05	14,70
36	0,809	0,655	20,59			13,48
30	0,866	0,750	17,55	84,65		13,16
24	0,914	0,835	15,01			12,53
18	0,951	0,905	13,5			12,21
12	0,978	0,957	8,34			7,98
6	0,995	0,989	5,18			5,12
0	1,000	1,000	4,58			4,58
-6	0,995	0,989	4,12			4,07
-12	0,978	0,957	3,79			3,63
-18	0,951	0,905	3,89			3,52
-24	0,914	0,835	4,24			3,54
-30	0,866	0,750	4,45			3,34
-36	0,809	0,655	4,53			2,96
-42	0,743	0,552	4,67			2,58
Σ(30)	10,407					
Σ(42)	13,511					107,39

L(30)= 8,1 km
L(42)= 10,4 km
Lef.= 10,4 km

Table 3.3 - Determination of the effective fetch length for directions S (left) and SSW (right)

S (180°)

Kut α (°)	cosα	cos²α	d (km)	Σd		d·cos²α
42	0,743	0,552	13,44		87,08	7,42
36	0,809	0,655	12,9			8,44
30	0,866	0,750	5,16	49,01		3,87
24	0,914	0,835	4,55			3,80
18	0,951	0,905	4,02			3,64
12	0,978	0,957	4,32			4,13
6	0,995	0,989	3,84			3,80
0	1,000	1,000	4,27			4,27
-6	0,995	0,989	4,5			4,45
-12	0,978	0,957	4,62			4,42
-18	0,951	0,905	4,81			4,35
-24	0,914	0,835	4,66			3,89
-30	0,866	0,750	4,26			3,20
-36	0,809	0,655	5,03			3,29
-42	0,743	0,552	6,7			3,70
Σ(30)	10,407					
Σ(42)	13,511					66,67

L(30)= 4,7 km
L(42)= 6,4 km
Lef.= 6,4 km

SSW (202,5°)

Kut α (°)	cosα	cos²α	d (km)	Σd		d·cos²α
42	0,743	0,552	4,18		73,62	2,31
36	0,809	0,655	4,19			2,74
30	0,866	0,750	3,83	53,62		2,87
24	0,914	0,835	4,31			3,60
18	0,951	0,905	4,44			4,02
12	0,978	0,957	4,58			4,38
6	0,995	0,989	4,43			4,38
0	1,000	1,000	4,56			4,56
-6	0,995	0,989	4,37			4,32
-12	0,978	0,957	4,78			4,57
-18	0,951	0,905	5,81			5,26
-24	0,914	0,835	6,07			5,07
-30	0,866	0,750	6,44			4,83
-36	0,809	0,655	6,12			4,01
-42	0,743	0,552	5,51			3,04
Σ(30)	10,407					
Σ(42)	13,511					59,96

L(30)= 5,2 km
L(42)= 5,4 km
Lef.= 5,4 km

Table 3.4 - Determination of the effective fetch length for directions SW (left) and WSW (right)

SW (225°)

Kut α (°)	cosα	cos²α	d (km)	Σd		d·cos²α
42	0,743	0,552	4,27		537,32	2,36
36	0,809	0,655	4,45			2,91
30	0,866	0,750	4,45	76,6		3,34
24	0,914	0,835	4,82			4,02
18	0,951	0,905	4,64			4,20
12	0,978	0,957	4,18			4,00
6	0,995	0,989	5,45			5,39
0	1,000	1,000	6			6,00
-6	0,995	0,989	6,88			6,80
-12	0,978	0,957	6,44			6,16
-18	0,951	0,905	5,47			4,95
-24	0,914	0,835	5,71			4,77
-30	0,866	0,750	22,56			16,92
-36	0,809	0,655	225			147,26
-42	0,743	0,552	227			125,36
Σ(30)	10,407					
Σ(42)	13,511					344,45

L(30)= 7,4 km
L(42)= 39,8 km
Lef.= 39,8 km

WSW (247,5°)

Kut α (°)	cosα	cos²α	d (km)	Σd		d·cos²α
42	0,743	0,552	4,72		1268,59	2,61
36	0,809	0,655	4,21			2,76
30	0,866	0,750	5,21	968,89		3,91
24	0,914	0,835	6,63			5,53
18	0,951	0,905	6,78			6,13
12	0,978	0,957	6,51			6,23
6	0,995	0,989	5,71			5,65
0	1,000	1,000	5,55			5,55
-6	0,995	0,989	6,4			6,33
-12	0,978	0,957	224,4			214,70
-18	0,951	0,905	226,7			205,05
-24	0,914	0,835	232			193,62
-30	0,866	0,750	243			182,25
-36	0,809	0,655	286,5			187,52
-42	0,743	0,552	4,27			2,36
Σ(30)	10,407					
Σ(42)	13,511					1030,19

L(30)= 93,1 km
L(42)= 93,9 km
Lef.= 93,9 km

Table 3.5 - Determination of the effective length of fetch for direction W

W (270°)

Kut α (°)	cosα	$\cos^2\alpha$	d (km)	Σd		$d\cdot\cos^2\alpha$
42	0,743	0,552	6,38		1237,3	3,52
36	0,809	0,655	6,42			4,20
30	0,866	0,750	5,69	1221,33		4,27
24	0,914	0,835	5,36			4,47
18	0,951	0,905	6,21			5,62
12	0,978	0,957	224			214,32
6	0,995	0,989	226			223,53
0	1,000	1,000	230			230,00
-6	0,995	0,989	240			237,38
-12	0,978	0,957	274			262,16
-18	0,951	0,905	4,82			4,36
-24	0,914	0,835	2,78			2,32
-30	0,866	0,750	2,47			1,85
-36	0,809	0,655	1,79			1,17
-42	0,743	0,552	1,38			0,76
Σ(30)	10,407					
Σ(42)	13,511					1199,93

L(30)= 117,4 km

L(42)= 91,6 km

Lef.= 117,4 km

3.1.1.2. Vis (Stiniva)

As already mentioned in point 2.2.3.2, the Stiniva beach aquatory on the island of Vis is exposed to winds from the second and third quadrants and consequent wind waves with different lengths of the fetch. In view of this, according to the criterion of fetch length and similarity of frequency of wind occurrence for a particular direction, certain sectors that are defined by the action of winds from the directions ESE, SE, SSE, S, SSW and SW will be defined.

Sector I is defined by the action of winds and consequent surface wind waves from the directions ESE and SE, sector II by the action of winds and consequent surface wind waves from the directions SSE and S, while sector III is defined by the action of winds and consequent surface wind waves from the directions SSW and SW.

For sector I and direction SE (135°), the effective fetch was calculated at 245.1 km (Table 3.6). For sector II, the longer effective fetch was calculated for the direction SSE (157.5°) and is 248.2 km (Tables 3.6 and 3.7). For sector III, the longer effective fetch was calculated for the direction SSW (202.5°) and is 177.4 km (Tables 3.7 and 3.8).

In figures 3.10 to 3.14 are given graphical representations of the placement of the central beam through the analyzed directions and beams with rotation ±6° from the central beam. The calculated values of the procedure for determining the effective length of the fetch for all individual directions are given in Tables 3.6 to 3.8.

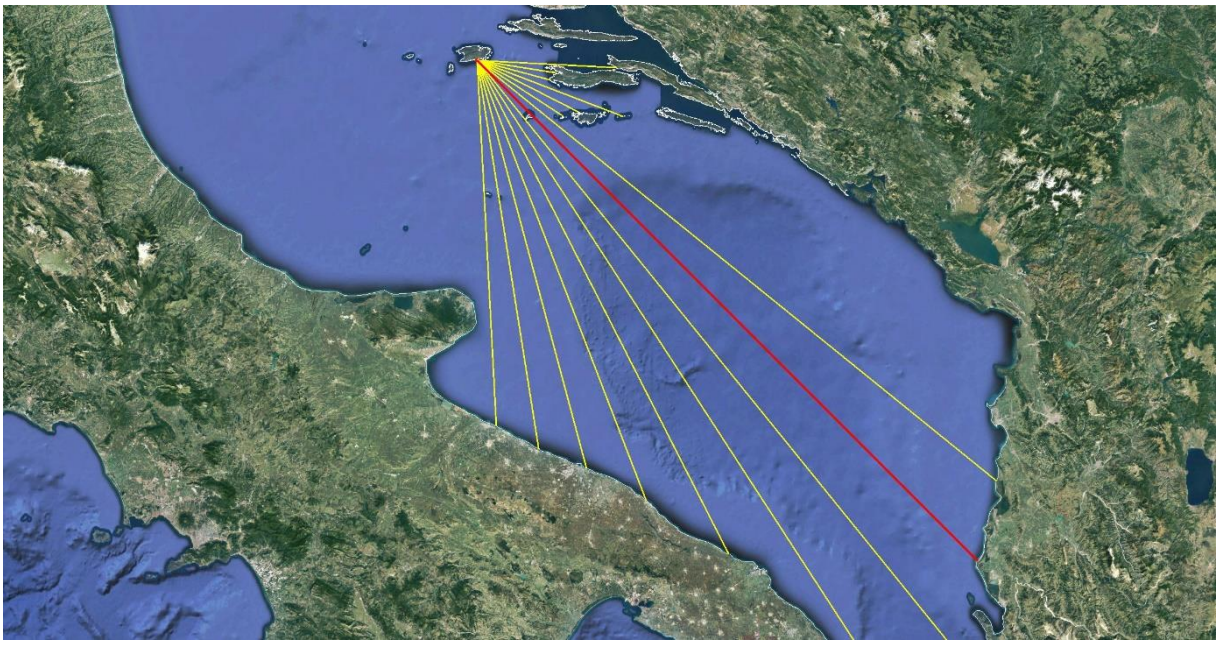

Figure 3.10 – Display of the central beam through the direction of SE (135°), and the beam with step ±6°

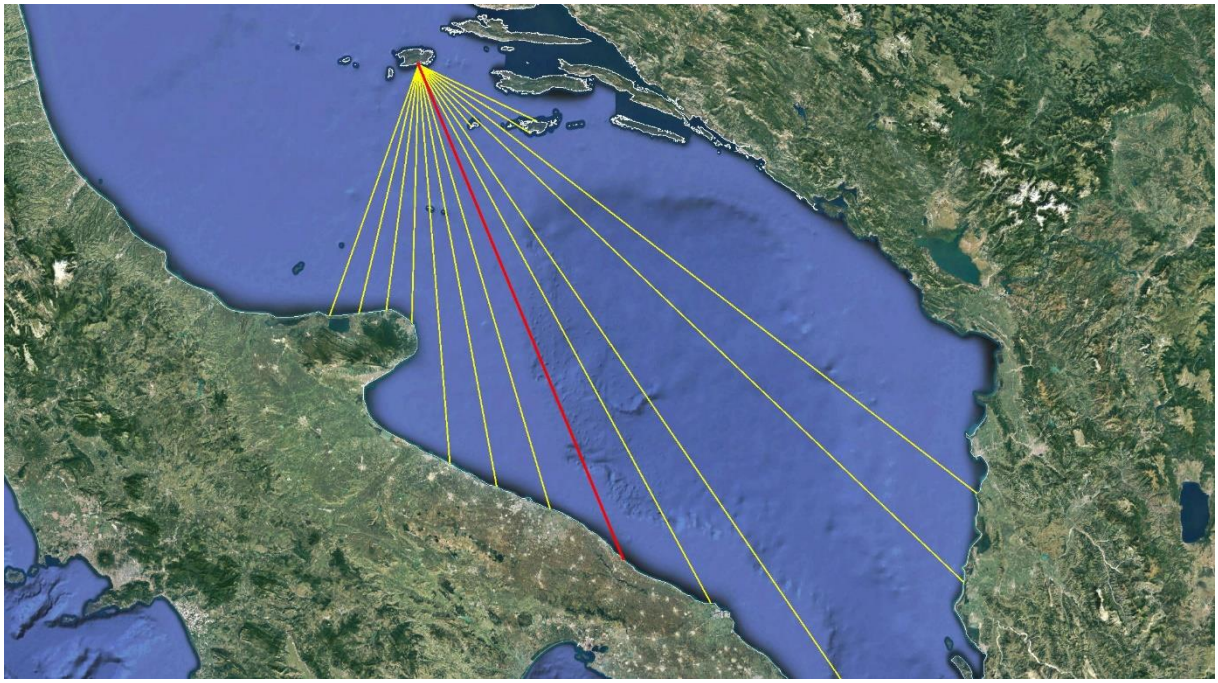

Figure 3.11 – Display of the central beam through the direction of SSE (157.5°), and the beam with step ±6°

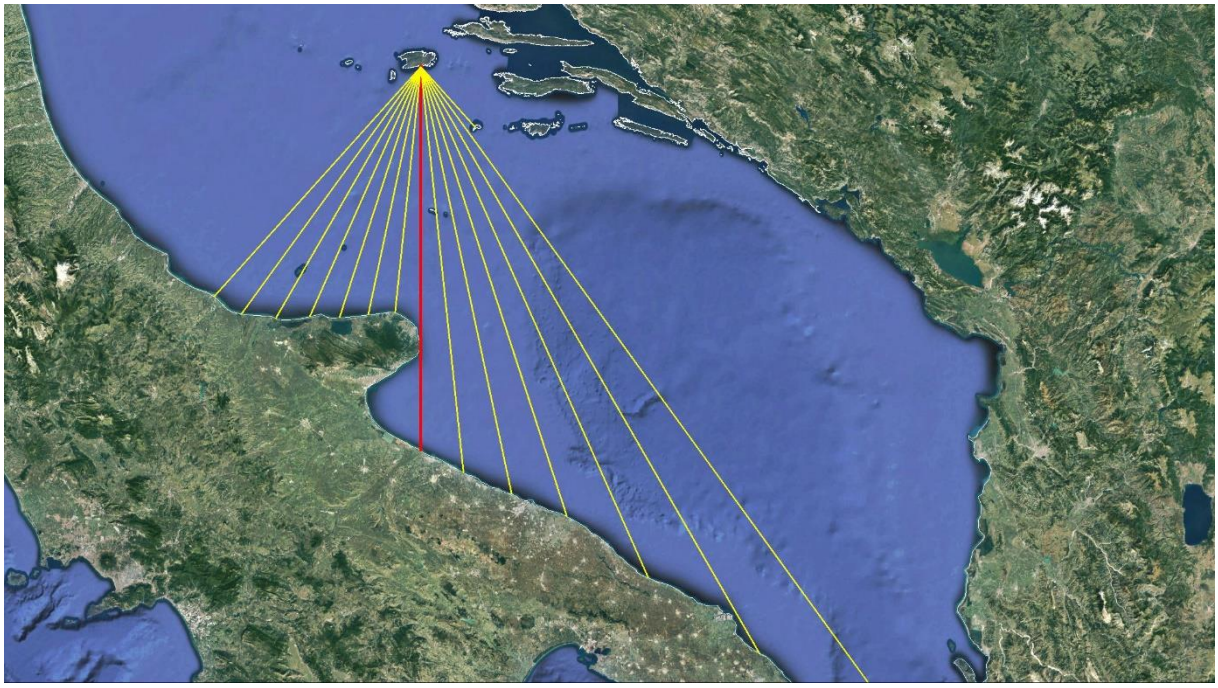

Figure 3.12 – Display of the central beam through direction S (180°), and the beam with step ±6°

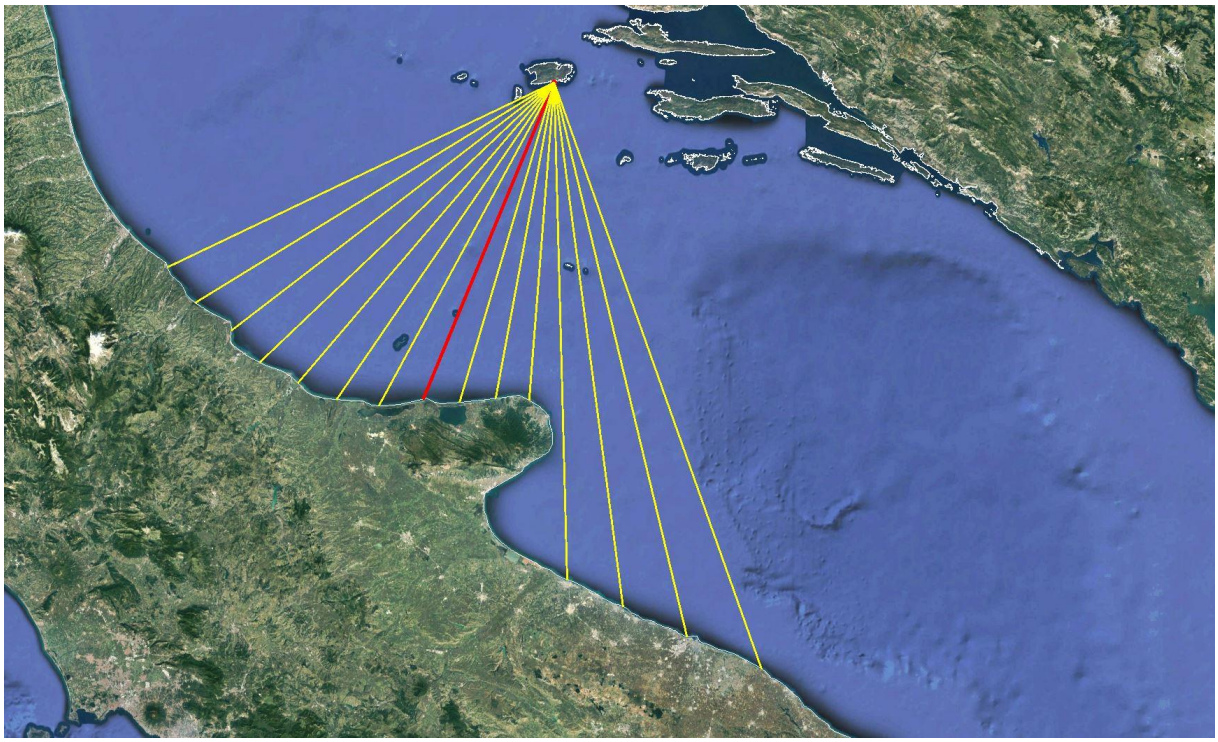

Figure 3.13 – Display of the central beam through the direction of SSW (202.5°), and the beam with step ±6°

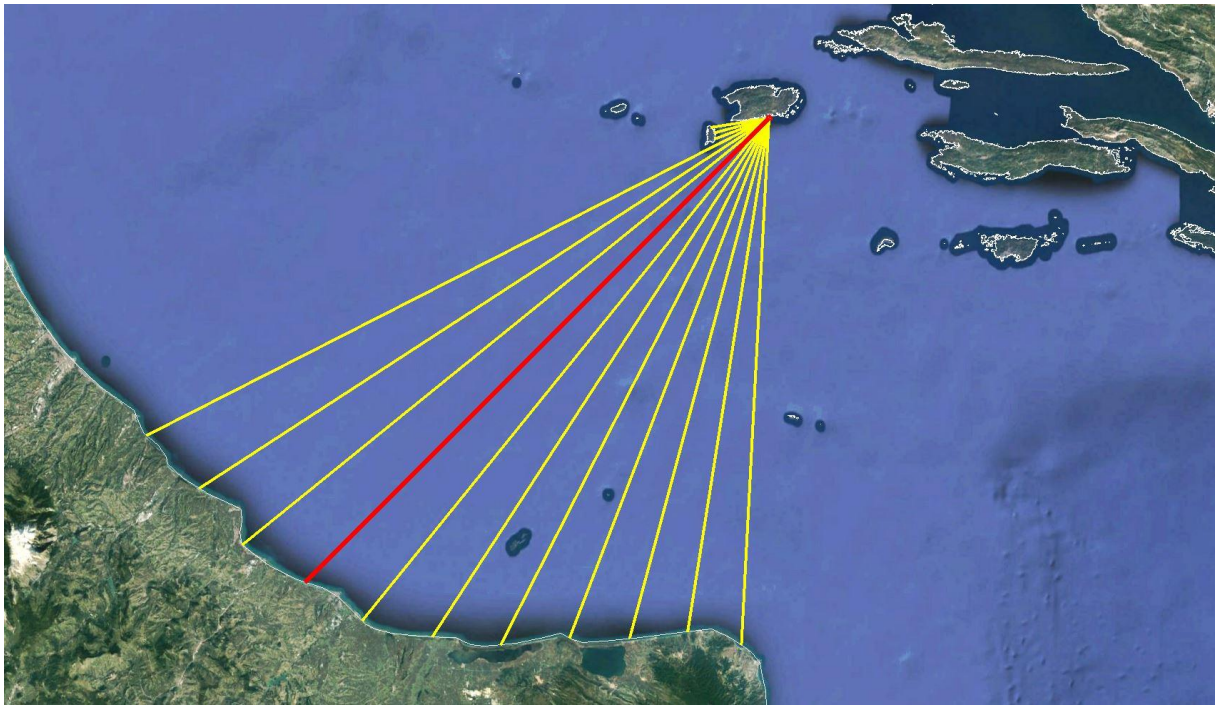

Figure 3.14 – Display of the central beam through the direction SW (225°), and the beam with step ±6°

Table 3.6 – Determination of the effective fetch length for directions SE (left) and SSE (right)

SE (135°)

Kut α (°)	cosα	cos²α	d (km)	Σd		d·cos²α
42	0,743	0,552	72,49		3058,72	40,03
36	0,809	0,655	41,45			27,13
30	0,866	0,750	39,26	2550,58		29,45
24	0,914	0,835	80,87			67,49
18	0,951	0,905	59,15			53,50
12	0,978	0,957	52,9			50,61
6	0,995	0,989	346,6			342,81
0	1,000	1,000	367			367,00
-6	0,995	0,989	443,6			438,75
-12	0,978	0,957	410			392,28
-18	0,951	0,905	287,5			260,05
-24	0,914	0,835	244,4			203,97
-30	0,866	0,750	219,3			164,48
-36	0,809	0,655	204,1			133,59
-42	0,743	0,552	190,1			104,99
Σ(30)	10,407					
Σ(42)	13,511					2676,12

L(30)= 245,1 km
L(42)= 226,4 km
Lef.= 245,1 km

SSE (157,5°)

Kut α (°)	cosα	cos²α	d (km)	Σd		d·cos²α
42	0,743	0,552	63,2		2961,12	34,90
36	0,809	0,655	63,17			41,35
30	0,866	0,750	339,8	2582,55		254,88
24	0,914	0,835	363			302,95
18	0,951	0,905	39,12			35,38
12	0,978	0,957	418			399,93
6	0,995	0,989	296			292,77
0	1,000	1,000	258,6			258,60
-6	0,995	0,989	223,7			221,26
-12	0,978	0,957	207,1			198,14
-18	0,951	0,905	193,1			174,66
-24	0,914	0,835	124,6			103,99
-30	0,866	0,750	119,5			89,63
-36	0,809	0,655	123,5			80,83
-42	0,743	0,552	128,7			71,08
Σ(30)	10,407					
Σ(42)	13,511					2560,33

L(30)= 248,2 km
L(42)= 219,2 km
Lef.= 248,2 km

Table 3.7 - Determination of the effective fetch length for directions S (left) and SSW (right)

S (180°)

Kut α (°)	cosα	cos²α	d (km)	Σd		d·cos²α
42	0,743	0,552	39,06		2819,86	21,57
36	0,809	0,655	425,6			278,56
30	0,866	0,750	326,8	2058,6		245,10
24	0,914	0,835	270			225,33
18	0,951	0,905	228,1			206,32
12	0,978	0,957	210,7			201,59
6	0,995	0,989	197			194,85
0	1,000	1,000	185			185,00
-6	0,995	0,989	119,2			117,90
-12	0,978	0,957	122,3			117,01
-18	0,951	0,905	127,3			115,14
-24	0,914	0,835	132			110,16
-30	0,866	0,750	140,2			105,15
-36	0,809	0,655	147,4			96,47
-42	0,743	0,552	149,2			82,40
Σ(30)	10,407					
Σ(42)	13,511					2302,56

L(30)= 197,8 km
L(42)= 208,7 km
Lef.= 208,7 km

SSW (202,5°)

Kut α (°)	cosα	cos²α	d (km)	Σd		d·cos²α
42	0,743	0,552	234,9		2397,2	129,73
36	0,809	0,655	215,2			140,85
30	0,866	0,750	199,7	1626		149,78
24	0,914	0,835	188			156,90
18	0,951	0,905	120,4			108,90
12	0,978	0,957	121,3			116,06
6	0,995	0,989	126			124,62
0	1,000	1,000	129,5			129,50
-6	0,995	0,989	139			137,48
-12	0,978	0,957	145,3			139,02
-18	0,951	0,905	149,3			135,04
-24	0,914	0,835	153,6			128,19
-30	0,866	0,750	153,9			115,43
-36	0,809	0,655	159,2			104,20
-42	0,743	0,552	161,9			89,41
Σ(30)	10,407					
Σ(42)	13,511					1905,10

L(30)= 156,2 km
L(42)= 177,4 km
Lef.= 177,4 km

Table 3.8 - Determination of the effective fetch length for direction SW

SW (225°)

Kut α (°)	cosα	cos²α	d (km)	Σd		d·cos²α
42	0,743	0,552	122,1		1598,47	67,43
36	0,809	0,655	120,3			78,74
30	0,866	0,750	124,7	1337,95		93,53
24	0,914	0,835	128,9			107,58
18	0,951	0,905	136,9			123,83
12	0,978	0,957	143,1			136,91
6	0,995	0,989	150			148,36
0	1,000	1,000	151,9			151,90
-6	0,995	0,989	157			155,28
-12	0,978	0,957	157,2			150,40
-18	0,951	0,905	161,8			146,35
-24	0,914	0,835	13,4			11,18
-30	0,866	0,750	13,05			9,79
-36	0,809	0,655	13,6			8,90
-42	0,743	0,552	4,52			2,50
Σ(30)	10,407					
Σ(42)	13,511					1392,68

L(30)= 128,6 km
L(42)= 118,3 km
Lef.= 128,6 km

3.1.1.3. Makarska Riviera (Podgora)

As already mentioned in point 2.2.3.3, Podgora beaches aquatory on the Makarska Riviera is exposed to winds from the second, third and fourth quadrants and consequent wind waves with different lengths of the fetch. In view of this, according to the criterion of fetch length and similarity of frequency of wind occurrence for a particular direction, certain sectors that are defined by the action of winds from the directions ESE, SE, SSE, SSW, SW, WSW, W and WNW will be defined.

Sector I is defined by the action of winds and consequent surface wind waves from the directions ESE and SE, sector II by the action of winds and consequent surface wind waves from the directions SSE and S, sector III by the action of winds and consequent surface wind waves from the directions SSW and SW, while sector IV is defined by the action of winds and consequent surface wind waves from directions WSW, W and WNW.

The longer effective fetch of sector I was calculated for the direction of SE (135°) and is 16.4 km (Table 3.9). For sector II, the longer effective fetch was calculated for the direction SSE (157.5°) and is 18.3 km (Tables 3.9 and 3.10). For sector III, the longer effective windward was calculated for the direction SW (202.5°) and is 18.6 km (Tables 3.10 and 3.11). For sector IV, the longest effective fetch is calculated for direction W (270°) and is 26.9 km (Tables 3.11 and 3.12).

In Figures 3.15 to 3.22, graphical representations of the central beam placement through the analyzed directions and beams with rotation ±6° from the central beam are given. The calculated values of the procedure for determining the effective length of the fetch for all individual directions are given in Tables 3.9 to 3.12.

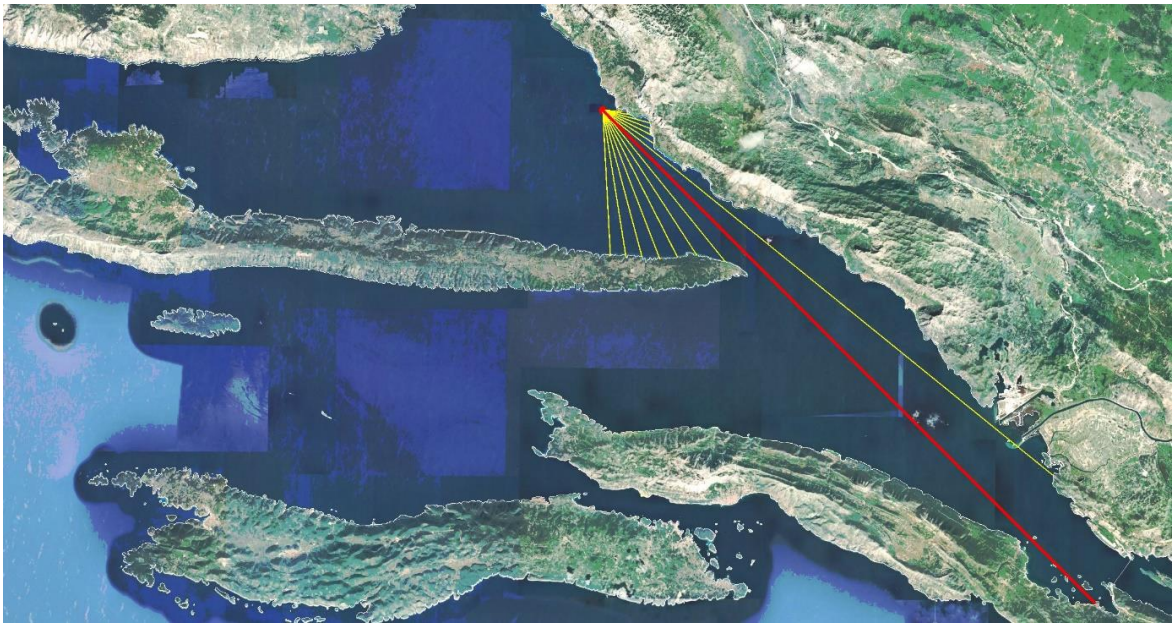

Figure 3.15 – Display of the central beam through the direction of SE (135°), and the beam striking ±6°

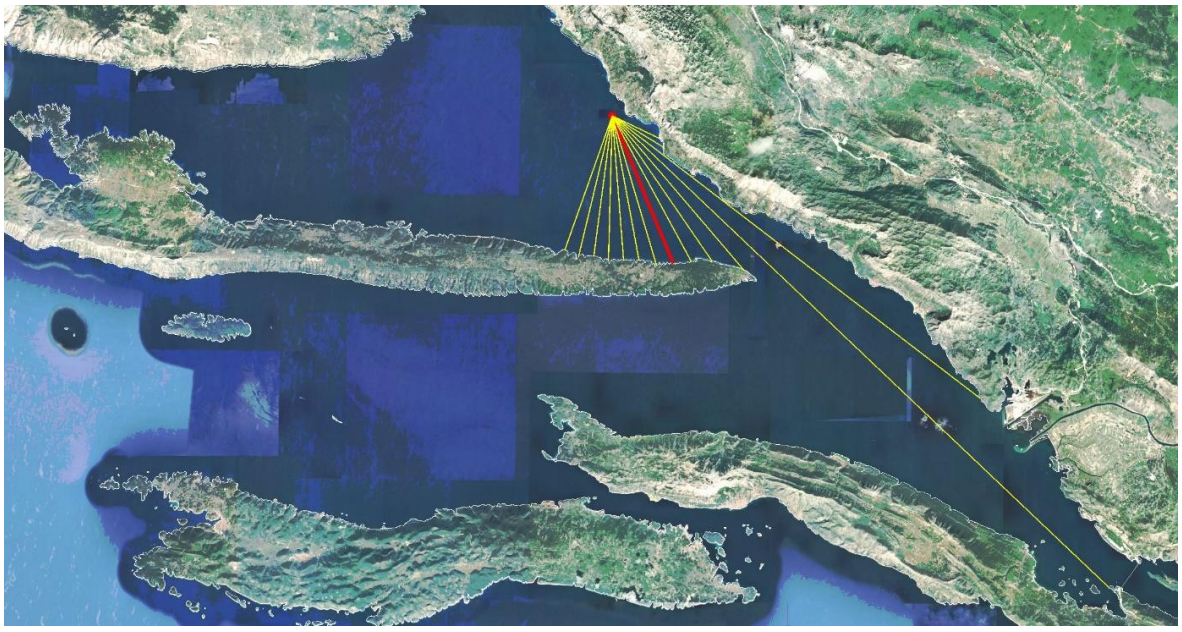

Figure 3.16 – Display of the central beam through the direction of SSE (157.5°), and the beam with a step ±6°

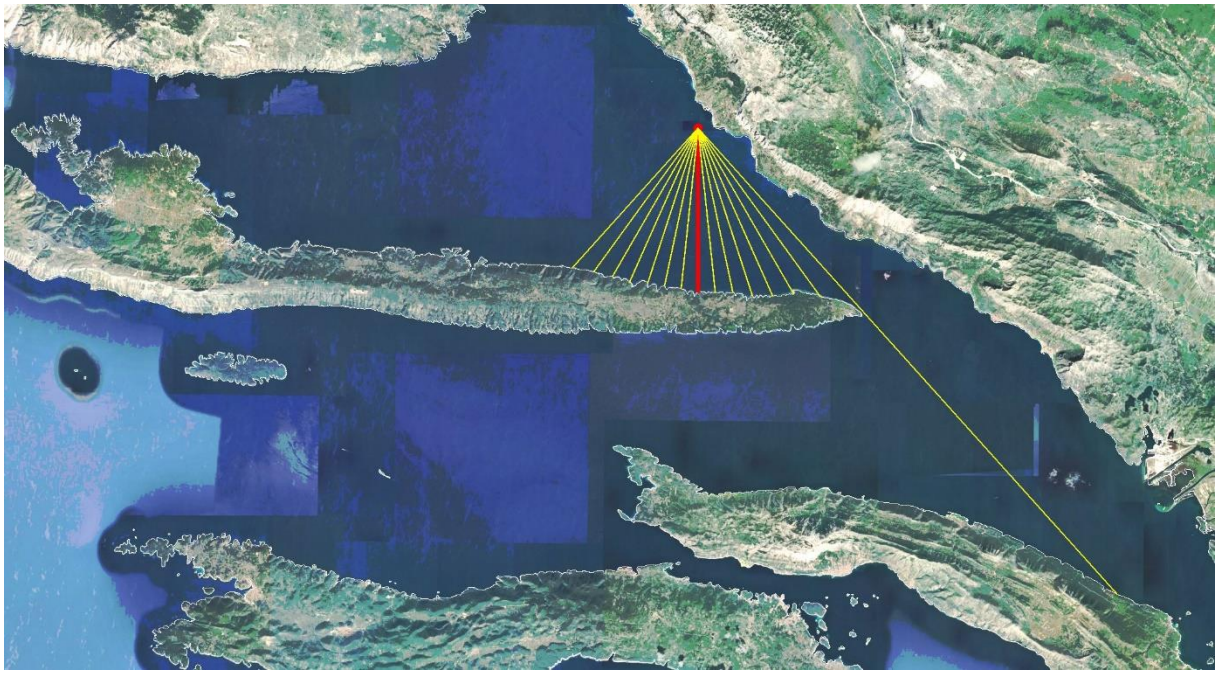

Figure 3.17 – Display of the central beam through direction S (180°), and beams with step ±6°

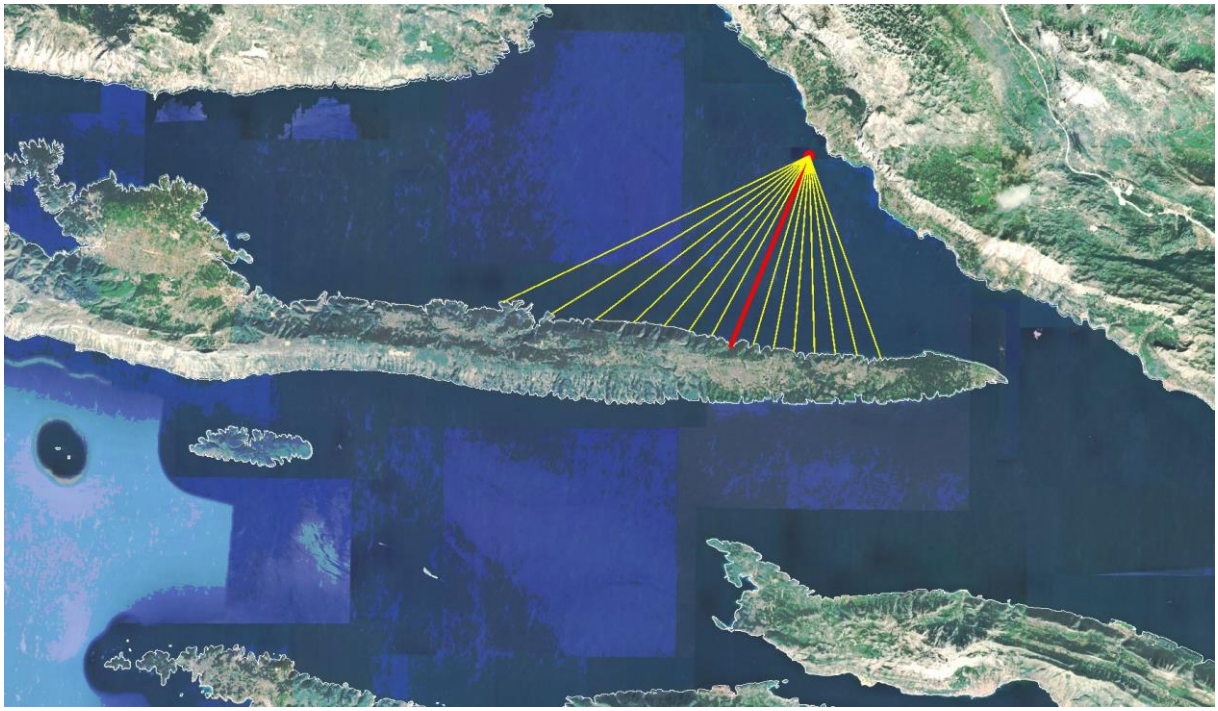

Figure 3.18 – Display of the central beam through the direction of SSW (202.5°), and the beam with a step ±6°

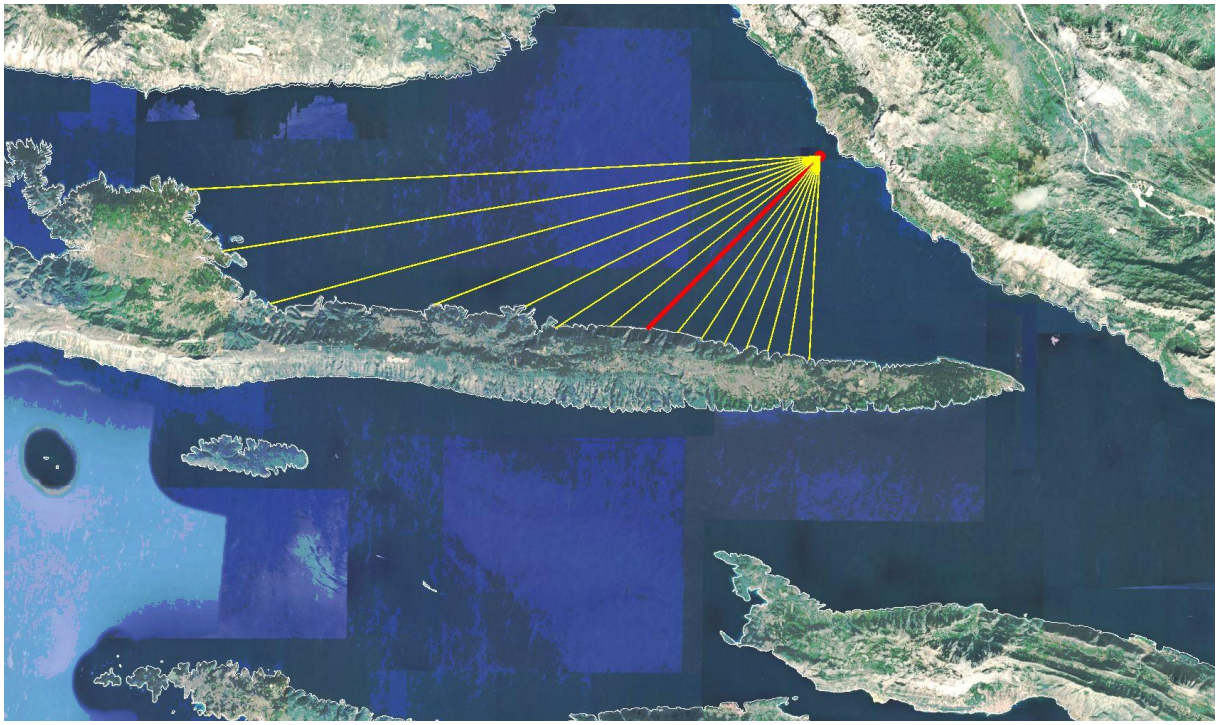

Figure 3.19 – Display of the central beam through the direction SW (225°), and the beam with step ±6°

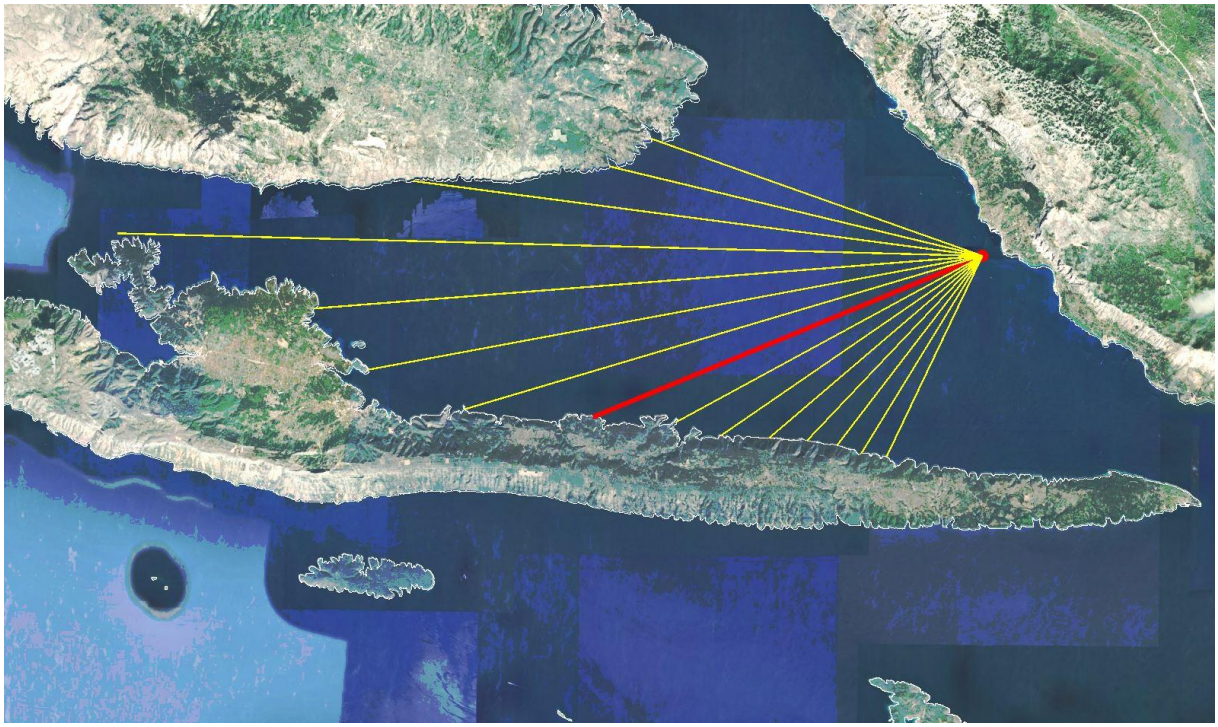

Figure 3.20 – Central beam display through WSW direction (247.5°), and beams with step ±6°

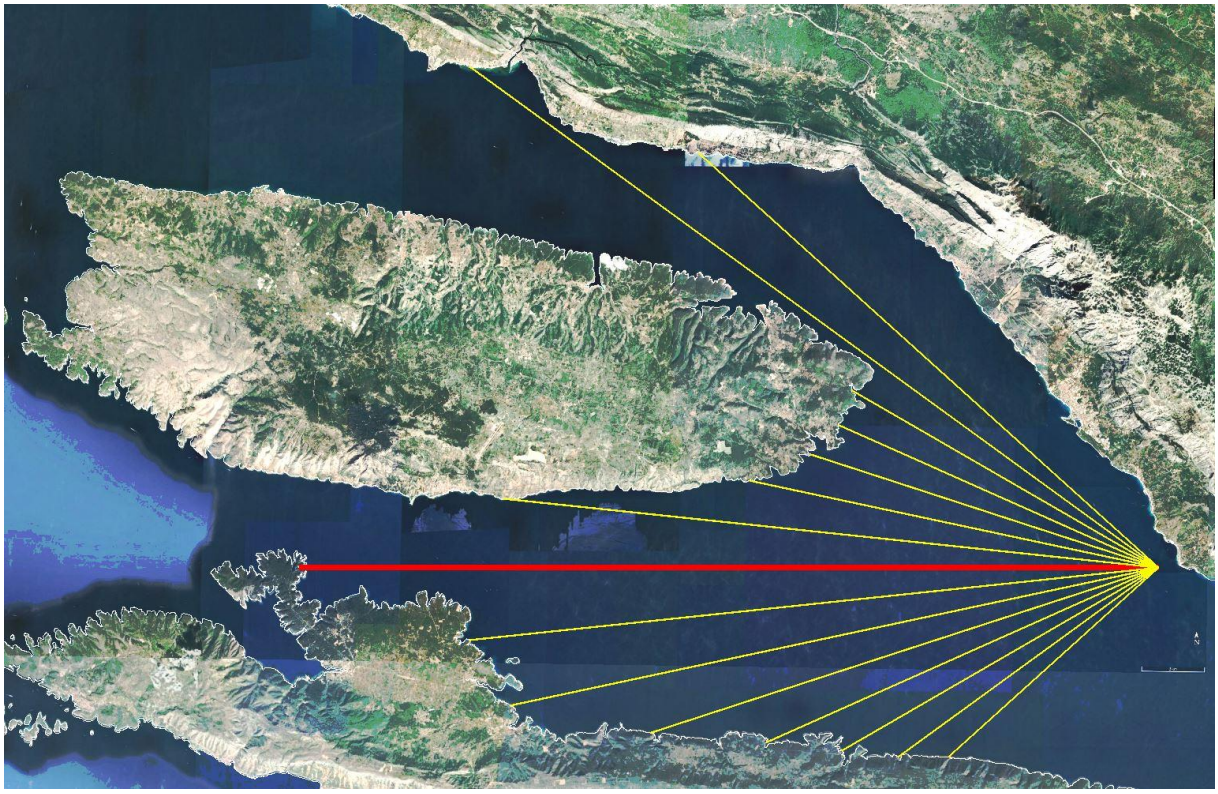

Figure 3.21 – Display of a central beam through direction W (270°), and a beam with a step ±6°

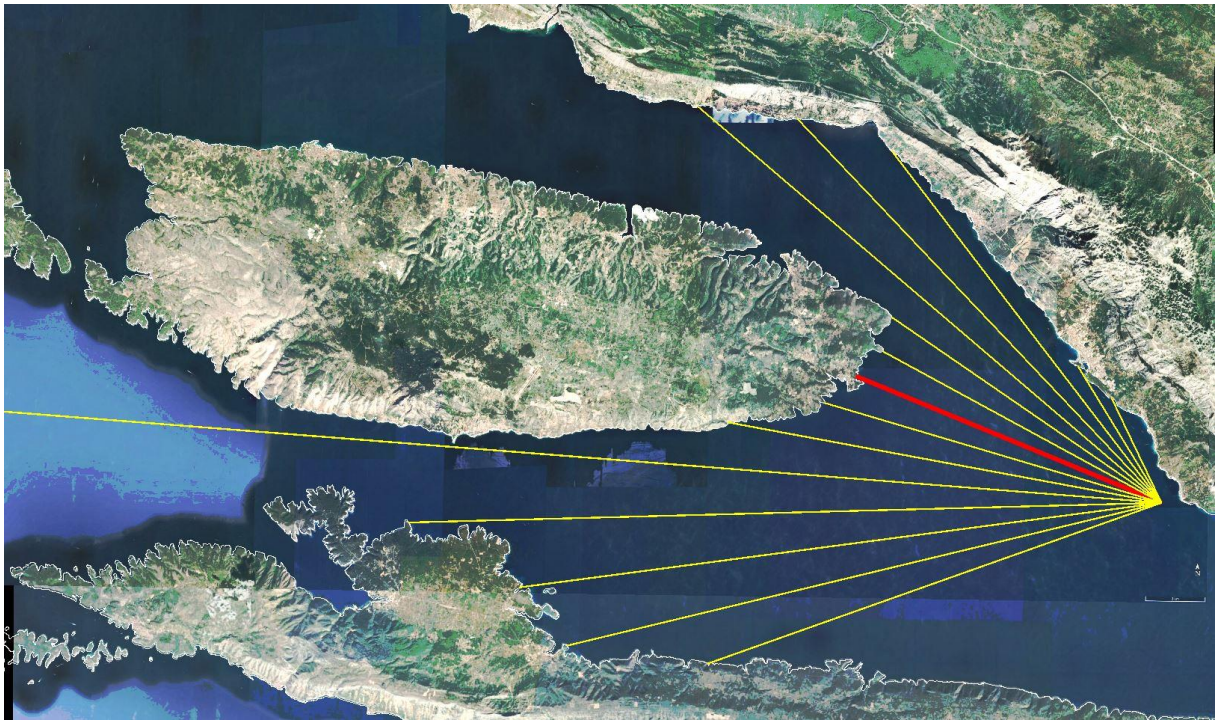

Figure 3.22 – Display of the central beam through the WNW direction (292.5°), and the beam with step ±6°

Table 3.9 - Determination of the effective fetch length for the directions SE (left) and SSE (right)

SE (135°)

Kut α (°)	cosα	cos²α	d (km)	Σd		d·cos²α
42	0,743	0,552	1,4			0,77
36	0,809	0,655	2,1			1,37
30	0,866	0,750	3,6			2,70
24	0,914	0,835	3,79			3,16
18	0,951	0,905	3,99			3,61
12	0,978	0,957	4,5			4,31
6	0,995	0,989	42,46	171,15	196,17	42,00
0	1,000	1,000	51,05			51,05
-6	0,995	0,989	14,27			14,11
-12	0,978	0,957	12,64			12,09
-18	0,951	0,905	12,07			10,92
-24	0,914	0,835	11,69			9,76
-30	0,866	0,750	11,09			8,32
-36	0,809	0,655	10,86			7,11
-42	0,743	0,552	10,66			5,89
Σ(30)	10,407					
Σ(42)	13,511					177,16

L(30)= 16,4 km
L(42)= 14,5 km
Lef.= 16,4 km

SSE (157,5°)

Kut α (°)	cosα	cos²α	d (km)	Σd		d·cos²α
42	0,743	0,552	3,85			2,13
36	0,809	0,655	4,41			2,89
30	0,866	0,750	34,06			25,55
24	0,914	0,835	50,36			42,03
18	0,951	0,905	14,96			13,53
12	0,978	0,957	12,98			12,42
6	0,995	0,989	12,18	190,21	219,54	12,05
0	1,000	1,000	11,71			11,71
-6	0,995	0,989	11,47			11,34
-12	0,978	0,957	10,78			10,31
-18	0,951	0,905	10,65			9,63
-24	0,914	0,835	10,68			8,91
-30	0,866	0,750	10,38			7,79
-36	0,809	0,655	10,62			6,95
-42	0,743	0,552	10,45			5,77
Σ(30)	10,407					
Σ(42)	13,511					183,01

L(30)= 18,3 km
L(42)= 16,2 km
Lef.= 18,3 km

Table 3.10 - Determination of the effective fetch length for directions S (left) and SSW (right)

S (180°)

Kut α (°)	cosα	cos²α	d (km)	Σd		d·cos²α
42	0,743	0,552	40,44		198,43	22,33
36	0,809	0,655	13,42			8,78
30	0,866	0,750	12,35	120,96		9,26
24	0,914	0,835	11,85			9,89
18	0,951	0,905	11,38			10,29
12	0,978	0,957	10,85			10,38
6	0,995	0,989	10,67			10,55
0	1,000	1,000	10,57			10,57
-6	0,995	0,989	10,42			10,31
-12	0,978	0,957	10,41			9,96
-18	0,951	0,905	10,51			9,51
-24	0,914	0,835	10,91			9,11
-30	0,866	0,750	11,04			8,28
-36	0,809	0,655	11,46			7,50
-42	0,743	0,552	12,15			6,71
Σ(30)	10,407					
Σ(42)	13,511					153,44

L(30)= 11,6 km
L(42)= 14,7 km
Lef.= 14,7 km

SSW (202,5°)

Kut α (°)	cosα	cos²α	d (km)	Σd		d·cos²α
42	0,743	0,552	11,47		182,2	6,33
36	0,809	0,655	10,97			7,18
30	0,866	0,750	10,68	125,44		8,01
24	0,914	0,835	10,56			8,81
18	0,951	0,905	10,48			9,48
12	0,978	0,957	10,49			10,04
6	0,995	0,989	10,52			10,41
0	1,000	1,000	11,08			11,08
-6	0,995	0,989	10,93			10,81
-12	0,978	0,957	11,38			10,89
-18	0,951	0,905	11,96			10,82
-24	0,914	0,835	12,96			10,82
-30	0,866	0,750	14,4			10,80
-36	0,809	0,655	16,18			10,59
-42	0,743	0,552	18,14			10,02
Σ(30)	10,407					
Σ(42)	13,511					146,08

L(30)= 12,1 km
L(42)= 13,5 km
Lef.= 13,5 km

Table 3.11 - Determination of the effective fetch length for directions SW (left) and WSW (right)

SW (225°)

Kut α (°)	cosα	cos²α	d (km)	Σd		d·cos²α
42	0,743	0,552	10,54		251,32	5,82
36	0,809	0,655	10,43			6,83
30	0,866	0,750	10,46	166,23		7,85
24	0,914	0,835	10,69			8,92
18	0,951	0,905	10,93			9,89
12	0,978	0,957	11,28			10,79
6	0,995	0,989	11,77			11,64
0	1,000	1,000	12,66			12,66
-6	0,995	0,989	14			13,85
-12	0,978	0,957	16,35			15,64
-18	0,951	0,905	17,13			15,49
-24	0,914	0,835	21,44			17,89
-30	0,866	0,750	29,52			22,14
-36	0,809	0,655	31,38			20,54
-42	0,743	0,552	32,74			18,08
Σ(30)	10,407					
Σ(42)	13,511					198,03

L(30)= 16,0 km
L(42)= 18,6 km
Lef.= 18,6 km

WSW (247,5°)

Kut α (°)	cosα	cos²α	d (km)	Σd		d·cos²α
42	0,743	0,552	10,79		306,38	5,96
36	0,809	0,655	11,23			7,35
30	0,866	0,750	11,57	248,76		8,68
24	0,914	0,835	12,35			10,31
18	0,951	0,905	13,59			12,29
12	0,978	0,957	15,36			14,70
6	0,995	0,989	16,88			16,70
0	1,000	1,000	20,4			20,40
-6	0,995	0,989	26,16			25,87
-12	0,978	0,957	30,25			28,94
-18	0,951	0,905	32,51			29,41
-24	0,914	0,835	41,92			34,98
-30	0,866	0,750	27,77			20,83
-36	0,809	0,655	18,57			12,15
-42	0,743	0,552	17,03			9,41
Σ(30)	10,407					
Σ(42)	13,511					257,97

L(30)= 23,9 km
L(42)= 22,7 km
Lef.= 23,9 km

European Regional Development Fund

Table 3.12 - Determination of the effective fetch length for directions W (left) and WNW (right)

W (270°)

Kut α (°)	cosα	cos²α	d (km)	Σd		d·cos²α
42	0,743	0,552	13,23		363,15	7,31
36	0,809	0,655	15,06			9,86
30	0,866	0,750	17,07	266,04		12,80
24	0,914	0,835	20,07			16,75
18	0,951	0,905	24,97			22,59
12	0,978	0,957	31			29,66
6	0,995	0,989	32,38			32,03
0	1,000	1,000	40,18			40,18
-6	0,995	0,989	30,77			30,43
-12	0,978	0,957	19,55			18,70
-18	0,951	0,905	17,11			15,48
-24	0,914	0,835	16,39			13,68
-30	0,866	0,750	16,55			12,41
-36	0,809	0,655	39,81			26,06
-42	0,743	0,552	29,01			16,02
Σ(30)	10,407					
Σ(42)	13,511					303,95

L(30)= 25,6 km
L(42)= 26,9 km
Lef.= 26,9 km

WNW (292,5°)

Kut α (°)	cosα	cos²α	d (km)	Σd		d·cos²α
42	0,743	0,552	23,77		343,92	13,13
36	0,809	0,655	30,15			19,73
30	0,866	0,750	31,97	276,36		23,98
24	0,914	0,835	37,14			31,00
18	0,951	0,905	42			37,99
12	0,978	0,957	21,76			20,82
6	0,995	0,989	17,33			17,14
0	1,000	1,000	16,31			16,31
-6	0,995	0,989	15,65			15,48
-12	0,978	0,957	16,14			15,44
-18	0,951	0,905	30,11			27,23
-24	0,914	0,835	26,11			21,79
-30	0,866	0,750	21,84			16,38
-36	0,809	0,655	7,89			5,16
-42	0,743	0,552	5,75			3,18
Σ(30)	10,407					
Σ(42)	13,511					284,76

L(30)= 26,6 km
L(42)= 25,5 km
Lef.= 26,6 km

3.1.1.4. Podstrana-Duće area

As already mentioned in point 2.2.3.4, the aquatory of the beaches in question on the Podstrana-Duće area are exposed to winds from the second, third and fourth quadrants and consequent wind waves with different lengths of the fetch. In view of this, according to the criterion of fetch length and similarity of frequency of wind occurrence for a particular direction, certain sectors that are defined by the action of winds from the directions ESE, SE, SSE, SSW, SW, WSW, W and WNW will be defined.

Sector I is defined by the action of winds and consequent surface wind waves from the directions ESE and SE, sector II by the action of winds and consequent surface wind waves from the directions SSE and S, sector III by the action of winds and consequent surface wind waves from the directions SSW and SW, while sector IV is defined by the action of winds and consequent surface wind waves from directions WSW, W and WNW.

The longer effective fetch of sector I was calculated for the direction of SE (135°) and is 14.8 km (Table 3.13). For sector II, the longer effective fetch was calculated for the direction SSE (157.5°) and is 13.8 km (Tables 3.13 and 3.14). For sector III, the longer effective fetch is calculated for the direction SW (225°)

and is 16.0 km (Tables 3.14 and 3.15). For sector IV, the longest effective fetch is calculated for direction W (270°) and is 23.8 km (Tables 3.15 and 3.16).

In figures 3.23 to 3.30 are graphical representations of the placement of the central beam through the analyzed directions and beams with rotation ±6° from the central beam. The calculated values of the procedure for determining the effective length of the fetch for all individual directions are given in Tables 3.13 to 3.16.

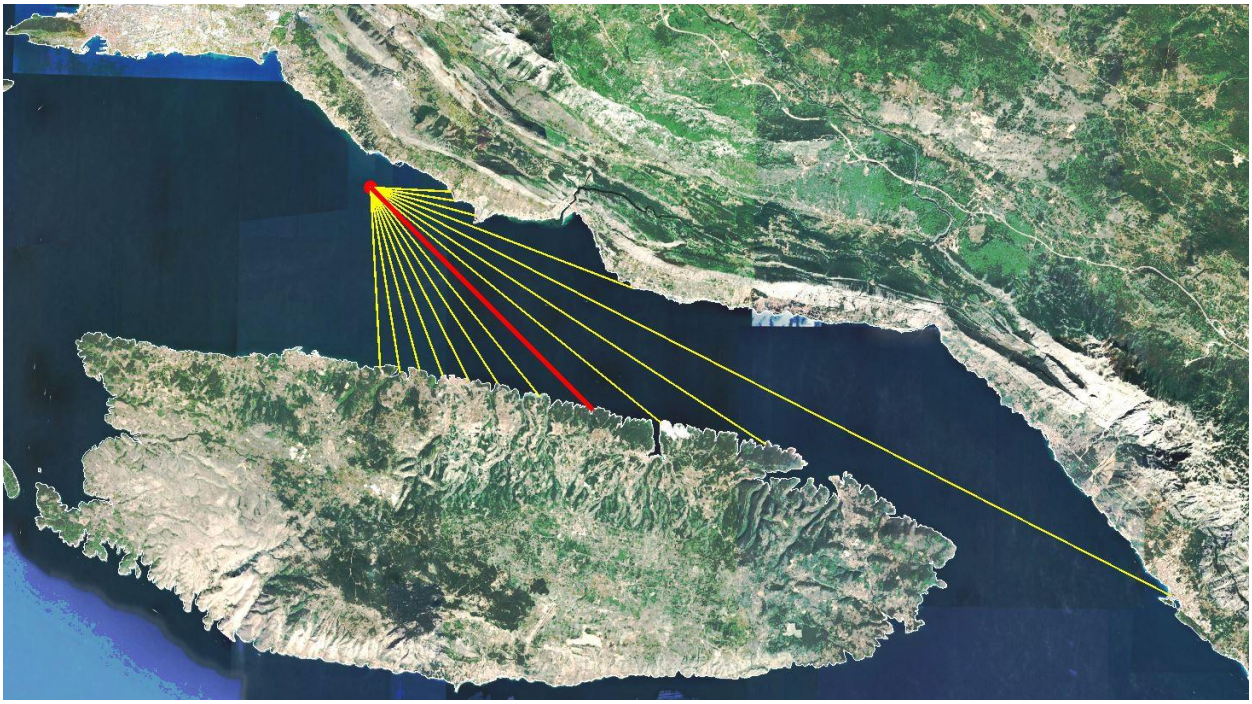

Figure 3.23 – Display of the central beam through the direction of the SE (135°), and the beam with step ±6°

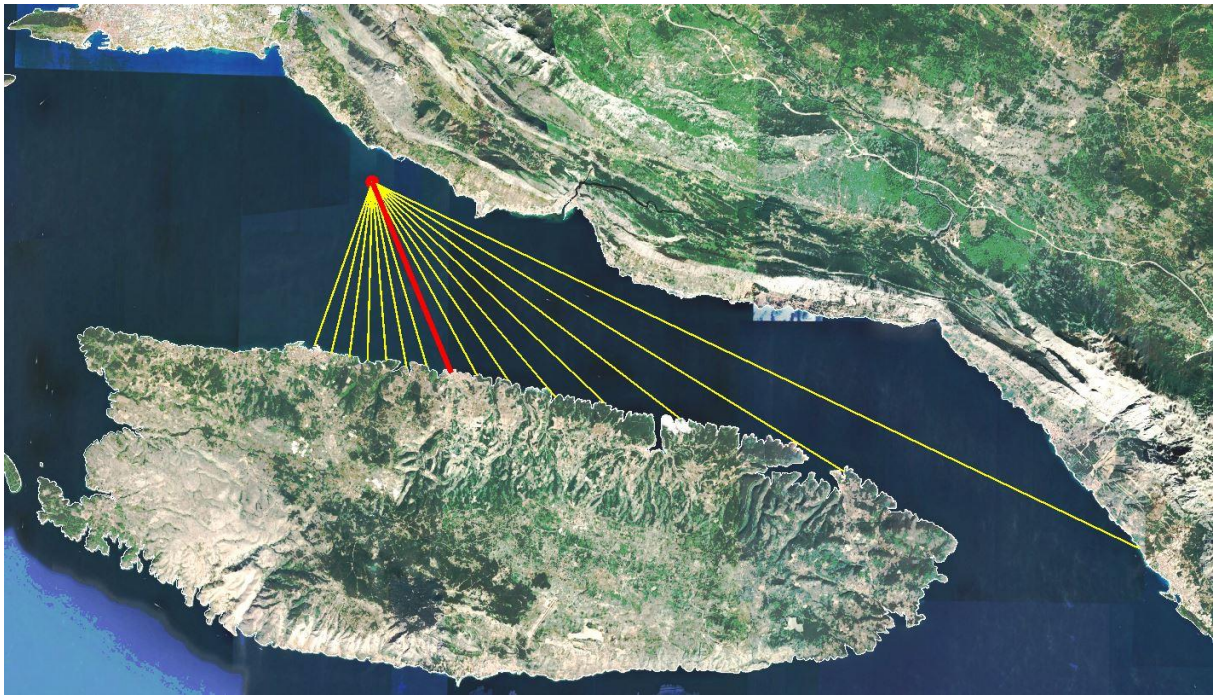

Figure 3.24 – Display of the central beam through the direction of the SSE (157.5°), and the beam with step ±6°

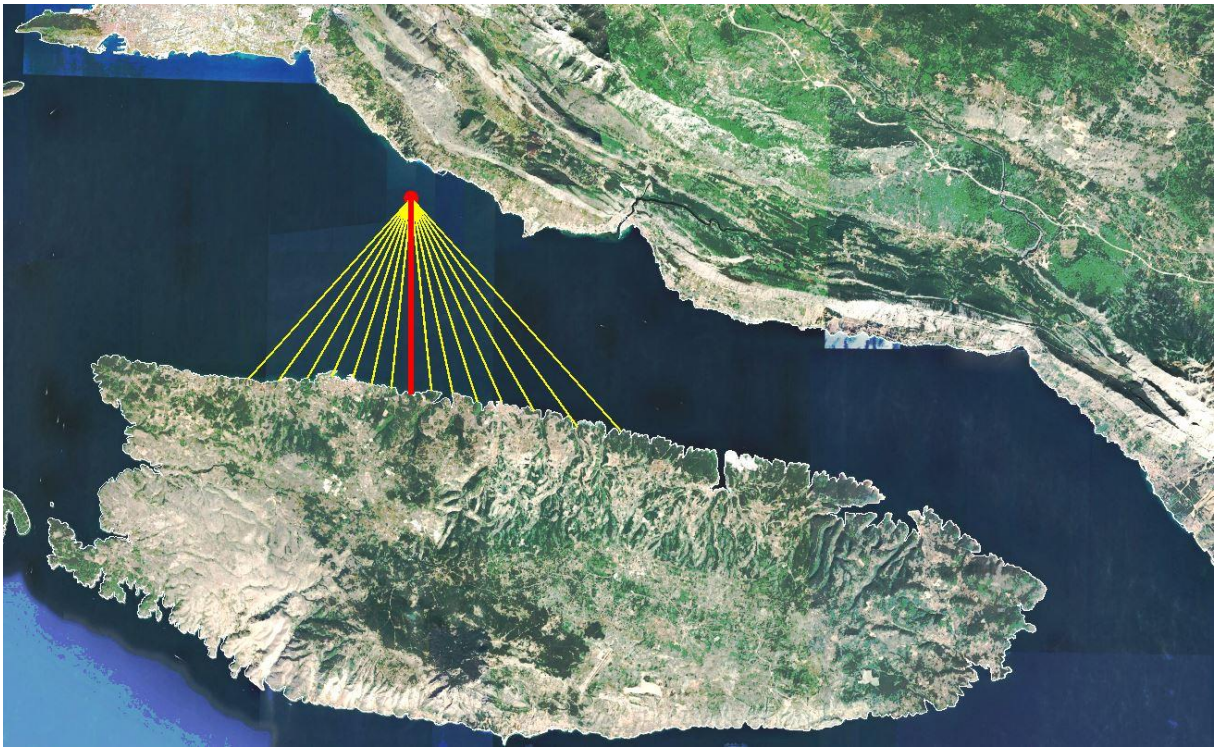

Figure 3.25 – Representation of the central beam through direction S (180°), and the beam with step ±6°

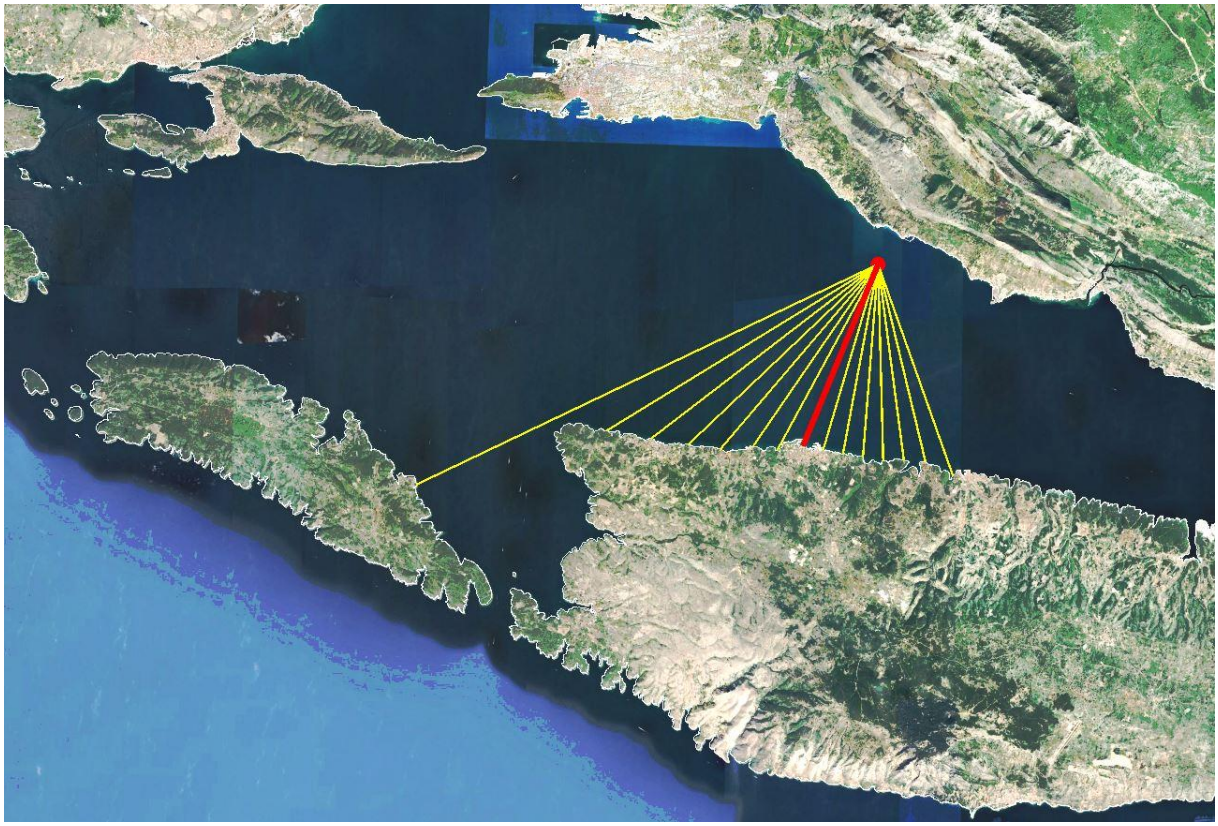

Figure 3.26 – Display of the central beam through the direction SSW (202.5°), and the beam with step ±6°

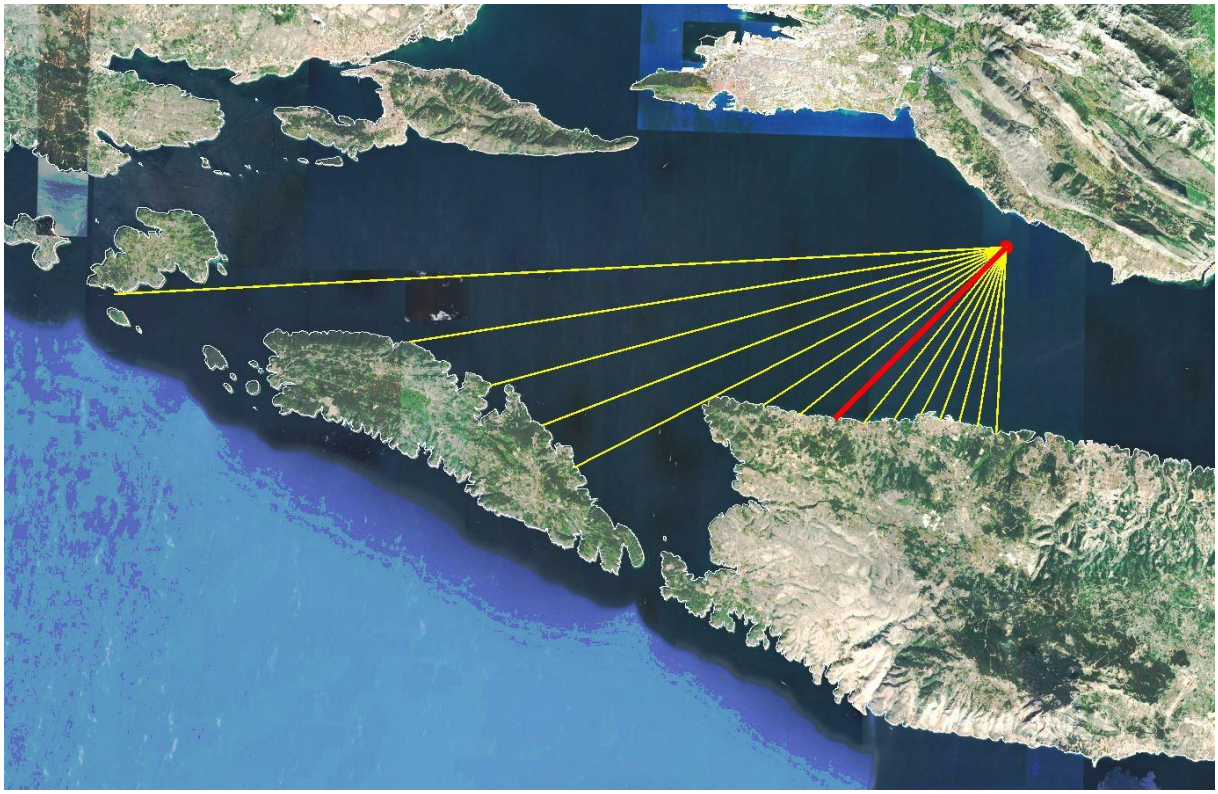

Figure 3.27 – Display of the central beam through direction SW (225°), and beams with step ±6°

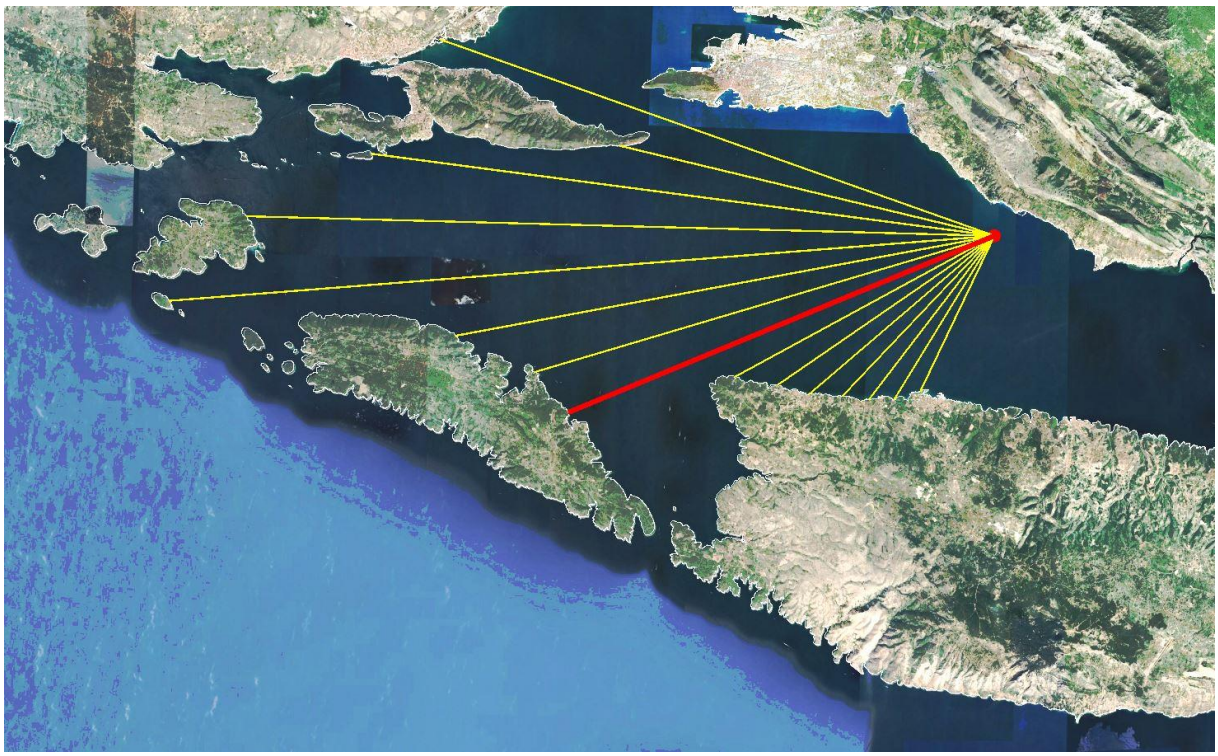

Figure 3.28 – Display of the central beam through the WSW direction (247.5°), and the beam with step ±6°

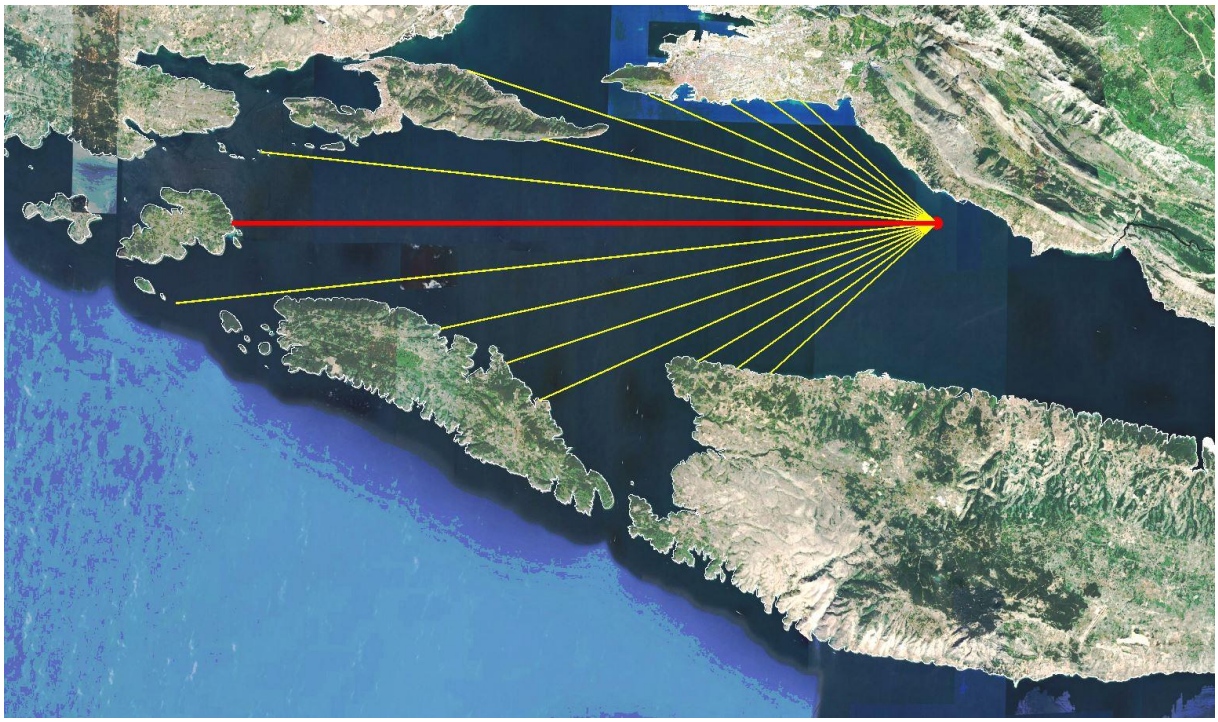

Figure 3.29 – Display of the central beam through the direction W (270°), and the beam with step ±6°

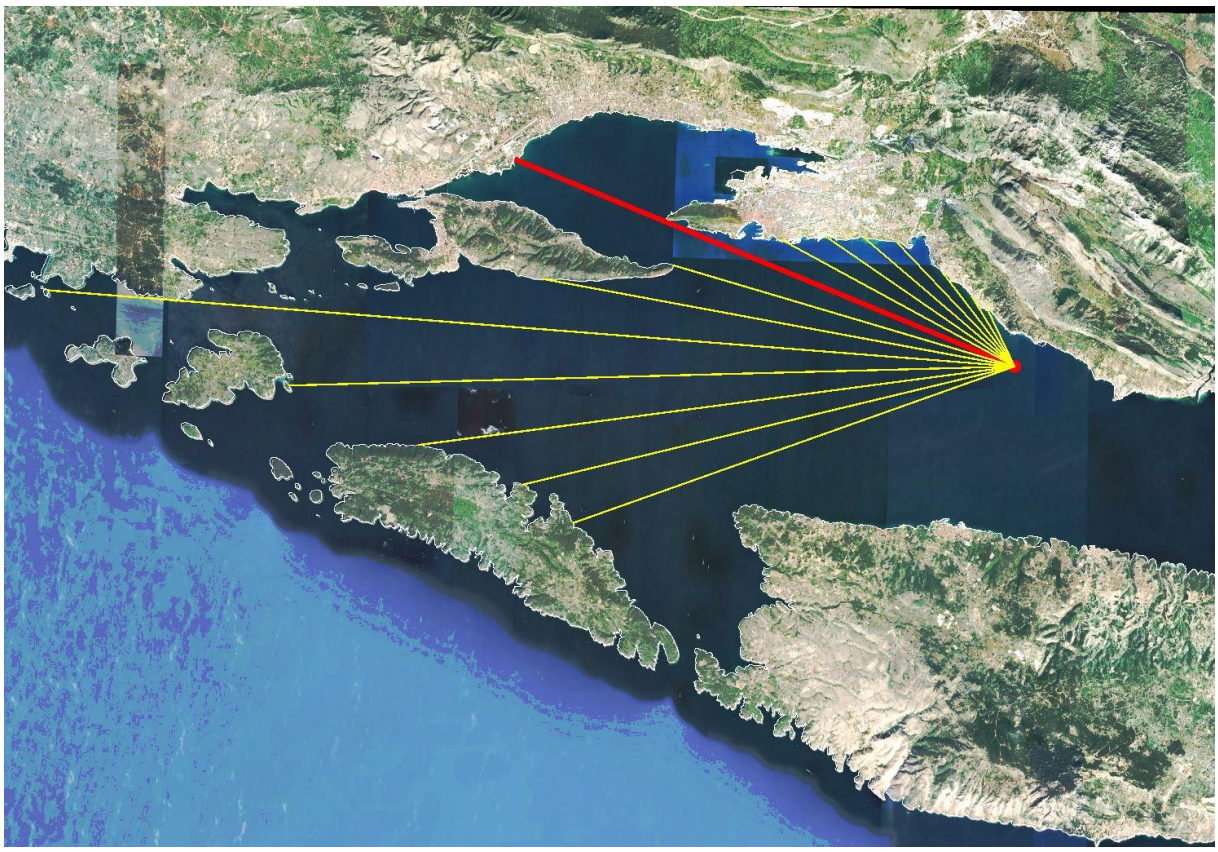

Figure 3.30 – Display of the central beam through the WNW direction (292.5°), and the beam with step ±6°

Table 3.13 - Determination of the effective length of the fetch for the directions SE (left) and SSE (right)

SE (135°)

Kut α (°)	cosα	cos²α	d (km)	Σd		d·cos²α
42	0,743	0,552	3,49			1,93
36	0,809	0,655	3,69			2,42
30	0,866	0,750	4,68			3,51
24	0,914	0,835	12,09			10,09
18	0,951	0,905	38,8			35,09
12	0,978	0,957	20,36			19,48
6	0,995	0,989	16,15	153,58	176,69	15,97
0	1,000	1,000	13,58			13,58
-6	0,995	0,989	11,63			11,50
-12	0,978	0,957	10,07			9,63
-18	0,951	0,905	9,36			8,47
-24	0,914	0,835	8,69			7,25
-30	0,866	0,750	8,17			6,13
-36	0,809	0,655	8,1			5,30
-42	0,743	0,552	7,83			4,32
Σ(30)	10,407					
Σ(42)	13,511					154,68

L(30)= 14,8 km
L(42)= 13,1 km
Lef.= 14,8 km

SSE (157,5°)

Kut α (°)	cosα	cos²α	d (km)	Σd		d·cos²α
42	0,743	0,552	36,78			20,31
36	0,809	0,655	23,96			15,68
30	0,866	0,750	16,74			12,56
24	0,914	0,835	13,84			11,55
18	0,951	0,905	12,24			11,07
12	0,978	0,957	10,41			9,96
6	0,995	0,989	9,52	111,11	186,95	9,42
0	1,000	1,000	8,91			8,91
-6	0,995	0,989	8,28			8,19
-12	0,978	0,957	8,14			7,79
-18	0,951	0,905	7,72			6,98
-24	0,914	0,835	7,7			6,43
-30	0,866	0,750	7,61			5,71
-36	0,809	0,655	7,61			4,98
-42	0,743	0,552	7,49			4,14
Σ(30)	10,407					
Σ(42)	13,511					143,67

L(30)= 10,7 km
L(42)= 13,8 km
Lef.= 13,8 km

Table 3.14 - Determination of the effective fetch length for directions S (left) and SSW (right)

S (180°)

Kut α (°)	cosα	cos²α	d (km)	Σd		d·cos²α
42	0,743	0,552	12,52			6,91
36	0,809	0,655	11,27			7,38
30	0,866	0,750	9,8			7,35
24	0,914	0,835	8,87			7,40
18	0,951	0,905	8,53			7,72
12	0,978	0,957	7,95			7,61
6	0,995	0,989	7,71	89,47	131,96	7,63
0	1,000	1,000	7,81			7,81
-6	0,995	0,989	7,63			7,55
-12	0,978	0,957	7,58			7,25
-18	0,951	0,905	7,51			6,79
-24	0,914	0,835	7,77			6,48
-30	0,866	0,750	8,31			6,23
-36	0,809	0,655	9,01			5,90
-42	0,743	0,552	9,69			5,35
Σ(30)	10,407					
Σ(42)	13,511					105,36

L(30)= 8,6 km
L(42)= 9,8 km
Lef.= 9,8 km

SSW (202,5°)

Kut α (°)	cosα	cos²α	d (km)	Σd		d·cos²α
42	0,743	0,552	8,84			4,88
36	0,809	0,655	8,01			5,24
30	0,866	0,750	7,77			5,83
24	0,914	0,835	7,73			6,45
18	0,951	0,905	7,63			6,90
12	0,978	0,957	7,59			7,26
6	0,995	0,989	7,62	94,28	143,8	7,54
0	1,000	1,000	7,73			7,73
-6	0,995	0,989	8,34			8,25
-12	0,978	0,957	8,71			8,33
-18	0,951	0,905	9,59			8,67
-24	0,914	0,835	10,31			8,60
-30	0,866	0,750	11,26			8,45
-36	0,809	0,655	12,52			8,19
-42	0,743	0,552	20,15			11,13
Σ(30)	10,407					
Σ(42)	13,511					113,46

L(30)= 9,1 km
L(42)= 10,6 km
Lef.= 10,6 km

Table 3.15 - Determination of the effective length of the fetch for directions SW (left) and WSW (right)

SW (225°)

Kut α (°)	cosα	cos²α	d (km)	Σd		d·cos²α
42	0,743	0,552	7,84			4,33
36	0,809	0,655	7,61			4,98
30	0,866	0,750	7,6			5,70
24	0,914	0,835	7,79			6,50
18	0,951	0,905	7,87			7,12
12	0,978	0,957	8,61			8,24
6	0,995	0,989	9,52	138,5	216,81	9,42
0	1,000	1,000	10,17			10,17
-6	0,995	0,989	11,2			11,08
-12	0,978	0,957	12,14			11,62
-18	0,951	0,905	20,35			18,41
-24	0,914	0,835	20,85			17,40
-30	0,866	0,750	22,4			16,80
-36	0,809	0,655	25,37			16,60
-42	0,743	0,552	37,49			20,70
Σ(30)	10,407					
Σ(42)	13,511					169,06

L(30)= 13,3 km
L(42)= 16,0 km
Lef.= 16,0 km

WSW (247,5°)

Kut α (°)	cosα	cos²α	d (km)	Σd		d·cos²α
42	0,743	0,552	7,71			4,26
36	0,809	0,655	8,6			5,63
30	0,866	0,750	9,23			6,92
24	0,914	0,835	9,89			8,25
18	0,951	0,905	10,92			9,88
12	0,978	0,957	11,8			11,29
6	0,995	0,989	13,24	220,47	280,37	13,10
0	1,000	1,000	20,64			20,64
-6	0,995	0,989	21,49			21,26
-12	0,978	0,957	24,55			23,49
-18	0,951	0,905	37,06			33,52
-24	0,914	0,835	33,51			27,97
-30	0,866	0,750	28,14			21,11
-36	0,809	0,655	17,27			11,30
-42	0,743	0,552	26,32			14,54
Σ(30)	10,407					
Σ(42)	13,511					233,14

L(30)= 21,2 km
L(42)= 20,8 km
Lef.= 21,2 km

Table 3.16 - Determination of the effective fetch length for directions W (left) and WNW (right)

W (270°)

Kut α (°)	cosα	cos²α	d (km)	Σd		d·cos²α
42	0,743	0,552	10,53			5,82
36	0,809	0,655	11,61			7,60
30	0,866	0,750	12,98			9,74
24	0,914	0,835	20,45			17,07
18	0,951	0,905	21,27			19,24
12	0,978	0,957	23,86			22,83
6	0,995	0,989	35,97	247,8	288,31	35,58
0	1,000	1,000	33,17			33,17
-6	0,995	0,989	31,95			31,60
-12	0,978	0,957	18,95			18,13
-18	0,951	0,905	23,19			20,98
-24	0,914	0,835	14,78			12,33
-30	0,866	0,750	11,23			8,42
-36	0,809	0,655	9,76			6,39
-42	0,743	0,552	8,61			4,75
Σ(30)	10,407					
Σ(42)	13,511					253,64

L(30)= 23,8 km
L(42)= 21,3 km
Lef.= 23,8 km

WNW (292,5°)

Kut α (°)	cosα	cos²α	d (km)	Σd		d·cos²α
42	0,743	0,552	21,21			11,71
36	0,809	0,655	22,91			14,99
30	0,866	0,750	27,21			20,41
24	0,914	0,835	32,86			27,42
18	0,951	0,905	43,91			39,72
12	0,978	0,957	21,69			20,75
6	0,995	0,989	16,13	210,73	261,44	15,95
0	1,000	1,000	24,49			24,49
-6	0,995	0,989	12			11,87
-12	0,978	0,957	10,41			9,96
-18	0,951	0,905	9			8,14
-24	0,914	0,835	7,76			6,48
-30	0,866	0,750	5,27			3,95
-36	0,809	0,655	3,73			2,44
-42	0,743	0,552	2,86			1,58
Σ(30)	10,407					
Σ(42)	13,511					219,87

L(30)= 20,2 km
L(42)= 19,4 km
Lef.= 20,2 km

3.1.1.5. Split (Kašjuni)

As already mentioned in point 2.2.3.5, the Kašjuni beach aquatory in Split is exposed to winds from the second, third and fourth quadrants and consequent wind waves with different lengths of the fetch. In view of this, according to the criterion of fetch length and similarity of frequency of wind occurrence for a particular direction, certain sectors that are defined by the action of winds from the directions ESE, SE, SSE, SSW, SW, WSW, W and WNW will be defined.

Sector I is defined by the action of winds and consequent surface wind waves from the directions ESE and SE, sector II by the action of winds and consequent surface wind waves from the directions SSE and S, sector III by the action of winds and consequent surface wind waves from the directions SSW and SW, while sector IV is defined by the action of winds and consequent surface wind waves from directions WSW, W and WNW.

The longer effective fetch of sector I was calculated for the direction of SE (135°) and is 23.0 km (Table 3.17). For sector II, the longer effective fetch was calculated for the direction SSE (157.5°) and is 21.3 km (Tables 3.17 and 3.18). For sector III, the longer effective fetch was calculated for the direction SSW (202.5°) and is 8.7 km (Tables 3.18 and 3.19). For sector IV, the longest effective fetch is calculated for direction W (270°) and is 6.3 km (Tables 3.19 and 3.20).

In figures 3.31 to 3.38, graphical representations of the central beam placement through the analyzed directions and beams with rotation correction are given $\pm 6°$ from the central beam. The calculated values of the procedure for determining the effective length of the fetch for all individual directions are given in Tables 3.17 to 3.20.

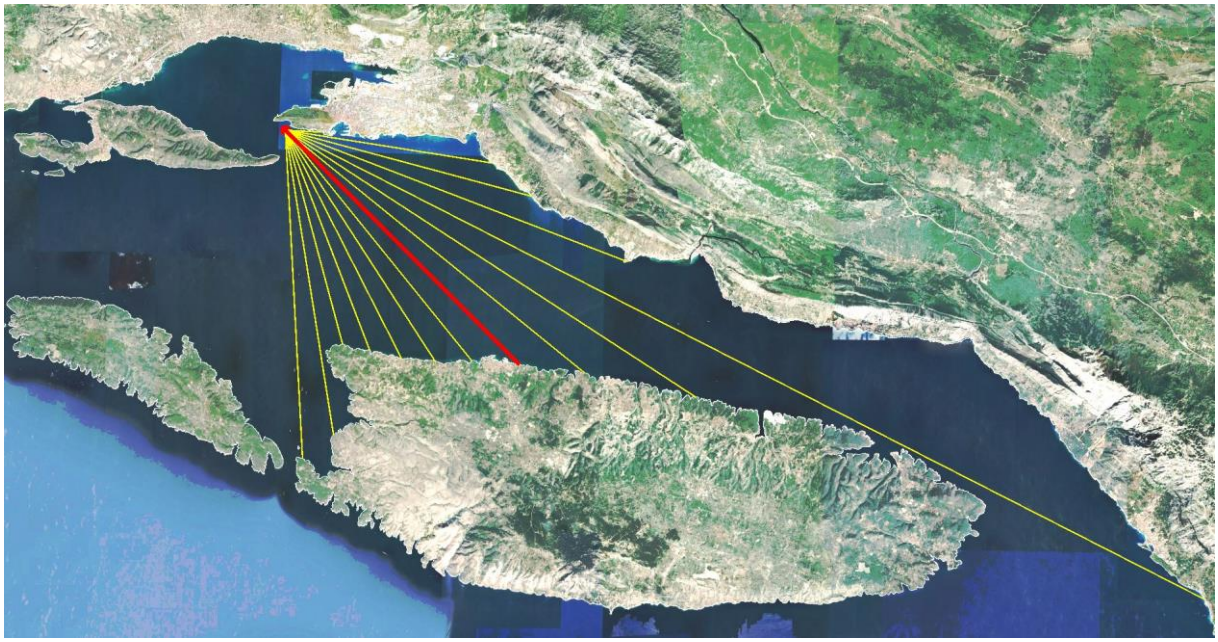

Figure 3.31 – Display of the central beam through the direction of the SE (135°), and the beam striking ±6°

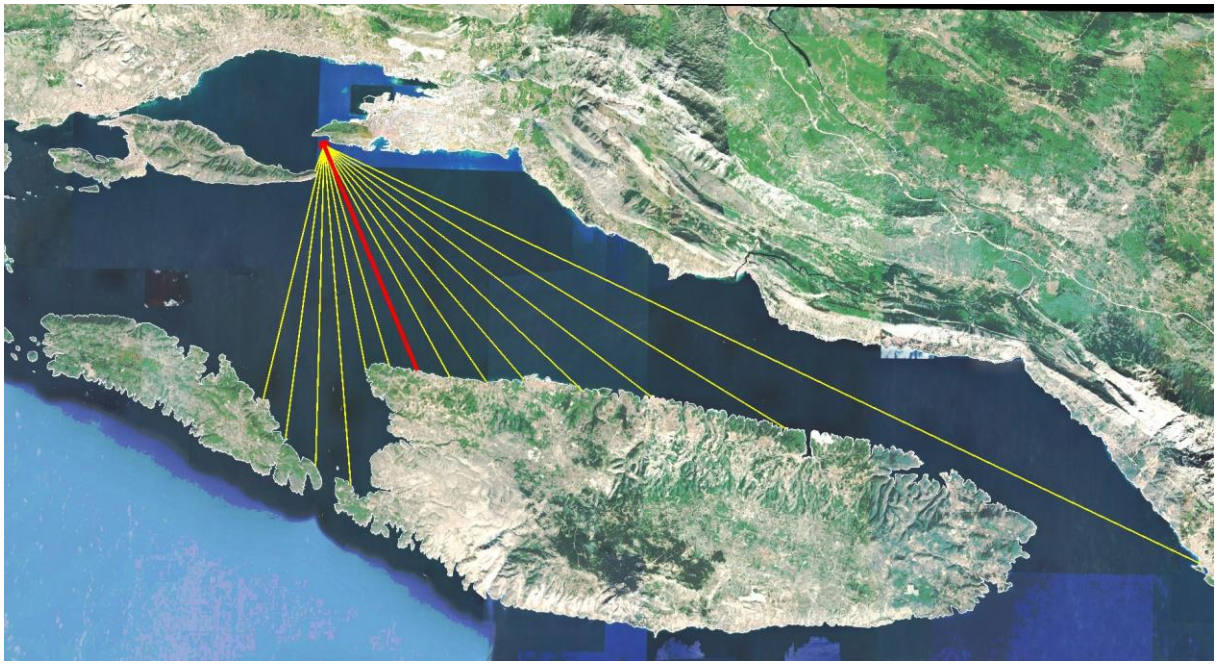

Figure 3.32 – Central beam display through SSE direction (157.5°), and beams with step ±6°

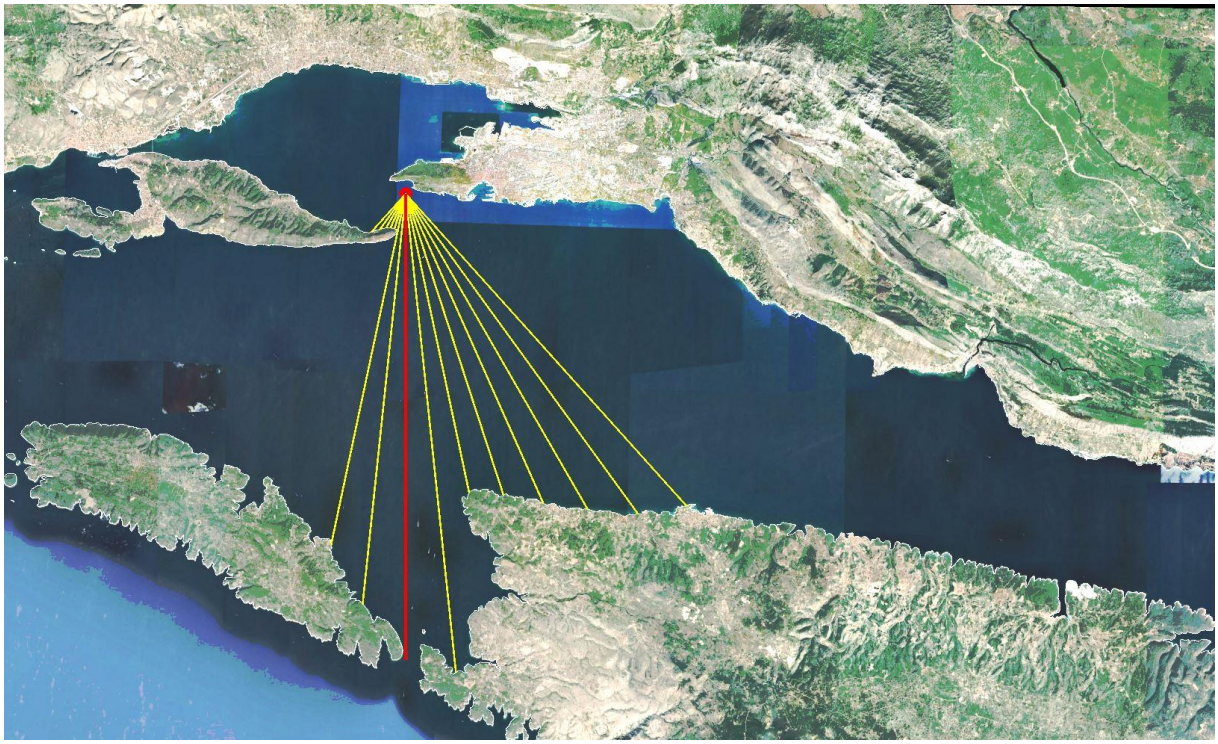

Figure 3.33 – Display of the central beam through direction S (180°), and beams with step ±6°

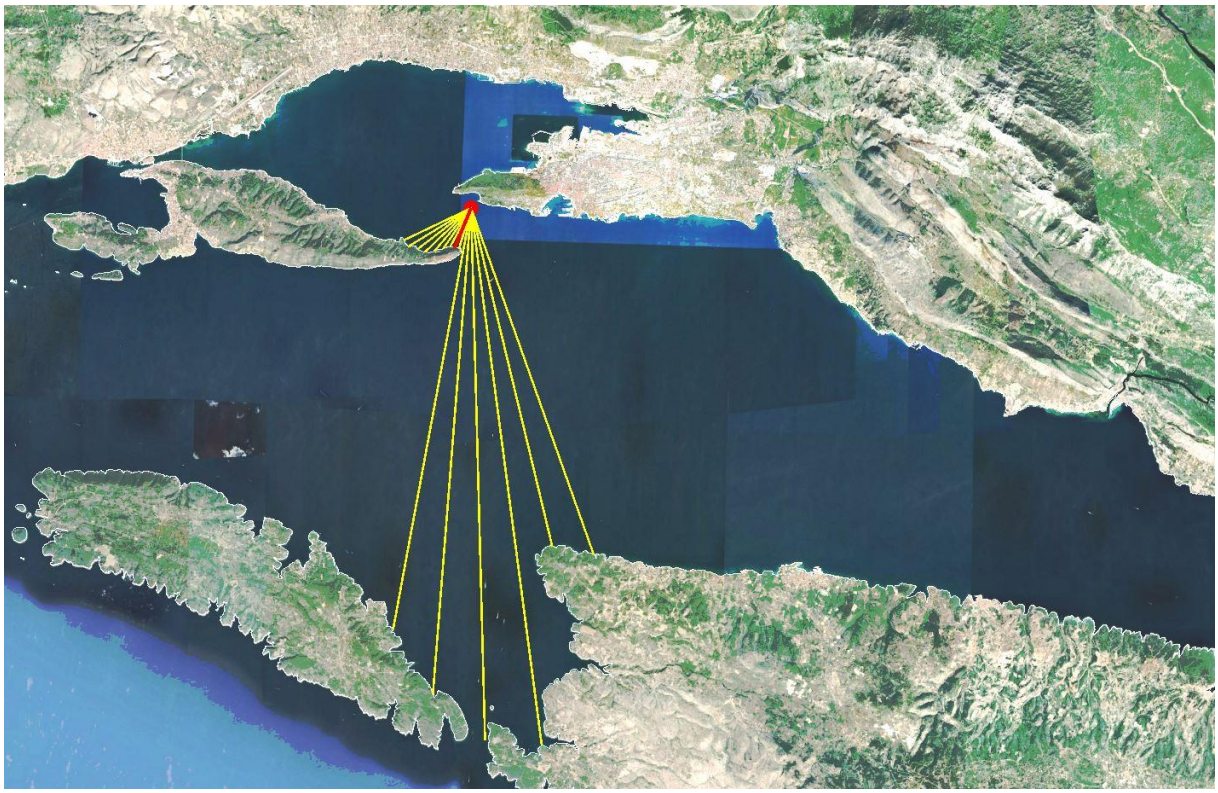

Figure 3.34 – Display of the central beam through the direction of SSW (202.5°), and the beam with step ±6°

Figure 3.35 – Display of the central beam through the direction SW (225°), and the beam with step ±6°

Figure 3.36 – Display of the central beam through the WSW (247.5°) direction, and the beam with step ±6°

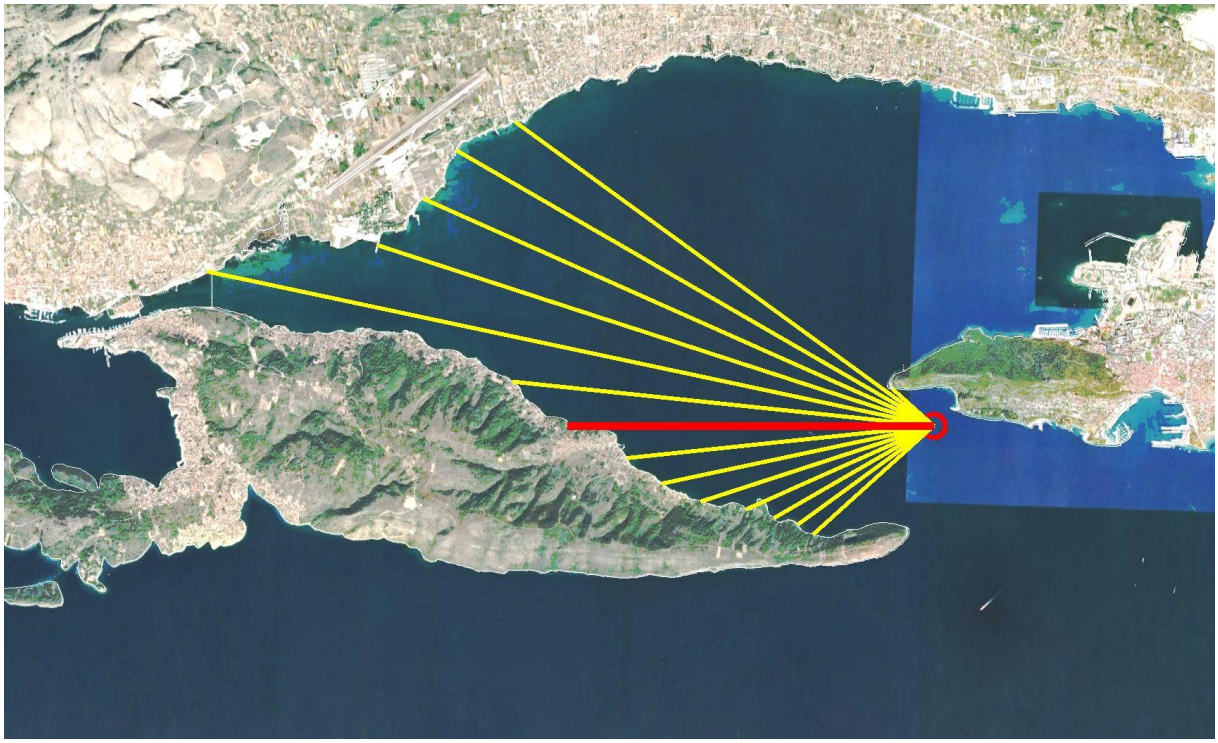

Figure 3.37 – Display of the central beam through direction W (270°), and the beam with step ±6°

Figure 3.38 – Display of the central beam through the WNW direction (292°), and the beam with a step ±6°

Table 3.17 - Determination of the effective fetch length for directions SE (left) and SSE (right)

SE (135°)

Kut α (°)	cosα	cos²α	d (km)	Σd		d·cos²α
42	0,743	0,552	2,16		289,86	1,19
36	0,809	0,655	11,98			7,84
30	0,866	0,750	14,72	239,02		11,04
24	0,914	0,835	21,13			17,63
18	0,951	0,905	59,54			53,85
12	0,978	0,957	28,25			27,03
6	0,995	0,989	22,21			21,97
0	1,000	1,000	19,08			19,08
-6	0,995	0,989	17,1			16,91
-12	0,978	0,957	15,86			15,17
-18	0,951	0,905	14,8			13,39
-24	0,914	0,835	13,55			11,31
-30	0,866	0,750	12,78			9,59
-36	0,809	0,655	17,76			11,62
-42	0,743	0,552	18,94			10,46
Σ(30)	10,407					
Σ(42)	13,511					248,09

L(30)= 23,0 km
L(42)= 21,5 km
Lef.= 23,0 km

SSE (157,5°)

Kut α (°)	cosα	cos²α	d (km)	Σd		d·cos²α
42	0,743	0,552	55,02		288,44	30,39
36	0,809	0,655	30,69			20,09
30	0,866	0,750	23,39	186,37		17,54
24	0,914	0,835	20,23			16,88
18	0,951	0,905	17,43			15,77
12	0,978	0,957	16,31			15,60
6	0,995	0,989	14,95			14,79
0	1,000	1,000	13,79			13,79
-6	0,995	0,989	13,05			12,91
-12	0,978	0,957	12,92			12,36
-18	0,951	0,905	19,32			17,48
-24	0,914	0,835	18,21			15,20
-30	0,866	0,750	16,77			12,58
-36	0,809	0,655	14,82			9,70
-42	0,743	0,552	1,54			0,85
Σ(30)	10,407					
Σ(42)	13,511					225,91

L(30)= 17,9 km
L(42)= 21,3 km
Lef.= 21,3 km

Table 3.18 - Determination of the effective fetch length for directions S (left) and SSW (right)

S (180°)

Kut α (°)	cosα	cos²α	d (km)	Σd		d·cos²α
42	0,743	0,552	17,56		170,09	9,70
36	0,809	0,655	16,54			10,83
30	0,866	0,750	15,21	131,95		11,41
24	0,914	0,835	14,16			11,82
18	0,951	0,905	13,24			11,98
12	0,978	0,957	12,78			12,23
6	0,995	0,989	20,12			19,90
0	1,000	1,000	19,46			19,46
-6	0,995	0,989	17,24			17,05
-12	0,978	0,957	14,99			14,34
-18	0,951	0,905	1,54			1,39
-24	0,914	0,835	1,56			1,30
-30	0,866	0,750	1,65			1,24
-36	0,809	0,655	1,87			1,22
-42	0,743	0,552	2,17			1,20
Σ(30)	10,407					
Σ(42)	13,511					145,06

L(30)= 12,7 km
L(42)= 12,6 km
Lef.= 12,7 km

SSW (202,5°)

Kut α (°)	cosα	cos²α	d (km)	Σd		d·cos²α
42	0,743	0,552	13,44		117,7	7,42
36	0,809	0,655	12,74			8,34
30	0,866	0,750	19,81	86,12		14,86
24	0,914	0,835	19,47			16,25
18	0,951	0,905	17,83			16,13
12	0,978	0,957	15,65			14,97
6	0,995	0,989	1,54			1,52
0	1,000	1,000	1,55			1,55
-6	0,995	0,989	1,61			1,59
-12	0,978	0,957	1,8			1,72
-18	0,951	0,905	2,06			1,86
-24	0,914	0,835	2,34			1,95
-30	0,866	0,750	2,46			1,85
-36	0,809	0,655	2,69			1,76
-42	0,743	0,552	2,71			1,50
Σ(30)	10,407					
Σ(42)	13,511					93,27

L(30)= 8,3 km
L(42)= 8,7 km
Lef.= 8,7 km

Table 3.19 - Determination of the effective fetch length for Directions SW (left) and WSW (right)

SW (225°)

Kut α (°)	cosα	cos²α	d (km)	Σd		d·cos²α
42	0,743	0,552	17,8		68,55	9,83
36	0,809	0,655	16,41			10,74
30	0,866	0,750	1,54	25,37		1,16
24	0,914	0,835	1,55			1,29
18	0,951	0,905	1,59			1,44
12	0,978	0,957	1,73			1,66
6	0,995	0,989	1,96			1,94
0	1,000	1,000	2,3			2,30
-6	0,995	0,989	2,46			2,43
-12	0,978	0,957	2,53			2,42
-18	0,951	0,905	2,73			2,47
-24	0,914	0,835	3,14			2,62
-30	0,866	0,750	3,84			2,88
-36	0,809	0,655	4,31			2,82
-42	0,743	0,552	4,66			2,57
Σ(30)	10,407					
Σ(42)	13,511					48,57

L(30)= 2,4 km
L(42)= 5,1 km
Lef.= 5,1 km

WSW (247,5°)

Kut α (°)	cosα	cos²α	d (km)	Σd		d·cos²α
42	0,743	0,552	1,58		62,02	0,87
36	0,809	0,655	1,68			1,10
30	0,866	0,750	1,91	39,63		1,43
24	0,914	0,835	2,25			1,88
18	0,951	0,905	2,42			2,19
12	0,978	0,957	2,47			2,36
6	0,995	0,989	2,74			2,71
0	1,000	1,000	3,04			3,04
-6	0,995	0,989	3,74			3,70
-12	0,978	0,957	4,15			3,97
-18	0,951	0,905	4,59			4,15
-24	0,914	0,835	5,69			4,75
-30	0,866	0,750	6,63			4,97
-36	0,809	0,655	10,59			6,93
-42	0,743	0,552	8,54			4,72
Σ(30)	10,407					
Σ(42)	13,511					48,77

L(30)= 3,8 km
L(42)= 4,6 km
Lef.= 4,6 km

Table 3.20 - Determination of the effective fetch length for directions W (left) and WNW (right)

W (270°)

Kut α (°)	cosα	cos²α	d (km)	Σd		d·cos²α
42	0,743	0,552	2,38		78,43	1,31
36	0,809	0,655	2,46			1,61
30	0,866	0,750	2,7	65,19		2,03
24	0,914	0,835	3,01			2,51
18	0,951	0,905	3,59			3,25
12	0,978	0,957	4,07			3,89
6	0,995	0,989	4,53			4,48
0	1,000	1,000	5,37			5,37
-6	0,995	0,989	6,2			6,13
-12	0,978	0,957	10,89			10,42
-18	0,951	0,905	8,58			7,76
-24	0,914	0,835	8,18			6,83
-30	0,866	0,750	8,07			6,05
-36	0,809	0,655	7,58			4,96
-42	0,743	0,552	0,82			0,45
Σ(30)	10,407					
Σ(42)	13,511					67,06

L(30)= 6,3 km
L(42)= 5,8 km
Lef.= 6,3 km

WNW (292,5°)

Kut α (°)	cosα	cos²α	d (km)	Σd		d·cos²α
42	0,743	0,552	3,46		71,38	1,91
36	0,809	0,655	3,98			2,60
30	0,866	0,750	4,47	62,73		3,35
24	0,914	0,835	4,67			3,90
18	0,951	0,905	6,06			5,48
12	0,978	0,957	11,4			10,91
6	0,995	0,989	9,84			9,73
0	1,000	1,000	8,23			8,23
-6	0,995	0,989	8,09			8,00
-12	0,978	0,957	7,71			7,38
-18	0,951	0,905	0,85			0,77
-24	0,914	0,835	0,74			0,62
-30	0,866	0,750	0,67			0,50
-36	0,809	0,655	0,62			0,41
-42	0,743	0,552	0,59			0,33
Σ(30)	10,407					
Σ(42)	13,511					64,12

L(30)= 6,0 km
L(42)= 5,3 km
Lef.= 6,0 km

3.1.2. Formation of wind pattern for long-term wave forecasts

The long-term forecast of significant Wave Height H_s^{PP} with return periods expressed in years (e.g., 5, 10, 100, etc.) is based on a sample of significant wave height *Hs*. This sample contains many *Hs* for short-term sea states (short-term wave situations) from the period 1990 - 2019.

Short-term wave situations represented by significant wave heights *Hs*, i.e., wave height sample *Hs*, are obtained by short-term wave forecasts from wind data. Such wind data represent a wind sample for long-term forecasts or summarizing speaking – a sample of significant wave heights (*Hs*) for a long-term wave forecast is obtained from a wind sample for a long-term wave forecast.

The wave height sample *Hs* is not formed by waves of quite small heights, which here means that the wind pattern is formed according to the threshold exceeding criterion from the wind contingency table, and the sample is formed only by data with wind strengths over a given threshold of 3 Bf.

Since the Hs sample for long-term forecast should represent individual short-term wave situations with larger waves (i.e., the wind that generates them), a sample threshold of 3 Bf (3.4-5.4 m/s) was taken. All

data with wind velocities over 3 Bf form a wind pattern because they contribute to the forecast of extremes, and data with wind velocities less than or equal to 3 Bf are dropped.

A pattern of wind velocities here is formed from the contingency table where hourly velocities are given, as is common for short-term wave forecast (WMO, 2006). They are about 5% less than 10-minute ones. Exceeding the "theoretical" forecast wave height is of the order of magnitude error in the reading of the forecast wave height from the forecast diagram used here - Groen-Dorrenstein, and recommended by the World Meteorological Organization (WMO).

Below is the formation of a wind pattern for a long-term wave forecast for each of the five locations of the selected beaches.

3.1.2.1. Brač (Zlatni rat)

The range of wind duration by Bf and sectors, for the location of Zlatni rat beach on Brač, is given in table 3.22. In addition, data are given on the duration of the wind required for the formation of waves of the fully developed sea (*Fully Arisen Sea* – FAS), which implies that the wave energy due to the wind is in balance with the energy transfer of individual wave components and the dissipation of energy due to wave breaking.

Table 3.21 – Fetches and wind durations required for fully developed seas

WIND STRENGHT (Bf)	SECTOR I		SECTOR II		SECTOR III		SECTOR IV	
	Fetch (km)	WIND DURATION FOR FAS (T_{FAS}) (h)	Fetch (km)	WIND DURATION FOR FAS (T_{FAS}) (h)	Fetch (km)	WIND DURATION FOR FAS (T_{FAS}) (h)	Fetch (km)	WIND DURATION FOR FAS (T_{FAS}) (h)
10								
9				≥ 1,10				
8		≥ 2,60		≥ 1,20				
7	28,3	≥ 2,80	10,4	≥ 1,40	39,8		117,4	
6		≥ 3,00		≥ 1,50		≥ 4,50		≥ 9,00
5		≥ 4,00		≥ 1,70		≥ 5,00		≥ 10,00
4		≥ 5,00		≥ 2,00		≥ 5,50		≥ 12,00

The wind pattern for short-term Hs wave forecasts is in fact represented by the wind contingence table 2.4a (DHMZ) divided into sectors (Table 3.22).

Table 3.22 – Wind pattern for Brač (Zlatni rat)

	DIRECTION	WIND STRENGHT (Bf)													SUM
		0	1	2	3	4	5	6	7	8	9	10	11	12	
	N	0	1875	607	768	307	62	3	0	1	0	0	0	0	3623
	NNE	0	628	340	682	682	543	290	186	96	24	15	1	2	3489
	NE	0	272	157	217	215	66	16	0	1	0	0	0	0	944
	ENE	0	753	653	950	607	66	3	1	1	0	0	0	0	3034
	E	0	433	219	94	10	0	1	0	0	0	0	0	0	757
sector I	ESE	0	877	1605	2158	583	44	2	2	1	0	0	0	0	5272
	SE	0	831	1079	1011	526	155	45	10	0	0	0	0	0	3657
sector II	SSE	0	703	1018	974	440	199	70	22	12	3	0	0	0	3441
	S	0	137	24	7	2	0	0	0	0	0	0	0	0	170
sector III	SSW	0	217	752	830	105	7	2	0	0	0	0	0	0	1913
	SW	0	138	170	159	66	2	0	0	0	0	0	0	0	535
sector IV	WSW	0	159	583	890	397	29	1	0	0	0	0	0	0	2059
	W	0	91	159	416	40	0	0	0	0	0	0	0	0	706
	WNW	0	199	186	255	240	57	3	3	0	0	0	0	0	943
	NW	0	168	74	52	22	1	2	0	0	0	0	0	0	319
	NNW	0	509	233	195	100	22	6	2	0	0	0	0	0	1067
	C	37	0	0	0	0	0	0	0	0	0	0	0	0	37
	SUM	37	7990	7859	9658	4342	1253	444	226	112	27	15	1	2	31966

3.1.2.2. Vis (Stiniva)

The range of wind duration by Bf and sectors, for the location of Zlatni rat beach on Brač, is given in table 3.23. In addition, data are given on the duration of the wind required for the formation of waves of the fully developed sea (*Fully Arisen Sea* – FAS), which implies that the wave energy due to the wind is in balance with the energy transfer of individual wave components and the dissipation of energy due to wave breaking.

Table 3.23 – Fetches and wind durations required for fully developed seas

WIND STRENGHT (Bf)	SECTOR I		SECTOR II		SECTOR III		SECTOR IV	
	Fetch (km)	WIND DURATION FOR FAS (T_{FAS}) (h)	Fetch (km)	WIND DURATION FOR FAS (T_{FAS}) (h)	Fetch (km)	WIND DURATION FOR FAS (T_{FAS}) (h)	Fetch (km)	WIND DURATION FOR FAS (T_{FAS}) (h)
10								
9								
8								
7	245,1		248,2		177,4		23	
6		≥ 16,00		≥ 16,00		≥ 12,00		≥ 2,80
5		≥ 18,00		≥ 18,00		≥ 13,00		≥ 3,10
4		≥ 20,00		≥ 24,00		≥ 18,00		≥ 3,50

The wind pattern for short-term *Hs* wave forecasts is in fact represented by wind contingency table 2.5a (DHMZ) divided into sectors (Table 3.24).

Table 3.24 – Wind pattern for Vis (Stiniva)

	DIRECTION	WIND STRENGHT (Bf)													SUM
		0	1	2	3	4	5	6	7	8	9	10	11	12	
	N	0	2230	2785	398	66	8	1	0	0	0	0	0	0	5488
	NNE	0	947	3174	621	155	44	2	0	0	0	0	0	0	4943
	NE	0	1022	2154	583	184	92	11	2	0	0	0	0	0	4048
	ENE	0	87	570	317	158	59	15	0	0	0	0	0	0	1206
	E	0	187	892	495	325	258	94	5	0	0	0	0	0	2256
sector I	ESE	0	31	307	311	250	148	27	0	0	0	0	0	0	1074
	SE	0	114	1134	792	408	153	14	0	0	0	0	0	0	2615
sector II	SSE	0	57	570	382	181	63	3	0	0	0	0	0	0	1256
	S	0	244	1234	434	190	69	2	0	0	0	0	0	0	2173
sector III	SSW	0	325	1303	326	82	31	2	0	0	0	0	0	0	2069
	SW	0	215	1454	244	42	7	2	0	0	0	0	0	0	1964
	WSW	0	30	259	87	7	2	0	0	0	0	0	0	0	385
	W	0	51	319	69	7	0	0	0	0	0	0	0	0	446
	WNW	0	14	143	48	3	1	0	0	0	0	0	0	0	209
	NW	0	152	676	173	15	0	0	0	0	0	0	0	0	1016
	NNW	0	461	880	248	38	6	1	0	0	0	0	0	0	1634
	C	86	0	0	0	0	0	0	0	0	0	0	0	0	86
	SUM	86	6167	17854	5528	2111	941	174	7	0	0	0	0	0	32868

3.1.2.3. Makarska Riviera (Podgora)

The range of wind duration by Bf and sectors, for the location of Zlatni rat beach on Brač, is given in table 3.25. In addition, data are given on the duration of the wind required for the formation of waves of the fully developed sea (*Fully Arisen Sea* – FAS), which implies that the wave energy due to the wind is in balance with the energy transfer of individual wave components and the dissipation of energy due to wave breaking.

Table 3.25 – Fetches and wind durations required for fully developed seas

WIND STRENGHT (Bf)	SECTOR I		SECTOR II		SECTOR III		SECTOR IV	
	Fetch (km)	WIND DURATION FOR FAS (T_{FAS}) (h)	Fetch (km)	WIND DURATION FOR FAS (T_{FAS}) (h)	Fetch (km)	WIND DURATION FOR FAS (T_{FAS}) (h)	Fetch (km)	WIND DURATION FOR FAS (T_{FAS}) (h)
10								
9								≥ 2,40
8		≥ 1,70		≥ 1,90				≥ 2,70
7	16,4	≥ 1,90	18,3	≥ 2,20	18,6		26,9	≥ 2,90
6		≥ 2,20		≥ 2,50		≥ 2,50		≥ 3,00
5		≥ 2,40		≥ 2,70		≥ 2,60		≥ 3,20
4		≥ 2,50		≥ 3,00		≥ 3,00		≥ 4,00

The wind pattern for short-term Hs wave forecasts is in fact represented by the wind contingency table 2.3a (DHMZ) divided into sectors (Table 3.26).

Table 3.26 – Wind pattern for Makarska Riviera (Podgora)

		WIND STRENGHT (Bf)													
	DIRECTION	0	1	2	3	4	5	6	7	8	9	10	11	12	SUM
	N	0	773	742	156	111	77	66	24	14	4	1	0	0	1968
	NNE	0	710	458	209	223	195	185	117	60	19	6	0	0	2182
	NE	0	626	349	138	158	141	145	88	55	22	3	0	0	1725
	ENE	0	663	361	139	95	81	82	37	25	8	0	0	0	1491
	E	0	852	866	308	149	62	23	4	0	0	0	0	0	2264
sector I	ESE	0	698	1312	957	538	206	44	6	0	0	0	0	0	3761
	SE	0	559	1137	682	494	189	65	3	1	0	0	0	0	3130
sector II	SSE	0	923	1444	759	416	176	73	13	1	0	0	0	0	3805
	S	0	710	954	86	22	2	0	1	0	0	0	0	0	1775
sector III	SSW	0	520	641	72	15	5	1	0	0	0	0	0	0	1254
	SW	0	435	688	105	12	1	2	0	0	0	0	0	0	1243
sector IV	WSW	0	532	964	124	22	2	1	1	0	1	0	0	0	1647
	W	0	297	486	106	30	13	2	0	0	0	0	0	0	934
	WNW	0	360	450	153	51	12	3	0	0	0	0	0	0	1029
	NW	0	440	451	123	55	12	1	0	0	0	0	0	0	1082
	NNW	0	706	1055	265	53	23	5	0	0	0	0	0	0	2107
	C	1024	0	0	0	0	0	0	0	0	0	0	0	0	1024
	SUM	1024	9804	12358	4382	2444	1197	698	294	156	54	10	0	0	32421

3.1.2.4. Podstrana-Duće area

The range of wind duration by Bf and sectors, for the location of Zlatni rat beach on Brač, is given in table 3.27. In addition, data are given on the duration of the wind required for the formation of waves of the fully developed sea (*Fully Arisen Sea* – FAS), which implies that the wave energy due to the wind is in balance with the energy transfer of individual wave components and the dissipation of energy due to wave breaking.

Table 3.27 – Fetches and wind durations required for a fully developed sea

WIND STRENGHT (Bf)	SECTOR I		SECTOR II		SECTOR III		SECTOR IV	
	Fetch (km)	WIND DURATION FOR FAS (T_{FAS}) (h)	Fetch (km)	WIND DURATION FOR FAS (T_{FAS}) (h)	Fetch (km)	WIND DURATION FOR FAS (T_{FAS}) (h)	Fetch (km)	WIND DURATION FOR FAS (T_{FAS}) (h)
10								
9		≥ 1,50		≥ 1,40				
8		≥ 1,70		≥ 1,50		≥ 1,70		
7	14,8	≥ 1,80	13,8	≥ 1,60	16	≥ 1,90	23,8	
6		≥ 2,00		≥ 1,70		≥ 2,10		≥ 2,80
5		≥ 2,20		≥ 1,90		≥ 2,30		≥ 3,10
4		≥ 2,50		≥ 2,40		≥ 2,90		≥ 3,50

The wind pattern for short-term Hs wave forecasts is in fact represented by the wind contingency table 2.2a (DHMZ) divided into sectors (Table 3.28).

Table 3.28 – Wind pattern for The Podstrana-Duće area

		WIND STRENGHT (Bf)													
	DIRECTION	0	1	2	3	4	5	6	7	8	9	10	11	12	SUM
	N	0	394	436	127	39	27	13	0	0	0	0	0	0	1036
	NNE	0	511	1347	967	987	900	325	89	26	5	3	0	0	5160
	NE	0	383	1105	603	272	224	84	20	2	3	1	0	0	2697
	ENE	0	616	1609	1082	599	550	188	45	6	3	0	0	0	4698
	E	0	406	627	260	125	54	12	1	0	0	0	0	0	1485
sector I	ESE	0	332	514	557	652	694	274	57	7	1	0	0	0	3088
	SE	0	218	267	239	332	434	219	64	13	2	0	0	0	1788
sector II	SSE	0	440	540	249	259	362	207	85	11	1	0	0	0	2154
	S	0	310	262	63	42	48	29	10	4	0	0	0	0	768
sector III	SSW	0	493	1174	533	74	36	23	10	2	0	0	0	0	2345
	SW	0	331	686	529	115	12	6	0	0	0	0	0	0	1679
sector IV	WSW	0	477	1080	779	127	10	1	0	0	0	0	0	0	2474
	W	0	154	183	60	12	0	0	0	0	0	0	0	0	409
	WNW	0	190	392	88	4	0	0	0	0	0	0	0	0	674
	NW	0	185	296	94	13	2	1	0	0	0	0	0	0	591
	NNW	0	443	579	171	40	13	3	0	0	0	0	0	0	1249
	C	576	0	0	0	0	0	0	0	0	0	0	0	0	576
	SUM	576	5883	11097	6401	3692	3366	1385	381	71	15	4	0	0	32871

3.1.2.5. Split (Kašjuni)

The range of wind duration by Bf and sectors, for the location of Zlatni rat beach on Brač, is given in table 3.27. In addition, data are given on the duration of the wind required for the formation of waves of the

fully developed sea (*Fully Arisen Sea* – FAS), which implies that the wave energy due to the wind is in balance with the energy transfer of individual wave components and the dissipation of energy due to wave breaking.

Table 3.29 – Fetches and wind durations required for a fully developed sea

WIND STRENGHT (Bf)	SECTOR I		SECTOR II		SECTOR III		SECTOR IV	
	Fetch (km)	WIND DURATION FOR FAS (T_{FAS}) (h)	Fetch (km)	WIND DURATION FOR FAS (T_{FAS}) (h)	Fetch (km)	WIND DURATION FOR FAS (T_{FAS}) (h)	Fetch (km)	WIND DURATION FOR FAS (T_{FAS}) (h)
10								
9		≥ 2,00		≥ 1,10				
8		≥ 2,10		≥ 1,20		≥ 1,00		
7	23	≥ 2,50	21,3	≥ 1,40	8,7	≥ 1,40	6,3	
6		≥ 2,80		≥ 1,50		≥ 1,50		≥ 1,00
5		≥ 3,00		≥ 1,70		≥ 1,60		≥ 1,30
4		≥ 4,00		≥ 2,00		≥ 2,00		≥ 1,50

The wind pattern for short-term wave forecasts *Hs* is in fact represented by the wind contingent table 2.2a (DHMZ) divided into sectors (Table 3.30).

Table 3.30 – Wind pattern for Split (Kašjuni)

	DIRECTION	WIND STRENGHT (Bf)													SUM
		0	1	2	3	4	5	6	7	8	9	10	11	12	
	N	0	394	436	127	39	27	13	0	0	0	0	0	0	1036
	NNE	0	511	1347	967	987	900	325	89	26	5	3	0	0	5160
	NE	0	383	1105	603	272	224	84	20	2	3	1	0	0	2697
	ENE	0	616	1609	1082	599	550	188	45	6	3	0	0	0	4698
	E	0	406	627	260	125	54	12	1	0	0	0	0	0	1485
sector I	ESE	0	332	514	557	652	694	274	57	7	1	0	0	0	3088
	SE	0	218	267	239	332	434	219	64	13	2	0	0	0	1788
sector II	SSE	0	440	540	249	259	362	207	85	11	1	0	0	0	2154
	S	0	310	262	63	42	48	29	10	4	0	0	0	0	768
sector III	SSW	0	493	1174	533	74	36	23	10	2	0	0	0	0	2345
	SW	0	331	686	529	115	12	6	0	0	0	0	0	0	1679
sector IV	WSW	0	477	1080	779	127	10	1	0	0	0	0	0	0	2474
	W	0	154	183	60	12	0	0	0	0	0	0	0	0	409
	WNW	0	190	392	88	4	0	0	0	0	0	0	0	0	674
	NW	0	185	296	94	13	2	1	0	0	0	0	0	0	591
	NNW	0	443	579	171	40	13	3	0	0	0	0	0	0	1249
	C	576	0	0	0	0	0	0	0	0	0	0	0	0	576
	SUM	576	5883	11097	6401	3692	3366	1385	381	71	15	4	0	0	32871

3.1.3. Calculation of significant wave heights for long return periods

After samples were formed for short-term wave forecasts, long-term forecasts of deepwater significant wave heights of *Hs* were also made for all formed sectors for each of the five (5) locations of the beaches in question. The result of the forecast is extreme significant wave heights of return periods PP= 5, 10, 20, 50 and 100 years, designated as H_S^{PP}.

3.1.3.1. Brač (Zlatni rat)

A sample of significant deepwater wave heights Hs for long-term forecast was formed from a wind sample, based on Table 3.22 and a calculated fetch, and using short-term wave forecast using the Groen-Dorrestein method (Table 3.31).

Table 3.31 – Sample of significant wave height Hs

	WIND STRENGHT (Bf)	4	5	6	7	8	9	10
SECTOR I	Fetch (km)	F1 = 28,3 km						
	FREQUENCY	1109	199	47	12	1	0	0
	H_S (m)	0,65	1,2	1,6	2	2,7	0	0
SECTOR II	Fetch (km)	F2 = 10,4 km						
	FREQUENCY	442	199	70	22	12	3	0
	H_S (m)	0,45	0,8	1	1,3	1,7	2	0
SECTOR III	Fetch (km)	F3 = 39,8 km						
	FREQUENCY	171	9	2	0	0	0	0
	H_S (m)	0,7	1,3	1,8	0	0	0	0
SECTOR IV	Fetch (km)	F4 = 117,4 km						
	FREQUENCY	437	29	1	0	0	0	0
	H_S (m)	1,85	1,8	2,6	0	0	0	0

For the sample of significant wave heights *Hs*, a long-term empirical probability was obtained, which adapts well to the direction. An adjustment of the theoretical Log-normal probability distribution was made to it. By extrapolating the theoretical Log-normal probability distribution (direction) into the area of low probability, i.e., long return periods, a long-term forecast was made.

Figures 3.39 and 3.40 show the probability distributions of random variables of significant wave height (Hs), and forecast values of significant wave heights H_S^{PP} at return periods PP = 100, 50, 25, 10 and 5 years.

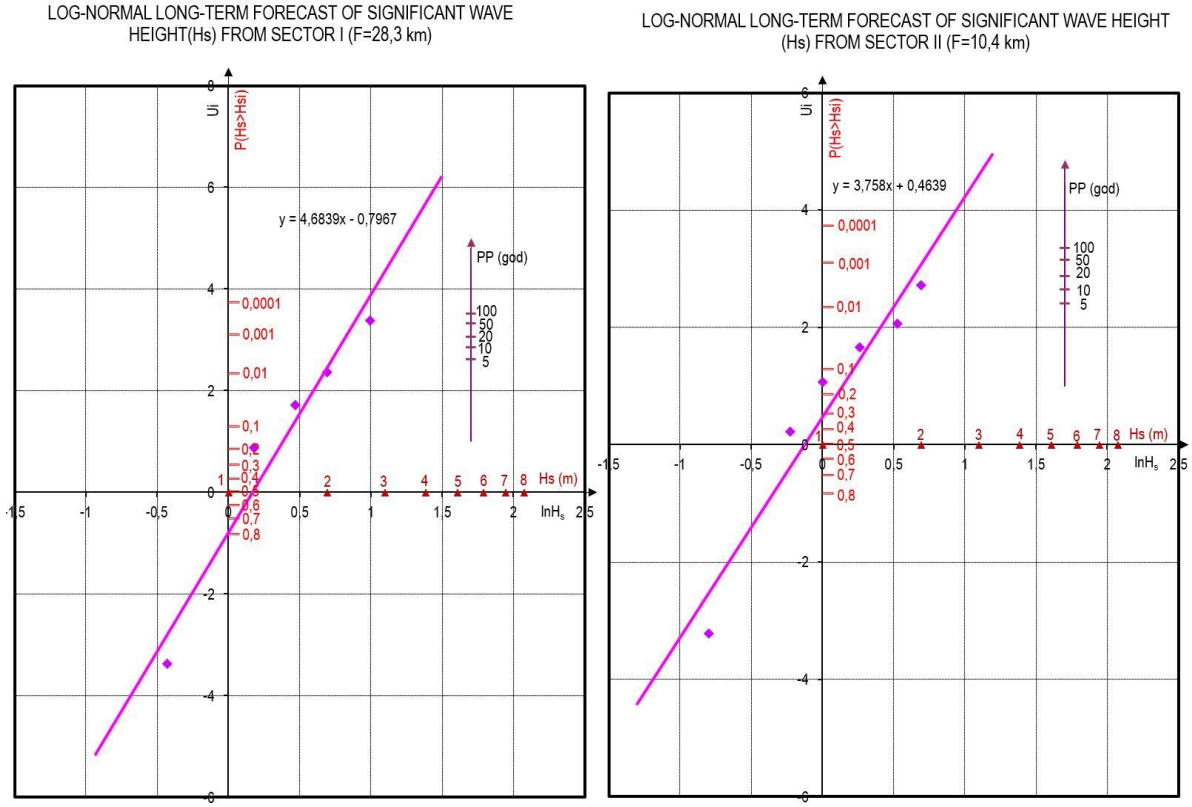

Figure 3.39 – Long-term distribution of significant wave height Hs for sectors I (left) and II (right)

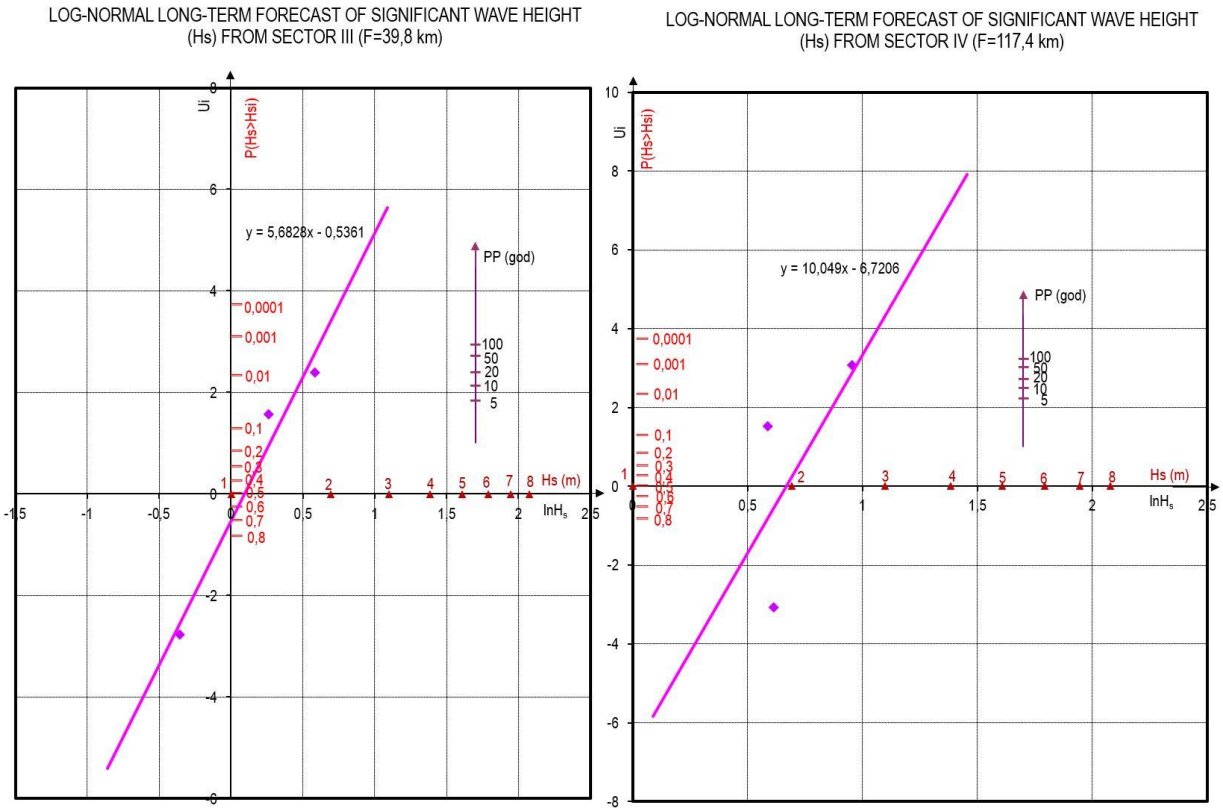

Figure 3.40 – Long-term distribution of significant wave height Hs for sectors III (left) i IV (right)

Table 3.32 gives long-term extreme significant (H_S^{PP}) by return periods forecast using probability distribution from Figures 3.39 and 3.40. Also, it gives associated values ($H_{1/10}$=1,27·H_s), ($H_{1/100}$=1,67·H_s) and maximum waves (H_{max}=1,8·H_s), mean wave periods (T_0) and wave lengths (L_0).

Table 3.32 – Adopted values of deepwater wave parameters for further analysis – Brač (Zlatni rat)

PP	SEKTOR I							SEKTOR II						
	H_S	$H_{1/10}$	$H_{1/100}$	H_{max}	T_0	L_0	T_p	H_S	$H_{1/10}$	$H_{1/100}$	H_{max}	T_0	L_0	T_p
	(m)	(m)	(m)	(m)	(s)	(m)	(s)	(m)	(m)	(m)	(m)	(s)	(m)	(s)
100	2,51	3,19	4,19	4,52	5,87	53,9	6,46	2,16	3,51	3,61	3,89	5,45	46,4	5,99
50	2,41	3,06	4,02	4,34	5,75	51,7	6,33	2,05	2,60	3,42	3,69	5,31	44,0	5,84
20	2,28	2,90	3,81	4,10	5,60	48,9	6,16	1,90	2,41	3,17	3,42	5,11	40,8	5,62
10	2,18	2,77	3,64	3,92	5,47	46,8	6,02	1,79	2,27	2,99	3,22	4,96	38,4	5,46
5	2,07	2,63	3,46	3,73	5,33	44,4	5,87	1,68	2,13	2,81	3,02	4,80	36,1	5,29

PP	SEKTOR III							SEKTOR IV						
	H_S	$H_{1/10}$	$H_{1/100}$	H_{max}	T_0	L_0	T_p	H_S	$H_{1/10}$	$H_{1/100}$	H_{max}	T_0	L_0	T_p
	(m)	(m)	(m)	(m)	(s)	(m)	(s)	(m)	(m)	(m)	(m)	(s)	(m)	(s)
100	1,84	2,99	3,07	3,31	5,03	39,5	5,53	2,69	3,42	4,49	4,84	6,08	57,7	6,69
50	1,77	2,25	2,96	3,19	4,93	38,0	5,43	2,63	3,34	4,39	4,73	6,01	56,5	6,61
20	1,68	2,13	2,81	3,02	4,80	36,1	5,29	2,56	3,25	4,28	4,61	5,93	55,0	6,52
10	1,60	2,03	2,67	2,88	4,69	34,3	5,16	2,50	3,18	4,18	4,50	5,86	53,7	6,45
5	1,52	1,93	2,54	2,74	4,57	32,6	5,03	2,44	3,10	4,07	4,39	5,79	52,4	6,37

3.1.3.2. Vis (Stiniva)

A sample of significant deepwater wave heights Hs for long-term forecast was formed from a wind sample, based on Table 3.24 and a calculated fetch, and using short-term wave forecast using the Groen-Dorrestein method (Table 3.33).

Table 3.33 – Sample of significant wave height Hs

	WIND STRENGHT (Bf)	4	5	6	7	8	9	10
SECTOR I	Fetch (km)	F1 = 245,1 km						
	FREQUENCY	658	301	41	0	0	0	0
	H_S (m)	1	2,1	3,2	0	0	0	0
SECTOR II	Fetch (km)	F2 = 248,2 km						
	FREQUENCY	371	132	5	0	0	0	0
	H_S (m)	0,9	2,1	3,2	0	0	0	0
SECTOR III	Fetch (km)	F3 = 177,4 km						
	FREQUENCY	124	38	4	0	0	0	0
	H_S (m)	0,9	2	2,9	0	0	0	0

For the sample of significant wave heights *Hs*, a long-term empirical probability was obtained, which adapts well to the direction. An adjustment of the theoretical Log-normal probability distribution was made to it. By extrapolating the theoretical Log-normal probability distribution (direction) into the area of low probability, i.e., long return periods, a long-term forecast was made.

Figures 3.41 and 3.42 show the probability distributions of random variables of significant wave height (*Hs*), and forecast values of significant wave heights H_S^{PP} at return periods PP = 100, 50, 25, 10 and 5 years.

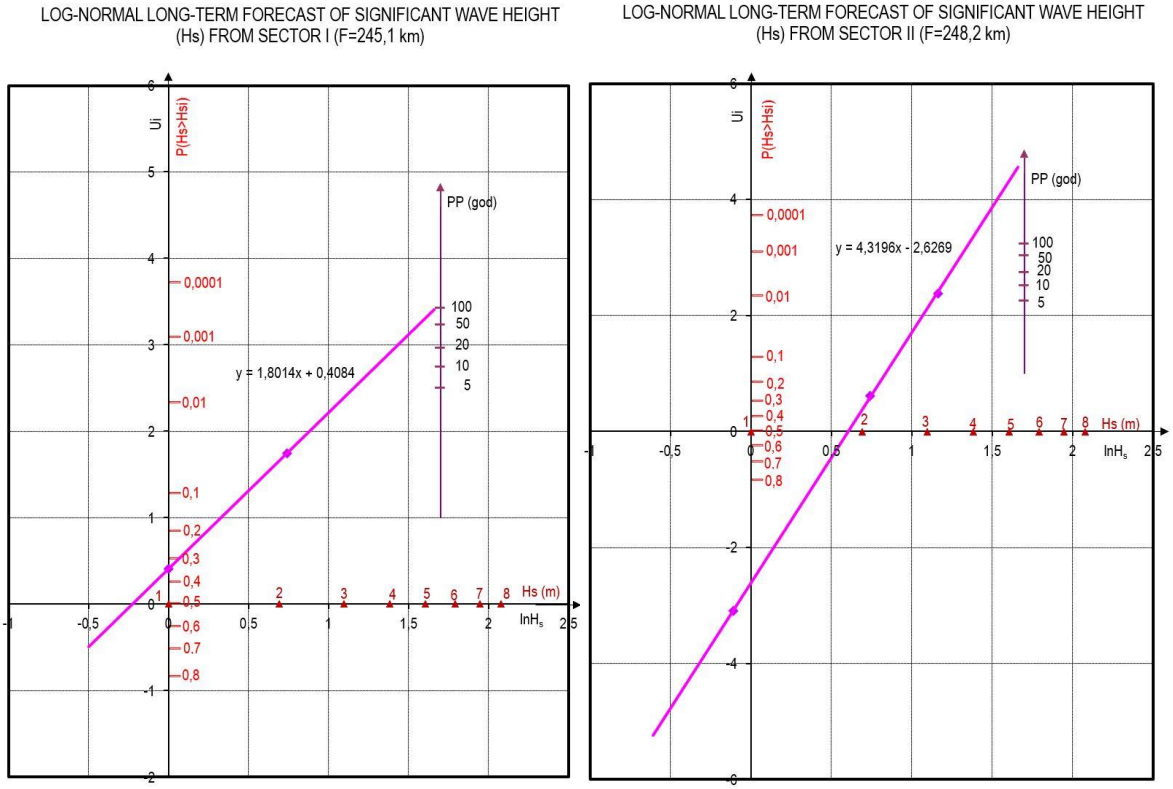

Figure 3.41 – Long-term distribution of significant Wave Height Hs for sectors I (left) and II (right)

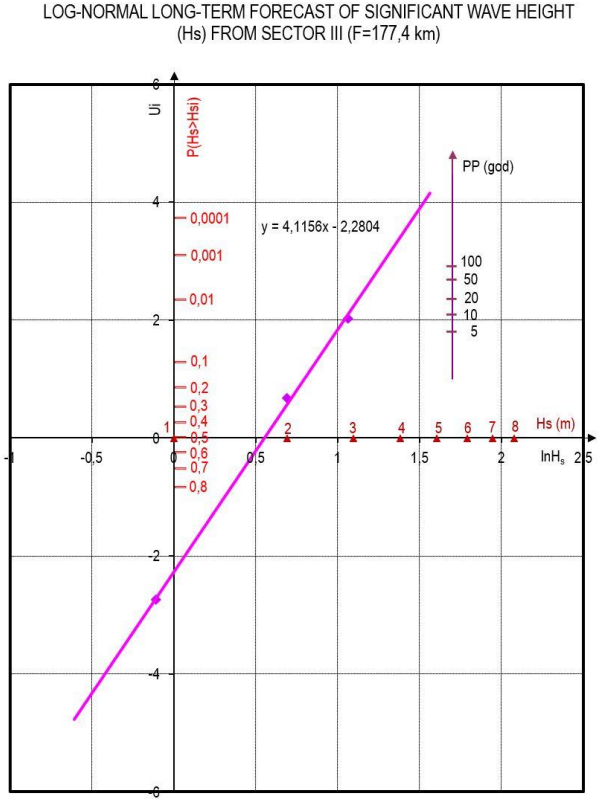

Figure 3.42 – Long-term distribution of significant Hs wave height for sector III

Table 3.34 gives long-term extreme significant (H_S^{PP}) by return periods forecast using probability distributions from Figures 3.41 and 3.42. Also, it gives associated values ($H_{1/10}$=1,27·H_s), ($H_{1/100}$=1,67·H_s) and maximum waves (H_{max}=1,8·H_s), mean wave periods (T_0) and wave lengths (L_0).

Table 3.35 – Adopted values of deepwater wave parameters for further analysis - Vis (Stiniva)

PP	SEKTOR I							SEKTOR II						
	H_S	$H_{1/10}$	$H_{1/100}$	H_{max}	T_0	L_0	T_p	H_S	$H_{1/10}$	$H_{1/100}$	H_{max}	T_0	L_0	T_p
	(m)	(m)	(m)	(m)	(s)	(m)	(s)	(m)	(m)	(m)	(m)	(s)	(m)	(s)
100	5,36	6,81	8,95	9,65	8,58	115,1	9,44	3,89	6,33	6,50	7,00	7,31	83,5	8,04
50	4,81	6,11	8,03	8,66	8,13	103,3	8,94	3,71	4,71	6,20	6,68	7,14	79,6	7,85
20	4,14	5,26	6,91	7,45	7,54	88,9	8,30	3,47	4,41	5,79	6,25	6,91	74,5	7,60
10	3,66	4,65	6,11	6,59	7,09	78,6	7,80	3,29	4,18	5,49	5,92	6,72	70,6	7,40
5	3,22	4,09	5,38	5,80	6,65	69,1	7,32	3,10	3,94	5,18	5,58	6,53	66,5	7,18

PP	SEKTOR III						
	H_S	$H_{1/10}$	$H_{1/100}$	H_{max}	T_0	L_0	T_p
	(m)	(m)	(m)	(m)	(s)	(m)	(s)
100	3,53	5,74	5,90	6,35	6,96	75,8	7,66
50	3,34	4,24	5,58	6,01	6,77	71,7	7,45
20	3,09	3,92	5,16	5,56	6,52	66,3	7,17
10	2,90	3,68	4,84	5,22	6,31	62,3	6,94
5	2,69	3,42	4,49	4,84	6,08	57,7	6,69

3.1.3.3. Makarska Riviera (Podgora)

A sample of significant deep-water wave heights *Hs* for long-term forecast was formed from a wind sample, based on Table 3.26 and a calculated fetch, and using short-term wave forecast using the Groen-Dorrestein method (Table 3.36).

Table 3.36 – Sample of significant wave height Hs

	WIND STRENGHT (Bf)	4	5	6	7	8	9	10
SECTOR I	Fetch (km)	F1 = 16,4 km						
	FREQUENCY	601	133	16	5	0	0	0
	H_S (m)	0,55	0,95	1,35	1,55	2,1	0	0
SECTOR II	Fetch (km)	F2 = 18,3 km						
	FREQUENCY	5838	4101	1241	276	68	15	2
	H_S (m)	0,55	0,95	1,35	1,7	2,3	0	0
SECTOR III	Fetch (km)	F3 = 18,6 km						
	FREQUENCY	215	62	13	1	0	0	0
	H_S (m)	0,55	1	1,3	0	0	0	0
SECTOR IV	Fetch (km)	F4 = 26,9 km						
	FREQUENCY	35	4	2	0	0	0	0
	H_S (m)	0,6	1,15	1,5	1,9	2,7	3	0

For the sample of significant wave heights Hs, a long-term empirical probability was obtained, which adapts well to the direction. An adjustment of the theoretical Log-normal probability distribution was made to it. By extrapolating the theoretical Log-normal probability distribution (direction) into the area of low probability, i.e., long return periods, a long-term forecast was made.

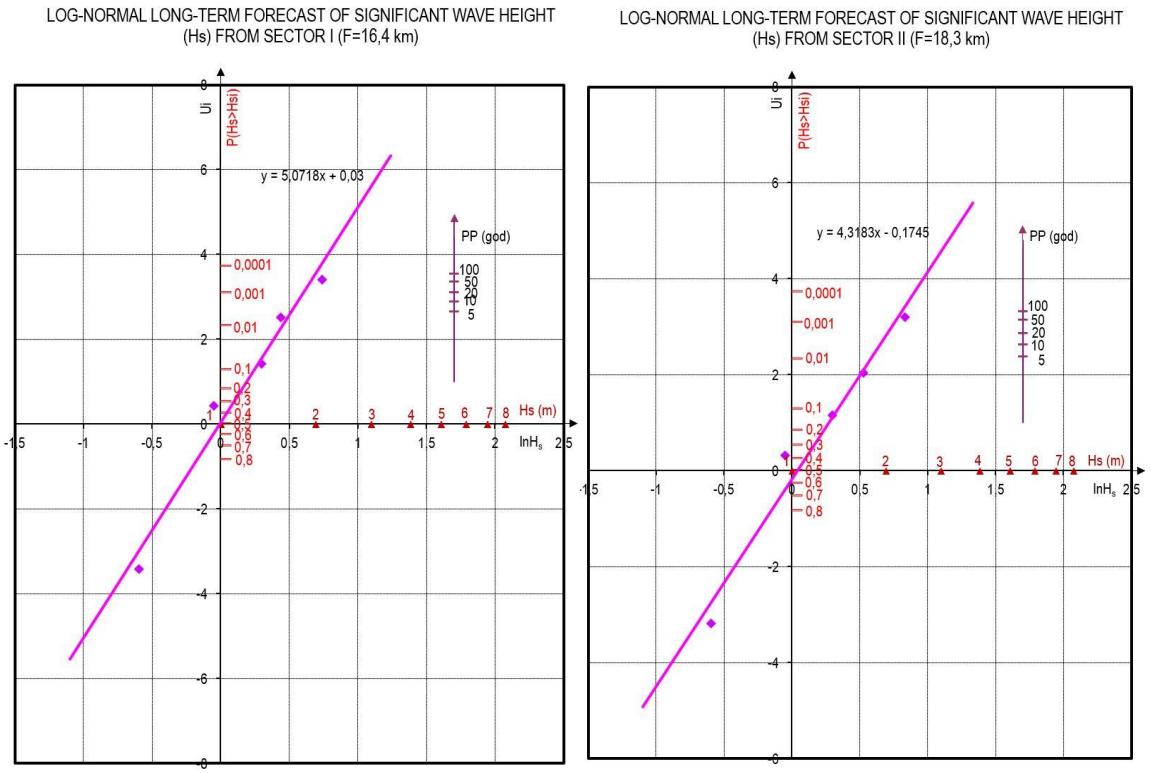

Figure 3.43 – Long-term distribution of significant wave height Hs for sectors I (left) and II (right)

Figures 3.43 and 3.44 show the probability distributions of random variables of significant wave height (*Hs*), and forecast values of significant wave heights H_S^{PP} at return periods PP = 100, 50, 25, 10 and 5 years.

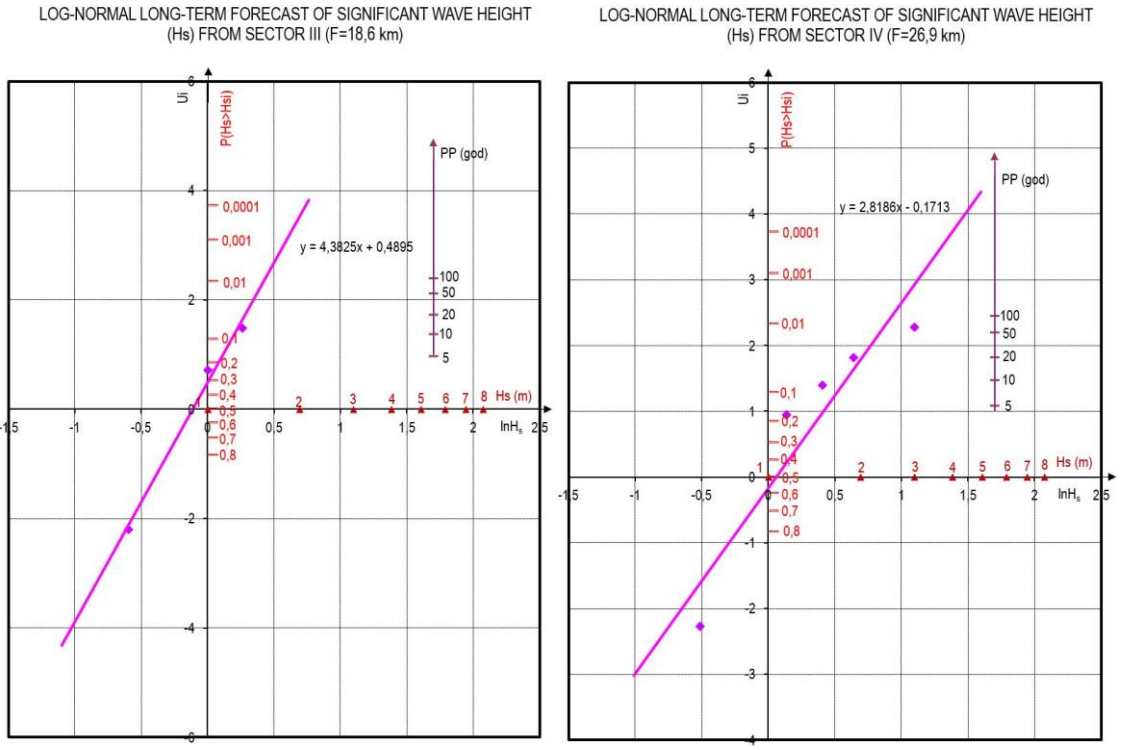

Figure 3.44 – Long-term distribution of significant wave height Hs for sectors II (left) i IV (right)

Table 3.37 gives long-term extreme significant (H_S^{PP}) by return periods forecast using probability distribution from Figures 3.43 and 3.44. Also, it gives associated values ($H_{1/10}$=1,27·H_s), ($H_{1/100}$=1,67·H_s) and maximum waves (H_{max}=1,8·H_s), mean wave periods (T_0) and wave lengths (L_0).

Table 3.37 – Adopted values of deep-water wave parameters for further analysis – Makarska Riviera (Podgora)

PP	SEKTOR I							SEKTOR II						
	H_S	$H_{1/10}$	$H_{1/100}$	H_{max}	T_0	L_0	T_p	H_S	$H_{1/10}$	$H_{1/100}$	H_{max}	T_0	L_0	T_p
	(m)	(m)	(m)	(m)	(s)	(m)	(s)	(m)	(m)	(m)	(m)	(s)	(m)	(s)
100	2,00	2,54	3,34	3,60	5,24	42,9	5,77	2,25	3,66	3,76	4,05	5,56	48,3	6,12
50	1,93	2,45	3,22	3,47	5,15	41,4	5,66	2,15	2,73	3,59	3,87	5,44	46,2	5,98
20	1,83	2,32	3,06	3,29	5,01	39,3	5,52	2,02	2,57	3,37	3,64	5,27	43,4	5,80
10	1,76	2,24	2,94	3,17	4,92	37,8	5,41	1,91	2,43	3,19	3,44	5,12	41,0	5,64
5	1,68	2,13	2,81	3,02	4,80	36,1	5,29	1,81	2,30	3,02	3,26	4,99	38,9	5,49

PP	SEKTOR III							SEKTOR IV						
	H_S	$H_{1/10}$	$H_{1/100}$	H_{max}	T_0	L_0	T_p	H_S	$H_{1/10}$	$H_{1/100}$	H_{max}	T_0	L_0	T_p
	(m)	(m)	(m)	(m)	(s)	(m)	(s)	(m)	(m)	(m)	(m)	(s)	(m)	(s)
100	1,54	2,51	2,57	2,77	4,60	33,1	5,06	2,54	3,23	4,24	4,57	5,91	54,5	6,50
50	1,45	1,84	2,42	2,61	4,46	31,1	4,91	2,32	2,95	3,87	4,18	5,65	49,8	6,21
20	1,33	1,69	2,22	2,39	4,28	28,6	4,70	2,02	2,57	3,37	3,64	5,27	43,4	5,80
10	1,23	1,56	2,05	2,21	4,11	26,4	4,52	1,79	2,27	2,99	3,22	4,96	38,4	5,46
5	1,12	1,42	1,87	2,02	3,92	24,0	4,32	1,56	1,98	2,61	2,81	4,63	33,5	5,09

3.1.3.4. Podstrana-Duće area

A sample of significant hs deep-water wave heights for long-term forecast was formed from a wind sample, based on Table 3.28 and a calculated fetch, and using short-term wave forecast using the Groen-Dorrestein method (Table 3.38).

Table 3.38 – Sample of significant wave height Hs

	WIND STRENGHT (Bf)	4	5	6	7	8	9	10
SECTOR I	Fetch (km)	F1 = 14,8 km						
	FREQUENCY	984	1128	493	121	20	3	0
	H_S (m)	0,55	0,9	1,25	1,5	2	2,4	0
SECTOR II	Fetch (km)	F2 = 13,8 km						
	FREQUENCY	301	410	236	95	15	1	0
	H_S (m)	0,5	0,85	1,1	1,4	1,9	2,2	0
SECTOR III	Fetch (km)	F3 = 16 km						
	FREQUENCY	189	48	29	10	2	0	0
	H_S (m)	0,55	0,95	1,3	1,6	2,1	0	0
SECTOR IV	Fetch (km)	F4 = 23,8 km						
	FREQUENCY	143	10	1	0	0	0	0
	H_S (m)	0,6	1,15	1,5	0	0	0	0

For the sample of significant wave heights *Hs*, a long-term empirical probability was obtained, which adapts well to the direction. An adjustment of the theoretical Log-normal probability distribution was made to it. By extrapolating the theoretical Log-normal probability distribution (direction) into the area of low probability, i.e., long return periods, a long-term forecast was made.

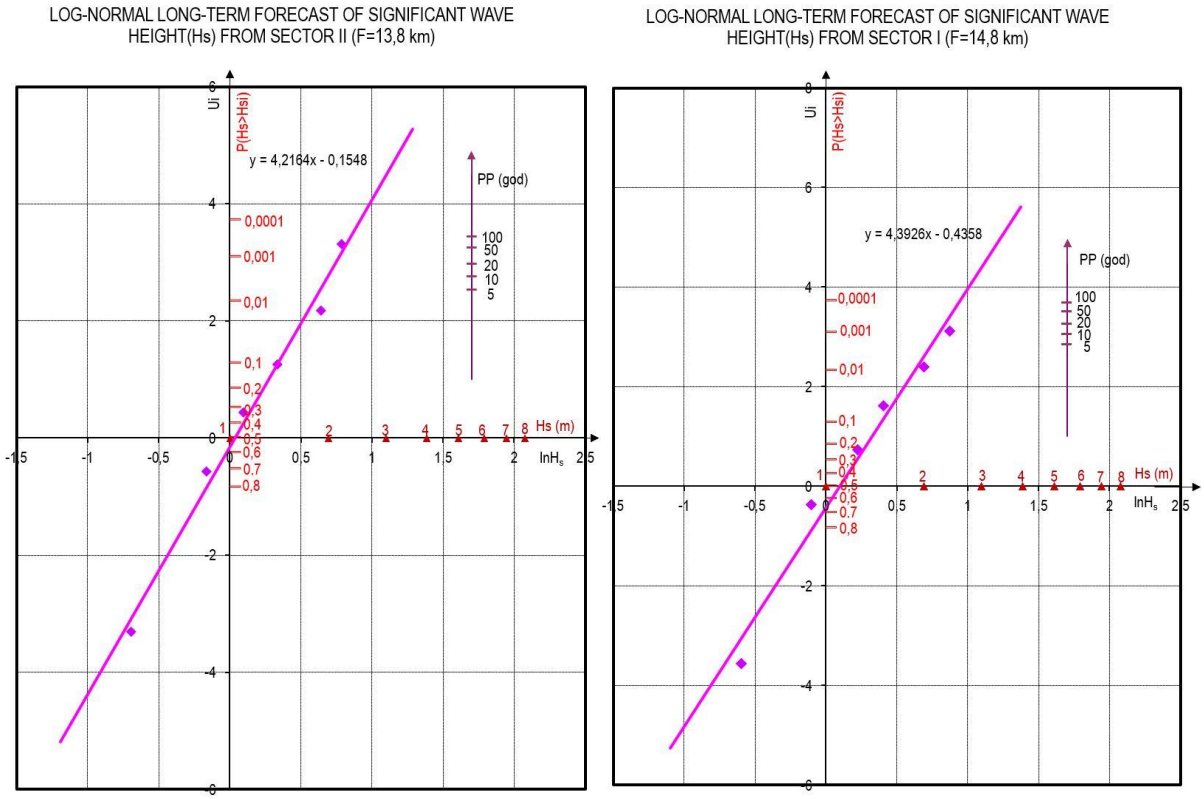

Figure 3.45 – Long-term distribution of significant wave height Hs for sectors I (left) and II (right)

Figures 3.45 and 3.46 show the probability distributions of random variables of significant wave height (*Hs*), and forecast values of significant wave heights H_S^{PP} at turnback periods PP = 100, 50, 25, 10 and 5 years.

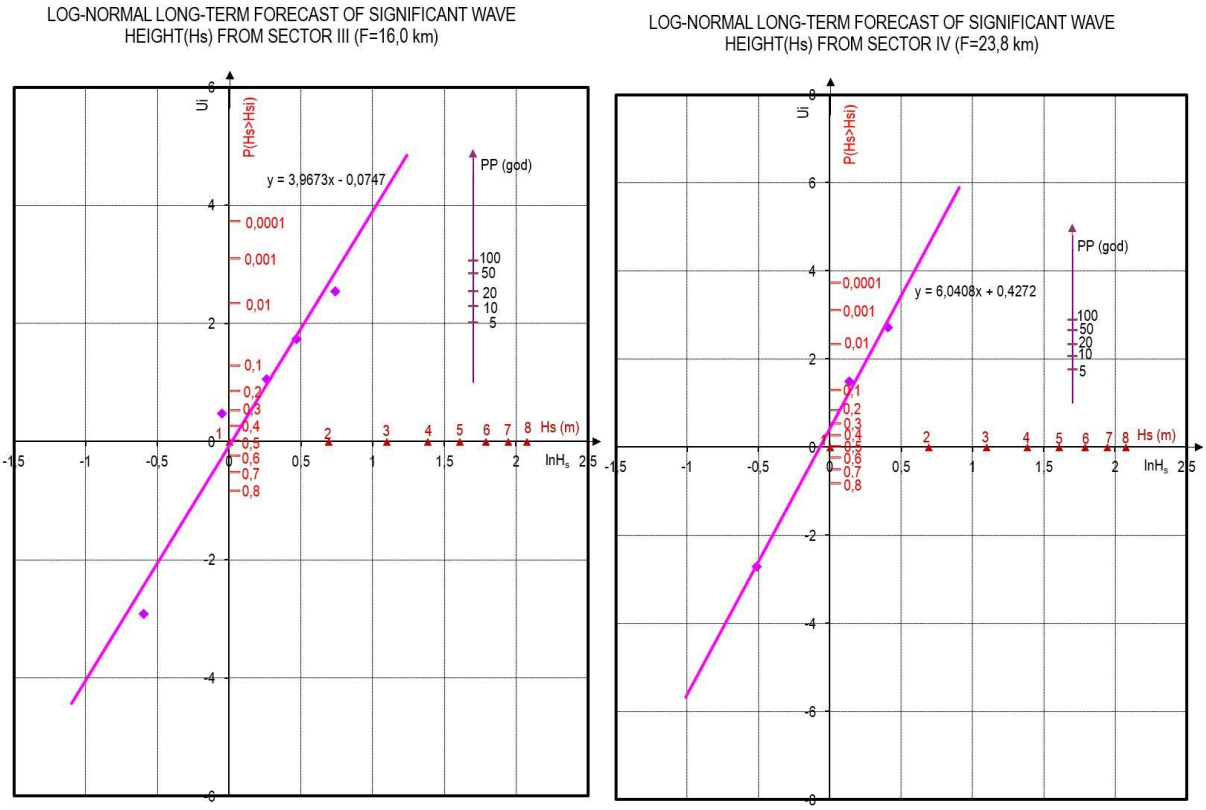

Figure 3.46 – Long-term distribution of significant Hs wave height for sectors III (left) and IV (right)

Table 3.39 gives long-term extreme significant (H_S^{PP}) by return periods forecast using probability distributions from Figures 3.45 and 3.46. Also, it gives associated values ($H_{1/10}$=1,27·H_s), ($H_{1/100}$=1,67·H_s) and maximum waves (H_{max}=1,8·H_s), mean wave periods (T_0) and wave lengths (L_0).

Table 3.39 – Adopted values of deepwater wave parameters for further analysis – Podstrana-Duće area

PP	SEKTOR I							SEKTOR II						
	H_S	$H_{1/10}$	$H_{1/100}$	H_{max}	T_0	L_0	T_p	H_S	$H_{1/10}$	$H_{1/100}$	H_{max}	T_0	L_0	T_p
	(m)	(m)	(m)	(m)	(s)	(m)	(s)	(m)	(m)	(m)	(m)	(s)	(m)	(s)
100	2,56	3,25	4,28	4,61	5,93	55,0	6,52	2,35	3,82	3,92	4,23	5,68	50,4	6,25
50	2,46	3,12	4,11	4,43	5,81	52,8	6,40	2,24	2,84	3,74	4,03	5,55	48,1	6,10
20	2,32	2,95	3,87	4,18	5,65	49,8	6,21	2,11	2,68	3,52	3,80	5,38	45,3	5,92
10	2,22	2,82	3,71	4,00	5,52	47,7	6,08	2,00	2,54	3,34	3,60	5,24	42,9	5,77
5	2,11	2,68	3,52	3,80	5,38	45,3	5,92	1,89	2,40	3,16	3,40	5,10	40,6	5,61

PP	SEKTOR III							SEKTOR IV						
	H_S	$H_{1/10}$	$H_{1/100}$	H_{max}	T_0	L_0	T_p	H_S	$H_{1/10}$	$H_{1/100}$	H_{max}	T_0	L_0	T_p
	(m)	(m)	(m)	(m)	(s)	(m)	(s)	(m)	(m)	(m)	(m)	(s)	(m)	(s)
100	2,21	3,60	3,69	3,98	5,51	47,4	6,06	1,82	2,31	3,04	3,28	5,00	39,1	5,50
50	2,09	2,65	3,49	3,76	5,36	44,9	5,90	1,73	2,20	2,89	3,11	4,88	37,1	5,36
20	1,94	2,46	3,24	3,49	5,16	41,6	5,68	1,61	2,04	2,69	2,90	4,70	34,6	5,17
10	1,82	2,31	3,04	3,28	5,00	39,1	5,50	1,52	1,93	2,54	2,74	4,57	32,6	5,03
5	1,70	2,16	2,84	3,06	4,83	36,5	5,32	1,42	1,80	2,37	2,56	4,42	30,5	4,86

3.1.3.5. Split (Kašjuni)

A sample of significant deepwater wave heights Hs for long-term forecast was formed from a wind sample, based on Table 3.30 and a calculated fetch, and using short-term wave forecast using the Groen-Dorrestein method (Table 3.40).

Table 3.40 – Sample of significant wave height Hs

	WIND STRENGHT (Bf)	4	5	6	7	8	9	10
SECTOR I	Fetch (km)	F1 = 23 km						
	FREQUENCY	984	1128	493	121	20	3	0
	H_S (m)	0,6	1,1	1,5	1,8	2,4	2,8	0
SECTOR II	Fetch (km)	F2 = 21,3 km						
	FREQUENCY	301	410	236	95	15	1	0
	H_S (m)	0,45	0,8	1	1,3	1,7	2	0
SECTOR III	Fetch (km)	F3 = 8,7 km						
	FREQUENCY	189	48	29	10	2	0	0
	H_S (m)	0,45	0,75	1	1,2	1,6	0	0
SECTOR IV	Fetch (km)	F4 = 6,3 km						
	FREQUENCY	143	10	1	0	0	0	0
	H_S (m)	0,35	0,6	0,85	0	0	0	0

For the sample of significant wave heights *Hs*, a long-term empirical probability was obtained, which adapts well to the direction. An adjustment of the theoretical Log-normal probability distribution was made to it. By extrapolating the theoretical Log-normal probability distribution (direction) into the area of low probability, i.e., long return periods, a long-term forecast was made.

Figures 3.47 and 3.48 show the probability distributions of random variables of significant wave height (*Hs*), and forecast values of significant wave heights H_S^{PP} at return periods PP = 100, 50, 25, 10 and 5 years.

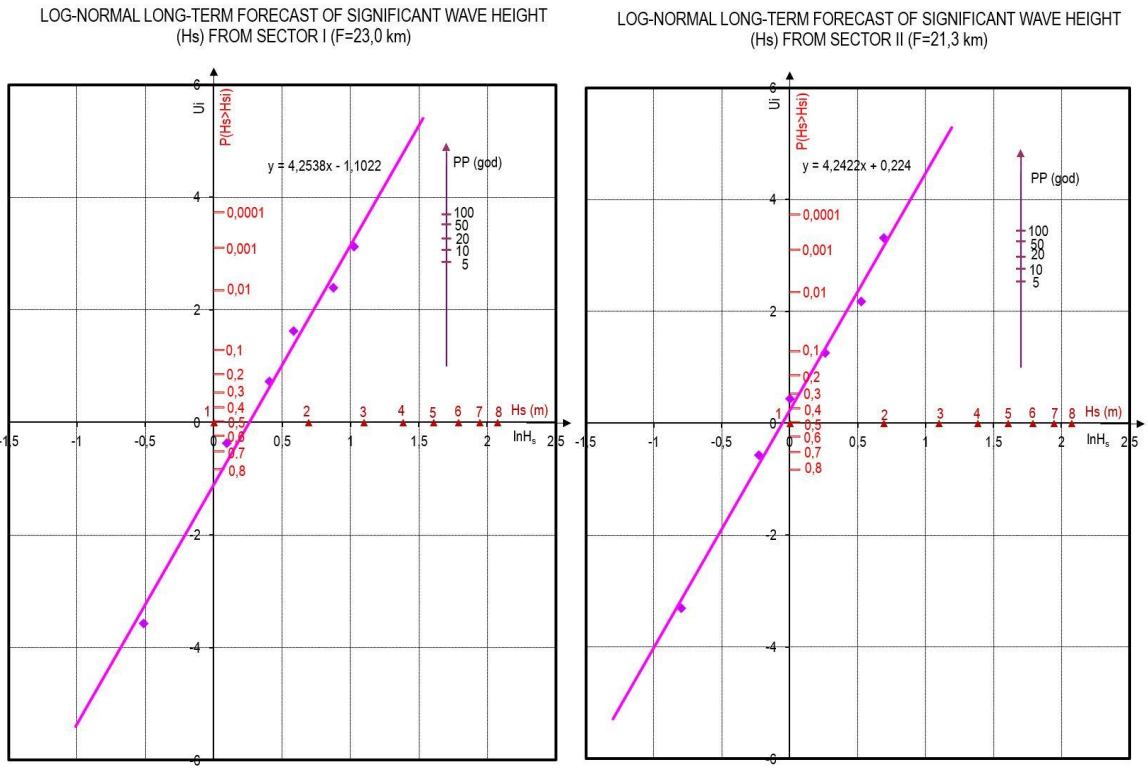

Figure 3.47 – Long-term distribution of significant Wave Height Hs for sectors I (left) and II (right)

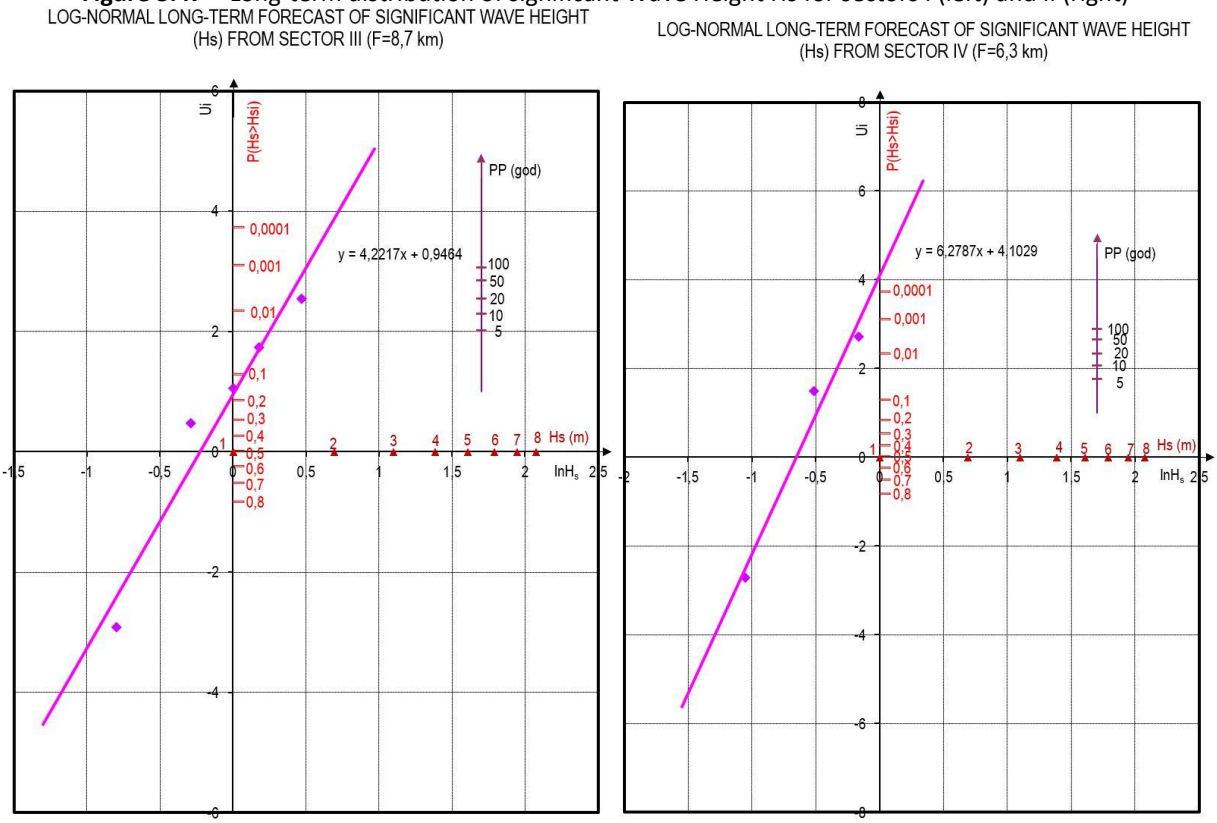

Figure 3.48 – Long-term distribution of significant Hs wave height for sectors III (left) and IV (right)

Table 3.41 provides long-term extreme significant (HSPP) by return periods forecast using the probability distribution from Figures 3.47 and 3.48. Also, it gives associated values ($H_{1/10}$=1,27·H_s), ($H_{1/100}$=1,67·H_s) and maximum waves (H_{max}=1,8·H_s), mean wave periods (T_0) and wave lengths (L_0).

Table 3.41 – Adopted values of deepwater wave parameters for further analysis – Split (Kašjuni)

PP	SEKTOR I							SEKTOR II						
	H_S	$H_{1/10}$	$H_{1/100}$	H_{max}	T_0	L_0	T_p	H_S	$H_{1/10}$	$H_{1/100}$	H_{max}	T_0	L_0	T_p
	(m)	(m)	(m)	(m)	(s)	(m)	(s)	(m)	(m)	(m)	(m)	(s)	(m)	(s)
100	3,09	3,92	5,16	5,56	6,52	66,3	7,17	2,14	3,48	3,57	3,85	5,42	45,9	5,97
50	2,96	3,76	4,94	5,33	6,38	63,5	7,02	2,04	2,59	3,41	3,67	5,29	43,8	5,82
20	2,79	3,54	4,66	5,02	6,19	59,9	6,81	1,92	2,44	3,21	3,46	5,14	41,2	5,65
10	2,66	3,38	4,44	4,79	6,05	57,1	6,65	1,82	2,31	3,04	3,28	5,00	39,1	5,50
5	2,53	3,21	4,23	4,55	5,90	54,3	6,49	1,72	2,18	2,87	3,10	4,86	36,9	5,35

PP	SEKTOR III							SEKTOR IV						
	H_S	$H_{1/10}$	$H_{1/100}$	H_{max}	T_0	L_0	T_p	H_S	$H_{1/10}$	$H_{1/100}$	H_{max}	T_0	L_0	T_p
	(m)	(m)	(m)	(m)	(s)	(m)	(s)	(m)	(m)	(m)	(m)	(s)	(m)	(s)
100	1,65	2,68	2,76	2,97	4,76	35,4	5,24	0,82	1,04	1,37	1,48	3,36	17,6	3,69
50	1,57	1,99	2,62	2,83	4,64	33,7	5,11	0,79	1,00	1,32	1,42	3,29	17,0	3,62
20	1,46	1,85	2,44	2,63	4,48	31,3	4,93	0,75	0,95	1,25	1,35	3,21	16,1	3,53
10	1,38	1,75	2,30	2,48	4,35	29,6	4,79	0,72	0,91	1,20	1,30	3,15	15,5	3,46
5	1,29	1,64	2,15	2,32	4,21	27,7	4,63	0,69	0,88	1,15	1,24	3,08	14,8	3,39

4. DETERMINATION OF GRANULOMETRIC COMPOSITION OF BEACHES

As shown below, the beaches that are the subject of the analysis of this study are made of granular material and according to the classification (Reeve, Chadwick and Fleming, 2004) given in chapter 5.2.1, belong to pebble beaches, where the grain size is predominantly greater than 2 mm.

The data on the composition of the beach, i.e., the size of the grain of the material from which it is composed, is an extremely important information because it defines the dominant type of transport of beach material that occurs on the analyzed beach and has a key significance on its morphology. As explained in detail in chapter 5.2.1, smaller beach material, such as sand, is subject to the so-called suspended transport of sediments, in which it is raised from the bottom due to the action of hydrodynamic forces and transferred by liquid (sea) above the bottom. In larger grain materials, sediment transport takes place by rolling or pushing the material along the bottom, when the natural resistance of the grain of the material at the bottom is exceeded (more details in Chapter 5). For this reason, it is very important to know the composition of the beach material, i.e., the range of grain sizes or its granulometric curve, which in practice is often expressed by the mean size of the D_{50} stone grain. D_{50} represents the diameter of the grain for which there is 50 percent of the grain of less, or larger, mass.

Also, the granulometric composition of the beach material, i.e., the data on the mean size of the D_{50} stone grain, is important because of the quantitative calculation of sediment transport potential and the calculation of the stable composition of beach material with which it should be fed to individual beaches exposed to increased erosion because of waves and the future consequences of climate changes.

Namely, the beach material is continuously exposed to hydrodynamic influences of varying intensity, as a result of which its gradual wear and shredding inevitably occurs. Where these influences are mild, the material experiences less intense shredding and remains stable and stable for a longer period, while in areas that are under stronger hydrodynamic influence, this process is intensified, with wear and shredding of beach material occurring faster. The wear of the material, of course, also depends on the type of stone material from which the body of the grainy beach is made, so the harder material will be more sustainable on these abrasive processes that shred it.

Once the grain of beach material, due to wear, is sufficiently chopped, it becomes subject to the suspended transport of sediments, which allows it to be taken away forever from the location of the beach in which it was until then. In this way, a gradual natural loss of beach material occurs, which is a process that, depending on the velocity of unfolding, is observed in the form of beach erosion. With the increase in the intensity of hydrodynamic influences, the intensity of erosion also increases, so it is logical to assume that the consequences of climate change will only further potentiate this problem.

Man can influence the reduction of this problem by applying two basic principles. The first is proactive action with the aim of reducing hydrodynamic impacts, employing protective coastal structures, and the second is a passive approach of nourishing lost (eroded) beach material. Practice has shown that the best results are achieved by combining both principles, where initial importance should be given to a proactive approach by employing protective coastal structures, because the degree of reduction of hydrodynamic impacts that exert wear of beach material and beach erosion depends on it.

What are the basic procedures for beach protection is explained in detail in chapter 5.5, and how the analysis necessary for their effective placement is performed, is shown by the methodology applied in this study, which resulted in the guidelines in question.

Below is an analysis of the existing granulometric compositions of the beaches in question (Institut IGH d.d., 2023), for the purpose of assessing the vulnerability of these beaches from erosion in their existing state and for predictions in the future related to the consequences of climate changes.

4.1. Field sampling

Two samples of beach material were taken from each of the five locations analyzed, with about 10 kilograms of material collected for each sample from a position directly on the coastline. The tool used was a shovel with a handle and a metal spatula for extracting sediments. The material was taken in such a way that the collection tool captures the complete sediment at a depth of approximately 30 centimeters, without unnecessary expansion of the excavation pit. The sediment was then collected in plastic bags and marked with a label for each of the locations. The coordinates of the locations of the samples collected are shown in Table 4.1 and in Figures 4.1 through 4.5.

Table 4.1 – Coordinates of locations of collected samples of beach material

LOCATION	COORDINATE	
Bol (Brač)	B1 – 43°15’21.51''N, 16°38'4.11''E	B2 – 43°15’21.55''N, 16°38'2.09''E
Stiniva (Vis)	S1 – 43°1’16.54''N, 16°10'17.49''E	S2 – 43°1’16.57''N, 16°10'18.28''E
Podgora	M1 – 43°14’23.45''N, 17°4'35.64''E	M2 – 43°14’2.86''N, 17°4'37.83''E
Podstrana	P1 – 43°29’11.30''N, 16°32'48.54''E	P2 – 43°28’56.85''N, 16°33'17.60''E
Kašjuni (Split)	K1 – 43°30’20.37''N, 16°24'2.13''E	K2 – 43°30’28.65''N, 16°23'55.27''E

Sampling of beach material was carried out in the spring period April-May 2023, so it can be said that the material at the sampling locations was in the condition expected after the winter period in which the most intense are the effects of severe and stormy weather that bring large waves to the beach shores. Given that there was no possibility to sampling beach material in another time period, such as after the summer and before the beginning of the winter season, which would certainly raise the level of confidence in the results of the granulometry test and improve the insight into the behavior of beach material during the year, this principle of sampling (twice a year) is recommended as one of the segments of control in the introduction of quality systematic monitoring of the situation on beaches proposed in the in the framework of these guidelines (more in Chapter 9).

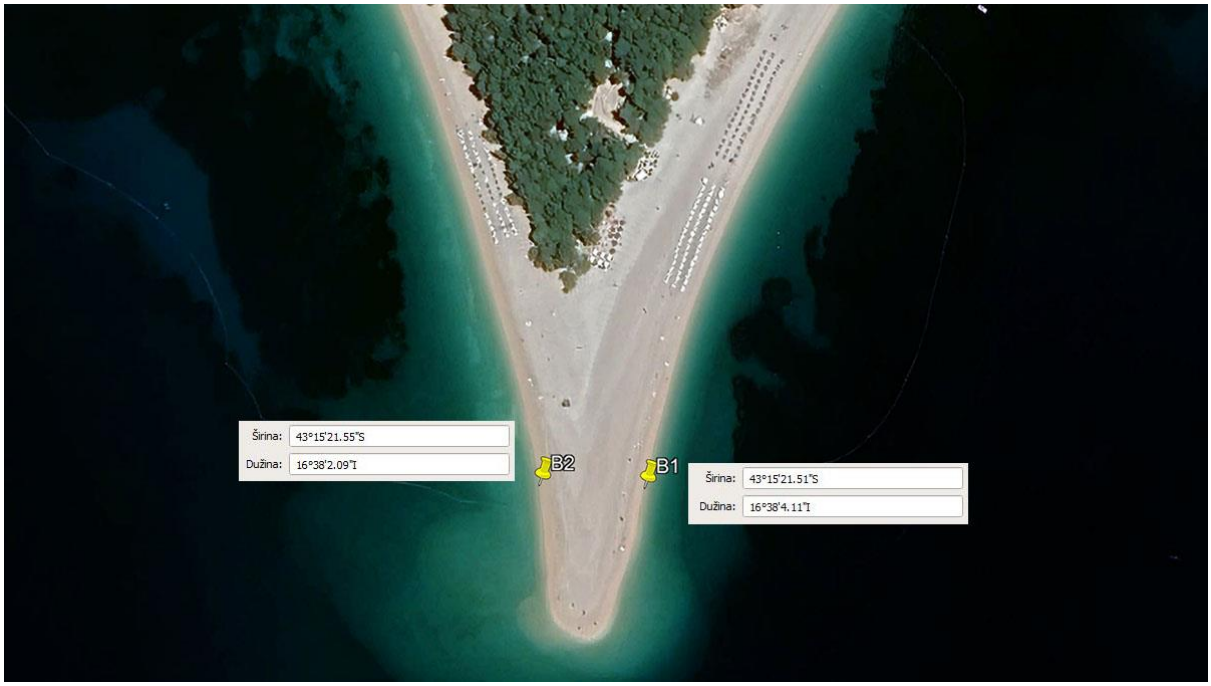

Figure 4.1 – Locations of sample collection of beach material for Zlatni rat beach (Brač)

After sampling, the samples were air-dried and analyzed by granulometric method of wet seeding in the laboratory of Institut IGH d.d. in Split. Analysis of each sample was carried out by sieving previously weighed material. After the finished sieving, the remains of the material remaining on each individual sieve were weighed, and their mass was recorded. The granulometric composition is shown by a diagram, where on the abscise is the diameter of the sieve opening, and on the ordinate is the passage through the sieve in percentages of the total mass of the sample. The results are points in the diagram that are connected make up the granulometric curve, which gives a picturesque idea of the distribution of grains by size in the observed pattern.

In addition to the data on the average grain size D_{50}, the parameters D_{60}, D_{30} i D_{10} are also determined. they are essential for the geomechanical classification of large-grained materials. They represent the diameters of the grain at 60, 30 i 10 the percentage pass and are determined by interpolation in the granulometric diagram. Argument $C_u = D_{60} / D_{10}$ it is called the coefficient of uniformity, and the parameter $C_c = (D_{30})2 / (D_{60} \times D_{10})$ coefficient of curvature.

European Regional Development Fund

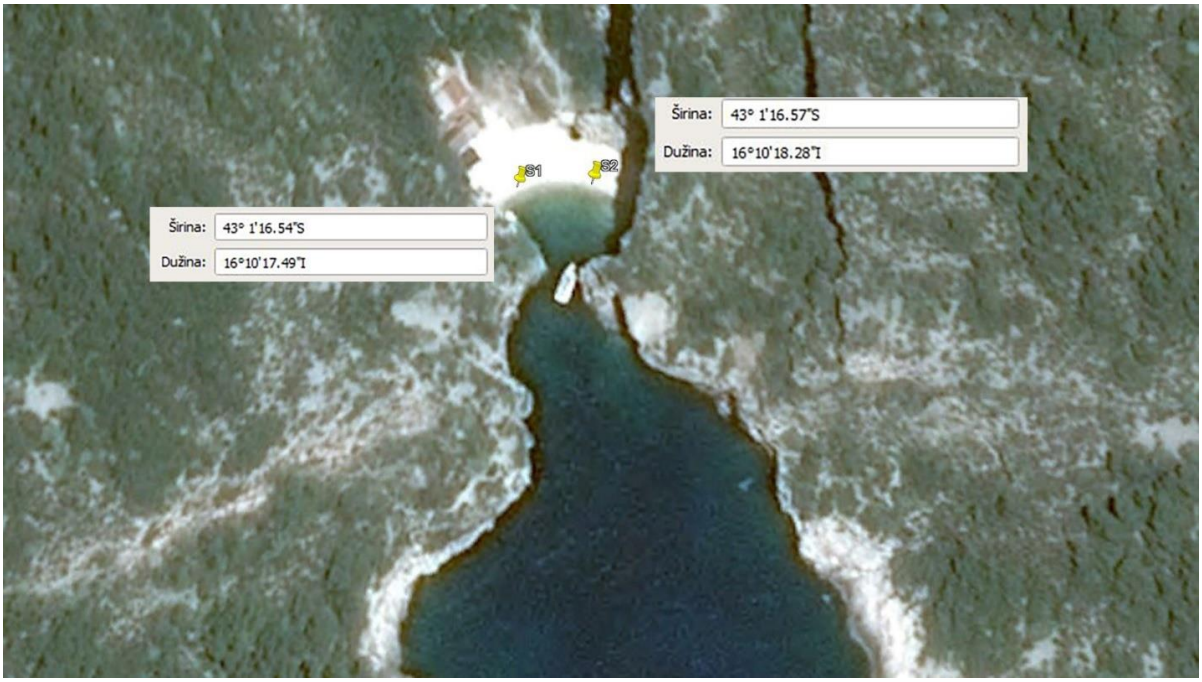

Figure 4.2 – Locations of sampling of beach material for Stiniva beach (Vis)

Figure 4.3 – Locations of sampling of beach material for Podgora beach (Makarska Riviera)

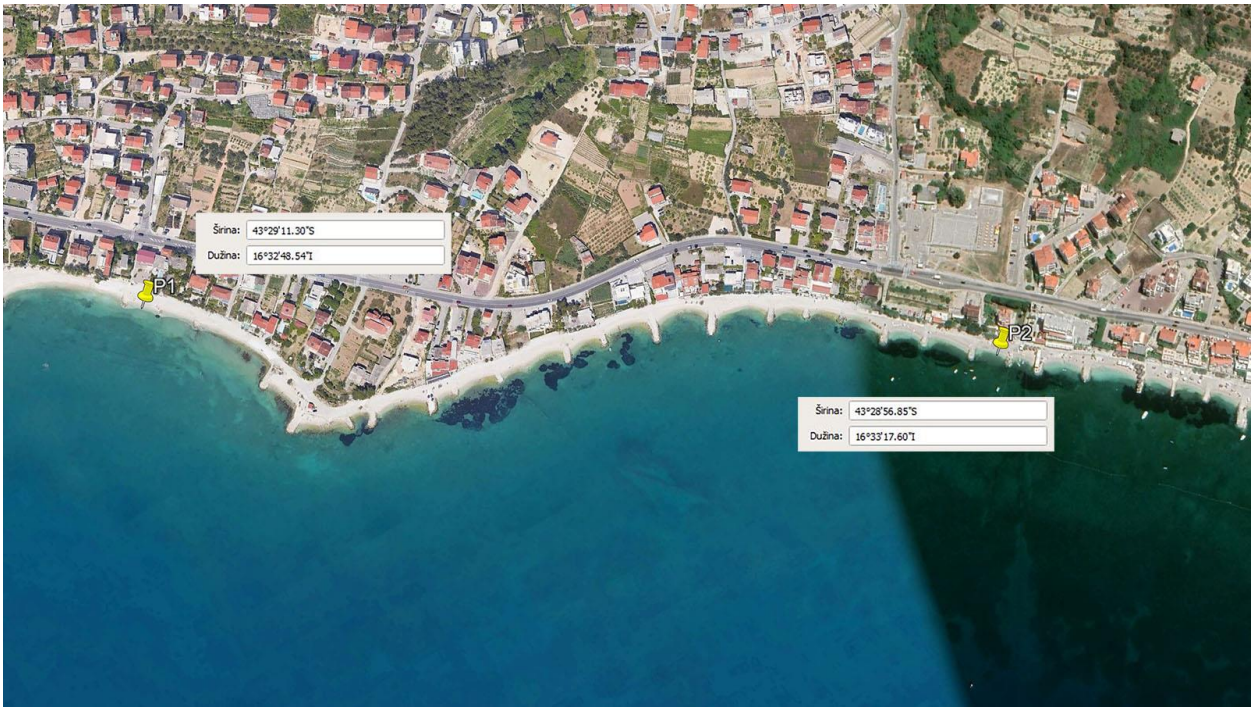

Figure 4.4 – Locations of sampling of beach material for Podstrana beach

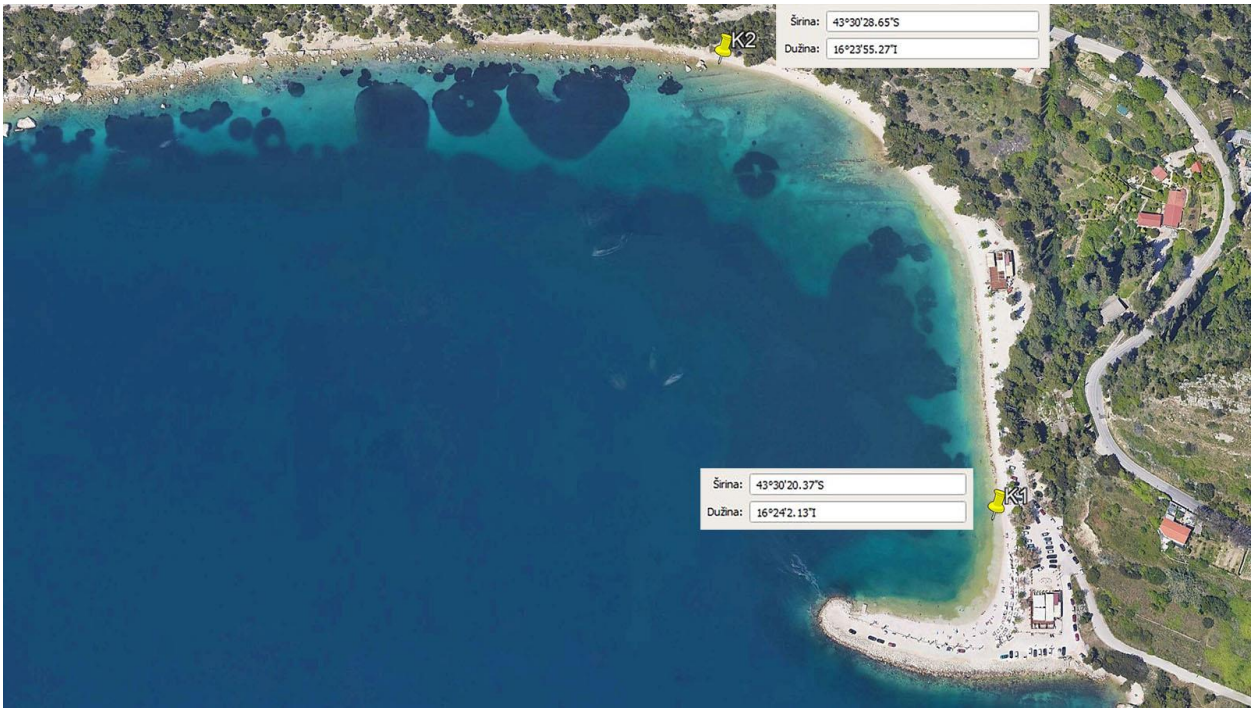

Figure 4.5 – Locations of sampling of beach material for Kašjuni beach (Split)

4.1.1. Zlatni rat (Brač)

On the beach Zlatni rat on Brač, beach material was sampled from the coastline, at the position of the east and west coast of the cape of the beach (figure 4.1). The sample collected on the east side of the cape is marked B1 (figure 4.6), while the pattern on the west side is marked B2 (figure 4.7). Visual

observation sampling of materials, it can be concluded that waves during the winter period applied smaller beach material to the coastal zone, while slightly larger material is noticeable already 1 to 2 meters from the coast to the sea. Also, the larger material is visible already a few meters from the coast to the mainland, while the flat part of the beach ridge is mostly covered with larger pebbles.

Figure 4.6 – Location of beach material Sampling B1 - Zlatni rat beach (Brač)

Figure 4.7 – Location of beach material B2 - Zlatni rat beach (Brač)

The granulometric composition of sample B1 (Figure 4.9) is shown in Figure 4.8. According to the results of the conducted test, **the mean grain size D_{50} is 2.7 mm**, while the coefficient of uniformity $C_u=D_{60}/D_{10}$=2,6.

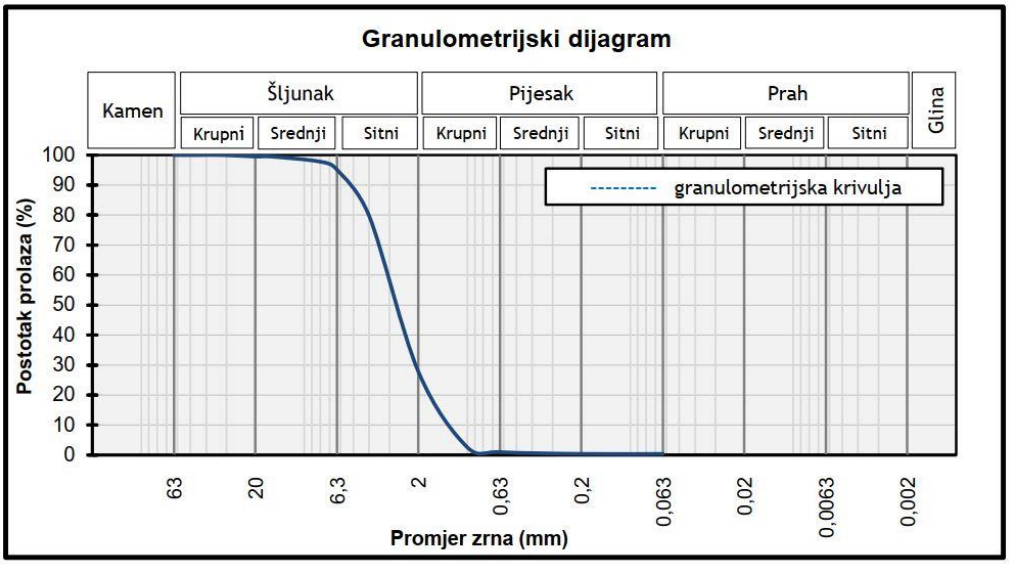

Prosijavanje	
Otvor sita (mm)	**Prolaz kroz sito** (%)
63	100,0
45	100,0
31,5	100,0
20	99,5
16	99,5
8	97,8
6,3	95,1
4	79,7
2	27,9
1	2,6
0,63	1,0
0,2	0,4
0,063	0,4

Areometriranje	
d_i (mm)	K (%)
0,02	-
0,0063	-
0,002	-
ρ_s (Mg/m^3)	
-	

UDIO FRAKCIJA (%)			
Krupnozrne		*Sitnozrne*	
Šljunak	**Pijesak**	**Prah**	**Glina**
72	28	-	-

d_i - *ekvivalentni promjer čestica*
K - *udio čestica manjih od* d_i

ρ_s - *gustoća areometriranih čestica prema HRN EN ISO 17892-3:2016*

DODATNI PODACI (*nisu u području akreditacije*)

Promjer najvećeg zrna, D_{max} (mm)	25
Promjer zrna s prolazom 60%, D_{60} (mm)	3,1
Promjer zrna s prolazom 30%, D_{30} (mm)	2,1
Promjer zrna s prolazom 10%, D_{10} (mm)	1,2

Napomena: Promjer zrna s prolazom 50%, D_{50} = 2,7 mm

Koeficijent uniformnosti:	
$C_u = D_{60} / D_{10}$	2,6

Koeficijent zakrivljenosti:	
$C_c = D_{30}^2 / (D_{60} \times D_{10})$	1,2

Odstupanja od norme: -

Figure 4.8 – Results of testing of granulometric composition of beach material sample B1 - Zlatni rat beach (Brač)

Figure 4.9 – Collected sample of beach material B1 - Zlatni rat beach (Brač)

The granulometric composition of sample B2 (Figure 4.11) is shown in Figure 4.10. According to the results of the test, **the mean grain size D_{50} is 5.6 mm**, while the coefficient of uniformity $C_u=D_{60}/D_{10}$=1,6.

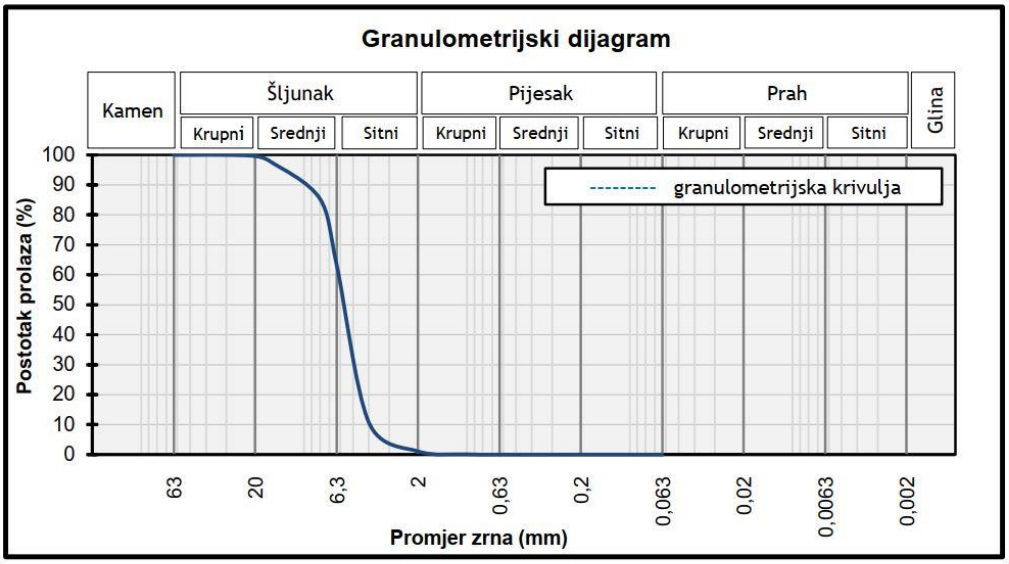

Prosijavanje	
Otvor sita (mm)	**Prolaz kroz sito** (%)
63	100,0
45	100,0
31,5	100,0
20	99,6
16	97,7
8	85,4
6,3	63,2
4	10,7
2	1,1
1	0,1
0,63	0,0
0,2	0,0
0,063	0,0

UDIO FRAKCIJA (%)			
Krupnozrne		*Sitnozrne*	
Šljunak	**Pijesak**	**Prah**	**Glina**
99	1	-	-

d_i - *ekvivalentni promjer čestica*
K - *udio čestica manjih od* d_i

Areometriranje	
d_i (mm)	K (%)
0,02	-
0,0063	-
0,002	-
ρ_s (Mg/m^3)	
-	

ρ_s - *gustoća areometriranih čestica prema HRN EN ISO 17892-3:2016*

DODATNI PODACI (*nisu u području akreditacije*)

Promjer najvećeg zrna, D_{max} (mm)	25
Promjer zrna s prolazom 60%, D_{60} (mm)	6,1
Promjer zrna s prolazom 30%, D_{30} (mm)	4,7
Promjer zrna s prolazom 10%, D_{10} (mm)	3,8

Napomena: Promjer zrna s prolazom 50%, D_{50} = 5,6 mm

Odstupanja od norme: -

Koeficijent uniformnosti: $C_u = D_{60} / D_{10}$	1,6

Koeficijent zakrivljenosti: $C_c = D_{30}^2 / (D_{60} \times D_{10})$	1,0

Figure 4.10 – Results of testing of granulometric composition of beach material Sample B2 - Zlatni rat beach (Brač)

Figure 4.11 – Collected sample of beach material B2 - Zlatni rat beach (Brač)

4.1.2. Stiniva (Vis)

Figure 4.12 – Location of beach material sampling S1 - Stiniva beach (Vis)

Figure 4.13 – Location of sampling of beach material S2 - Stiniva beach (Vis)

On the beach Stiniva on Vis, sampling of beach material from the coastline was carried out, in two positions marked in Figure 4.2. The sample collected on the western part of the beach is marked with the Mark S1 (figure 4.12), while the pattern on the eastern part is marked with the mark S2 (figure 4.13). Visual observation during material sampling, it can be concluded that there is no significant impact of waves at the beach location during the winter period, and that the beach material is quite uniform in size throughout the entire surface of the beach in the mainland and underwater part. It is mostly a larger material and pebbles.

The granulometric composition of sample S1 (Figure 4.15) is shown in Figure 4.14. According to the results of the test, **the mean grain size D_{50} is 22.3 mm**, while the coefficient of uniformity $C_u=D_{60}/D_{10}$=1,8.

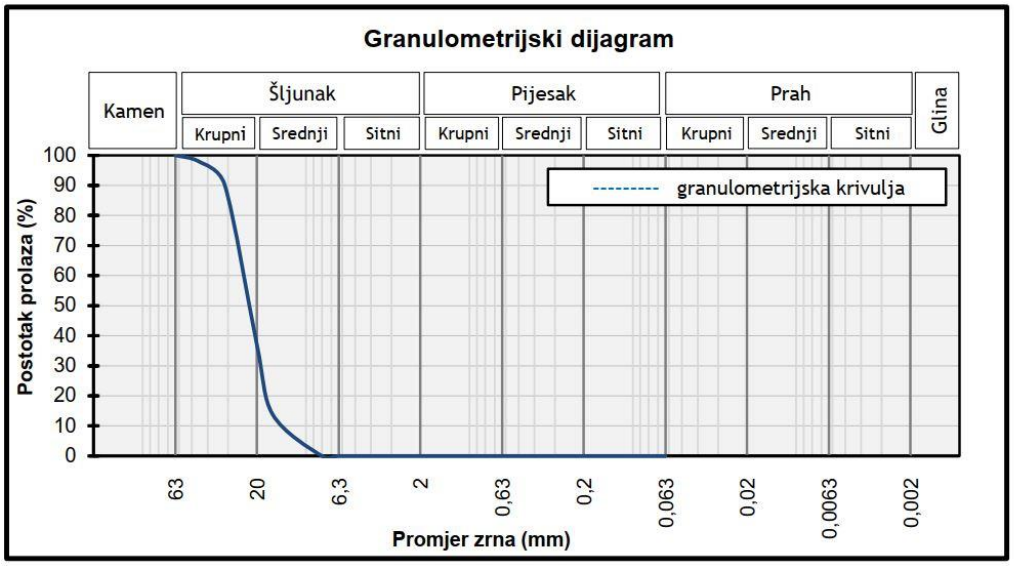

Prosijavanje	
Otvor sita (mm)	**Prolaz kroz sito** (%)
63	100,0
45	97,9
31,5	90,3
20	37,1
16	13,8
8	0,0
6,3	0,0
4	0,0
2	0,0
1	0,0
0,63	0,0
0,2	0,0
0,063	0,0

UDIO FRAKCIJA (%)			
Krupnozrne		*Sitnozrne*	
Šljunak	**Pijesak**	**Prah**	**Glina**
100	0	-	-

d_i - *ekvivalentni promjer čestica*
K - *udio čestica manjih od* d_i

Areometriranje	
d_i (mm)	**K** (%)
0,02	-
0,0063	-
0,002	-
ρ_s (Mg/m^3)	
-	

ρ_s - *gustoća areometriranih čestica prema HRN EN ISO 17892-3:2016*

DODATNI PODACI (*nisu u području akreditacije*)

Promjer najvećeg zrna, D_{max} (mm)	60
Promjer zrna s prolazom 60%, D_{60} (mm)	24,3
Promjer zrna s prolazom 30%, D_{30} (mm)	18,7
Promjer zrna s prolazom 10%, D_{10} (mm)	13,2

Napomena: Promjer zrna s prolazom 50%, D_{50} = 22,3 mm

Koeficijent uniformnosti:	
$C_u = D_{60} / D_{10}$	1,8

Koeficijent zakrivljenosti:	
$C_c = D_{30}^2 / (D_{60} \times D_{10})$	1,1

Odstupanja od norme: -

Figure 4.14 – Results of testing the granulometric composition of a sample of beach material S1 – Stiniva beach (Vis)

Figure 4.15 – Collected sample of beach material S1 - Stiniva beach (Vis)

The granulometric composition of the Sample S2 (Figure 4.17) is shown in Figure 4.16. According to the results of the test, **the mean grain size D_{50} is 13.7 mm**, while the coefficient of uniformity $C_u=D_{60}/D_{10}$=1,9.

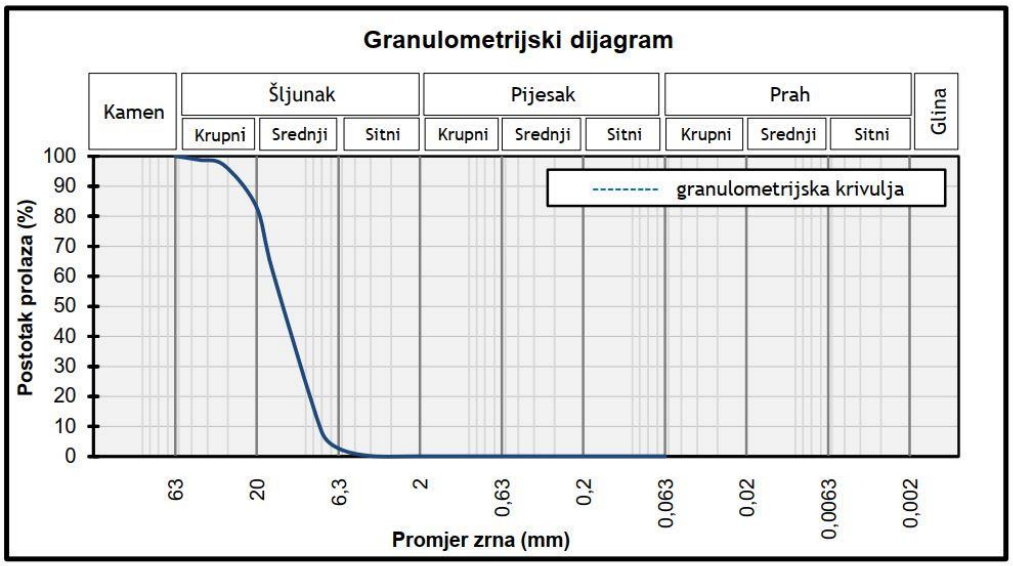

Prosijavanje	
Otvor sita (mm)	**Prolaz kroz sito** (%)
63	100,0
45	98,8
31,5	96,9
20	83,0
16	61,9
8	8,3
6,3	2,7
4	0,2
2	0,1
1	0,1
0,63	0,1
0,2	0,1
0,063	0,1

UDIO FRAKCIJA (%)			
Krupnozrne		*Sitnozrne*	
Šljunak	**Pijesak**	**Prah**	**Glina**
100	0	-	-

d $_i$ *- ekvivalentni promjer čestica*
K *- udio čestica manjih od* ***d*** $_i$

Areometriranje	
d $_i$ (mm)	***K*** (%)
0,02	-
0,0063	-
0,002	-
ρ_s (Mg/m^3)	
-	

ρ_s *- gustoća areometriranih čestica prema HRN EN ISO 17892-3:2016*

DODATNI PODACI (*nisu u području akreditacije*)

Promjer najvećeg zrna, D_{max} (mm)	60
Promjer zrna s prolazom 60%, D_{60} (mm)	15,6
Promjer zrna s prolazom 30%, D_{30} (mm)	10,6
Promjer zrna s prolazom 10%, D_{10} (mm)	8,2

Napomena: Promjer zrna s prolazom 50%, D_{50} = 13,7 mm

Koeficijent uniformnosti:	
$C_u = D_{60} / D_{10}$	1,9

Koeficijent zakrivljenosti:	
$C_c = D_{30}^2 / (D_{60} \times D_{10})$	0,9

Odstupanja od norme: -

Figure 4.16 – Results of testing of granulometric composition of sample beach material S2 – Stiniva beach (Vis)

Figure 4.17 – Collected sample of beach material S2 - Stiniva beach (Vis)

4.1.3. Podgora (Makarska rivijera)

Figure 4.18 – Location of beach material Sample M1 - Podstrana beach (Makarska Riviera)

On the beach Podgora on the Makarska Riviera, sampling of beach material was carried out, in two positions shown in Figure 4.3. The sample collected on the northern part of the beach marked with the mark M1 (figure 4.18), while the pattern on the southern part of the beach is marked with the mark M2 (figure 4.19). Visual observations when sampling materials, it can be concluded that waves during the winter period only slightly pronouncedly applied smaller beach material into the coastal zone, while somewhat larger material can be observed somewhat further from the coastline to land and to the sea. The material is mixed in terms of shape, where rounded pebbles are observed that represent the beach material that has been present on the site for a long time and that has been shaped by the sea, while the material of more angular grain shapes is the material brought by the recent nourishment of the beach.

Figure 4.19 – Location of beach material Sample M2 - Beach Podstrana (Makarska Riviera)

The granulometric composition of sample M1 (Figure 4.21) is shown in Figure 4.20. According to the results of the test, **the mean grain size D_{50} is 11.7 mm**, while the coefficient of uniformity $C_u=D_{60}/D_{10}$=4,6.

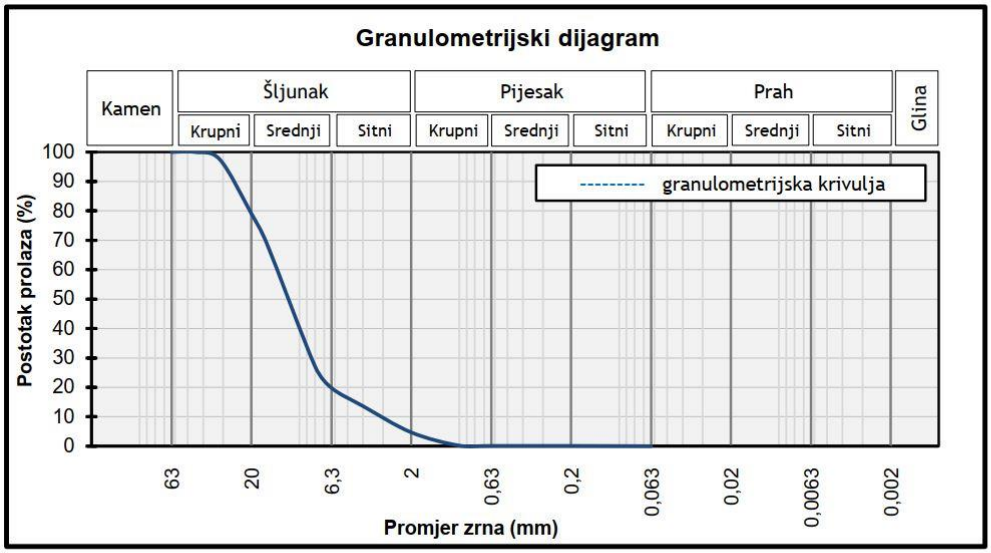

Prosijavanje	
Otvor sita (mm)	**Prolaz kroz sito** (%)
63	100,0
45	100,0
31,5	97,5
20	79,1
16	68,9
8	27,2
6,3	19,8
4	13,6
2	4,7
1	0,2
0,63	0,1
0,2	0,1
0,063	0,0

Areometriranje	
d_i (mm)	K (%)
0,02	-
0,0063	-
0,002	-
ρ_s (Mg/m^3)	
-	

UDIO FRAKCIJA (%)			
Krupnozrne		*Sitnozrne*	
Šljunak	**Pijesak**	**Prah**	**Glina**
95	5	-	-

d_i - *ekvivalentni promjer čestica*
K - *udio čestica manjih od* d_i

ρ_s - *gustoća areometriranih čestica prema HRN EN ISO 17892-3:2016*

DODATNI PODACI (*nisu u području akreditacije*)

Promjer najvećeg zrna, D_{max} (mm)	40
Promjer zrna s prolazom 60%, D_{60} (mm)	13,8
Promjer zrna s prolazom 30%, D_{30} (mm)	8,4
Promjer zrna s prolazom 10%, D_{10} (mm)	3,0

Napomena: Promjer zrna s prolazom 50%, D_{50} = 11,7 mm

Koeficijent uniformnosti:	
$C_u = D_{60} / D_{10}$	4,6

Koeficijent zakrivljenosti:	
$C_c = D_{30}^2 / (D_{60} \times D_{10})$	1,7

Odstupanja od norme: -

Figure 4.20 – Results of testing the granulometric composition of the sample of beach material M1 – Podgora beach

Figure 4.21 – Collected sample of beach material M1 - Podstrana beach (Makarska Riviera)

The granulometric composition of sample M2 (Figure 4.23) is shown in Figure 4.22. According to the results of the test, **the mean grain size D_{50} is 11.7 mm**, while the coefficient of uniformity $C_u=D_{60}/D_{10}$=4,6.

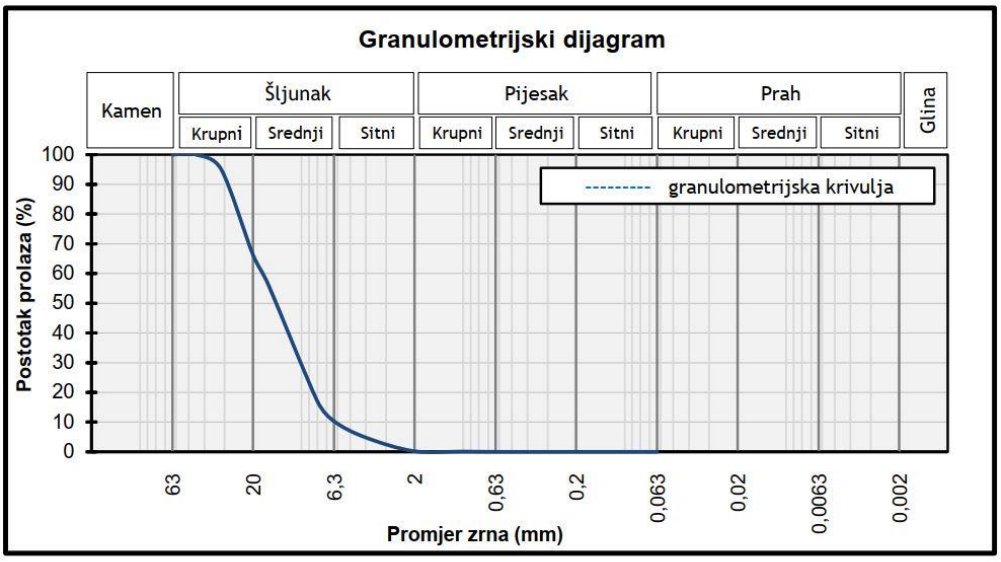

Prosijavanje	
Otvor sita (mm)	**Prolaz kroz sito** (%)
63	100,0
45	100,0
31,5	95,1
20	66,3
16	56,0
8	17,1
6,3	10,3
4	4,8
2	0,2
1	0,1
0,63	0,0
0,2	0,0
0,063	0,0

UDIO FRAKCIJA (%)			
Krupnozrne		*Sitnozrne*	
Šljunak	**Pijesak**	**Prah**	**Glina**
100	0	-	-

d_i - *ekvivalentni promjer čestica*
K - *udio čestica manjih od* d_i

Areometriranje	
d_i (mm)	K (%)
0,02	-
0,0063	-
0,002	-
ρ_s (Mg/m^3)	
-	

ρ_s - *gustoća areometriranih čestica prema HRN EN ISO 17892-3:2016*

DODATNI PODACI (*nisu u području akreditacije*)

Promjer najvećeg zrna, D_{max} (mm)	40
Promjer zrna s prolazom 60%, D_{60} (mm)	17,4
Promjer zrna s prolazom 30%, D_{30} (mm)	10,1
Promjer zrna s prolazom 10%, D_{10} (mm)	6,1

Napomena: Promjer zrna s prolazom 50%, D_{50} = 14,4 mm

Koeficijent uniformnosti:	
$C_u = D_{60} / D_{10}$	2,9

Koeficijent zakrivljenosti:	
$C_c = D_{30}^2 / (D_{60} \times D_{10})$	1,0

Odstupanja od norme: -

Figure 4.22 – Results of testing of granulometric composition of beach material sample M2 – Podgora beach

Figure 4.23 – Collected sample of beach material M2 - Podstrana beach (Makarska Riviera)

4.1.4. Podstrana-Duće area

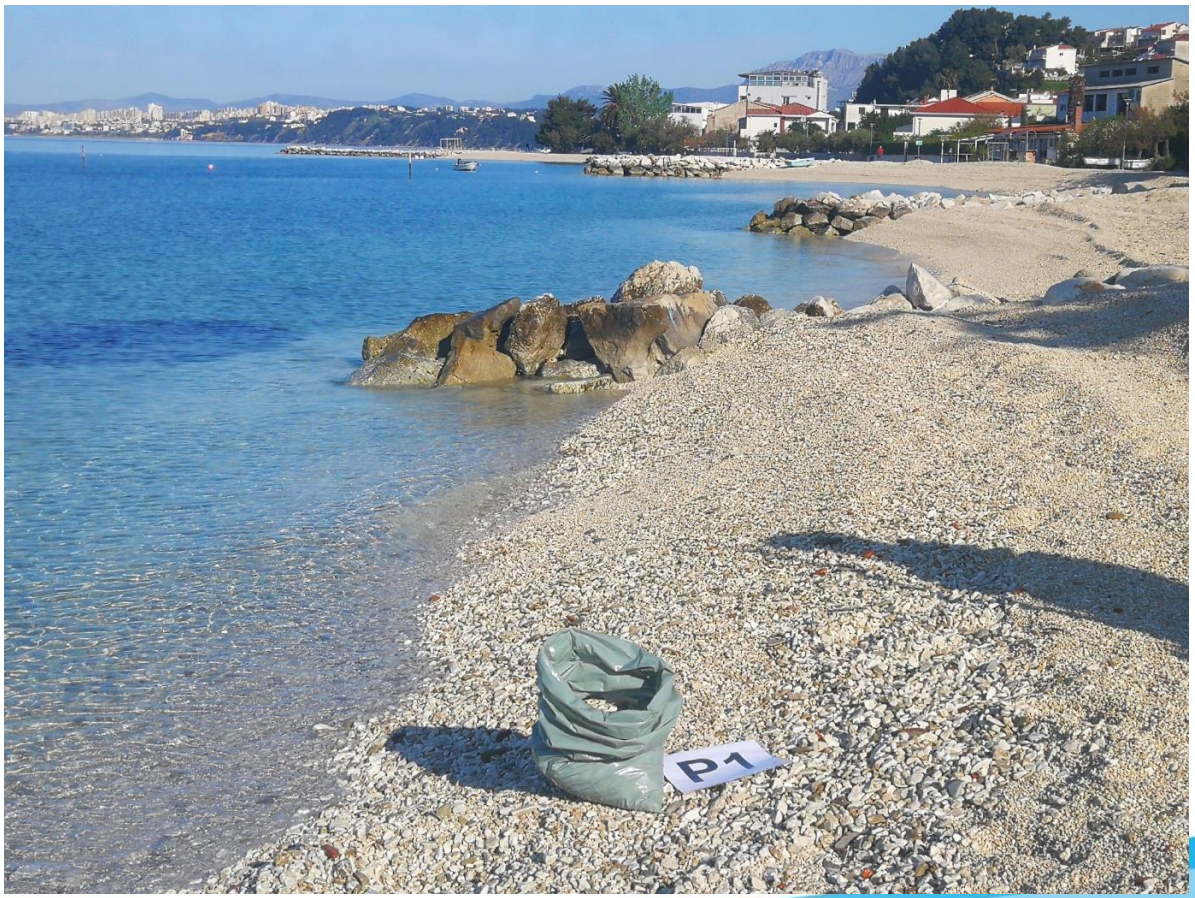

Figure 4.24 – Location of beach material sampling P1 - Podstrana beach

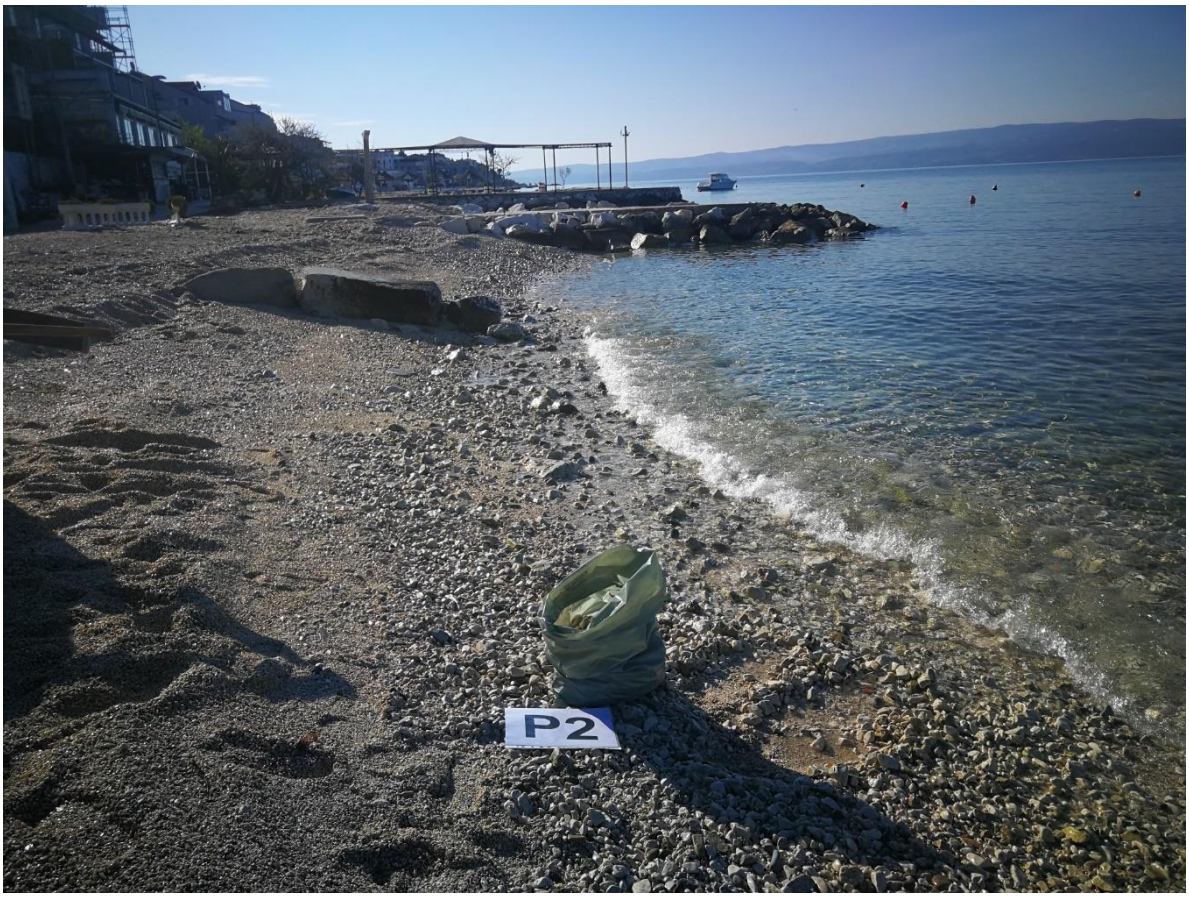

Figure 4.25 – Location of beach material sampling P2 - Podstrana beach

On the beach Podstrana, sampling of beach material was carried out, in two positions shown in Figure 4.4. The sample collected on the western part of the beach is marked P1 (Figure 4.24), while the sample on the eastern part of the beach is marked p2 (figure 4.25). Visual observations when sampling materials, it can be concluded that waves during the winter period significantly applied smaller beach material to the coastal zone, while significantly larger material can be observed a little further from the coastline to the sea. In the mainland, too, a large amount of smaller material is noticeable, which is assumed to have been prepared to feed the beach before the summer season. In general, the existing material on the beach gives the impression of too small material for the location, while the larger material is usually more angular in shape, from which it can be hinted that it was brought by the recent nourishment of the beach because the sea failed to shape it.

The granulometric composition of the sample P1 (Figure 4.27) is shown in Figure 4.26. According to the results of the test, **the mean grain size D_{50} is 14.6 mm**, while the coefficient of uniformity $C_u=D_{60}/D_{10}$=3,8.

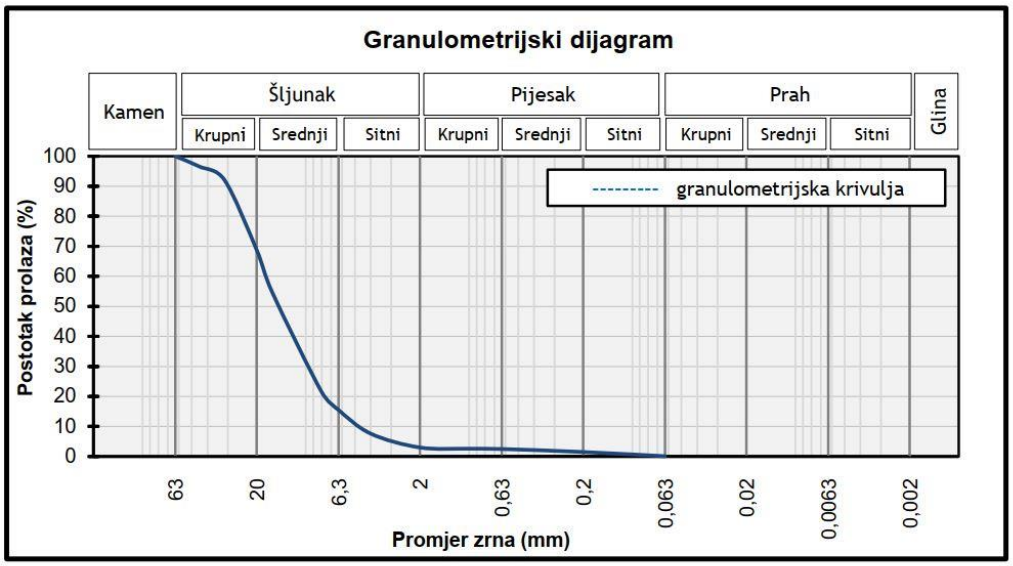

Prosijavanje	
Otvor sita (mm)	**Prolaz kroz sito** (%)
63	100,0
45	96,6
31,5	92,1
20	68,8
16	54,5
8	21,5
6,3	15,5
4	7,6
2	3,0
1	2,6
0,63	2,5
0,2	1,5
0,063	0,1

Areometriranje	
d_i (mm)	**K** (%)
0,02	-
0,0063	-
0,002	-
ρ_s (Mg/m^3)	
-	

UDIO FRAKCIJA (%)			
Krupnozrne		*Sitnozrne*	
Šljunak	**Pijesak**	**Prah**	**Glina**
97	3	-	-

d_i - *ekvivalentni promjer čestica*
K - *udio čestica manjih od* d_i

ρ_s - *gustoća areometriranih čestica prema HRN EN ISO 17892-3:2016*

DODATNI PODACI (*nisu u području akreditacije*)

Promjer najvećeg zrna, D_{max} (mm)	49
Promjer zrna s prolazom 60%, D_{60} (mm)	17,4
Promjer zrna s prolazom 30%, D_{30} (mm)	9,6
Promjer zrna s prolazom 10%, D_{10} (mm)	4,6

Napomena: Promjer zrna s prolazom 50%, D_{50} = 14,6 mm

Koeficijent uniformnosti:	
$C_u = D_{60} / D_{10}$	3,8

Koeficijent zakrivljenosti:	
$C_c = D_{30}^2 / (D_{60} \times D_{10})$	1,2

Odstupanja od norme: -

Figure 4.26 – Results of testing the granulometric composition of a sample of beach material P1 – Podstrana beach

Slika 4.27 – Prikupljeni uzorak plažnog materijala P1 - plaža Podstrana

The granulometric composition of sample P1 (Figure 4.29) is shown in Figure 4.28. According to the results of the test, **the mean grain size D_{50} is 22.9 mm**, while the coefficient of uniformity $C_u=D_{60}/D_{10}$=6,2.

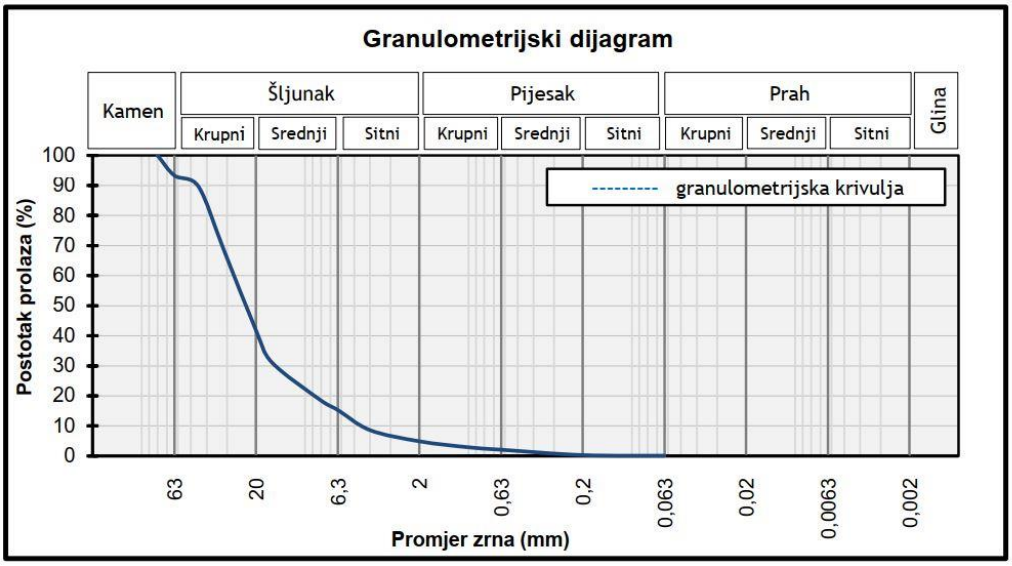

Prosijavanje	
Otvor sita (mm)	**Prolaz kroz sito** (%)
63	93,3
45	89,7
31,5	68,7
20	41,9
16	31,2
8	18,5
6,3	15,3
4	8,6
2	4,9
1	2,9
0,63	2,1
0,2	0,3
0,063	0,1

UDIO FRAKCIJA (%)			
Krupnozrne		*Sitnozrne*	
Šljunak	**Pijesak**	**Prah**	**Glina**
88	5	-	-

d_i - *ekvivalentni promjer čestica*
K - *udio čestica manjih od* d_i

Areometriranje	
d_i (mm)	**K** (%)
0,02	-
0,0063	-
0,002	-
ρ_s (Mg/m^3)	
-	

DODATNI PODACI (*nisu u području akreditacije*)

Promjer najvećeg zrna, D_{max} (mm)	80
Promjer zrna s prolazom 60%, D_{60} (mm)	27,2
Promjer zrna s prolazom 30%, D_{30} (mm)	15,0
Promjer zrna s prolazom 10%, D_{10} (mm)	4,4

ρ_s - *gustoća areometriranih čestica prema HRN EN ISO 17892-3:2016*

Koeficijent uniformnosti:	
$C_u = D_{60} / D_{10}$	6,2

Koeficijent zakrivljenosti:	
$C_c = D_{30}^2 / (D_{60} \times D_{10})$	1,9

Napomena: Promjer zrna s prolazom 50%, D_{50} = 22,9 mm

Odstupanja od norme: -

Figure 4.28 – Results of testing of granulometric composition of beach material sample P2 – Podstrana beach

Figure 4.29 – Collected sample of beach material P2 - Podstrana beach

4.1.5. Kašjuni (Split)

Figure 4.30 – Location of beach material sampling K1 - Kašjuni beach (Split)

On the beach Kašjuni in Split, sampling of beach material was carried out, at two positions shown in Figure 4.5. The sample collected on the southern part of the beach marked with the mark K1 (Figure 4.30), while the sample in the northern part of the beach is marked with the mark K2 (figure 4.31). Visual observations when sampling material, it can be concluded that waves during the winter period significantly applied smaller beach material to the coastal zone, while slightly larger material can be observed a little further from the coastline to the sea, especially in the northern part of the beach. In the mainland part of the southern and central part of the beach, too, a large amount of smaller material is noticeable, which was brought as a supplement of the beach relatively recently (in the past few years). Furthermore, the central part of the beach in an estimated length of 100 meters is lined with larger stone blocks (about 100-200 kg), so it is practically lost as a beach for swimmers. The assumption is that this intervention tried to prevent the erosion of the beach, which is the most intense in this part. In general, the material found on the beach gives the impression of too small material for the location, while the larger material is usually more angular in shape, from which it can be hinted that it was brought by the recent nourishment of the beach because the sea failed to shape it.

Figure 4.31 – Location of beach material Sampling K2 - Kašjuni beach (Split)

The granulometric composition of the Sample K1 (Figure 4.33) is shown in Figure 4.32. According to the results of the test, **the mean grain size D_{50} is 5.2 mm**, while the coefficient of uniformity $C_u=D_{60}/D_{10}$=2,9.

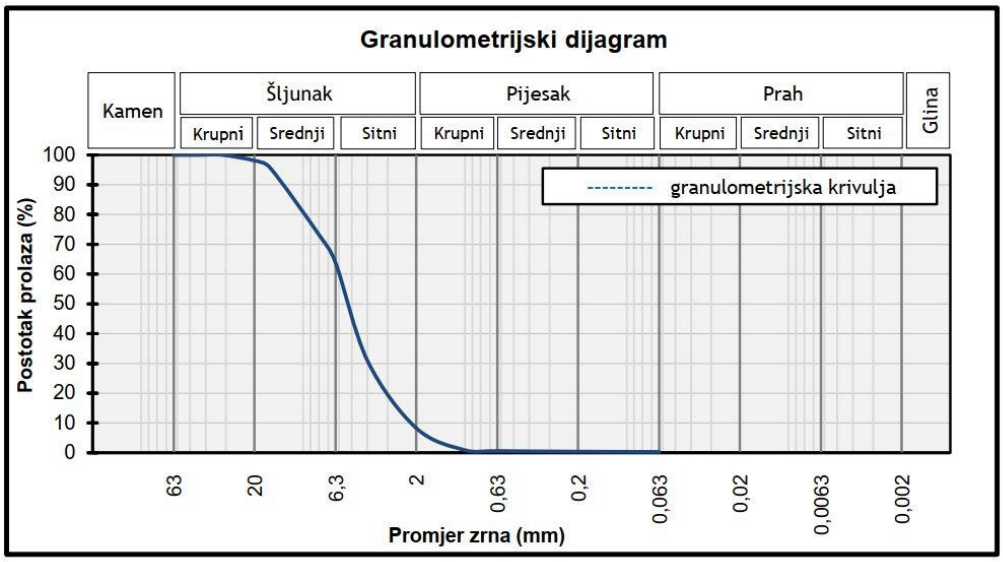

Prosijavanje	
Otvor sita (mm)	**Prolaz kroz sito** (%)
63	100,0
45	100,0
31,5	100,0
20	98,1
16	95,7
8	73,3
6,3	63,8
4	30,9
2	8,3
1	0,9
0,63	0,6
0,2	0,4
0,063	0,3

UDIO FRAKCIJA (%)			
Krupnozrne		*Sitnozrne*	
Šljunak	**Pijesak**	**Prah**	**Glina**
92	8	-	-

d_i - *ekvivalentni promjer čestica*
K - *udio čestica manjih od* d_i

Areometriranje	
d_i (mm)	**K** (%)
0,02	-
0,0063	-
0,002	-
ρ_s (Mg/m^3)	
-	

ρ_s - *gustoća areometriranih čestica prema HRN EN ISO 17892-3:2016*

DODATNI PODACI (*nisu u području akreditacije*)

Promjer najvećeg zrna, D_{max} (mm)	25
Promjer zrna s prolazom 60%, D_{60} (mm)	6,0
Promjer zrna s prolazom 30%, D_{30} (mm)	3,9
Promjer zrna s prolazom 10%, D_{10} (mm)	2,1

Napomena: Promjer zrna s prolazom 50%, D_{50} = 5,2 mm

Koeficijent uniformnosti:	
$C_u = D_{60} / D_{10}$	2,9

Koeficijent zakrivljenosti:	
$C_c = D_{30}^2 / (D_{60} \times D_{10})$	1,2

Odstupanja od norme: -

Figure 4.32 – Results of testing the granulometric composition of the beach material sample K1 – Kašjuni beach (Split)

Figure 4.33 – Collected sample of beach material K1 - Kašjuni beach (Split)

The granulometric composition of the Sample K2 (Figure 4.34) is shown in Figure 4.33. According to the results of the test, **the mean grain size D_{50} is 18.5 mm**, while the coefficient of uniformity $C_u=D_{60}/D_{10}$=2,9.

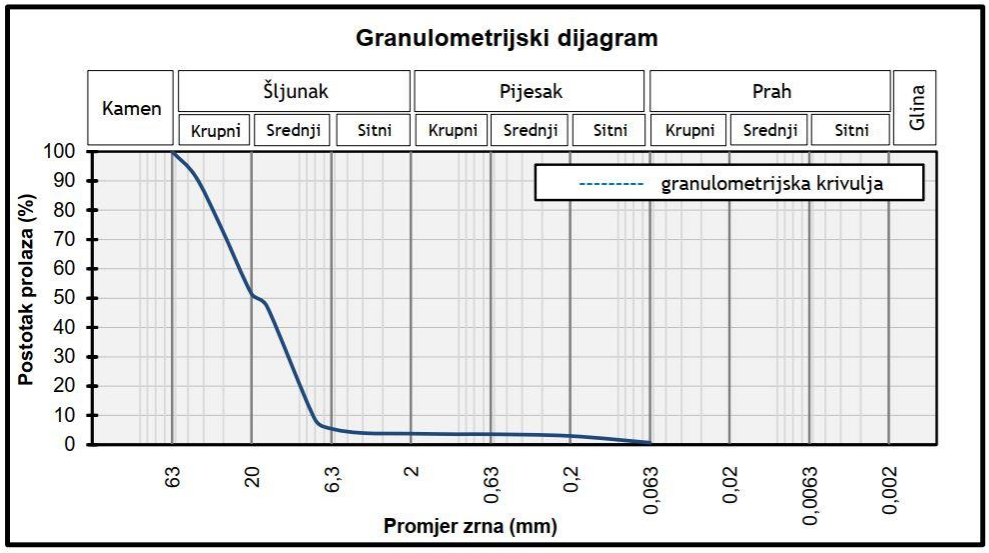

Prosijavanje	
Otvor sita (mm)	**Prolaz kroz sito** (%)
63	100,0
45	91,6
31,5	74,9
20	51,5
16	47,2
8	8,7
6,3	5,5
4	4,0
2	3,8
1	3,6
0,63	3,6
0,2	3,0
0,063	0,7

Areometriranje	
d_i (mm)	K (%)
0,02	-
0,0063	-
0,002	-
ρ_s (Mg/m^3)	
-	

UDIO FRAKCIJA (%)			
Krupnozrne		*Sitnozrne*	
Šljunak	**Pijesak**	**Prah**	**Glina**
96	3	-	-

d_i - *ekvivalentni promjer čestica*
K - *udio čestica manjih od* d_i

ρ_s - *gustoća areometriranih čestica prema HRN EN ISO 17892-3:2016*

DODATNI PODACI (*nisu u području akreditacije*)

Promjer najvećeg zrna, D_{max} (mm)	60
Promjer zrna s prolazom 60%, D_{60} (mm)	23,6
Promjer zrna s prolazom 30%, D_{30} (mm)	11,7
Promjer zrna s prolazom 10%, D_{10} (mm)	8,2

Napomena: Promjer zrna s prolazom 50%, D_{50} = 18,5 mm

Koeficijent uniformnosti: $C_u = D_{60} / D_{10}$	2,9

Koeficijent zakrivljenosti: $C_c = D_{30}^2 / (D_{60} \times D_{10})$	0,7

Odstupanja od norme: -

Figure 4.34 – Results of testing of granulometric composition of a sample of beach material K2 – Kašjuni beach (Split)

European Regional Development Fund

Figure 4.35 – Collected sample of beach material K2 - Kašjuni beach (Split)

4.2. Conclusion on testing the granulometric composition of beaches

The examination showed that all the beaches in question are made of granular material and according to the classification (Reeve, Chadwick and Fleming, 2004) belong to pebble beaches, where the grain size is predominantly more than 2 mm.

The aim of the tests carried out on the existing granulometric composition of the beaches in question was to determine the basic indicators based on which it is possible to give an assessment of hydraulic and hydrodynamic parameters that affect physical processes of crucial importance for morphological and erosive changes taking place on them. As the most important indicator, the average sizes of stone grains are determined D_{50} for each of the beaches, based on which the type of mechanism (modality) of sediment transport on each beach can be estimated, and quantitative calculation of sediment transport potential and calculation of the stable composition of beach material with which the nourishment of individual beaches should be carried out.

Also, granulometric testing determined 10% cumulative passages on the sieve D_{10}, based on which it is possible to define the degree of permeability (porosity) of beach material K (section 5.3), which is a parameter of particular importance in the analysis of the graduation of beach material (Table 4.2) and the intensity of wave energy absorption by infiltration. Beaches with well-graded materials have lower porosity and less absorb wave energy by infiltrating the sea than those with less graded materials that better absorb wave energy by infiltration. If the material is labeled as uniformly graded, then the porosity, i.e., its degree of absorption of wave energy, increases proportionally with the size of the material.

Table 4.2 – Classification of coarse-grained materials by graduation

GRADUATION	C_u	C_c
Good	> 15	1 do 3
Mean	6 do 15	< 1
Weak	3 do 6	< 1
Uniformly	< 3	< 1
Discontinued	> 15	< 0,5

In conclusion, based on the results of laboratory tests and granulometric analysis, it can be concluded that the sampled beach materials, collected at five locations in question, are predominantly uniform to weakly graded gravel, with the parameters expressed in Table 4.3.

Table 4.3 – Recapitulation of beach material test results

Uzorak	Description of materials	C_u	C_c	D_{50}
Zlatni rat beach (Brač)				
B1	Uniformly graded gravel	2,6	1,2	2,7
B2	Uniformly graded gravel	1,6	1,0	5,6
Beach Stiniva (Vis)				
S1	Uniformly graduated sandy gravel	1,8	1,1	22,3
S2	Uniformly graded gravel	1,9	0,9	13,7
Beach Podgora				
M1	Weakly graduated gravel	4,6	1,7	11,7
M2	Uniformly graded gravel	2,9	1,0	14,4
Beach Podstrana				
P1	Weakly graduated gravel	3,8	1,2	14,6
P2	Medium graduated gravel	6,2	1,9	22,9
Kašjuni Beach (Split)				
K1	Uniformly graded gravel	1,8	1,1	22,3
K2	Uniformly graded gravel	1,9	0,9	13,7

5. PROCESSES AFFECTING BEACHES AND THE BASICS OF BEACH PROTECTION

Beaches are areas at the borders of land and sea that, in terms of considering this study, are built of sedimentary granular material. These contact spaces are influenced by numerous natural physical processes, many of which are erosive in character, and can come from land and/or from the sea. As the most dominant influential processes for beaches in the Croatian part of the Adriatic Sea in general, which have the greatest erosive impact are surface sea waves.

Sea waves are a process of periodic wavering of the physical surface of the sea, which is reflected in the oscillation of water particles under the action of excitating and soothing forces. The excitating forces are pulsating and often random in nature, such as the wind blowing force which is the primary excitation force of windy sea waves. In general, surface sea waves can be classified according to Figure 5.1.

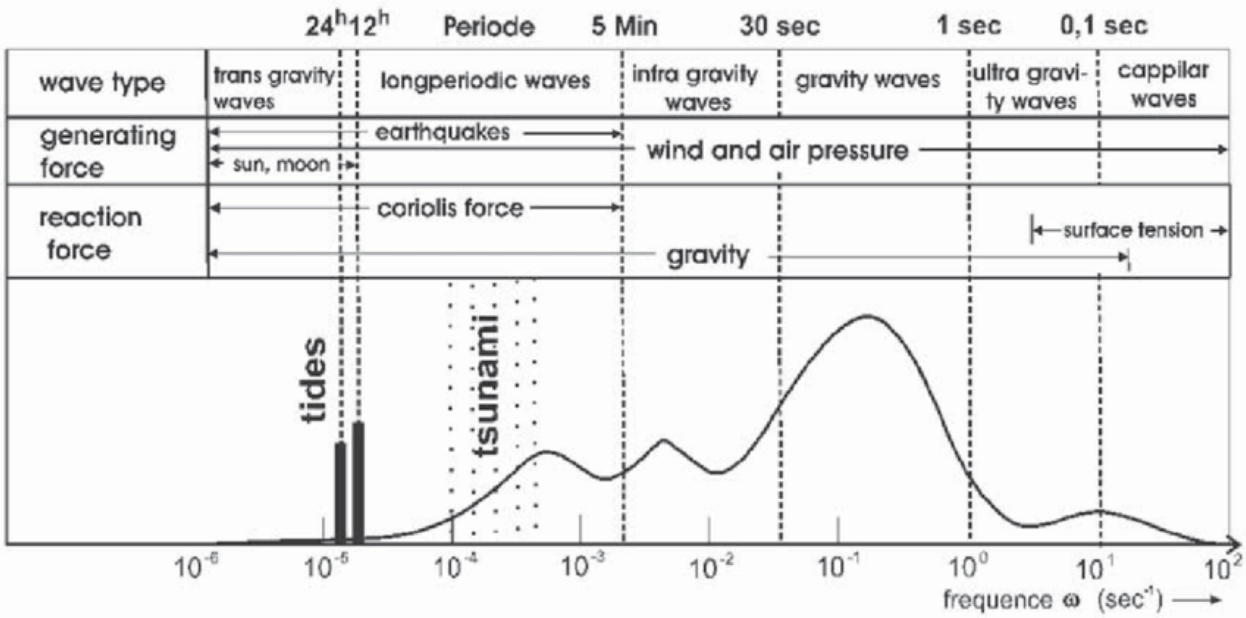

Figure 5.1 – Classification of surface sea waves

As already mentioned, sea wind waves are the primary driving force for increasingly significant processes occurring on beaches. They form them, shape them, cause erosion of beach material on their surfaces and contribute to the fact that the beaches are under constant dynamic influences that cause spatial displacement and shaping of beach material and thus constantly affect their morphology.

In order to understand the physical processes caused by real sea waves on the beach, it is necessary to understand the basic principles of wave theory describing the so-called ideal waves (linear wave theory).

5.1. Basic wave processes

5.1.1. Fundaments of (linear) wave theory

The ideal wave is a very restrictive physical or mathematical model of the real wave, and the restrictiveness is reflected in the fact that it is an ideal wave relative to the real wave of two-dimensional, monochromatic, simple and constant heights. Ideal waves can primarily be divided into waves of short periods, such as wind waves and waves of long periods, such as tides. The characteristic of short waves is

that they have a movement mainly of the surface layer of the sea, while the deep layers are significantly less or not moving at all. In waves of long periods, movements affect the entire sea mass in depth.

Elementary particles of water in a wave move in circular or elliptical trajectories, depending on the depth in which they are located. When the wave length ratio (*d/L*) is greater than 0.5, then it is a circular trajectory, and as the wave encounters a shallower sea, the trajectories turn elliptical. These elliptical trajectories in a very shallow sea become so "flattened", that almost only horizontal motions occur (Figure 5.2).

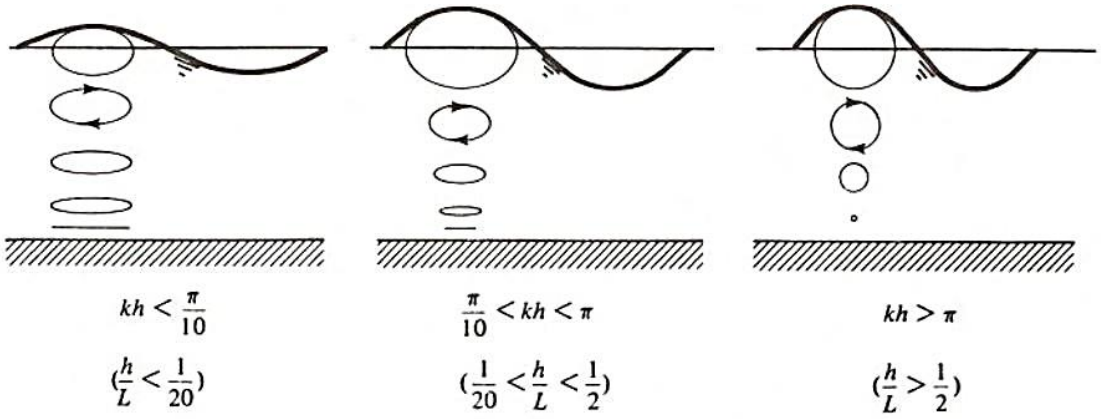

Figure 5.2 – Paths of water particles at waves with respect to sea depth (Dean R.G., Dalrymple R.A., 2007)

Only ideal waves can be fully described in a deterministic way, through the laws of wave mechanics, where it is necessary to determine the shape of the physical surface of the sea or the wave profile, and the way particles move below the wave profile.

The most basic parameters for describing the wave profile are the height *of H* (m), length *L* (m) and period *T* (s) wave. Wave amplitude *a* = *H/2* (m) is the maximum displacement of the physical surface of a sea or wave profile from the mean wave. The wave period is the time between two consecutive passes of a wave ridge through the same point. Wave height and length are depth-dependent parameters, while the wave period does not change with respect to the depth of the sea. Wave stride is the ratio of wavelength and altitude (*H/L*). The wave propagation rate is *c* = *L/T* (m/s).

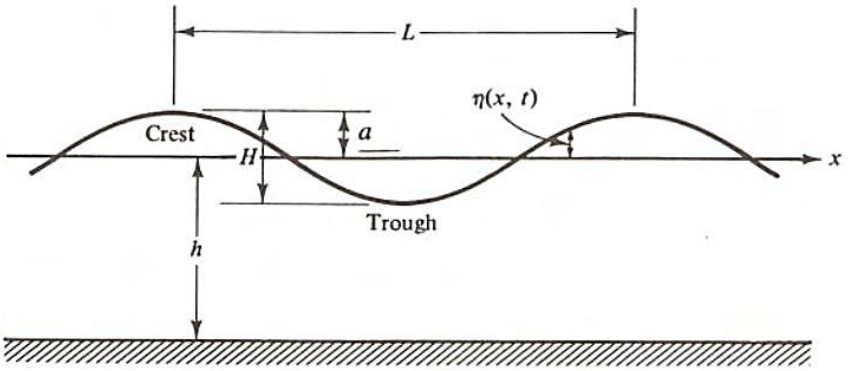

Figure 5.3 – Basic parameters for the definition of ideal wave and parameters (Dean R.G., Dalrymple R.A., 2007)

The equation of the height position of the wave traveling from left to right relative to the mean sea level has a positive sign and depends on the distance in the direction of propagation of the wave *x* and time *t*. If the wave direction is opposite, the sign is negative:

$$\eta = a\cos(kx - \omega t) = \frac{H}{2}\cos\left(\frac{2\pi\, x}{L} - \frac{2\pi\, t}{T}\right)$$

where:

a – wave amplitude (m),
k - wave number (rad/m),
ω - wave angular frequency (rad/s).
H - wave height (m),
L – wave length (m),
T - wave period (s).

5.1.2. Wave shoaling and refraction

The total energy transmitted by the wave is formed by potential energy as a result of the vertical rise of the sea surface and kinetic energy generated by the motion of wave particles:

$$E_{uk} = \overline{PE} + \overline{KE} = \frac{1}{8}\rho g H^2$$

As the deepwater wave approaches the coast, there is an increasing impact of the bottom, manifested through changes in wave parameters and the direction of motion of wave rays. Below are described the mechanisms of wave transformations in the zone of influence of the seabed.

Shoaling is a phenomenon that occurs when a wave encounters the shore and in doing so the entire wave energy is transferred towards the shore, which means that the flow of energy is constant regardless of the distance of the wave ridge from the shore:

$$EC_g = E\, nC = const.$$

where C_g – the velocity of a group of waves.

If the equation for wave energy is included, you get:

$$nCH^2 = n_1 C_1 H^2{}_1 = n_2 C_2 H^2{}_2 = n_0 C_0 H^2{}_0 = const.$$

from which it follows that the ratio of any two wave heights can be represented as:

$$\frac{H_2}{H_1} = \sqrt{\frac{n_1}{n_2}\frac{C_1}{C_2}}$$

In general, using wave height in deep sea H_0 it is possible to obtain wave height H at any depth:

$$\frac{H}{H_0} = \sqrt{\frac{n_0}{n}\frac{C_0}{C}} = \sqrt{\frac{1}{2}\frac{1}{n}\frac{1}{\mathrm{tg\,h}(kd)}} = \frac{H}{H_0{}'} = K_S$$

where K_S - the interference coefficient that in the deep sea is 1.0, and with depth it decreases to a value of 0.91, after which it rises to infinity as the depth of the sea goes towards zero.

Refraction occurs when waves meet in the zone of shallower sea where depths become less than half of the wavelength ($L/2$), that is, when waves begin to "feel" the bottom. Outside that zone, the wavefronts are relatively flat and regular. Entering the shallower zone, the structures of particle trajectories along the depth elongate (fig. 5.4), the wave velocity decreases, and the wavefronts begin to rotate. Part of the

wave front closer to the shallower sea experiences a greater loss of wave velocity and rotates more towards the shallows. In general, the wave tends to rotate to such an extent that its front becomes parallel to the contour of the bottom.

Provided that the law of conservation between rays of mutual distance *b* applies, the following follows:

$$nCH^2b = n_1C_1H^2{}_1b_1 = n_2C_2H^2{}_2b_2 = n_0C_0H^2{}_0b_2 = const.$$

from which the ratio of any two wave heights can be shown as:

$$\frac{H_2}{H_1} = \sqrt{\frac{n_1}{n_2}\frac{C_1}{C_2}}\sqrt{\frac{b_1}{b_2}}$$

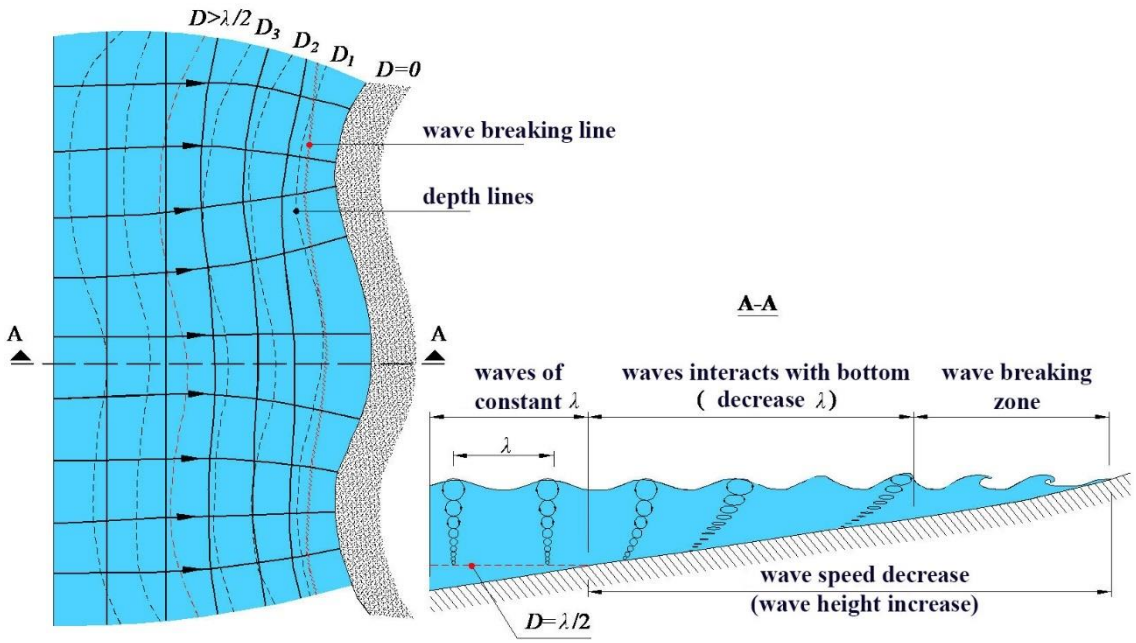

Figure 5.4 – Refractive process (Pernat Z., Vranješ M., 2012)

In general, using wave height in deep sea H_0 it is possible to obtain wave height *H* at any depth:

$$\frac{H}{H_0} = \sqrt{\frac{n_0}{n}\frac{C_0}{C}}\sqrt{\frac{b_1}{b_2}} = \sqrt{\frac{1}{2}\frac{1}{n}\frac{1}{\text{tg h}(kd)}}\sqrt{\frac{b_0}{b}} = K_S \cdot K_R$$

The wave propagation equation reads:

$$\frac{\partial}{\partial x}(k\ sin\alpha) - \frac{\partial}{\partial y}(k\ cos\alpha) = 0$$

and since for a coast that is placed perpendicular to the x axis there is no change in the y direction, it follows:

$$k\ sin\alpha = const.$$

Considering that the wave period is constant, it follows Snell's law of wave breaking:

$$k\ sin\alpha = \frac{sin\alpha}{C} = konst.$$

using which the angles of encountering the wave are calculated:

$$\frac{sin\alpha}{sin\alpha_0} = \frac{C}{C_0} = tanh\frac{2\pi d}{L}$$

Given that each wave beam is refracted according to the same law, the distance of the air in the direction of providing the coast remains constant:

$$\frac{b}{cos\alpha} = const.$$

$$\sqrt{\frac{b_1}{b_2}} = \sqrt{\frac{cos\alpha_1}{cos\alpha_2}}$$

where *is the* K_r refractive coefficient

$$K_R = \sqrt{\frac{b_0}{b}} = \sqrt{\frac{cos\alpha_0}{cos\alpha}}$$

5.1.3. Wave diffraction

When waves in their propagation encounter an obstacle, such as a breakwater or a protective groyne of a beach, they begin to turn around that obstacle, that is, their fronts begin to rotate around it. When turning around the obstacle, in addition to the transfer of energy in the direction of wave propagation, there is a transfer of energy and perpendicular to the direction of the wave (along the wave front). This process is known as wave diffraction.

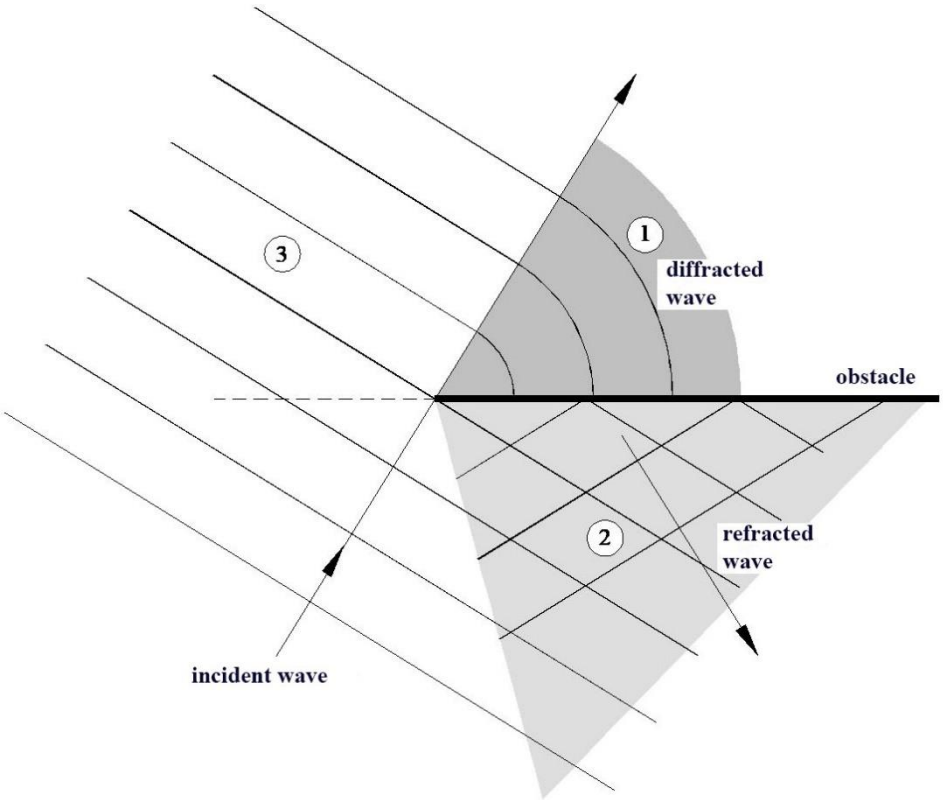

Figure 5.5 – Diffraction process (Pernat Z., Vranješ M., 2012)

Although in nature it mainly takes place simultaneously with refraction, for the purpose of consideration it is taken that there is no change in depth, so refraction is not present. The case of pure diffraction is shown in Figure 5.5, where incoming deepwater waves encounter an obstacle at the top that is the dividing area of shadow and zone of undisturbed incoming waves. Wave beams are swayed and directed towards the shadow zone, where energy transfer occurs. So, according to this, three characteristic zones occur (Figure 5.5):

1. "shadow" zone, in which diffraction occurs
2. zone in which incident and reflected waves interacts
3. zone of undisturbed incident waves.

The diffraction coefficient K_D is obtained from the nomogram, and multiplied by the wave height of the incident wave results in the wave height in the shadow zone:

$$K_D = \frac{H}{H_S}$$

The calculation of wave height due to the simultaneous action of interference, refraction and diffraction can be carried out according to:

$$\frac{H}{H_0} = K_S \cdot K_R \cdot K_D$$

5.1.4. Wave reflection

When a wave encounters an impermeable vertical barrier, a total reflection of the total energy of the incident wave occurs, which after reflection superimposes (adds up) with the energy of the incident wave, forming a complete standing wave characterized by a maximum height in the amount of double the wave height of the incident wave 2*Hi*.

The *Cr* reflection coefficient can range from zero to one and represents the proportion of the total amount of energy of the incoming wave reflected from the structure, the reflected wave of which is superimposed with the incoming wave, and the wave load on the structure increases:

$$C_R = \frac{H_R}{H_I}$$

where:

H_R - height of the reflected wave (m),

H_I - the height of the incident wave (m).

Due to their natural position and materials, beaches are very good energy dissipators of the incident wave, so they have very low values of reflection coefficient. For variable parameters of incident waves, the beach changes the geometry and reflection coefficient.

5.1.5. Wave breaking

Wave breaking occurs when the wave steepness, i.e. the wavelength-to-wavelength ratio (*H/L*), is exceeded. According to Galvin, there are four types of wave breaking (Figure 5.6):

1. overflow at a very slight slope of the bottom (transferred fracture),
2. fracture by pushing with a covered air bubble at a steep slope of the bottom,
3. the decaying fracture as a transitional form and a breakthrough wave,
4. rise at a very steep slope.

When a wave break will occur depends on the criterion of maximum wave steepness:

- for the deep sea: $\left(\frac{H_0}{L_0}\right)_{max} = \frac{1}{7} = 0{,}142$

- for shallow sea: $\left(\frac{H}{L}\right)_{max} = \frac{1}{7}\frac{2\pi d}{L}$

- Miche's general expression: $\left(\frac{H}{L}\right)_{max} = \frac{1}{7} tgh\left(\frac{2\pi d}{L}\right)$

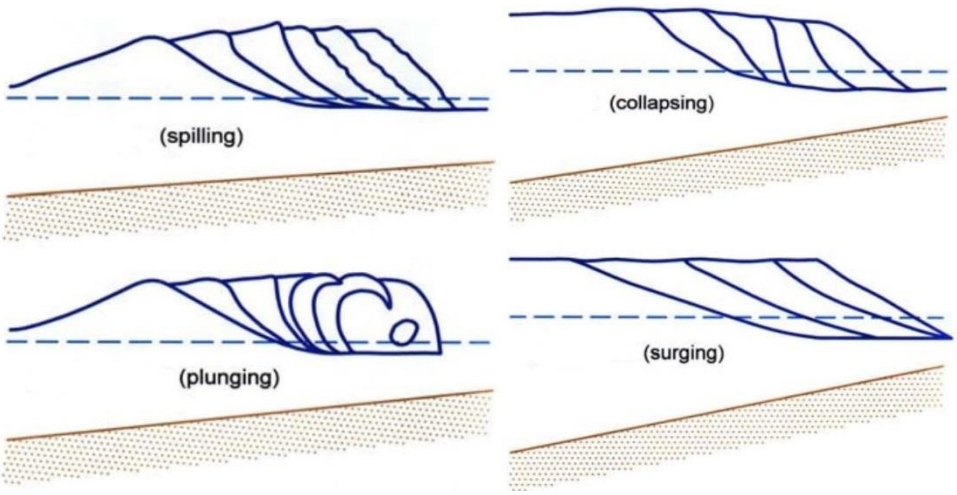

Figure 5.6 – Wave breaking types according to Galvin (Pršić M., 2008)

5.2. Sediment transport

Wave breaking near the coast contributes to various combinations of horizontal and vertical motions, which cause the transport of beach sediments. Sometimes this transport results only in the local rhythmic movement of grained material from one position to another, and such transport does not pose a greater threat to beach erosion. On the other hand, excessive transport of materials is possible, whereby beach material is continuously lost permanently, as a result of which there is a significant erosion of the beach over a longer period.

In order to determine the potential of erosion hazard caused by the transport of sediments to the beach in question, it is necessary to carry out the procedure of estimating the rate of sediment transport – a process that primarily takes place within the wave breaking zone. This is the most important physical process that affects the morphology of beaches from granular materials, and determines whether the beach will erode, whether material accumulates on it or remains stable over a long period of time (Reeve, Chadwick and Fleming, 2004).

Waves that act on the beaches, daily and even multiple times in one day, change directions and intensities. If this process is observed over a longer period, it is possible to predict the resulting vector of transport of sediments, based on the frequency of the appearance of waves from a particular direction. If, over a longer observed period, it is determined that waves from one direction are more frequent and more intense than waves from other directions, it can be determined with very high certainty the direction of the resulting vector in which sediment transport and beach erosion will occur during this period. In contrast, if it is found that there is a tendency to balance the appearance of waves from different directions over a longer period, it may indicate that the considered beach is in a state of natural balance, which contributes to its stability in terms of erosion of beach material over time.

If a high rate of sediment transport is detected on the beach, in order to ensure its sustainability, it is necessary to ensure the stability of the beach material, i.e., prevent its gradual degradation over a longer period. This is achieved by employing protective coastal structures, in the form of protective groynes, underwater reefs, etc., which protect the beach from erosion due to hydrodynamic influences, and by choosing the appropriate granulometric composition of the beach material for its nourishment.

5.2.1. Types of sediment transport and types of beaches by granulometric composition

There are two basic types of sediment transport, which depend on the type or size of the material from which the beach is made. The first type is the so-called suspended transport of sediments, in which (smaller) sediment is raised from the bottom due to the action of hydrodynamic forces and transferred by liquid (sea) above the bottom. This type of sediment transport is characteristic for beaches built of finer grains, like sands. The second type is the transport of sediments that takes place by rolling or pushing sediments along the bottom, when the natural resistance of the grain of the material at the bottom is exceeded, that is, the critical shear force.

In order to be able to distinguish which process of transporting sediments will be dominant on the considered beach, it is necessary to know the composition of the beach, that is, the range of grain sizes or the granulometric curve of the material. It is common for beach material to consist of a certain range of grain sizes, which is expressed by the medium size of D_{50} stone grain. D_{50} represents the diameter of the grain for which there is 50 percent of the grain of less, or larger, mass.

Depending on the granulometric composition, beaches made of granular materials can be classified as (Reeve, Chadwick and Fleming, 2004):

1. Sand: grain size 0.0625 to 2 mm
2. Gravel: grain size greater than 2 mm
3. Mixed.

The characteristic profile of a pebble and mixed pebble-sandy beach is shown in Figure 5.7, together with the average granulometric composition of the materials of such beaches.

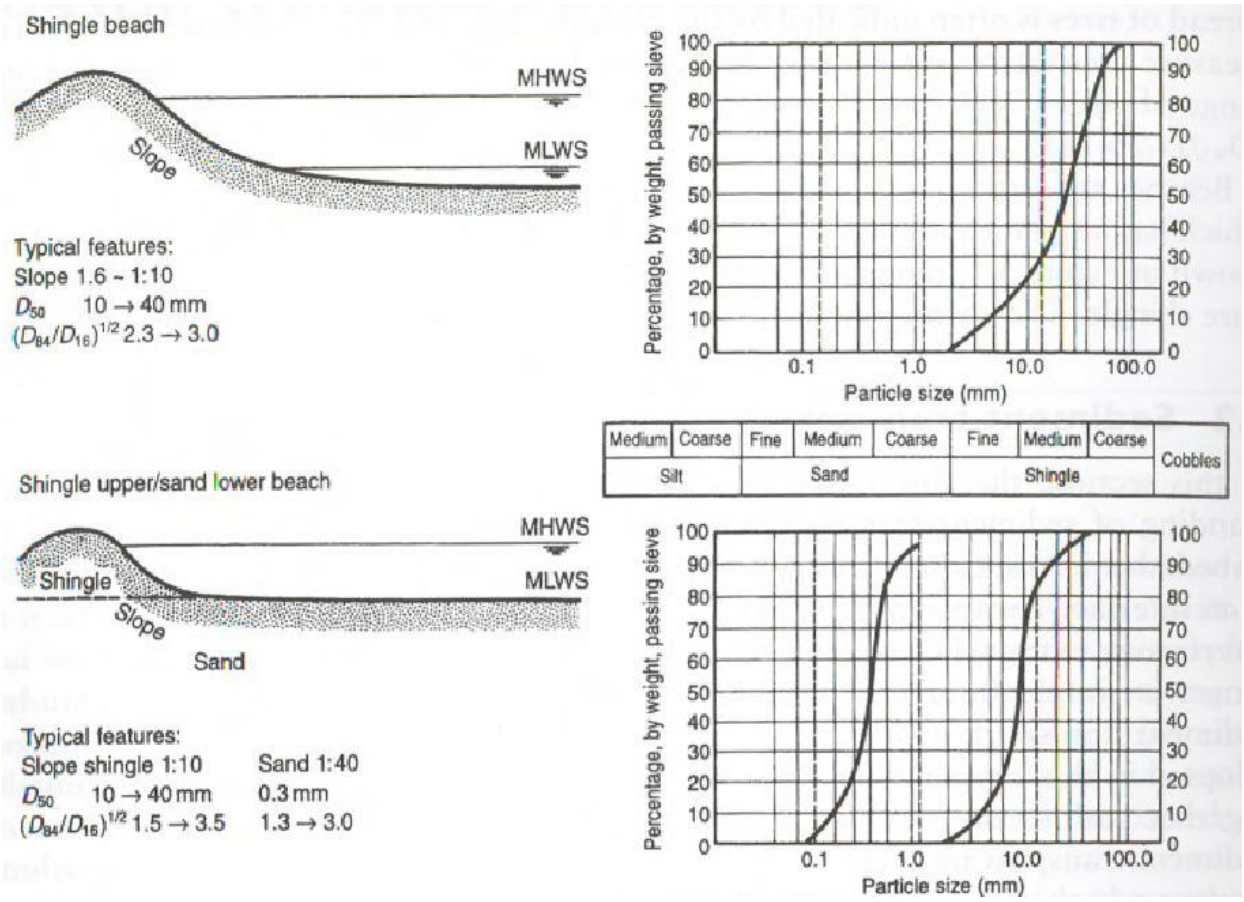

Figure 5.7 Characteristic profiles and granulometric composition of pebble and pebble-sandy beaches (Reeve, Chadwick and Fleming, 2004)

5.2.2. Calculation of sediment transport potential

In order to calculate the potential of sediment transport for a particular point on the considered beach, it is necessary to know the wave height parameter *Hs* at that point, which indicates the potential amount of energy that waves bring to the shore (Pernat Ž., Vranješ M, 2012). Furthermore, the wave power parameter, i.e., wave energy flow P_l, is also important, which serves to estimate the size of the potential transport of beach material due to wave-induced currents. As the dominant currents due to waves and the greatest transmission of beach material occur in the wave breaking zone, it is of particular interest to observe the above parameters precisely in this area.

The wave height *Hs* at the breaking point of the wave is directly related to the power of the wave:

$$P_l = \frac{\rho g}{16} H_{sb}^2 C_{gb} sin2\alpha_b$$

where C_{gb} is the local group wave velocity, α_b the angle between the wave direction and the direction of the bottom slope at the breaking point of the wave.

Based on the data on the power of the P_l wave, it is possible to determine the amount of its potential volumetric transport Q_l for a certain granulometric composition of the beach material:

$$Q_l = \frac{K}{(\rho_s - \rho)g(1-n)} P_l$$

where *K* is the dimensionless empirical coefficient dependent on the granulometric composition of the beach material, *n*=0.4, *ρs* is the spatial density of beach sediment, and ρ_s is the spatial density of the sea.

In order to obtain all the necessary data for the calculation of volumetric transport, it is necessary to carry out numerical wave modeling, and for the considered points to read the required parameters from the modeling results.

The calculation of sediment transport potential for all five locations of the beaches in question is given in chapter 7.1 of this study.

5.2.3. Calculation of stable composition of beach material

As already stated, the dominant physical process that contributes to the beach material transport is the action of waves, especially in the wave breaking zone. For gravel beaches, which are the subject of the analysis of this study, the transport of beach material that takes place by rolling and/or pushing along the bottom is dominant, and the transport of particles in suspended fluid is less present. The transport of materials by rolling and/or pushing occurs when the so-called moving threshold, which represents the natural resistance of the material, i.e., the grain of the beach material at the bottom, is exceeded, whereby the shear force τ_0 occurs, which is equivalent to the force acting on the exposed grain surface (Figure 5.8). This force is also called the critical shear force τ_{cr}.

Waves create a turbulent flow as a result of which vortexes are created, while at the level of the grains of the beach material there is still a small zone (layer) within which the stationary flow takes place. However, it is very unstable because vortices of turbulent flow occasionally penetrate it and disrupt its stability. The difference in moments between these two layers creates shear forces that create new additional vortices. Therefore, the grains of the beach material are subjected to a fluctuating impulse force and when this force is large enough to move the grain, the rolling process occurs. As this process expands, it becomes more complex, as moving grains hit each other. By increasing the shear stress, the process of moving the grain penetrates the deeper layers of the beach's bulk material. To simplify this complex process, it can be approximated as a series of grain layers sliding relative to each other, with a linear velocity distribution (Figure 5.9).

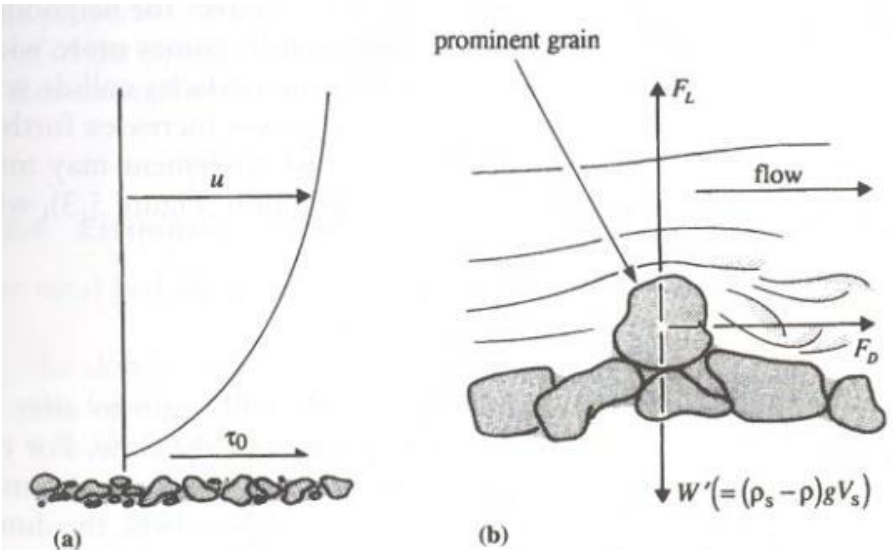

Figure 5.8 - The forces of the fluid that cause the material to move (a) the shear force to the granular bottom; (b) force on a single grain (Reeve, Chadwick and Fleming, 2004)

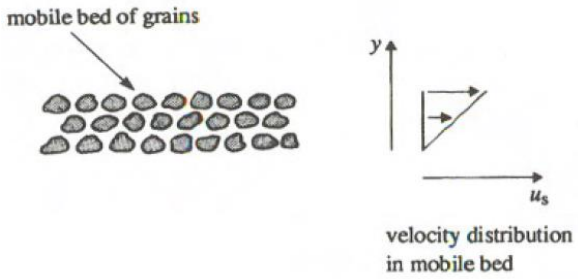

Figure 5.9 – Simplified representation of grain layers of beach material (Reeve, Chadwick and Fleming, 2004)

Under the action of waves, the velocity at the bottom varies in size and direction, and therefore a very small oscillatory boundary layer occurs (several mm to several cm thick). The result is the occurrence of shear stress at the bottom of a much larger amount than that occurring under the stationary flow of an equivalent flow rate.

Striking strain on the bottom can be expressed as:

$$\tau_{ws} = 0{,}5 \cdot \rho \cdot f_w \cdot u_d^2$$

where *the* u_d is the bottom orbital wave velocity and *fw* is the friction factor. For group turbulent streaming applies (Soulsby, 1997):

$$f_{wr} = 1{,}39 \cdot \left(\frac{a}{z_0}\right)^{-0{,}52}$$

where:

$a = u_d \cdot \frac{T}{2\pi}$ – wave amplitude

$z_0 = \frac{k_s}{30}$

$k_s = 2{,}5 \cdot D_{50}$

A good indicator of the relationship of shear force to gravitational forces is the so-called Shield parameter, which for the boundary conditions of the grain displacement becomes a "critical" Shield parameter:

$$\theta_{cr} = \frac{\tau_{cr}}{(\rho_s - \rho) \cdot gD_{50}}$$

or:

$$\theta_{cr} = \frac{0{,}3}{(1 + 1{,}2D^*)} + 0{,}055 \cdot [1 - \exp(-0{,}02D^*)]$$

where ρ_s is the density of stone material beach embankment, ρ density of the sea, and

$$D^* = \left[\frac{g \cdot (s-1)}{\nu^2}\right]^{\frac{1}{3}} \cdot D_{50}$$

$$s = \frac{\rho_s}{\rho}$$

$\nu = \frac{\mu}{\rho}$ – sea kinematic viscosity.

For the action of waves, the following relation applies:

$$\theta_{ws} = \frac{\tau_{ws}}{(\rho_s - \rho) \cdot gD_{50}}$$

The size of the transport of beach material can be expressed by the dimensionless demersal transport factor (Soulsby, 1997):

$$\emptyset = 5{,}1 \cdot (\theta_{ws} - \theta_{cr})^{\frac{3}{2}}$$

If this dimensionless factor is zero, then there is no possibility of displacement or transport of sedimentary beach material. Given that this factor depends, among other things, on the middle diameter of the grain of beach material D_{50}, it can be determined based on the size of the beach material (D_{50}), which will be stable in the conditions of detected demersal orbital wave velocities u_d.

Determination of granulometric composition for all five locations of the beaches in question is given in Chapter 4, and the calculation of stable beach material in Chapter 7.2 of this study.

5.3. Influence of the composition of the beach

When considering the impact of the composition of the beach on the basic processes that occur on them, the determination of the type of beach material from which a particular beach is made is crucial. As already stated, the basic division of beaches made of granular materials is into: sandy, gravel and mixed. The division depends on the granulometric composition of the beach material, that is, on the grain size in this material (section 5.2.1).

In specific cases, five pilot locations, i.e., beaches in Split-Dalmatia County, which are the subject of analysis in this study, these are gravel beaches, which is confirmed by granulometric tests of existing beach material (chapter 4).

In addition to the modality of transport of beach sediments that occurs due to the action of waves (section 5.2.2), the composition of beach material also affects some other significant physical processes that take place on beaches.

One of the most important such physical processes are morphological changes in granular beaches, which occur primarily due to the action of waves, and depend on the composition of the beach, i.e., on its degree of permeability (Jamal M.H., 2011). The degree of permeability *K*, is also known as hydraulic conductivity, which is a measure of the possibility of fluid passing through permeable material. The mean permeability level for sand is about 0.001 m/s, while for gravel it can range from 0.01 to 1.

The permeability of the material (beach) depends on the porosity, grain size and its graduation, and can be measured using piezometers in the field or calculated via Hazen's formula (Jamal M.H., 2011):

$$K = A_p \cdot D_{10}^2$$

where *K* – permeability in mm/s, *Ap* – constant (10-15 $mm^{-1}s^{-1}$) and *D10* – 10% cumulative passage on the sieve when analyzing sample material in mm.

In the analysis carried out for the five beach sites in question, the range of measured data on D_{10} beach materials ranged from 1.2 to 13.2, which means that the permeability of the beaches in question ranges from 0.014 to 1.7, corresponding to the classification of beach material and the beaches themselves as gravel.

Also, the data on the graduation of beach material is of particular importance, so beaches with well-graded materials have less porosity and less absorb wave energy by infiltrating the sea than those with poorly graded materials that better absorb wave energy by infiltration.

5.4. Impact of climate changes

5.4.1. General

Climate change[1] and its impact is difficult to assess. However, meteorological data that have been monitored since the 19th century from several stations in Croatia provide reliable documentation of long-term climate trends.

During the period 1961-2010, the trends of medium, medium minimum and mid-maximum air temperatures show warming throughout Croatia. Trends in annual air temperature are positive and statistically significant, and the changes are greater in the continental part of the country, than on the coast and in the Dalmatian interior. The greatest changes (rise) were exposed to the maximum air temperature.

During the period 1961-2010, annual amounts of total precipitation in the Republic of Croatia show the prevailing statistically insignificant trends that are positive in the eastern plains (increase) and negative in other areas of Croatia (decrease). Weak trends are noticeable in most seasons, but the exception is

[1] taken from the Seventh National Report of the Republic of Croatia under the United Nations Framework Convention on Climate Change (UNFCCC), (MZOE, 2018); The results of climate modelling on the HPC Velebit system for the purpose of drafting the Strategy for Adaptation to Climate Change of the Republic of Croatia until 2040 and with a view to 2070 and the Action Plan (Subactivity 2.2.1.), (CFCA, 2017))

summer precipitation, which has a clearly highlighted negative trend throughout the country (decrease). In the fall, there are weak mixed trends, and the increase in rainfall in the interior is mainly caused by a rise in the number of days with large daily rainfall. During the winter, precipitation trends are not significant and are mostly negative in the southern and eastern regions, and in the remaining part of the country they are of mixed omen. In the spring, the results show that there are no marked changes in the total amount of precipitation in the southern and eastern parts of the country, while a negative trend (decrease) is present in the remaining area.

5.4.2. Sea level rise

Sea level rise[2] has accelerated in recent decades. As a result of global warming, there is a decrease in snow cover, especially in spring and summer, and melting ice. There has also been a rise in global sea levels caused by melting terrestrial ice and the heat expansion of the oceans due to its heating. Global mean sea level rise is 2.9 +/- 0.4 mm/year, while the mean level of the Adriatic Sea is 2.2 +/- 0.4 mm/yr. At the tide gauge in the port of Split, the trend of mean sea level rise in the period from 1955 to 2009 was 0.59 mm/year, while the trend of mean sea level rise in the period from 1993 to 2009 is 4.15 mm/yr.

Sea levels are rising faster than IPCC estimates, and rapid sea level rise has been recorded in the last fifteen years, about 30-35 cm/100 years. The eastern coast of the Adriatic is not as endangered as some other areas in the world and the Mediterranean, but as well as on a global level, there has been an accelerated increase in the level of the Adriatic in the last 15 years, but with large interannual variations.

The current trend of absolute sea level across Europe[3] based on satellite measurements shows that in the County area there is a pronounced increase of 3 to 4 mm per year. When, in addition to the projected projections of sea level rise, the impacts of occasional extreme sea levels in the range of 0.84 m to 1.15 m are added, extreme intermittent sea levels are obtained at the end of the century in the range of about 1.4 m to 2.2 m (Draft RH Strategy for Adaptation to Climate Change). Since 1955, when measurements began at the Tideographic Station Split, in November 2019 the highest sea level of 91.1 cm above the mean sea level was measured. Given the expected trend of sea level rise, and the fact that small sea level rise increases the frequency of extreme levels, such phenomena will be more frequent, especially in the second half of this century. In the long run, sea level rise is potentially one of the most expensive effects of climate change on the entire Croatian coast.

In addition to sea level rise, sea temperature rises and increased evaporation and decrease in fresh water inflow can be expected. Projections of temperature rise for the Mediterranean for 2100 vary between +1.8°C and +3.5°C on average compared to the period between 1961 and 1990. Expected sea level rise, as well as the effects of future tides, waves and storm slowdowns will also have an impact on coastal infrastructure (ports, marinas, coasts), with cities and coastal settlements being the most at risk.

The negative impact of sea level rise and especially stormy weather is expected on sea shores, which will be exposed to increased erosion (abrasion) due to sea level rise, as well as other morphological changes in terms of changes in their geometry, which can lead to their complete disappearance.

[2] data on previous level changes must be taken from Kilić et al. (2014.)

[3] Taken from the Marine Environment and Coastal Management Plan of Split-Dalmatia County (item 3.3.4 Effects of climate change at the level of Split-Dalmatia County)

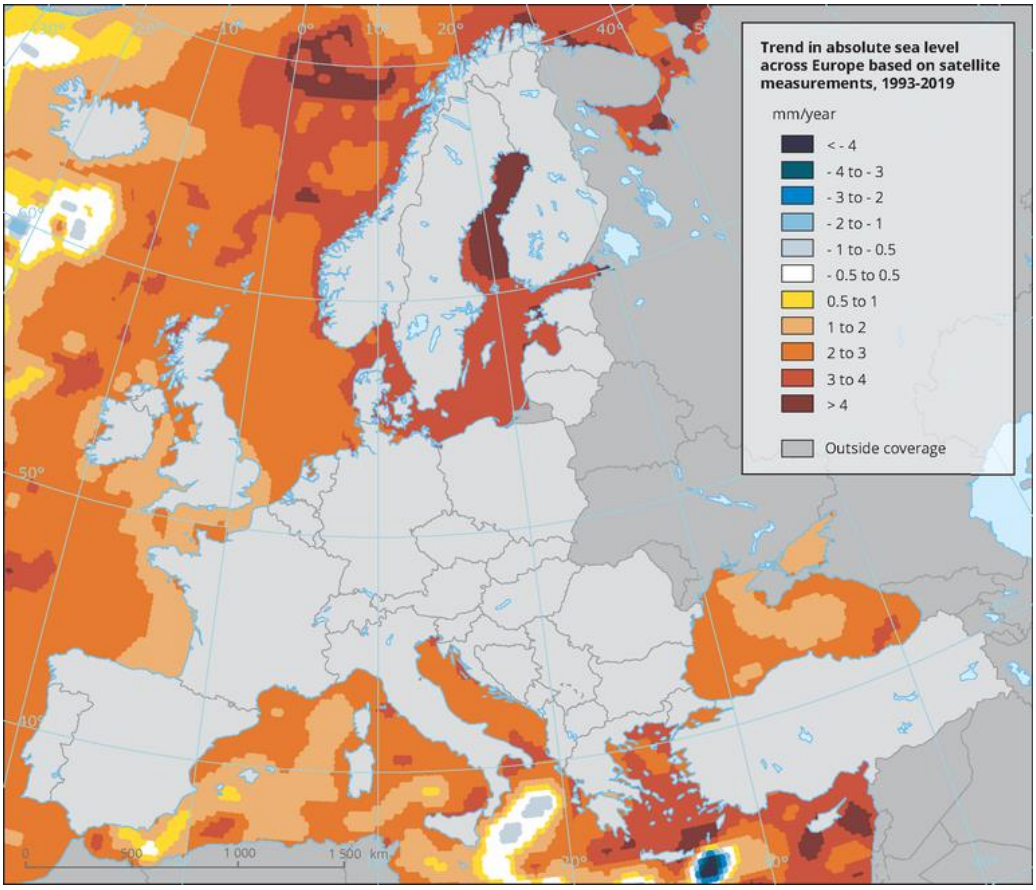

Figure 5.10 – Trends in mean sea level based on satellite measurements in 1993-2019 (*https://www.eea.europa.eu/data-and-maps/figures/trend-in-absolute-sea-level*)

5.4.3. Changes in precipitation characteristics

In addition to increasing the intensity and length of dry periods, because of climate changes, the intensity of short-term heavy rainfall is expected [4]to increase, thus increasing the risk of flash floods characterized by high water velocities that can cause great damage and erosive processes in locations where they were not previously pronounced. A milder increase in the number of days is also expected with extreme precipitation in autumn and winter in the southern regions, especially in the central and southern Adriatic. Higher volumes and irregular frequencies of increased rainfall affect existing stormwater collection and drainage infrastructure, whose capacity has been surpassed by the high rate of urbanization over the past 50 years.

5.4.4. Impact of climate changes on beaches

As already stated, the negative impacts of the consequences of climate change, especially the impact of sea level rise and the occurrence of stormy weather, will be particularly noticeable and visible on beaches, especially from granular materials (Codignotto J.O. et al, 2012). In addition to the increased erosion that will intensify due to these influences, it is expected that there are increased changes in their morphology and composition, which can lead to their complete degradation, and even complete disappearance (Bruun

[4] Taken from the Marine Environment and Coastal Management Plan of Split-Dalmatia County (item 3.3.4 Effects of climate change at the level of Split-Dalmatia County)

P., 1962, Schwartz M.L., 1967). When analyzing these potential problems in the coastal area, it is important to detect and categorize zones or beaches, given the degree of threat due to potential changes, for which it will be necessary to adopt general plans for their preservation, but also concrete technical solutions that would reduce the potential of their erosion for the current and future situation.

Given that wind surface waves are the main driving forces of changes in the morphology of beaches made of granular materials, it is necessary to know the basic principles of physical processes by which they put pressure on beaches coastal systems at their encounter in the coastal area. This issue is explained in more detail in Chapter 5.1. Furthermore, given that waves are also the main generators of sediment transport, which is the primary process that causes erosion of beaches from granular materials, chapter 5.2 describes this process.

If the conditions of the main driving forces of sediment transport and changes in the morphology of beaches change, and the increase in sea level is certainly one of the most important factors for this, then in the analysis for the assessment of the degree of beach vulnerability it is necessary to consider these changes in sea level as a result of climate changes. The general characteristics of the morphology of beaches made of granular materials, as well as the basics of their protection are given in the next chapter (chapter 5.5), while the conclusions of the analyses conducted in this study are combined through the adopted guidelines in order to reduce beach erosion due to the consequences of climate changes.

In order to provide concrete technical solutions in order to minimize these problems brought by climate changes, and primarily the problem of beach erosion from granular materials, it is necessary to apply the methodology proposed here, which includes a detailed analysis of each beach zone that is intended to be protected.

5.5. Beach morphology and basics of beach protection

On beaches made of granular materials where the process of erosion has been detected, i.e., the potential of erosion due to the incident waves, appropriate protective measures should be taken in order to prevent their complete degradation and disappearance. For this purpose, protective coastal structures are applied in the form of protective groynes, underwater reefs and tombolos, that change the wave conditions and hydrodynamic conditions in the aquatory and contribute to the general protection and preservation of the beach.

Given the significant impact these structures can have on the coastal environment, they should be only considered as the part of a holistic adaptive governance policy. Such a policy should consider the local characteristics of the location on which they are built and the potential impacts on the entire coastline. The construction of groynes, tombolos and underwater reefs can be integrated into local beach landscaping programs, complement other green measures and be part of integrated coastal area management plans (Climate-ADAPT).

Stakeholder involvement generally does not play a major role in the technical design and construction of protective coastal structures unless they are part of a broader coastal defense plan. However, these measures may raise concerns about possible environmental impacts on the marine ecosystem and visual impacts on the coastal landscape. Conflicts can arise between different groups and economic sectors: the tourism sector generally benefits from protected beaches or safer tourist berths, while local communities may be concerned about changing coastal landscapes, habitat loss and biodiversity, and environmental

impacts in general. Such conflicts require the active involvement of all stakeholders, including local authorities, coastal communities, tourism operators, research institutions and/or non-governmental organizations (Climate ADAPT).

5.5.1. Beach morphology

In coastal areas, the profile and shape of beaches made of granular materials depend on sedimentary transport processes generated by the natural forces of waves and currents, on the supply of sediments and their natural or artificial restoration, and on natural geological and artificially created coastal structures (groynes, underwater reefs, tombolos...).

Beaches made of granular materials are an important form of natural protection of the coastal area, but also significant urban areas, agricultural areas, natural habitats, recreational and ecological goods from the aggressive action of waves. Understanding the morphological behavior of beaches made of granular materials is important in response to short-term and long-term ensuring their sustainability.

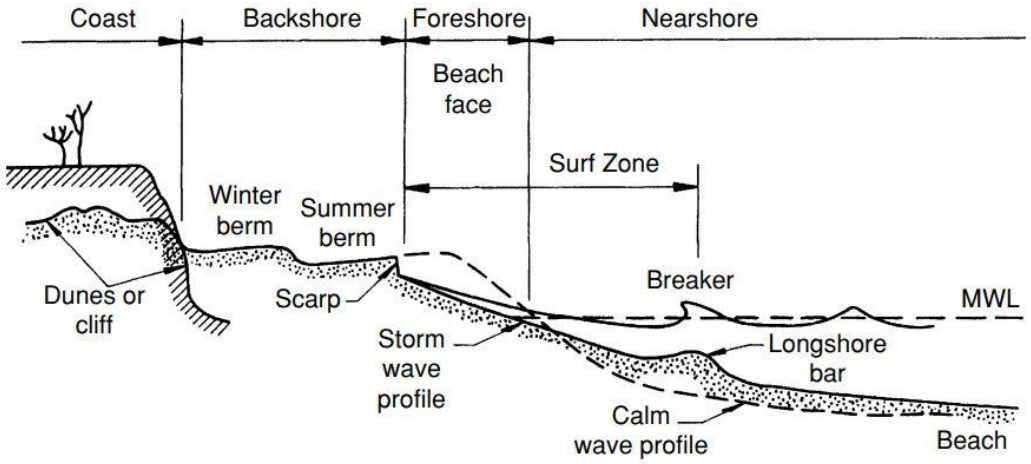

Figure 5.11 – Layout of a typical beach profile for illustration and terminology definition (Sorensen R.M., 2006)

What the typical profile of the beach made of granular material looks like is visible from the idealized characteristic cross-section in Figure 5.11. What is significant to note in the illustration above are the two characteristic profiles of beaches that occur during the two, for the beach, the most important periods of the year. These are the so-called "storm profile" of the beach, which occurs mainly during the winter months (full line), and the so-called "calm profile" of the beach, which mostly occurs during the remaining part of the year (dashed line). Namely, during a relatively long period of lower wave intensity, beach material is slowly transported to the mainland, which contributes to a steeper profile of the beach. With the appearance of larger and steeper waves, which mainly occur during the winter months, beach material is transported towards the sea, which contributes to the formation of the beach profile of a smaller slope (Sorensen R.M., 2006).

Also, the shape of the face of the beach depends on the size of the beach material from which it is made. Beaches with larger material tend to create steeper profiles, while beach profiles composed of finer material are mostly milder. This is completely noticeable in sandy beaches, which are very mild, almost horizontal slopes.

Variations in wave parameters and sea level significantly affect the profile of the beach, so the term equilibrium profile of the beach is often used in practice, as a measure of sustainability, i.e., the stability

of the beach in relation to the grain size of the beach composition. The formula based on which it is possible to obtain a beach profile in relation to the grain size of the beach material (medium diameter of grain D_{50}) reads (Dean R.G., Dalrymple R.A., 2007):

$$z = A \cdot y^{\frac{2}{3}}$$

where:

z – depth

A – experimentally obtained coefficient depending on the rate of deposition of beach material grains (from diagram, Dean R.G., Dalrymple R.A., 2007)

y – horizontal distance from the coastline (position of depth z)

The complexity of coastal processes makes it difficult to accurately predict the morphological response to changing wave conditions and sea level. In general, during wavy conditions, the stimulus of sediment transfer along the beach shore from granular materials in the wave zone, is caused by an asymmetry in the flow rate. This process contributes to changes in the volume and surfaces of the underwater and altitude of the beach, increasing the steepness of the face of the beach and raising the height of its berm.

Although steeper beaches are relatively more stable to waves, during periodic extreme storm events, larger waves degrade the face of the beach, creating significant erosion. The material accumulated in the beach's berm then acts as a source of sediment during this period, but some stronger storms can cause complete degradation of the beach, taking the material to the deeper parts of the seabed. If such events happen several times a year, the beach practically disappears in just a few years.

Due to this dynamic nature of the process on beaches made of granular materials, it is crucial to understand these physical processes, and to establish reliable techniques for forecasting and preventing adverse impacts, and ensuring the sustainability of beaches in times that bring increasingly pronounced extreme events.

5.5.2. Protective groynes

Groyne is a protective coastal structure built perpendicular to the coastline, in order to reduce the coastal transport of beach material. They are usually applied as a series of groynes that forms a system working together to protect the beach from erosion. As a building material for the construction of groynes, stone or concrete is commonly used. In Croatia, stone is predominantly used because the groynes built from it are more durable and absorb more wave energy due to their permeable nature.

Groynes "catch" the sediments of the beach moving along the coast in wave breaking zones due to the action of waves and thus protect the beach from erosion, and their effectiveness depends on the length and position (figure 5.12). If applied as independent element of protection (without underwater reef) they can cause additional problems in the form of a stronger accumulation of beach material on the mainland part of the beach, and more intensive transport of material away from the coastline to the deeper sea, especially during stormy events. Therefore, it is very important to perform an analysis of their functionality for the relevant wave conditions at the setup location.

Groyne is an active protective structure that extends from the shore into the sea, usually vertically or slightly obliquely relative to the coast. Adequate sediment supply and the existence of medium-strong coastal sediment transport are the main conditions for groyne efficiency.

Groynes partially dissipate the energy of motion of the sea during conditions of weak and moderate waves, which leads to natural nutrition and favorable shaping of the beach. However, in the case of storm waves, and especially those that come to the shore approximately vertically, the protective role of the groyne decreases and the coast is under the direct influence of waves, which contributes to increased beach erosion, especially if they are not built in a common system with submarine thresholds.

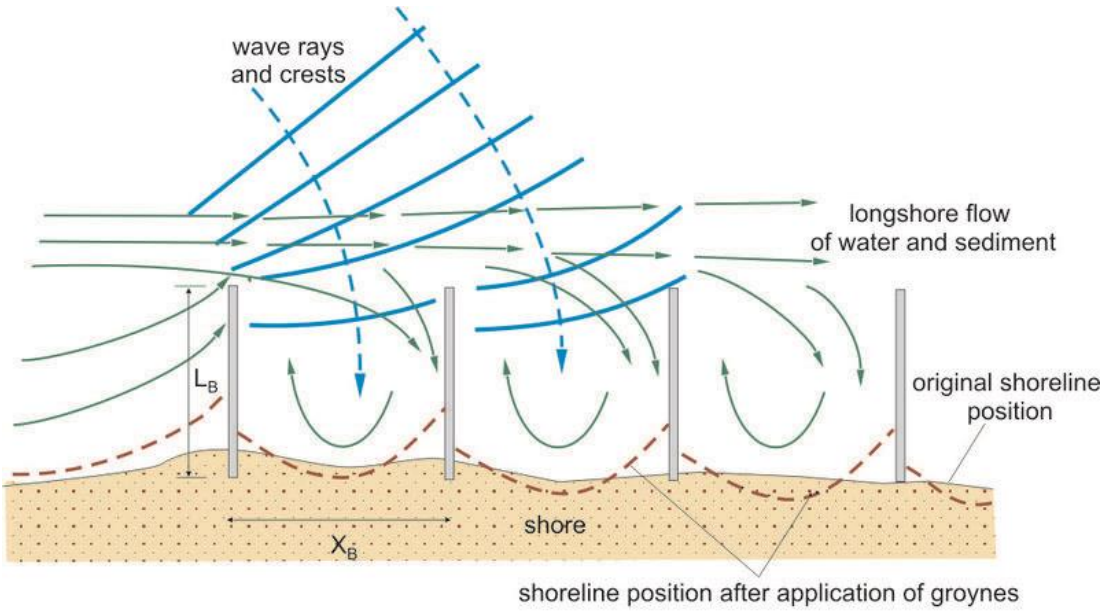

Figure 5.12 - Scheme of interaction of groynes, waves, currents and shore (Coastal Wiki)

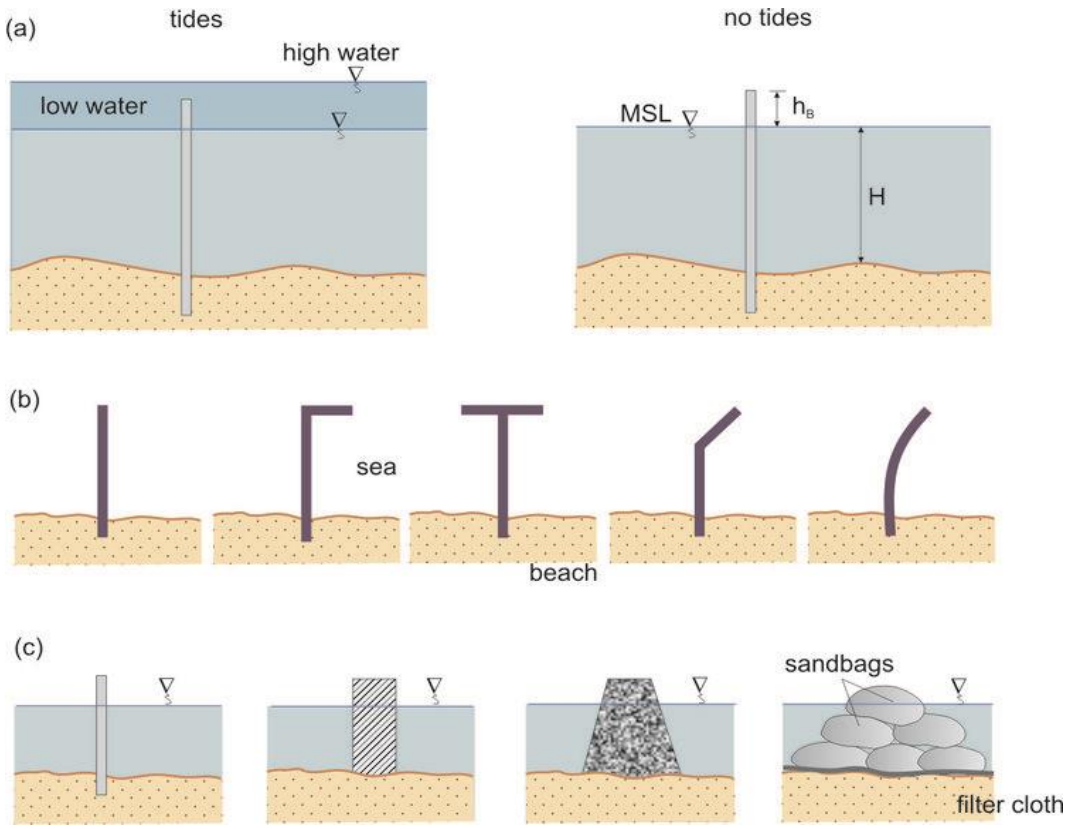

Figure 5.13 – Types and shapes of groynes (Coastal Wiki)

Because of this, groynes, which are the most widely used protective coastal structures, when applied as the only measure of coastal protection, are very often not a particularly effective solution for a long period of time. However, when groyne solutions are applied in combination with other measures to protect the coast from erosion, such as the construction of underwater reefs and proper nourishment, then their full effectiveness is demonstrated.

The design of groynes (floor plan, length, height, cross-section, slope to the shore) affects the morphology of the coast, and their effectiveness, in addition to the above geometric parameters, depends on marine levels, dominant waves and sediment stocks in the wave breaking zone.

The protection of coast with groyne is generally designed as protection with a group of groynes. The scheme of groyne interaction is shown in Figure 5.12. While one groyne causes coastal erosion on the leeward side, erosion in the case of a group of groynes is shifted to the leeward side of the entire system. Erosion also occurs in the immediate vicinity of the groyne, especially when the dominant direction of the waves is perpendicular to the shore. In the space of the sea between the groynes, compensatory and turbulent flows along the groyne occur, causing local erosion of the seabed and loss of material towards the deep sea. During severe storms with high and long waves, groynes become "too short" compared to the width of the wave breaking zone, so erosion occurs around them. In conditions of gentle waves, groynes become "long" (lengths comparable to the width of the wave breaking zone), which favors the accumulation of material towards the coast and the expansion of the beach. Therefore, when designing it is necessary to make an optimal balance between these influences and the geometry of the pen, based on the detailed analysis of the wavefield with a numerical model.

An appropriate choice of shape, dimensions and position of the groyne is essential for the effectiveness of coastal protection. The length of the groyne is usually associated with the mean width of the wave

breaking zone and the spacing along the shore in the pen field. The active length of the groyne increases with increasing the angle of encounter of the wave. Groynes are most effective if they do not trap the entire stream of sediment along the coast. Numerous studies and observations suggest that the length of the groyne towards the sea should not exceed 40-50% of the width of the storm zone of wave breaking. The effectiveness of groynes also depends on their permeability. Groynes that are structurally permeable or submerged allow greater sediment transfer along the coast.

In general, groynes are designed with an elevation around *hs* =0.5 - 1.0 m above mean sea level (SRM). Groynes that are too high cause more significant wave reflection, resulting in local erosion. Given the floor plan shape, the groynes can be flat, curved, L-shaped, T-shaped or Y-shaped. The most popular shapes and types of groynes are schematically shown in Figure 5.13.

5.5.3. Protective tombolos

Tombolo is a protective coastal structure (a type of separate breakwater) built parallel to the coastline in its vicinity, which serves to reduce the coastal transport of beach material. It primarily protects the beach by reducing the incoming wave energy lost on its hull (in the form of wave breaking), but also shapes the beach due to the waves bending around its regions, forming a recognizable shape of the double-sided beach in its leeward side (figure 5.14).

The design of tombolos, i.e., detailed selection of their length, distance from the shore, and the number and distance between individual tombolos, regulates the way of establishing the desired pattern of accumulation of beach material

The general rule of their placement says that they need to be placed at a distance depending on the position of the wave breaking zone, that is, in a zone away from the coast less than half of the dimensionless width of the wave breaking zone $x^*=x/x_{80}$ <0.5 (Figure 5.14), where x - is the distance of the tombolo from the shore, and x_{80} – the distance of the wave breaking zone (approximately 80% of coastal transport takes place in this area).

The effect of the tombolos on the formation and protection of beaches is reflected in the appearance of diffraction behind its ends, whereby the potential of material transport is reduced due to a decrease in wave energy and captures the material that forms a recognizable shape of the double-sided beach (Figure 5.15). Like protective groynes, it is also possible to apply a protective tombolo in a row, whereby the protection of a longer stretch of coast line is carried out, while the impacts on the beaches remain approximately like that of a single structure.

Given the complexity of hydrodynamic processes that occur with the introduction of these protective structures in the coastal waters, which fundamentally affect the processes by which the beach is formed, it is necessary to carry out numerical modeling within the design to achieve their optimal design.

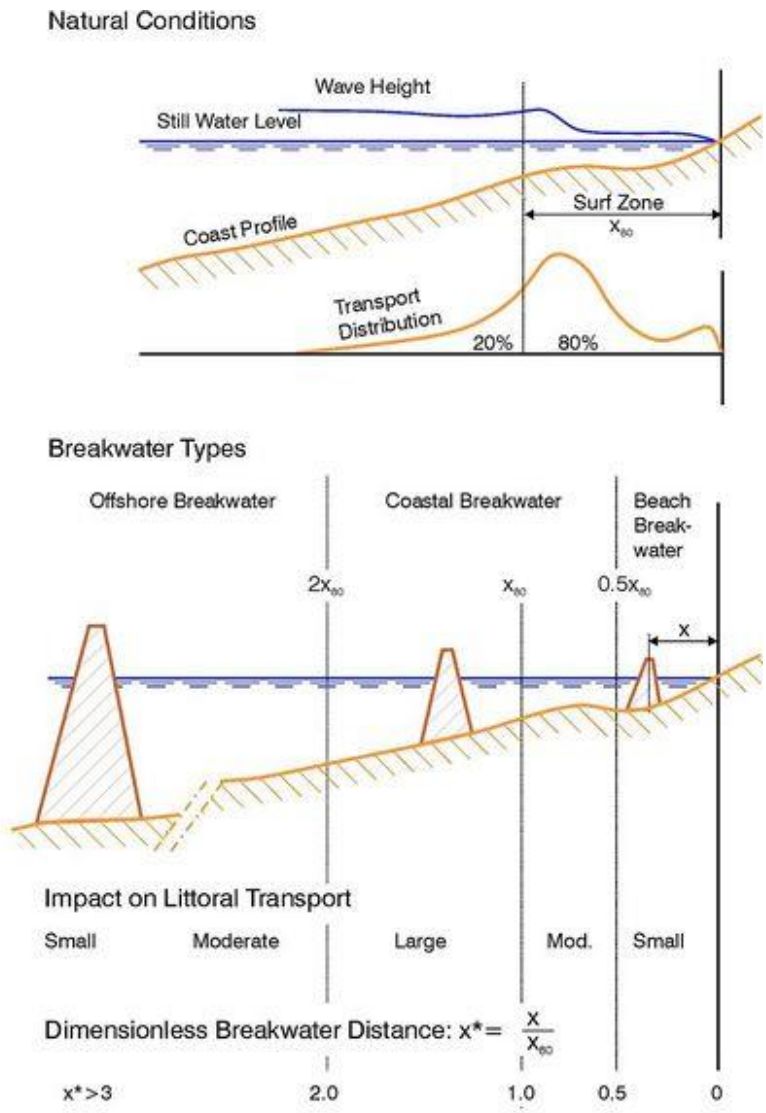

Figure 5.14 – Types of separate breakwaters (Coastal Wiki)

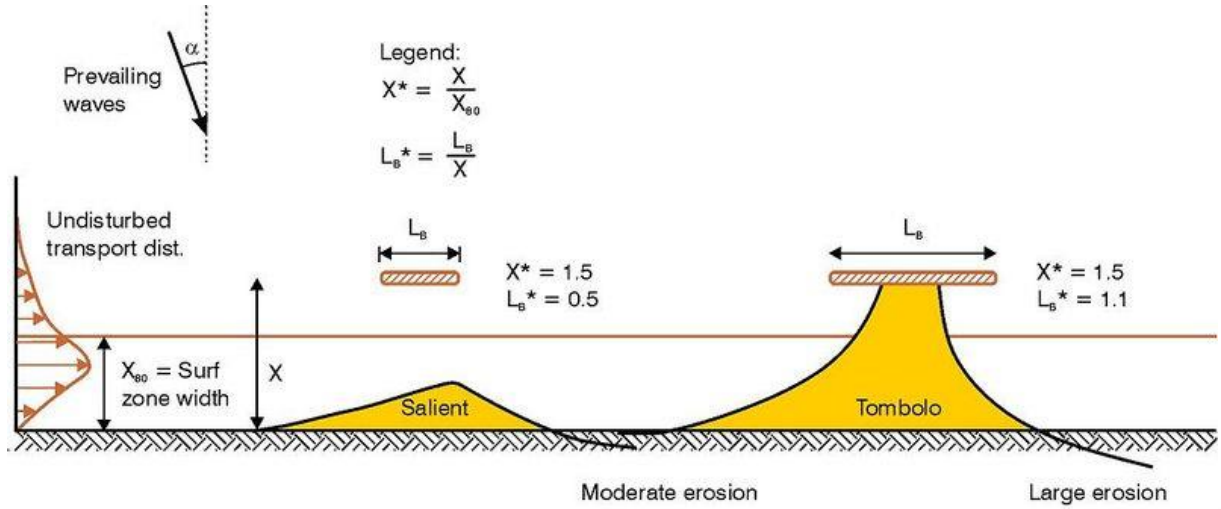

Figure 5.15 – Definition of parameters characterizing separate breakwaters (Coastal Wiki)

5.5.4. Protective underwater reefs

Underwater reefs are artificial underwater dikes made of stone, with a top below sea level (Figure 5.16). They are usually performed parallel to the coast, and are very effective in protective systems with protective groynes. They are less spatially intrusive than tombolos and (depending on orientation) can have a greater and more favorable impact on coastal processes than tombolos. Like tombolos, underwater reefs reduce wave energy (primarily by wave breaking), thus protecting the beach from erosion.

Underwater reefs function by causing wave breaking in the zone of their placement, allowing at the same time a certain transmission of waves (*Ht*), thus achieving a milder and more favorable wave image on the beach in its hinterland. The capacity of sediment transport behind the undersea threshold is significantly reduced, and by detailed analysis and selection of geometric parameters, primarily by choosing the plan position, and the width (*B*) and the height of the berm threshold (*Rc*), its effectiveness in protecting the beach is regulated in relation to preventing the material from being carried into the deeper sea and excessive pushing to land.

They are more favorable compared to protective tombolos and from a visual aspect, because they do not obscure the view as a tombolo, and are significantly cheaper than them. Also, they achieve a very good degree of protection of the beach from erosion in a less spatially intrusive way, and contribute to a better state of circulation of the coastal sea and have a smaller impact on animal habitats than tombolos.

The characteristic cross-section of the underwater reef (Figure 5.16) varies depending on the materials used and the main function of the structure. The width of the top of the underwater reef (*B*) must be large enough to disperse the wave energy (Pilarczyk, 1996), and the peak elevation (*Rc*) selected in such a way as to ensure that incoming waves break on it (Sawaragi T., 1995). Otherwise, the underwater reef does not have its primary function.

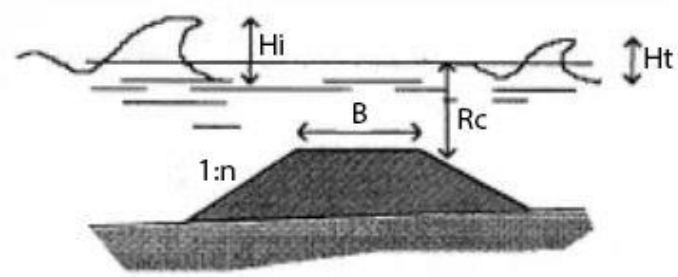

Figure 5.16 – Typical cross-section of the underwater reef (Sawaragi T., 1995)

The correct selection of the geometry of the underwater reef depends, first, on the detailed knowledge of the wave conditions of the location where they are placed, primarily the knowledge of the zone in which the wave breaking occurs. Therefore, as part of the design, it is necessary to carry out numerical wave modeling, in order to confirm the correctness of the given solutions.

5.5.5. Beach nourishment

Beach nourishment is the artificial backfilling of stone beach material on the eroded coast in order to maintain the amount of material at the base of the coast, thus compensating for natural erosion and to a

greater or lesser extent protect the area from storm surges and the effects of climate change. This is also the most common method used to control erosion caused by storm events (Hanson H. et al., 2002), and to the Croatian public these procedures are known based on a bad examples that have an extremely negative impact on the environment. Also, in the Croatian coast, a trend of increasing the total amount of material and the total cost of nourishment beaches in Croatia has been observed, which is evident from the diagram in Figure 5.17 (Carević D. et al., 2022).

For nourishment it is necessary to use material that will ensure the sustainability of the beach in question on the one hand, and comfortable use on the other. So far, it has been the practice that the beach nourishment was carried out solely with the aim of maintaining and expanding the size of the beach areas for tourist and recreational purposes, and the material was mostly inadequate to the conditions in which the beach is located, which would ultimately only further worsen the situation on the ground. All this contributed to a very negative they were embanking dredging materials (sand, gravel, small pebbles) from the source area (offshore, near the mainland or inland) in order to feed the beach where erosion occurs.

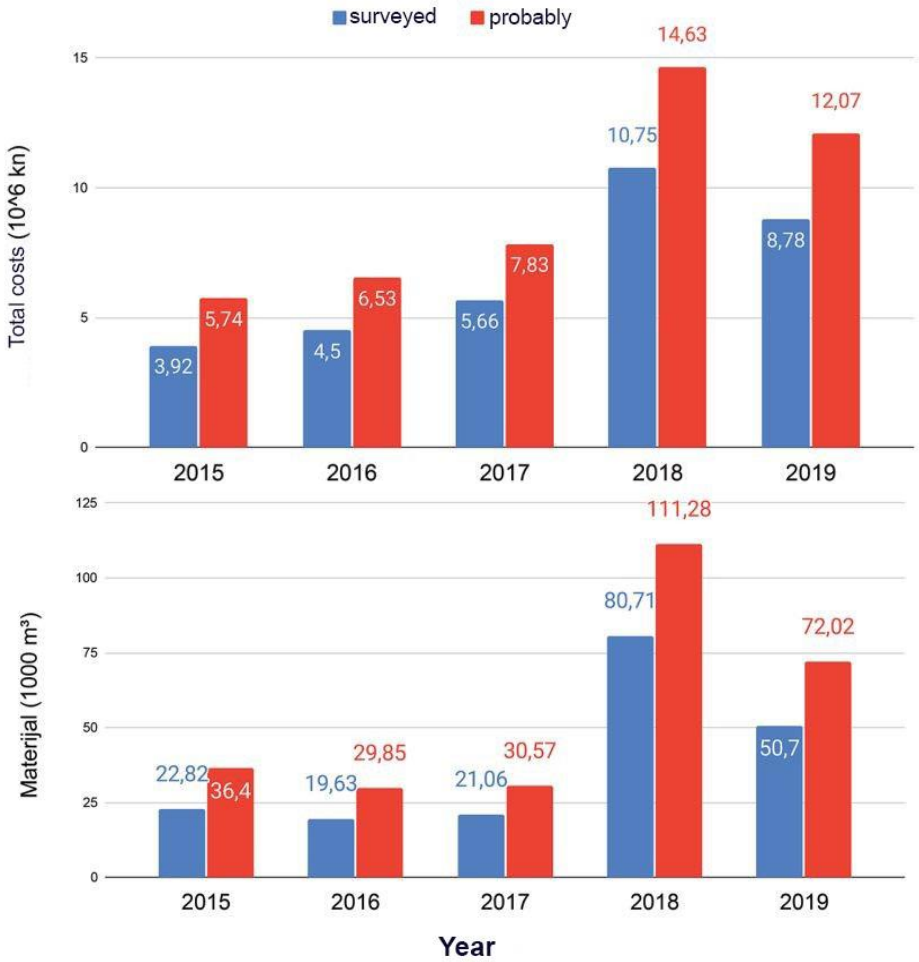

Figure 5.17 – Total cost of nourishment in Croatia – above, total amount of material used in nourishment in Croatia – down (Carević D. et al., 2022)

In conditions when local government units do not have projects or do not find financial resources for the realization of projects that solve the problem of beach erosion in integrated manner, the initially cheaper practice *of ad hoc* backfilling materials along the coastline is resorted to. So, nourished beaches generally do not have the required stability and resistance to the influence of waves, and they last at best one

summer season, when winter storms for the most part simply "take them away" (Granum Salis Cooperative, 2021). This bad practice has a far greater negative impact on the environment than the implementation of integral solutions to protect the coastal zone from erosion, due to the negative impact of inappropriate (finer) eroded material that affects the surrounding benthic habitats. Also, although initially more expensive, integral solutions are ultimately more economically viable than ad *hoc* solutions (Cooperative Granum Salis, 2021).

Considering that Split-Dalmatia County is located just behind Zadar County in terms of the amount of material consumed and funds for beach nourishment in the period 2015. to 2019. (Table 5.1), as well as by the area of the total zones in the period 1968. to 2020. (Table 5.2), the adoption of these guidelines represents a necessity without any alternative.

It is very important to point out that the beach nourishment itself cannot stop beach erosion, but only, unless other protective interventions are undertaken (construction of groynes, underwater reefs...), temporarily solves the lack of sediment, which mainly requires repeated interventions. There are several beach nourishment techniques, which are used throughout Europe and the world:

1. Beach nourishment, whereby beach material is applied to places in the coastal area of the beach where erosion occurs, in order to compensate for coastal erosion and restore the recreational value of the beach. Waves after backfilling, by their action, perform the movement of material into the underwater world and land.
2. Beach nourishment, whereby beach material is applied in the hinterland of the coastline (the part of the beach above the coast, which is exposed to waves only in extreme cases) to strengthen the beach against erosion and puncture in the event of a storm.
    - Beach nourishment, whereby beach material is applied in the immediate seabed of the beach. In this way, the wave energy that is relaxed before the coastline is reduced, while reducing the potential erosion of the beach.

County	No. of Munic.	No.of Beach.	No.of nourished Beaches	No.of surveyed Beaches	% nourished Beaches out of surveyed	% nourished Beaches out of total No.	Total nourishm. expenses [kn]	Total material [m3]
Dubrovačko-neretvanska	18	278	28	205	13,7	10,1	1.596.461,20	4.182,00
Ličko-senjska	3	181	15	60	25	8,3	637.000,00	4.900,00
Splitsko-dalmatinska	32	347	26	206	12,6	7,5	8.090.718,41	54.889,41
Šibensko-kninska	10	142	27	81	33,3	19	4.310.369,24	30.026,21
Istarska	21	250	35	239	14,6	14	2.427.748,36	8.944,53
Primorsko-goranska	20	406	58	345	16,8	14,3	4.068.070,50	17.849,11
Zadarska	26	300	67	264	25,4	22,3	12.448.394,51	74.088,99
Ukupno	130	1904	256	1400	18,3	13,4	33.578.762,22	194.880,25

Table 5.1 – Data on beach nourishment by county in the period 2015.-2019. (Et al., 2023)

County	Beach category	Port category	City area category	Industry category	Total No. of locations	Total area [km2]
Istarska	96	46	25	4	171	0,974
Primorsko-goranska	44	35	30	5	114	1,073
Ličko-senjska	41	24	15	2	82	0,202
Zadarska	136	107	60	6	309	2,092
Šibensko-kninska	20	17	8	2	47	0,593
Splitsko-dalmatinska	68	30	28	4	130	2,000
Dubrovačko-neretvanska	80	44	46	3	173	0,579
Total No. of locations	485	303	212	26	1026	7,513
Total area [km2]	1,859	3,107	1,677	0,869		

Table 5.2 – Backfilling of the coastline in the period 1968.-2020. (Et al., 2023)

In practice, a combination of different beach nourishment techniques is very often used, and in combination with the execution of protective coastal structures, such as groynes, tombolos and underwater reefs, the best results are achieved to protect beaches from erosion.

In order to determine the best way to determine the method of nourishment, but also the optimal system of constructions for the protection of the beach, it is necessary to know in detail the physical and morphological processes that are behind the potential of erosion, and with the help of numerical modeling techniques confirm the solutions that are intended to be applied.

As limiting factors of beach nourishment are of the utmost importance (AdriaAdapt):

1. Impacts on marine ecosystems, from small interstitial organisms to large mobile organisms, at different trophic levels. Negative impacts on benthic (macro-, meio- and micro-) organisms can be recorded in the form of important changes in community composition, abundance, and biodiversity. Moreover, the direct and indirect effects of nourishment have also been noted on types of commercial fishing (such as bivalvemous, crustaceans, sponges, bottom fish, etc.).
2. Certain negative effects on the coastal ecosystem: biota backfilling and habitat loss in coastal sandbars and coastal seabed can occur. Smaller particles contribute to the turbidity and clogging of fish gills, and have adverse effects on plankton larvae, mollusks, etc. According to some studies, particles smaller than 0.063 mm floating and covering a wide area around beaches have significant adverse effects.
3. Serious impacts on protected species (such as *Pinna nobilis*) and important marine habitats (such as *Posidonia oceanica* meadows*).*
4. Proper nourishment time – usually carried out in the spring, after winter storms (which erode the beach) and before the summer season.
5. Higher costs over time and due to re-disruption of ecosystems, if performed as an independent erosion rehabilitation intervention (without protective coastal buildings).
6. Finding sources with enough quality material for nourishment. The nourishment material should match the source material in size, color and composition. Practice shows that the use of finer material than necessary leads to a more frequent need for nourishment due to more intense erosion, which affects the overall cost.
7. A beach nourishment must be integrated into a broader approach to coastal planning.

In order to obtain adequate material for the nourishment of a particular beach, and bearing in mind the necessity of ensuring its sufficient stability and sustainability, as explained in Chapter 5.2, appropriate calculations should be made (days in Chapter 7.2 for each of the five sites concerned). Given that this is an extremely complex process, which depends on a whole range of influential factors and differs for each separate location of the beach, without detailed numerical modeling it is not possible to fully understand this problem, nor to solve it successfully.

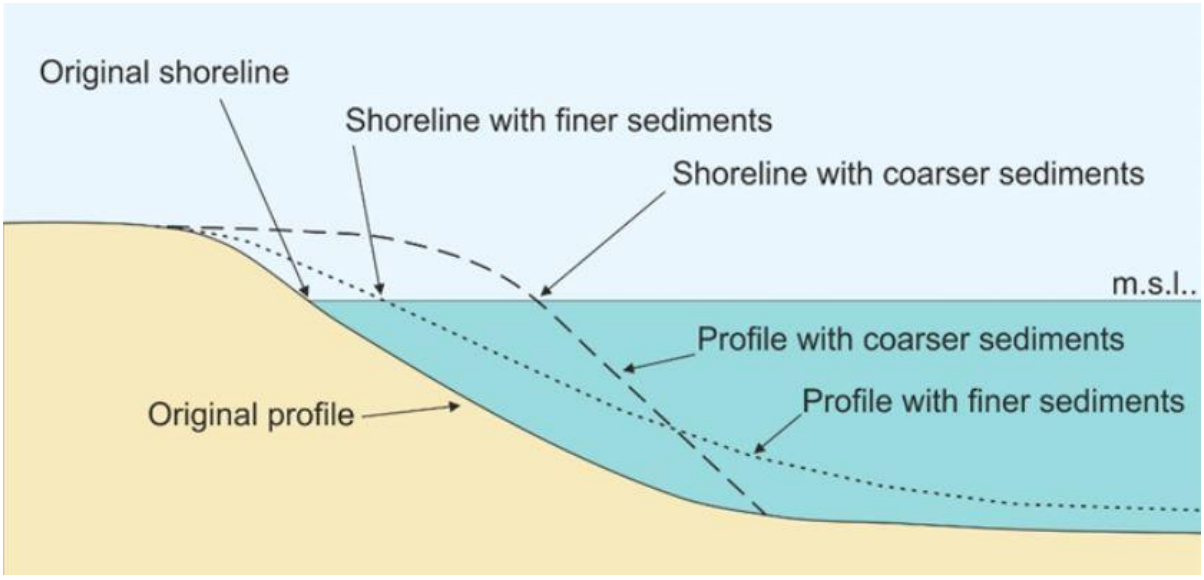

Figure 5.18 – Beach profiles relative to feed grain size (AdriaAdapt)

If the parameters of waves that can occur in a certain area in a certain period are known, numerical wave simulations can be performed from which the values of the wave bottom orbital velocities (*Ud*) are obtained, based on which it is possible to calculate the value of the previously mentioned driving forces of transport of beach material. Based on this, it is possible to calculate the granulometric composition, i.e., the mean diameter of the grain D_{50} beach embankment, which will be stable for the relevant dominant wave influences at the location of the beach in question. The formation of typical profiles of the beach depending on the size of the material it is fed with are shown in Figure 5.18.

6. NUMERICAL MODELING

6.1. Mathematical wave model

6.1.1. Applied numerical model

For wave analysis, a numerical model based on the iterative solving of a modified elliptical partial differential equation of a slight slope was used, by finite element method, developed under the name CGWAVE at the University of Maine in collaboration with the U.S. Army Corps of Engineers - Waterways Experiment Station.

It is a model for estimating wavefields in ports, in open coastal areas, bays (bays), around islands, fixed and floating structures (Demirbilek Z.-Panchang V.G, 1998). This numerical model considers all significant wave transformation processes occurring in the coastal area (diffraction, refraction, reflection), the state of the sea beyond the port itself, and can include a whole host of other important factors such as nonlinear wave breaking processes, friction along the bottom and nonlinear wave scattering (Chhabra N., 2004, Li D., 2002; Demirbilek Z.-Panchang V.G, 1998).

A numerical procedure of finite triangular elements with linear approximation of functions was applied, which are generated automatically by applying the Surface Water Modeling System (SMS) (Jones N.L., 1992). The model can analyze spectral wave conditions.

The U.S. Army Corps of Engineers brings a whole range of projects that have been explored, in terms of wavering, by the CGWAVE model, where by the results of numerical modeling were compared with the results on physical models and from field measurements. In this way, this numerical model has been proven to be a valuable tool. In addition to the above examples, there are other numerous studies in the literature, which calibrated and perfected the model in question (Panchang V.G. et al., 2000; Zubier K. et al., 2003; Li D., 2002; Chhabra N., 2004; Zhang J., 2007).

Before solving the equations, it is necessary to specify only the area (aquatory) of the model, which is discretized by three-junction triangle finite elements. The area is determined by a three-dimensional (geodetically recorded) substrate of the area, and by setting the coastal edge and open boundary.

The geodetic background contains data on the horizontal coordinates (x, y) of the recorded points and their depth (z). The coastal edge shall be determined by the single sea level elevation and the marginal conditions described in point 6.1.3.1.

The sea level elevation defines a horizontal plane that, by intersecting with a three-dimensional bathymetric surface, creates a coastal edge. Control of the coastal edge thus obtained from the model is carried out in relation to the geodetically recorded line of the coastal edge. In places where the bathymetric surface and the horizontal surface defined by the sea level elevation do not intersect, the vertical coastal edge is defined.

The open boundary shall be set by a circular arc segment (point 6.1.3.2) at which boundary conditions are set.

The size of the finite elements depends on the local wavelength which again depends on the local depth. The user himself selects the resolution of the finite element network, and a minimum of 8-10 points per wavelength is recommended (Demirbilek Z.-Panchang V.G, 1998; Liu S., Sun B., 2006; Zhang J., 2007). In areas of major changes in bottom topography or wave amplitudes, a finer grid is required, which is why

the smallest finite element is defined, in order to create an optimal finite element network. This ensures that the wave components of the given spectrum with the lowest wavelength are also considered when solving.

The input parameters of a significant wave are the amplitude (*a*), the direction of the wave and the period (*T*). In the case of spectral description of wave conditions, the direction, significant wave height (*Hs*), peak period (*Tp*), as well as the standard parameters of the selected spectrum are set. The energy spectrum defined in this way is broken down into the desired number of monochromatic components by direction and frequency.

6.1.2. Basic process equation

The approximation of wave motion in the coastal area can be given by the equation of a slight slope (Berkhoff J.C.W., 1972; Berkhoff J.C.W., 1976), which in its basic form reads:

$$\nabla \cdot \left(CC_g \nabla \phi\right) + \omega^2 \frac{C_g}{C} \phi = 0$$

where *C* is the wave velocity, C_g is the wave group velocity, $\phi(x, y)$ a complex two-dimensional potential, a ω circular frequency ($\omega = 2\pi/T$; *T*–wave period). An equation is an elliptical partial differential two-dimensional equation that gives solutions to unknown potentials $\phi(x, y)$ in the horizontal plane. The equation applies to the condition of a slight slope of the bottom, that is, for $|\nabla D| / kD << 1$ (*D*-depth, *k*-wave number) (Zhang J, 2007). It includes all forms of coastal wave transformation, such as diffraction, refraction, impact of shoal and reflection.

In order to include nonlinear processes in the model, such as wave breaking and friction along the bottom, the basic equation is expanded (Booij N, 1981; Demirbilex Z.-Panchang V.G, 1998):

$$\nabla \cdot \left(CC_g \nabla \phi\right) + \left(\omega^2 \frac{C_g}{C} + iC_g \omega W_d \right) \phi = 0$$

where W_d is a coefficient that combines the impact of wave breaking and friction along the bottom.

For the equation to be applied to real, irregular bottoms, with different and steeper slopes, the following formulation is used (Chandrasekera C.N.-Cheung K.F., 1997):

$$\nabla \cdot \left(CC_g \nabla \phi\right) + \left[\omega^2 \frac{C_g}{C} + d_1 \nabla^2 D + d_2 \left(\nabla D\right)^2 \right] \phi = 0$$

With the applied numerical model CGWAVE, after the boundary conditions are set, the equation of a slight slope in the inner region of the model is solved, which is discretized by a network of triangular finite elements.

6.1.3. Boundary conditions

For the process equation to be solved in the given area of the model, it is necessary to set boundary conditions across the entire (closed) boundary of the model. They represent a mathematical description of the physical properties of the edges of the model in two-dimensional space. With the third dimension of the model, i.e., depth at each point of the model, boundary conditions are crucial for correctly creating the model of real reality of the waters being tested.

There are two types of boundary conditions – boundary conditions at the open border and coastal boundary conditions.

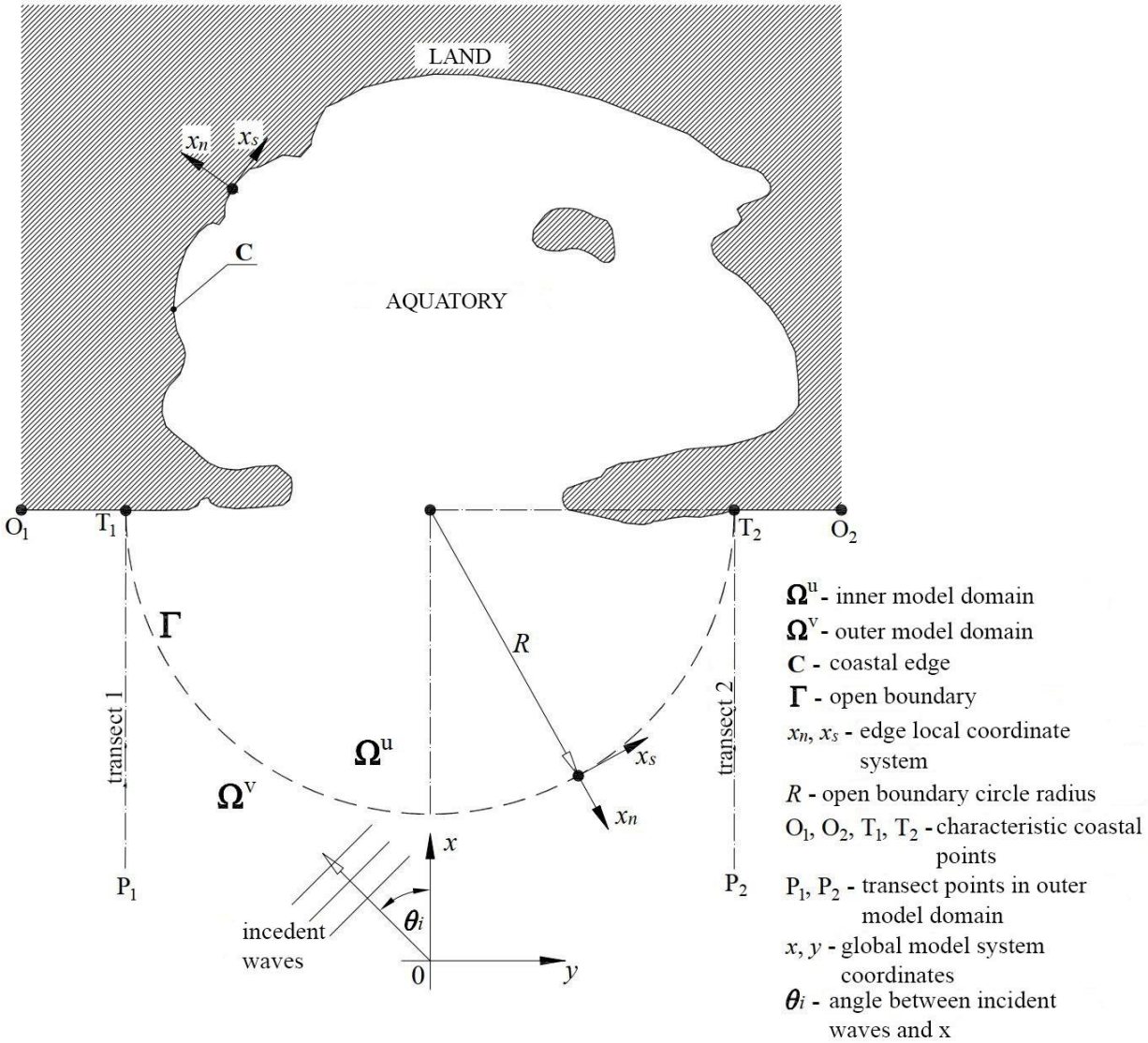

Figure 6.1 – Model domain definition

6.1.3.1. Coastal boundary conditions

If an incident and reflected wave is observed near the coastal edge, the total potential can be recorded

as:

$$\phi = ae^{ik\left(x_n \cos\delta_i + x_s \sin\delta_i\right)} + aK_r e^{ik\left(-x_n \cos\delta_i + x_s \sin\delta_i + \delta\right)}$$

where the δ_i angle of the incident wave is to the coastal edge (Figure 6.2), and *the δ* is the phase shift between the incident wave and the reflected wave. x_n and x_s are the coordinates of the local system on the edge (Figure 6.2).

As the angle of the incident wave δ_i is not known in advance, it is necessary to determine it. For the marginal coastal element (Figure 6.2), with a defined angle of incident wave to the shore, the marginal condition reads as follows:

$$\left.\begin{aligned} \frac{\partial\phi}{\partial x_n} &= ik\cos\delta_i \frac{1-K_r}{1+K_r}\phi \\ \frac{\partial\phi}{\partial x_s} &= ik\sin\delta_i\phi \end{aligned}\right\}$$

or:

$$\frac{1}{\phi}\frac{\partial\phi}{\partial x} = \frac{1}{|\phi|}\frac{\partial|\phi|}{\partial x} + i\frac{\partial S}{\partial x}$$

where $S(x,y) = \arg(\phi)$ is the phase function of the complex potential ϕ. Now the edge condition can be written:

$$\left.\begin{aligned} \frac{\partial S}{\partial x_n} &= k\cos\delta_i \frac{1-K_r}{1+K_r} \\ \frac{\partial S}{\partial x_s} &= k\sin\delta_i \end{aligned}\right\}$$

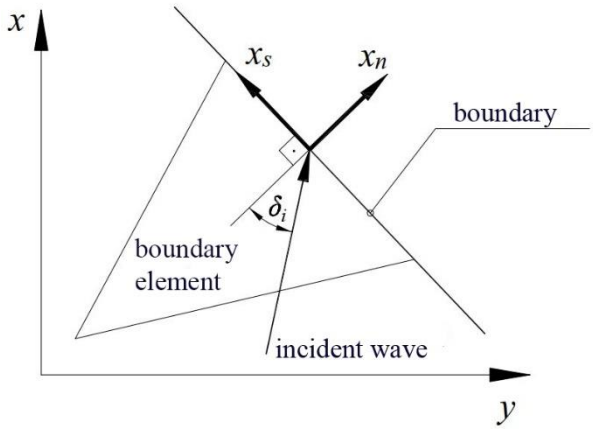

Figures 6.2 – Boundary element and direction of the incident wave to the edge

the angle of the incident wave to the shore gets from the expression:

$$\tan\delta_i = \frac{\partial S/\partial x_s}{\partial S/\partial x_n + k(2K_r/1+K_r)\cos\delta_i} \qquad (x_n = 0)$$

The problem of obtaining an incident angle δ_i is solved by an iterative procedure. The equation of a slight slope is solved and S0 ϕ_0 is obtained, including the initial incident angle δ_0. The values δ_0, ϕ_1 and *S1*, and so on are used until the convergence criterion is achieved:

$$\sqrt{(\delta_n - \delta_{n-1})^2} \le 0{,}01$$

Below are given all the marginal conditions used, i.e., reflection coefficients (*Kr*) for the predicted impermeable coastal structures for each of the analyzed locations, which were selected based on experience, and based on literature (Thompson E.F., 1996; Goda Y., 2000; CEM, 2003).

6.1.3.1.1. Brač (Zlatni rat)

For conducting numerical simulations for the location of Zlatni rat beach on the island of Brač, reflection coefficients (coastal boundary conditions) were used as shown in Figure 6.3

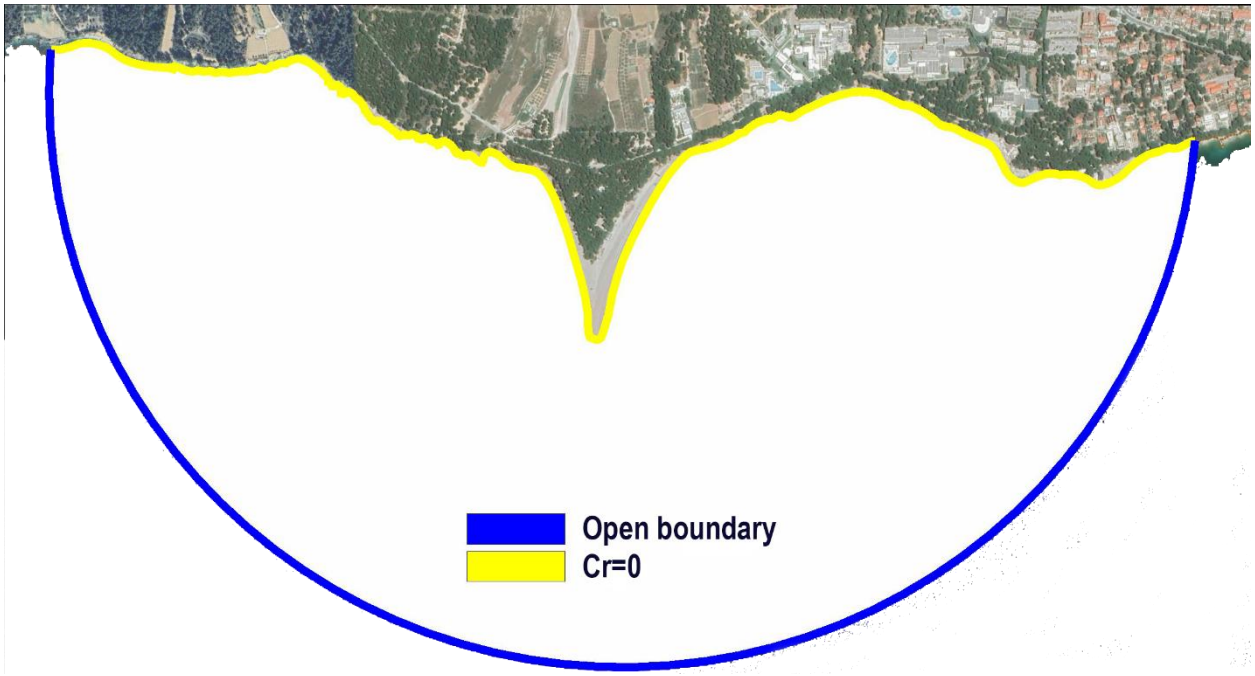

Figure 6.3 – Used coastal boundary conditions - reflection coefficients (Kr) for Zlatni rat beach (Brač)

6.1.3.1.2. Vis (Stiniva)

For conducting numerical simulations for the location of Stiniva beach on the island of Vis, reflection coefficients (coastal boundary conditions) were used as shown in Figure 6.4.

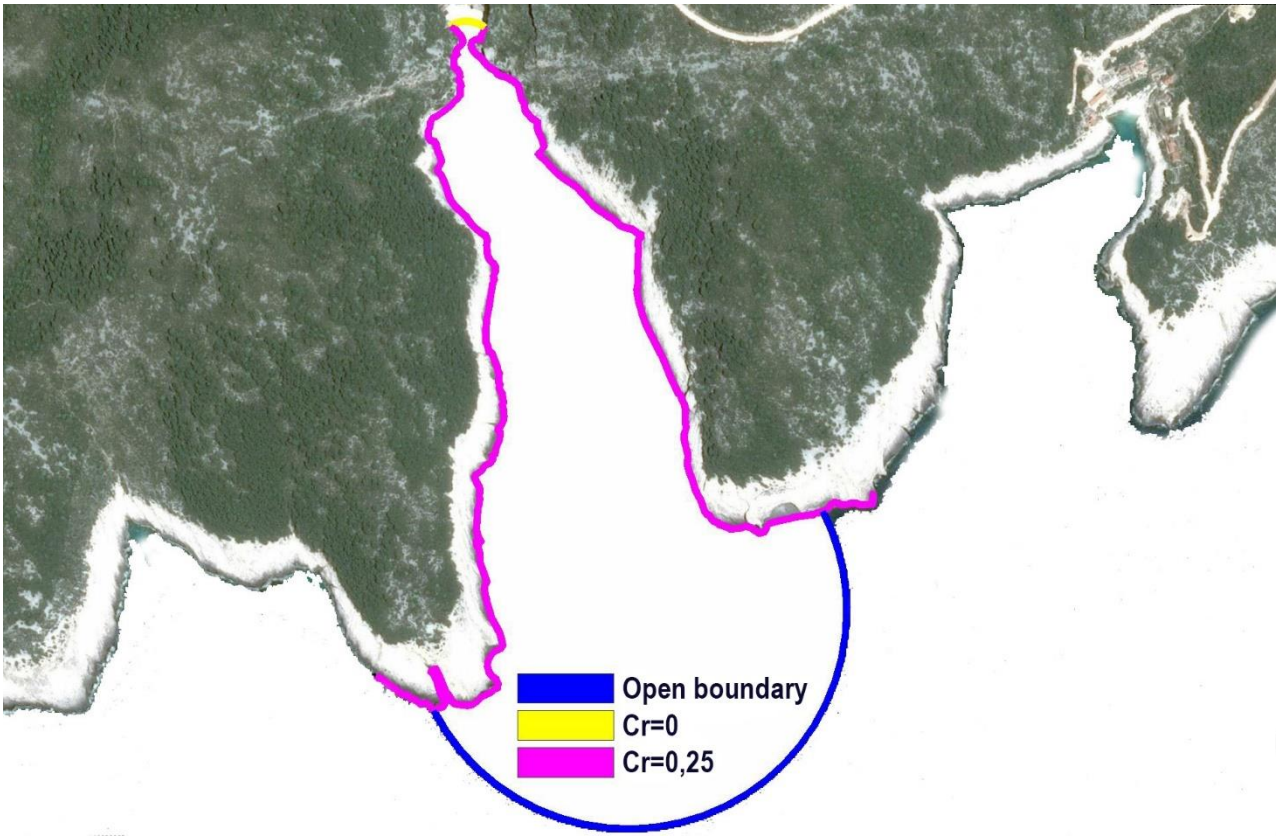

Figure 6.4 – Used coastal boundary conditions - reflection coefficients (Kr) for Stiniva beach (Vis)

6.1.3.1.3. Makarska Riviera (Podgora)

For conducting numerical simulations for the location of Podgora beach on the Makarska Riviera, reflection coefficients (coastal boundary conditions) were used as shown in Figure 6.5.

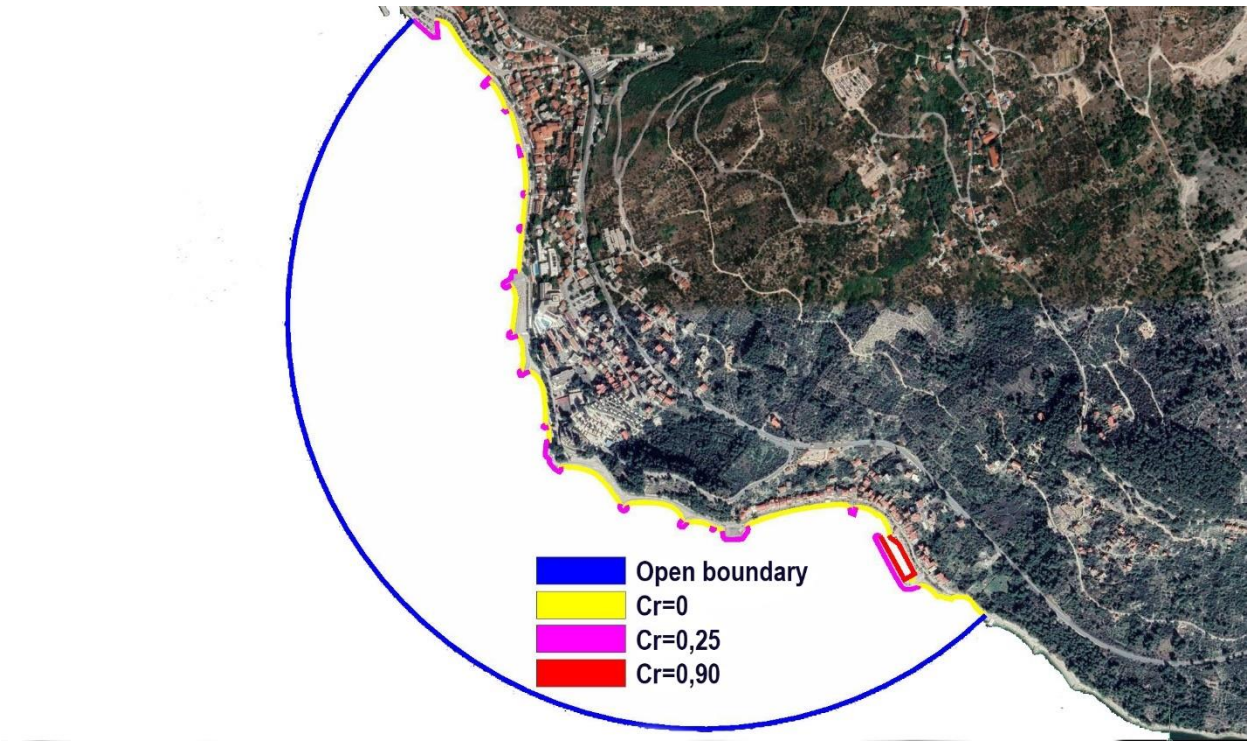

Figure 6.5 – Used coastal boundary conditions - reflection coefficients (Kr) for Podgora beach (Makarska Riviera)

6.1.3.1.4. Podstrana-Duće area

For conducting numerical simulations for the location of beaches on the Podstrana-Duće area, reflection coefficients (coastal boundary conditions) were used as shown in Figure 6.6.

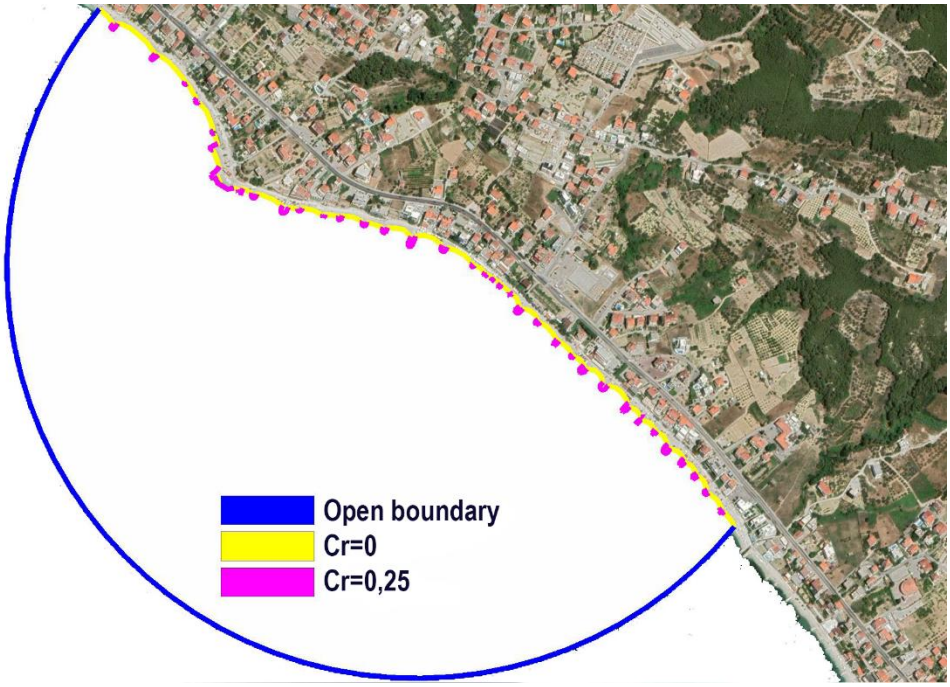

Figure 6.6 – Used coastal boundary conditions - reflection coefficients (Kr) for beaches on the Podstrana-Duće area

6.1.3.1.5. Split (Kašjuni)

For conducting numerical simulations for the location of Kašjuni beach in Split, reflection coefficients (coastal boundary conditions) were used as shown in Figure 6.7.

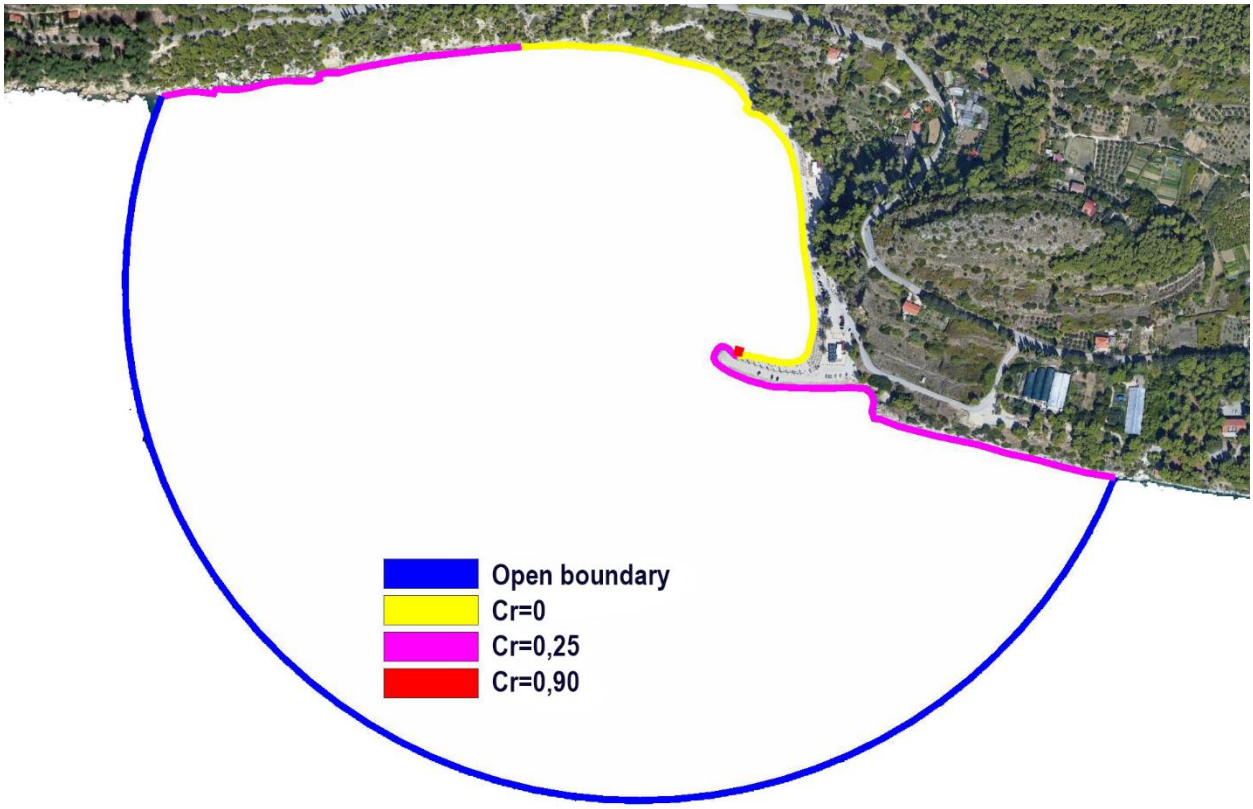

Figure 6.7 – Used coastal boundary conditions - reflection coefficients (Kr) for Kašjuni beach (Split

6.1.3.2. Open boundary conditions

The boundary conditions on the open boundary of the model represent the line where incoming waves are generated operating in the considered created model area.

A two-dimensional complex potential $\phi(x,y)$, at the open boundary of Γ, can be expressed as:

$$\phi = \phi^0 + \phi^s$$

where is ϕ^0 the sum of the potential of the incident wave and reflected wave, and ϕ^s is the potential of the scattered wave. Since it is not possible to give a simple expression for the sum ϕ^0, due to the influence of external bathymetry, it is necessary to make a simplification in the display of the bathymetry of the outer region Ωv using a 1D cross-section (Panchang V.G. et al., 2000 and 2005), (figure 6.8).

With this simplification, the sum of the components of incident (incoming) and reflected waves can be shown as:

$$\phi^0 = \phi^I + \phi^r = \phi(x)e^{ik_y y}$$

and get a solution from the one-dimensional form of the equation of a slight slope:

$$\frac{d}{dx}\left(CC_g\frac{d\phi(x)}{dx}\right)+\left(\left(k^2-k_y^2\right)CC_g+i\omega W_d\right)\phi(x)=0$$

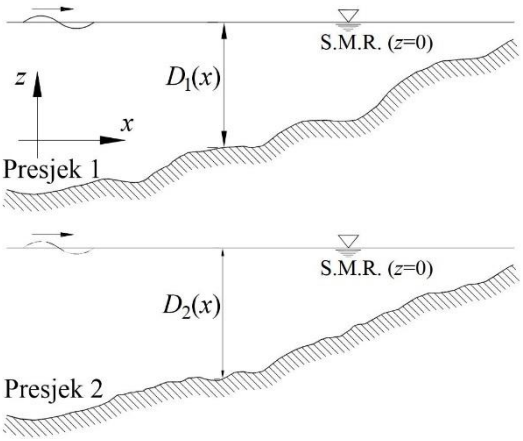

Figure 6.8 - 1D crossections

By the solution of this expression, with marginal conditions for point *P1* (Figure 6.1):

$$\frac{\partial\phi(x)}{\partial x}=ik\cos\theta_i(-i\frac{g}{\omega}2a_i-\phi(x))$$

I point *T1* (Figure 6.1):

$$\frac{\partial\phi(x)}{\partial x}=\left(i\sqrt{k^2-k_y^2}\frac{1-K_re^{ik\delta}}{1+K_re^{ik\delta}}\right)\phi(x)$$

solutions for cross-sections 1 and 2 [$\phi_1(x),\phi_2(x)$]are obtained. In order to obtain the required ϕ^0 along the segment of the open border circle, these two solutions are transversely translated between these two cross-sections, and the solutions are interpolated to the open border:

$$\phi^0=\left(\frac{1+y/R}{2}\phi_1(x)+\frac{1-y/R}{2}\phi_2(x)\right)e^{ik_yy}$$

For the description of the component of the scattered wave in the 2D region, a parabolic approximation is applied:

$$\frac{\partial\phi^s}{\partial x_n}=p\phi^s+q\frac{\partial^2\phi^s}{\partial x_s^2}$$

where:

$$p=ik-\frac{1}{2R}+\frac{i}{8kR^2}$$

$$q = \frac{i}{2k}$$

R is the radius of the circle.

The parabolic approximation allows scattered waves to exit the Ωu region only through a limited opening (~45°) around the dominant direction of the scattered waves. This direction is not known in advance, and due to the satisfaction of the Sommerfeld radiation condition, scattered waves must move radially towards infinity, so the center of the scattering is selected and the circle segment is used as an open boundary.

It is assumed that the bulk of the scattering occurs within the port itself (Ωu area) and/or due to structures and banks, so the direction of the scattered waves at each point of the open border can be assumed as radial (perpendicular to the tangent of the circle).

For an open border, the marginal condition is used as for the coastal edge but of a lower order. It includes the angle of incident waves and treats the open boundary as fully permeable (*Kr* = 0), and in the case of a slight slope of the bottom and when the scattered waves are unexpressed and spread from the immediate vicinity of the center of the circle reads:

$$\frac{\partial \phi^s}{\partial x_n} = \left(ik - \frac{1}{2R} \right) \phi^s$$

As it is true $\phi^s = \phi - \phi^0$, inclusion gives the total marginal condition for the open border:

$$\frac{\partial \phi}{\partial x_n} = \left(ik - \frac{1}{2R} \right) \left(\phi - \phi^0 \right) + \frac{\partial \phi^0}{\partial x_n}$$

where the sizes associated with are ϕ^0 obtained from:

$$\phi^0 = \phi^I + \phi^r = \phi(x) e^{ik_y y}$$

6.1.3.2.1. Brač (Zlatni rat)

On the lines of generating a numerical model (open border) for the analysis of Zlatni rat beach on the island of Brač, boundary conditions are defined by selecting deep-water incident spectra with statistical characteristics and feedback periods shown in Figures 6.9 to 6.12, and obtained based on making a long-term wave forecast (chapter 3.1).

Selected base directions from individual sectors for which numerical wave simulations will be performed are **ESE (112.5°), SSE (157.5°**), **SW (225°)** and **WSW (247.5°)**. Although there is a high probability that the realistic directions of wind waves at the location deviate a few degrees from those chosen here, each of these directions was chosen for several reasons.

The ESE direction (112.5°) was chosen because wind data (Table 2.4) indicate that wind from this direction is the most dominant in sector I, and the fetch (Tables 3.1 and 3.2) for the development of waves from this direction is longer than the wind direction of SE (135°). In addition, the waves from this direction will

have a significant impact on the hydrodynamic state of the waves in the considered area than other directions from the sector, including on the morphology of the beach itself.

The direction of SSE (157.5°) was chosen because wind data (Table 2.4) indicate that the wind from this direction is the most dominant in sector II, and the fetch (Tables 3.2 and 3.3) is for the development of waves from this direction longer than the direction of wind S (180°).

The direction of SW (225°) was chosen because wind data (Table 2.4) indicate that wind from this direction is the most dominant in sector III, and the fetch (Tables 3.3 and 3.4) for the development of waves from this direction is longer than the wind direction SSW (202.5°).

The WSW direction (247.5°) was chosen because wind data (Table 2.4) indicate that wind from this direction is the most dominant in sector IV, although the fetch (Tables 3.4 and 3.5) for the development of waves from this direction is slightly shorter than the wind direction W (270°).

It should be especially emphasized that when modeling the waves of these types of waters, which are usually exposed to wind waves with a variation of the basic direction at the local level, wave conditions are described by the energy spectrum with a certain directional dispersion around the basic direction of incident waves (Goda Y., 2000). For this case, a ±30° directional dispersion was selected around the basic directions of incident waves, since about 85% of the wave energy is propagated in this zone. Thus, in numerical simulations, all directional wave components in a total angle of 60° were considered, which represents an additional degree of safety.

For all selected directions, numerical simulations will be conducted with wave parameters for a return period of 50 years.

Figures 6.9 to 6.12 give the energy distributions of the incident wave spectrums used with respect to the frequency range. In all numerical simulations, the frequency part of the spectrum from fmin= 0.08 Hz to fmax= 0.6 Hz was used, i.e., the wave spectrum obtained by the superposition of monochromatic wave components with a minimum period from Tmin = 1.67 s to waves with a maximum period of Tmax = 12.5 s. The peak periods *of the Tp* spectrum are calculated by the expression $Tp = 1.1*T0$.

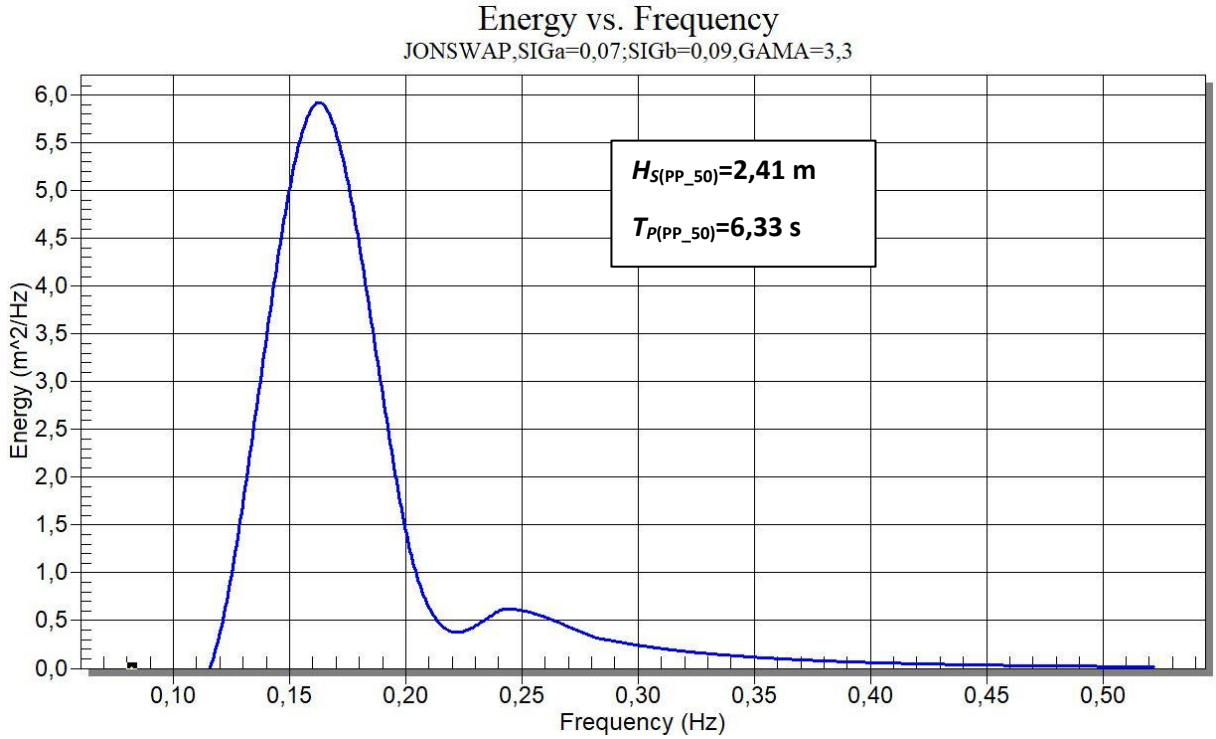

Figure 6.9 – Power diagram of deepwater incident wave spectrum with statistical characteristics for a 50-year return period for sector I (JONSWAP spectrum; γ = 3.3; directional dispersion ±300) for direction ESE (112.5°)

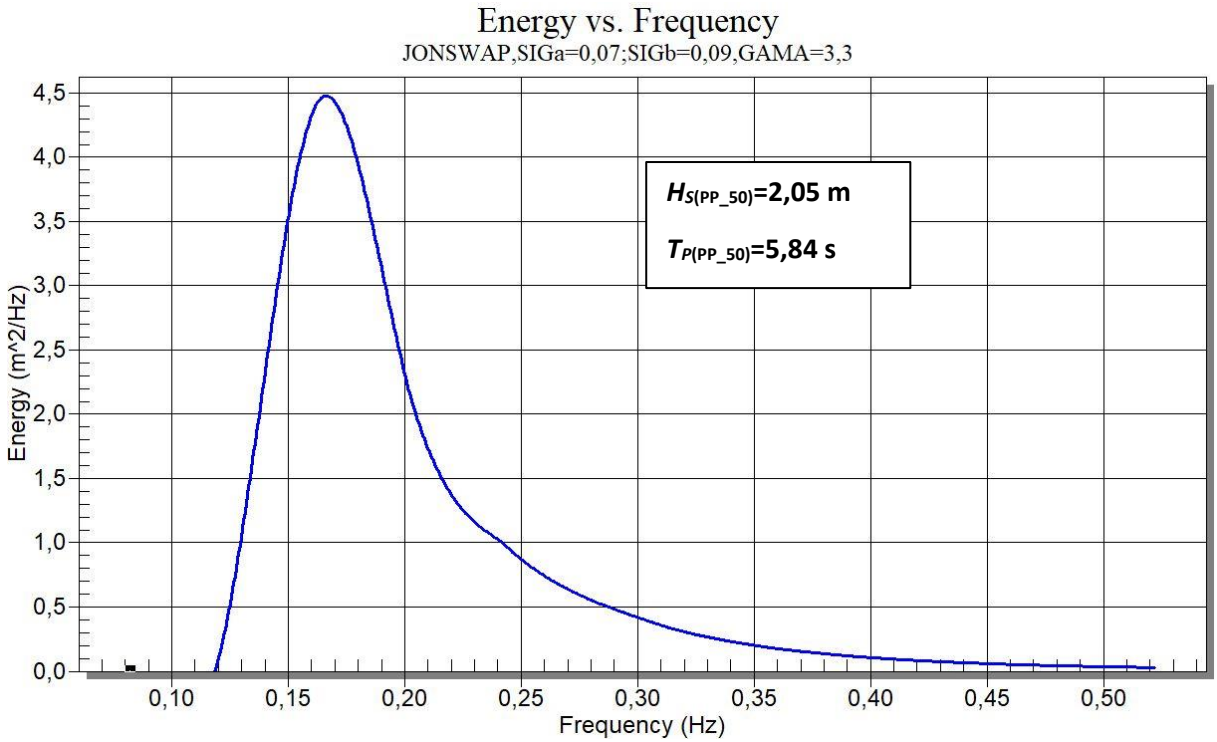

Figure 6.10 – Power diagram of deep-water incident wave spectrum with statistical characteristics for a 50-

year return period for sector II (JONSWAP spectrum; γ= 3.3; directional dispersion ±300) for SSE direction (157.5°)

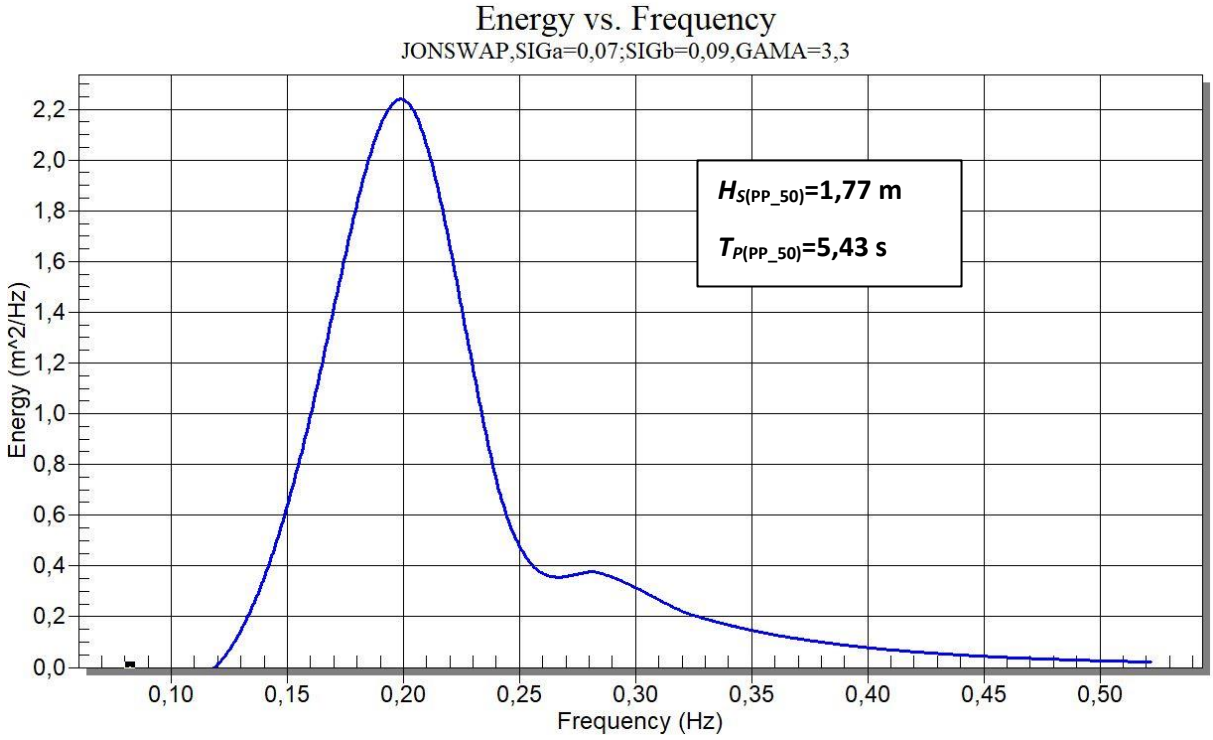

Figure 6.11 – Power diagram of deepwater incident wave spectrum with statistical characteristics for a 50-year return period for sector III (JONSWAP spectrum; γ = 3.3; directional dispersion ±300) for direction SW (225°)

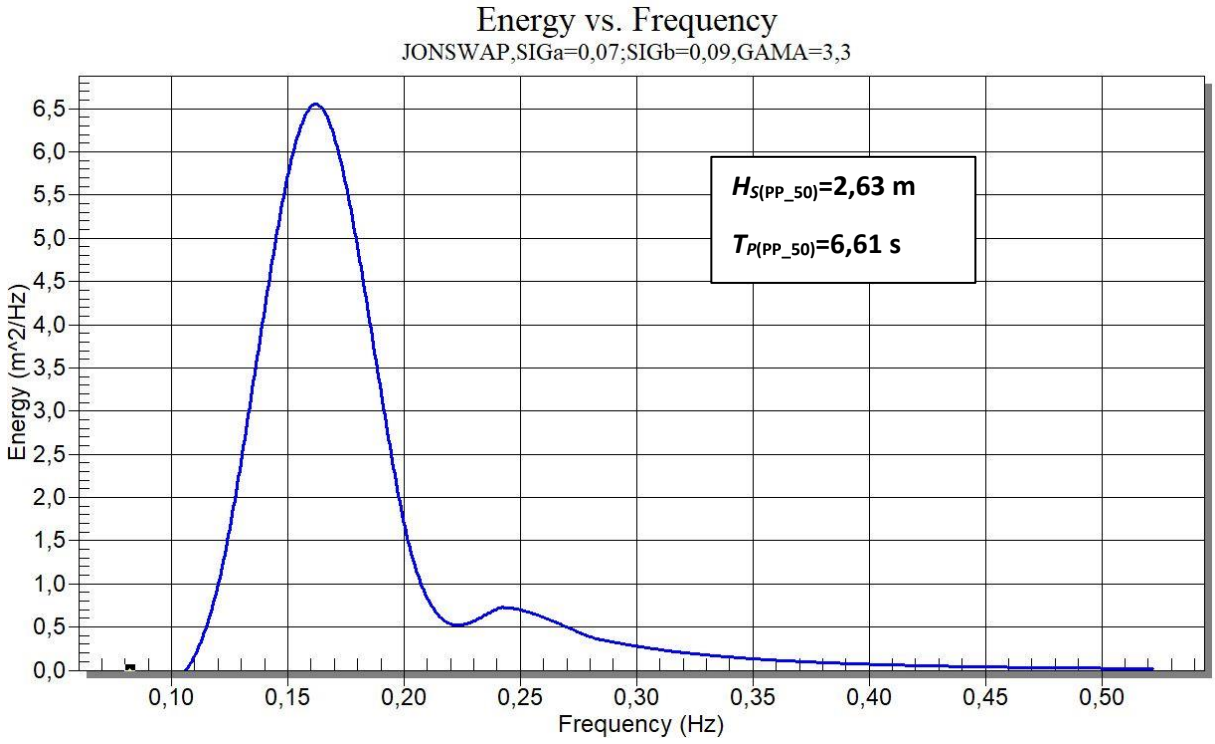

Figure 6.12 – Power diagram of deepwater incident wave spectrum with statistical characteristics for a 50-year return period for sector IV (JONSWAP spectrum; γ = 3.3; directional dispersion ±300) for WSW direction (247.5^o)

6.1.3.2.2. Vis (Stiniva)

On the line of generating a numerical model (open border) for the analysis of Stiniva beach on the island of Vis, boundary conditions are defined by selecting deep-water incident spectra with statistical characteristics and feedback periods shown in Figure 6.13, and obtained based on the long-term wave forecast (chapter 3.1).

The orientation of Stiniva beach and its location within a deep bay contributes to the oncoming waves from all three considered wind wave sectors roughly encountering its coast at the same angle. In such a situation, it is a reasonable estimate to analyze the hydrodynamic state of the waves in the considered area and the impact on its morphology only for waves with the calculated maximum wave parameters.

The basic direction from sector II was chosen for which numerical simulations of the waves will be performed, which is **SE (135°)**. Although there is a high probability that the real directions of wind waves at the site deviate several degrees from those selected here, this direction was chosen because wind data (Table 2.5) indicate that the wind from this direction is the most dominant in sector I. In addition, the waves from this direction will have a significant impact on the hydrodynamic state of the waves in the considered area than other directions from the sector, and the morphology of the beach itself.

It should be especially emphasized that when modeling the waves of these types of waters, which are usually exposed to wind waves with a variation of the basic direction at the local level, wave conditions are described by the energy spectrum with a certain directional dispersion around the basic direction of incident waves (Goda Y., 2000). For this case, a ±30° directional dispersion was selected around the basic directions of incident waves, since about 85% of the wave energy is propagated in this zone. Thus, in numerical simulations, all directional wave components in a total angle of 60o were considered, which represents an additional degree of safety.

For the chosen direction, numerical simulations will be conducted with wave parameters for a return period of 50 years.

In Figure 6.13 days is the energy distribution of the incident wave spectrum used with respect to the frequency range. In all numerical simulations, the frequency part of the spectrum from fmin= 0.08 Hz to fmax= 0.6 Hz was used, i.e., the wave spectrum obtained by the superposition of monochromatic wave components with a minimum period from Tmin = 1.67 s to waves with a maximum period of Tmax = 12.5 s. The peak periods *of the Tp* spectrum are calculated by the expression *Tp* = 1.1**T0*.

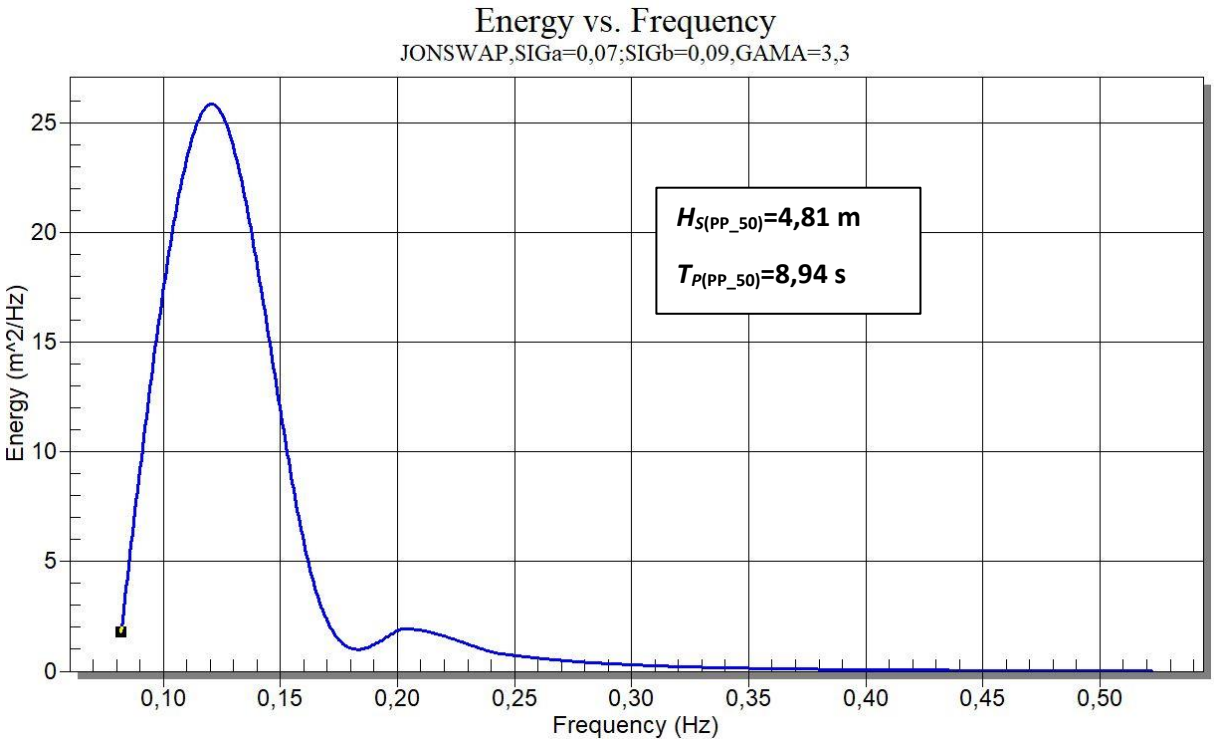

Figure 6.13 – Power diagram of deepwater incident wave spectrum with statistical characteristics for a 50-year return period for sector I (JONSWAP spectrum; γ = 3.3; directional dispersion ±300) for direction SE (135°)

6.1.3.2.3. Makarska Riviera (Podgora)

On the lines of generating a numerical model (open border) for the analysis of Podgora beach on the Makarska Riviera, boundary conditions are defined by selecting deep-water incident spectra with statistical characteristics and feedback periods shown in figures 6.14 to 6.16, and obtained based on making a long-term wave forecast (chapter 3.1).

The selected basic directions from individual sectors for which numerical valve simulations will be performed are **SSE (157.5°)**, **SW (225°)** and **W (270°)**. Although there is a high probability that the realistic directions of wind waves at the location deviate a few degrees from those chosen here, each of these directions was chosen for several reasons.

Although wind data (Table 2.3) indicate that wind from the direction of SE (135°) is the most dominant in sector I, due to the specific disposition of the location concerned, the direction of SSE (157.5°) was chosen to conduct the wave simulations, which shows a more significant impact than the direction of SE (135°) from Sector I.

The Direction SW (225°) was chosen because wind data (Table 2.3) indicate that the wind from this direction is the most dominant in Sector III, and the fetch (Tables 3.10 and 3.11) is for the development of waves from this direction longer than the wind direction SSW (202.5°).

Direction W (270°) was chosen because wind data (Table 2.3) indicate that wind from this direction is the most dominant in sector IV, and the fetch (Tables 3.11 and 3.12) is for the development of waves from this direction longer than the directions of winds WSW (247.5°) and WNW (292.5°).

It should be especially emphasized that when modeling the waves of these types of waters, which are

usually exposed to wind waves with a variation of the basic direction at the local level, wave conditions are described by the energy spectrum with a certain directional dispersion around the basic direction of incident waves (Goda Y., 2000). For this case, a ±30° directional dispersion was selected around the basic directions of incident waves, since about 85% of the wave energy is propagated in this zone. Thus, in numerical simulations, all directional wave components in a total angle of 60o were considered, which represents an additional degree of safety.

For all selected directions, numerical simulations will be conducted with wave parameters for a return period of 50 years.

Figures 6.14 to 6.16 give the energy distributions of the incident wave spectrums used with respect to the frequency range. In all numerical simulations, the frequency part of the spectrum from fmin= 0.08 Hz to fmax= 0.6 Hz was used, i.e., the wave spectrum obtained by the superposition of monochromatic wave components with a minimum period from Tmin = 1.67 s to waves with a maximum period of Tmax = 12.5 s. The peak periods *of the Tp* spectrum are calculated by the expression *Tp* = 1.1**T0*.

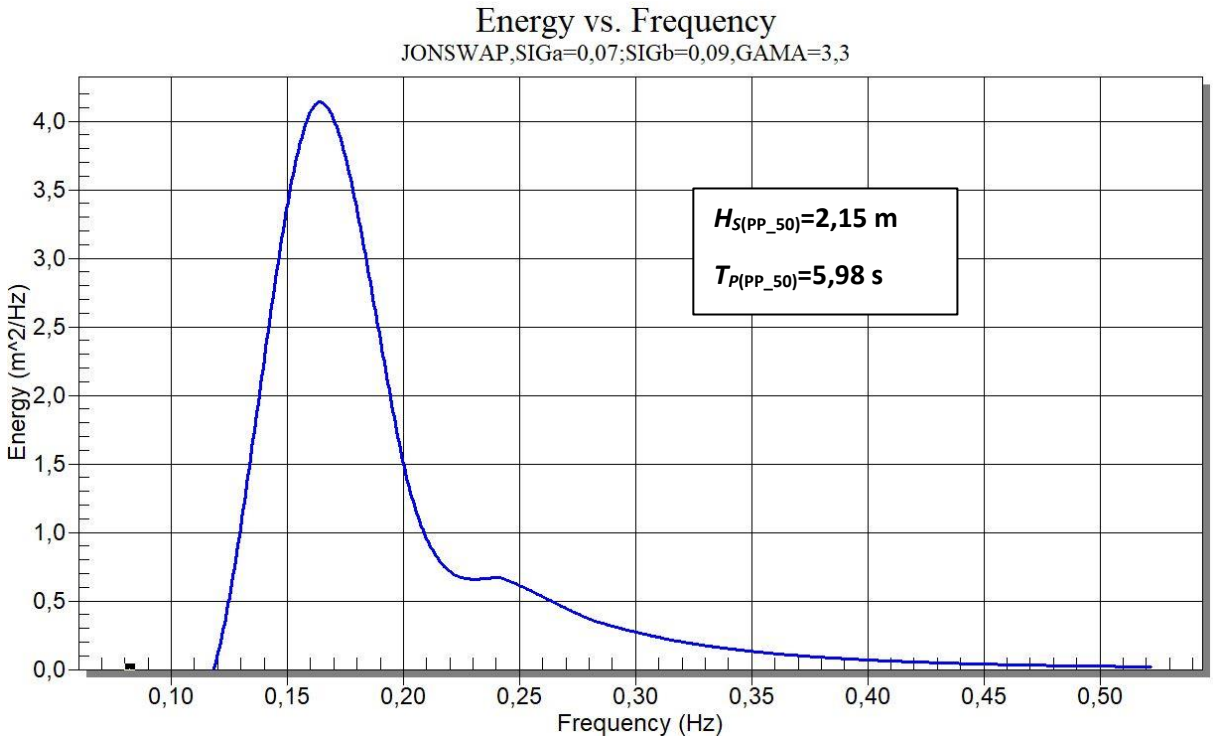

Figure 6.14 – Power diagram of deepwater incident wave spectrum with statistical characteristics for return period of 50 years for sector II (JONSWAP spectrum; γ = 3.3; directional dispersion ±300) for SSE direction (157.5°)

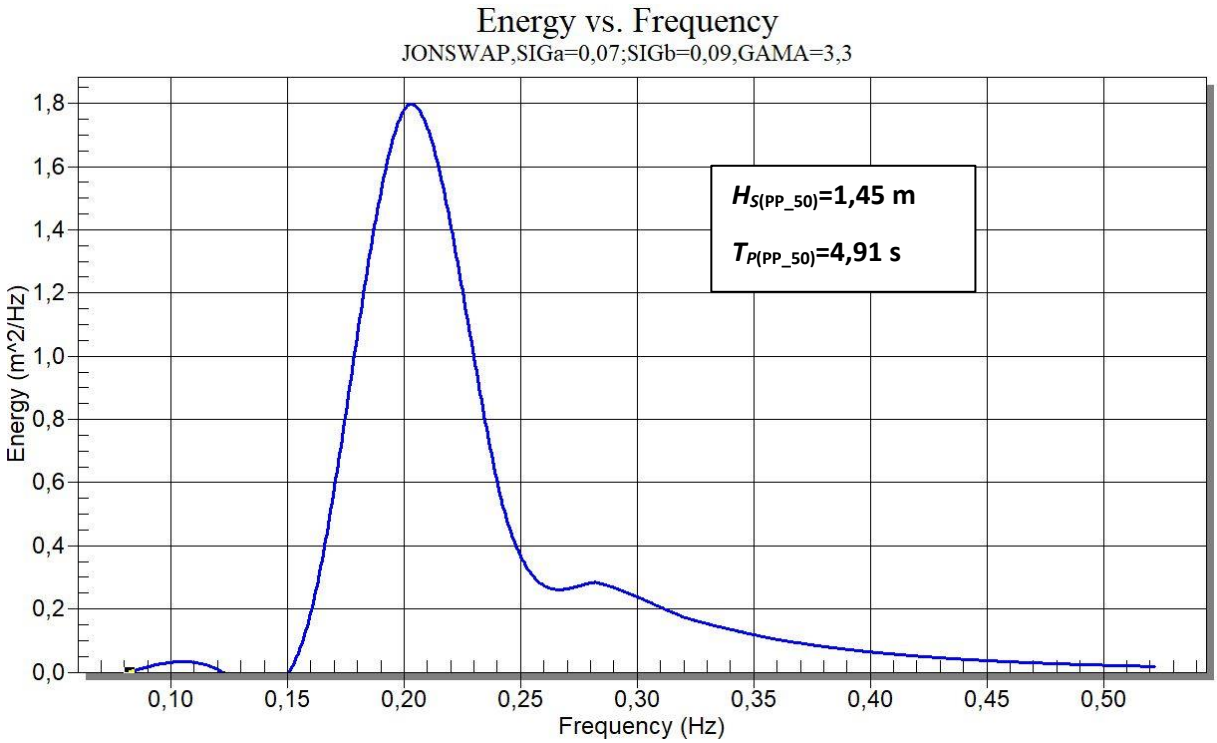

Figure 6.15 – Power diagram of the deepwater incident wave spectrum with statistical characteristics for 50-year return period for sector III (JONSWAP spectrum; γ = 3.3; directional dispersion ±300) for direction SW (225°)

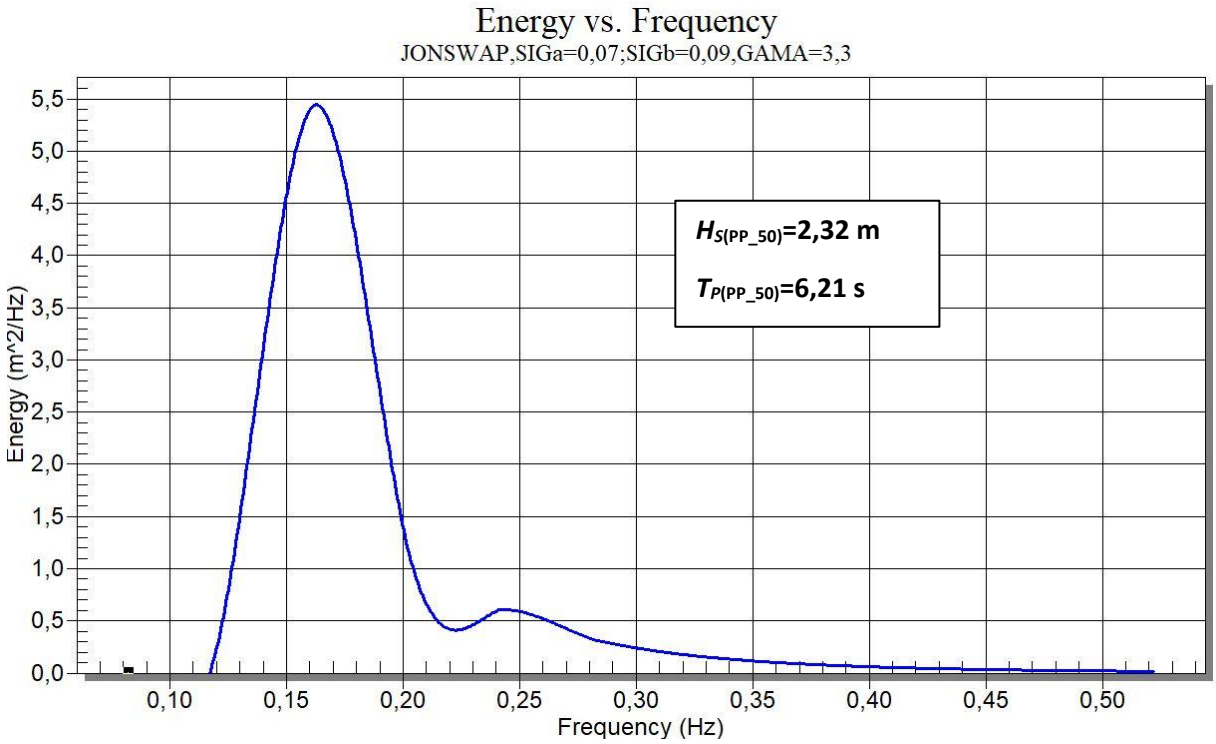

Figure 6.16 – Power diagram of the deepwater incident wave spectrum with statistical characteristics for a

50-year return period for sector IV (JONSWAP spectrum; γ = 3.3; directional dispersion ±300) for direction W (270^o)

6.1.3.2.4. Podstrana-Duće area

On the lines of generating a numerical model (open border) for the analysis of the beach on the Podstrana-Duće area, boundary conditions are defined by selecting deep-water incident spectra with statistical characteristics and feedback periods shown in Figures 6.17 to 6.19, and obtained based on making a long-term wave forecast (chapter 3.1).

Selected basic directions from individual sectors for which numerical wave simulations will be performed are **SE (135°), SSW (202.5°)** and **W (270°)**. Although there is a high probability that the realistic directions of wind waves at the location deviate a few degrees from those chosen here, each of these directions was chosen for several reasons.

The SE direction (135°) was chosen because wind data (Table 2.2) indicate that wind from this direction is the most dominant in sector I.

The direction of SSW (202.5°) was chosen because wind data (Table 2.2) indicate that wind from this direction is the most dominant in Sector III, although the fetch (Tables 3.14 and 3.15) for the development of waves from this direction is slightly shorter than the direction of wind SW (225°).

The w direction (270°) was chosen even though wind data (Table 2.2) indicate that the wind from the WSW direction (247.5°) is the most dominant in sector IV, because considering the orientation of the beach and the longest calculated fetch (Tables 3.15 and 3.16) has the greatest impact on the beaches concerned.

It should be emphasized that when modeling the waves of these types of waters, which are usually exposed to wind waves with a variation of the basic direction at the local level, wave conditions are described by the energy spectrum with a certain directional dispersion around the basic direction of incident waves (Goda Y., 2000). For this case, a ±30° directional dispersion was selected around the basic directions of incident waves, since about 85% of the wave energy is propagated in this zone. Thus, in numerical simulations, all directional wave components in a total angle of 60o were considered, which represents an additional degree of safety.

For all selected directions, numerical simulations will be conducted with wave parameters for a return period of 50 years.

Figures 6.17 to 6.19 give the energy distributions of the incident wave spectrums used with respect to the frequency range. In all numerical simulations, the frequency part of the spectrum from fmin=0.08 Hz to fmax=0.6 Hz was used, i.e., the wave spectrum obtained by the superposition of monochromatic wave components with a minimum period from Tmin =1.67 s to waves with a maximum period of Tmax = 12.5 s. The peak periods *of the Tp* spectrum are calculated by the expression *Tp* = 1.1**T0*.

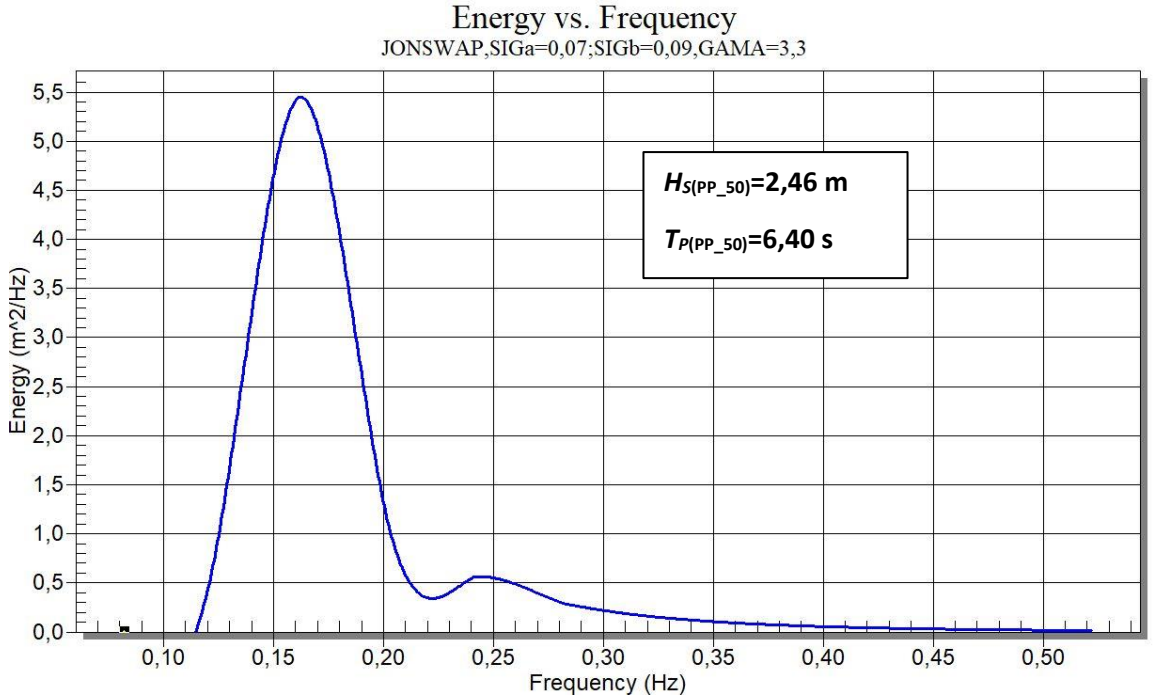

Figure 6.17 – Power diagram of deepwater incident wave spectrum with statistical characteristics for a 50-year return period for sector I (JONSWAP spectrum; γ = 3.3; directional dispersion ±300) for direction SE (135°)

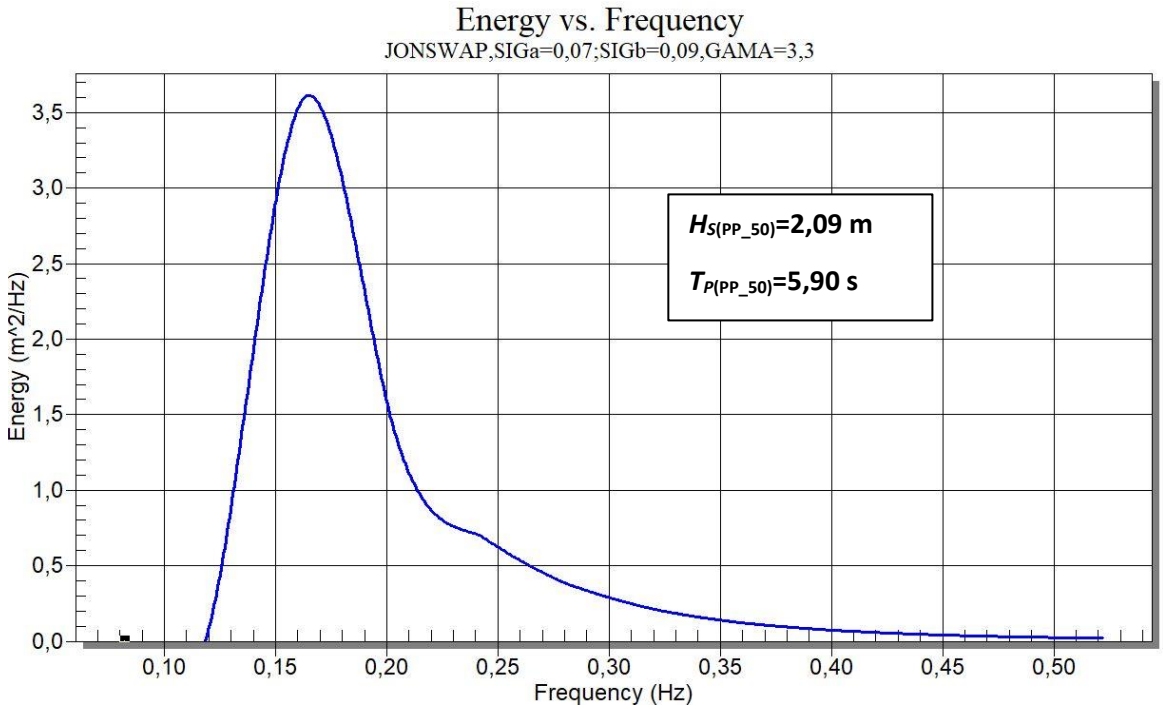

Figure 6.18 – Power diagram of deepwater incident wave spectrum with statistical characteristics for return period of 50 years for sector III (JONSWAP spectrum; γ = 3.3; directional dispersion ±300) for direction SSW (202.5°)

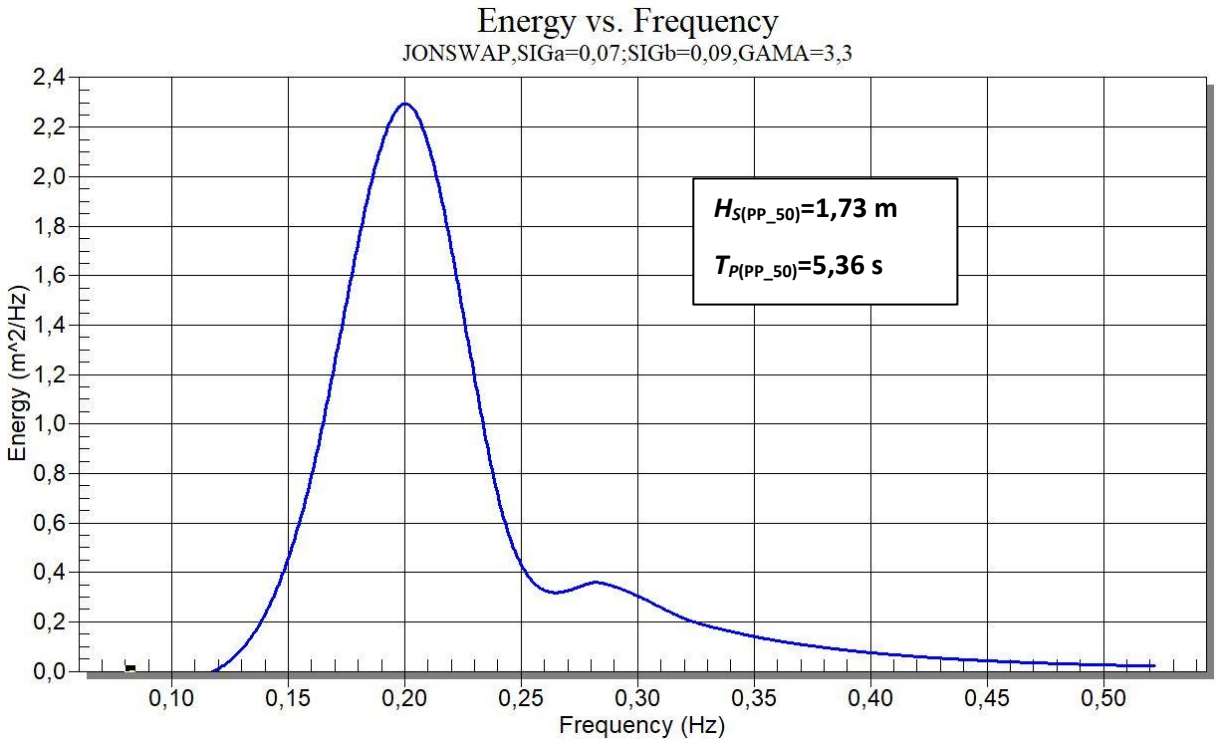

Figure 6.19 – Power diagram of the deepwater incident wave spectrum with statistical characteristics for a 50-year return period for sector IV (JONSWAP spectrum; γ = 3.3; directional dispersion ±300) for direction W (270^o)

6.1.3.2.5. Split (Kašjuni)

On the lines of generating a numerical model (open border) for the analysis of Kašjuni beach in Split, boundary conditions are defined by selecting deep-water incident spectra with statistical characteristics and feedback periods shown in Figures 6.20 and 6.21, and obtained based on the preparation of long-term wave forecast (chapter 3.1).

The selected basic directions from individual sectors for which numerical wave simulations will be performed are **SSW (202.5°)** and **W (270°)**. Although there is a high probability that the realistic directions of wind waves at the location deviate a few degrees from those chosen here, each of these directions was chosen for several reasons.

The direction of SSW (202.5°) was chosen because wind data (Table 2.2) indicate that wind from this direction is the most dominant in sector III, and the fetch (Tables 3.18 and 3.19) is for the development of waves from this direction longer than the wind direction SW (225°).

The w direction (270°) was chosen even though wind data (Table 2.2) indicate that the wind from the WSW direction (247.5°) is the most dominant in sector IV, because considering the orientation of the beach and the longest calculated fetch (Tables 3.19 and 3.20) has the greatest impact on the beach in question.

It should be especially emphasized that when modeling the waves of these types of waters, which are usually exposed to wind waves with a variation of the basic direction at the local level, wave conditions are described by the energy spectrum with a certain directional dispersion around the basic direction of

incident waves (Goda Y., 2000). For this case, a ±30° directional dispersion was selected around the basic directions of incident waves, since about 85% of the wave energy is propagated in this zone. Thus, in numerical simulations, all directional wave components in a total angle of 60o were considered, which represents an additional degree of safety.

For all selected directions, numerical simulations will be conducted with wave parameters for a return period of 50 years.

Figures 6.20 and 6.21 give the energy distributions of the incident wave spectrums used with respect to the frequency range. In all numerical simulations, the frequency part of the spectrum from fmin= 0.08 Hz to fmax= 0.6 Hz was used, i.e., the wave spectrum obtained by the superposition of monochromatic wave components with a minimum period from Tmin = 1.67 s to waves with a maximum period of Tmax = 12.5 s. The peak periods *of the Tp* spectrum are calculated by the expression *Tp* = 1.1**T0*.

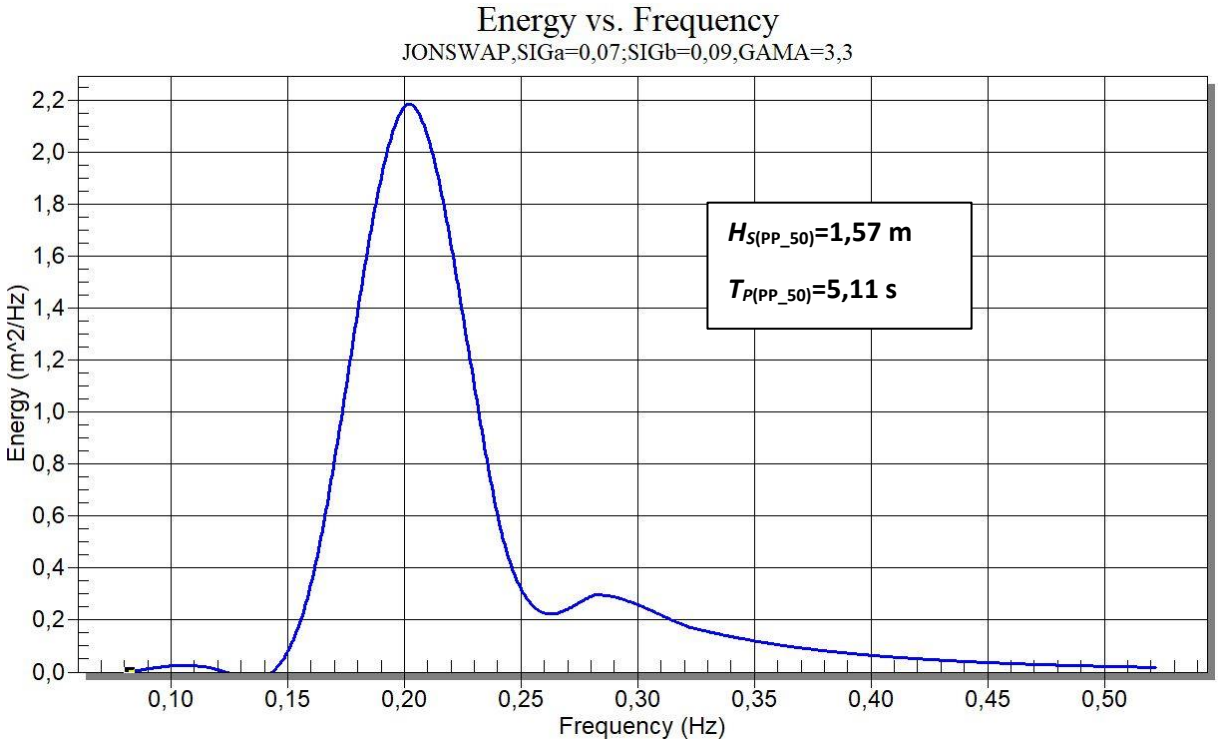

Figure 6.20 – Power diagram of the deepwater incident wave spectrum with statistical characteristics for 50-year return period for sector III (JONSWAP spectrum; γ = 3.3; directional dispersion ±300) for direction SSW (202.5°)

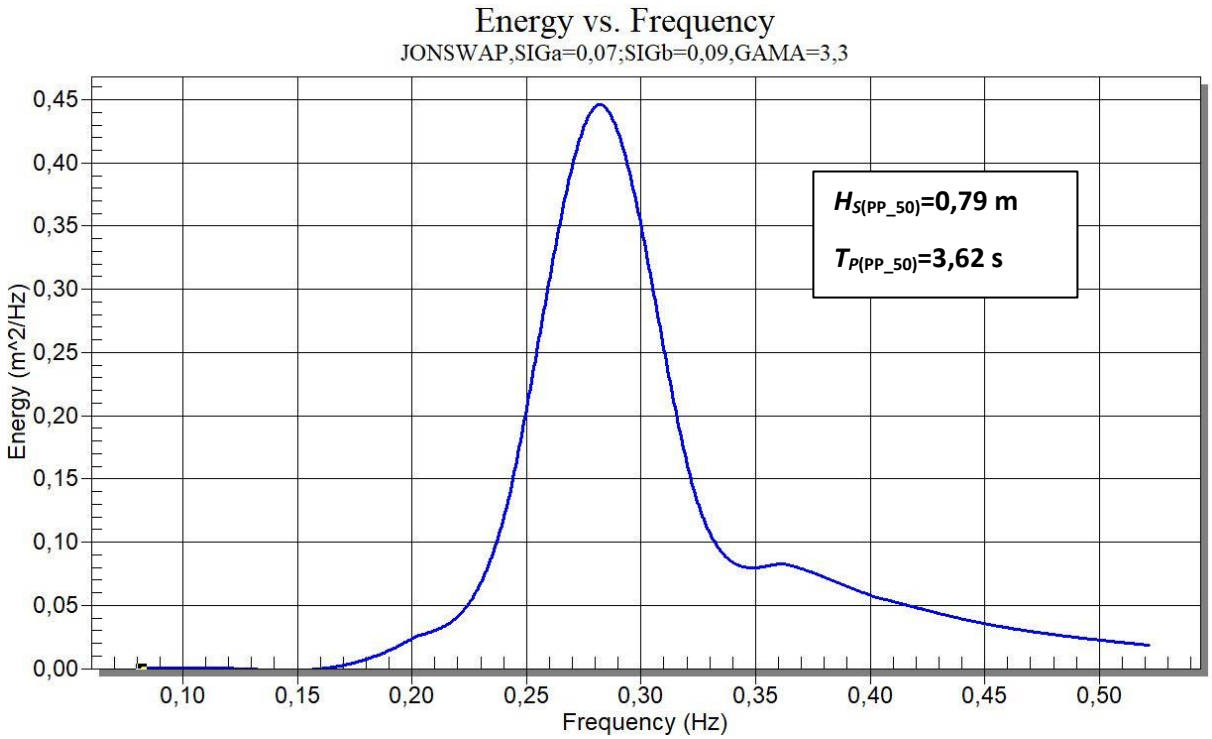

Figure 6.21 – Power diagram of the deepwater incident wave spectrum with statistical characteristics for a 50-year return period for sector IV (JONSWAP spectrum; γ= 3.3; directional dispersion ±300) for direction W (270°)

6.2. Performed numerical simulations labels and parameters

For the purpose of analysis, numerical modeling of wave deformations was carried out for the existing state of each of the five selected beach locations. For each of the locations, modeling was performed with two sea levels, with the mean sea level and the absolute maximum, in accordance with the official hydrographic data on the relevant sea levels for the Split-Dalmatia County.

For the location of the Zlatni rat beach on the island of Brač, a total of eight (8) numerical simulations were performed for the existing state, two simulations each for two sea levels (mean sea level and absolute maximum) for each of the four selected directions of incoming waves.

For the location of Stiniva beach on the island of Vis, a total of two (2) numerical simulations were performed for the existing state, one simulation each for two sea levels (mean sea level and absolute maximum) for the selected direction of incoming waves.

For the location of Podgora beach on the Makarska Riviera, six (6) numerical simulations were performed for the existing state, two simulations for two sea levels (mean sea level and absolute maximum) for each of the three selected directions of incoming waves. Also, an additional one (1) numerical simulation was performed with a proposal for a conceptual solution of protective coastal construction interventions in the control zone for the dominant direction of incoming waves for the control area (SSE, 157.5°), with the sea level corresponding to the absolute maximum. So, a total of seven (7) numerical simulations were performed for the location of the Podgora beach on the Makarska Riviera.

For the location of the beaches on the Podstrana-Duće area, six (6) numerical simulations were performed

for the existing state, two simulations each for two sea levels (mean sea level and absolute maximum) for each of the three selected directions of incoming waves. Also, three (3) additional numerical simulations were performed with a proposal for a conceptual solution of protective coastal construction interventions in the control zone for all analyzed directions of incoming waves for the control area (SE, 135°; SSW, 202.5°; W, 270°), with the sea level corresponding to the absolute maximum. Therefore, a total of eight (9) numerical simulations were performed for the location of the beaches on the Podstrana-Duće area.

For the Kašjuni beach location in Split, four (4) numerical simulations were performed for the existing state, two simulations each for two sea levels (mean sea level and absolute maximum) for each of the two selected directions of incoming waves. Also, two (2) additional numerical simulations were performed with a proposal for a conceptual solution of protective coastal construction interventions for both analyzed directions of incoming waves (SSW, 202.5°; W, 270°) with the sea level corresponding to the absolute maximum. So, a total of six (6) numerical simulations were performed for the location of Kašjuni beach in Split.

A list of all conducted numerical wave simulations with associated simulation marks, beach location, state of construction, wave direction, boundary conditions at the boundary of the generation of incoming waves, and sea level is given in table 6.1.

Table 6.1 – List of performed numerical simulations

SIMUL.	LOCATION	STATE	DIRECTION, MEAN ANGLE	BOUNDARY CONDITIONS	SEA LEVEL
A1	Zlatni rat	existing	ESE, 112,5°	H_s=2,41 m; T_p =6,33 s	SRM
A2	Zlatni rat	existing	SSE, 157,5°	H_s=2,05 m; T_p =5,84 s	SRM
A3	Zlatni rat	existing	SW, 225°	H_s=1,77 m; T_p =5,43 s	SRM
A4	Zlatni rat	existing	WSW, 247,5°	H_s=2,63 m; T_p =6,61 s	SRM
A5	Zlatni rat	existing	ESE, 112,5°	H_s=2,41 m; T_p =6,33 s	Aps.max.
A6	Zlatni rat	existing	SSE, 157,5°	H_s=2,05 m; T_p =5,84 s	Aps.max.
A7	Zlatni rat	existing	SW, 225°	H_s=1,77 m; T_p =5,43 s	Aps.max.
A8	Zlatni rat	existing	WSW, 247,5°	H_s=2,63 m; T_p =6,61 s	Aps.max.

A9	Stiniva	existing	SE, 135°	H_s=4,81 m; T_p =8,94 s	SRM
A10	Stiniva	existing	SE, 135°	H_s=4,81 m; T_p =8,94 s	Aps.max.
A11	Podgora	existing	SSE, 157,5°	H_s=2,15 m; T_p =5,98 s	SRM
A12	Podgora	existing	SW, 225°	H_s=1,45 m; T_p =4,91 s	SRM
A13	Podgora	existing	W, 270°	H_s =2,32 m; T_p =6,21 s	SRM
A14	Podgora	existing	SSE, 157,5°	H_s=2,15 m; T_p =5,98 s	Aps.max.
A15	Podgora	existing	SW, 225°	H_s=1,45 m; T_p =4,91 s	Aps.max.
A16	Podgora	existing	W, 270°	H_s =2,32 m; T_p =6,21 s	Aps.max.
A17	Podgora	conceptual sol.	SSE, 157,5°	H_s=2,15 m; T_p =5,98 s	Aps.max.
A18	Podstrana	existing	SE, 135°	H_s =2,46 m; T_p =6,40 s	SRM
A19	Podstrana	existing	SSW, 202,5°	H_s =2,09 m; T_p =5,90 s	SRM
A20	Podstrana	existing	W, 270°	H_s =1,73 m; T_p =5,36 s	SRM
A21	Podstrana	existing	SE, 135°	H_s =2,46 m; T_p =6,40 s	Aps.max.
A22	Podstrana	existing	SSW, 202,5°	H_s =2,09 m; T_p =5,90 s	Aps.max.
A23	Podstrana	existing	W, 270°	H_s =1,73 m; T_p =5,36 s	Aps.max.
A24	Podstrana	conceptual sol.	SE, 135°	H_s =2,46 m; T_p =6,40 s	Aps.max.
A25	Podstrana	conceptual sol.	SSW, 202,5°	H_s =2,09 m; T_p =5,90 s	Aps.max.
A26	Podstrana	conceptual sol.	W, 270°	H_s =1,73 m; T_p =5,36 s	Aps.max.
A27	Kašjuni	existing	SSW, 202,5°	H_s =1,57 m; T_p =5,11 s	SRM
A28	Kašjuni	existing	W, 270°	H_s =0,79 m; T_p =3,62 s	SRM
A29	Kašjuni	existing	SSW, 202,5°	H_s =1,57 m; T_p =5,11 s	Aps.max.
A30	Kašjuni	existing	W, 270°	H_s =0,79 m; T_p =3,62 s	Aps.max.
A31	Kašjuni	conceptual sol.	SSW, 202,5°	H_s =1,57 m; T_p =5,11 s	Aps.max.
A32	Kašjuni	conceptual sol.	W, 270°	H_s =0,79 m; T_p =3,62 s	Aps.max.

6.3. Modeling results

Keeping in mind the goals that this study wants to achieve, which is primarily the adoption of guidelines for dimensioning and designing beaches made of granular materials, which would increase the level of protection against erosion, and the sustainable and resilient development of the coastal area of Split-Dalmatia County, and in accordance with capabilities of the applied numerical wave model (CGWAVE), the output results of the modeling are presented in several ways. As already mentioned before, in order

to make quality and consistent conclusions, which will ultimately result in coherent and applicable guidelines, it is necessary to ensure a complete understanding of the physical natural processes and impacts that occur on beaches made of granular materials.

This approach to problem solving and the proposed methodology ensure that the default existing beach systems can be upgraded with new conceptual solutions for construction interventions in the coastal area, with the goal of increasing the resistance and sustainability of beach systems in relation to the consequences of climate change.

Therefore, the results of the conducted numerical modeling of the waves, which are given below for each of the subject beaches separately, serve to give pictorial representations of the primary influences that exert erosive processes on beaches made of granular materials.

Here, the field representations of significant wave heights (Hs) are primarily important, which clearly represent the spatial occurrence and distribution of wave impacts in the considered water areas, as the main driving forces under whose influence erosive processes occur on beaches made of granular materials.

Furthermore, it is very important to know the ways of propagation of waves from certain directions, especially when they come towards the land, that is, towards the beach itself. As explained in detail in Chapter 5 of this study, intuitively it is only possible to guess how the complex interplay of numerous transformation and deformation processes of incoming waves will take place, and therefore numerical modeling is necessary in order to determine the resulting state waves fully realistically, especially in areas close to the coast. This is particularly important from the point of view of determining the primary vectors that determine the direction and amount of the potential of beach material transfer, and thus the potential of erosion and sustainability of the considered beach.

Last, but not least, are representations of the zone of potential wave breaking. As explained in detail in chapter 5 of this study, most of the erosive processes of granular beaches occur within this zone, because these are the zones where most of the wave energy of incoming waves is released, due to numerous combinations of horizontal and vertical movements that cause the transport of beach sediments. For this reason, it is very important to know which beach zones are particularly exposed and threatened by the occurrence of this wave impact, in order to be able to fully see and understand the main physical processes and provide concrete solutions that eliminate existing problems with erosion, but also reduce the risk for their potential occurrence in the future due to the consequences of climate change.

In order to keep the focus on important things, and considering the relatively large number of conducted numerical simulations, the results (fields of significant wave heights, current wave contours and wave breaking zones) are not presented for all conducted numerical simulations. Namely, in the following representations, the field displays of significant wave heights and current wave contours for numerical simulations with the sea level corresponding to the absolute maximum are not included, because they are almost identical to those performed based on the mean sea level. In contrast to that, the results of the wave breaking zones are shown for all simulations, because as explained before, it is a crucially important data, based on which potential erosive processes can be clearly observed.

6.3.1. Brač (Zlatni rat)

In accordance with the previously stated, a total of eight (8) numerical simulations were conducted for the subject area of Zlatni rat beach on Brač, and below are the following results:

1. Figure 6.22 – Current wave outline for simulation A1 – the existing state of Zlatni rat beach (Brač) with wave parameters from the direction of ESE (112.5°), 50-year return period (Hs=2.41 m; Tp=6.33 s) and sea level corresponding to the middle sea level (SRM)
2. Figure 6.23 – Field of significant wave heights for simulation A1 – the existing state of Zlatni rat beach (Brač) with wave parameters from the direction of ESE (112.5°), 50-year return period (Hs=2.41 m; Tp=6.33 s) and sea level corresponding to middle sea level (SRM)
3. Figure 6.24 – Wave breaking zone for simulation A1 – the existing state of Zlatni rat beach (Brač) with wave parameters from the Direction of ESE (112.5°), 50-year return period (Hs=2.41 m; Tp=6.33 s) and sea level corresponding to the middle sea level (SRM)
4. Figure 6.25 – Wave breaking zone for simulation A5 – the existing state of Zlatni rat beach (Brač) with wave parameters from the Direction of ESE (112.5°), 50-year return period (Hs=2.41 m; Tp=6.33 s) and sea level corresponding to absolute maximum
5. Figure 6.26 – Current wave outline for simulation A2 – the existing state of Zlatni rat beach (Brač) with wave parameters from the direction of SSE (157.5°), 50-year return period (Hs=2.05 m; Tp=5.84 s) and sea level corresponding to middle sea level (SRM)
6. Figure 6.27 – Field of significant wave heights for simulation A2 – the existing state of Zlatni rat beach (Brač) with wave parameters from the direction of SSE (157.5°), 50-year return period (Hs=2.05 m; Tp=5.84 s) and sea level corresponding to middle sea level (SRM)
7. Figure 6.28 – Wave breaking zone for simulation A2 – the existing state of Zlatni rat beach (Brač) with wave parameters from the Direction of SSE (157.5°), 50-year return period (Hs=2.05 m; Tp=5.84 s) and sea level corresponding to middle sea level (SRM)
8. Figure 6.29 – Wave breaking zone for simulation A6 – the existing state of Zlatni rat beach (Brač) with wave parameters from the Direction of SSE (157.5°), 50-year return period (Hs=2.05 m; Tp=5.84 s) and sea level corresponding to absolute maximum
9. Figure 6.30 – Current wave outline for simulation for Simulation A3 – the existing state of Zlatni rat beach (Brač) with wave parameters from the direction of SW (225°), 50-year return period (Hs=1.77 m; Tp=5.43 s) and sea level corresponding to the middle sea level (SRM)
10. Figure 6.31 – Field of significant wave heights for simulation A3 – the existing state of Zlatni rat beach (Brač) with wave parameters from the direction of SW (225°), 50-year return period (Hs=1.77 m; Tp=5.43 s) and sea level corresponding to the middle sea level (SRM)
11. Figure 6.32 – Wave breaking zone for simulation A3 – the existing state of Zlatni rat beach (Brač) with wave parameters from the direction of SW (225°), 50-year return period (Hs=1.77 m; Tp=5.43 s) and sea level corresponding to the middle sea level (SRM)
12. Figure 6.33 – Wave breaking zone for simulation A7 – the existing state of Zlatni rat beach (Brač) with wave parameters from the Direction of SW (225°), 50-year return period (Hs=1.77 m; Tp=5.43 s) and sea level corresponding to absolute maximum
13. Figure 6.34 – Current wave outline for simulation for simulation A4 – existing state of Zlatni rat beach (Brač) with wave parameters from WSW direction (247.5°), 50-year return period (Hs=2.63 m; Tp=6.61 s) and sea level corresponding to middle sea level (SRM)

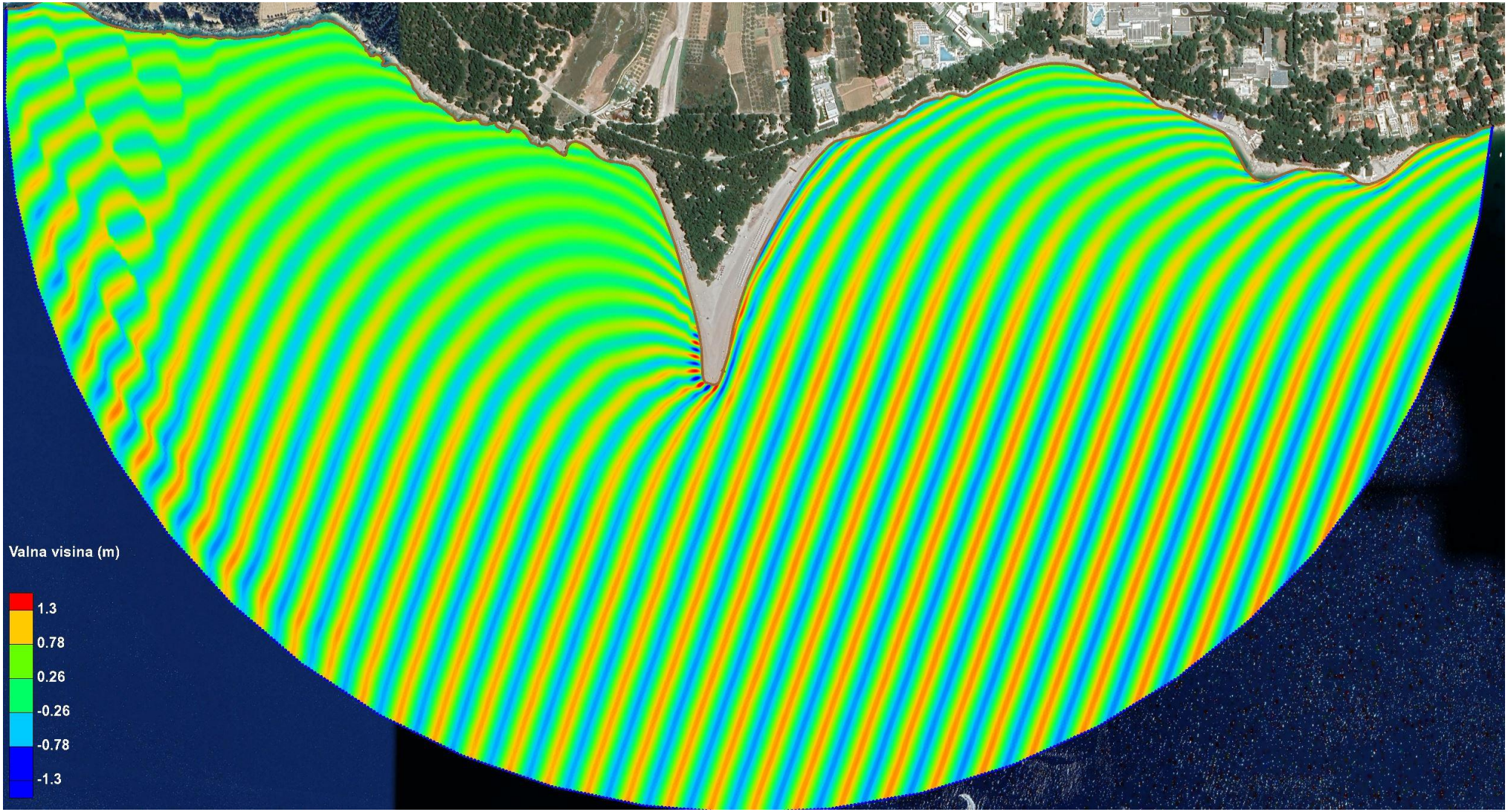

Figure 6.22 – Current wave outline for simulation **A1** – the existing state of Zlatni rat beach (Brač) with wave parameters from the direction of ESE (112.5°), 50-year return period (Hs=2.41 m; Tp=6.33 s) and sea level corresponding to middle sea level (SRM)

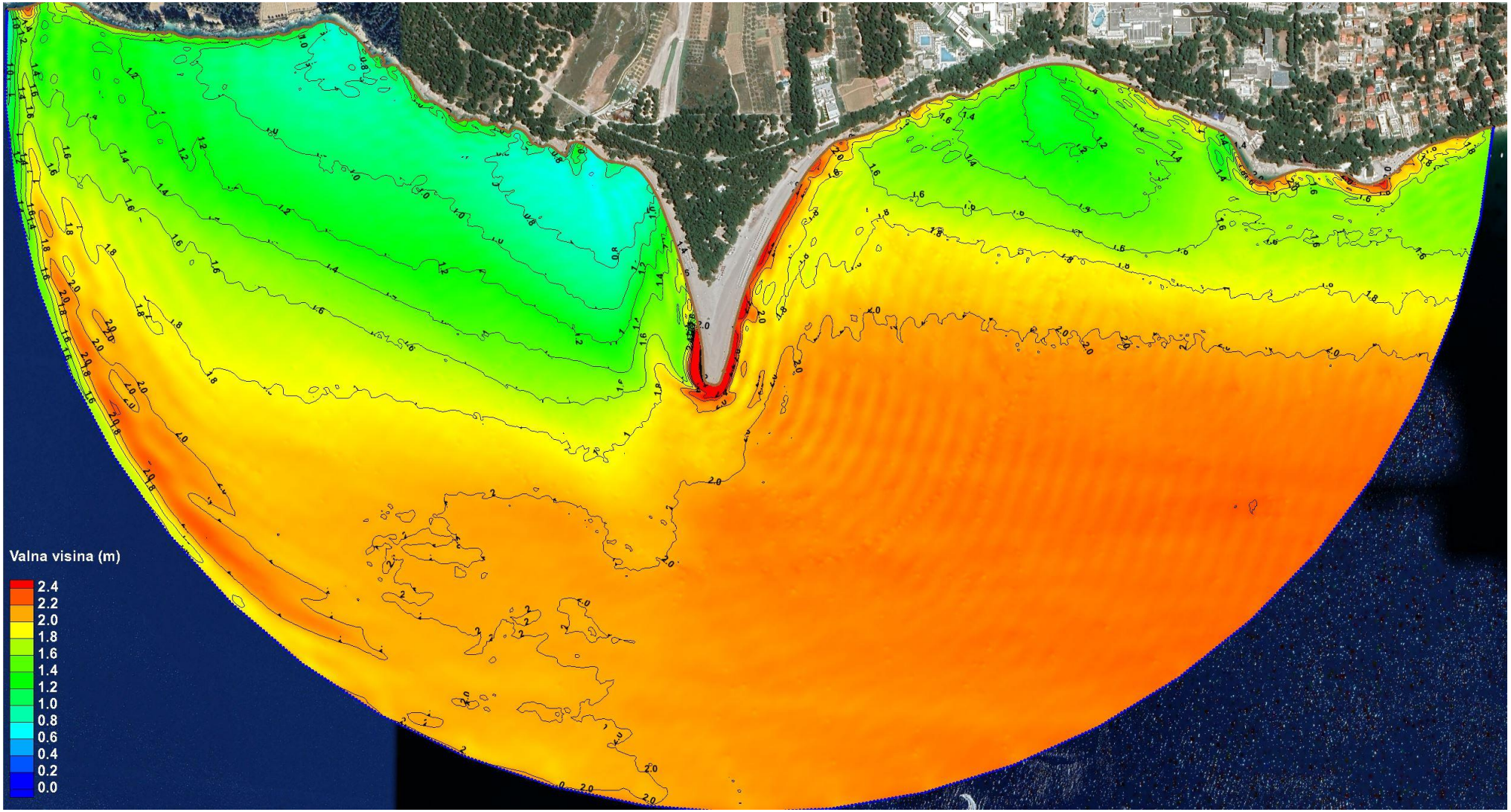

Figure 6.23 – Field of significant wave heights for simulation **A1** – the existing state of Zlatni rat beach (Brač) with wave parameters from the direction of ESE (112.5°), 50-year return period (Hs=2.41 m; Tp=6.33 s) and sea level corresponding to middle sea level (SRM)

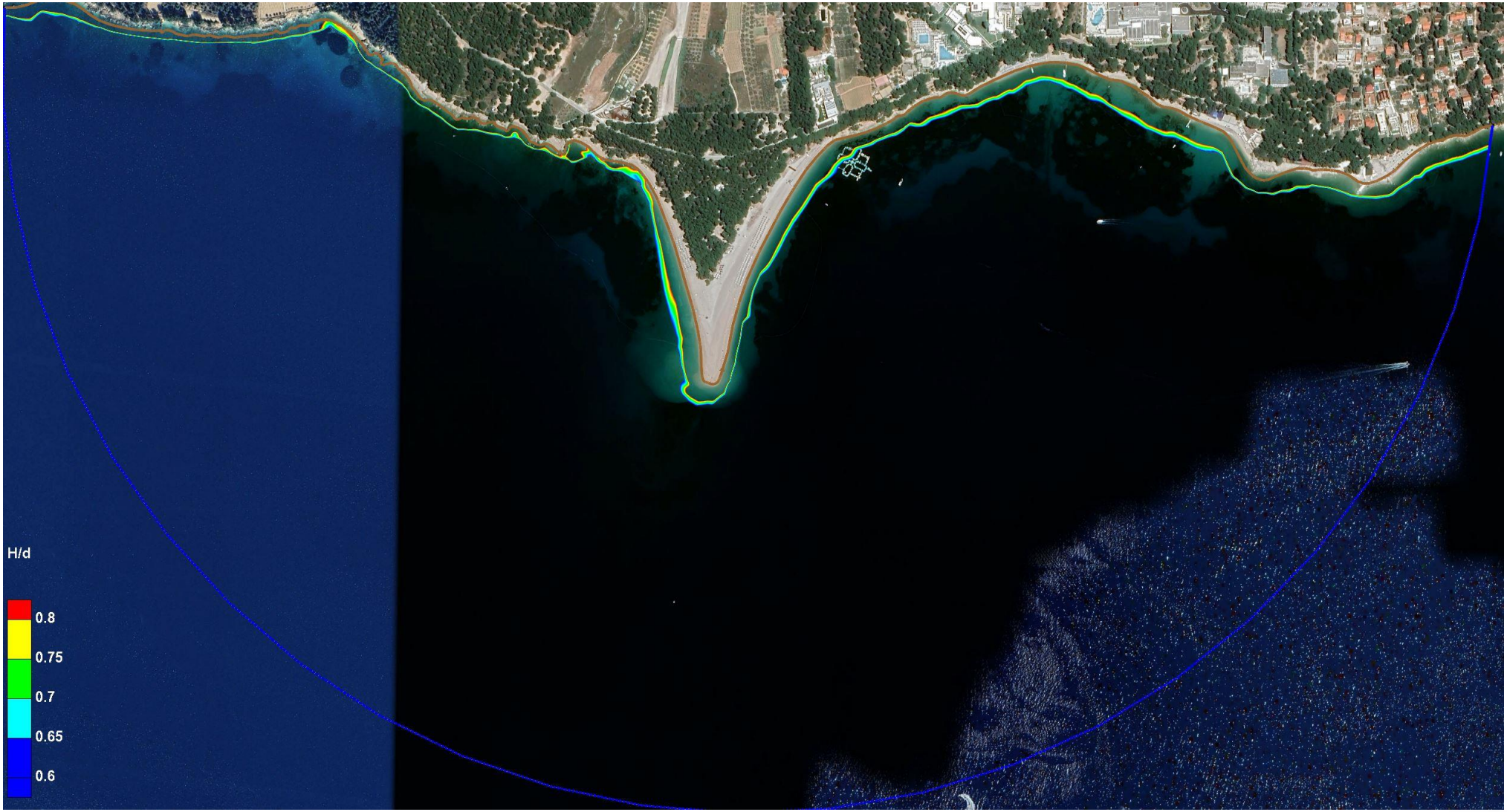

Figure 6.24 – Wave breaking zone for simulation **A1** – the existing state of Zlatni rat beach (Brač) with wave parameters from the Direction of ESE (112.5°), 50-year return period (Hs=2.41 m; Tp=6.33 s) and sea level corresponding to the middle sea level (SRM)

Figure 6.25 – Wave breaking zone for simulation **A5** – the existing state of Zlatni rat beach (Brač) with wave parameters from the direction of ESE (112.5°), 50-year return period (Hs=2.41 m; Tp=6.33 s) and sea level corresponding to **absolute maximum**

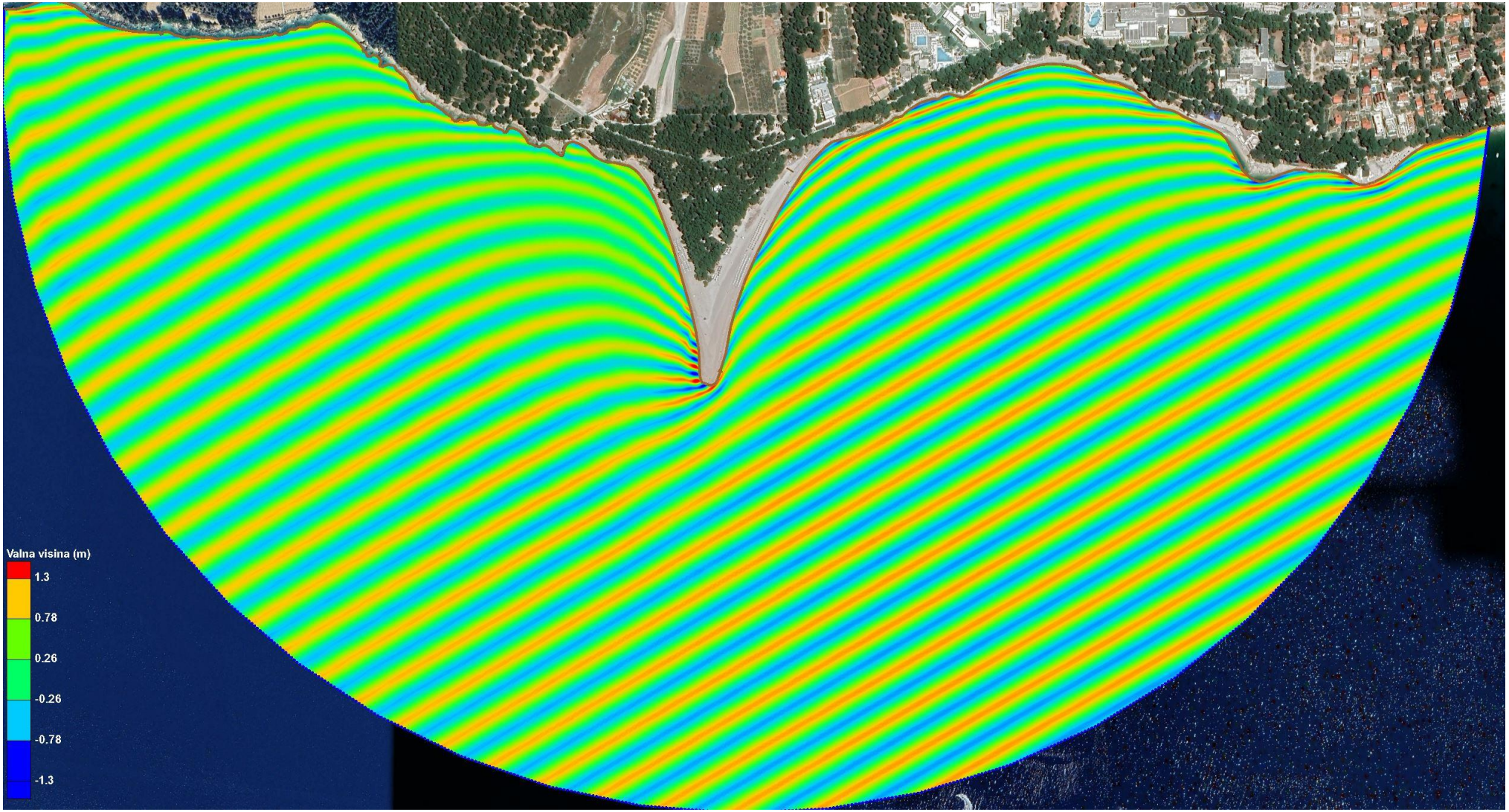

Figure 6.26 – Current wave outline for simulation **A2** – the existing state of Zlatni rat beach (Brač) with wave parameters from the direction of SSE (157.5°), 50-year return period (Hs=2.05 m; Tp=5.84 s) and sea level corresponding to middle sea level (SRM)

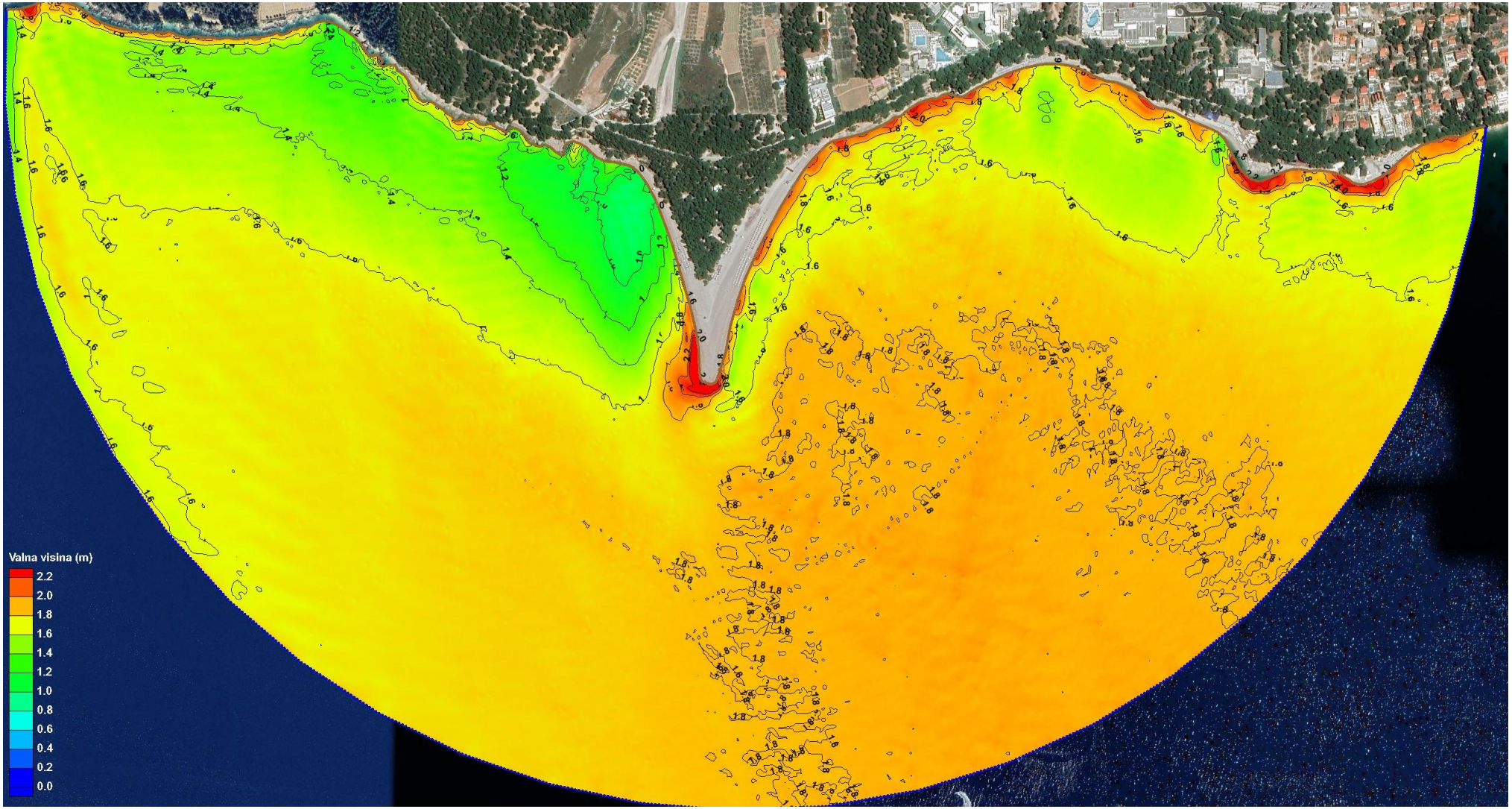

Figure 6.27 – Field of significant wave heights for simulation **A2** – the existing state of Zlatni rat beach (Brač) with wave parameters from the direction of SSE (157.5°), 50-year return period (Hs=2.05 m; Tp=5.84 s) and sea level corresponding to middle sea level (SRM)

Figure 6.28 – Wave breaking zone for simulation **A2** – the existing state of Zlatni rat beach (Brač) with wave parameters from the direction of SSE (157.5°), 50-year return period (Hs=2.05 m; Tp=5.84 s) and sea level corresponding to middle sea level (SRM)

Figure 6.29 – Wave breaking zone for simulation **A6** – the existing state of Zlatni rat beach (Brač) with wave parameters from the direction of SSE (157.5°), 50-year return period (Hs=2.05 m; Tp=5.84 s) and sea level corresponding to **absolute maximum**

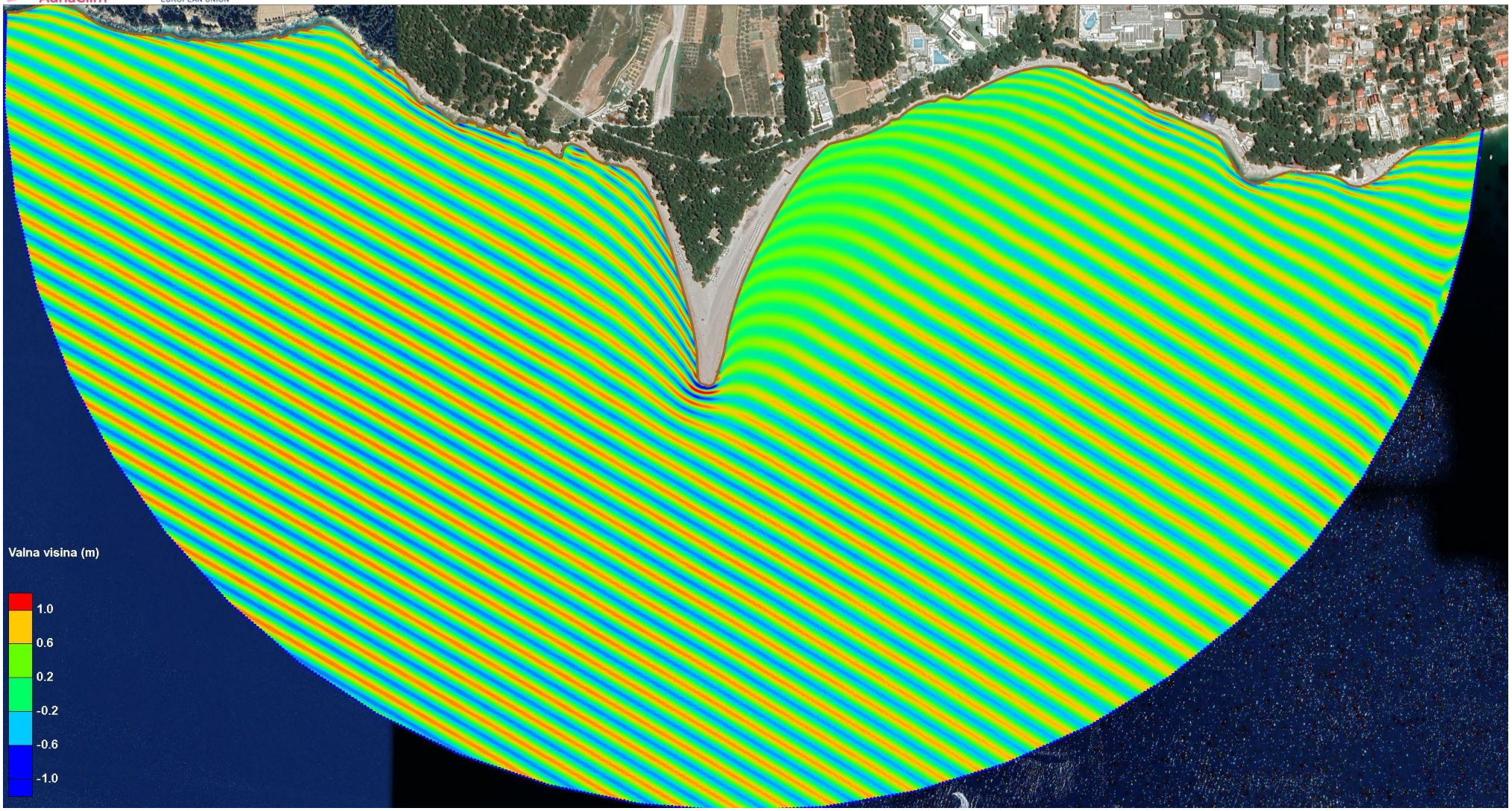

Figure 6.30 – Current wave outline for simulation for Simulation A3 – the existing state of Zlatni rat beach (Brač) with wave parameters from the direction of SW (225°), 50-year return period (Hs=1.77 m; Tp=5.43 s) and sea level corresponding to the middle sea level (SRM)

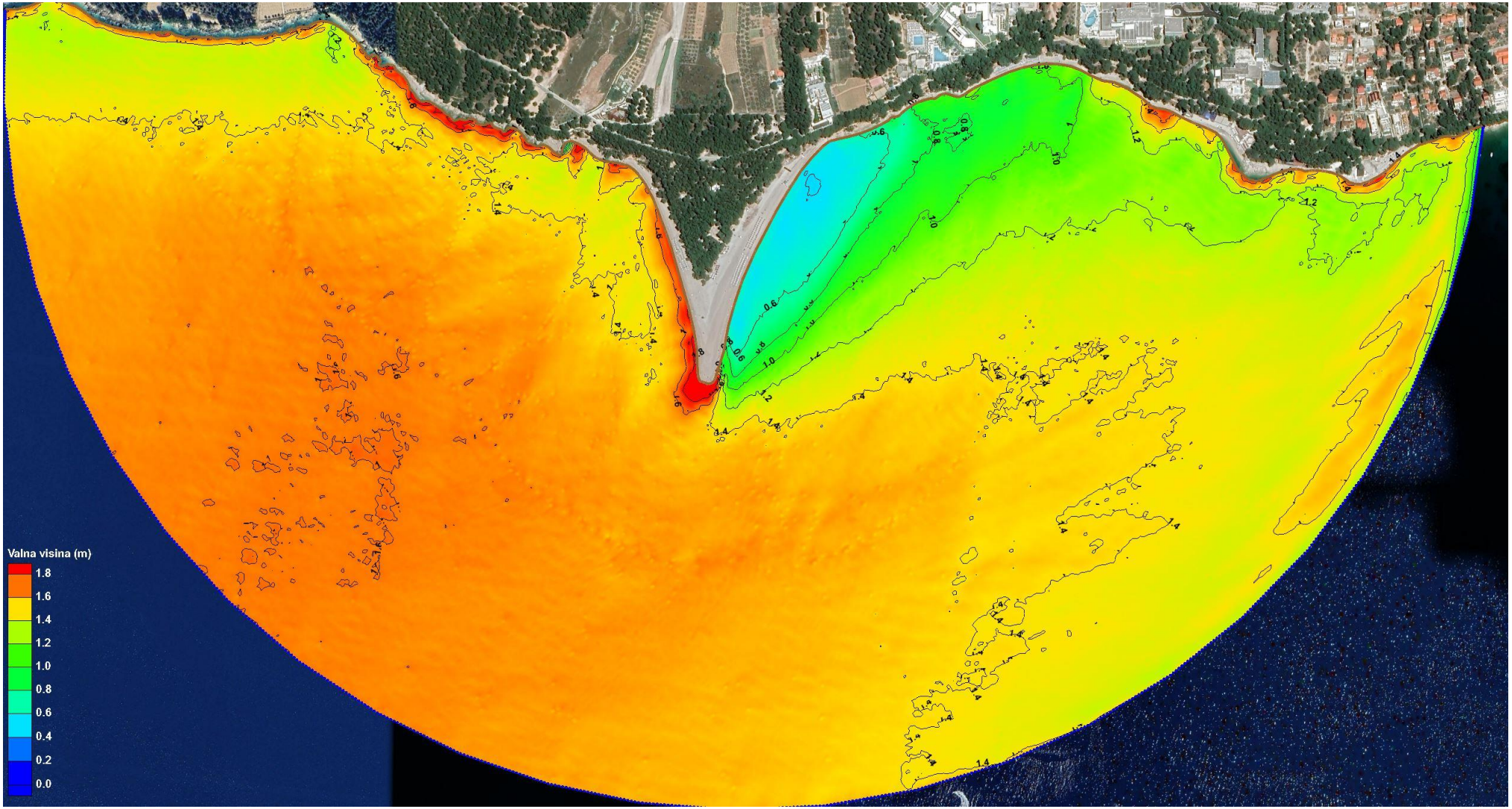

Figure 6.31 – Field of significant wave heights for simulation **A3** – the existing state of Zlatni rat beach (Brač) with wave parameters from the direction of SW (225°), 50-year return period (Hs=1.77 m; Tp=5.43 s) and sea level corresponding to the middle sea level (SRM)

Figure 6.32 – Wave breaking zone for simulation **A3** – the existing state of Zlatni rat beach (Brač) with wave parameters from the direction of SW (225°), 50-year return period (Hs=1.77 m; Tp=5.43 s) and sea level corresponding to middle sea level (SRM)

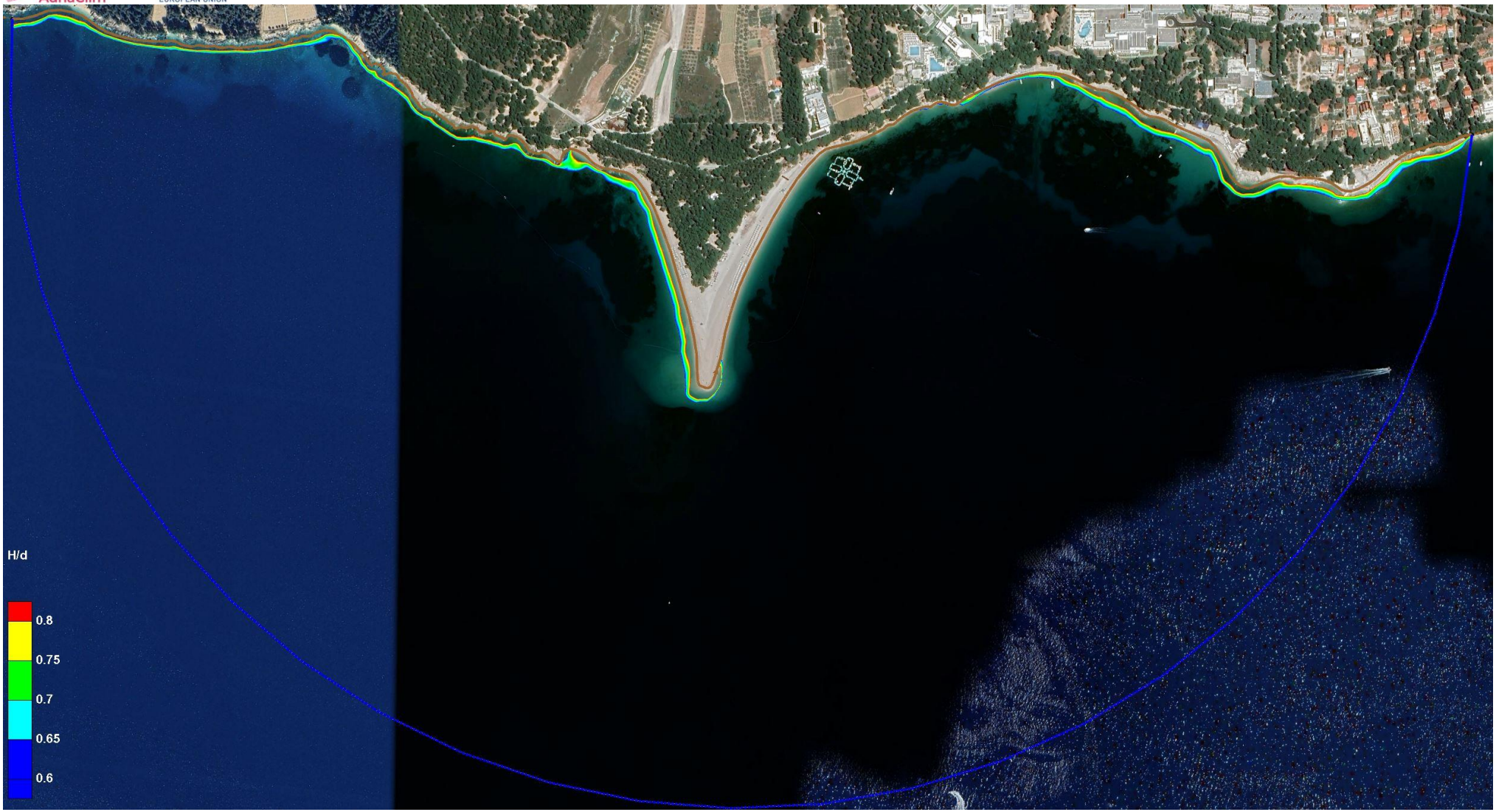

Figure 6.33 – Wave breaking zone for simulation **A7** – the existing state of Zlatni rat beach (Brač) with wave parameters from the direction of SW (225°), 50-year return period (Hs=1.77 m; Tp=5.43 s) and sea level corresponding to **absolute maximum**

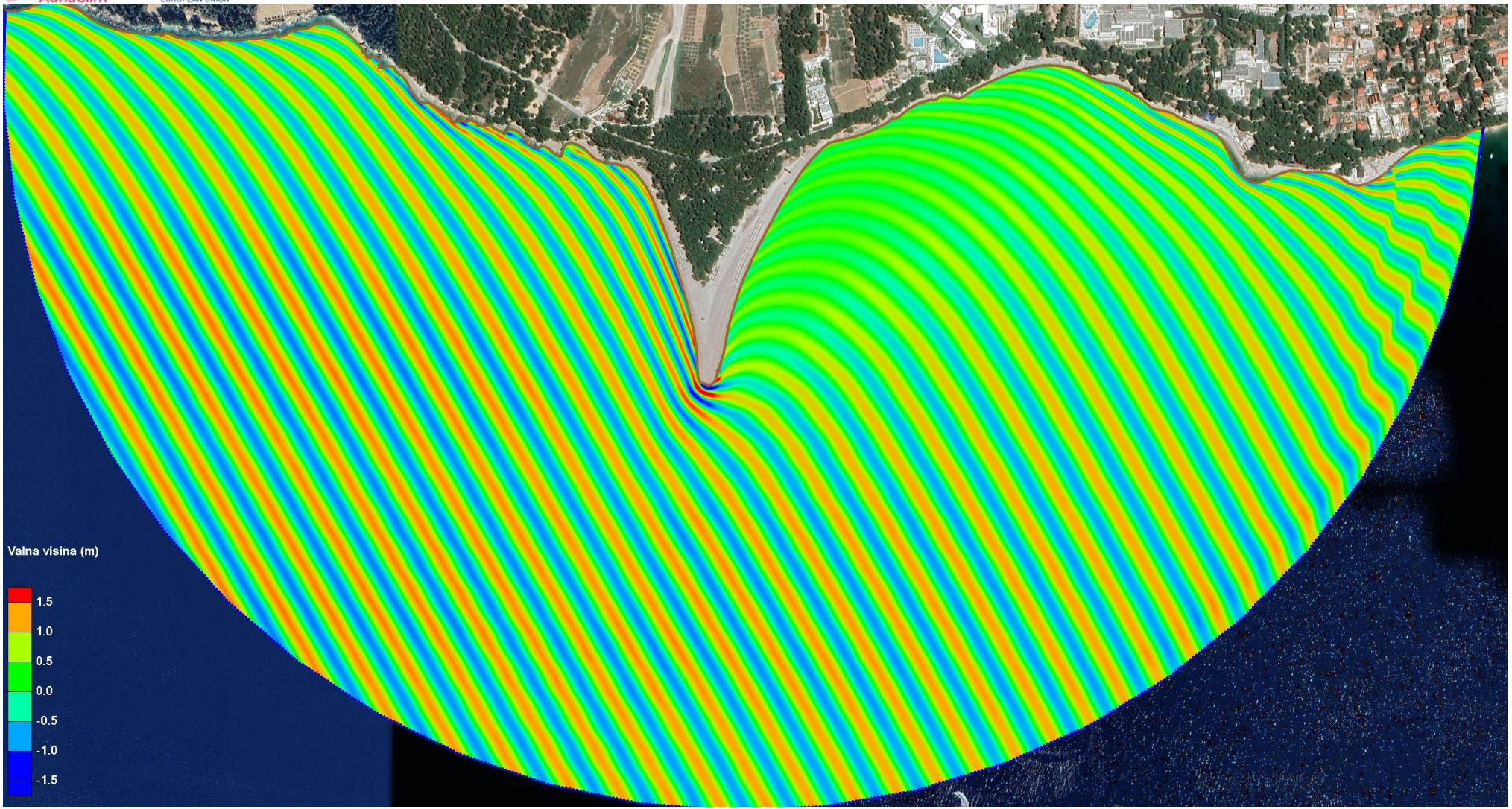

Figure 6.34 – Current wave outline for simulation for simulation **A4** – existing state of Zlatni rat beach (Brač) with wave parameters from WSW direction (247.5°), 50-year return period (Hs=2.63 m; Tp=6.61 s) and sea level corresponding to middle sea level (SRM)

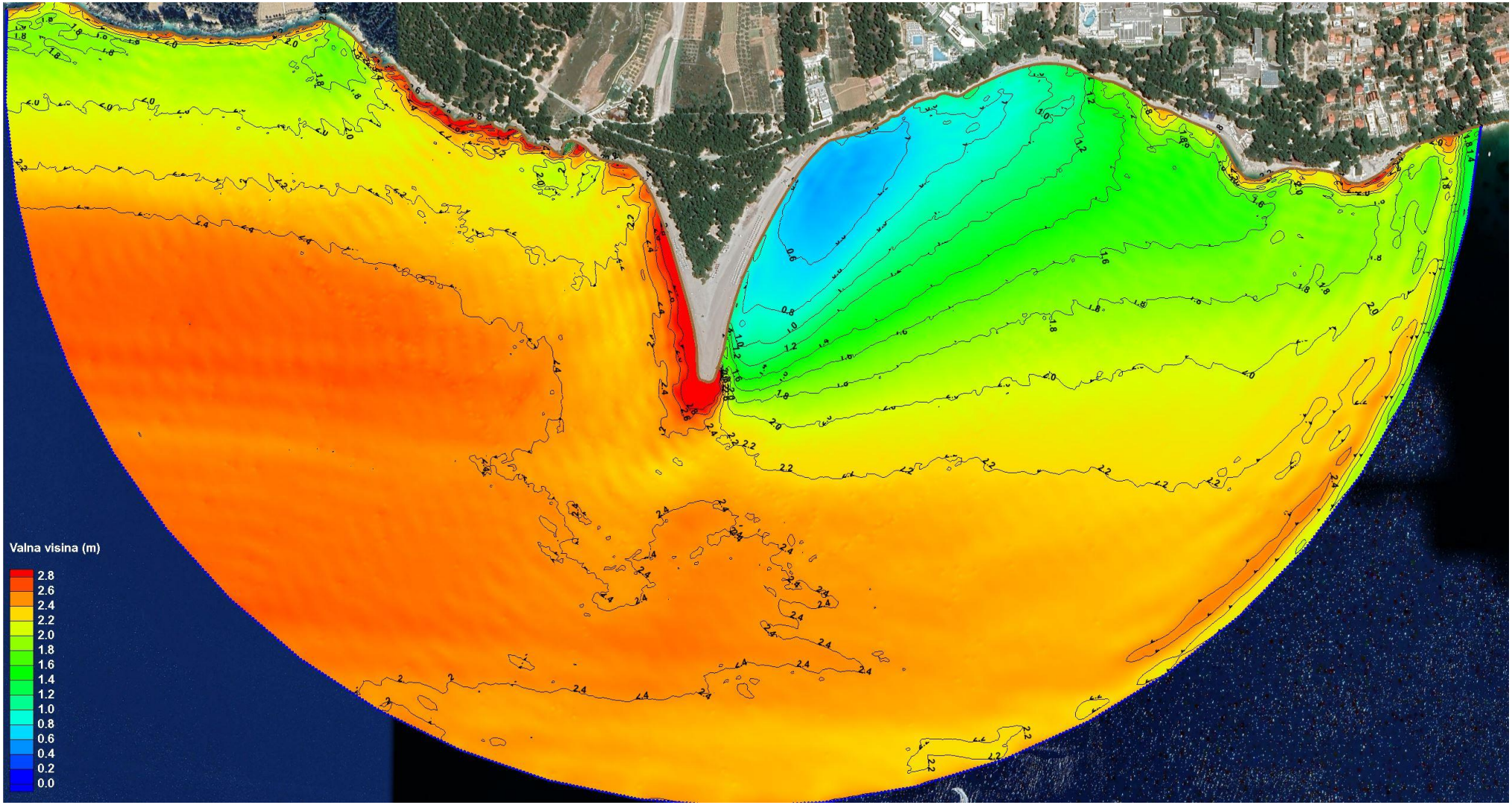

Figure 6.35 – Field of significant wave heights for simulation **A4** – the existing state of Zlatni rat beach (Brač) with wave parameters from WSW direction (247.5°), 50-year return period (Hs=2.63 m; Tp=6.61 s) and sea level corresponding to middle sea level (SRM)

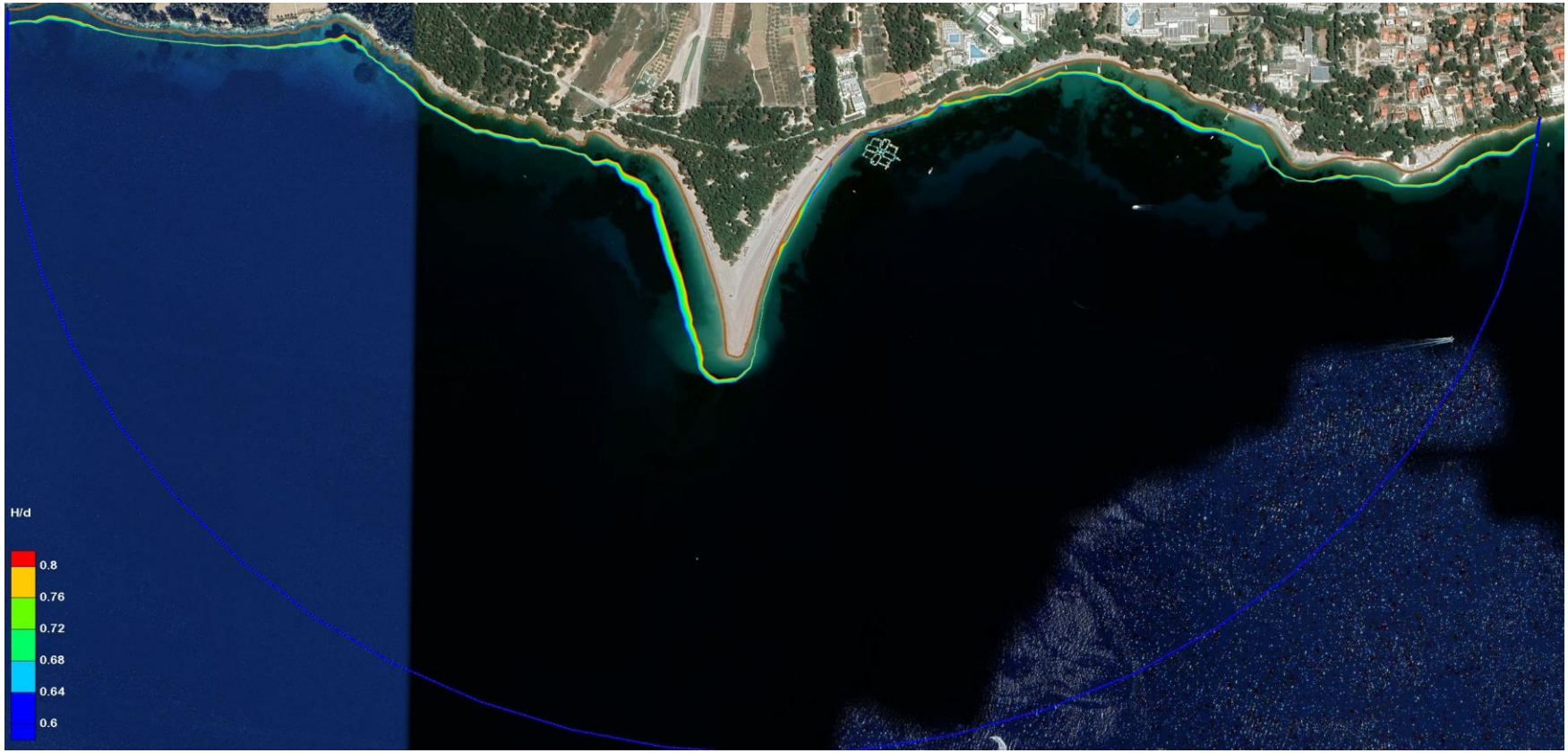

Figure 6.36 – Wave breaking zone for simulation **A4** – the existing state of Zlatni rat beach (Brač) with wave parameters from the WSW direction (247.5°), a 50-year return period (Hs=2.63 m; Tp=6.61 s) and sea level corresponding to the middle sea level (SRM)

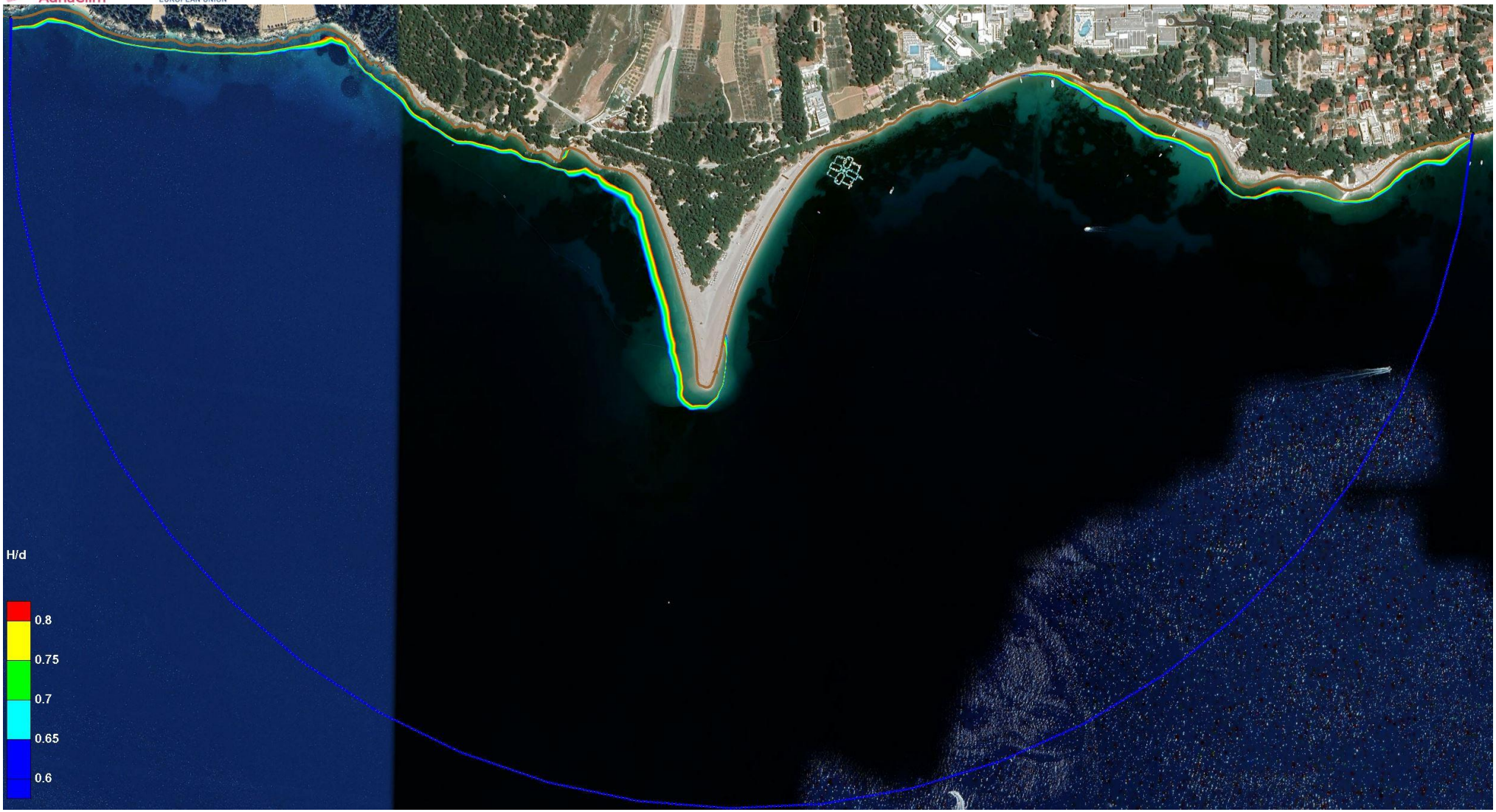

Figure 6.37 – Wave breaking zone for simulation **A8** – the existing state of Zlatni rat beach (Brač) with wave parameters from wsw (247.5°), 50-year turnback period (Hs=2.63 m; Tp=6.61 s) and sea level corresponding to **absolute maximum**

6.3.2. Vis (Stiniva)

In accordance with the previously stated, a total of two (2) numerical simulations were conducted for the Stiniva beach on Vis in question, and the following results are given below:

1. Figure 6.38 – Current wave outline for simulation for simulation A9 – existing state of Stiniva beach (Vis) with wave parameters from the direction of SE (135°), 50-year return period (Hs=4.81 m; Tp=8.94 s) and sea level corresponding to middle sea level (SRM)
2. Figure 6.39 – Field of significant wave heights for simulation A9 – the existing state of Stiniva beach (Vis) with wave parameters from the direction of se (135°), 50-year return period (Hs=4.81 m; Tp=8.94 s) and sea level corresponding to middle sea level (SRM)
3. Figure 6.40 – Wave breaking zone for simulation A9 – existing state of Stiniva beach (Vis) with wave parameters from the direction of SE (135°), 50-year turnback period (Hs=4.81 m; Tp=8.94 s) and sea level corresponding to middle sea level (SRM)

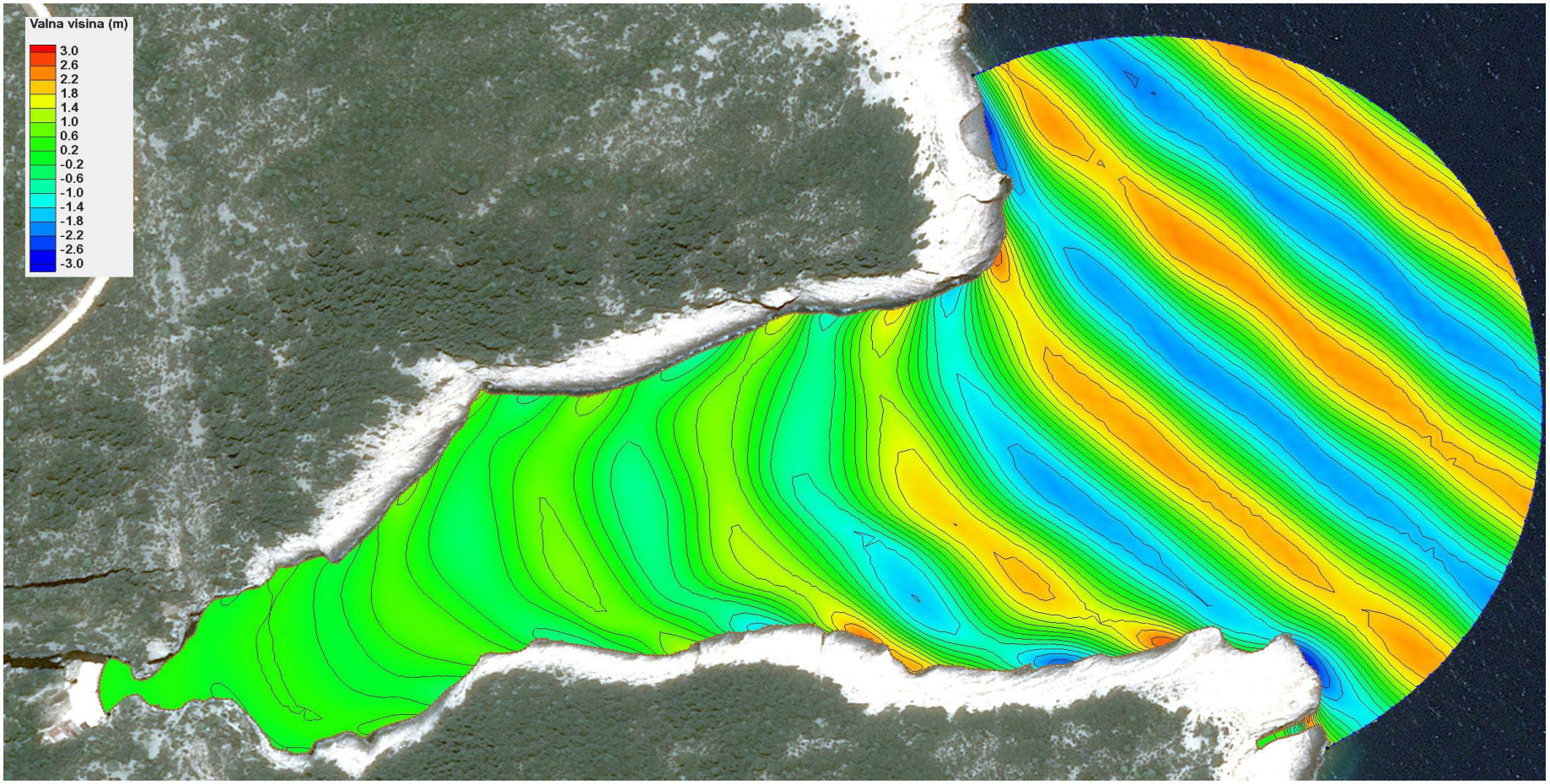

Figure 6.38 – Current wave outline for simulation for simulation **A9** – existing state of Stiniva beach (Vis) with wave parameters from the direction of SE (135°), 50-year return period (Hs=4.81 m; Tp=8.94 s) and sea level corresponding to middle sea level (SRM)

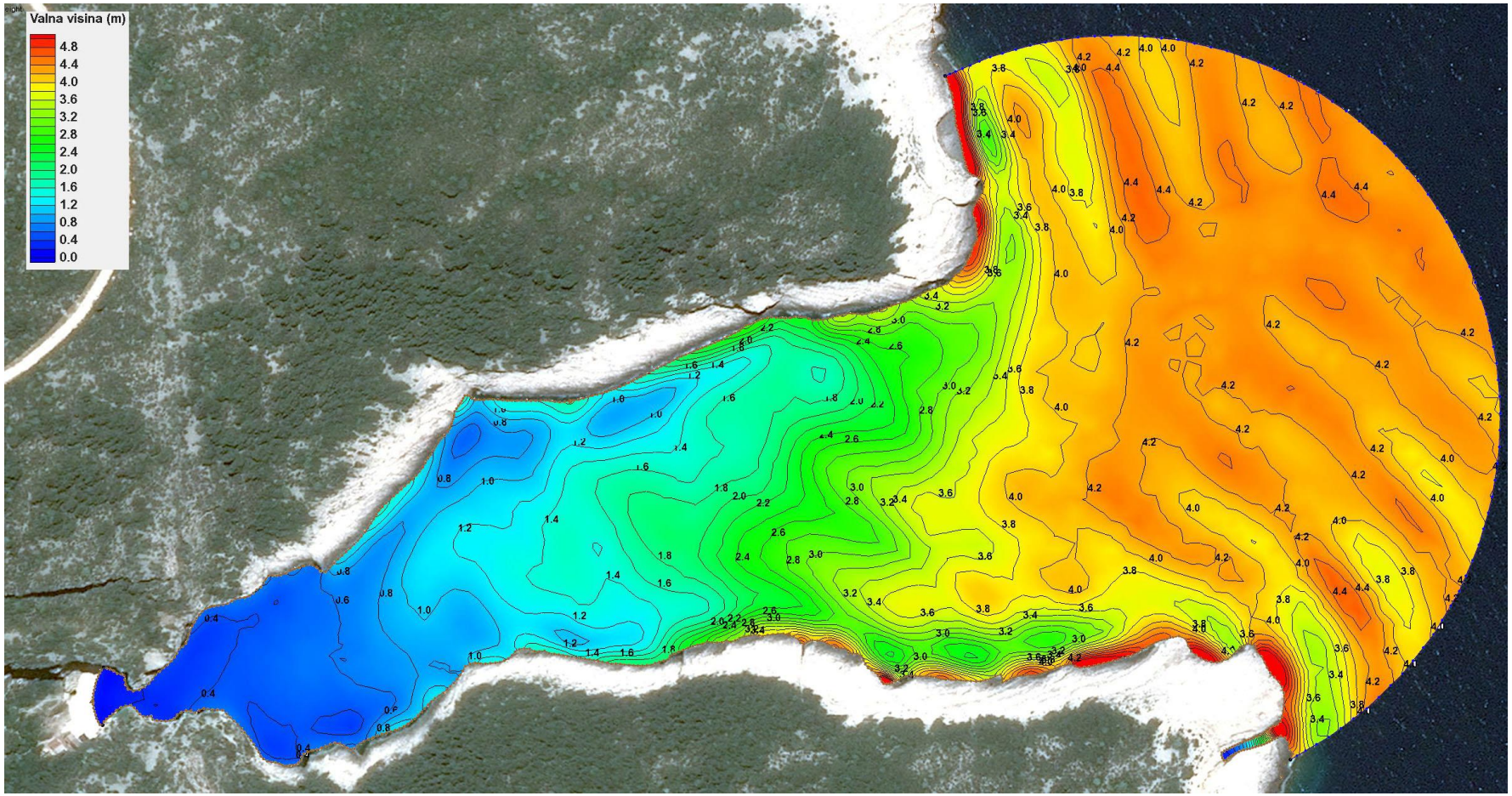

Figure 6.39 – Field of significant wave heights for simulation **A9** – the existing state of Stiniva beach (Vis) with wave parameters from the direction of se (135°), 50-year return period (Hs=4.81 m; Tp=8.94 s) and sea level corresponding to middle sea level (SRM)

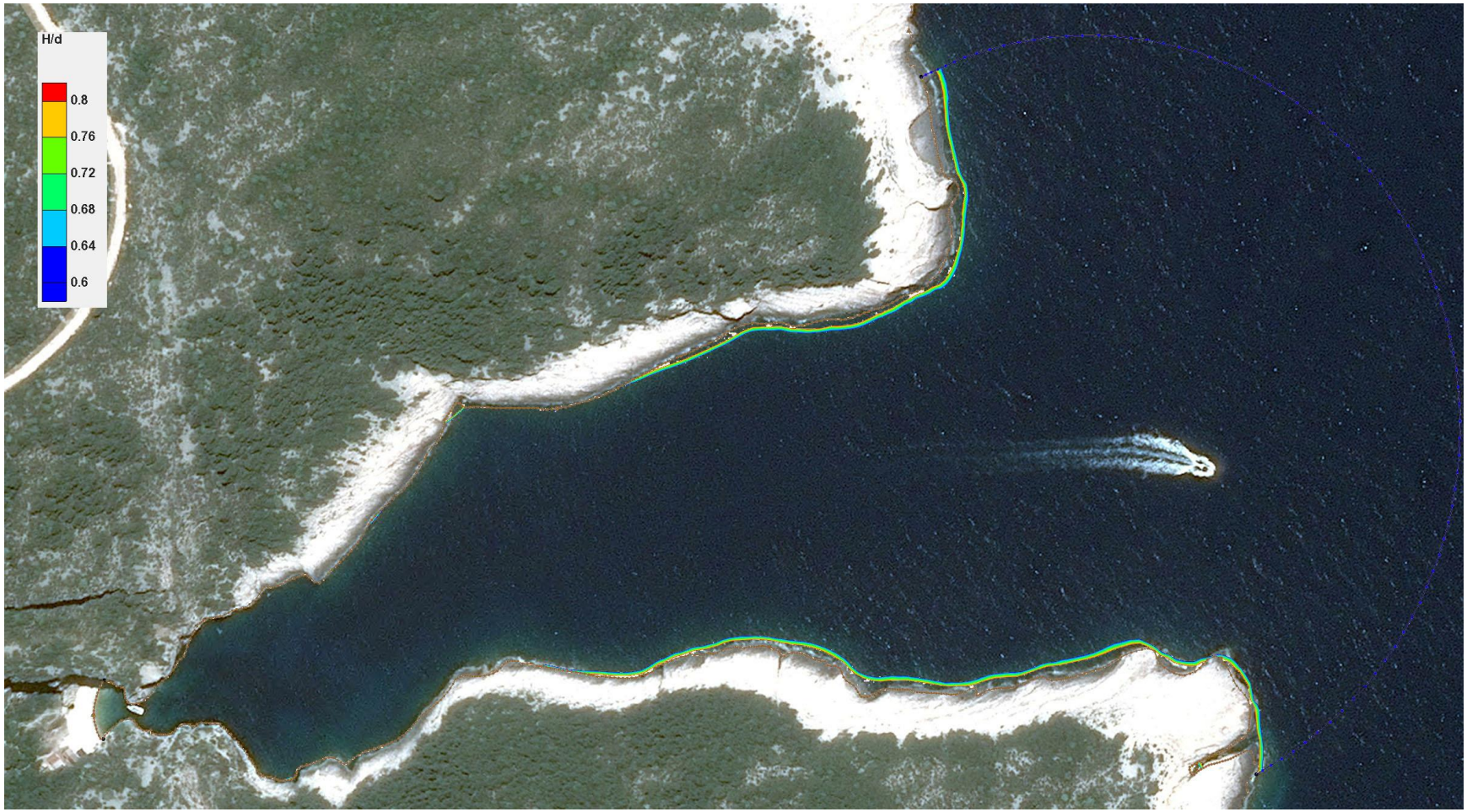

Figure 6.40 – Wave breaking zone for simulation **A9** – existing state of Stiniva beach (Vis) with wave parameters from the direction of SE (135°), 50-year return period (Hs=4.81 m; Tp=8.94 s) and sea level corresponding to middle sea level (SRM)

6.3.3. Makarska Riviera (Podgora)

In accordance with the above, a total of seven (7) numerical simulations were conducted for the area of Podgora beach on the Makarska Riviera, and below are the following results:

1. Figure 6.41 – Current wave outline for Simulation A11 – existing state of Podgora beach (Makarska Riviera) with wave parameters from the Direction of SSE (157.5°), 50-year return period (Hs=2.15 m; Tp=5.98 s) and sea level corresponding to middle sea level (SRM)
2. Figure 6.42 – Field of significant wave heights for simulation A11 – the existing state of Podgora beach (Makarska Riviera) with wave parameters from the Direction of SSE (157.5°), 50-year return period (Hs=2.15 m; Tp=5.98 s) and sea level corresponding to middle sea level (SRM)
3. Figure 6.43 – Wave breaking zone for simulation A11 – the existing state of Podgora beach (Makarska Riviera) with wave parameters from the Direction of the SSE (157.5°), a 50-year return period (Hs=2.15 m; Tp=5.98 s) and sea level corresponding to the Middle Sea Level (SRM)
4. Figure 6.44 – Wave breaking zone for simulation A14 – existing state of Podgora beach (Makarska Riviera) with wave parameters from the Direction of SSE (157.5°), 50-year return period (Hs=2.15 m; Tp=5.98 s) and sea level corresponding to absolute maximum
5. Figure 6.45 – Wave breaking zone for Simulation A17 – conceptual design for the control area (indicated by a yellow arrow) of Podgora beach (Makarska Riviera) with wave parameters from the Direction of SSE (157.5°), 50-year return period (Hs=2.15 m; Tp=5.98 s) and sea level corresponding to absolute maximum
6. Figure 6.46 – Current wave outline for A12 simulation – existing state of Podgora beach (Makarska Riviera) with wave parameters from SW direction (225°), 50-year return period (Hs=1.45 m; Tp=4.91 s) and sea level corresponding to middle sea level (SRM)
7. Figure 6.47 – Field of significant wave heights for simulation A12 – the existing state of Podgora beach (Makarska Riviera) with wave parameters from the direction of SW (225°), 50-year return period (Hs=1.45 m; Tp=4.91 s) and sea level corresponding to the middle sea level (SRM)
8. Figure 6.48 – Wave breaking zone for simulation A12 – existing state of Podgora beach (Makarska Riviera) with wave parameters from the direction of SW (225°), 50-year return period (Hs=1.45 m; Tp=4.91 s) and sea level corresponding to middle sea level (SRM)
9. Figure 6.49 – Wave breaking zone for simulation A15 – the existing state of Podgora beach (Makarska Riviera) with wave parameters from the Direction of SW (225°), a 50-year turnback period (Hs=1.45 m; Tp=4.91 s) and a sea level corresponding to the absolute maximum
10. Figure 6.50 – Current wave outline for simulation A13 – existing state of Podgora beach (Makarska Riviera) with wave parameters from w direction (270°), 50-year return period (Hs=2.32 m; Tp=6.21 s) and sea level corresponding to middle sea level (SRM)
11. Figure 6.51 – Field of significant wave heights for simulation A13 – existing state of Podgora beach (Makarska Riviera) with wave parameters from w direction (270°), 50-year return period (Hs=2.32 m; Tp=6.21 s) and sea level corresponding to middle sea level (SRM)
12. Figure 6.52 – Wave breaking zone for simulation A13 – the existing state of Podgora beach (Makarska Riviera) with wave parameters from the direction W (270°), a 50-year return period (Hs=2.32 m; Tp=6.21 s) and sea level corresponding to the middle sea level (SRM)
13. Figure 6.53 – Wave breaking zone for simulation A16 – existing state of Podgora beach (Makarska Riviera) with wave parameters from w direction (270°), 50-year return period (Hs=2.32 m; Tp=6.21 s) and sea level corresponding to absolute maximum

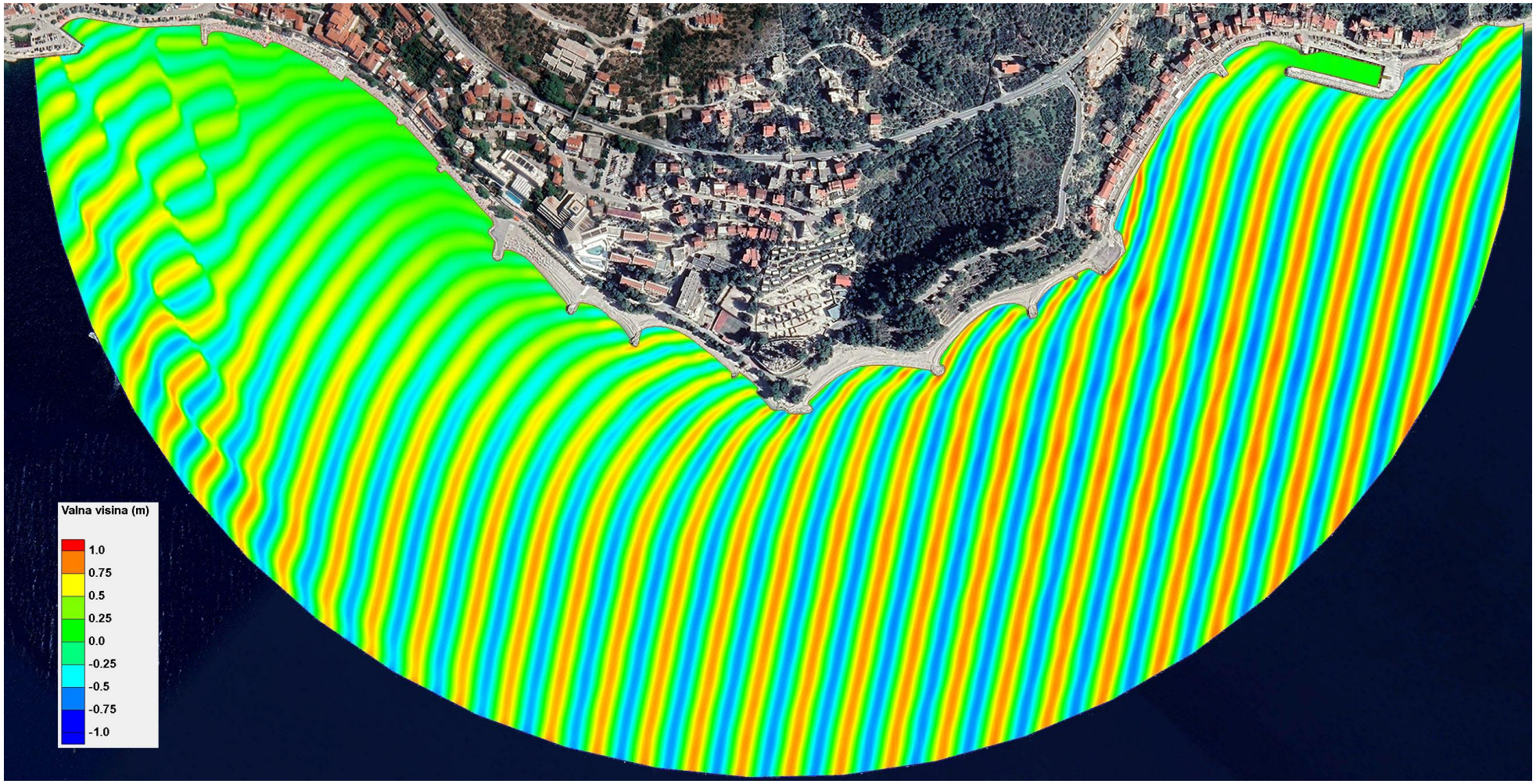

Figure 6.41 – Current wave outline for Simulation **A11** – existing state of Podgora beach (Makarska Riviera) with wave parameters from the Direction of SSE (157.5°), 50-year return period (Hs=2.15 m; Tp=5.98 s) and sea level corresponding to middle sea level (SRM)

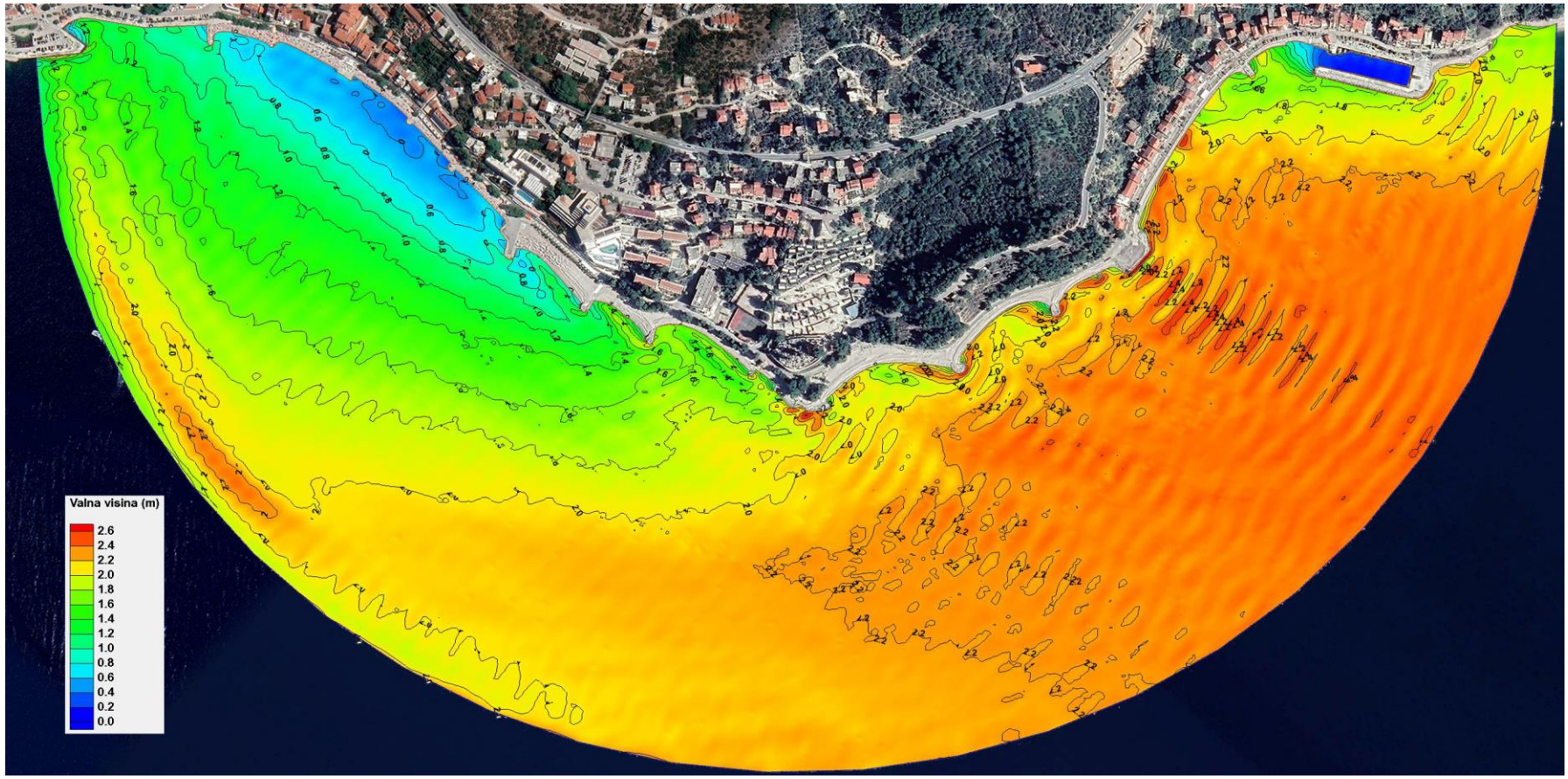

Figure 6.42 – Field of significant wave heights for simulation **A11** – the existing state of Podgora beach (Makarska Riviera) with wave parameters from the Direction of SSE (157.5°), 50-year return period (Hs=2.15 m; Tp=5.98 s) and sea level corresponding to middle sea level (SRM)

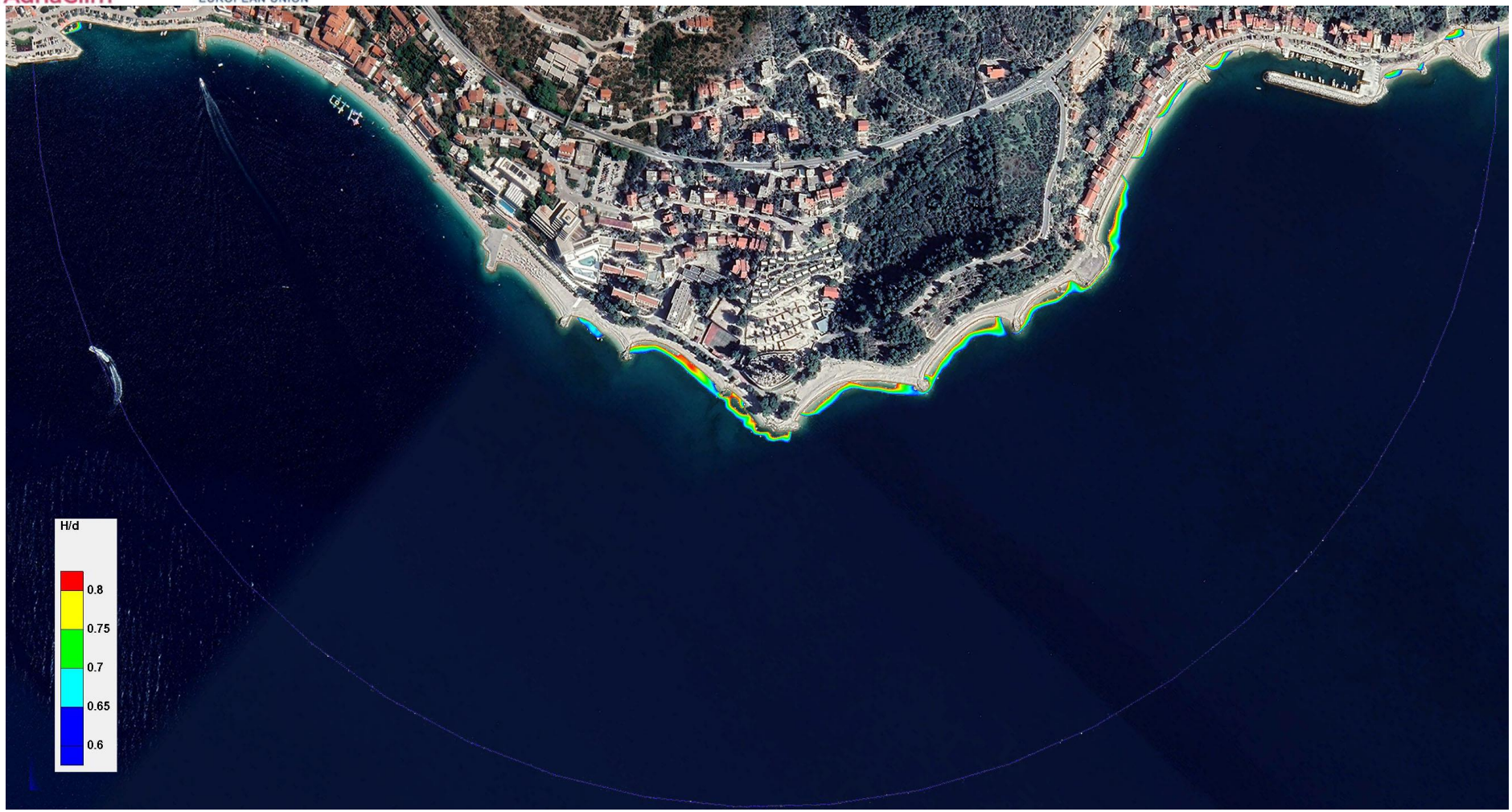

Figure 6.43 – Wave breaking zone for simulation **A11** – the existing state of Podgora beach (Makarska Riviera) with wave parameters from the Direction of the SSE (157.5°), a 50-year return period (Hs=2.15 m; Tp=5.98 s) and sea level corresponding to the Middle Sea Level (SRM)

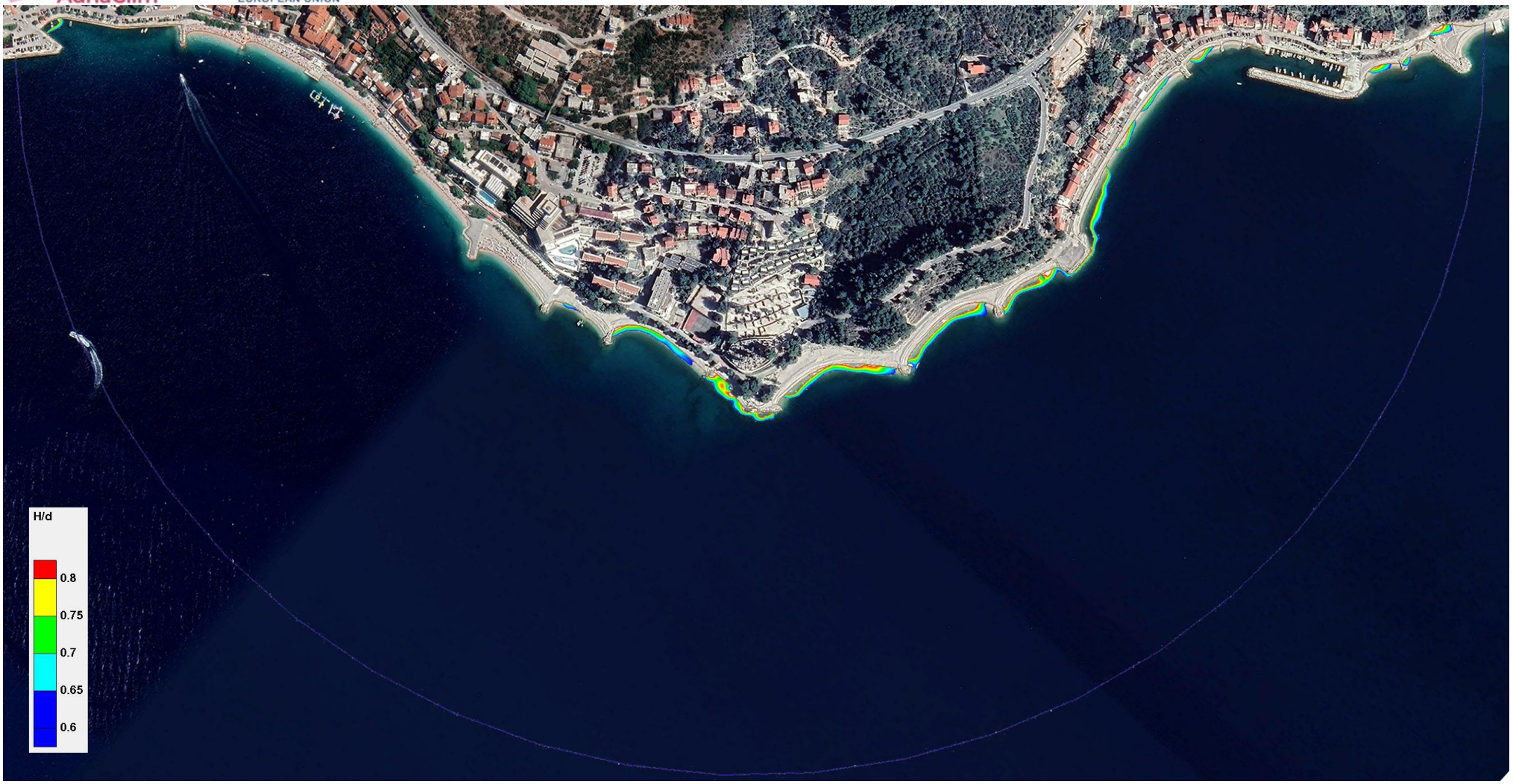

Figure 6.44 – Wave breaking zone for simulation **A14** – existing state of Podgora beach (Makarska Riviera) with wave parameters from the Direction of SSE (157.5°), 50-year turnback period (Hs=2.15 m; Tp=5.98 s) and sea level corresponding to **absolute maximum**

Figure 6.45 – Wave breaking zone for Simulation **A17** – **conceptual design** for the control area (indicated by a yellow arrow) of Podgora beach (Makarska Riviera) with wave parameters from the Direction of SSE (157.5°), 50-year return period (Hs=2.15 m; Tp=5.98 s) and sea level corresponding to **absolute maximum**

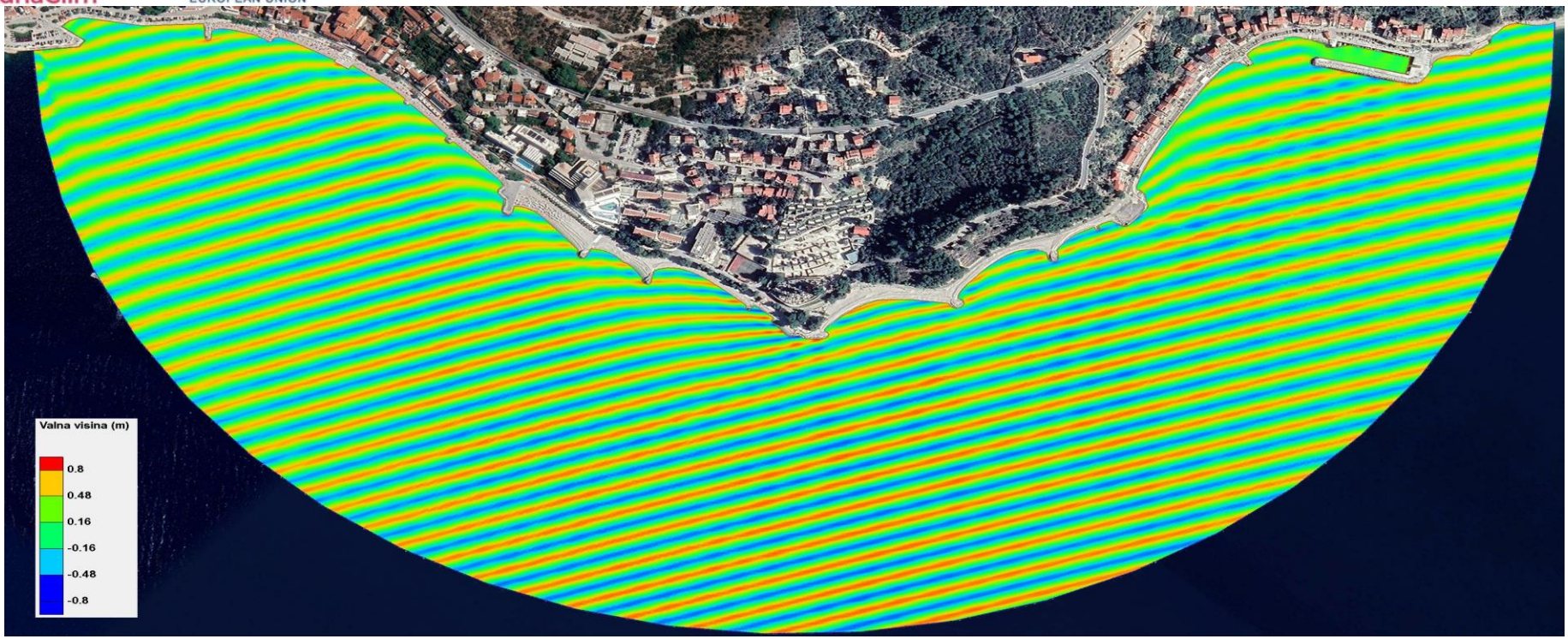

Figure 6.46 – Current wave outline for A12 simulation – existing state of Podgora beach (Makarska Riviera) with wave parameters from SW direction (225°), 50-year return period (Hs=1.45 m; Tp=4.91 s) and sea level corresponding to middle sea level (SRM)

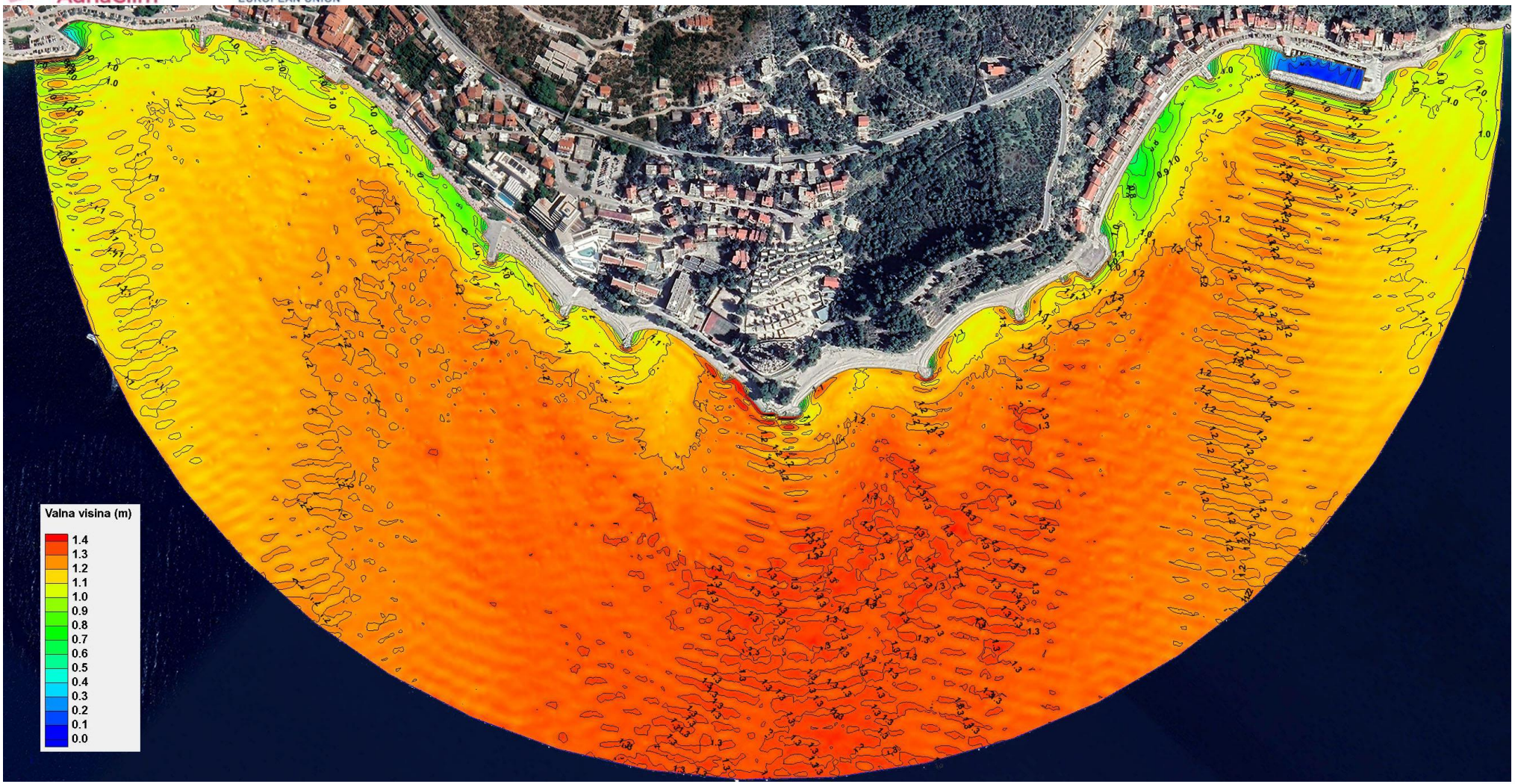

Figure 6.47 – Field of significant wave heights for simulation **A12** – the existing state of Podgora beach (Makarska Riviera) with wave parameters from the Direction of SW (225°), 50-year return period (Hs=1.45 m; Tp=4.91 s) and sea level corresponding to the Middle Sea Level (SRM)

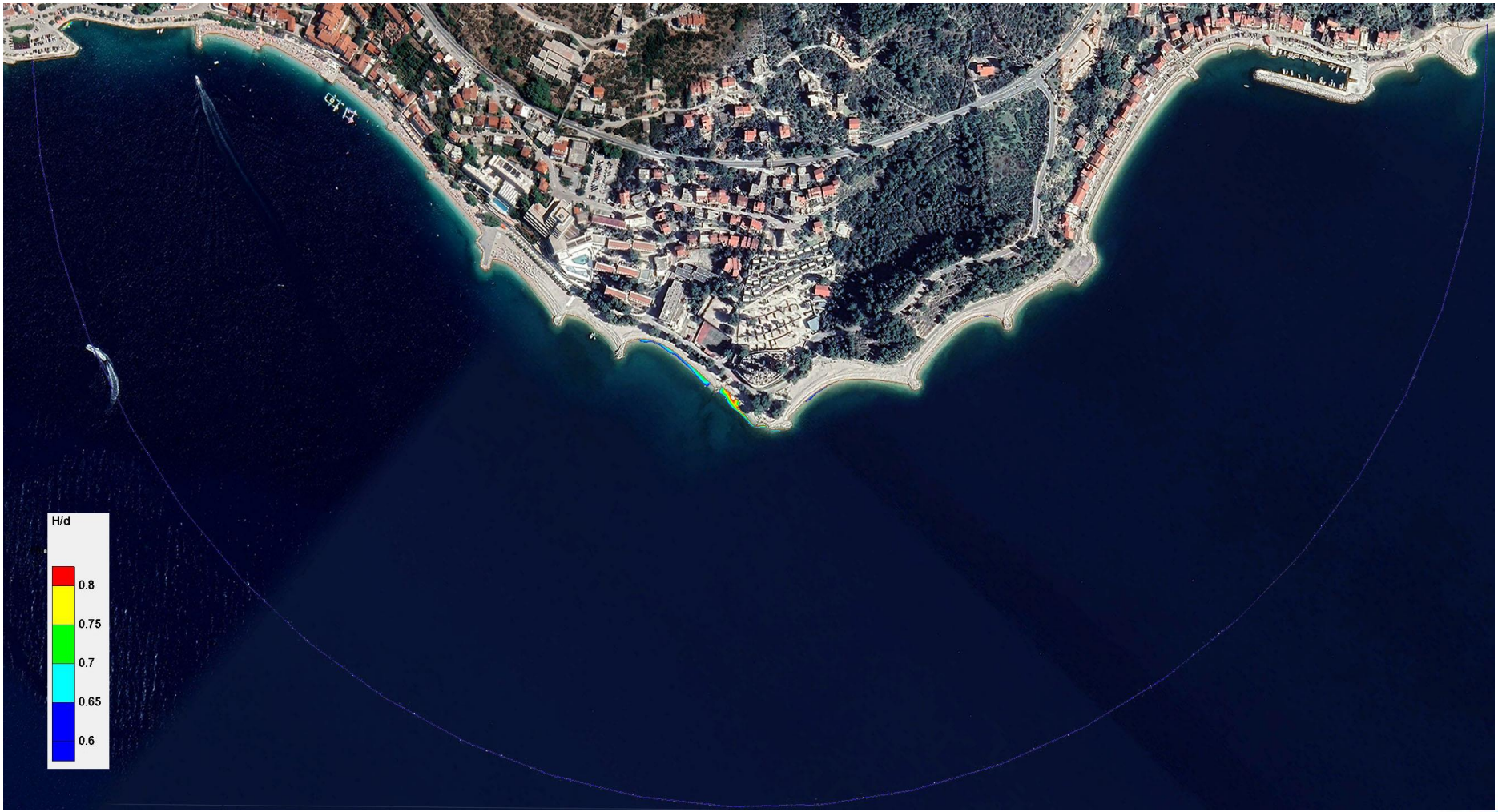

Figure 6.48 – Wave breaking zone for simulation **A12** – existing state of Podgora beach (Makarska Riviera) with wave parameters from the direction of SW (225°), 50-year return period (Hs=1.45 m; Tp=4.91 s) and sea level corresponding to middle sea level (SRM)

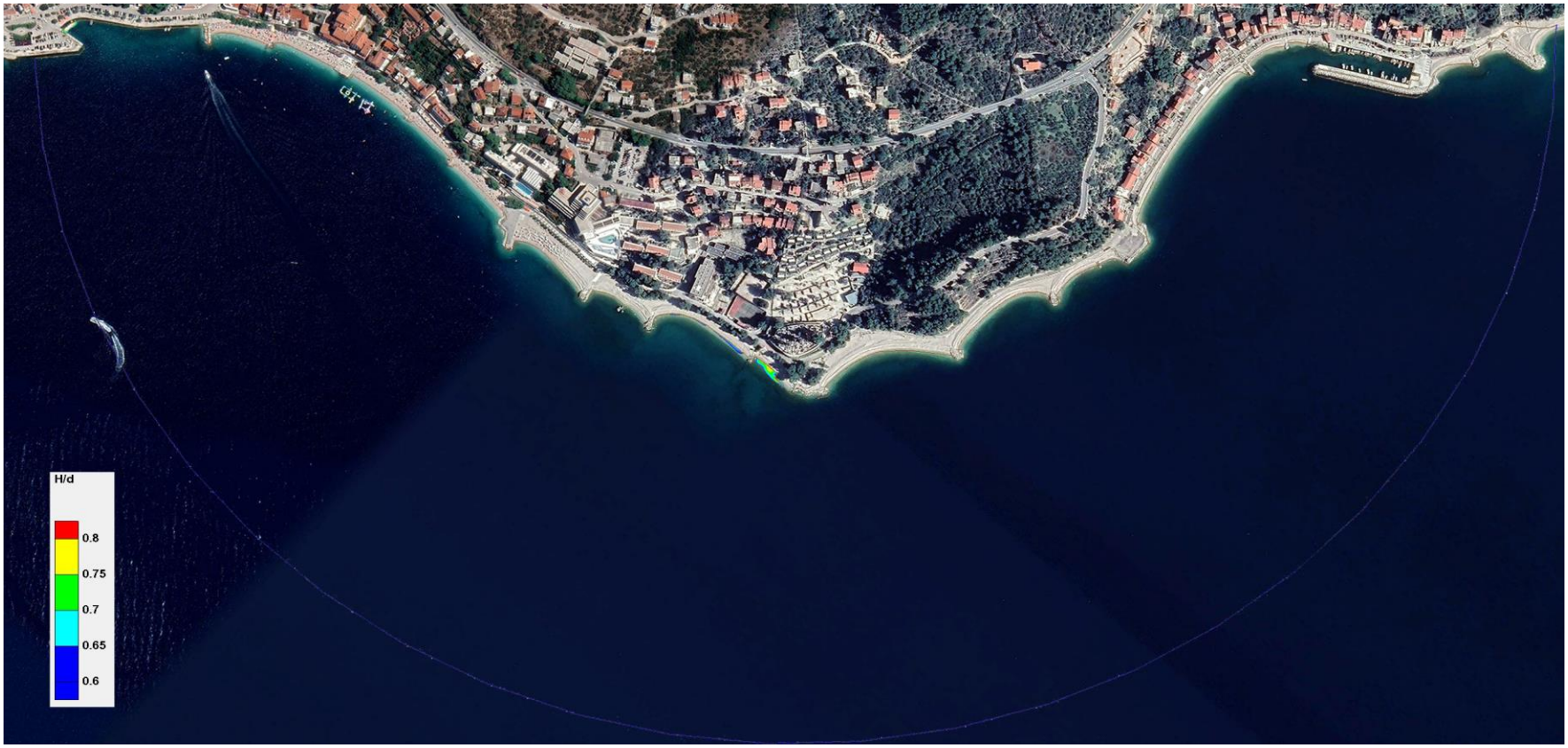

Figure 6.49 – Wave breaking zone for simulation **A15** – the existing state of Podgora beach (Makarska Riviera) with wave parameters from the Direction of SW (225°), a 50-year turnback period (Hs=1.45 m; Tp=4.91 s) and a sea level corresponding to **the absolute maximum**

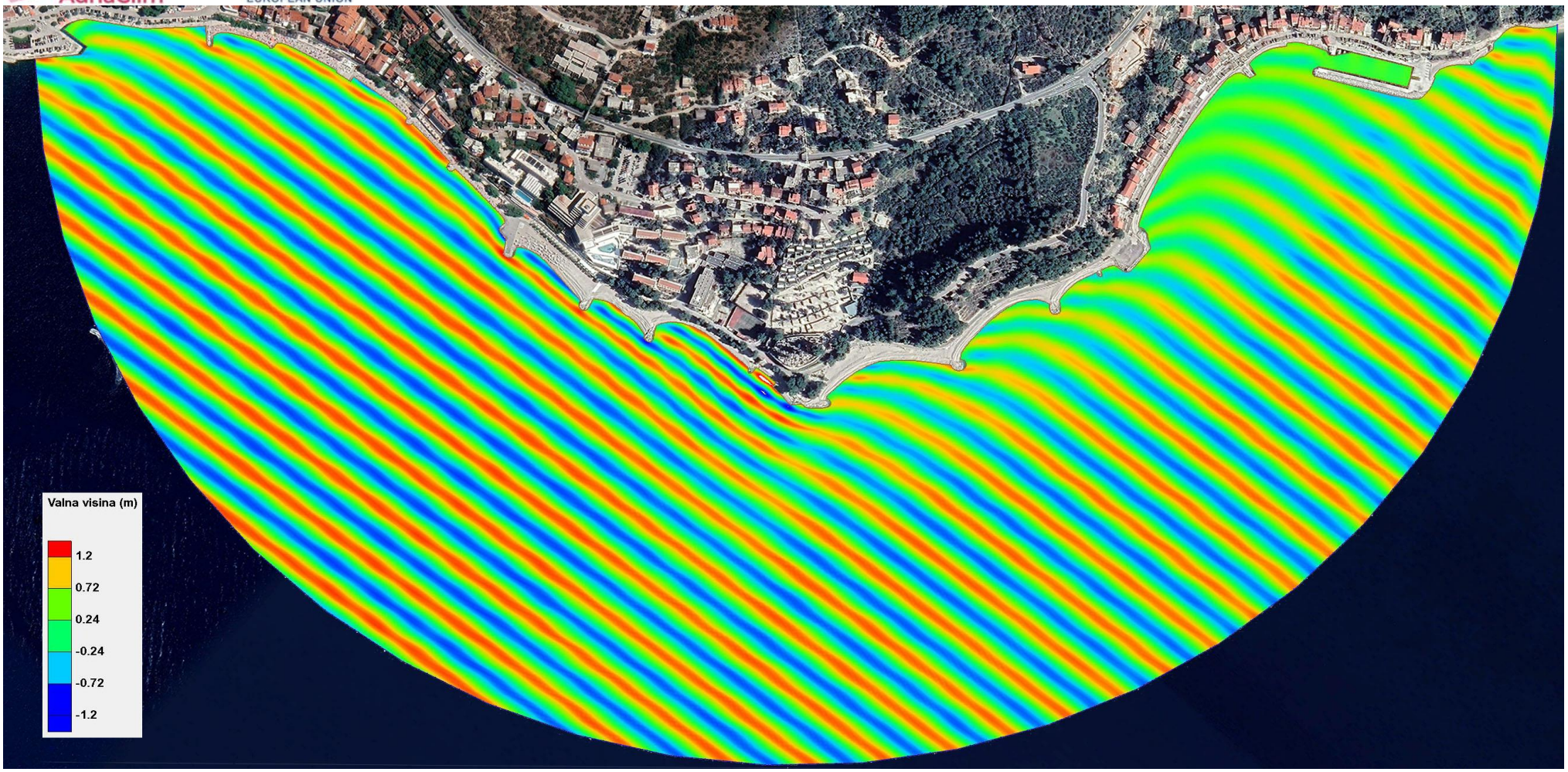

Figure 6.50 – Current wave outline for simulation **A13** – existing state of Podgora beach (Makarska Riviera) with wave parameters from w direction (270°), 50-year return period (Hs=2.32 m; Tp=6.21 s) and sea level corresponding to middle sea level (SRM)

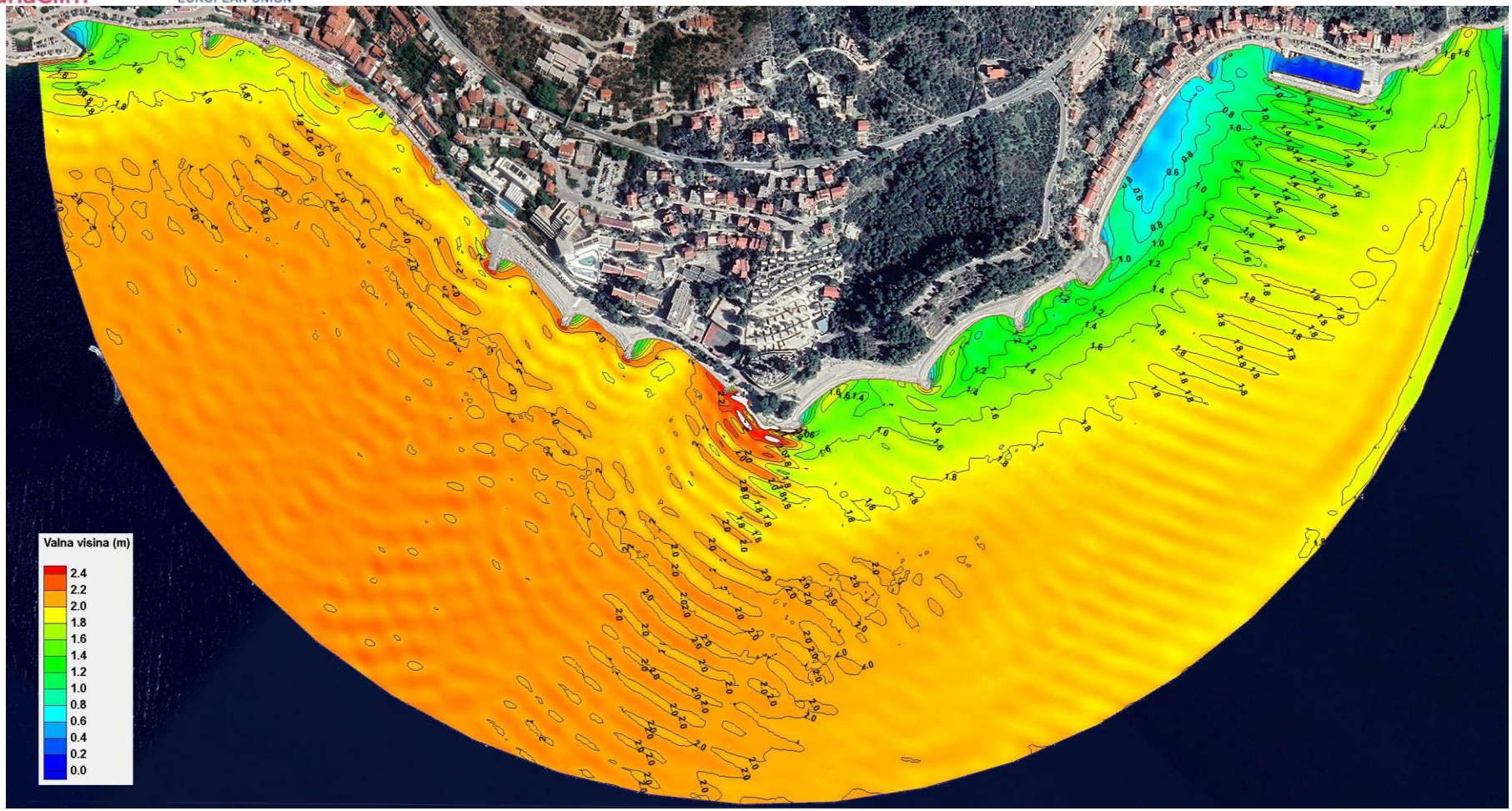

Figure 6.51 – Field of significant wave heights for simulation **A13** – existing state of Podgora beach (Makarska Riviera) with wave parameters from w direction (270°), 50-year return period (Hs=2.32 m; Tp=6.21 s) and sea level corresponding to middle sea level (SRM)

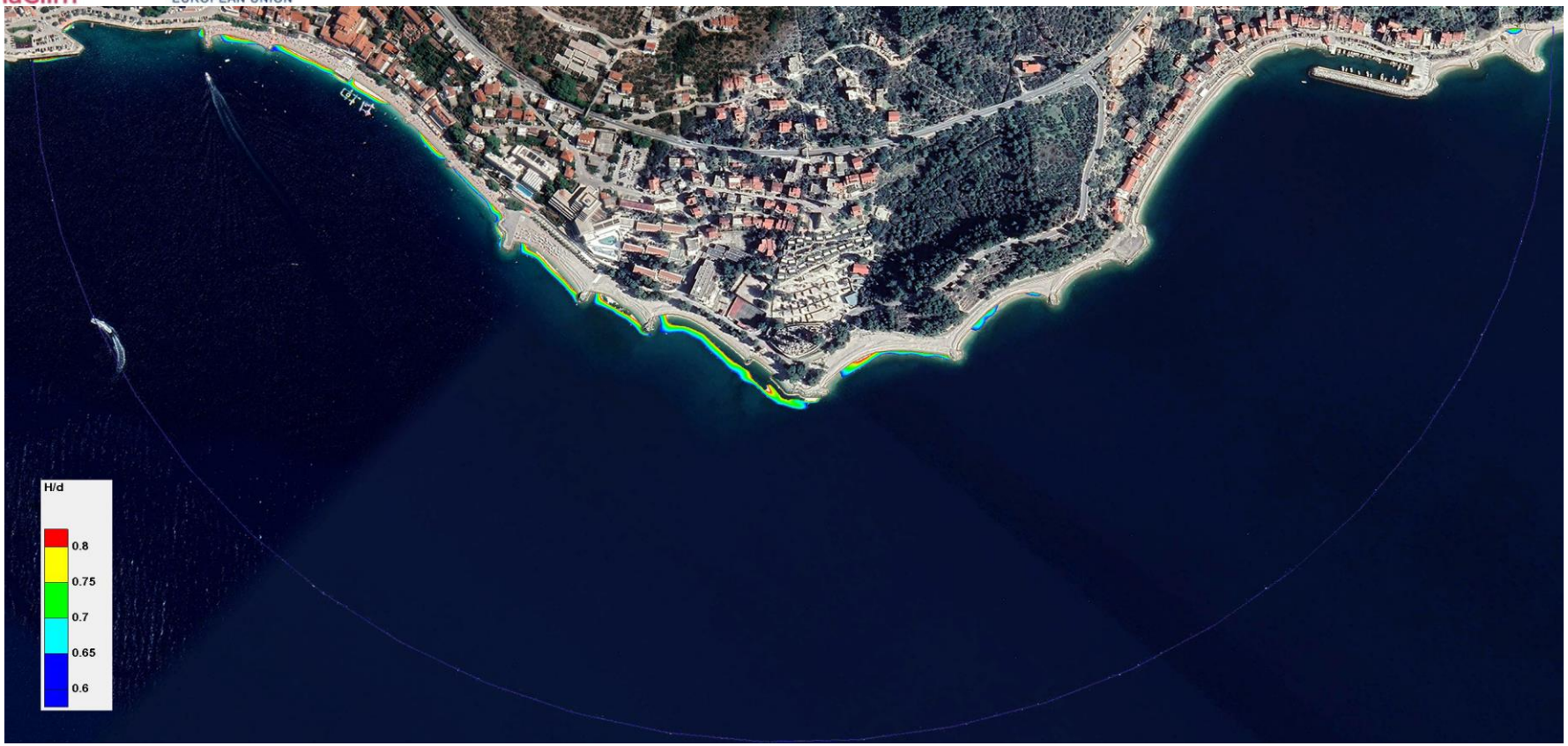

Figure 6.52 – Wave breaking zone for simulation **A13** – the existing state of Podgora beach (Makarska Riviera) with wave parameters from the direction W (270°), a 50-year return period (Hs=2.32 m; Tp=6.21 s) and sea level corresponding to the middle sea level (SRM)

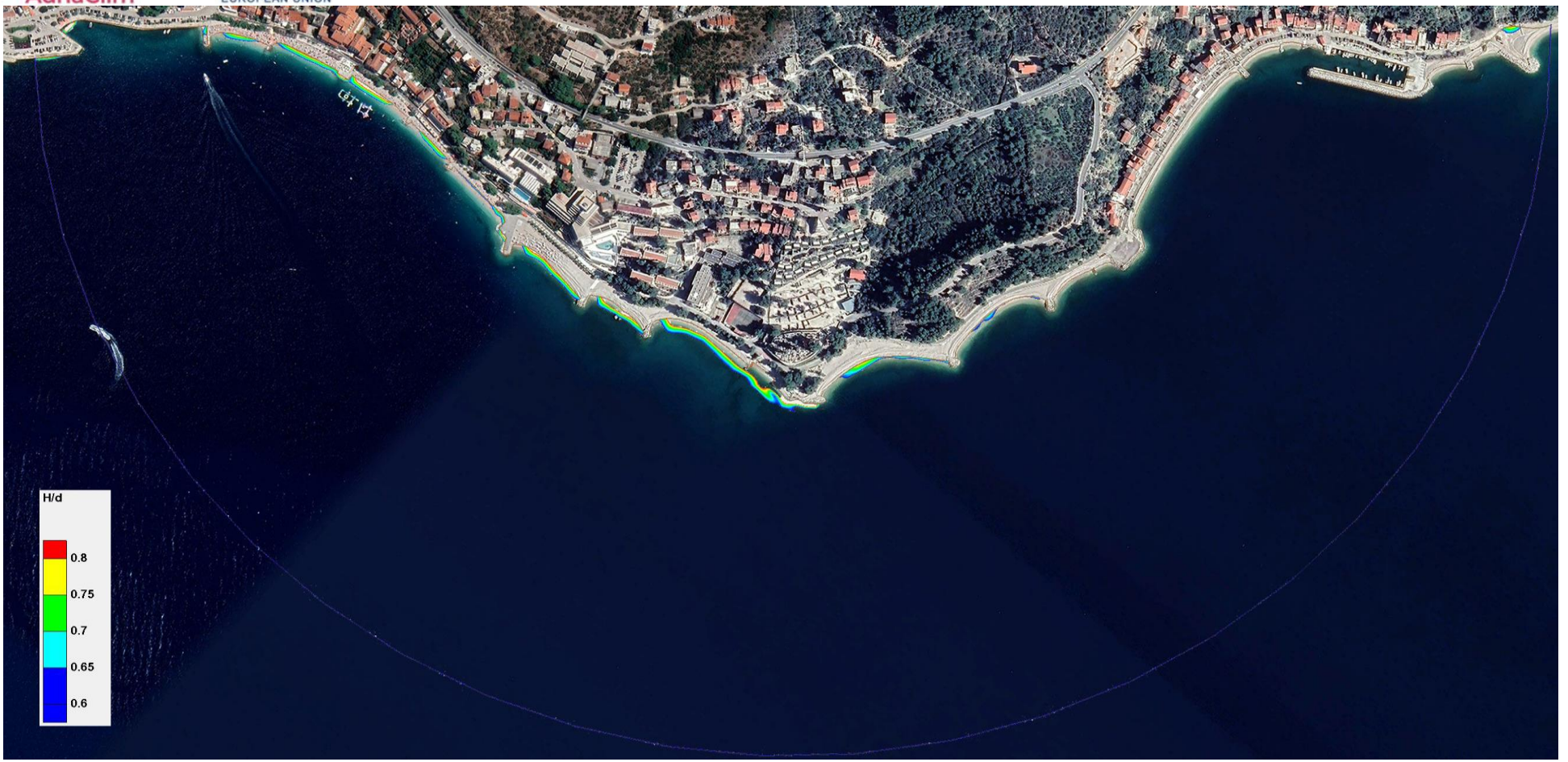

Figure 6.53 – Wave breaking zone for simulation **A16** – the existing state of Podgora beach (Makarska Riviera) with wave parameters from w direction (270°), 50-year return period (Hs=2.32 m; Tp=6.21 s) and sea level corresponding to **absolute maximum**

6.3.4. Podstrana-Duće area

In accordance with the previously stated, a total of nine (9) numerical simulations were conducted for the area of beaches on the Podstrana-Duće area, and below are the following results:

1. Figure 6.54 – Current wave outline for simulation A18 – the existing state of the beach on the Podstrana-Duće area with wave parameters from the direction of SE (135°), a 50-year return period (Hs=2.46 m; Tp=6.40 s) and sea level corresponding to the middle sea level (SRM)
2. Figure 6.55 – Field of significant wave heights for simulation A18 – the existing state of the beach on the Podstrana-Duće area with wave parameters from the direction of SE (135°), a 50-year return period (Hs=2.46 m; Tp=6.40 s) and sea level corresponding to the middle sea level (SRM)
3. Figure 6.56 – Wave breaking zone for simulation A18 – the existing state of the beach on the Podstrana-Duće area with wave parameters from the direction of the SE (135°), a 50-year return period (Hs=2.46 m; Tp=6.40 s) and sea level corresponding to the middle sea level (SRM)
4. Figure 6.57 – Wave breaking zone for simulation A21 – the existing state of the beach on the Podstrana-Duće area with wave parameters from the SE direction (135°), a 50-year return period (Hs=2.46 m; Tp=6.40 s) and a sea level corresponding to the absolute maximum
5. Figure 6.58 – Wave breaking zone for Simulation A24 – conceptual design for the control area (marked with a yellow arrow) for the beach on the Podstrana-Duće area with wave parameters from the SE direction (135°), a 50-year return period (Hs=2.46 m; Tp=6.40 s) and a sea level corresponding to the absolute maximum
6. Figure 6.59 – Current wave outline for Simulation A19 – the existing state of the beach on the Podstrana-Duće area with wave parameters from the Direction of SSW (202.5°), a 50-year return period (Hs=2.09 m; Tp=5.90 s) and sea level corresponding to the Middle Sea Level (SRM)
7. Figure 6.60 – Field of significant wave heights for simulation A19 – the existing state of the beach on the Podstrana-Duće area with wave parameters from the direction of SSW (202.5°), a 50-year return period (Hs=2.09 m; Tp=5.90 s) and sea level corresponding to the middle sea level (SRM)
8. Figure 6.61 – Wave breaking zone for simulation A19 – the existing state of the beach on the Podstrana-Duće area with wave parameters from the direction of SSW (202.5°), a 50-year turnback period (Hs=2.09 m; Tp=5.90 s) and sea level corresponding to the middle sea level (SRM)
9. Figure 6.62 – Wave breaking zone for simulation A22 – the existing state of the beach on the Podstrana-Duće area with wave parameters from the Direction of SSW (202.5°), a 50-year return period (Hs=2.09 m; Tp=5.90 s) and a sea level corresponding to the absolute maximum
10. Figure 6.63 – Wave breaking zone for Simulation A25 – conceptual design for the control area (marked with a yellow arrow) of the beach on the Podstrana-Duće area with wave parameters from the Direction of SSW (202.5°), 50-year return period (Hs=2.09 m; Tp=5.90 s) and sea level corresponding to absolute maximum
11. Figure 6.64 – Current wave outline for A20 simulation – the existing state of the beach on the Podstrana-Duće area with wave parameters from w direction (270°), 50-year return period (Hs=1.73 m; Tp=5.36 s) and sea level corresponding to middle sea level (SRM)
12. Figure 6.65 – Field of significant wave heights for simulation A20 – the existing state of the beach on the Podstrana-Duće area with wave parameters from the direction W (270°), a 50-year return period (Hs=1.73 m; Tp=5.36 s) and sea level corresponding to the middle sea level (SRM)
13. Figure 6.66 – Wave breaking zone for simulation A20 – the existing state of the beach on the Podstrana-Duće area with wave parameters from the direction W (270°), a 50-year return period (Hs=1.73 m; Tp=5.36 s) and sea level corresponding to the middle sea level (SRM)
14. Figure 6.67 – Wave breaking zone for Simulation A23 – the existing state of the beach on the Podstrana-Duće area with wave parameters from the direction W (270°), a 50-year return period (Hs=1.73 m; Tp=5.36 s) and a sea level corresponding to the absolute maximum
15. Figure 6.68 – Wave breaking zone for Simulation A26 – conceptual design for the control area (indicated by a yellow arrow) of the beach on the Podstrana-Duće area with wave parameters from w direction (270°), 50-year return period (Hs=1.73 m; Tp=5.36 s) and sea level corresponding to absolute maximum

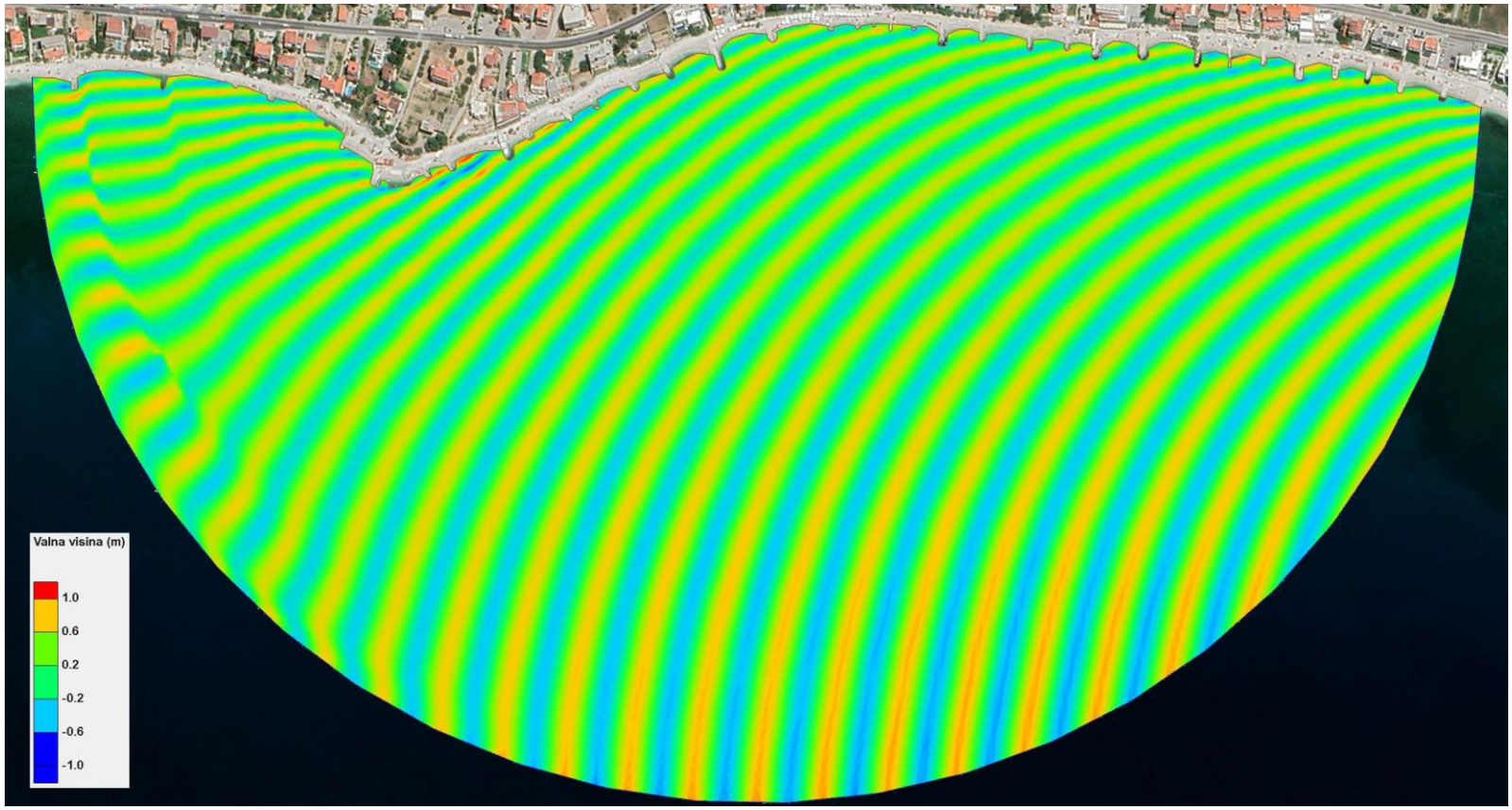

Figure 6.54 – Current wave outline for simulation **A18** – the existing state of the beach on the Podstrana-Duće area with wave parameters from the direction of SE (135°), a 50-year return period (Hs=2.46 m; Tp=6.40 s) and sea level corresponding to the middle sea level (SRM)

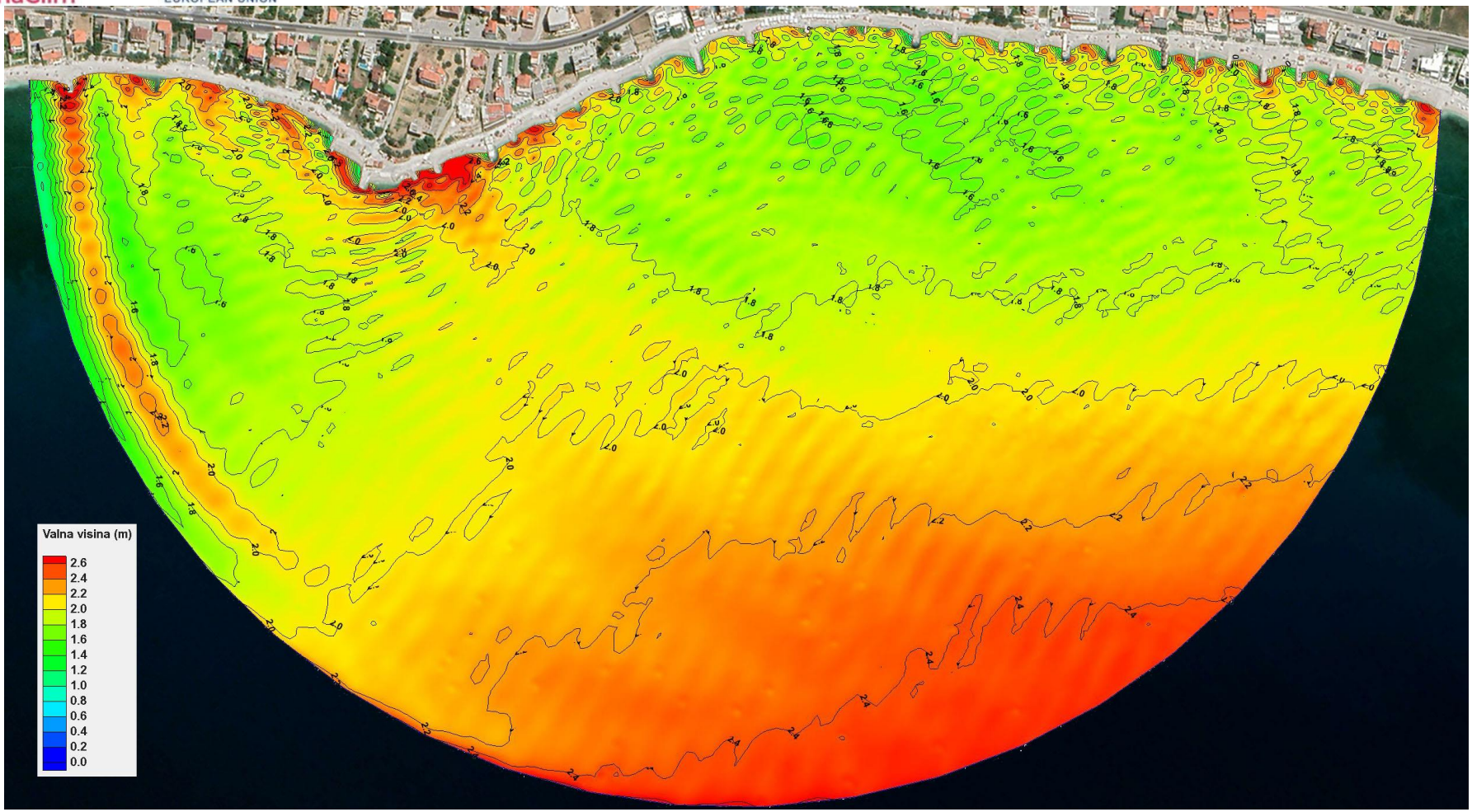

Figure 6.55 – Field of significant wave heights for simulation **A18** – the existing state of the beach on the Podstrana-Duće area with wave parameters from the direction of SE (135°), a 50-year return period (Hs=2.46 m; Tp=6.40 s) and sea level corresponding to the middle sea level (SRM)

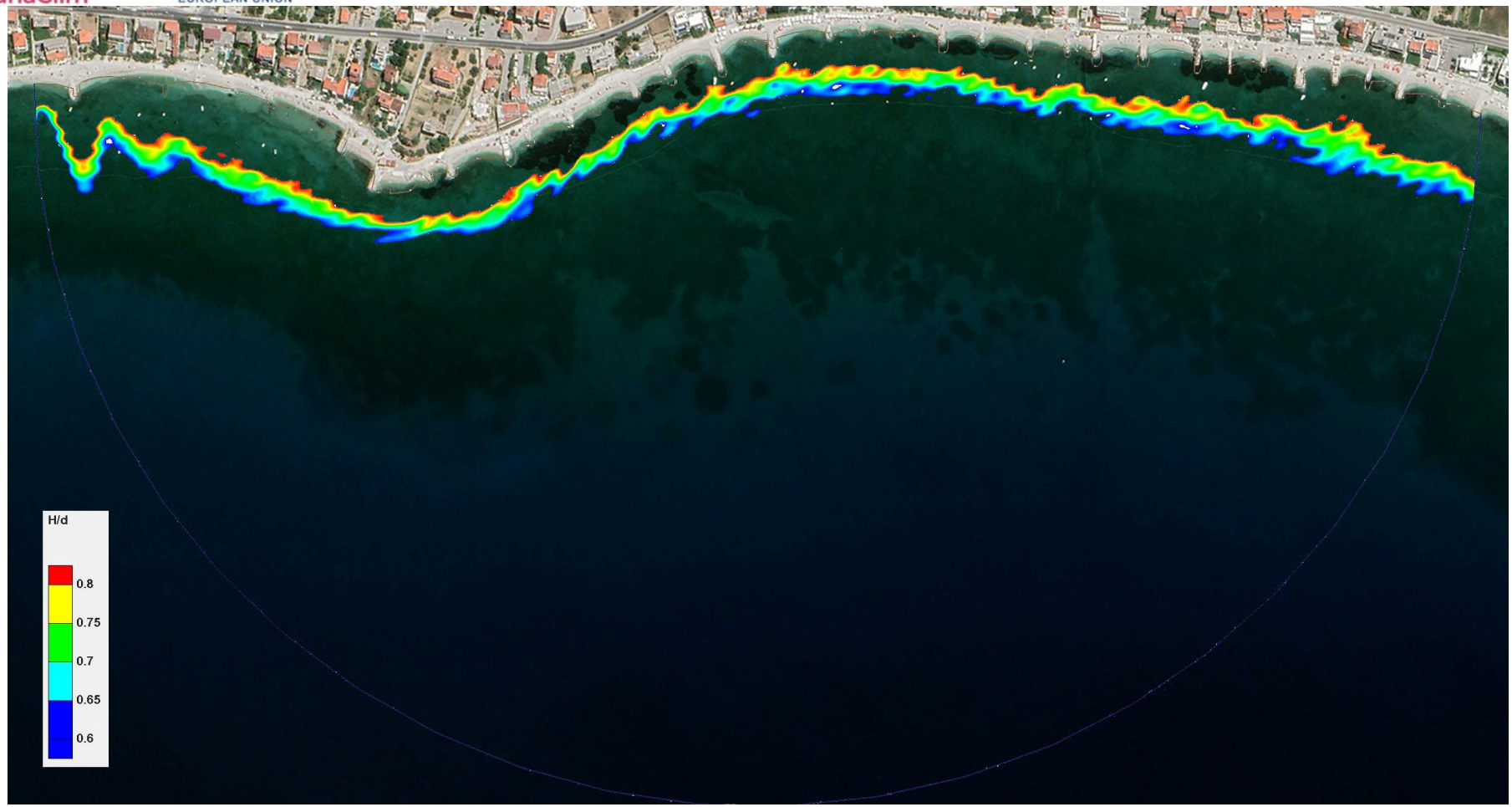

Figure 6.56 – Wave breaking zone for simulation **A18** – the existing state of the beach on the Podstrana-Duće area with wave parameters from the direction of the SE (135°), a 50-year return period (Hs=2.46 m; Tp=6.40 s) and sea level corresponding to the middle sea level (SRM)

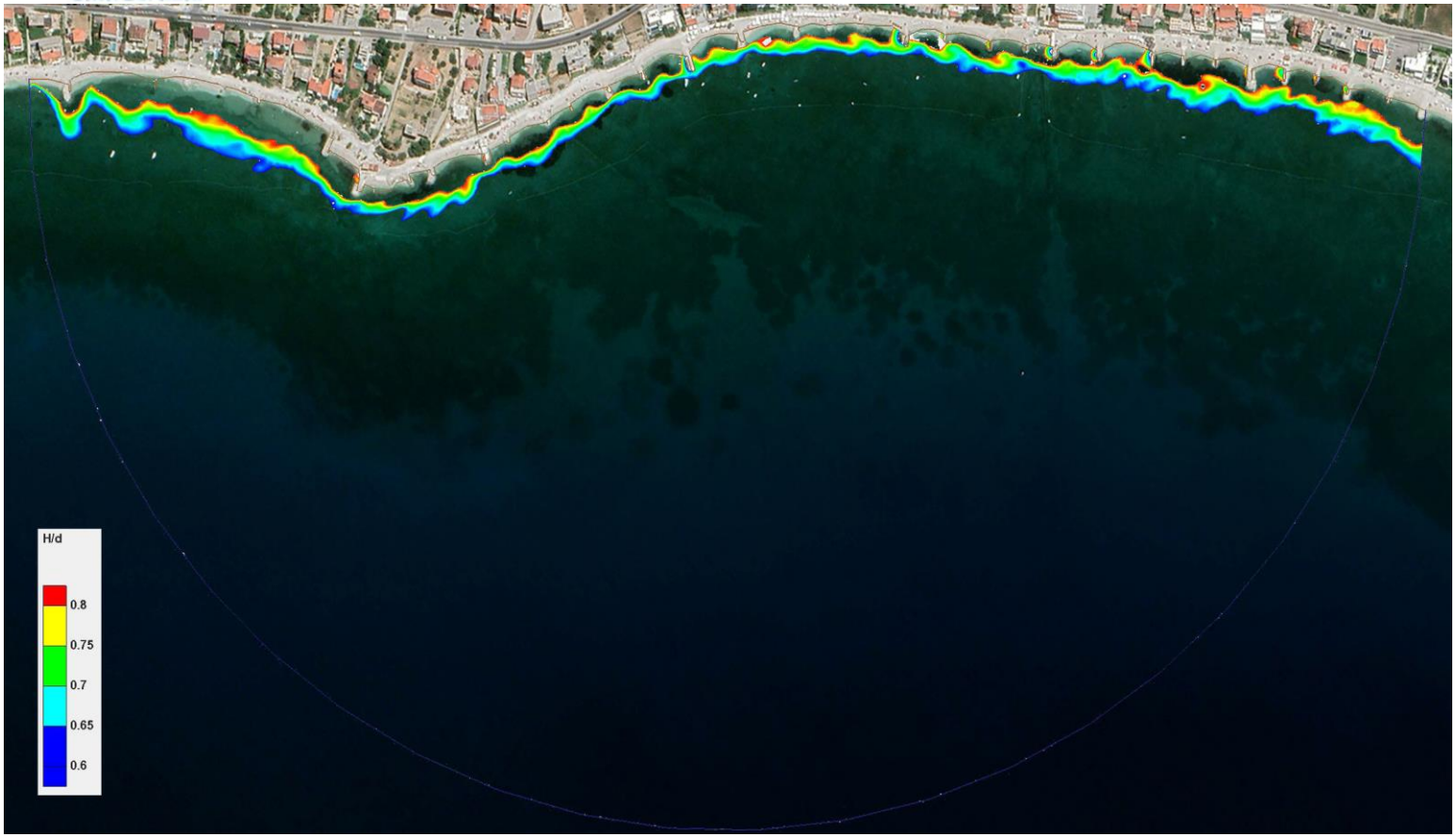

Figure 6.57 – Wave breaking zone for simulation **A21** – the existing state of the beach on the Podstrana-Duće area with wave parameters from the SE direction (135°), a 50-year return period (Hs=2.46 m; Tp=6.40 s) and a sea level corresponding to **the absolute maximum**

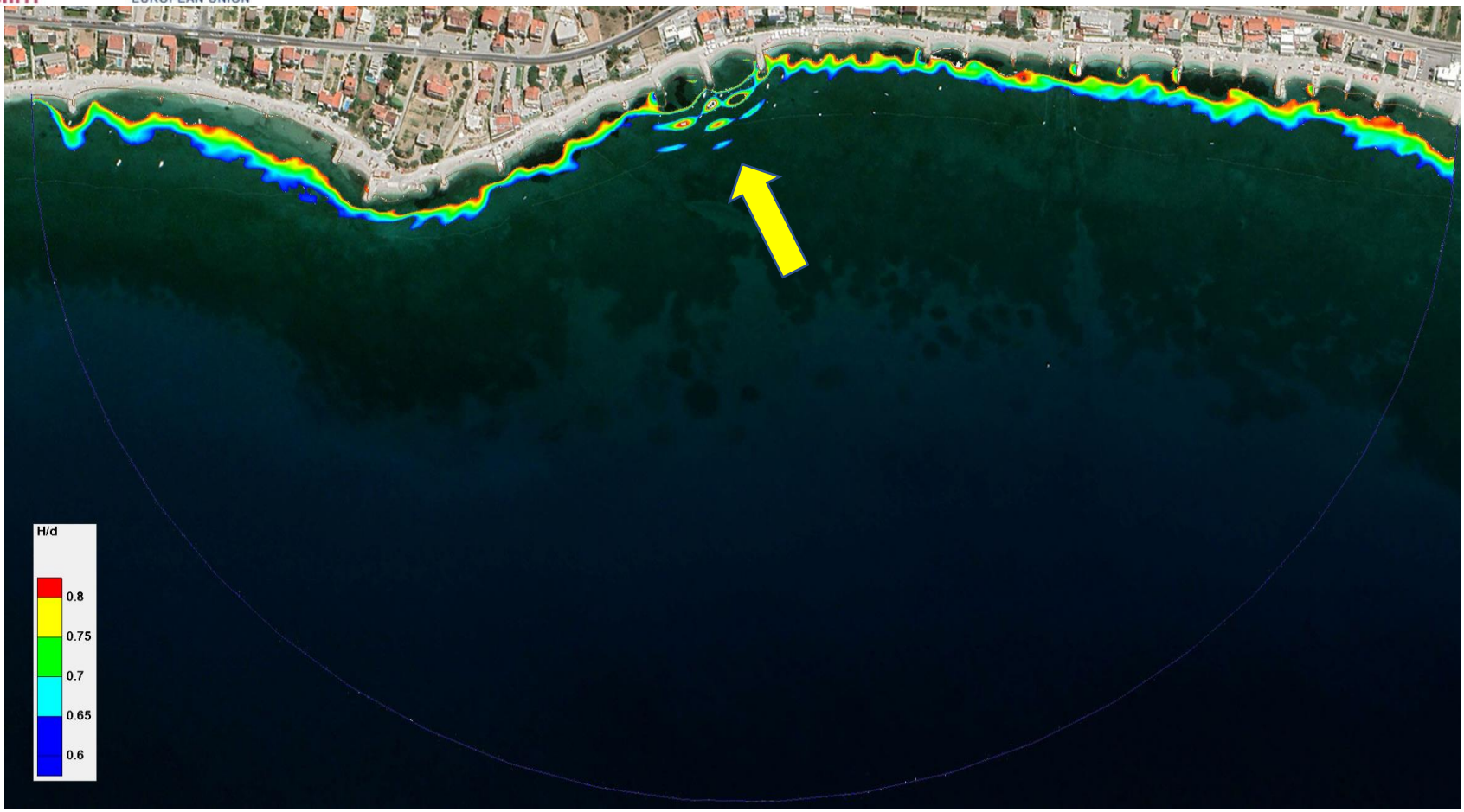

Figure 6.58 – Wave breaking zone for Simulation **A24** – **conceptual design** for the control area (marked with a yellow arrow) for the beach on the Podstrana-Duće area with wave parameters from the SE direction (135°), a 50-year return period (Hs=2.46 m; Tp=6.40 s) and a sea level corresponding to **the absolute maximum**

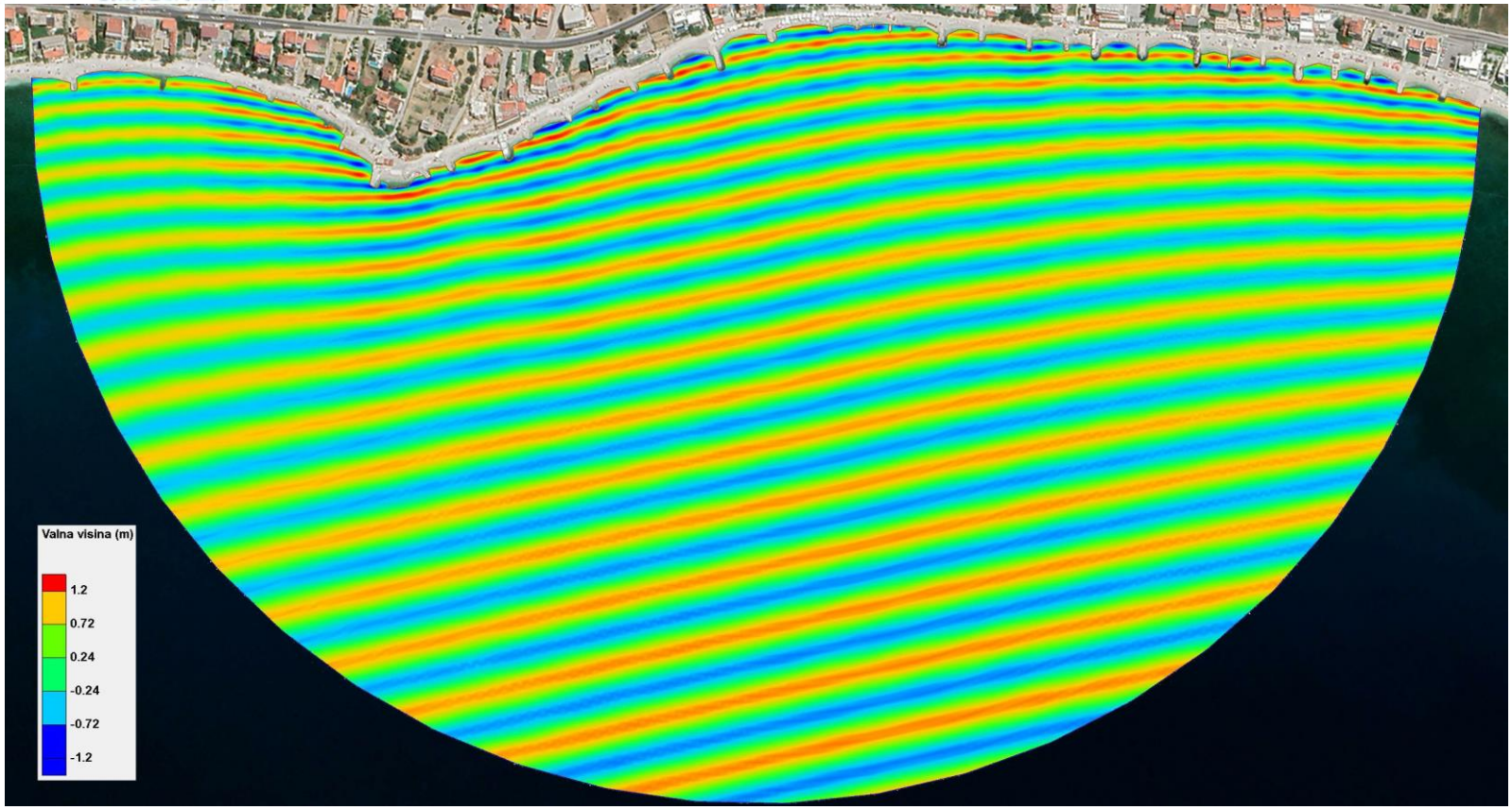

Figure 6.59 – Current wave outline for Simulation **A19** – the existing state of the beach on the Podstrana-Duće area with wave parameters from the Direction of SSW (202.5°), a 50-year return period (Hs=2.09 m; Tp=5.90 s) and sea level corresponding to the Middle Sea Level (SRM)

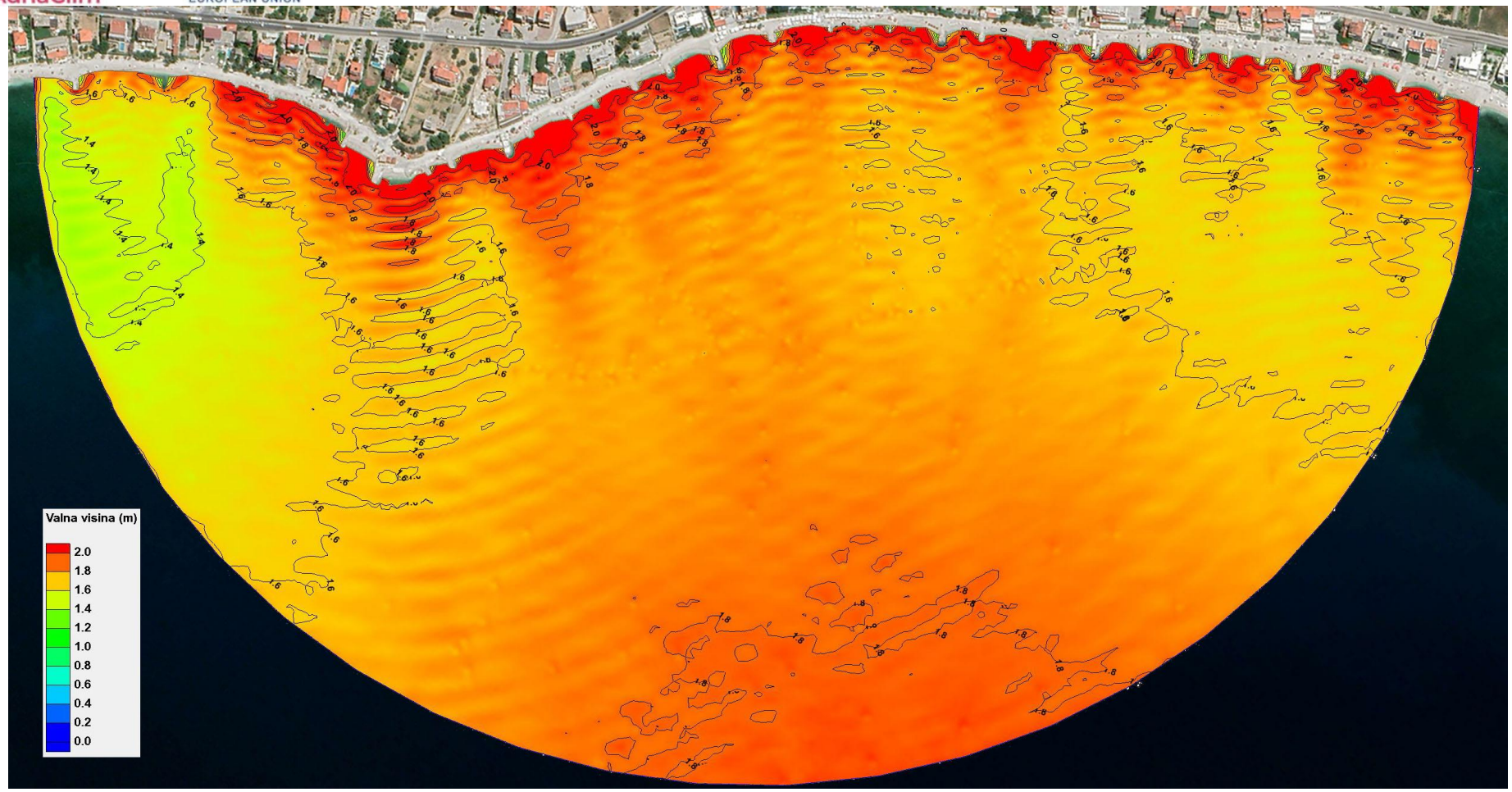

Figure 6.60 – Field of significant wave heights for simulation **A19** – the existing state of the beach on the Podstrana-Duće area with wave parameters from the direction of SSW (202.5°), a 50-year return period (Hs=2.09 m; Tp=5.90 s) and sea level corresponding to the middle sea level (SRM)

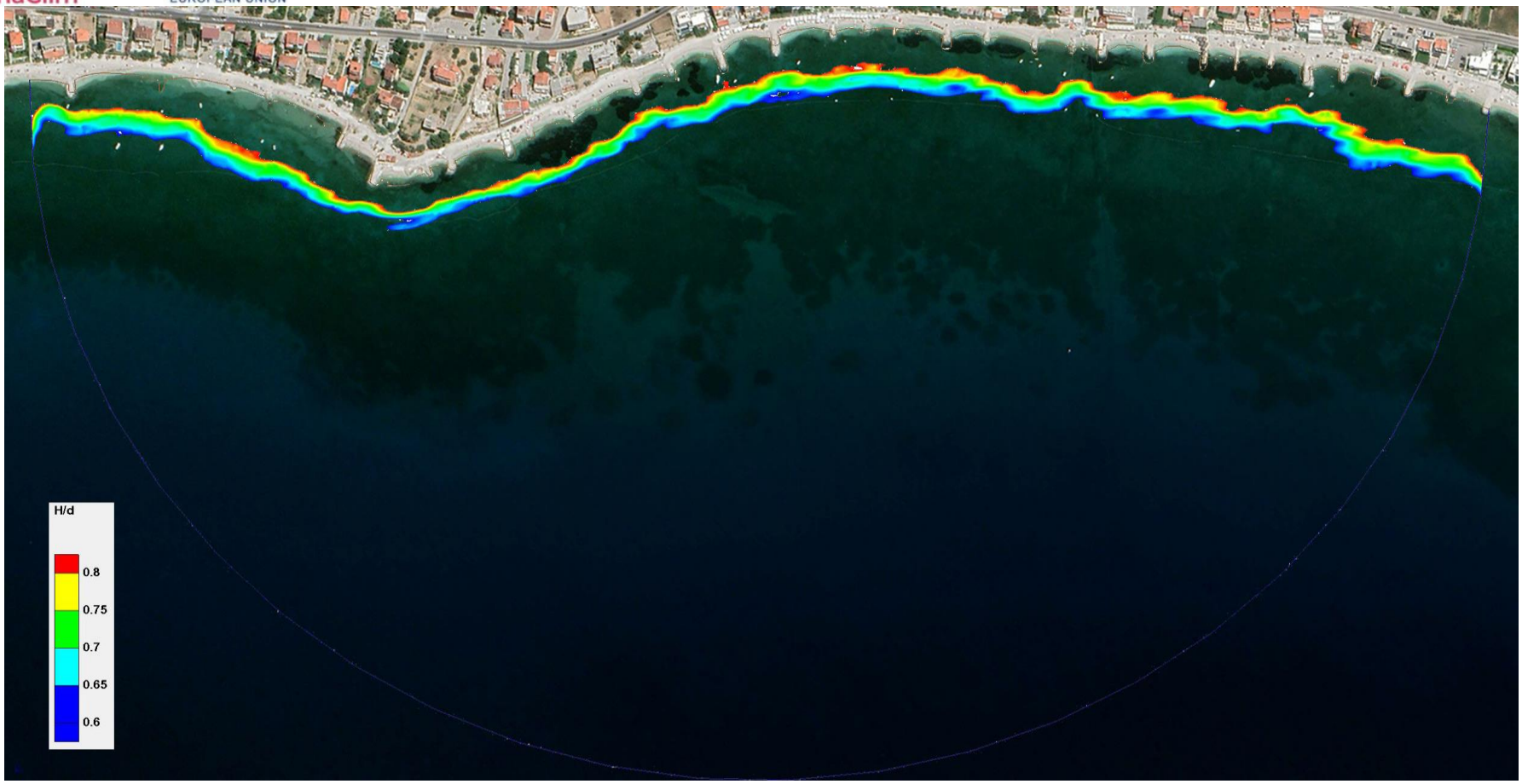

Figure 6.61 – Wave breaking zone for simulation **A19** – the existing state of the beach on the Podstrana-Duće area with wave parameters from the direction of SSW (202.5°), a 50-year turnback period (Hs=2.09 m; Tp=5.90 s) and sea level corresponding to the middle sea level (SRM)

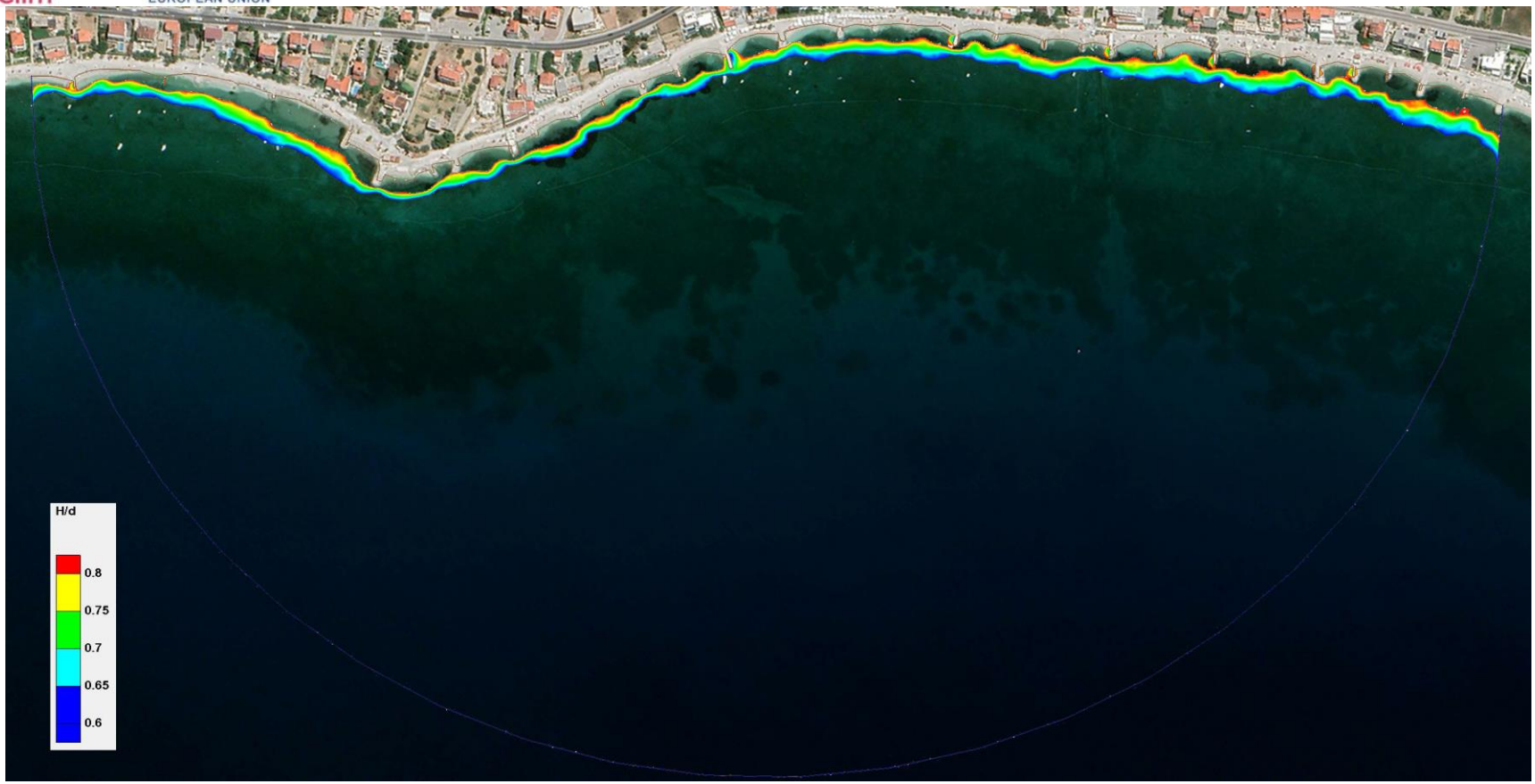

Figure 6.62 – Wave breaking zone for simulation **A22** – the existing state of the beach on the Podstrana-Duće area with wave parameters from the Direction of SSW (202.5°), a 50-year return period (Hs=2.09 m; Tp=5.90 s) and a sea level corresponding to **the absolute maximum**

Figure 6.63 – Wave breaking zone for Simulation **A25** – **conceptual design** for the control area (marked with a yellow arrow) of the beach on the Podstrana-Duće area with wave parameters from the Direction of SSW (202.5°), 50-year return period (Hs=2.09 m; Tp=5.90 s) and sea level corresponding to **absolute maximum**

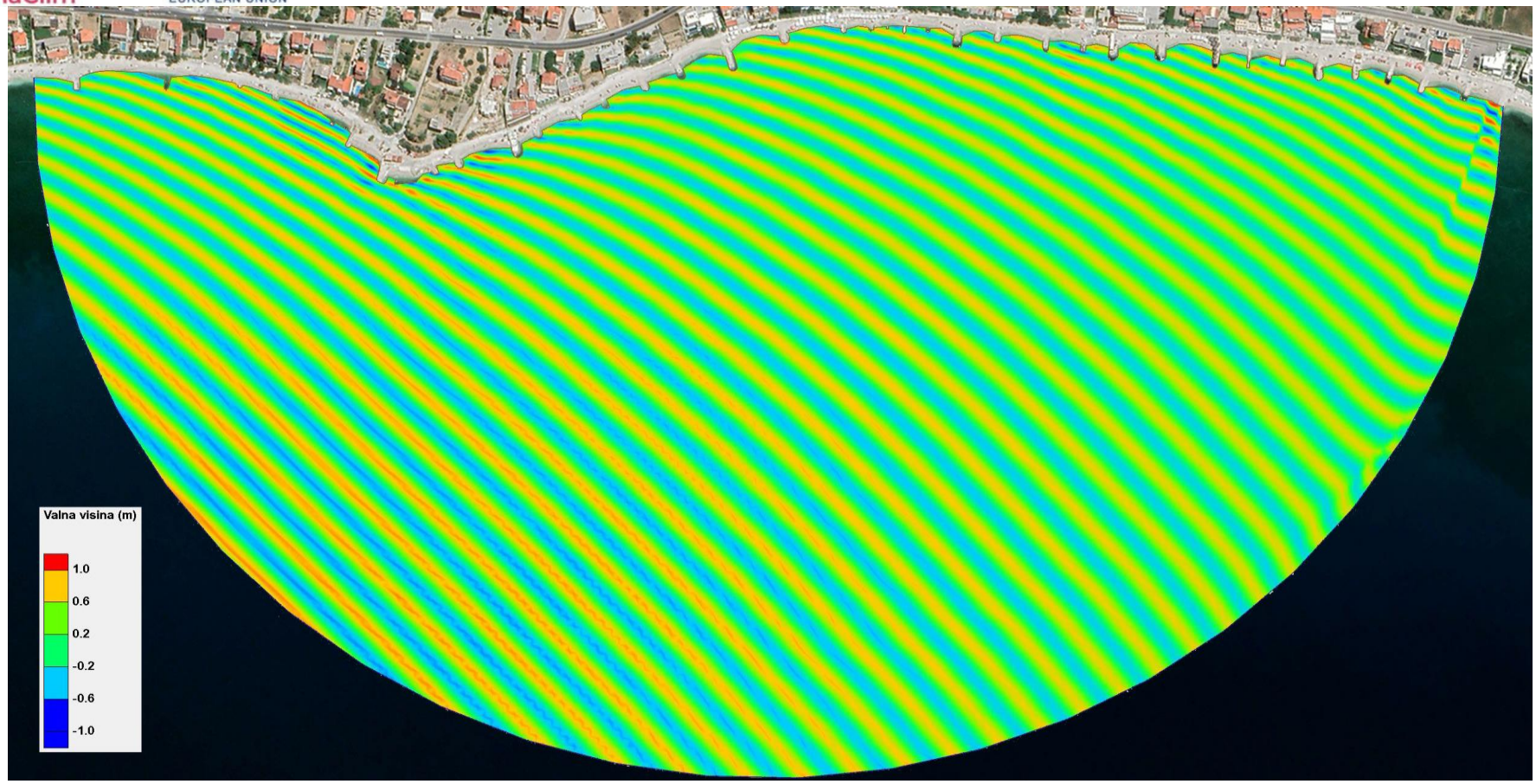

Figure 6.64 – Current wave outline for A20 simulation – the existing state of the beach on the Podstrana-Duće area with wave parameters from w direction (270°), 50-year return period (Hs=1.73 m; Tp=5.36 s) and sea level corresponding to middle sea level (SRM)

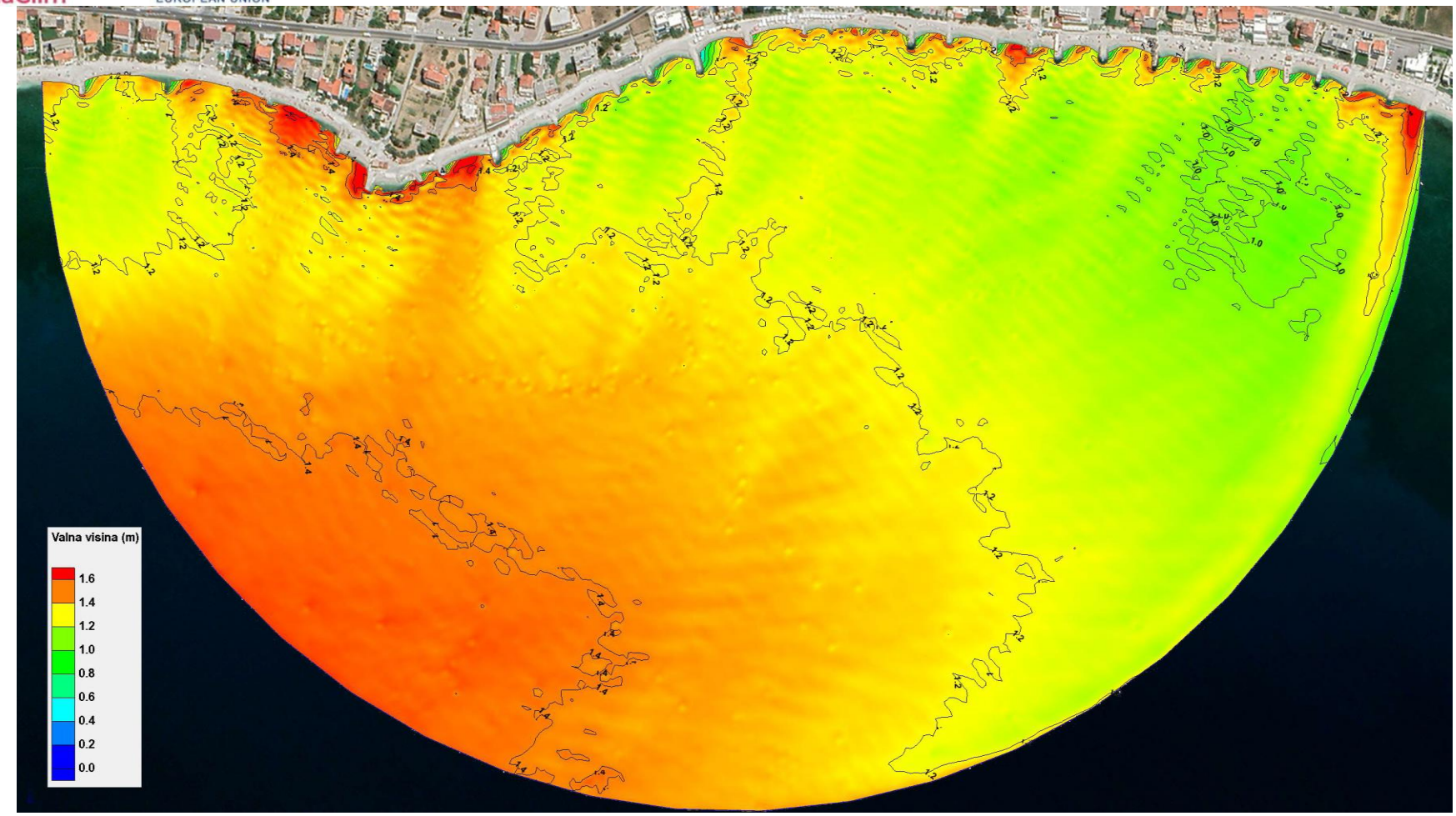

Figure 6.65 – Field of significant wave heights for simulation **A20** – the existing state of the beach on the Podstrana-Duće area with wave parameters from the direction W (270°), a 50-year return period (Hs=1.73 m; Tp=5.36 s) and sea level corresponding to the middle sea level (SRM)

Figure 6.66 – Wave breaking zone for simulation **A20** – the existing state of the beach on the Podstrana-Duće area with wave parameters from the direction W (270°), a 50-year return period (Hs=1.73 m; Tp=5.36 s) and sea level corresponding to the middle sea level (SRM)

Figure 6.67 – Wave breaking zone for Simulation **A23** – the existing state of the beach on the Podstrana-Duće area with wave parameters from the direction W (270°), a 50-year return period (Hs=1.73 m; Tp=5.36 s) and a sea level corresponding to **the absolute maximum**

Figure 6.68 – Wave breaking zone for Simulation **A26** – **conceptual design** for the control area (indicated by a yellow arrow) of the beach on the Podstrana-Duće area with wave parameters from w direction (270°), 50-year return period (Hs=1.73 m; Tp=5.36 s) and sea level corresponding to **absolute maximum**

6.3.5. Split (Kašjuni)

In accordance with the previously stated, a total of six (6) numerical simulations were conducted for the area of Kašjuni beach in Split, and below are the following results:

1. Figure 6.69 – Current wave outline for A27 simulation – the existing state of Kašjuni beach in Split with wave parameters from the Direction of SSW (202.5°), 50-year return period (Hs=1.57 m; Tp=5.11 s) and sea level corresponding to the Middle Sea Level (SRM)
2. Figure 6.70 – Field of significant wave heights for simulation A27 – the existing state of Kašjuni beach in Split with wave parameters from the Direction of SSW (202.5°), 50-year return period (Hs=1.57 m; Tp=5.11 s) and sea level corresponding to the Middle Sea Level (SRM)
3. Figure 6.71 – Wave breaking zone for simulation A27 – the current situation of Kašjuni beach in Split with wave parameters from the Direction of SSW (202.5°), 50-year return period (Hs=1.57 m; Tp=5.11 s) and sea level corresponding to middle sea level (SRM)
4. Figure 6.72 – Wave breaking zone for simulation A29 – the existing state of Kašjuni beach in Split with wave parameters from the Direction of SSW (202.5°), a 50-year return period (Hs=1.57 m; Tp=5.11 s) and a sea level corresponding to the absolute maximum
5. Figure 6.73 – Wave breaking zone for simulation A31 – conceptual design of Kašjuni beach in Split with wave parameters from the Direction of SSW (202.5°), 50-year turnback period (Hs=1.57 m; Tp=5.11 s) and sea level corresponding to absolute maximum
6. Figure 6.74 – Current wave outline for simulation A28 – existing state of Kašjuni beach in Split with wave parameters from w direction (270°), 50-year return period (Hs=0.79 m; Tp=3.62 s) and sea level corresponding to middle sea level (SRM)
7. Figure 6.75 – Field of significant wave heights for simulation A28 – the existing state of Kašjuni beach in Split with wave parameters from w direction (270°), 50-year return period (Hs=0.79 m; Tp=3.62 s) and sea level corresponding to middle sea level (SRM)
8. Figure 6.76 – Wave breaking zone for simulation A28 – the existing state of Kašjuni beach in Split with wave parameters from w direction (270°), 50-year return period (Hs=0.79 m; Tp=3.62 s) and sea level corresponding to middle sea level (SRM)
9. Figure 6.77 – Wave breaking zone for A30 simulation – the existing state of Kašjuni beach in Split with wave parameters from w direction (270°), 50-year return period (Hs=0.79 m; Tp=3.62 s) and sea level corresponding to absolute maximum
10. Figure 6.78 – Wave breaking zone for simulation A32 – conceptual design of Kašjuni beach in Split with wave parameters from W direction (270°), 50-year return period (Hs=0.79 m; Tp=3.62 s) and sea level corresponding to absolute maximum

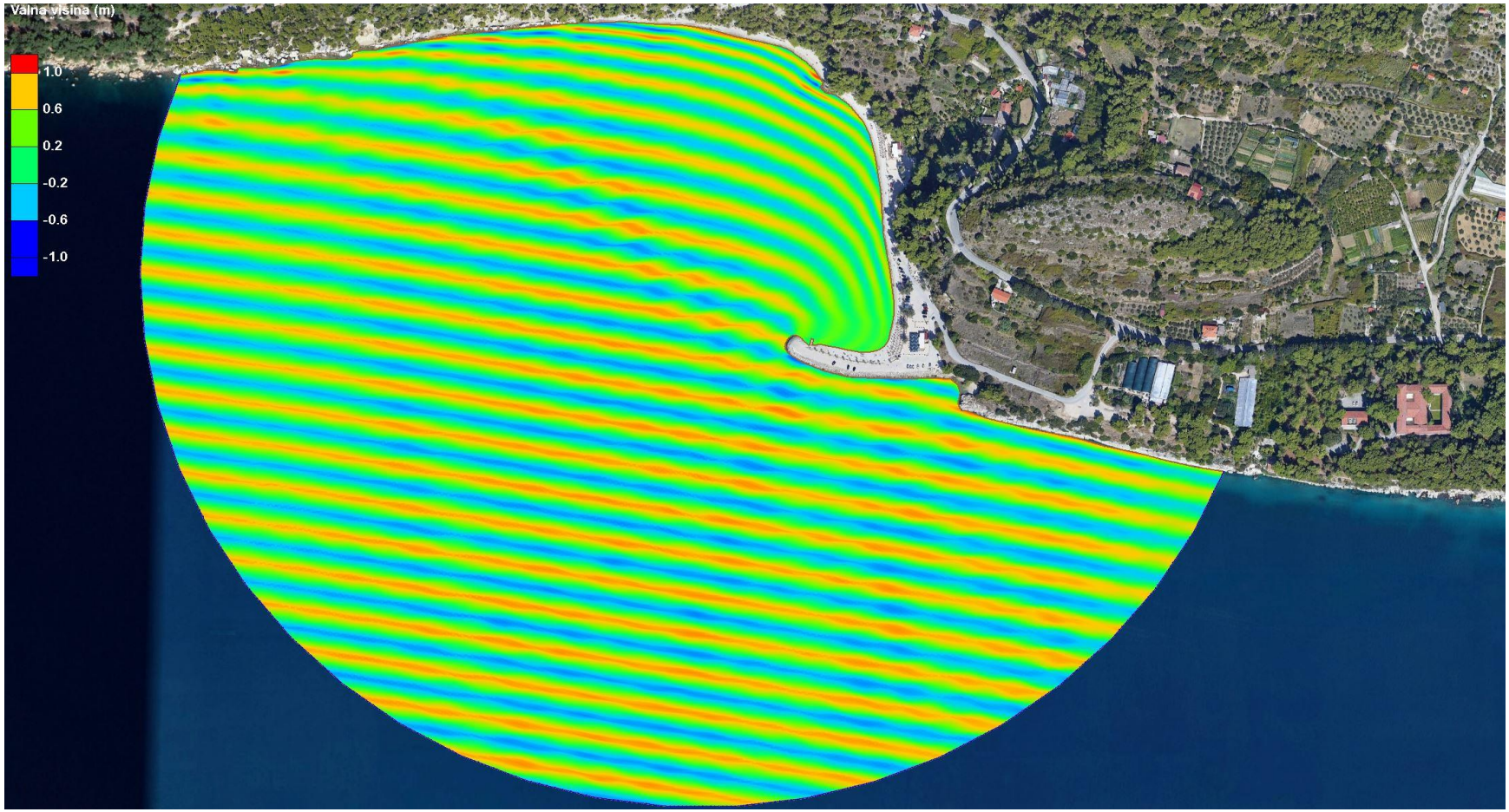

Figure 6.69 – Current wave outline for A27 simulation – the existing state of Kašjuni beach in Split with wave parameters from the Direction of SSW (202.5°), 50-year return period (Hs=1.57 m; Tp=5.11 s) and sea level corresponding to the Middle Sea Level (SRM)

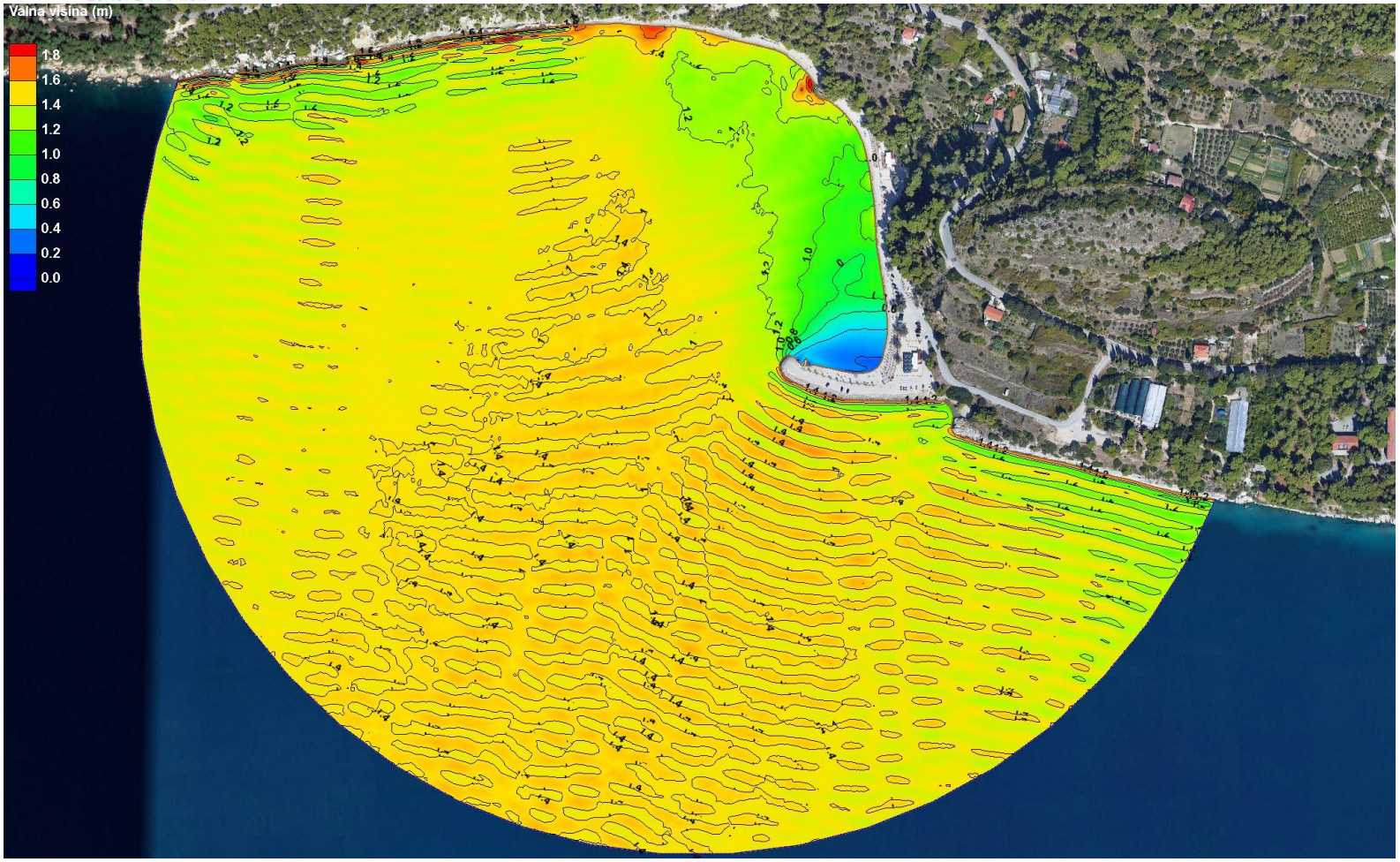

Figure 6.70 – Field of significant wave heights for simulation **A27** – the existing state of Kašjuni beach in Split with wave parameters from the Direction of SSW (202.5°), 50-year return period (Hs=1.57 m; Tp=5.11 s) and sea level corresponding to the Middle Sea Level (SRM)

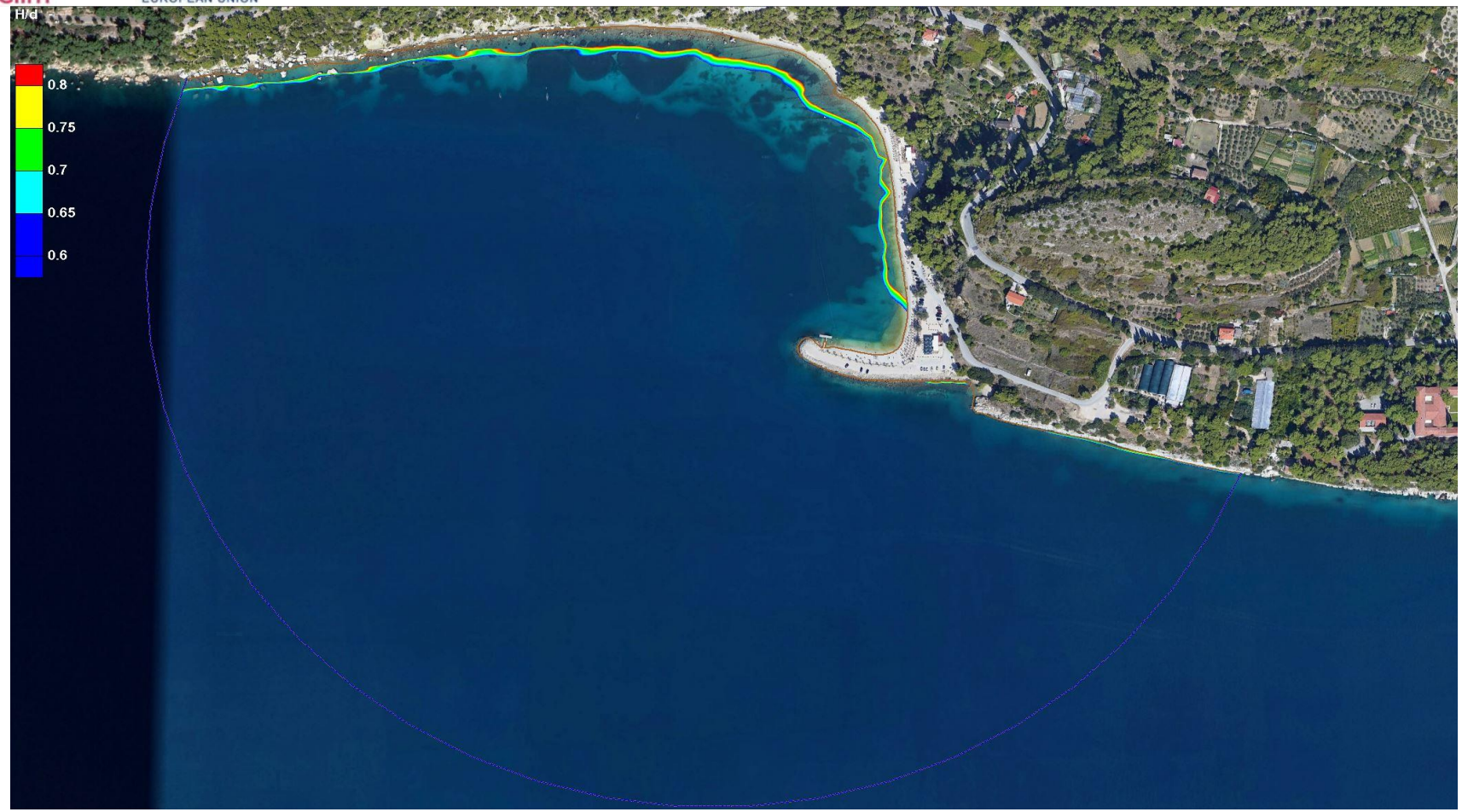

Figure 6.71 – Wave breaking zone for simulation **A27** – the existing state of Kašjuni beach in Split with wave parameters from the Direction of SSW (202.5°), 50-year return period (Hs=1.57 m; Tp=5.11 s) and sea level corresponding to middle sea level (SRM)

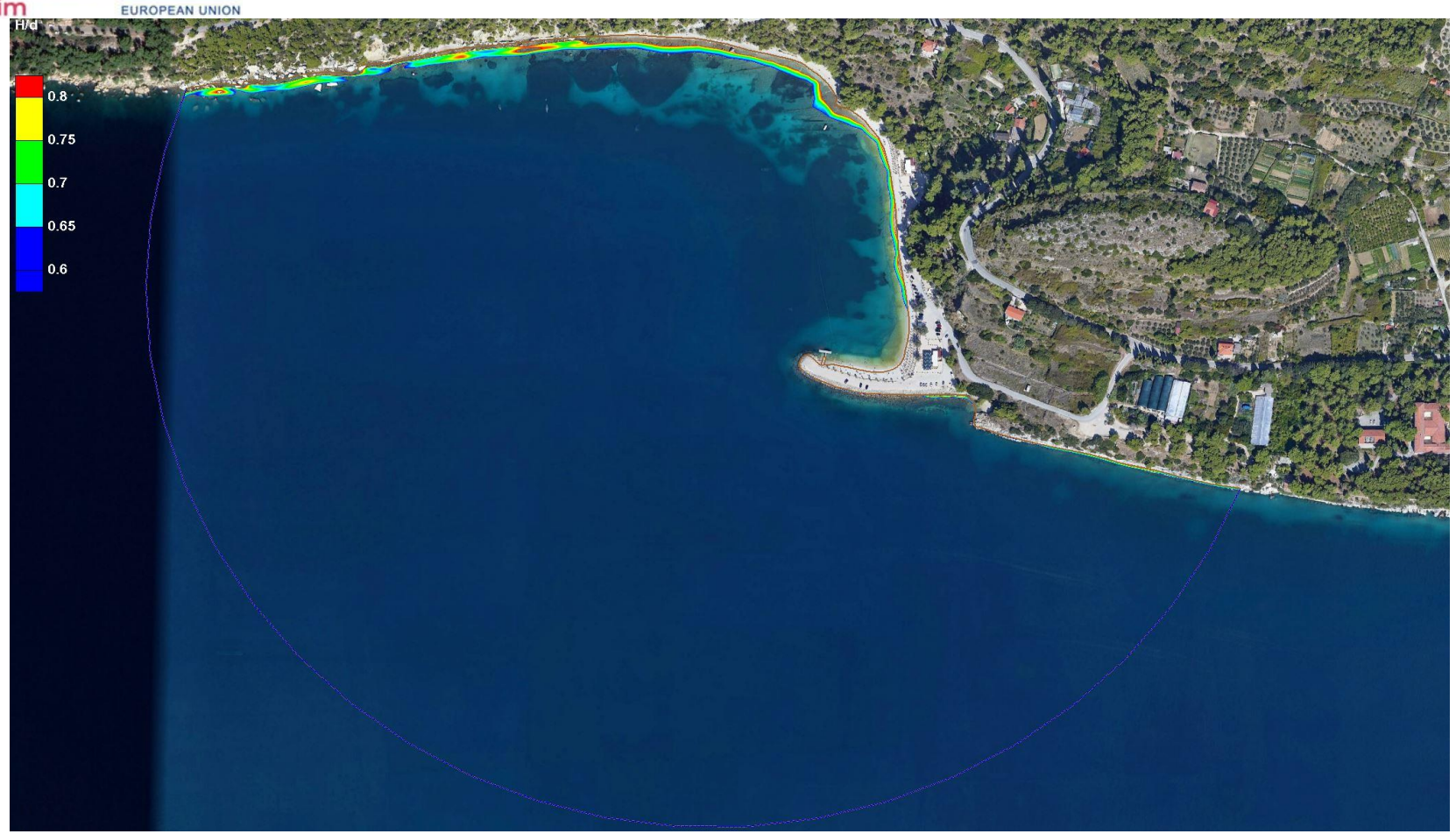

Figure 6.72 – Wave breaking zone for simulation **A29** – the existing state of Kašjuni beach in Split with wave parameters from the Direction of SSW (202.5°), 50-year return period (Hs=1.57 m; Tp=5.11 s) and sea level corresponding to **absolute maximum**

Figure 6.73 – Wave breaking zone for simulation **A31** – **conceptual design of** Kašjuni beach in Split with wave parameters from the Direction of SSW (202.5°), 50-year turnback period (Hs=1.57 m; Tp=5.11 s) and sea level corresponding to **absolute maximum**

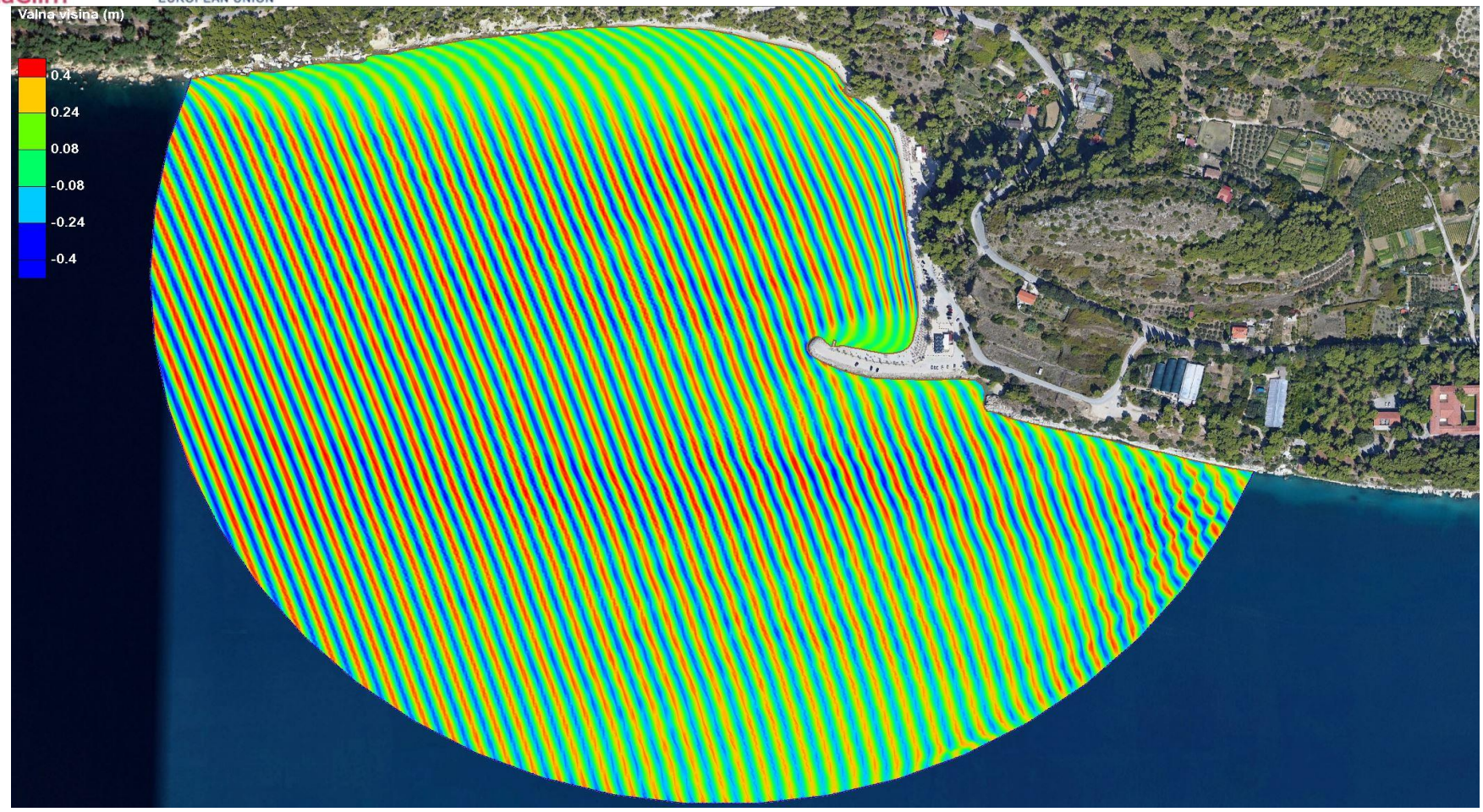

Figure 6.74 – Current wave outline for A28 simulation – the existing state of Kašjuni beach in Split with wave parameters from w direction (270°), 50-year return period (Hs=0.79 m; Tp=3.62 s) and sea level corresponding to middle sea level (SRM)

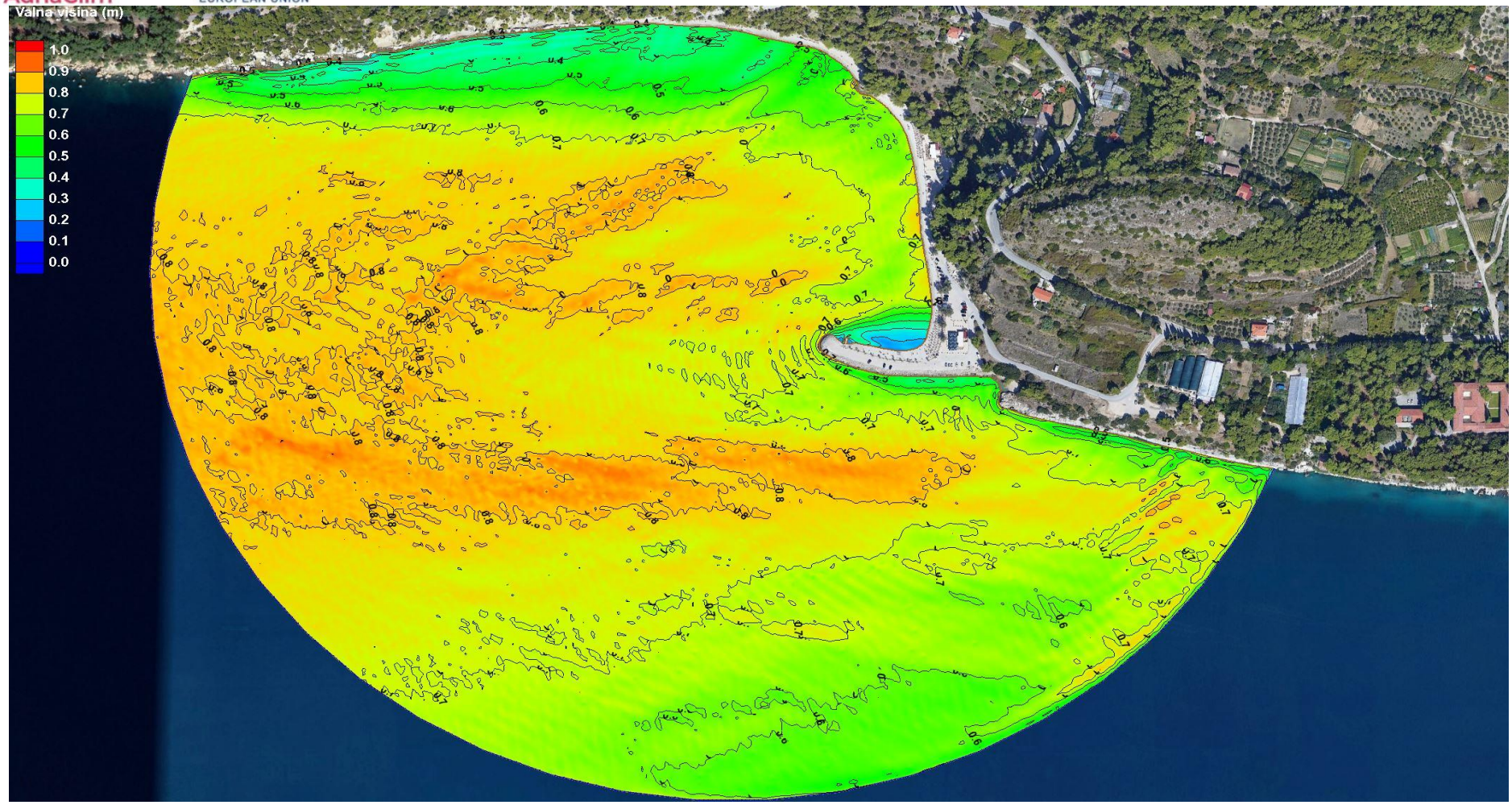

Figure 6.75 – Field of significant wave heights for simulation **A28** – the existing state of Kašjuni beach in Split with wave parameters from w direction (270°), 50-year return period (Hs=0.79 m; Tp=3.62 s) and sea level corresponding to middle sea level (SRM)

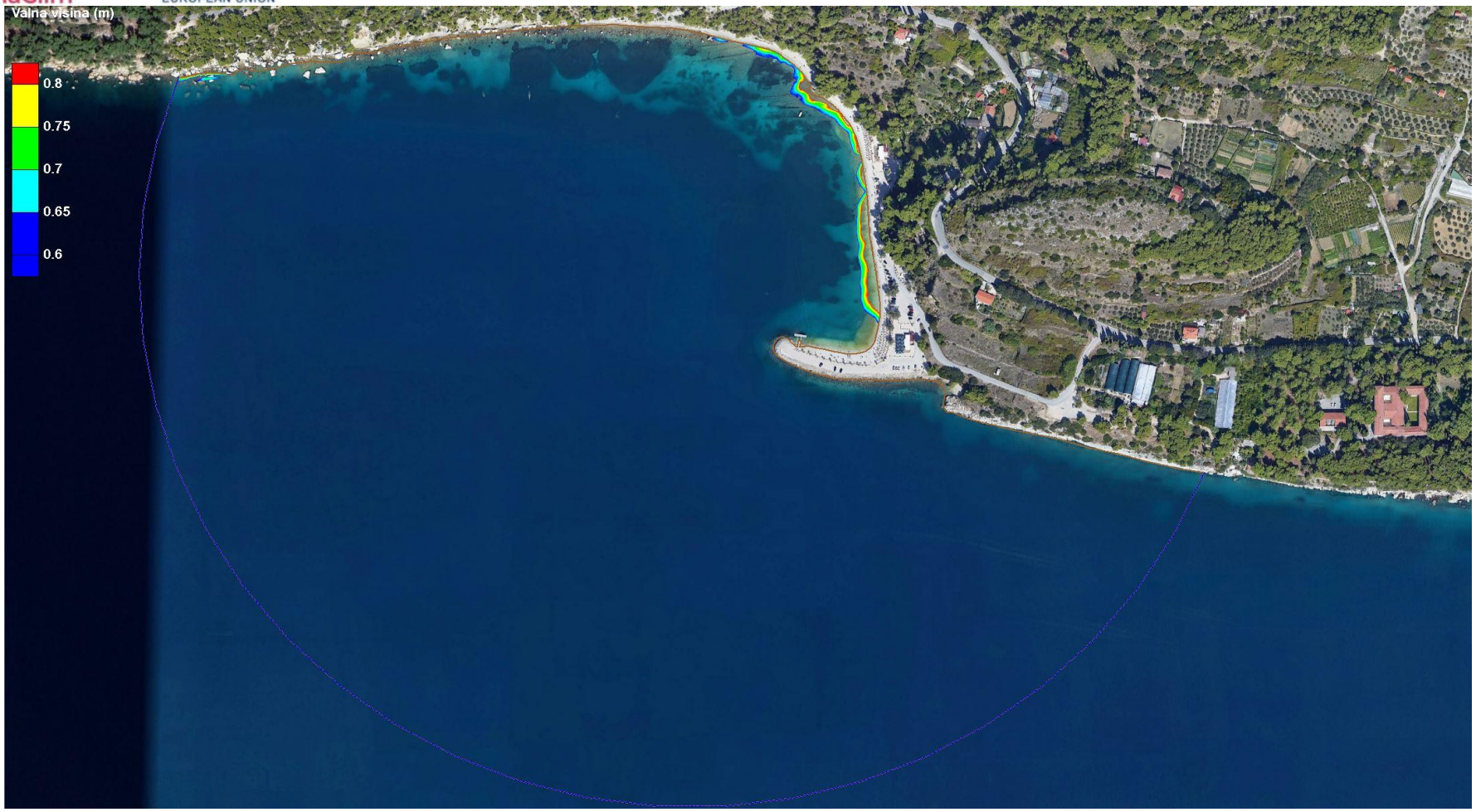

Figure 6.76 – Wave breaking zone for simulation **A28** – the existing state of Kašjuni beach in Split with wave parameters from w direction (270°), 50-year return period (Hs=0.79 m; Tp=3.62 s) and sea level corresponding to middle sea level (SRM)

Figure 6.77 – Wave breaking zone for simulation **A30** – the existing state of Kašjuni beach in Split with wave parameters from w direction (270°), 50-year return period (Hs=0.79 m; Tp=3.62 s) and sea level corresponding to **absolute maximum**

Figure 6.78 – Wave breaking zone for simulation **A32** – **conceptual design** of Kašjuni beach in Split with wave parameters from W direction (270°), 50-year return period (Hs=0.79 m; Tp=3.62 s) and sea level corresponding to **absolute maximum**

7. CALCULATION OF TRANSPORT POTENTIAL AND STABLE COMPOSITION OF BEACH MATERIAL

7.1. Calculation of transport potential of the beach material

As explained in Chapter 5.3 of this study, in order to calculate the potential of sediment transport for a particular point on the considered beach, it is necessary to know the wave height parameter *Hs* at that point, which indicates the potential amount of energy that waves bring to the shore, with the help of which the wave energy *flow can be calculated*, which serves to estimate the size of the potential transport of beach material due to wave-induced currents (Pernat Ž., Vranješ M, 2012).

The calculation of the transport potential of beach material was carried out for the current condition of all five locations of the beaches in question, but only for smaller control areas, whose positions are indicated in the following chapters for each of the beaches. Considering the size of the coastal zones considered, the aim of this study is not to provide ready-made design solutions for the entire coastal zones concerned, but exclusively to implement procedures for defining guidelines and methodologies for their implementation. Furthermore, due to the complexity of the task, which requires that, based on a detailed analysis of the results of potential transfer (transmission) for the existing state, solutions be provided that will improve the detected condition, the procedure of checking the potential transfer (transmission) of beach material for the existing state and for the proposed construction solutions in control areas has been applied, with a comparison of the results and the assessment of the degree of improvement. The exception is Kašjuni beach in Split, for which, due to its relatively small size, an integral solution has been given.

This methodological approach provides the basic prerequisites for making quality and consistent conclusions, as a necessary and stable basis for the development of general, but also detailed guidelines for the dimensioning and design of beaches made of granular materials, with the goal of conservation and sustainable and resilient development of the coastal area of Split-Dalmatia County.

7.1.1. Zlatni rat (Brač)

In accordance with table 6.1, a total of 8 numerical wave simulations (simulations A1 to A8) were conducted for Zlatni rat beach on Brač, and the results of the simulations are shown in Figures 6.22 to 6.37. For further analysis and calculation of the transport potential of beach material of the beach in question, two control areas were selected, shown in Figure 7.1.

Given that Zlatni rat beach is an extremely sensitive natural phenomenon and protected landscape (just like Stiniva beach), the methodology applied to other beaches that are the subject of analysis of this study, which aims to improve the level of sustainability and resilience of the beach in question, *a priori* did not include the development of a proposal for the conceptual design of construction works in the area or underwater of the beach, but only an evaluation of the potential impacts, in this particular case the calculation of the potential of the transfer (transmission) of beach material only for the current situation.

Control areas for Zlatni rat beach were selected on both sides of the cape with individual lengths of 200 m each (Figure 7.1). In accordance with the results of numerical modeling with wave parameters from the directions ESE (112.5°) and WSW (247.5°), which are the most dominant for the beach in question, the results for the existing situation (Figures 6.24 and 6.25, and 6.36 and 6.37) with both analyzed sea level (SRM and absolute maximum) show that wave breaking occurs in the immediate

vicinity of the coastline, which indicates a significant probability of increased potential of beach material transfer and beach erosion. The results of numerical simulations for the direction of ESE (112.5°) with a sea level corresponding to the absolute maximum show that the refractive zone of incoming waves from this direction moves as much as 5 meters towards land in relation to the simulation with a sea level corresponding to the middle sea level (SRM). This is evident from Figure 8.4, which shows the positions of wave zones for simulations with different sea levels.

It is a similar situation for numerical simulations for WSW direction (157.5°). The results of the simulation with a sea level corresponding to the absolute maximum show that the refractive zone of incoming waves from this direction moves as much as 20 meters towards land compared to the simulation with a sea level corresponding to the middle sea level (SRM). This is evident from Figure 8.9, which shows the positions of wave zones for simulations with different sea levels.

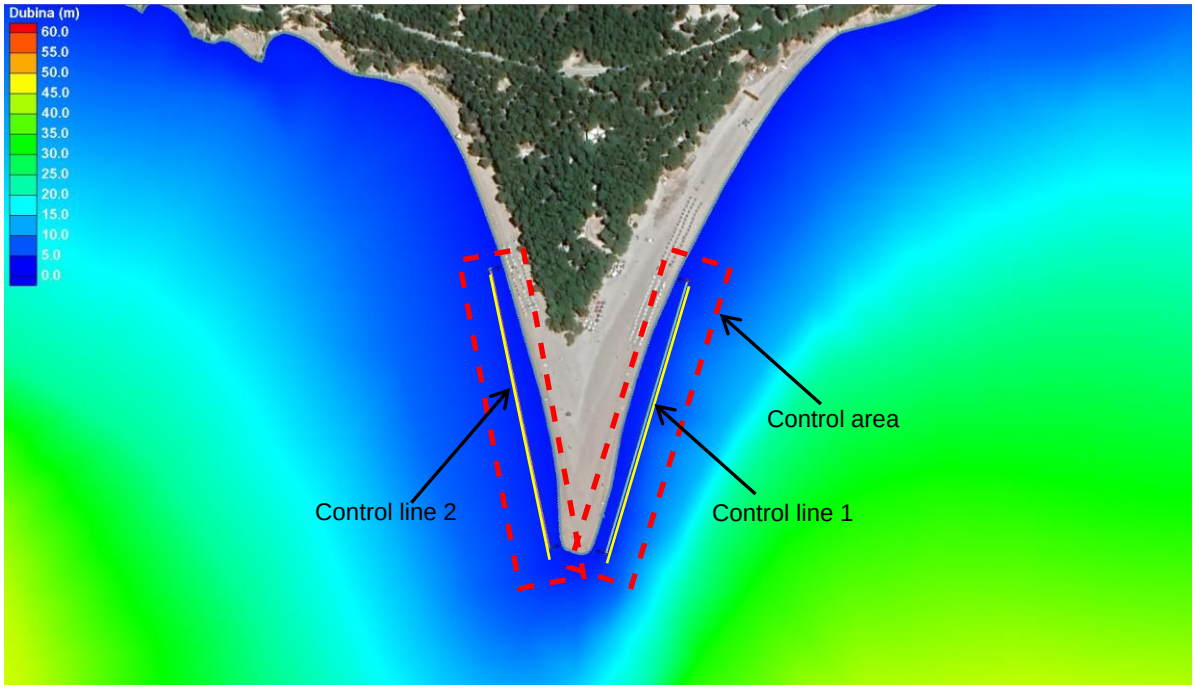

Figure 7.1 – Control area and control lines for the existing state of Zlatni rat beach (Brač)

In the control areas, control lines were determined in which parameters were observed crucial for determining the transport potential of beach material, namely wave height *Hs* and wave power *PI*. The parameters were monitored for numerical simulations with sea level corresponding to the absolute maximum for the existing state.

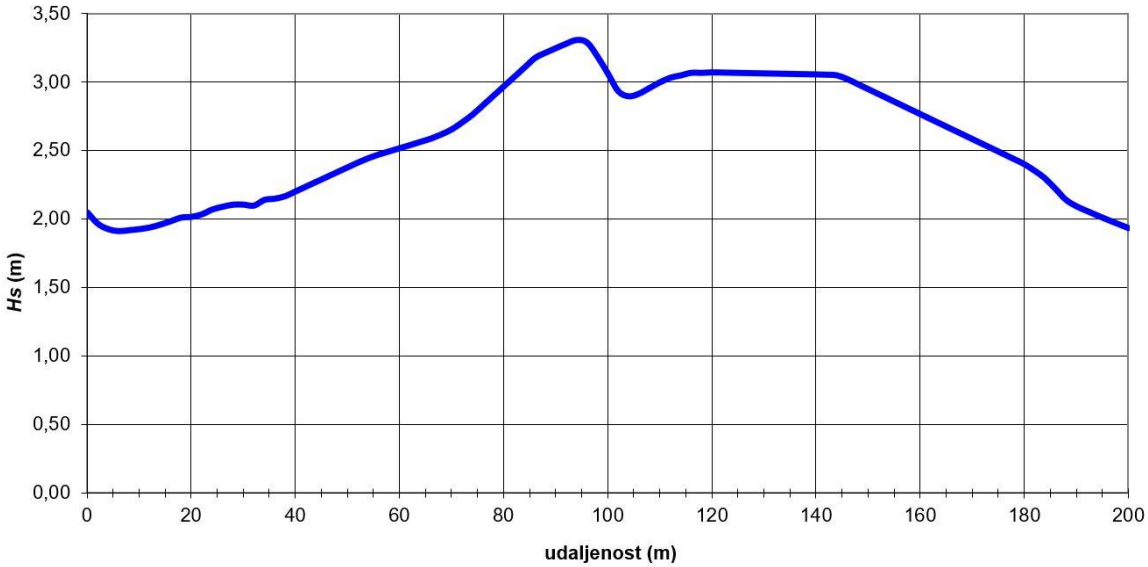

Figure 7.2 – Variation of Wave Heights *Hs* for the existing state and direction ESE (112.5°) in the control line 1 of Zlatni rat beach (Brač)

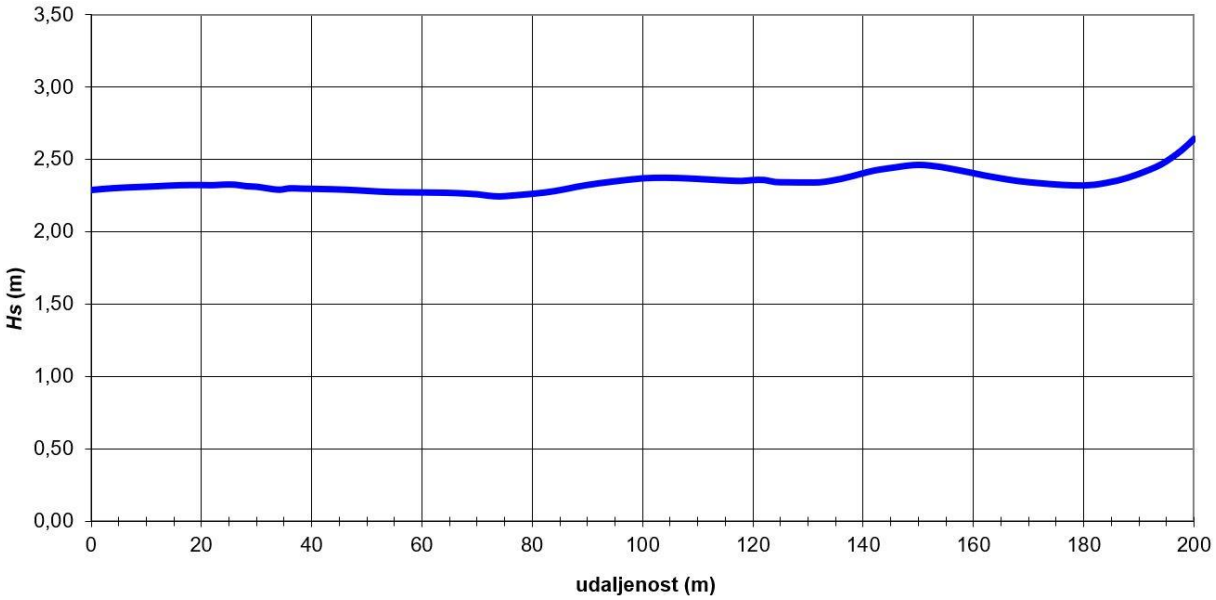

Figure 7.3 – Variation of Hs wave heights for the existing state and direction WSW (247.5°) in the control line 2 of Zlatni rat beach (Brač)

The results of the analysis show that in both control areas there are parts of the coast with possible problems with the transmission (adoption and removal) of beach material, and are reflected in increased values of wave power *PI* (Figures 7.4 and 7.5). The most pronounced problem occurs, as expected, at the very top of cape Zlatni rat beach, where the values of wave power *PI* reach approximately 1.6x103 N/s for both analyzed wave directions. This area (the tip of the cape) is also the most exposed part of the actual situation on the ground, where due to the most pronounced action of waves and the interaction of numerous related physical processes, the known motion of beach material and the change of orientation of the top of the beach occurs during the year.

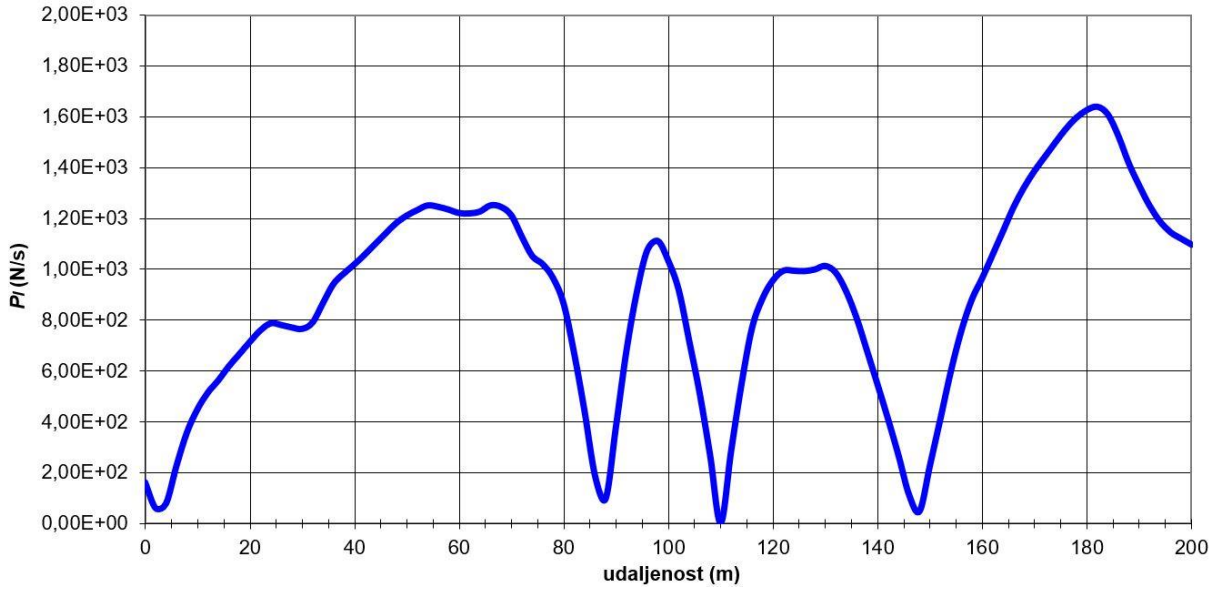

Figure 7.4 – Variation of the wave power *Pl* for the existing state and direction ESE (112.5°) in the control line 1 of Zlatni rat beach (Brač)

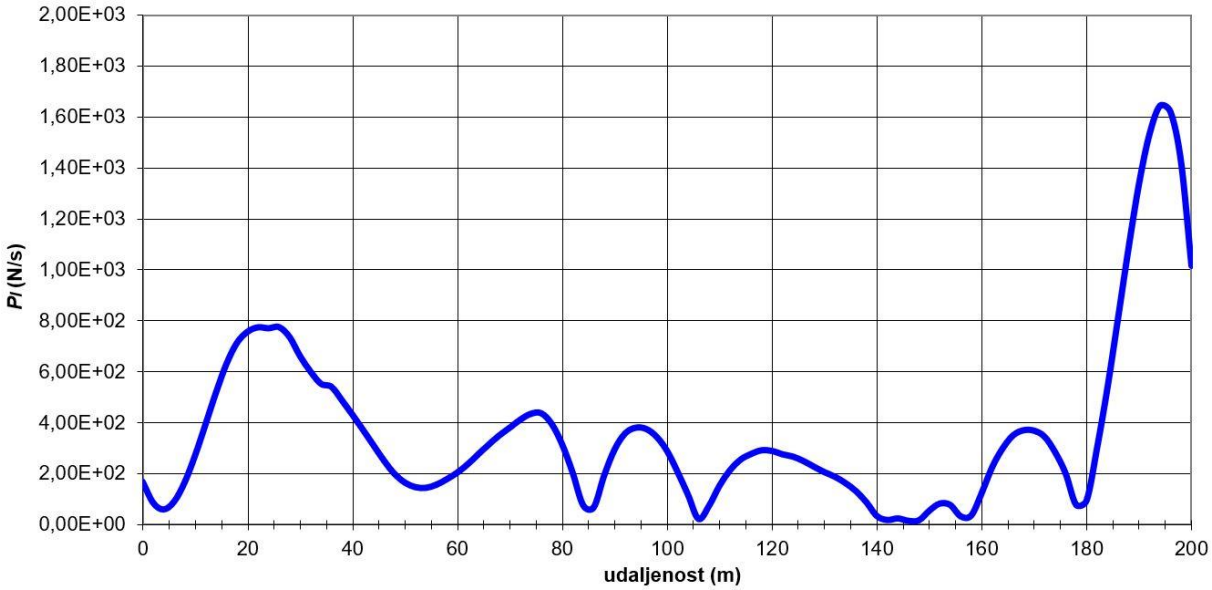

Figure 7.5 – Variation of wave power *Pl* for the existing state and direction WSW (247.5°) in the control line 2 of Zlatni rat beach (Brač)

Based on all the above, it can be concluded that the conducted analysis procedures for the control areas of Zlatni rat beach on Brač pointed to the necessity of raising the level of sustainability and resilience of the coastal zone in question, and confirmed the correctness of the applied methodology. As previously stated, the methodological approach given for Zlatni rat beach differs from the other considered beaches, which does not diminish the fact that based on the conducted analysis, quality bases were obtained for making equally high-quality and consistent conclusions, as a necessary and stable basis for the development of general, but also more detailed guidelines for sizing and designing beaches made of granular materials. In solving the issue of sustainability and resilience of Zlatni rat

beach on Brač, it is necessary to apply a somewhat different strategy compared to other considered beaches, without construction interventions in the area and / or underwater of the beach in question, with the goal of conservation and sustainable and resilient development of the entire coastal area (more on this in chapter 9).

7.1.2. Stiniva (Vis)

In accordance with table 6.1, a total of 2 numerical wave simulations (Simulations A9 and A10) were conducted for Stiniva beach on Vis, and the results of the simulations are shown in Figures 6.38 to 6.40. For further analysis and calculation of the potential transfer (transmission) of beach material of the beach in question, the control area shown in Figure 7.6 was selected.

Considering that Stiniva beach, as well as Zlatni rat beach is an extremely sensitive natural phenomenon and protected landscape, the methodology applied to other beaches that are the subject of this study, which aims to improve the level of sustainability and resilience of the beach in question, *a priori* did not include the development of a proposal for the conceptual design of construction works in the area or seabed of the beach, but only an evaluation of the potential impacts, in this particular case the calculation of the potential of the transfer (transmission) of beach material only for the current situation.

The control area for Stiniva beach was selected within the waters of the 20 m long beach itself (Figure 7.6). In accordance with the results of numerical modelling that are dominant for the control area concerned, the results for the existing situation (Figure 6.40) with both analyzed sea level (SRM and absolute maximum) show that wave breaking does not occur in the immediate vicinity of the coastline, indicating a low potential of transfer (transmission) of beach material and beach erosion. This is evident from Figure 8.12, which does not notice the appearance of a wave regression zone in the area of the waters of the beach itself, nor in its immediate vicinity.

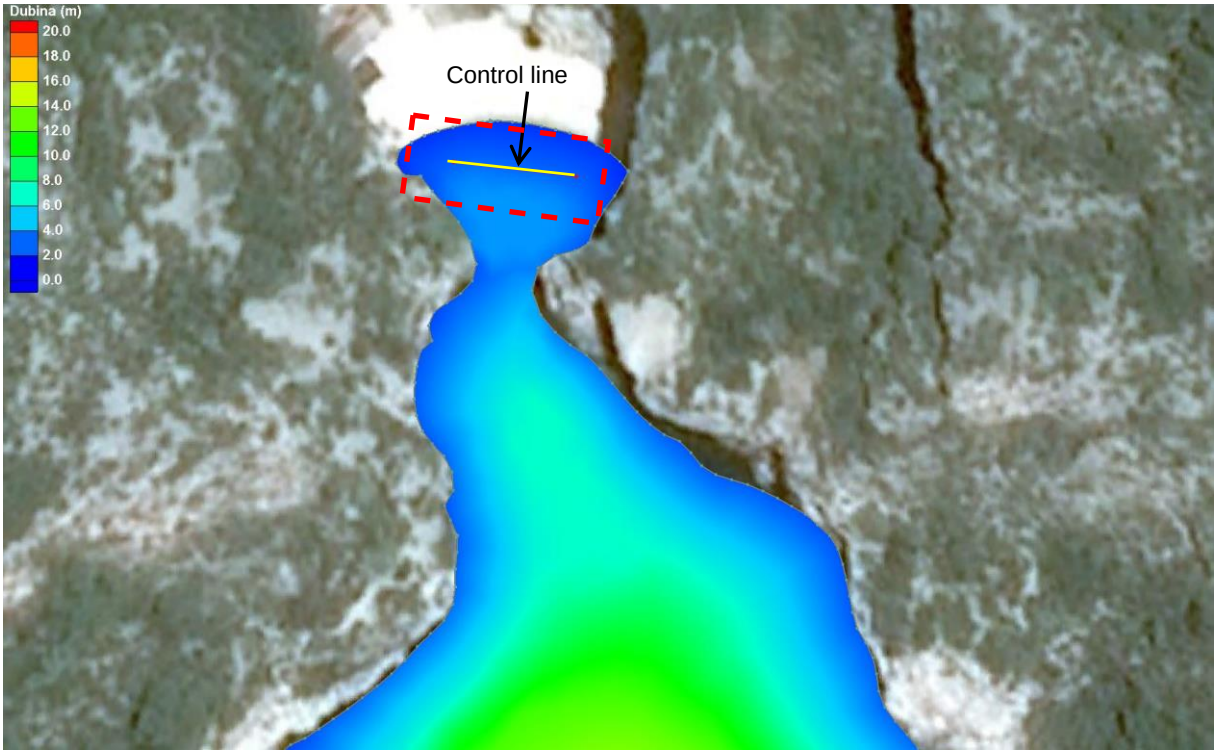

Figure 7.6 – Control area and control line for the existing state of Stiniva beach (Vis)

In the control area, a control line was determined in which parameters were observed crucial for determining the transport potential of beach material, namely wave height *Hs* and wave power *PI*. The parameters were monitored for numerical simulations with sea level corresponding to the absolute maximum for the existing state.

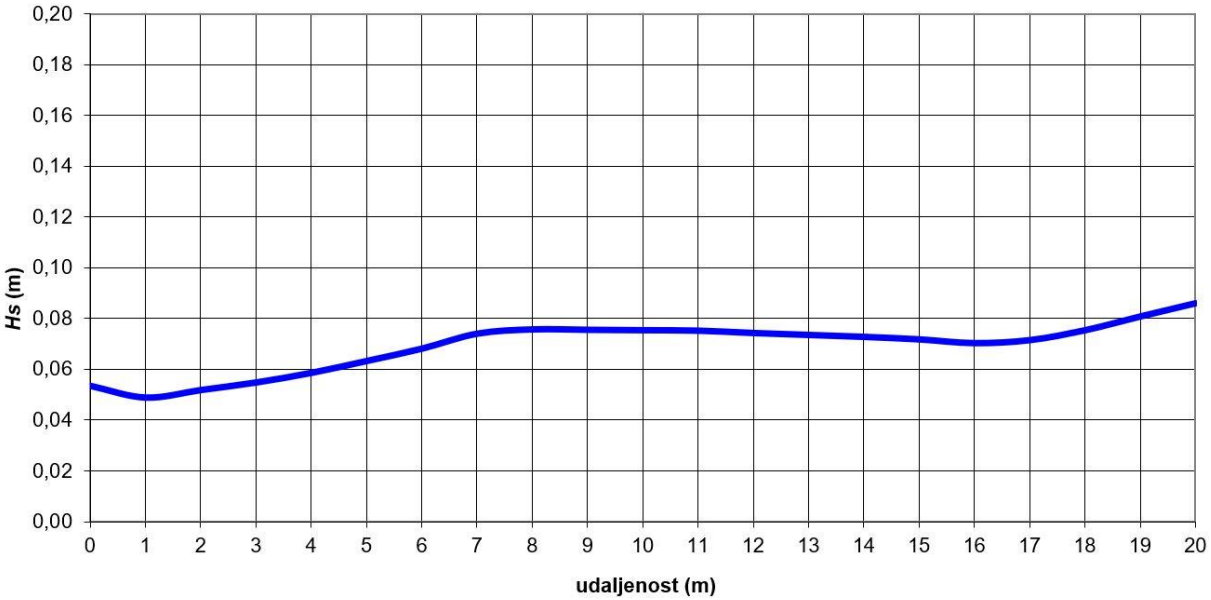

Figure 7.7 – Variation of Hs wave heights for the existing state in the control line of Stiniva beach (Vis)

The results of the analysis show that in the control area there are no parts of the coast that could have potential problems with the transmission (adoption and removal) of beach material, and is reflected in extremely low values of wave power *PI* (Figure 7.8), which amount to a maximum of 0.5 N / s. This trend certainly occurs in the actual state, because there are no noticeable parts of the coast on the ground that can be safely claimed to be susceptible to the process of transmission (transmission) of beach materials.

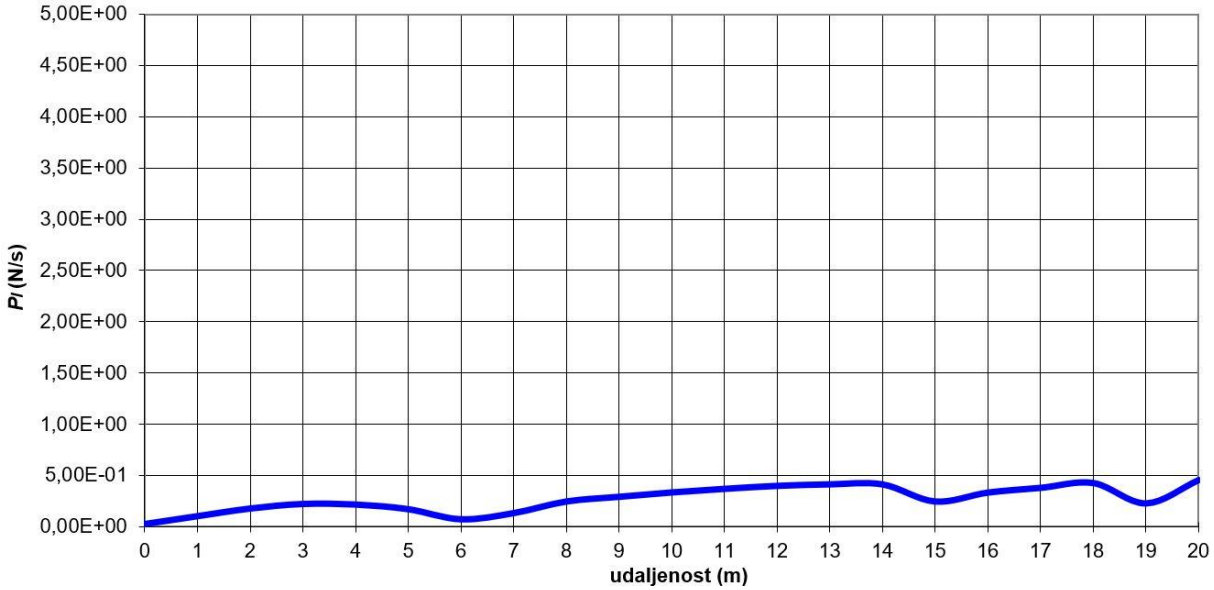

Figure 7.8 – Variation of the wave power Pl for the existing state in the control line of Stiniva beach (Vis)

Based on all the above, it can be concluded that the analysis procedures conducted for the control area of Stiniva beach on Vis indicated that it is not necessary to take any specific actions to raise the level of sustainability and resistance of the coastal zone in question due to the potential transfer (transmission) of beach material, and confirmed the correctness of the applied methodologies. As previously stated, the methodological approach given for Stiniva beach (and Zlatni rat) differs from other considered beaches, which does not diminish the fact that based on the analysis, quality bases were obtained for making equally high-quality and consistent conclusions, as a necessary and stable basis for the development of general, but also more detailed guidelines for the dimensioning and design of beaches made of granular materials. In solving the issue of sustainability and resilience of Stiniva beach on Vis, it is necessary to apply a somewhat different strategy compared to other considered beaches, without construction interventions in the area and / or underwater of the beach in question, with the goal of preserving and sustainable and resilient development of the entire coastal area (more on this in chapter 9).

7.1.3. Podgora (Makarska Riviera)

In accordance with table 6.1, a total of 7 numerical simulations of valves (simulations A11 to A17) were conducted for Podgora beach on the Makarska Riviera, and the results of the simulations are shown in Figures 6.41 to 6.53. For further analysis and calculation of the potential transfer (transmission) of beach material of the beach in question, a control area was selected, shown in Figures 7.9 and 7.10. As previously emphasized, the aim of the analysis is not to provide design solutions for the entire coastal zone, but to provide procedures for defining guidelines and methodologies for their implementation in a smaller area, which can then be applied throughout the coastal zone. The methodology applied in the control area of Podgora beach concerned, i.e., the sequence of analysis procedures for establishing design guidelines, aims to improve the level of sustainability and resilience across the entire coastal zone of the beach concerned.

The control area for the Beach Podgora was selected in the southern part of the coastal belt of the beach in question, with an approximate length of 130 m. The coast in the control area is bordered by

two smaller stone groynes. In accordance with the results of numerical modelling with wave parameters from the direction of SSE (157.5°), which are dominant for the control area concerned, the results for the existing situation (Figures 6.43 and 6.44) with both analyzed sea level (SRM and absolute maximum) show that wave breaking occurs in the immediate vicinity of the coastline, indicating an increased transport potential of beach material and beach erosion. The results of numerical simulations with a sea level corresponding to the absolute maximum show that the wave breaking zone of incident waves from this direction moves as much as 5 meters towards land compared to the simulation with the sea level corresponding to the Middle Sea Level (SRM). This is visible from Figure 8.17, which shows the positions of wave zones for simulations with different sea levels.

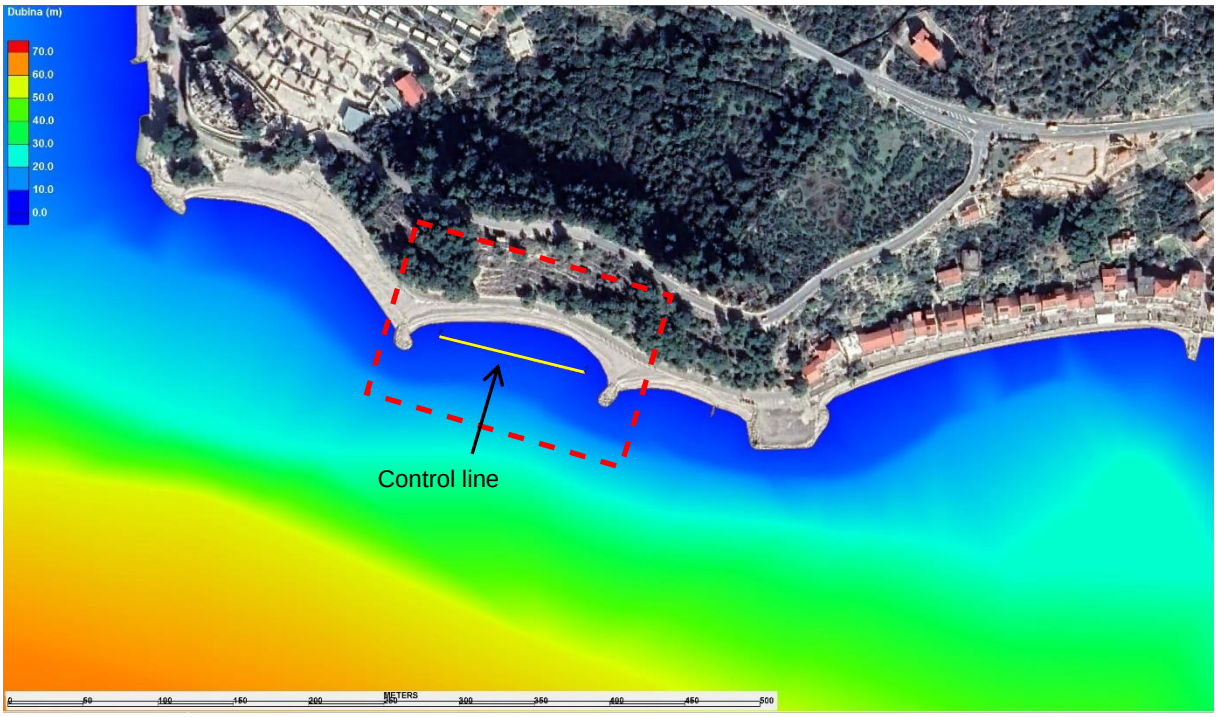

Figure 7.9 – Control area and control line for the existing state of Podgora beach (Makarska Riviera)

The results of the analysis for the existing situation showed that in the control area there are parts of the coast with possible problems with the transport of beach material, and are reflected in the increased values of the wave power *Pl* (figure 7.12). The most pronounced problem occurs in the far eastern part of the control line, where the values of wave power *Pl* reach approximately 2.5x103 N /s. This area is also the most exposed part of the actual situation on the ground, so the proposal of the conceptual solution should eliminate this problem, while considering that construction interventions do not worsen the condition of the wavefield in the considered waters.

Based on the results of numerical simulations and detected problems, a proposal for the control area of Podgora beach was made in order to eliminate them, and raise the general level of sustainability and resilience of the beach. The proposal of the conceptual design is conceived using the basic protective building and technical principles (more in Chapter 5), and it is about the applying of an underwater stone reef at the appropriate distance and depth, and additional plan correction of two existing stone groynes with the addition supplementation of the beach with appropriate beach material. Sizing the details of all parameters of the technical solution (width of berm, height of the berm, slope, granulation of stone blocks, slope of the face of the beach, granulometric composition of

beach material...), should be the subject of technical and project documentation for the realization of this project, based on the guidelines given by this study.

The ground plan disposition of the interventions made in the area and waters of the control area of Podgora beach in question is shown in Figure 7.10. In the control area, a control line was determined in which parameters were observed crucial for determining the transport potential of beach material, namely wave height *Hs* and wave power *Pl*. The parameters were monitored for numerical simulations with a sea level corresponding to the absolute maximum, for the existing state and conceptual design.

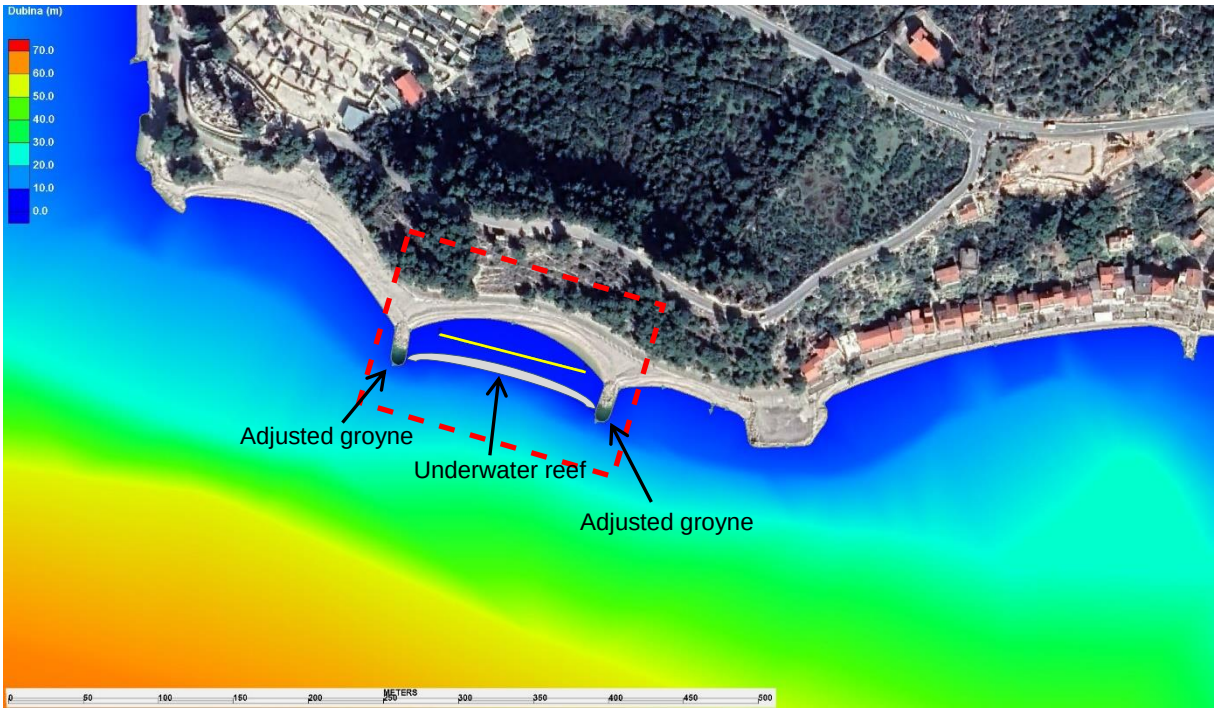

Figure 7.10 – Control area and control line for the conceptual design of the beach Podgora (Makarska Riviera)

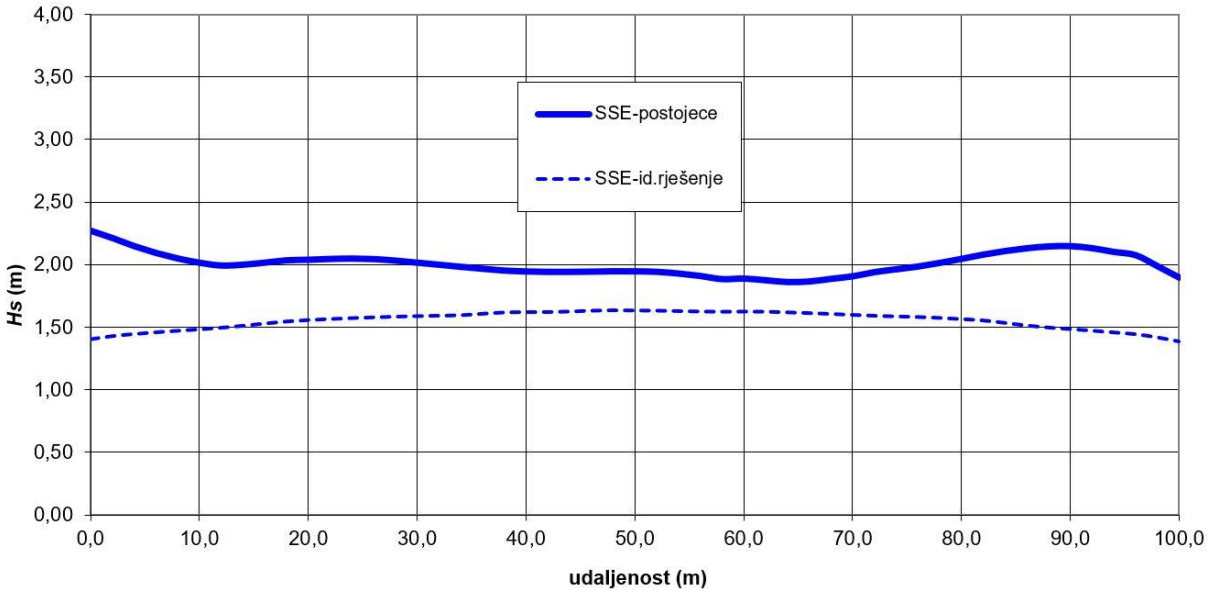

Figure 7.11 – Variation of Wave Heights *Hs* for the existing state and conceptual design in the control line of

Podgora beach (Makarska Riviera) for the direction of waves SSE (157.5°)

The results of the numerical simulation A17 with the conceptual design of the coastal zone in the control area of Podgora beach (with the sea level corresponding to the absolute maximum) show a significant shift of the wave breaking zone from the incident direction of the SSE (157.5°) towards the open sea, i.e., at the position of the set undersea threshold (Figure 6.45). This is especially evident from figure 8.17. This situation indicates a significant improvement in the situation in the control area for the conceptual design compared to the current situation. If we look at the wave power values *PI* now, it is noticed that they are significantly smaller along the entire control line with a maximum of approximately $1.2x10^3$ N/s, which is more than twice less than for the existing state of the coastal belt (Figure 7.12). Also, variations of wave heights Hs in the control line show a significant decrease for the conceptual design compared to the existing state (Figure 7.11).

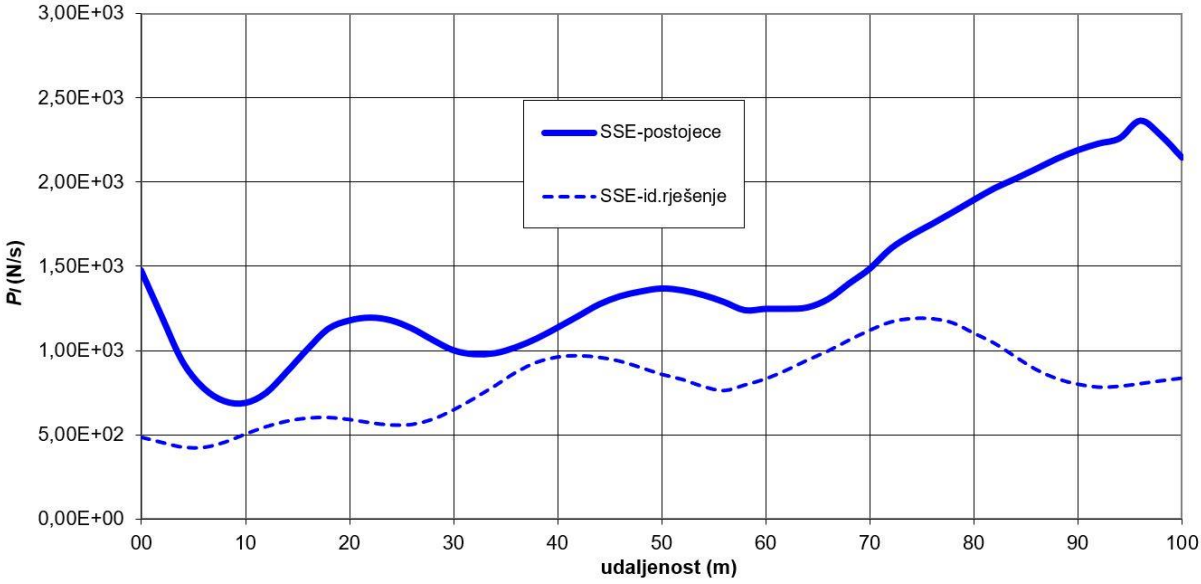

Figure 7.12 – Variation of the wave power Pl for the existing state situation and conceptual design in the control line of the beach Podgora (Makarska Riviera) for the direction of the waves SSE (157.5°)

Based on all the above, it can be concluded that the conducted analysis procedures for the control area of Podgora beach on the Makarska Riviera showed the correctness of the applied methodology, which resulted in a solution that will undoubtedly raise the level of sustainability and resistance of the coastal zone of the control area. The methodological approach presented in the analysis of the control area provides the basis for the adoption of quality and consistent conclusions, as a necessary and stable basis for the development of general, but also more detailed guidelines for the dimensioning and design of beaches made of granular materials, with the goal of conservation and sustainable and resilient development of the entire coastal area of Podgora and Split-Dalmatia County.

7.1.4. Podstrana-Duće area

In accordance with table 6.1, a total of 9 numerical simulations of valves (simulations A18 to A26) were conducted for beaches on the Podstrana-Duće area, and the results of the simulations are shown in Figures 6.54 to 6.68. For further analysis and calculation of the transport potential of beach material of the beach in question, the control area was selected, shown in Figures 7.13 and 7.14. As previously

emphasized, the aim of the analysis is not to provide design solutions for the entire coastal zone, but to provide procedures for defining guidelines and methodologies for their implementation in a smaller area, which can then be applied throughout the coastal zone. The methodology applied in the control area of Podstrana beach concerned, i.e., the sequence of analysis procedures for establishing design guidelines, aims to improve the level of sustainability and resilience across the entire coastal zone of the beach concerned.

The control area for Podstrana beach was selected in an area called Grljevac, approximately 120 m long. The coast in the control area is divided into two separate beaches with three stone groynes. In accordance with the results of numerical modelling with wave parameters from the direction of SE (135°), which are dominant for the control area in question, the results for the existing situation (Figures 6.56 and 6.57) with both analyzed sea level (SRM and absolute maximum) indicate that wave breaking occurs in the immediate vicinity of the coastline, which indicates an increased transport potential of beach material and beach erosion. The results of numerical simulations with a sea level corresponding to the absolute maximum show that the refractive zone of incident waves from this direction moves as much as 30 meters towards land in relation to the simulation with the sea level corresponding to the middle sea level (SRM). This is evident from Figure 8.25, which shows the positions of wave zones for simulations with different sea levels.

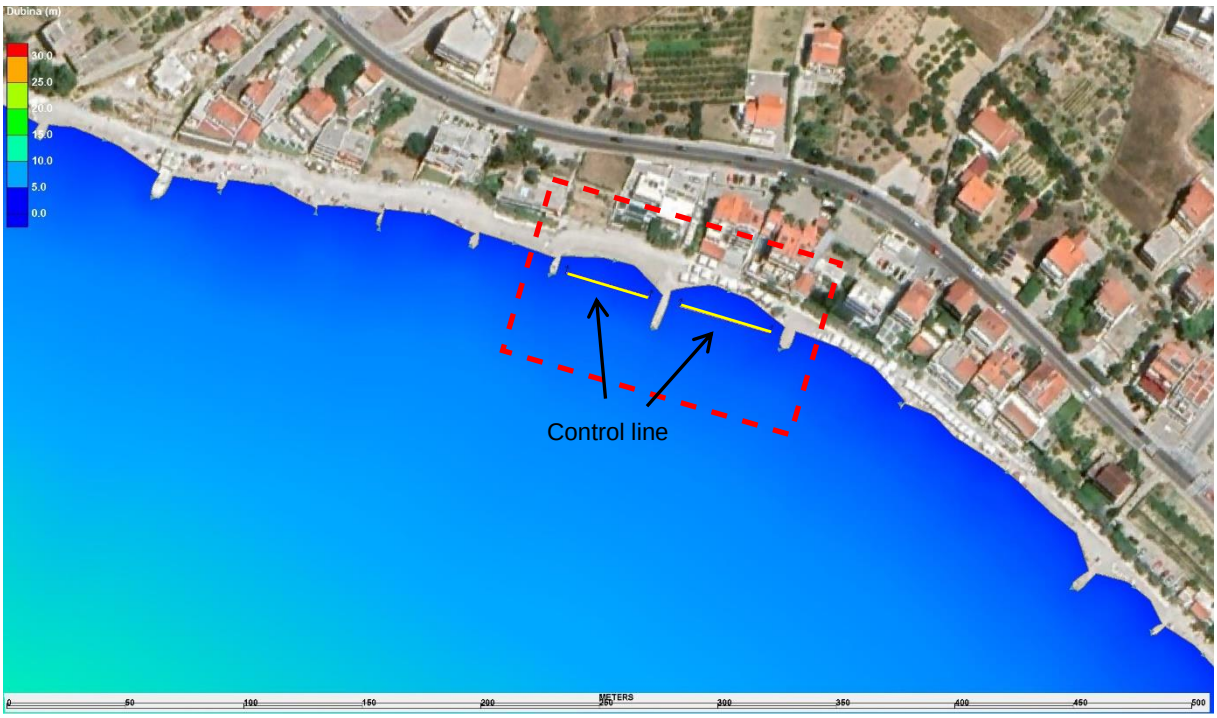

Figure 7.13 – Control area and control lines for the existing state of the Podstrana beach

The results of the analysis for the existing situation show that in the control area there are parts of the coast with possible problems with the transport of beach material, and are reflected in the increased values of the wave power *PI* (figure 7.16). The problem arises in both analyzed beaches, somewhat more pronounced for the western beach, where the wave power values of *PI* reach approximately $3.0x10^3$ N/s. This area is also the most exposed part of the actual situation on the ground, so the proposal of the conceptual solution is necessary to eliminate this problem, while considering that construction interventions do not worsen the condition of the wave field in the considered waters.

Based on the results of numerical simulations and detected problems, a proposal for the conceptual design was made for the control area of Podstrana beach in order to eliminate them, and raise the general level of sustainability and resilience of the beach. The proposal of the conceptual design is conceived by applying the basic construction and technical principles (more in chapter 5), and it is about setting the underwater stone reefs at the appropriate distance and depth, and additional plan correction of the three existing stone groynes with the addition (supplementation) of the beach with appropriate beach material. Sizing the details of all parameters of the technical solution (berm width of underwater reefs, berm height, slopes, granulation of stone blocks, slope of the face of the beach, granulometric composition of beach material...) should be the subject of technical and project documentation for the realization of this project, based on the guidelines given by this study.

The ground plan disposition of the interventions made in the space and waters of the control area in question is shown in Figure 7.14. In the control area, two control lines were determined in the direction in which the parameters were observed crucial for determining the transport potential of beach material, namely the wave height *Hs* and the power of the wave *PI*. The parameters were monitored for numerical simulations with a sea level corresponding to the absolute maximum, for the existing state and conceptual design.

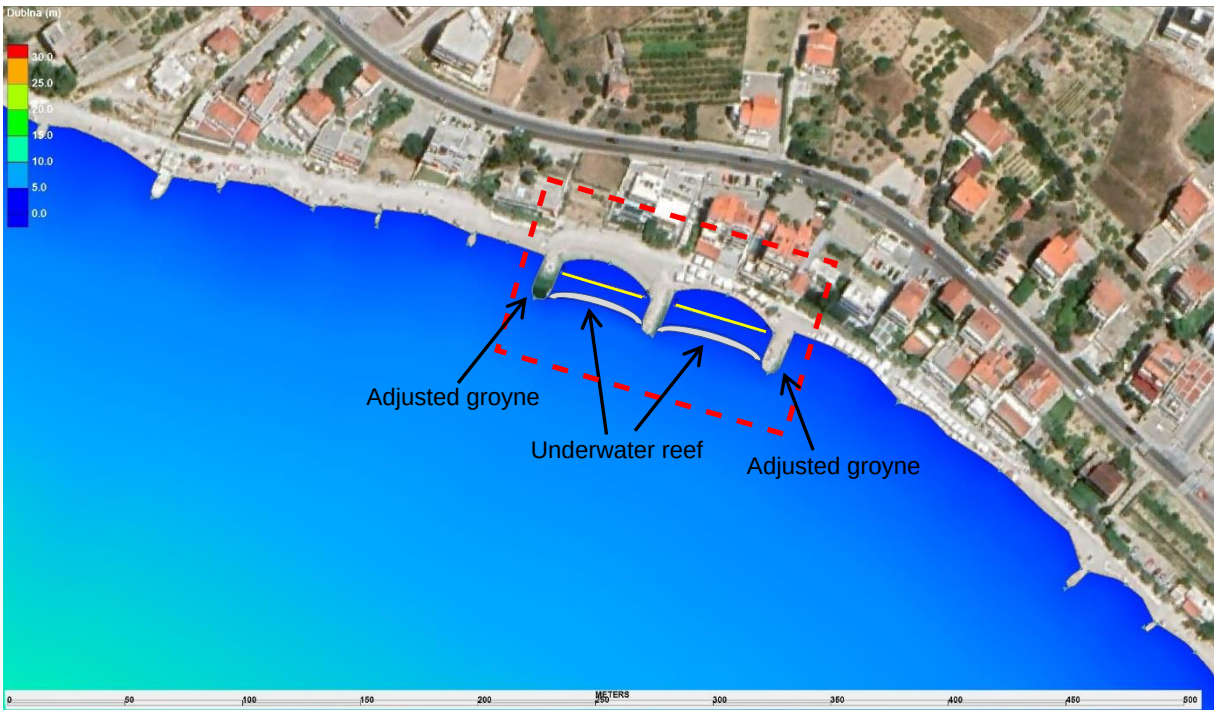

Figure 7.14 – Control area and control lines for the conceptual design of the Beach Podstrana

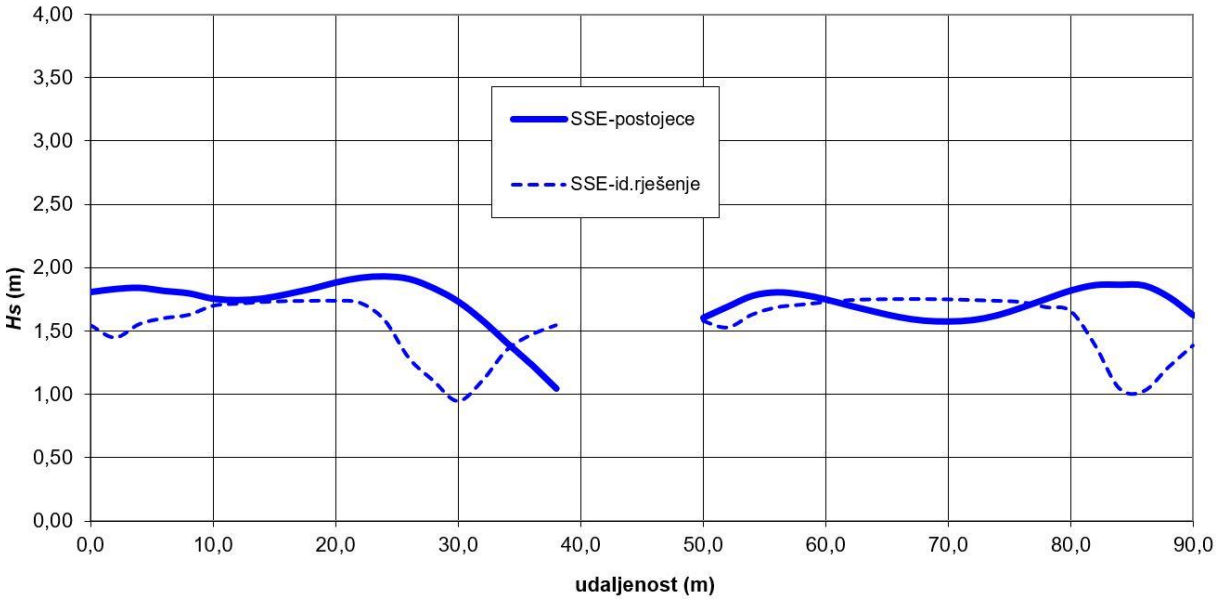

Figure 7.15 – Variation of Wave Heights *Hs* for the existing state and conceptual design in the control lines of the Beach Podstrana for the wave direction OF SE (135°)

The results of the numerical simulation A24 with the conceptual design of the coastal zone (with a sea level corresponding to the absolute maximum) in the control area of Podstrana beach show a significant shift of the wave breaking zone from the incident direction of the SE (135°) towards the open sea, i.e., at the position of the set undersea threshold (Figure 6.58). This is even better seen in Figure 8.25, where it is observed that the wave breaking zone from this direction moves towards the open sea by 19 meters compared to the simulation for the existing state with a sea level corresponding to the absolute maximum. This situation undoubtedly indicates a significant improvement in the situation in the control area for the proposal of the conceptual design in relation to the current situation. If we look at the wave power values of *PI*, it is noticed that they are significantly smaller in the entire length of both control lines with a maximum of approximately 1.8x103 N/s and for the most part around zero, which is significantly less than for the existing state of the coastal belt (Figure 7.16). Also, variations of wave heights Hs in the control line show a certain decrease for the conceptual design compared to the existing state (Figure 7.15).

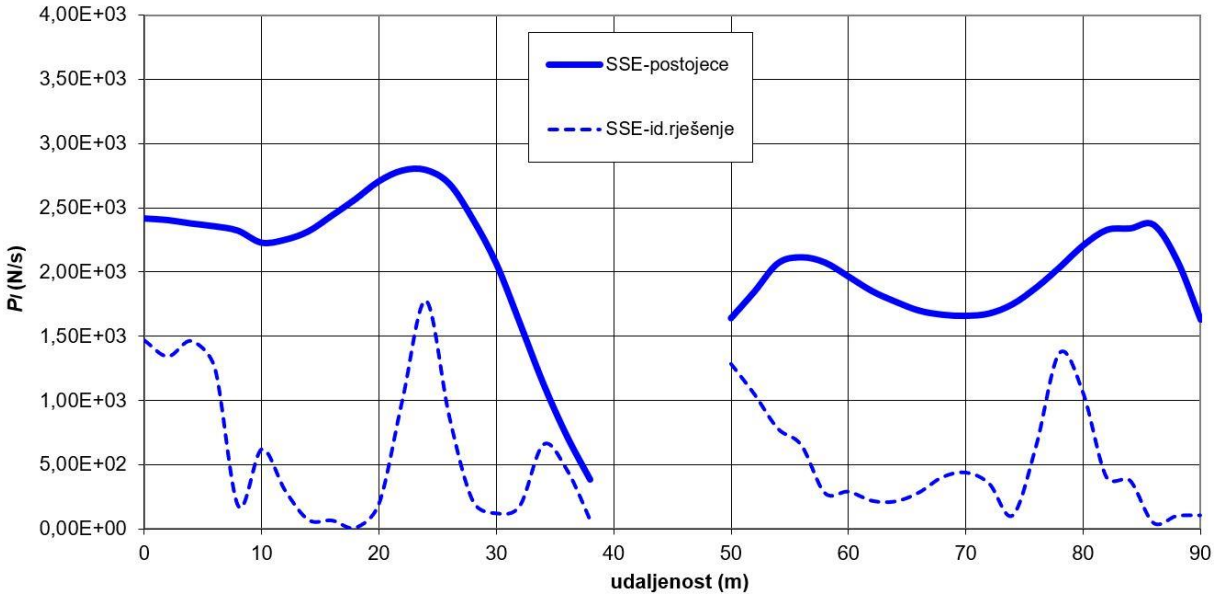

Figure 7.16 – Variation of the wave power Pl for the existing state and conceptual design in the control lines of the Podstrana beach for wave direction SE (135°)

Based on all the above, it can be concluded that the analysis procedures conducted for the control area of Podstrana beach have shown the correctness of the applied methodology, which resulted in a solution that will undoubtedly raise the level of sustainability and resilience of the coastal zone of the control area in question. The methodological approach presented in the analysis of the control area provides the basis for the adoption of quality and consistent conclusions, as a necessary and stable basis for the development of general, but also more detailed guidelines for the dimensioning and design of beaches made of granular materials, with the goal of conservation and sustainable and resilient development of the entire coastal area of Podstrana and Split-Dalmatia County.

7.1.5. Kašjuni (Split)

In accordance with table 6.1, a total of 6 numerical wave simulations (Simulations A27 to A32) were conducted for Kašjuni beach in Split, and the results of the simulations are shown in Figures 6.69 to 6.78. For further analysis and calculation of the transport potential of beach material, two control areas were selected, shown in Figures 7.17 and 7.18.

In accordance with the results of numerical modeling with wave parameters from the direction of SSW (202.5°), which are dominant for the coastal zone concerned, the results for the existing state (Figures 6.71 and 6.72) with both analyzed sea level (SRM and absolute maximum) indicate that wave breaking occurs in the immediate vicinity of the coastline, and even on the coast, which indicates an increased transport potential of beach material and beach erosion. The results of numerical simulations with a sea level corresponding to the absolute maximum show that the wave breaking zone of incident waves from this direction moves as much as 18-20 meters towards land compared to the simulation with the sea level corresponding to the middle sea level (SRM). This is evident from Figures 8.36 and 8.37, which show the positions of wave breaking zones for simulations with different sea levels.

Although it was previously emphasized that the aim of the analysis is not to provide design solutions for entire coastal zones, but to provide procedures for defining guidelines and methodologies for their implementation in a smaller area, which can then be applied on the entire coastal zone, given the size

of the beach in question, the proposal of the conceptual technical solution was given for the entire coastal area of the beach, to establish design guidelines, with a view to improving the level of sustainability and resilience of the beach in question.

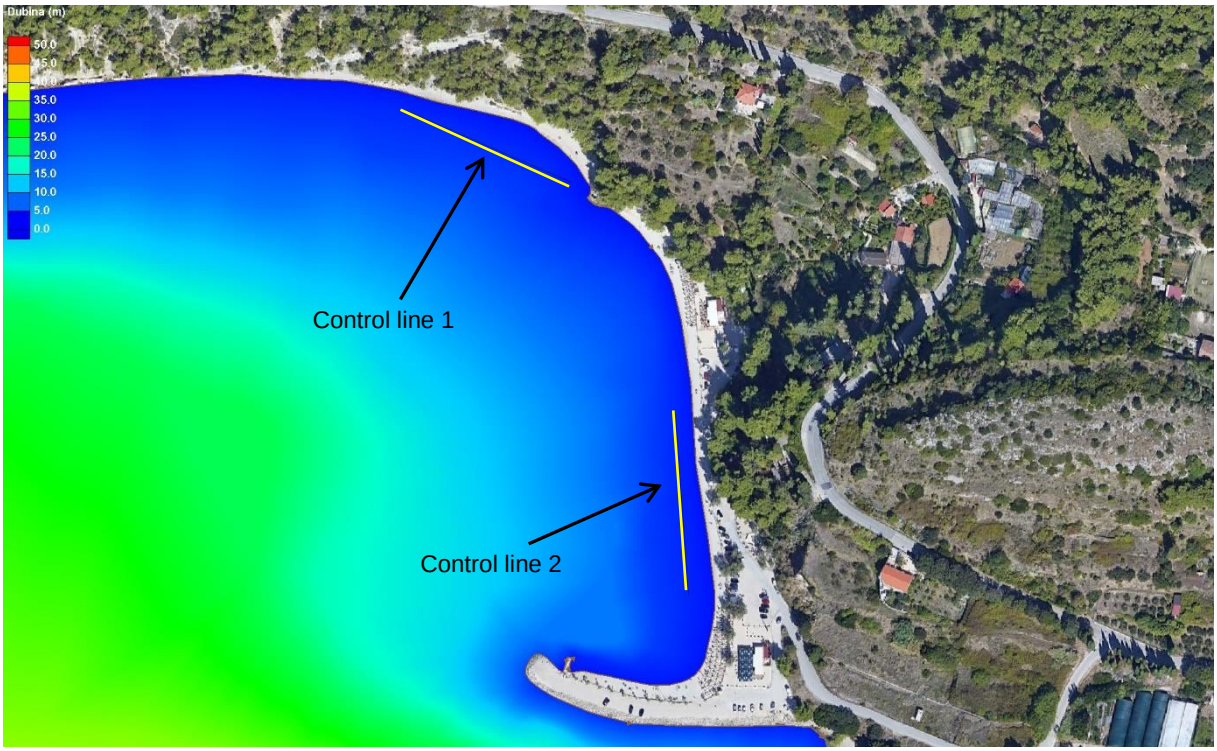

Figure 7.17 – Control area and control lines for the existing state of Kašjuni beach in Split

The results of the analysis for the current situation show that in the control area there are parts of the coast with possible problems with the transmission (adoption and removal) of beach material, and are reflected in the increased values of the wave power *PI* (Figures 7.21 and 7.21). The problem arises in both analyzed beach control lines, somewhat more pronounced for the control line 2, where the values of wave power *PI* reach approximately 7.0×10^2 N/s. This area is also the most exposed part of the actual situation on the ground, so the proposal of the conceptual solution should eliminate this problem, while considering that construction interventions do not worsen the condition of the wavefield in the considered waters.

Based on the results of numerical simulations and detected problems, a proposal for the conceptual design was made for the Kašjuni beach area in order to eliminate them, and raise the general level of sustainability and resilience of the beach. The proposal of the conceptual design is conceived using the basic construction and technical principles (more in Chapter 5), and it is about setting up an underwater stone reef at the appropriate distance and depth, and the construction of a groyne on the north side of the bay, on its western part with the addition (nourishment) of the beach with appropriate beach material. Sizing the details of all parameters of the technical solution (berm width of underwater reef, berm height, slopes, granulation of stone blocks, slope of the face of the beach, granulometric composition of beach material...) should be the subject of technical and project documentation for the realization of this project, based on the guidelines given by this study.

The ground plan disposition of the interventions made in the space and waters of the control area in question is shown in Figure 7.18. In accordance with the previously stated, the entire Kašjuni beach

represents a control area in which two control lines are set up in which the parameters are observed crucial for determining the transport potential of beach material, namely wave height *Hs* and wave power *PI*. The parameters were monitored for numerical simulations with a sea level corresponding to the absolute maximum, for the existing state and conceptual design.

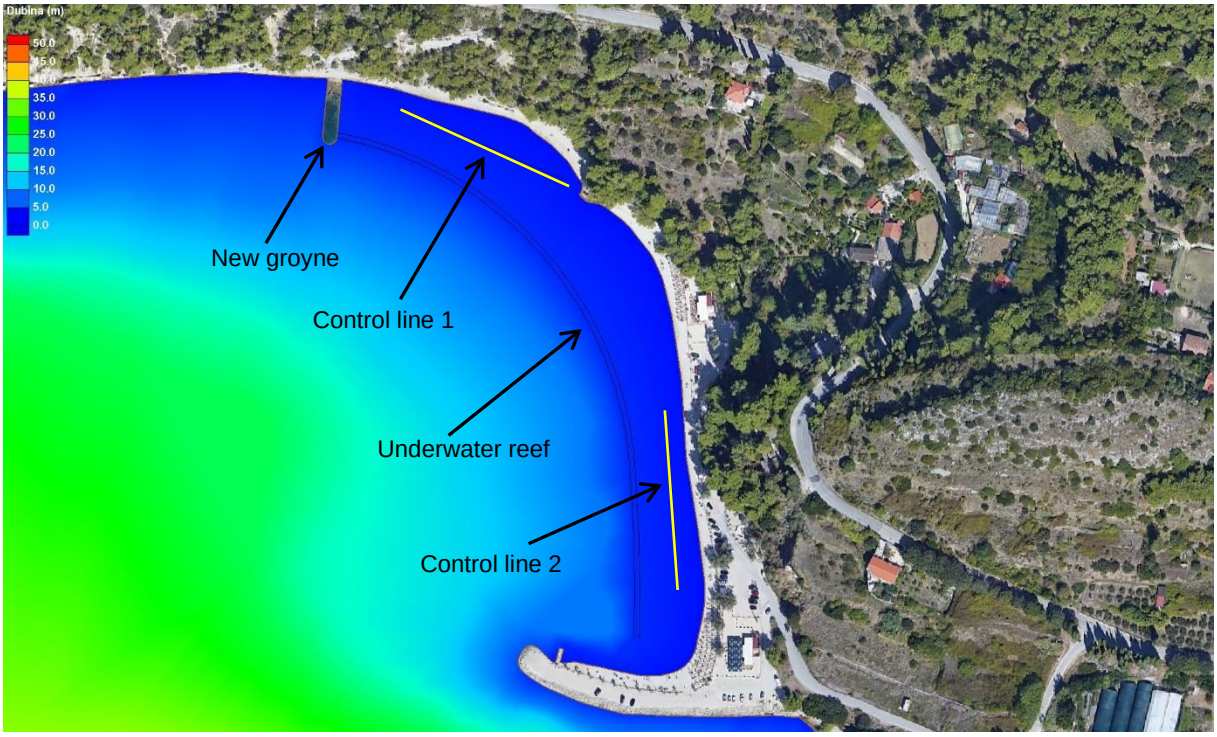

Figure 7.18 – Control area and control lines for the conceptual design of Kašjuni beach in Split

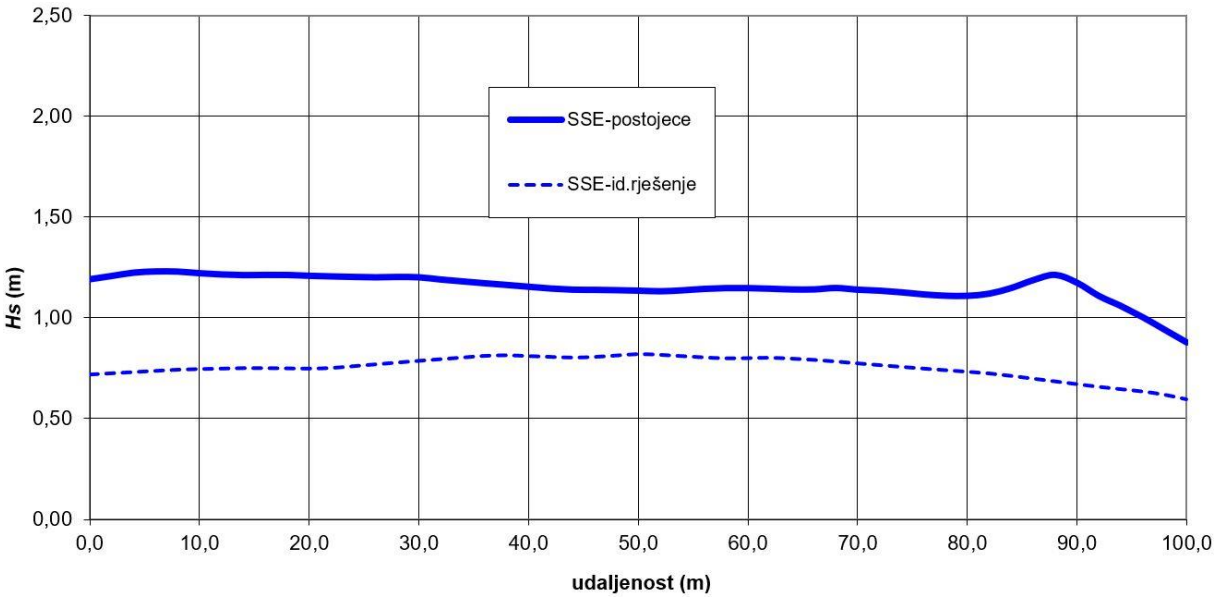

Figure 7.19 – Variation of Wave Heights *Hs* for the existing state and conceptual design in the control line 1 of Kašjuni beach in Split for wave direction SSW (202.5°)

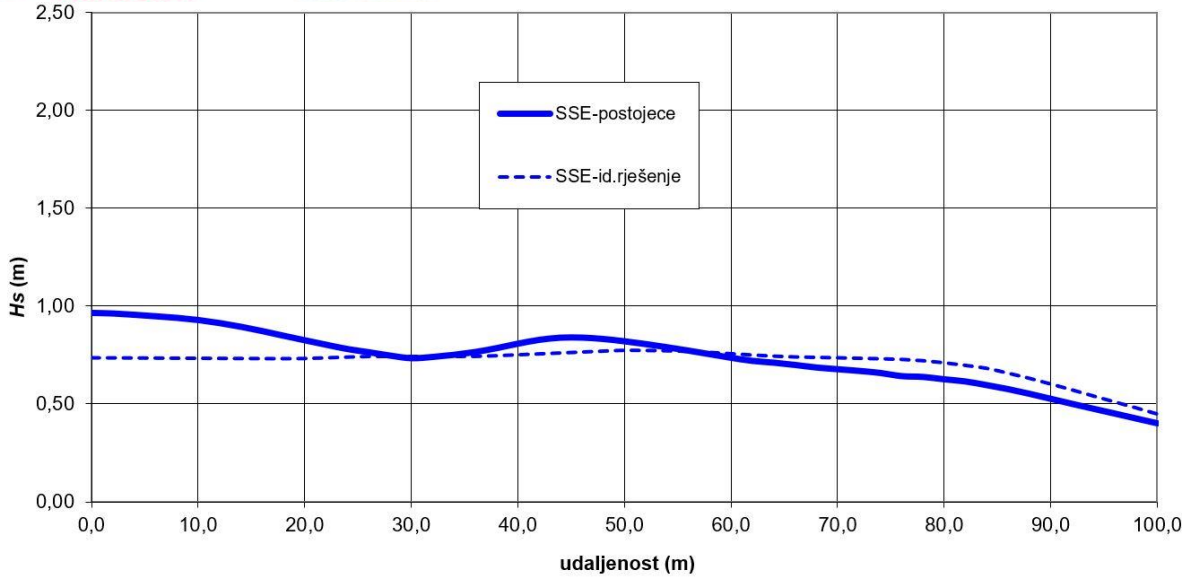

Figure 7.20 – Variation of wave heights *Hs* for the existing state and conceptual design in the control line 2 of Kašjuni beach in Split for wave direction SSW (202.5°)

The results of the numerical simulation A31 with the conceptual design of the coastal belt (with a sea level corresponding to the absolute maximum) in the control area of Kašjuni beach show a significant shift of the wave breaking zone from the incident direction SSW (202.5°) towards the open sea, i.e., at the position of the set underwater reef (Figure 6.73). This is even better seen in Figures 8.36 and 8.37, where it is observed that the wave breaking zone from this direction moves towards the open sea by 6-20 meters compared to the simulation for the existing state with a sea level corresponding to the absolute maximum. This situation undoubtedly indicates a significant improvement in the situation in the control area for the proposal of the conceptual design in relation to the existing state. If we look at the wave power values *Pl* now, it is noticed that they are significantly smaller in the entire length of both control lines with a maximum of approximately $1.8x10^2$ N/s and mostly around zero, which is significantly less than for the existing state of the coastal belt (figures 7.21 and 7.22). Also, the wave height variations of Hs in the control lines show a certain decrease for the conceptual design in the control line 1 relative to the existing state (Figure 7.19), while in the control line 2 the condition remains approximately the same compared to the existing state (figure 7.20).

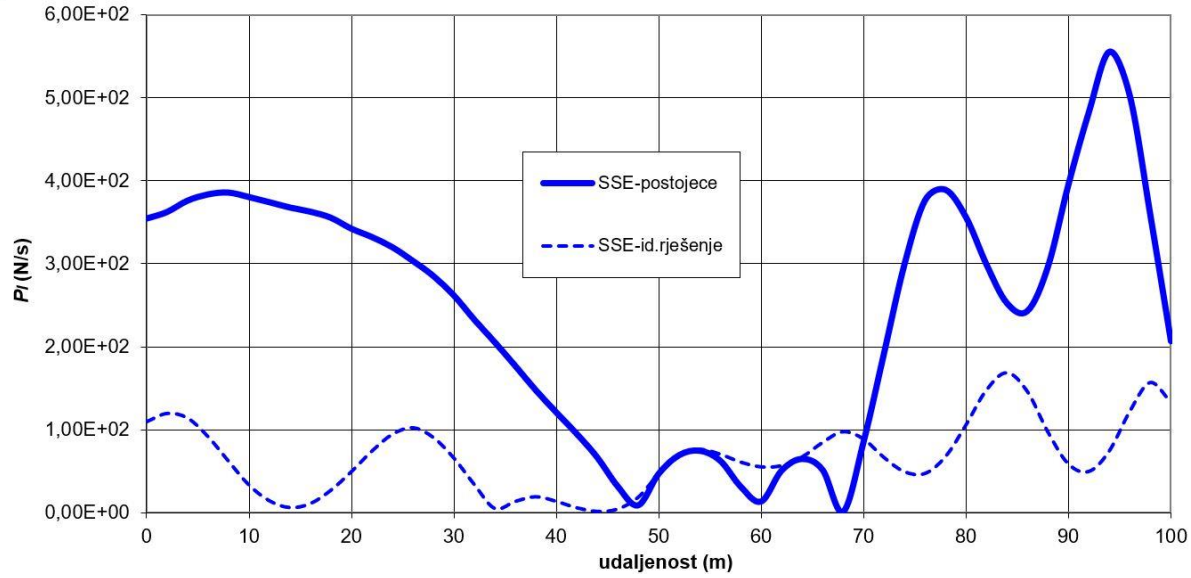

Figure 7.21 – Variation of Wave Heights *Hs* for the existing state and conceptual design in the control line 1 of Kašjuni beach in Split for wave direction SSW (202.5°)

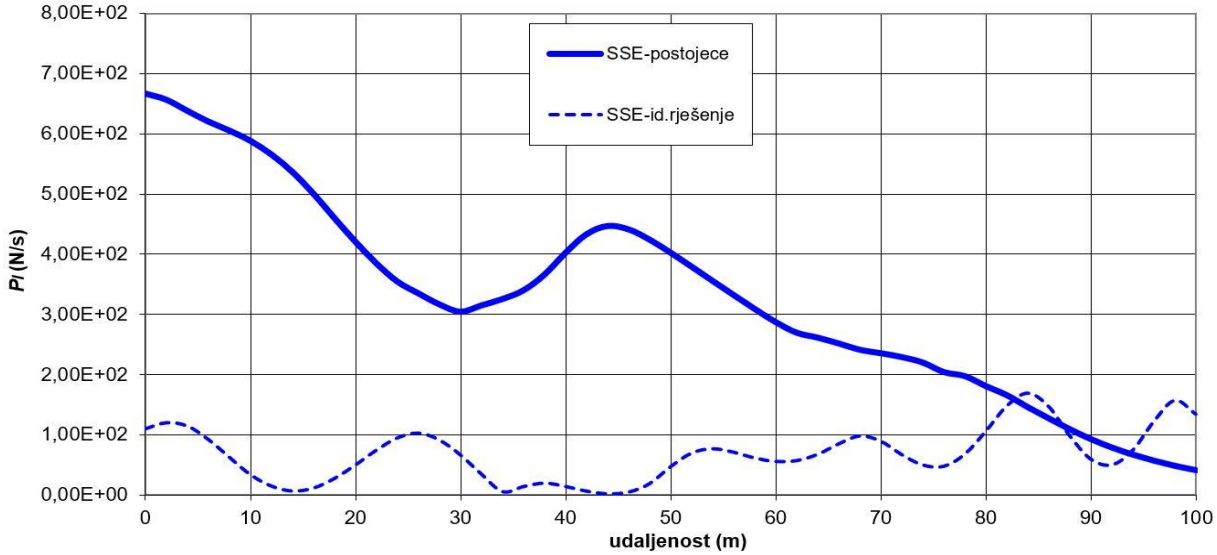

Figure 7.22 – Variation of the wave power Pl for the existing state and conceptual design in the control line 2 of Kašjuni beach in Split for wave direction SSW (202.5°)

Based on all the above, it can be concluded that the conducted analysis procedures for the Kašjuni beach area in Split showed the correctness of the applied methodology, which resulted in a solution that will undoubtedly raise the level of sustainability and resilience of the coastal zone in question. The methodological approach presented in the analysis of the control area provides the basis for the adoption of high-quality and consistent conclusions, as a necessary and stable basis for the development of general, but also more detailed guidelines for the dimensioning and design of beaches made of granular materials, with the goal of conservation and sustainable and resilient development of the coastal area of Kašjuni Beach and Split-Dalmatia County.

7.2. Calculation of stable composition of beach material

As previously explained in Chapter 5.2 of this study, in order to ensure the sustainability of beaches from granular materials, it is necessary to ensure the stability of the material from which the beach is made, i.e., to prevent the possibility of its erosion, due to complex physical processes that occur when waves meet the shore. It is primarily about the influence of the complex interaction of the processes of refraction, diffraction and wave reflection, whereby the incoming waves due to the action of the bottom develop a tendency to break precisely in the zones just before the coastline of the beach or on its coastline, causing stochastic processes due to which the driving forces that carry out the transport or transfer (transmission) of the grained material of the beach develop.

Given that this is an extremely complex process, which depends on a whole range of influential factors and differs for each separate location of the beach, without detailed numerical modeling it is not possible to fully understand this problem, nor to solve it successfully. If the parameters of waves that can occur in a certain area in a certain period are known, numerical wave simulations can be performed from which the values of the bottom orbital wave velocities of *Ud* are obtained, based on which it is possible to calculate the value of the previously mentioned driving forces of the transport of beach material. Based on this, it is possible to calculate the granulometric composition, i.e., the mean diameter of the grain D_{50} beach embankment, which will be stable for the relevant dominant wave influences at the location of the beach in question. Such a procedure was carried out for all five locations of the beaches in question, in order to show the correctness of the proposed methodology.

7.2.1. Zlatni rat (Brač)

From the results of numerical modelling of waves for sea level corresponding to middle sea level (SRM), depictions of bottom orbital wave velocities U_d for incoming waves from ese (112.5°), SSE (157.5°), SW (225°) and WSW (247.5°) are obtained, and figure 7.23 gives results only for the direction of WSW waves (247.5°) which have the greatest impact and also give the highest demersal orbital wave velocities, and are therefore authoritative for determining the stable composition of beach material.

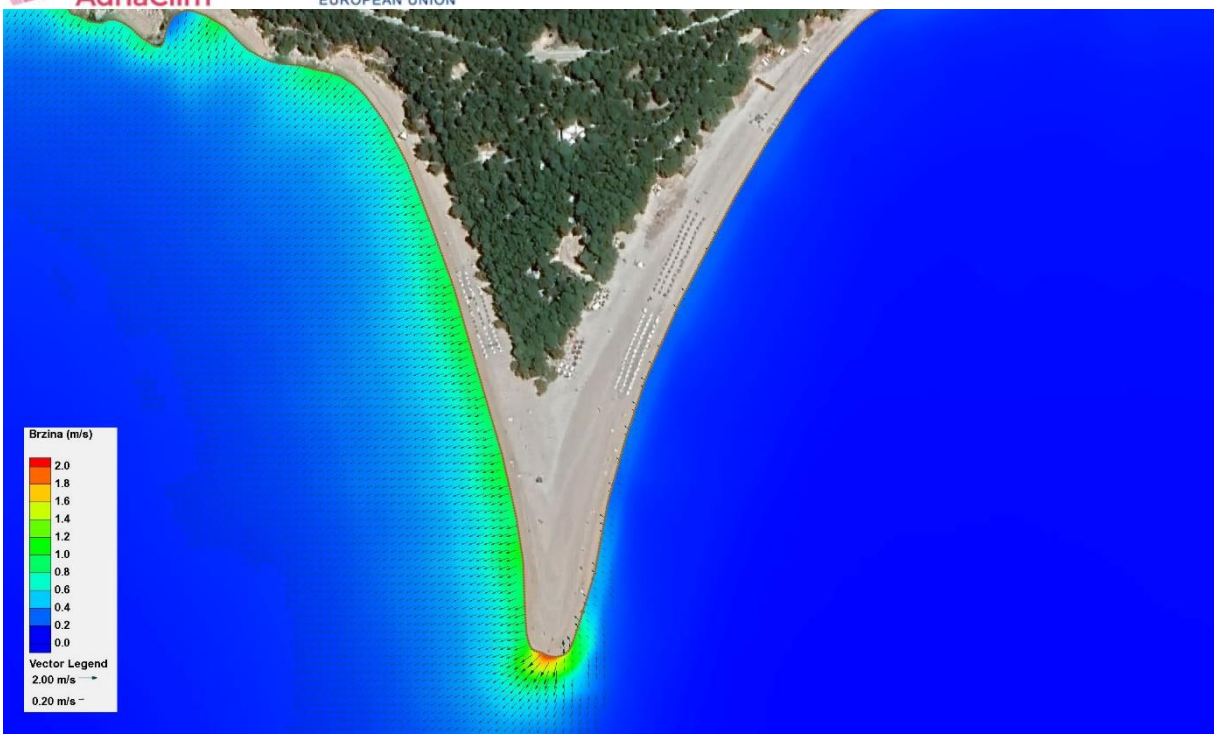

Figure 7.23 – Velocity field *ud* and vectors for simulation A4 - the existing state of Zlatni rat beach (Brač) with wave parameters from the WSW direction (247.5°) and the sea level corresponding to the middle sea level (SRM)

As explained in Chapter 5.2.3 of this study, based on the bottom orbital wave velocities *Ud*, it is possible to calculate the value of the driving forces that cause the transport of the beach material, and consequently calculate the granulometric composition, i.e., the mean diameter of the grain D_{50} the beach embankment, which will be stable for the relevant dominant wave influences at the location of the beach in question and with which the beach in question should be nourished.

The calculation of dimensionless demersal transport of beach material is made based on the results of a numerical simulation that gives the most unfavorable picture of the field of demersal orbital wave velocities, i.e., for the one that gives the highest demersal orbital velocities of ud waves. It is a numerical simulation of the A4 mark (the existing state of the Zlatni rat beach on Brač with wave parameters from the WSW direction (247.5°) and the sea level corresponding to the middle sea level - SRM). The calculation was carried out for a certain range of medium-sized D_{50} grains and detected range of bottom orbital wave velocities occurring in the subject region (Figure 7.23) based on the results of conducted numerical simulations of waves.

Table 7.1 – Calculation of dimensionless bottom transport of beach material for Zlatni rat beach (Brač)

D_{50} = 10,0 mm

u	k_s	z_0	a	f_w	τ_{ws}	θ_{ws}	u_s*	D*	θ_{cr}	$\theta_{ws} - \theta_{cr}$	Ø
(m/s)		(m)	(m)		(N/m^2)		(m/s)				
0,6	0,025	0,0008333	1,261	0,0309	5,705	0,0358	0,075	203,13	0,0553	-0,0194	bez pomaka
0,8	0,025	0,0008333	1,682	0,0266	8,734	0,0549	0,092	203,13	0,0553	-0,0004	bez pomaka
1	0,025	0,0008333	2,102	0,0237	12,151	0,0763	0,109	203,13	0,0553	0,0210	0,015564
1,2	0,025	0,0008333	2,522	0,0215	15,915	0,1000	0,124	203,13	0,0553	0,0447	0,048165
1,4	0,025	0,0008333	2,943	0,0199	19,994	0,1256	0,140	203,13	0,0553	0,0703	0,095052

D_{50} = 25,0 mm

u	k_s	z_0	a	f_w	τ_{ws}	θ_{ws}	u_s*	D*	θ_{cr}	$\theta_{ws} - \theta_{cr}$	Ø
(m/s)		(m)	(m)		(N/m^2)		(m/s)				
0,6	0,063	0,0020833	1,261	0,0497	9,188	0,0231	0,095	507,83	0,0555	-0,0324	bez pomaka
0,8	0,063	0,0020833	1,682	0,0428	14,064	0,0353	0,117	507,83	0,0555	-0,0202	bez pomaka
1	0,063	0,0020833	2,102	0,0381	19,568	0,0492	0,138	507,83	0,0555	-0,0063	bez pomaka
1,2	0,063	0,0020833	2,522	0,0347	25,629	0,0644	0,158	507,83	0,0555	0,0089	0,004282
1,4	0,063	0,0020833	2,943	0,0320	32,197	0,0809	0,177	507,83	0,0555	0,0254	0,020646

D_{50} = 40,0 mm

u	k_s	z_0	a	f_w	τ_{ws}	θ_{ws}	u_s*	D*	θ_{cr}	$\theta_{ws} - \theta_{cr}$	Ø
(m/s)		(m)	(m)		(N/m^2)		(m/s)				
0,6	0,100	0,0033333	1,261	0,0635	11,732	0,0184	0,107	812,53	0,0553	-0,0369	bez pomaka
0,8	0,100	0,0033333	1,682	0,0546	17,958	0,0282	0,132	812,53	0,0553	-0,0271	bez pomaka
1	0,100	0,0033333	2,102	0,0487	24,986	0,0392	0,156	812,53	0,0553	-0,0161	bez pomaka
1,2	0,100	0,0033333	2,522	0,0443	32,725	0,0514	0,179	812,53	0,0553	-0,0039	bez pomaka
1,4	0,100	0,0033333	2,943	0,0408	41,111	0,0646	0,200	812,53	0,0553	0,0092	0,004534

D_{50} = 55,0 mm

u	k_s	z_0	a	f_w	τ_{ws}	θ_{ws}	u_s*	D*	θ_{cr}	$\theta_{ws} - \theta_{cr}$	Ø
(m/s)		(m)	(m)		(N/m^2)		(m/s)				
0,6	0,138	0,0045833	1,261	0,0749	13,844	0,0158	0,116	1117,23	0,0552	-0,0394	bez pomaka
0,8	0,138	0,0045833	1,682	0,0645	21,193	0,0242	0,144	1117,23	0,0552	-0,0310	bez pomaka
1	0,138	0,0045833	2,102	0,0574	29,486	0,0337	0,169	1117,23	0,0552	-0,0216	bez pomaka
1,2	0,138	0,0045833	2,522	0,0522	38,619	0,0441	0,194	1117,23	0,0552	-0,0111	bez pomaka
1,4	0,138	0,0045833	2,943	0,0482	48,515	0,0554	0,217	1117,23	0,0552	0,0002	0,000012

D_{50} = 70,0 mm

u	k_s	z_0	a	f_w	τ_{ws}	θ_{ws}	u_s*	D*	θ_{cr}	$\theta_{ws} - \theta_{cr}$	Ø
(m/s)		(m)	(m)		(N/m^2)		(m/s)				
0,6	0,175	0,0058333	1,261	0,0849	15,694	0,0141	0,124	1421,93	0,0552	-0,0411	bez pomaka
0,8	0,175	0,0058333	1,682	0,0731	24,024	0,0216	0,153	1421,93	0,0552	-0,0336	bez pomaka
1	0,175	0,0058333	2,102	0,0651	33,425	0,0300	0,180	1421,93	0,0552	-0,0252	bez pomaka
1,2	0,175	0,0058333	2,522	0,0592	43,778	0,0393	0,206	1421,93	0,0552	-0,0159	bez pomaka
1,4	0,175	0,0058333	2,943	0,0546	54,997	0,0493	0,231	1421,93	0,0552	-0,0058	bez pomaka

Range of demersal orbital velocities u_d: **0,6 – 1,4** m/s

Medium grain size range D_{50}: **10 – 70** mm

ρ_s = 2650 kg/m^3

ρ = 1027 kg/m^3

T = 6,60 s

v = 1,36E-06 m^2/s

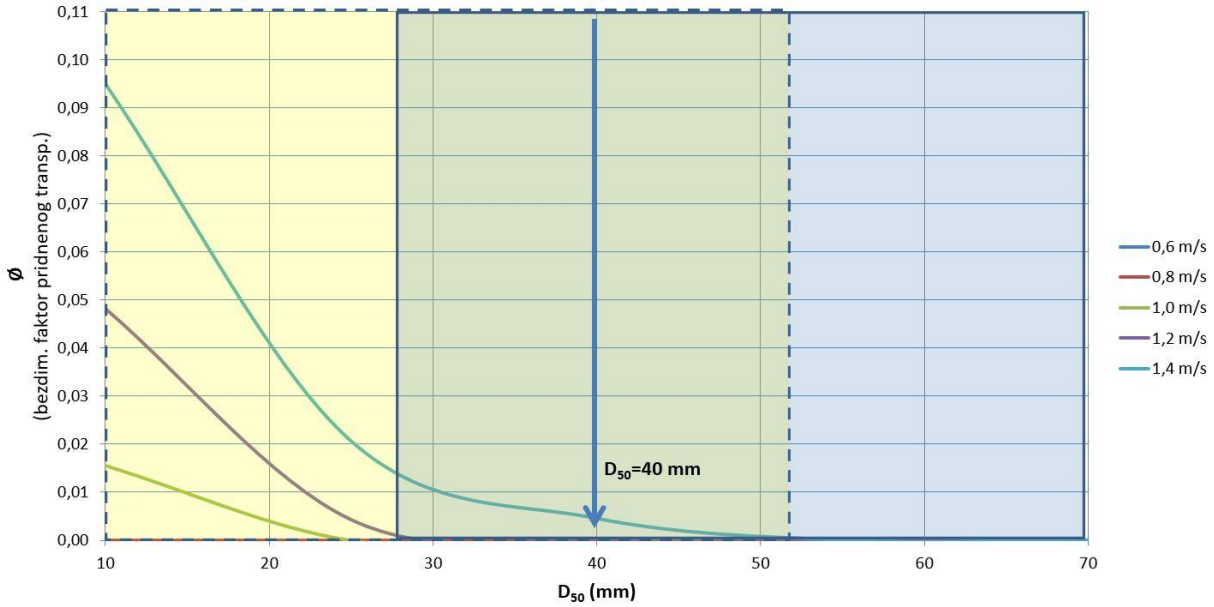

Figure 7.24 – diagram for calculating the size of medium grain beach material *D50* for Zlatni rat beach (Brač)

In accordance with the implemented calculation, according to Table 7.1, for the lower orbital velocity range *of limbs of* 0.6 – 1.4 m/s and the medium grain *size Range* D_{50} of 10 – 70 mm, **the stable composition of beach material for Zlatni rat beach on Brač can be defined as rock material medium grain *size* D_{50} = 40 mm, with a range of 28 – 52 mm**, as seen from the diagram in Figure 7.24.

7.2.2. Stiniva (Vis)

From the results of numerical modelling of waves for sea level corresponding to the middle sea level (SRM), an overview of the field of bottom orbital wave velocities u_d for incident waves from the direction of SE (135°) was obtained - Figure 7.25. As explained in Chapter 5.2.3 of this study, based on the bottom orbital wave velocities *Ud*, it is possible to calculate the value of the driving forces that cause the transport of the beach material, and consequently and budgetarily determine the granulometric composition, i.e., the mean diameter of the grain D_{50} beach embankment, which will be stable for the relevant dominant wave influences at the location of the beach in question.

Given the extremely low resulting demersal orbital wave velocities for incoming waves from the analyzed direction, which are less than 0.1 m/s, the calculation of determining the stable composition of the beach material does not make sense, because it would lead to the definition of fine material. As the beach is under extremely little influence of the incident waves, in terms of bottom orbital wave velocities, it can be concluded that the existing beach material is not in danger of transmission (transmission) due to the action of waves, so further calculation has not been carried out, and the determination of the material with which the potential nourishment of the beach will be carried out, was determined on the basis of the existing granulometric composition of the beach (chapter 4).

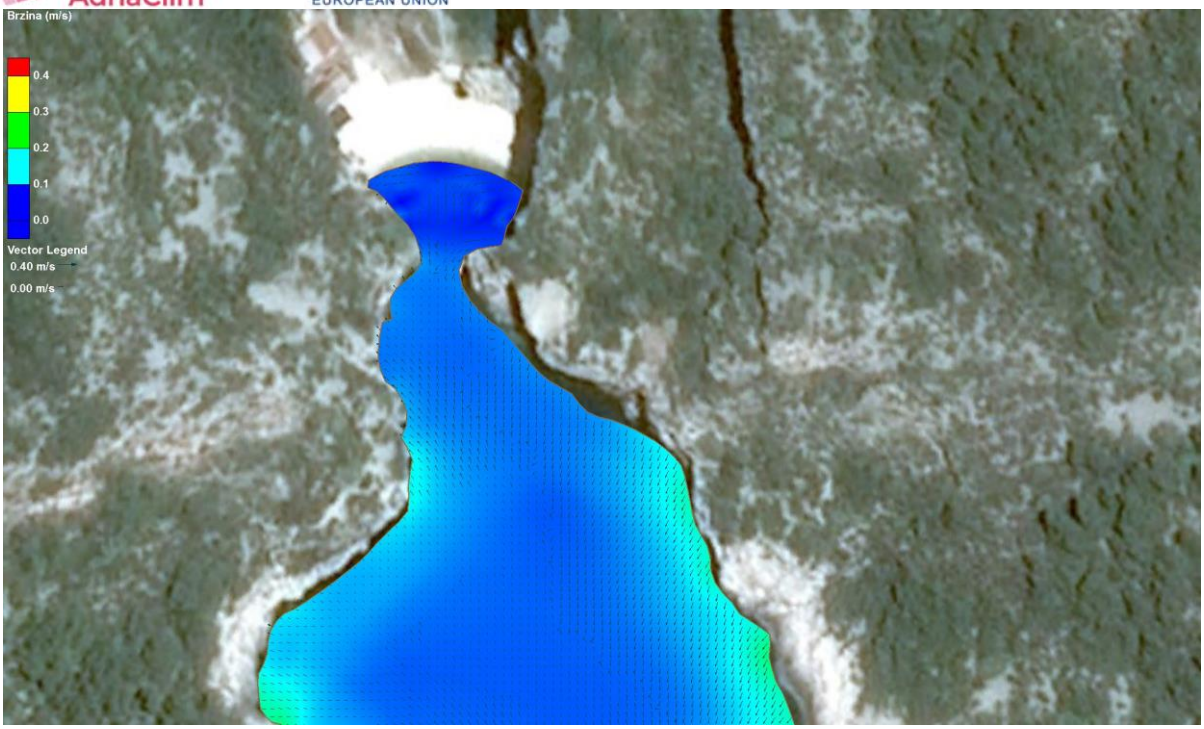

Figure 7.25 – Velocity field *Ud* i vectors for simulation A9 - the existing state of the beach Stiniva (Vis) with wave parameters from the direction of se (135°) and the sea level corresponding to the middle sea level (SRM)

7.2.3. Podgora (Makarska Riviera)

From the results of numerical modelling of waves for sea level corresponding to the middle sea level (SRM), depictions of the bottom orbital wave velocities for incident waves Ud from the directions SSE (157.5°), SW (225°) and W (270°) are obtained, and in Figure 7.26 the results are given only for the direction of waves W (270°) which have the greatest impact and at the same time give the highest demersal orbital wave velocities, and are therefore authoritative for determining the stable composition of beach material.

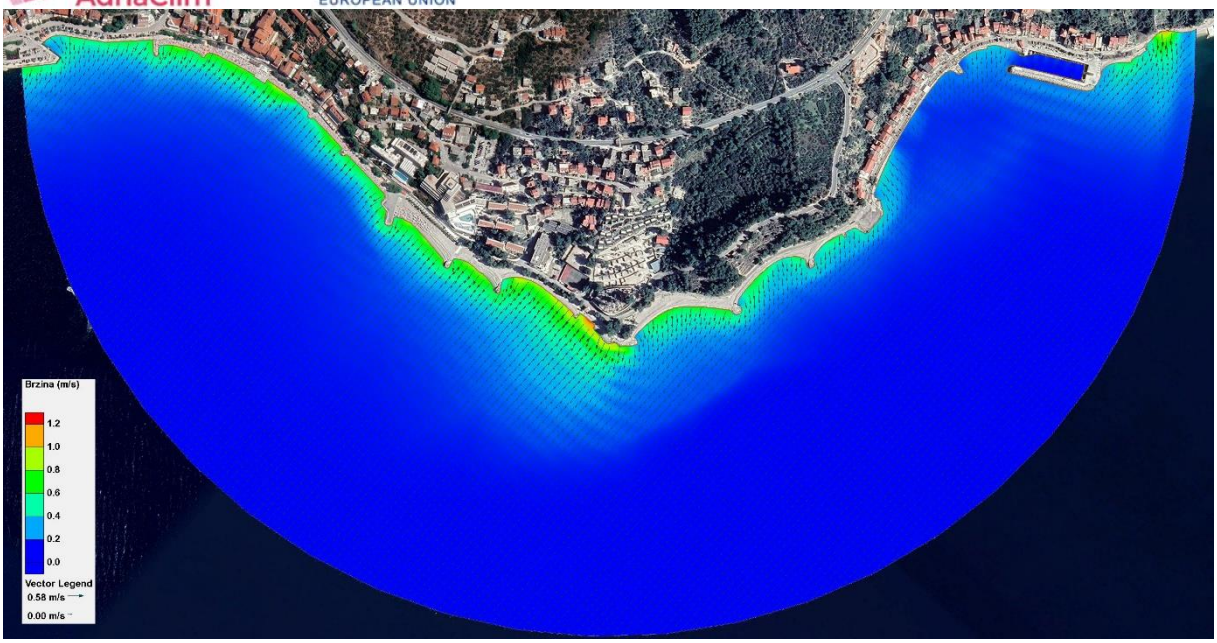

Figure 7.26 – Velocity field *Ud* and simulation vectors A13 - existing state of Podgora beach (Makarska Riviera) with wave parameters from direction W (270°) and sea level corresponding to middle sea level (SRM)

As explained in Chapter 5.2.3 of this study, based on the bottom orbital wave velocities Ud, it is possible to calculate the value of the driving forces that cause the transport or transfer (transmission) of the beach material, and consequently calculate the granulometric composition, i.e., the mean diameter of the grain $D5_0$ beach embankment, which will be stable for the relevant dominant wave influences at the location of the beach in question.

The calculation of dimensionless demersal transport of beach material is made based on the results of a numerical simulation that gives the most unfavorable picture of the field of demersal orbital wave velocities, i.e., for the one that gives the highest demersal orbital velocities. It is a numerical simulation of the a13 mark (the existing state of the Beach Podgora on the Makarska Riviera with wave parameters from the direction W (270°) and the sea level corresponding to the middle sea level -SRM). The calculation was carried out for a certain range of medium-sized D_{50} grains and detected range of demersal orbital wave velocities occurring in the subject region (Figure 7.26) based on the results of conducted numerical simulations of the waves.

Table 7.2 – Calculation of dimensionless bottom transport of beach material for Beach Podgora (Makarska Riviera)

D_{50} = 10,0 mm

u	k_s	z_0	a	f_w	τ_{ws}	θ_{ws}	u_s*	D*	θ_{cr}	$\theta_{ws} - \theta_{cr}$	Ø
(m/s)		(m)	(m)		(N/m^2)		(m/s)				
0,4	0,025	0,0008333	0,764	0,0400	3,284	0,0227	0,057	196,89	0,0552	-0,0325	bez pomaka
0,6	0,025	0,0008333	1,146	0,0324	5,984	0,0414	0,076	196,89	0,0552	-0,0138	bez pomaka
0,8	0,025	0,0008333	1,529	0,0279	9,160	0,0633	0,095	196,89	0,0552	0,0081	0,003724
1	0,025	0,0008333	1,911	0,0249	12,744	0,0881	0,112	196,89	0,0552	0,0329	0,030406
1,2	0,025	0,0008333	2,293	0,0226	16,691	0,1154	0,128	196,89	0,0552	0,0602	0,075254

D_{50} = 15,0 mm

u	k_s	z_0	a	f_w	τ_{ws}	θ_{ws}	u_s*	D*	θ_{cr}	$\theta_{ws} - \theta_{cr}$	Ø
(m/s)		(m)	(m)		(N/m^2)		(m/s)				
0,4	0,038	0,0012500	0,764	0,0494	4,054	0,0187	0,063	295,33	0,0557	-0,0370	bez pomaka
0,6	0,038	0,0012500	1,146	0,0400	7,388	0,0340	0,085	295,33	0,0557	-0,0217	bez pomaka
0,8	0,038	0,0012500	1,529	0,0345	11,309	0,0521	0,105	295,33	0,0557	-0,0036	bez pomaka
1	0,038	0,0012500	1,911	0,0307	15,735	0,0725	0,124	295,33	0,0557	0,0168	0,011107
1,2	0,038	0,0012500	2,293	0,0279	20,609	0,0950	0,142	295,33	0,0557	0,0393	0,039669

D_{50} = 20,0 mm

u	k_s	z_0	a	f_w	τ_{ws}	θ_{ws}	u_s*	D*	θ_{cr}	$\theta_{ws} - \theta_{cr}$	Ø
(m/s)		(m)	(m)		(N/m^2)		(m/s)				
0,4	0,050	0,0016667	0,764	0,0574	4,709	0,0163	0,068	393,78	0,0556	-0,0393	bez pomaka
0,6	0,050	0,0016667	1,146	0,0465	8,580	0,0296	0,091	393,78	0,0556	-0,0260	bez pomaka
0,8	0,050	0,0016667	1,529	0,0400	13,134	0,0454	0,113	393,78	0,0556	-0,0102	bez pomaka
1	0,050	0,0016667	1,911	0,0357	18,274	0,0631	0,134	393,78	0,0556	0,0075	0,003334
1,2	0,050	0,0016667	2,293	0,0324	23,934	0,0827	0,153	393,78	0,0556	0,0271	0,022743

D_{50} = 30,0 mm

u	k_s	z_0	a	f_w	τ_{ws}	θ_{ws}	u_s*	D*	θ_{cr}	$\theta_{ws} - \theta_{cr}$	Ø
(m/s)		(m)	(m)		(N/m^2)		(m/s)				
0,4	0,075	0,0025000	0,764	0,0709	5,814	0,0134	0,075	590,66	0,0554	-0,0420	bez pomaka
0,6	0,075	0,0025000	1,146	0,0574	10,594	0,0244	0,102	590,66	0,0554	-0,0310	bez pomaka
0,8	0,075	0,0025000	1,529	0,0494	16,217	0,0374	0,126	590,66	0,0554	-0,0181	bez pomaka
1	0,075	0,0025000	1,911	0,0440	22,563	0,0520	0,148	590,66	0,0554	-0,0034	bez pomaka
1,2	0,075	0,0025000	2,293	0,0400	29,552	0,0681	0,170	590,66	0,0554	0,0127	0,007261

D_{50} = 35,0 mm

u	k_s	z_0	a	f_w	τ_{ws}	θ_{ws}	u_s*	D*	θ_{cr}	$\theta_{ws} - \theta_{cr}$	Ø
(m/s)		(m)	(m)		(N/m^2)		(m/s)				
0,4	0,088	0,0029167	0,764	0,0768	6,299	0,0124	0,078	689,11	0,0554	-0,0429	bez pomaka
0,6	0,088	0,0029167	1,146	0,0622	11,478	0,0227	0,106	689,11	0,0554	-0,0327	bez pomaka
0,8	0,088	0,0029167	1,529	0,0536	17,571	0,0347	0,131	689,11	0,0554	-0,0207	bez pomaka
1	0,088	0,0029167	1,911	0,0477	24,446	0,0483	0,154	689,11	0,0554	-0,0071	bez pomaka
1,2	0,088	0,0029167	2,293	0,0434	32,019	0,0632	0,177	689,11	0,0554	0,0079	0,003554

D_{50} = 50,0 mm

u	k_s	z_0	a	f_w	τ_{ws}	θ_{ws}	u_s*	D*	θ_{cr}	$\theta_{ws} - \theta_{cr}$	Ø
(m/s)		(m)	(m)		(N/m^2)		(m/s)				
0,4	0,125	0,0041667	0,764	0,0925	7,582	0,0105	0,086	984,44	0,0553	-0,0448	bez pomaka
0,6	0,125	0,0041667	1,146	0,0749	13,817	0,0191	0,116	984,44	0,0553	-0,0362	bez pomaka
0,8	0,125	0,0041667	1,529	0,0645	21,151	0,0292	0,144	984,44	0,0553	-0,0260	bez pomaka
1	0,125	0,0041667	1,911	0,0574	29,428	0,0407	0,169	984,44	0,0553	-0,0146	bez pomaka
1,2	0,125	0,0041667	2,293	0,0522	38,544	0,0533	0,194	984,44	0,0553	-0,0020	bez pomaka

Range of demersal orbital velocities u_d: **0,4 – 1,2** m/s

Medium grain size range D_{50}: **10 – 50** mm

ρ_s = 2500 kg/m^3

ρ = 1025 kg/m^3

T = 6,00 s

ν = 1,36E-06 m^2/s

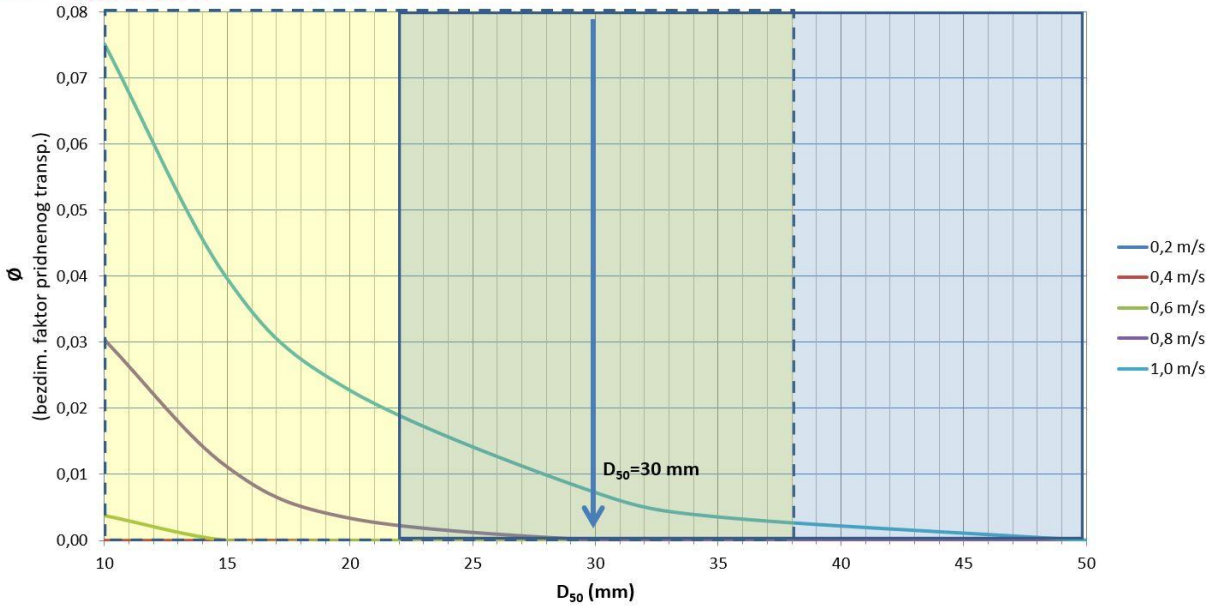

Figure 7.27 – diagram for calculating the size of medium grain beach material D_{50} for Podgora beach (Makarska Riviera)

In accordance with the implemented calculation, according to Table 7.2, for the bottom orbital velocity range *Ud* 0.4 – 1.2 m/s and the D_{50} medium grain size range of 10 – 50 mm, **the stable composition of the beach material Podgora on the Makarska Riviera can be defined as a rock material of medium grain size D_{50} = 30 mm, with a range of 22 – 38 mm**, as seen from the diagram in Figure 7.27.

7.2.4. Podstrana-Duće area

From the results of numerical modelling of waves for sea level corresponding to the middle sea level (SRM), depictions of the bottom orbital wave velocities *Ud* for incident waves from the directions SE (135°), SSW (202.5°) and W (270°) are obtained, and in Figure 7.28 the results are given only for the direction of waves SSW (202.5°) which has the greatest impact and also gives the highest demersal orbital wave velocities, and are therefore authoritative for determining the stable composition of beach material.

As explained in the introduction to Chapter 5.2.3 of this study, based on the bottom orbital wave velocities Ud, it is possible to calculate the value of the driving forces that cause the transport of the beach material, and consequently and budgetarily determine the granulometric composition, i.e., the mean diameter of the grain D_{50} beach embankment, which will be stable for the relevant dominant wave influences at the location of the beach in question.

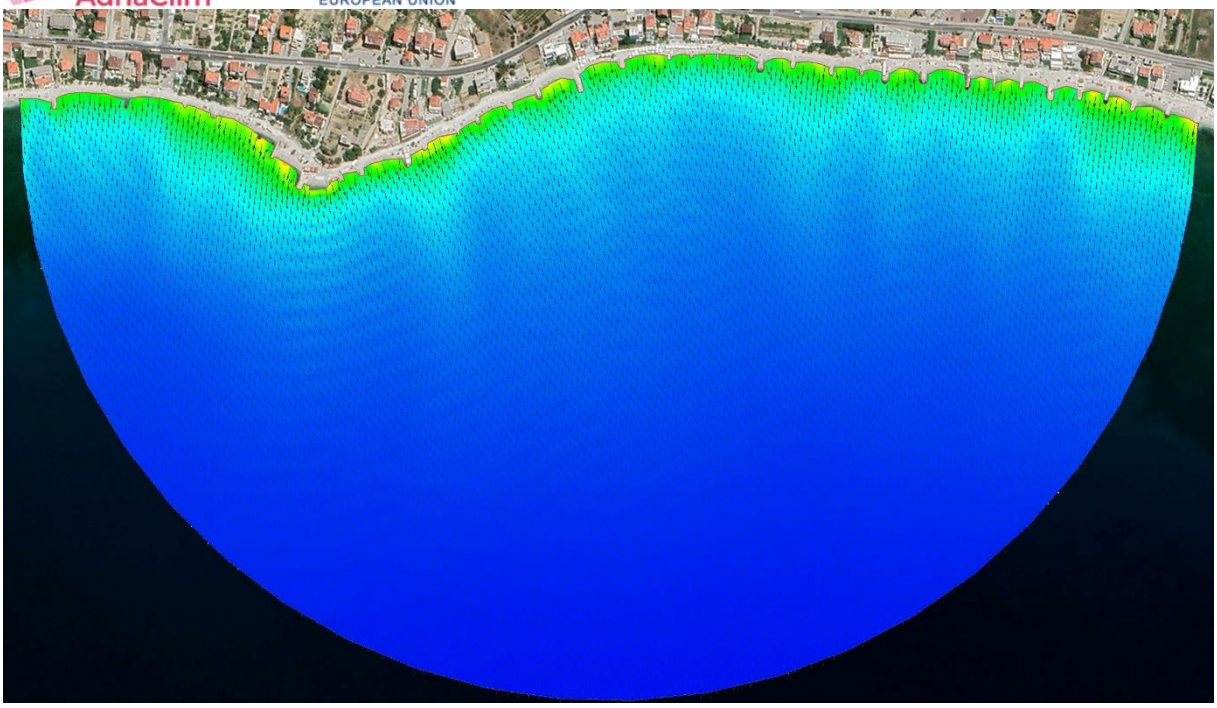

Slika 7.28 – Field velocity *Ud* and vectors for simulation A20 - the existing state condition of the beaches on the Podstrana-Duće area with wave parameters from the direction of SSW (202.5°) and the sea level corresponding to the middle sea level (SRM)

The calculation of dimensionless demersal transport of beach material is made based on the results of a numerical simulation that gives the most unfavorable picture of the field of demersal orbital wave velocities, i.e., for the one that gives the highest demersal orbital velocities of limb waves. It is a numerical simulation of the A20 mark (the existing state of the beaches on the Podstrana-Duće area with wave parameters from the direction W (270°) and the sea level corresponding to the middle sea level -SRM). The calculation was carried out for a certain range of medium grain size D_{50} and detected range of demersal orbital velocities of waves occurring in the subject area (Figure 7.28) based on the results of conducted numerical simulations of waves.

Range of demersal orbital velocities u_d: **0,4 – 1,2** m/s
Medium grain size range D_{50}: **10 – 50** mm

ρ_s = 2500 kg/m^3
ρ = 1025 kg/m^3
T = 5,80 s
v = 1,36E-06 m^2/s

Table 7.3 – Calculation of dimensionless bottom transport of beach material for beaches on the Podstrana-Duće area

D_{50} = 10,0 mm

u	k_s	z_0	a	f_w	τ_{ws}	θ_{ws}	u_s*	D*	θ_{cr}	$\theta_{ws} - \theta_{cr}$	Ø
(m/s)		(m)	(m)		(N/m^2)		(m/s)				
0,4	0,025	0,0008333	0,739	0,0408	3,342	0,0231	0,057	196,89	0,0552	-0,0321	bez pomaka
0,6	0,025	0,0008333	1,108	0,0330	6,090	0,0421	0,077	196,89	0,0552	-0,0131	bez pomaka
0,8	0,025	0,0008333	1,478	0,0284	9,322	0,0644	0,095	196,89	0,0552	0,0092	0,004526
1	0,025	0,0008333	1,847	0,0253	12,970	0,0896	0,112	196,89	0,0552	0,0344	0,032605
1,2	0,025	0,0008333	2,217	0,0230	16,988	0,1174	0,129	196,89	0,0552	0,0622	0,079136

D_{50} = 15,0 mm

u	k_s	z_0	a	f_w	τ_{ws}	θ_{ws}	u_s*	D*	θ_{cr}	$\theta_{ws} - \theta_{cr}$	Ø
(m/s)		(m)	(m)		(N/m^2)		(m/s)				
0,4	0,038	0,0012500	0,739	0,0503	4,126	0,0190	0,063	295,33	0,0557	-0,0367	bez pomaka
0,6	0,038	0,0012500	1,108	0,0408	7,519	0,0346	0,086	295,33	0,0557	-0,0210	bez pomaka
0,8	0,038	0,0012500	1,478	0,0351	11,511	0,0530	0,106	295,33	0,0557	-0,0027	bez pomaka
1	0,038	0,0012500	1,847	0,0312	16,015	0,0738	0,125	295,33	0,0557	0,0181	0,012410
1,2	0,038	0,0012500	2,217	0,0284	20,975	0,0966	0,143	295,33	0,0557	0,0409	0,042256

D_{50} = 20,0 mm

u	k_s	z_0	a	f_w	τ_{ws}	θ_{ws}	u_s*	D*	θ_{cr}	$\theta_{ws} - \theta_{cr}$	Ø
(m/s)		(m)	(m)		(N/m^2)		(m/s)				
0,4	0,050	0,0016667	0,739	0,0584	4,792	0,0166	0,068	393,78	0,0556	-0,0391	bez pomaka
0,6	0,050	0,0016667	1,108	0,0473	8,733	0,0302	0,092	393,78	0,0556	-0,0254	bez pomaka
0,8	0,050	0,0016667	1,478	0,0408	13,368	0,0462	0,114	393,78	0,0556	-0,0094	bez pomaka
1	0,050	0,0016667	1,847	0,0363	18,599	0,0643	0,135	393,78	0,0556	0,0087	0,004107
1,2	0,050	0,0016667	2,217	0,0330	24,360	0,0842	0,154	393,78	0,0556	0,0286	0,024620

D_{50} = 30,0 mm

u	k_s	z_0	a	f_w	τ_{ws}	θ_{ws}	u_s*	D*	θ_{cr}	$\theta_{ws} - \theta_{cr}$	Ø
(m/s)		(m)	(m)		(N/m^2)		(m/s)				
0,4	0,075	0,0025000	0,739	0,0722	5,917	0,0136	0,076	590,66	0,0554	-0,0418	bez pomaka
0,6	0,075	0,0025000	1,108	0,0584	10,783	0,0248	0,103	590,66	0,0554	-0,0306	bez pomaka
0,8	0,075	0,0025000	1,478	0,0503	16,506	0,0380	0,127	590,66	0,0554	-0,0174	bez pomaka
1	0,075	0,0025000	1,847	0,0448	22,965	0,0529	0,150	590,66	0,0554	-0,0025	bez pomaka
1,2	0,075	0,0025000	2,217	0,0408	30,078	0,0693	0,171	590,66	0,0554	0,0139	0,008328

D_{50} = 35,0 mm

u	k_s	z_0	a	f_w	τ_{ws}	θ_{ws}	u_s*	D*	θ_{cr}	$\theta_{ws} - \theta_{cr}$	Ø
(m/s)		(m)	(m)		(N/m^2)		(m/s)				
0,4	0,088	0,0029167	0,739	0,0782	6,411	0,0127	0,079	689,11	0,0554	-0,0427	bez pomaka
0,6	0,088	0,0029167	1,108	0,0633	11,682	0,0231	0,107	689,11	0,0554	-0,0323	bez pomaka
0,8	0,088	0,0029167	1,478	0,0545	17,883	0,0353	0,132	689,11	0,0554	-0,0201	bez pomaka
1	0,088	0,0029167	1,847	0,0485	24,881	0,0491	0,156	689,11	0,0554	-0,0062	bez pomaka
1,2	0,088	0,0029167	2,217	0,0442	32,588	0,0643	0,178	689,11	0,0554	0,0090	0,004344

D_{50} = 50,0 mm

u	k_s	z_0	a	f_w	τ_{ws}	θ_{ws}	u_s*	D*	θ_{cr}	$\theta_{ws} - \theta_{cr}$	Ø
(m/s)		(m)	(m)		(N/m^2)		(m/s)				
0,4	0,125	0,0041667	0,739	0,0941	7,717	0,0107	0,087	984,44	0,0553	-0,0446	bez pomaka
0,6	0,125	0,0041667	1,108	0,0762	14,063	0,0194	0,117	984,44	0,0553	-0,0358	bez pomaka
0,8	0,125	0,0041667	1,478	0,0656	21,527	0,0298	0,145	984,44	0,0553	-0,0255	bez pomaka
1	0,125	0,0041667	1,847	0,0584	29,952	0,0414	0,171	984,44	0,0553	-0,0139	bez pomaka
1,2	0,125	0,0041667	2,217	0,0532	39,229	0,0542	0,196	984,44	0,0553	-0,0010	bez pomaka

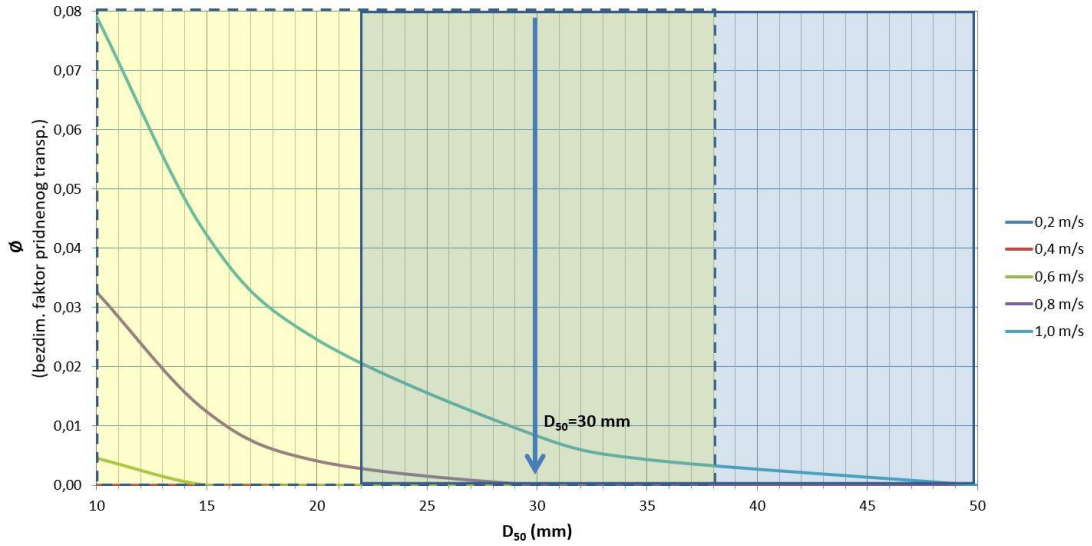

Figure 7.29 – diagram for calculating the size of medium grain beach material *D50* for beaches on the Podstrana-Duće area

In accordance with the budget carried out, according to Table 7.3, for the bottom orbital velocity range *Ud* 0.4 – 1.2 m/s and a medium grain size range D_{50} of 10 – 50 mm, **the stable composition of the beach material Podstrana can be defined as medium grain rock material D_{50} = 30 mm, with a range of 22 – 38 mm**, as is evident from the diagram in Figure 7.29.

7.2.5. Kašjuni (Split)

From the results of numerical modelling of waves for sea level corresponding to the middle sea level (SRM), representations of the bottom orbital wave velocities *Ud* for incident waves from the directions SSW (202.5°) and W (270°) are obtained, and in Figure 7.30 the results are given only for the direction of waves SSW (202.5°) which has the greatest impact and also gives the highest demersal orbital wave velocities, and are therefore authoritative for determining the stable composition of beach material.

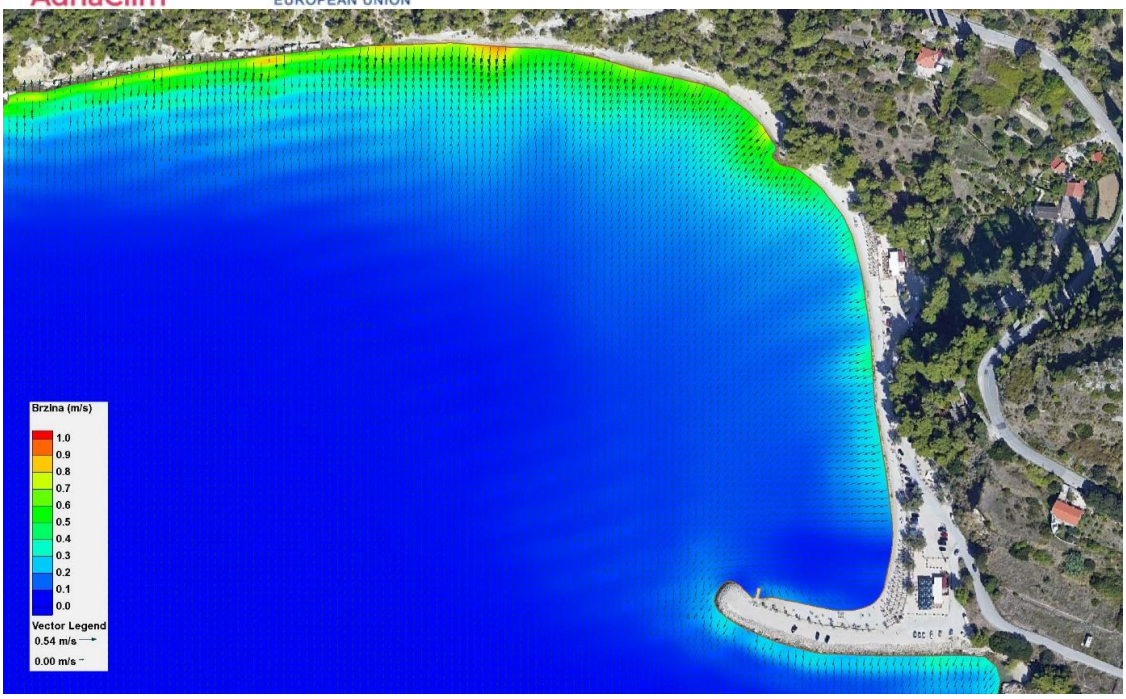

Figure 7.30 – Field velocity *Ud* and vectors for simulation A27 - the existing state of Kašjuni beach in Split with wave parameters for direction of SSW (202.5°) and the sea level corresponding to the middle sea level (SRM)

As explained in the introduction to Chapter 5.2.3 of this study, based on the bottom orbital wave velocities Ud, it is possible to calculate the value of the driving forces that cause the transport of the beach material, and consequently and budgetarily determine the granulometric composition, i.e., the mean diameter of the grain D_{50} beach embankment, which will be stable for the relevant dominant wave influences at the location of the beach in question.

The calculation of dimensionless demersal transport of beach material is made based on the results of a numerical simulation that gives the most unfavorable picture of the field of demersal orbital wave velocities, i.e., for the one that gives the highest demersal orbital velocities of limb waves. It is a numerical simulation of the A27 mark (the existing state of Kašjuni beach in Split with wave parameters from the direction of SSW (202.5°) and the sea level corresponding to the middle sea level -SRM). The calculation was carried out for a certain range of medium grain *D50* grain and detected range of demersal orbital wave velocities occurring in the subject area (Figure 7.30) based on the results of conducted numerical simulations of waves.

Table 7.4 – Calculation of dimensionless bottom transport of beach material for Kašjuni beach (Split)

D_{50} = 10,0 mm

u	k_s	z_0	a	f_w	τ_{ws}	θ_{ws}	u_s*	D*	θ_{cr}	$\theta_{ws} - \theta_{cr}$	Ø
(m/s)		(m)	(m)		(N/m^2)		(m/s)				
0,2	0,025	0,0008333	0,318	0,0631	1,294	0,0089	0,036	196,89	0,0552	-0,0462	bez pomaka
0,4	0,025	0,0008333	0,637	0,0440	3,610	0,0249	0,059	196,89	0,0552	-0,0302	bez pomaka
0,6	0,025	0,0008333	0,955	0,0357	6,579	0,0455	0,080	196,89	0,0552	-0,0097	bez pomaka
0,8	0,025	0,0008333	1,274	0,0307	10,070	0,0696	0,099	196,89	0,0552	0,0144	0,008816
1	0,025	0,0008333	1,592	0,0273	14,011	0,0968	0,117	196,89	0,0552	0,0416	0,043332

D_{50} = 15,0 mm

u	k_s	z_0	a	f_w	τ_{ws}	θ_{ws}	u_s*	D*	θ_{cr}	$\theta_{ws} - \theta_{cr}$	Ø
(m/s)		(m)	(m)		(N/m^2)		(m/s)				
0,2	0,038	0,0012500	0,318	0,0779	1,598	0,0074	0,039	295,33	0,0557	-0,0483	bez pomaka
0,4	0,038	0,0012500	0,637	0,0544	4,457	0,0205	0,066	295,33	0,0557	-0,0352	bez pomaka
0,6	0,038	0,0012500	0,955	0,0440	8,123	0,0374	0,089	295,33	0,0557	-0,0183	bez pomaka
0,8	0,038	0,0012500	1,274	0,0379	12,434	0,0573	0,110	295,33	0,0557	0,0016	0,000324
1	0,038	0,0012500	1,592	0,0338	17,300	0,0797	0,130	295,33	0,0557	0,0240	0,018975

D_{50} = 20,0 mm

u	k_s	z_0	a	f_w	τ_{ws}	θ_{ws}	u_s*	D*	θ_{cr}	$\theta_{ws} - \theta_{cr}$	Ø
(m/s)		(m)	(m)		(N/m^2)		(m/s)				
0,2	0,050	0,0016667	0,318	0,0905	1,856	0,0064	0,043	393,78	0,0556	-0,0492	bez pomaka
0,4	0,050	0,0016667	0,637	0,0631	5,177	0,0179	0,071	393,78	0,0556	-0,0377	bez pomaka
0,6	0,050	0,0016667	0,955	0,0511	9,434	0,0326	0,096	393,78	0,0556	-0,0230	bez pomaka
0,8	0,050	0,0016667	1,274	0,0440	14,440	0,0499	0,119	393,78	0,0556	-0,0057	bez pomaka
1	0,050	0,0016667	1,592	0,0392	20,091	0,0694	0,140	393,78	0,0556	0,0138	0,008279

D_{50} = 25,0 mm

u	k_s	z_0	a	f_w	τ_{ws}	θ_{ws}	u_s*	D*	θ_{cr}	$\theta_{ws} - \theta_{cr}$	Ø
(m/s)		(m)	(m)		(N/m^2)		(m/s)				
0,2	0,063	0,0020833	0,318	0,1017	2,084	0,0058	0,045	492,22	0,0555	-0,0497	bez pomaka
0,4	0,063	0,0020833	0,637	0,0709	5,814	0,0161	0,075	492,22	0,0555	-0,0394	bez pomaka
0,6	0,063	0,0020833	0,955	0,0574	10,594	0,0293	0,102	492,22	0,0555	-0,0262	bez pomaka
0,8	0,063	0,0020833	1,274	0,0494	16,217	0,0448	0,126	492,22	0,0555	-0,0107	bez pomaka
1	0,063	0,0020833	1,592	0,0440	22,563	0,0624	0,148	492,22	0,0555	0,0069	0,002904

D_{50} = 30,0 mm

u	k_s	z_0	a	f_w	τ_{ws}	θ_{ws}	u_s*	D*	θ_{cr}	$\theta_{ws} - \theta_{cr}$	Ø
(m/s)		(m)	(m)		(N/m^2)		(m/s)				
0,2	0,075	0,0025000	0,318	0,1118	2,291	0,0053	0,047	590,66	0,0554	-0,0501	bez pomaka
0,4	0,075	0,0025000	0,637	0,0779	6,392	0,0147	0,079	590,66	0,0554	-0,0407	bez pomaka
0,6	0,075	0,0025000	0,955	0,0631	11,648	0,0268	0,107	590,66	0,0554	-0,0286	bez pomaka
0,8	0,075	0,0025000	1,274	0,0544	17,830	0,0411	0,132	590,66	0,0554	-0,0143	bez pomaka
1	0,075	0,0025000	1,592	0,0484	24,807	0,0571	0,156	590,66	0,0554	0,0017	0,000365

D_{50} = 35,0 mm

u	k_s	z_0	a	f_w	τ_{ws}	θ_{ws}	u_s*	D*	θ_{cr}	$\theta_{ws} - \theta_{cr}$	Ø
(m/s)		(m)	(m)		(N/m^2)		(m/s)				
0,2	0,088	0,0029167	0,318	0,1211	2,483	0,0049	0,049	689,11	0,0554	-0,0505	bez pomaka
0,4	0,088	0,0029167	0,637	0,0845	6,925	0,0137	0,082	689,11	0,0554	-0,0417	bez pomaka
0,6	0,088	0,0029167	0,955	0,0684	12,620	0,0249	0,111	689,11	0,0554	-0,0304	bez pomaka
0,8	0,088	0,0029167	1,274	0,0589	19,318	0,0381	0,137	689,11	0,0554	-0,0172	bez pomaka
1	0,088	0,0029167	1,592	0,0524	26,877	0,0531	0,162	689,11	0,0554	-0,0023	bez pomaka

Range of demersal orbital velocities u_d: **0,2 – 1,0** m/s
Medium grain size range D_{50}: **10 – 35** mm

ρ_s = 2500 kg/m^3
ρ = 1025 kg/m^3
T = 5,00 s
v = 1,36E-06 m^2/s

European Regional Development Fund

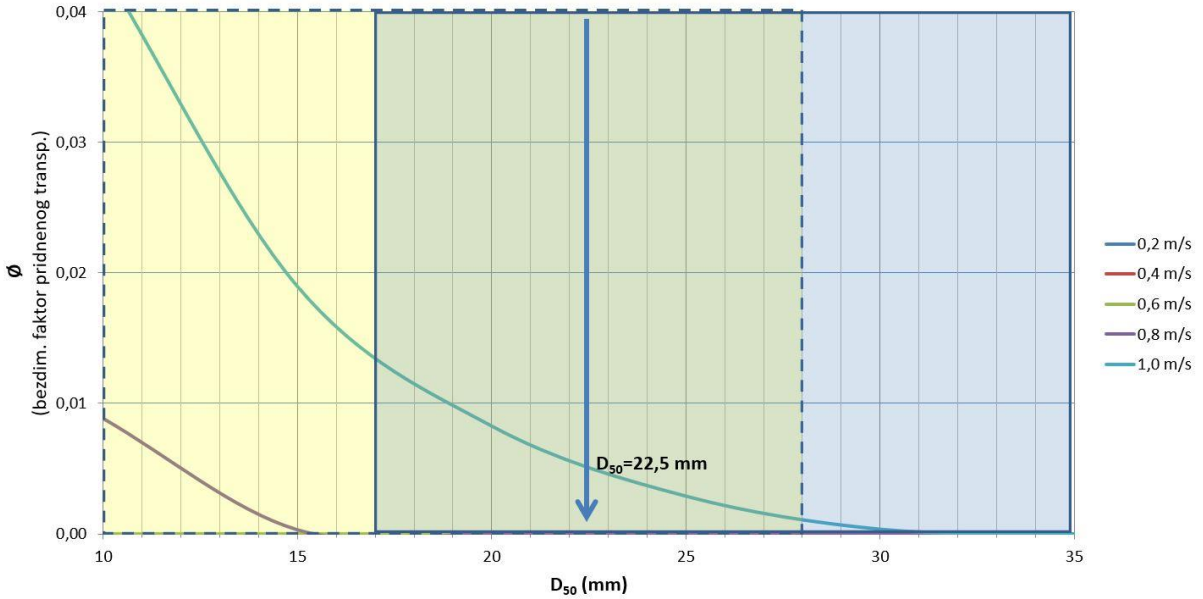

Figure 7.31 – diagram for calculating the size of medium grain beach material *D50* for Kašjuni beach (Split)

In accordance with the implemented calculation, according to Table 7.4, for the bottom orbital wave velocity Ud range 0.2 – 1.0 m/s and the Medium Grain D_{50} range of 10 – 35 mm, **the stable composition of the beach material for Kašjuni Beach in Split can be defined as a medium-sized rock material D_{50} = 22.5 mm, with a range of 17 – 28 mm**, as shown from the diagram in Figure 7.31.

8. ANALYSIS OF THE NUMERICAL MODELING AND CALCULATING RESULTS

8.1. Zlatni rat (Brač)

8.1.1. Analysis of the numerical modeling results

Numerical wave simulations for Zlatni rat beach on the island of Brač were conducted for four directions of the incident waves. These are the following wave directions: ESE (112.5°), SSE (157.5°), SW (225°) and WSW (247.5°). Numerical simulations with two sea levels were performed for each of these directions, for the mean sea level (SRM) and the absolute maximum, all in accordance with Table 6.1.

8.1.1.1. Analysis of wave propagation results and wave height fields

In addition to the two-dimensional representation of wave height fields given in Chapter 6 of this study, two control cross-sections of individual lengths of 100 meters (Figure 8.1) were set up in which a detailed observation of wave height variations for simulations with individual directions of incident waves for the mean sea level of SRM was performed (Figures 8.2 and 8.3).

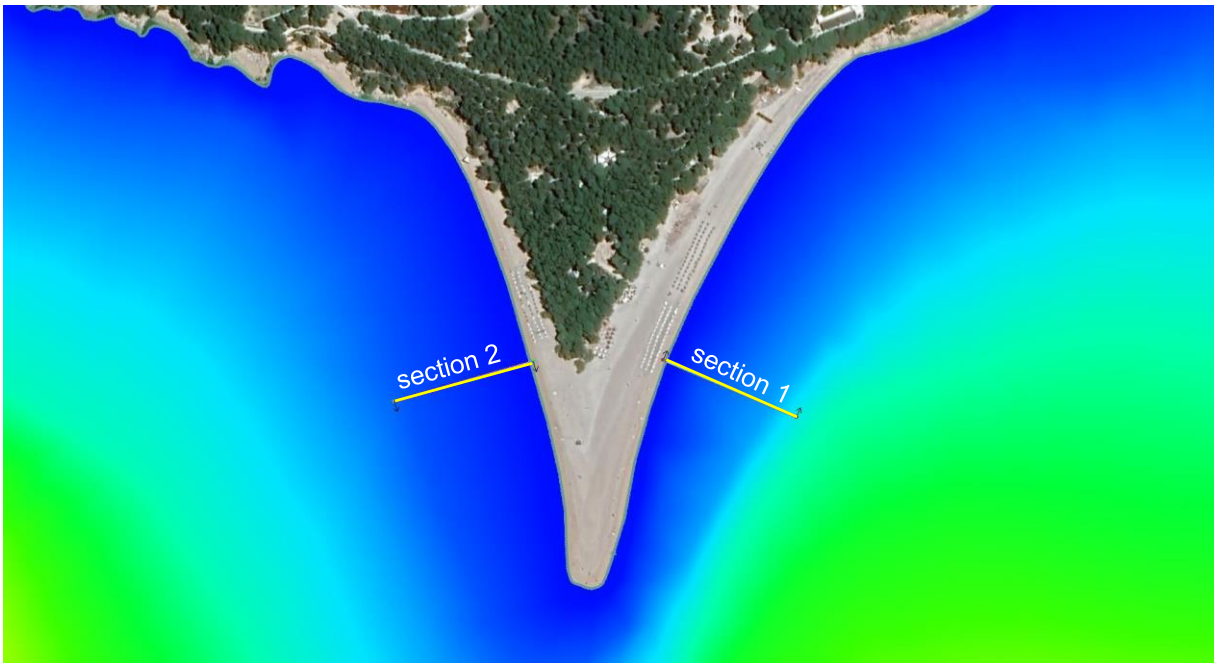

Figure 8.1 – Position of control cross-sections for Zlatni rat beach (Brač)

The results of numerical modeling for simulation A1 (existing state, direction ESE, SRM) show the expected direct exposure of the eastern part of Zlatni rat beach and its very top to the incident waves. In accordance with the display of fields of significant wave heights (Figure 6.23), it is evident that the highest wave heights occur in the immediate vicinity of the eastern coastline of the beach, and at the top of the cape. Also, wave heights are increased from the west side of the cape near its peak, and the reason for this is visible from the image of the current wave outline (Figure 6.22), where the tendency to rotate wave fronts around the tip of the cape due to transformation processes of diffraction and refraction of waves is observed. In this area, the wave experiences certain transformations and deformations, not losing significantly on wave energy.

The results of numerical modeling for simulation A2 (existing state, direction SSE, SRM) show exposure of the eastern part of the beach, but in the part towards the mainland and the mainland part of the

beach itself to the incoming waves. In accordance with the display of fields of significant wave heights (Figure 6.27), it is evident that the highest wave heights appear precisely in the mentioned eastern mainland part of the beach, and at the very top of the cape of the beach. Also, wave heights are increased from the west side of the cape near its peak, and the reason for this is visible from the image of the current wave outline (Figure 6.26), where the tendency to rotate wave fronts around the tip of the cape is observed due to transformation processes of diffraction and wave breaking. In this area, the wave experiences certain transformations and deformations, not losing significantly on wave energy.

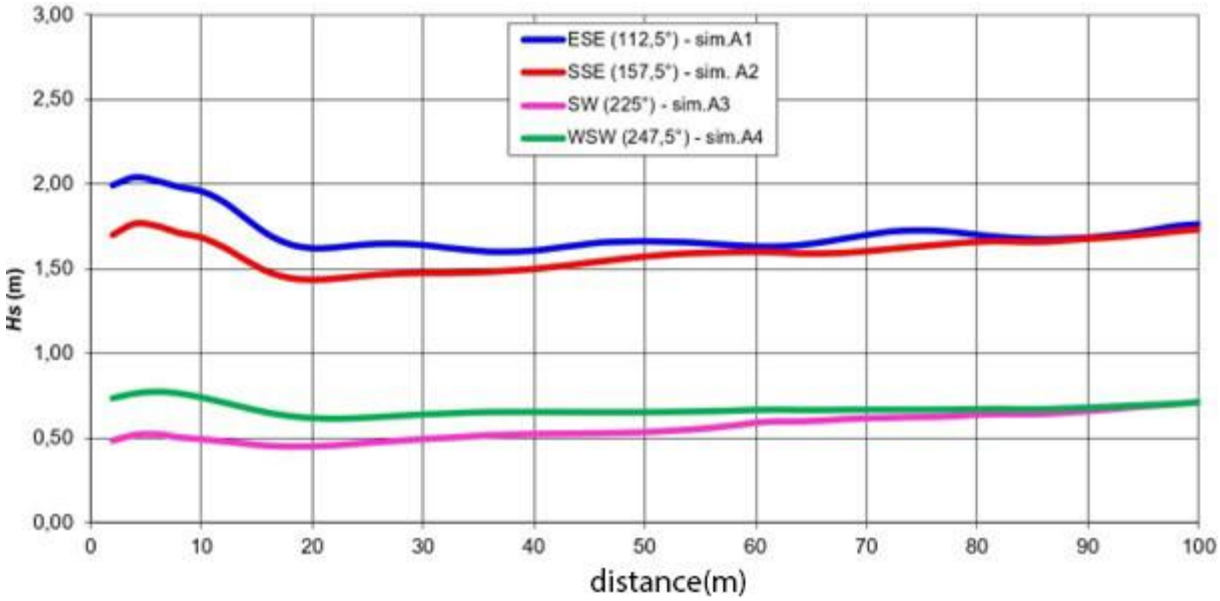

Figure 8.2 – Variation of wave heights *Hs* in control cross-section 1, Zlatni rat (Brač)

The results of numerical modeling for simulation A3 (existing state, direction SW, SRM) show the expected direct exposure of the western part of Zlatni rat beach and its peak to the incident waves. In accordance with the display of fields of significant wave heights (Figure 6.31), it is evident that the highest wave heights appear in the immediate vicinity of the western coastline of the beach, and at the top of the cape. The eastern coast of the beach is relatively well sheltered, and in this part, there is no significant increase in wave heights. From the picture of the current wave outline (Figure 6.30), there is only a very mild tendency to rotate the wave fronts around the top of the beach, while most of the wave energy, after passing the tip of the cape, is directed towards the eastern mainland part of the beach.

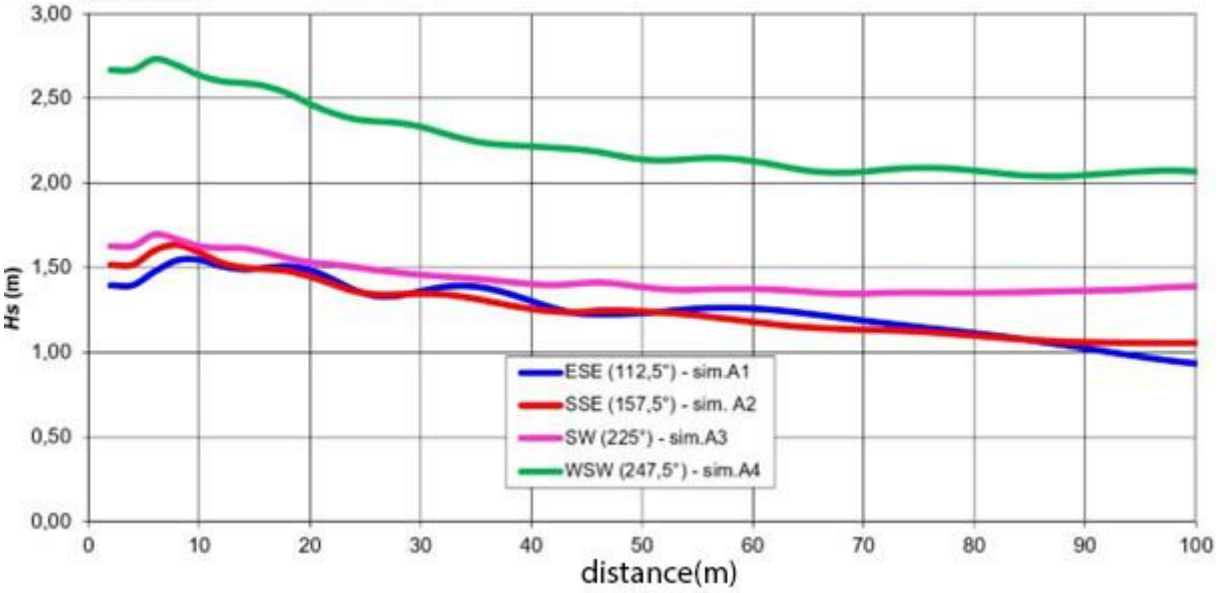

Figure 8.3 – Variation of wave heights *Hs* in control cross-section 2, Zlatni rat (Brač)

The results of numerical modeling for simulation A4 (existing state, direction WSW, SRM) show the expected direct exposure of the western part of Zlatni rat beach and its peak to the incident waves. In accordance with the display of fields of significant wave heights (Figure 6.35), it is evident that the highest wave heights appear in the immediate vicinity of the western coastline of the beach, and at the top of the cape. The eastern coast of the beach is relatively well sheltered, and in this part, there is no significant increase in wave heights. From the picture of the current wave outline (Figure 6.34), one can see only a very slight tendency to rotate wave fronts around the top of the beach.

In conclusion, regarding the analysis of the propagation of waves and wave heights for the Zlatni rat beach on the island of Brač, it can be said that Zlatni rat beach on the island of Brač is under the considerable influence of the incident waves. The results of the numerical analysis undoubtedly indicate a very high degree of exposure of certain parts of the beach, especially the very top of the beach and the zone in its immediate vicinity, looking from both sides. Therefore, it can be concluded that Zlatni rat beach, and especially the part in the zone of its peak, experiences significant hydrodynamic influences, which have great importance on the morphology of the beach and the dynamics of its beach material. This is very well visible in the actual situation on the ground, where the dynamic process of alternating shifting of the top of the beach due to the waves that occur during the year is evident.

8.1.1.2. Analysis of wave breaking zone results

For the analysis of the wave breaking zone, as the main cause of beach erosion from granular materials, the results of simulations conducted with the same directions of incoming waves for different sea levels will be compared. A comparison of these results gave an answer to the question of how much potential sea level rise, as a result of climate change, will have an impact on the beach in question.

In addition to the two-dimensional representation of wave breaking zones given in Chapter 6 of this study, two control sections of individual lengths of 100 meters (Figure 8.1) were set up in which detailed observation and comparison of the position of the wave breaking zone for simulations of one direction and different sea levels (Figures 8.4 to 8.9) were carried out.

As can be seen from Figures 6.24 and 6.25, wave breaking zones for ese direction (112.5°) and both analyzed sea levels, reveal that wave breaking occurs on both sides of cape Zlatni rat beach, with wave breaking zones on its eastern side much closer to the coastline itself, which is to be expected because

incoming waves directly encounter that side of the coastline. Due to the rotation of the waves around the top of the cape, which is visible from Figure 6.22, the waves due to the transformations they experience, primarily due to the processes of refraction and diffraction, lose at the wave height, but still have enough energy to break them in the immediate vicinity of the coastline of the beach. However, these wave breaking zones on the west side of cape Zlatni rat beach are somewhat further away from the coastline compared to the wave breaking zones that occur on its eastern side. This is best evident from the control sections, from which it is observed that for simulation with elevated sea level, i.e., with a level corresponding to the absolute maximum, the wave breaking zone on the east side of the cape, i.e., for the control section 1, was shifted towards the coastal line by approximately 5 meters in relation to the simulation with sea level corresponding to the middle sea level (SRM) (Figure 8.4). Namely, for the simulation with medium sea distance (SRM), the wave breaking zone occurs some 17 meters, and for the simulation with an absolute maximum at approximately 12 meters from the coastline. For control cross-section 2, placed on the west side of the cape, an even more drastic shift of the wave breaking zone towards the shore in the amount of 18 meters is noticeable (Figure 8.5). Here, the wave breaking zone for simulation with sea level corresponding to the middle sea level (SRM) occurs about 31 meters from the coast, and for simulation with an absolute maximum at approximately 13 meters from the coastline.

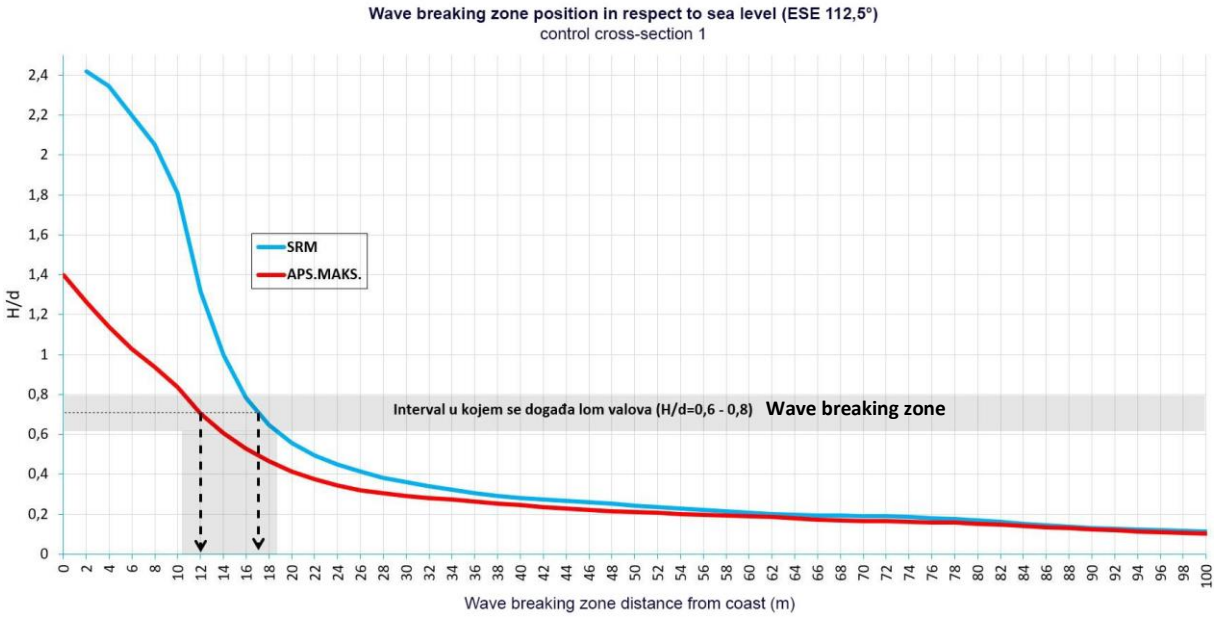

Figure 8.4 – Position of the wave breaking zone relative to sea level for the direction of ESE waves (112,5°) for cross-section 1, Zlatni rat (Brač)

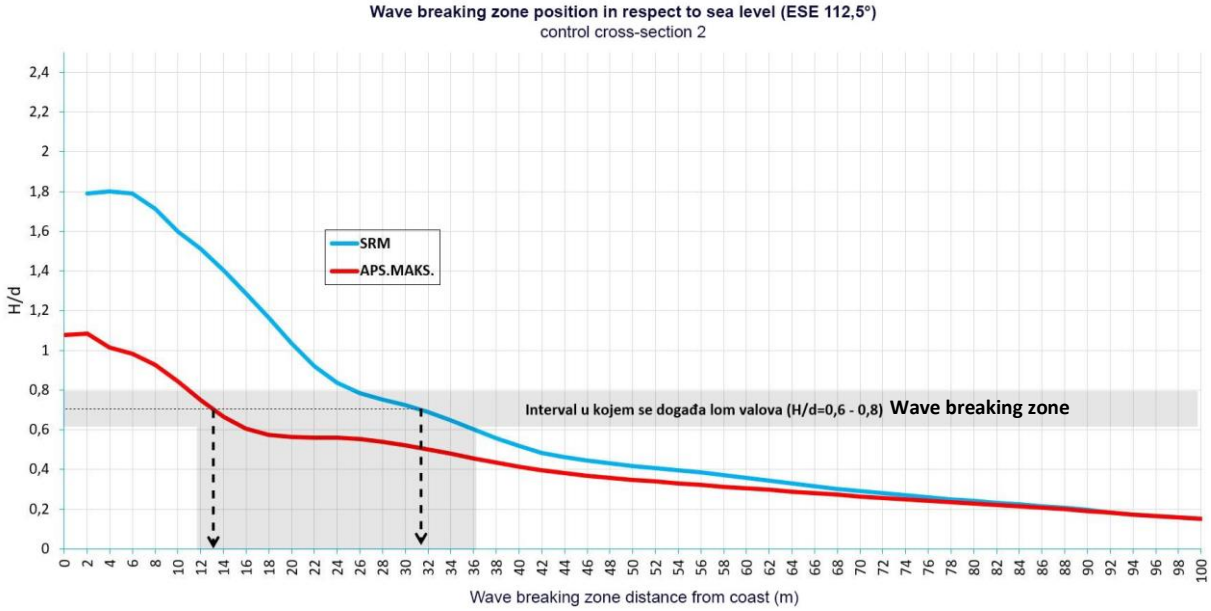

Figure 8.5 – Position of wave breaking zone relative to sea level for wave direction ESE (112.5°) for cross-section 2, Zlatni rat (Brač)

A similar situation arises in the second analyzed direction of the incoming waves, which is the direction of the SSE (157.5°). There is also, this time from figures 6.28 and 6.29, visible how the wave break occurs on both sides of the cape Zlatni rat beach. Also, just as with the simulation with incoming waves from the direction of ESE (112.5°), the wave breaking zones on its eastern side are much closer to the coastal line itself, which is to be expected because this side of the coastline is more exposed to incoming waves. And here, from Figure 6.26, there is a noticeable rotation of waves around the cape, where the waves due to the transformations they experience, primarily due to the processes of refraction and diffraction, lose at wave height, but still have enough energy to occur their fracture in the immediate vicinity of the coastline of the beach. The same as in the previous case, the wave breaking zones on the west side of Cape Zlatni rat beach are somewhat further away from the coastline compared to the wave breaking zones occurring from its eastern side. If we look at the control cross-sections, it is noticed that for simulation with elevated sea level, i.e., with a level corresponding to the absolute maximum, the wave breaking zone is shifted towards the coastal line by approximately 5 meters in relation to the simulation with sea level corresponding to the middle sea level (SRM) (Figure 8.6). Namely, for the simulation with medium sea distance (SRM), the wave breaking zone occurs some 16 meters, and for the simulation with an absolute maximum at approximately 11 meters from the coastline. For the control cross-section 2, placed on the west side of the cape, an even more drastic shift of the wave breaking zone towards the shore in the amount of 18 meters is noticeable (Figure 8.7). Here, the wave breaking zone for simulation with sea level corresponding to the middle sea level (SRM) occurs about 30 meters from the coast, and for simulation with an absolute maximum at approximately 12 meters from the coastline.

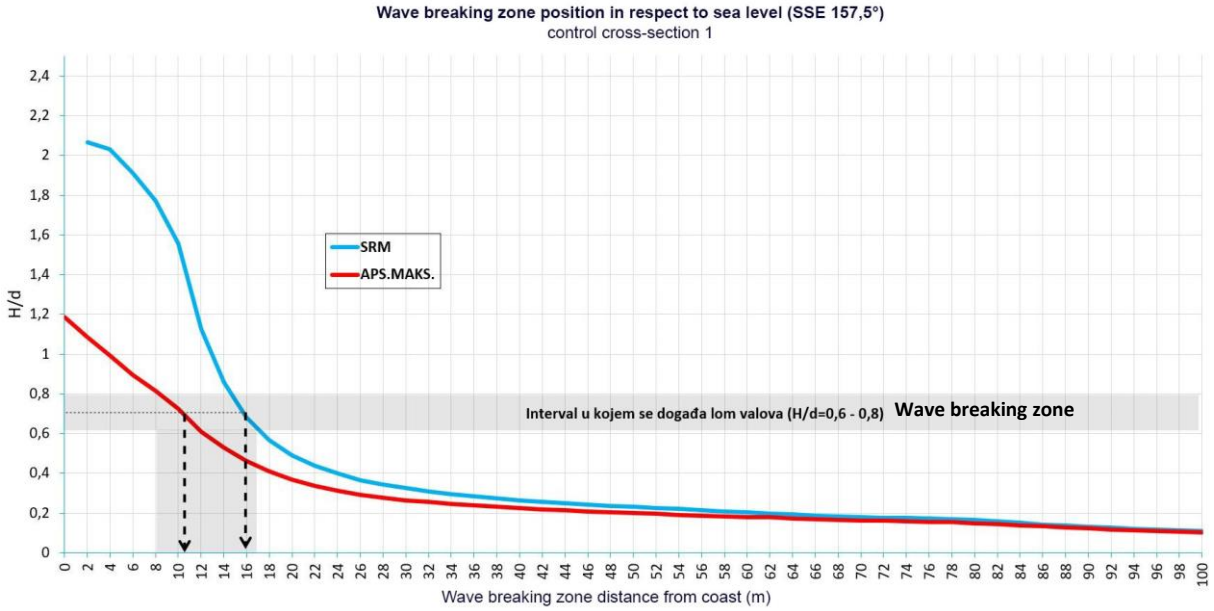

Figure 8.6 – Position of wave breaking zone relative to sea level for SSE wave direction (157,5°) for cross-sectional cross-section 1, Zlatni rat (Brač)

Figure 8.7 – Position of the wave breaking zone relative to sea level for the wave direction of SSE (157,5°) for cross-section 2, Zlatni rat (Brač)

Simulations with incoming waves from the direction of the SW (225°) wave breaking zone are somewhat different from the previous two analyzed directions (Figures 6.32 and 6.33), given the directionality of incoming waves. It is evident that the wave break primarily occurs on the west side of the cape Zlatni rat beach, while on the east side it occurs only in the immediate vicinity of the peak. For this reason, here it is possible to observe the position of the wave breaking zone only for the control section 2, placed on the west side of the cape of the beach. From cross-section 2 (Figure 8.8), it is evident that for a simulation with elevated sea level, i.e., with a level corresponding to the absolute maximum, the wave breaking zone shifted towards the coastal line by more than 20 meters in relation to the simulation with sea level corresponding to the middle sea level (SRM) (Figure 8.8). Specifically, for simulation with medium sea level (SRM), the wave breaking zone occurs about 34 meters from the

shore, and for simulation with an absolute maximum at approximately 14 meters from the coastline.

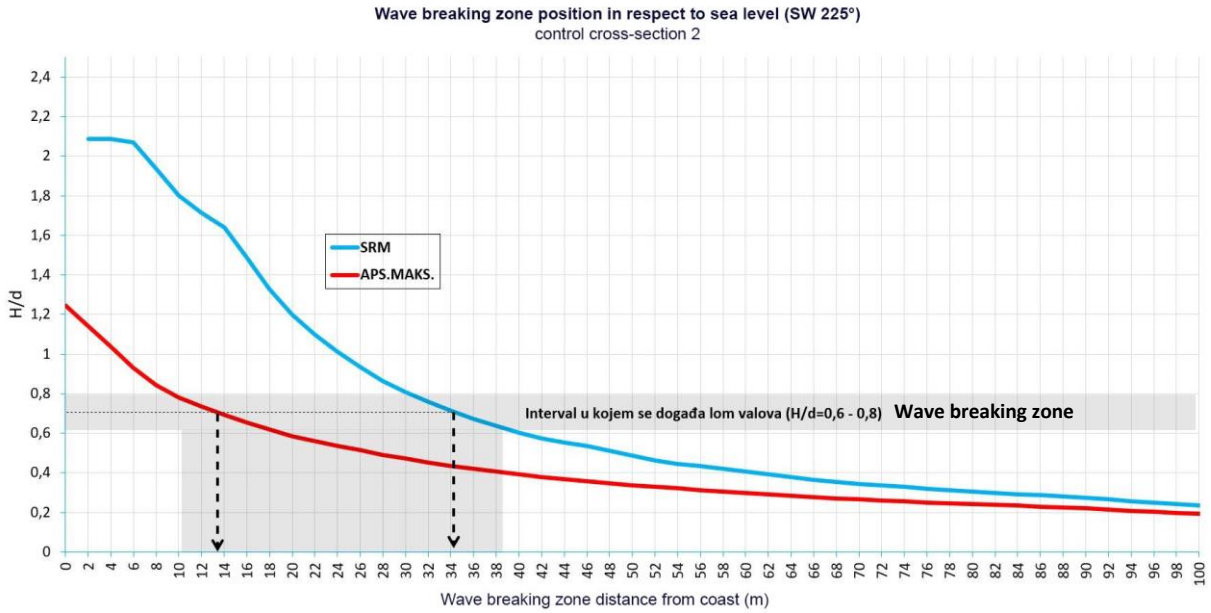

Figure 8.8 – Position of wave breaking zone relative to sea level for wave direction SW (225°) for cross-sectional cross-section 2, Zlatni rat (Brač)

For simulations with incoming waves from the WSW (247.5°) wave breaking zones are like the previously analyzed direction SW (225°). From Figures 6.36 and 6.37, it is evident that the wave break occurs primarily from the western side of cape Zlatni rat beach, and for simulation with medium sea distance (SRM) and on its eastern side on a somewhat smaller scale. For simulation with absolute maximum, the wave breaking zone occurs primarily on the west side of the cape of the beach, while on the eastern side it occurs only in the immediate vicinity of the peak. Because of all the above, the position of the wave breaking zone is also observed here only for the control section 2, placed on the west side of the cape of the beach. From cross-section 2, it is evident that for a simulation with elevated sea level, i.e., with a level corresponding to the absolute maximum, a wave breaking zone shifted towards the coastal line by approximately 20 meters in relation to the simulation with sea level corresponding to the middle sea level (SRM) (Figure 8.9). Specifically, for the simulation with medium sea distance (SRM), the wave breaking zone occurs about 53 meters from the coast, and for the simulation with an absolute maximum at approximately 33 meters from the coastline.

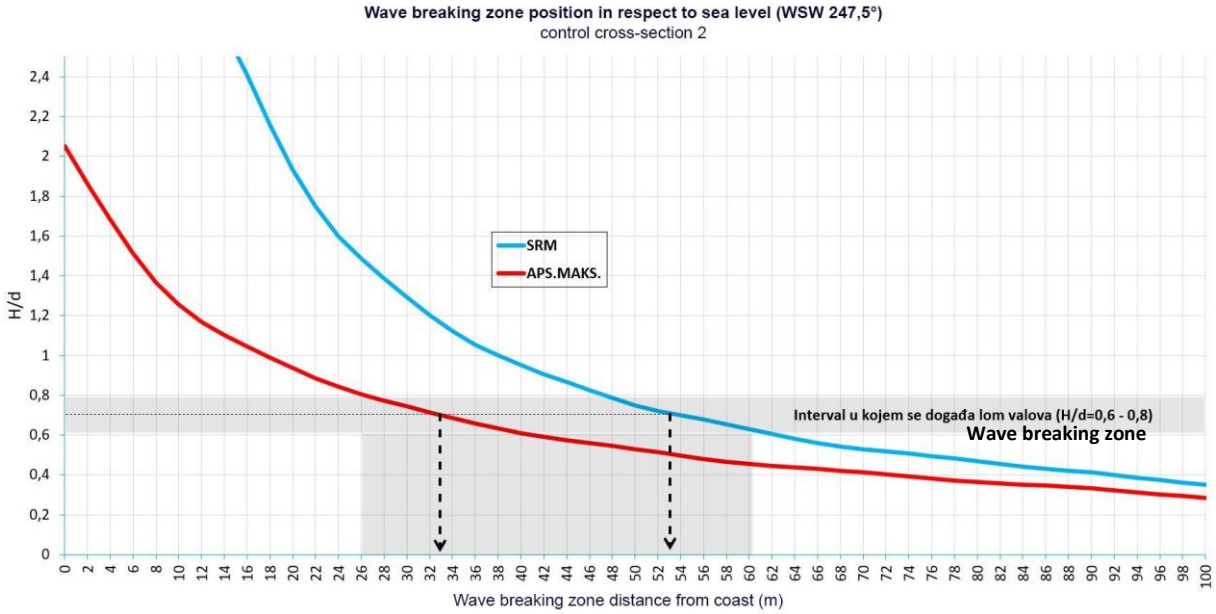

Figure 8.9 – Position of wave breaking zone relative to sea level for wave direction WSW (225°) for cross-section 2, Zlatni rat (Brač)

In conclusion, regarding the analysis of the occurrence of wave breaking zone for Zlatni rat beach on the island of Brač, it can be said that Zlatni rat beach on the island of Brač is under the considerable influence of wave breaking process, which is one of the most important erosive processes for grainy beaches. The results of the numerical analysis undoubtedly point to a very high degree of beach vulnerability due to potential sea level rise, as a result of climate change. This is reflected in the drastic shift of wave breaking zones towards the coast for all conducted numerical simulations with a sea level corresponding to the absolute maximum. Thus, it can be concluded that the beach in the coming period, if predictions regarding sea level rise are realized, will be under increasing erosive pressure, which could ultimately result in its complete degradation and disappearance unless timely activities are undertaken.

8.1.2. Analysis of the potential transport of beach material calculation results

In order to calculate the potential of sediment transport for a particular point on the considered beach, it is necessary to know the wave height parameter *Hs* at that point, which indicates the potential amount of energy that waves bring to the shore, with the help of which the wave energy flow can be calculated *Pl*, which serves to estimate the size of the potential transport of beach material due to wave-induced currents (Pernat Ž., Vranješ M, 2012).

Based on the analysis given in Chapter 7.1.1. of this study, a very high potential for the transport of beach material for the existing situation was determined for the Zlatni rat beach on Brač. The analysis looked at two dominant directions of incoming waves (ESE and WSW), and observed variations in wave power *Pl* along two set control lines of individual lengths of 200 meters, detecting increased values in both control lines.

In conclusion, regarding the analysis of the potential transport of beach material calculation results for Zlatni rat beach on the island of Brač, it can be said that Zlatni rat beach is under considerable hydrodynamic influence that contributes to its high potential of transporting sedimentary material from which it is made.

8.2. Stiniva (Vis)

8.2.1. Analysis of the numerical modeling results

Numerical simulations of waves for Stiniva beach on the island of Vis were conducted for one direction of incident waves, and it is the direction of SE (135°), for which numerical simulations were performed with two sea levels, for the mean sea level (SRM) and the absolute maximum, all in accordance with Table 6.1.

8.2.1.1. Analysis of wave propagation results and wave height fields

In addition to the two-dimensional representation of wave height fields given in chapter 6 of this study, a 40-meter-long control cross-section (Figure 8.10) was set up in which a detailed observation of wave height variations was performed to simulate incoming waves with medium sea level - SRM (Figure 8.11).

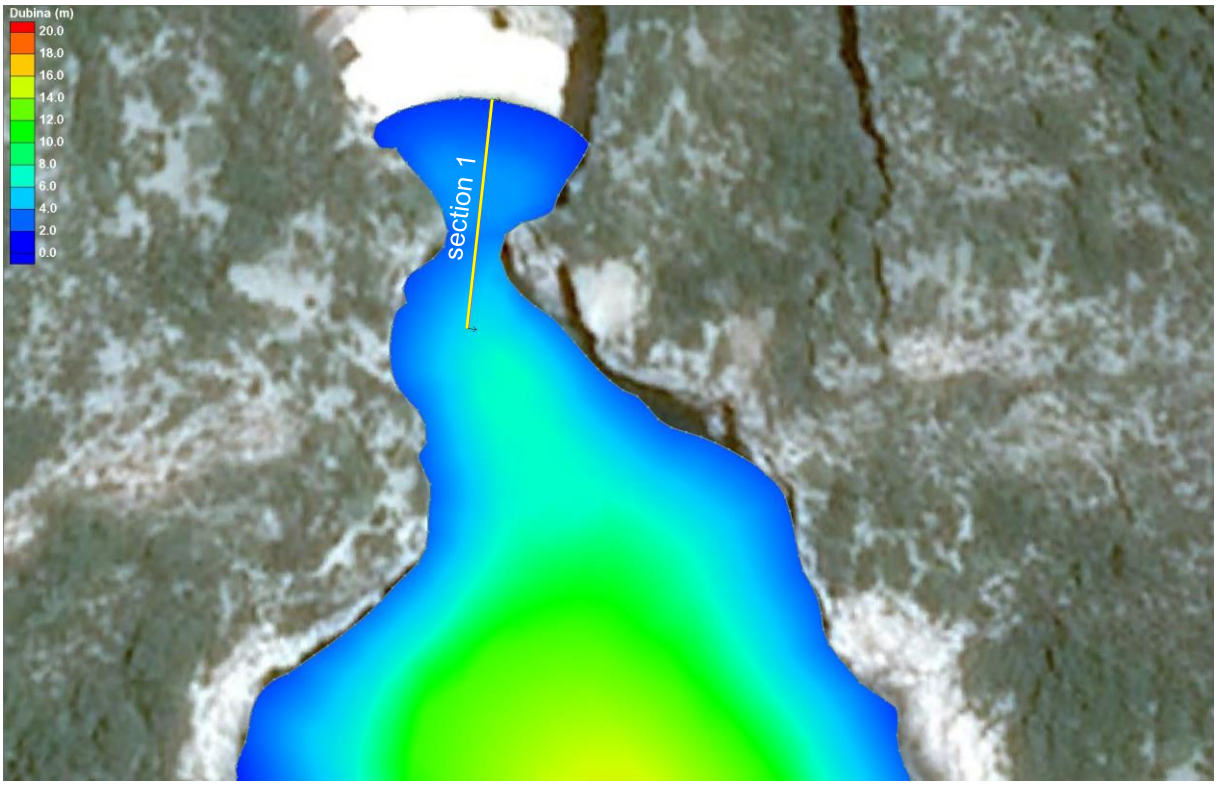

Figure 8.10 – Position of cross-section for Stiniva beach (Vis)

The results of numerical modeling for simulation A9 (existing state, direction SE, SRM) show the expected direct exposure of the outer parts of the bay within which there is also the waters of Stiniva beach itself to the incident waves. In accordance with the display of fields of significant wave heights (Figure 6.39), it is evident that the highest wave heights appear at the entrance to the bay, especially in the immediate vicinity of its west coast. Looking towards the bottom of the bay, and the waters of Stiniva beach, wave heights drastically decrease, both due to deformations and transformations of waves, and due to the encounter of waves in the much shallower sea. This is evident from the picture of the current wave outline (Figure 6.38), where the tendency of wave fronts to rotate towards both shores of the bay is observed, due to the processes, which significantly reduces wave energy, contributing to a relatively complete reduction of waves at the very entrance to the waters of Stiniva beach and inside it. How much the wave energy reduction is best illustrated by the diagram of wave

height variation in the set control cross-section (Figure 8.11).

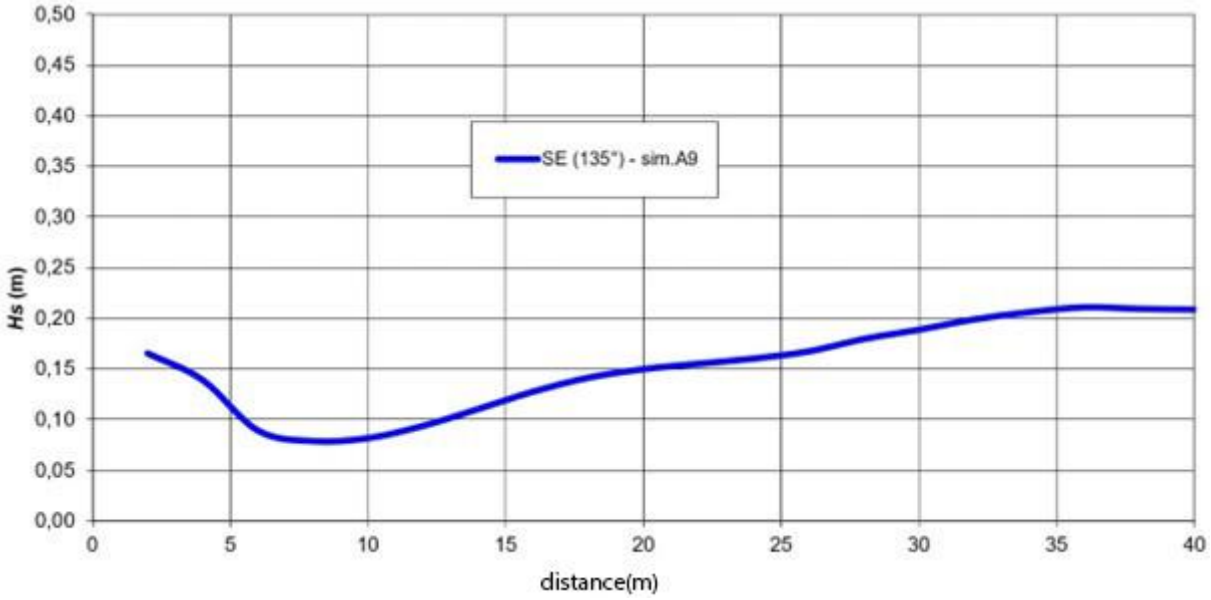

Figure 8.11 – Variation of wave heights *Hs* in control cross-section 1, Zlatni rat (Brač)

In conclusion, regarding the analysis of the propagation of waves and wave height fields for Stiniva beach on the island of Vis, it can be said that the wider aquatory of Stiniva beach, i.e. the bay within which it is located, is under the considerable influence of the incident waves, but the the beach itself is excellently protected and completely without the influence of waves. The results of the numerical analysis, undoubtedly indicate an extremely low degree of exposure of the beach to the incident waves. Thus, it can be concluded that Stiniva beach does not experience significant hydrodynamic influences, which could have an impact on the morphology of the beach and the dynamics of its beach material. This is very well visible in the actual state, because on the location there are no areas that can be safely stated to be under the significant influence of the action of waves.

8.2.1.2. Analysis of wave breaking zone results

In addition to the two-dimensional representation of wave height fields given in chapter 6 of this study, a control cross-section 40 meters long (Figure 8.10) was set up in which a detailed observation and comparison of the position of the wave breaking zone for simulations of one direction and different sea levels was performed (Figure 8.12).

As can be seen from Figure 8.12, for the conducted numerical simulations for the direction of SE (135°) from both analyzed sea level (mean sea level – SRM and absolute maximum), the results of the analysis reveal that wave breaking cannot be detected anywhere in the control cross-section.

In conclusion, regarding the analysis of the occurrence of the wave breaking zone for Stiniva beach on the island of Vis, it can be said that Stiniva beach is not affected by the wave breaking process, which is one of the most important erosive processes for grainy beaches. The results of the conducted numerical analysis undoubtedly indicate a very low degree of beach vulnerability due to potential sea level rise, as a result of climate change. Therefore, it can be concluded that the beach in the coming period, if predictions regarding sea level rise come true, will remain in approximately the same state in terms of erosive pressure due to hydrodynamic action of the sea.

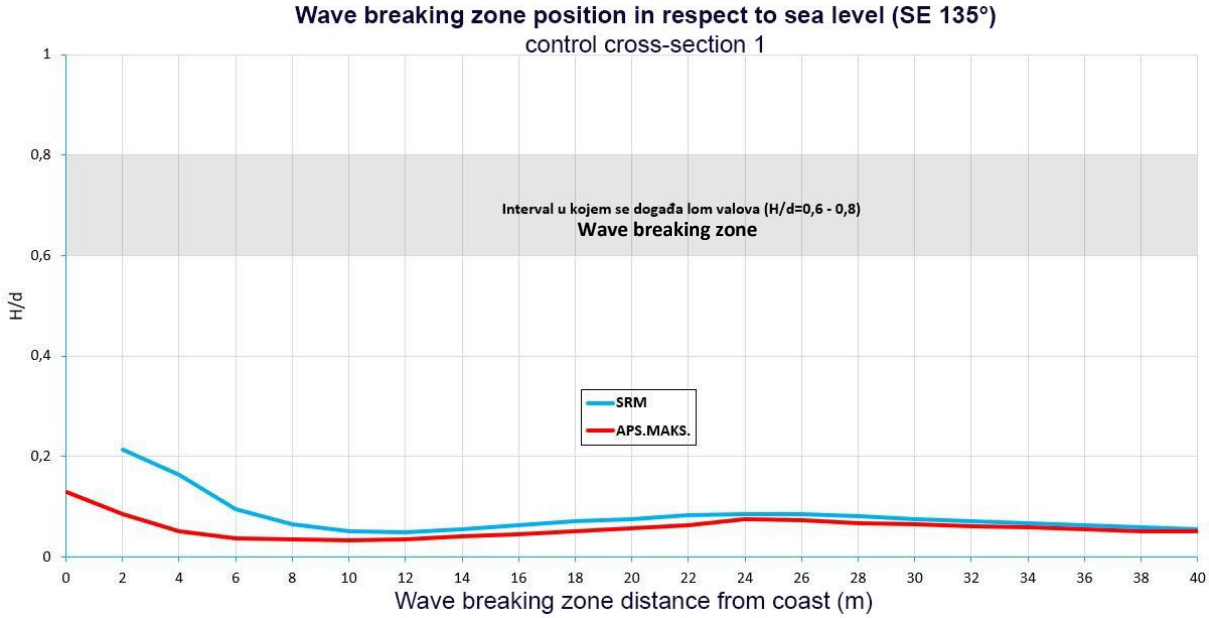

Figure 8.12 – Position of wave breaking zone relative to sea level for wave direction SE (135°) for cross-sectional control, Stiniva (Vis)

8.2.2. Analysis of the potential transport of beach material calculation results

In order to calculate the potential of sediment transport for a particular point on the considered beach, it is necessary to know the wave height parameter *Hs* at that point, which indicates the potential amount of energy that waves bring to the shore, with the help of which the wave energy *flow can be calculated Pl*, which serves to estimate the size of the potential transport of beach material due to wave-induced currents (Pernat Ž., Vranješ M, 2012).

Based on the analysis given in Chapter 7.1.2 of this study, a very low potential for the transport of beach material for the existing state was determined for the beach Stiniva on Vis. In the analysis, the dominant direction of incident waves (SE) was considered, and variations in the power of the Pl wave along the set control cross-section 20 meters long were observed, where extremely small values were detected.

In conclusion, regarding the analysis of the potential transport of beach material calculation results for Stiniva beach on the island of Vis, it can be said that Stiniva beach is under a slight hydrodynamic influence that contributes to its low potential for the transport of sedimentary material from which it is made.

8.3. Podgora (Makarska Riviera)

8.3.1. Analysis of the numerical modeling results

Numerical simulations of waves for Podgora beach on the Makarska Riviera were conducted for three directions of incident waves. These are the following wave directions: SSE (157.5°), SW (225°) and W (270°). Numerical simulations with two sea levels were performed for each of these directions, for the mean sea level (SRM) and the absolute maximum, all in accordance with Table 6.1.

Simulations were carried out for the existing state and the proposal of the conceptual design. Namely, based on the results of numerical simulations and detected problems, a proposal for the control area of Podgora beach was made in order to eliminate them, and raise the general level of sustainability and resilience of the beach. The conceptual design is conceived using basic construction and technical

principles (more in chapter 5), and it is about setting up an underwater stone reef at the appropriate distance and depth, and additional plan correction of two existing stone groynes with addition nourishment of the beach with appropriate beach material.

8.3.1.1. Analysis of wave propagation results and wave height fields

In addition to the two-dimensional representation of wave height fields given in Chapter 6 of this study, three control cross-sections of individual lengths of 100 meters (Figure 8.13) were set up in which a detailed observation of wave height variations for simulations with individual directions of incident waves for the mean sea level of SRM was performed (Figures 8.14 to 8.16).

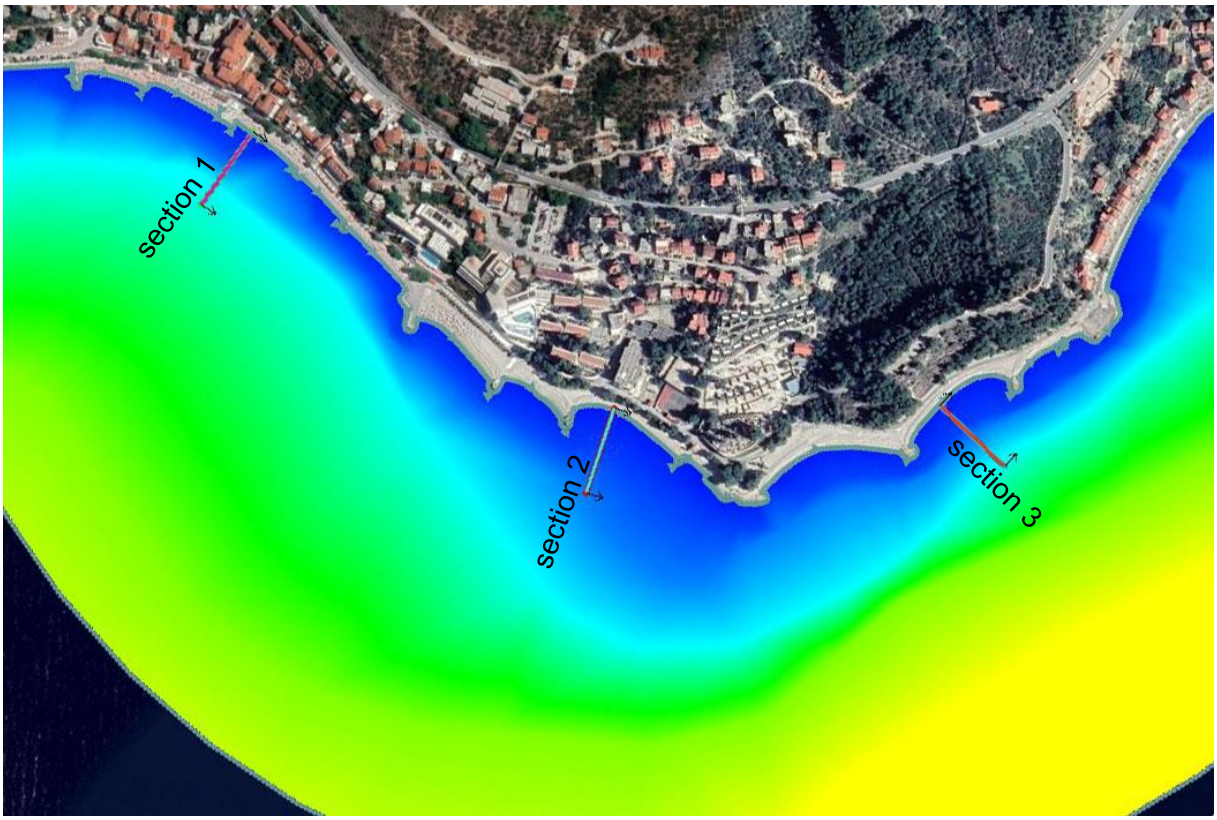

Figure 8.13 – Position of control sections for Podgora beach (Makarska Riviera)

The results of numerical modeling for simulation A11 (existing state, direction SSE, SRM) show the expected direct exposure of the southern part of Podgora beach to the incident waves. In accordance with the display of fields of significant wave heights (Figure 6.42), it is evident that the highest wave heights occur in the immediate vicinity of the southern coastline of the beach.

The northern part of the coast, which is laid in a north-south direction, is quite protected from waves from this direction, and the reason for this is visible from the picture of the current wave outline (Figure 6.41), where the tendency to rotate the wave fronts due to transformational processes of diffraction and refraction of waves is observed. In this area, the wave experiences transformations and deformations, more significantly losing on wave energy.

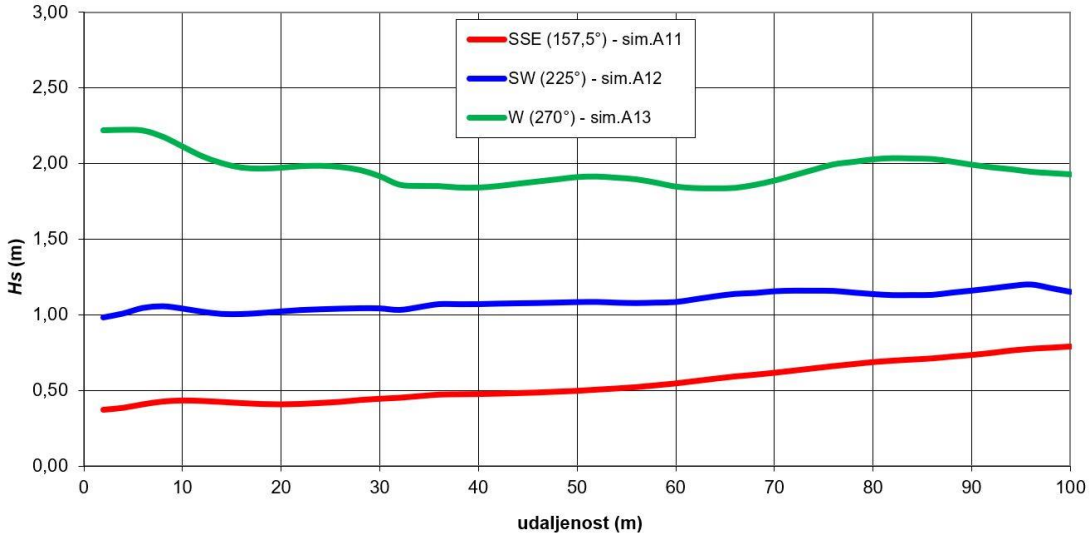

Figure 8.14 – Variation of wave heights *Hs* in control cross-section 1, Podgora (Makarska Riviera)

The results of numerical modeling for simulation A12 (existing state, direction SW, SRM) show the expected direct exposure of the entire coastal belt of the Podgora beach in question to the incoming waves. In accordance with the display of fields of significant wave heights (Figure 6.47), it is evident that the highest wave heights appear in the immediate vicinity of the southern cape of the beach, which divides the beach into northern and southern parts. The reason for this is particularly evident from the picture of the current wave outline (Figure 6.46), where the tendency of direct waves from this direction to the cape is observed, and the slight rotation of the wave fronts in the rest of the coastal belt due to transformation processes of diffraction and refraction of waves. It can be said that for this wave direction, waves bring approximately uniform wave energy throughout the coastal zone in question.

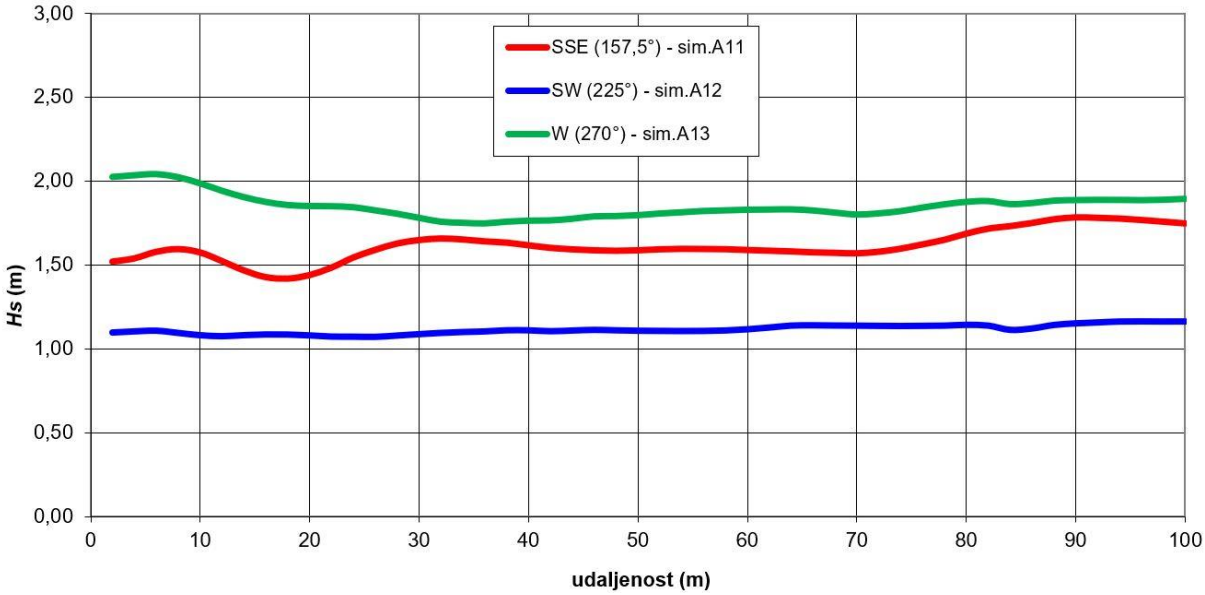

Figure 8.15 – Variation of wave heights *Hs* in control cross-section 2, Podgora (Makarska Riviera)

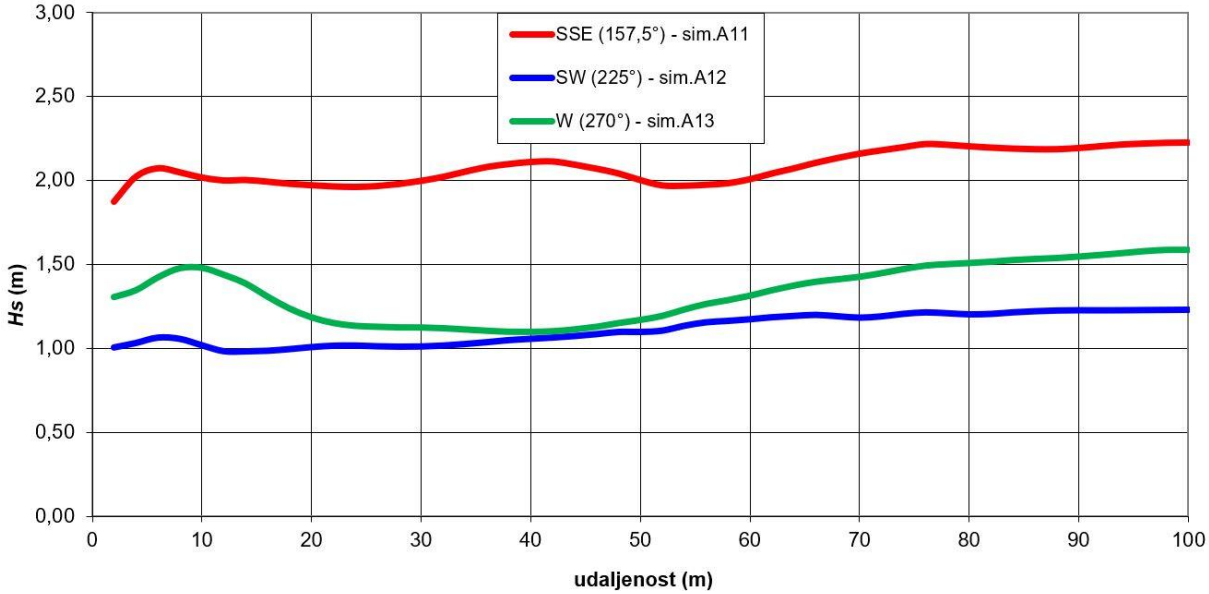

Figure 8.16 – Variation of Wave Heights *Hs* in Control Cross Section 3, Podgora (Makarska Riviera)

The results of numerical modeling for simulation A13 (existing state, direction W, SRM) show the expected direct exposure of the part of the beach that is laid in the north-south direction, especially its southern cape to the incoming waves. In accordance with the display of fields of significant wave heights (Figure 6.51), it is evident that the highest wave heights appear in the immediate vicinity of the coast laid in the north-south direction and the cape on its southern part. The southern part of the beach is quite protected from waves from this direction, and the reason for this is visible from the picture of the current wave outline (Figure 6.50), where the tendency to rotate wave fronts due to transformational processes of diffraction and wave breaking is observed. In this area, the wave experiences transformations and deformations, more significantly losing on wave energy.

In conclusion, regarding the analysis of the propagation of waves and wavefields for the Beach Podgora on the Makarska Riviera, it can be said that Podgora beach is under the considerable influence of the incident waves. The results of the numerical analysis undoubtedly indicate a very high degree of exposure of the entire coastal zone, which implies the conclusion that it experiences large hydrodynamic influences, which have a significant impact on its beach material. This is very well visible in the real state, where the dynamic process of continuously pushing the beach material to the shore and simultaneously carrying it to the deeper sea during the year is evident.

8.3.1.2. Analysis of wave breaking zone results

For the analysis of the wave breaking zone, as the main cause of beach erosion from granular materials, the results of simulations that were conducted with the same directions of incident waves for different sea levels were compared. The comparison of these results gave an answer to the question of how much potentially raising sea levels, as a result of climate change, will have an impact on the beach in question.

In addition, in addition to the two-dimensional representation of wave breaking zones given in Chapter 6 of this study, two control sections of individual lengths of 100 meters (Figure 8.13) were set up in which a detailed observation and comparison of the position of the wave breaking zone for simulations of one direction and different sea levels was carried out (Figures 8.17 to 8.19).

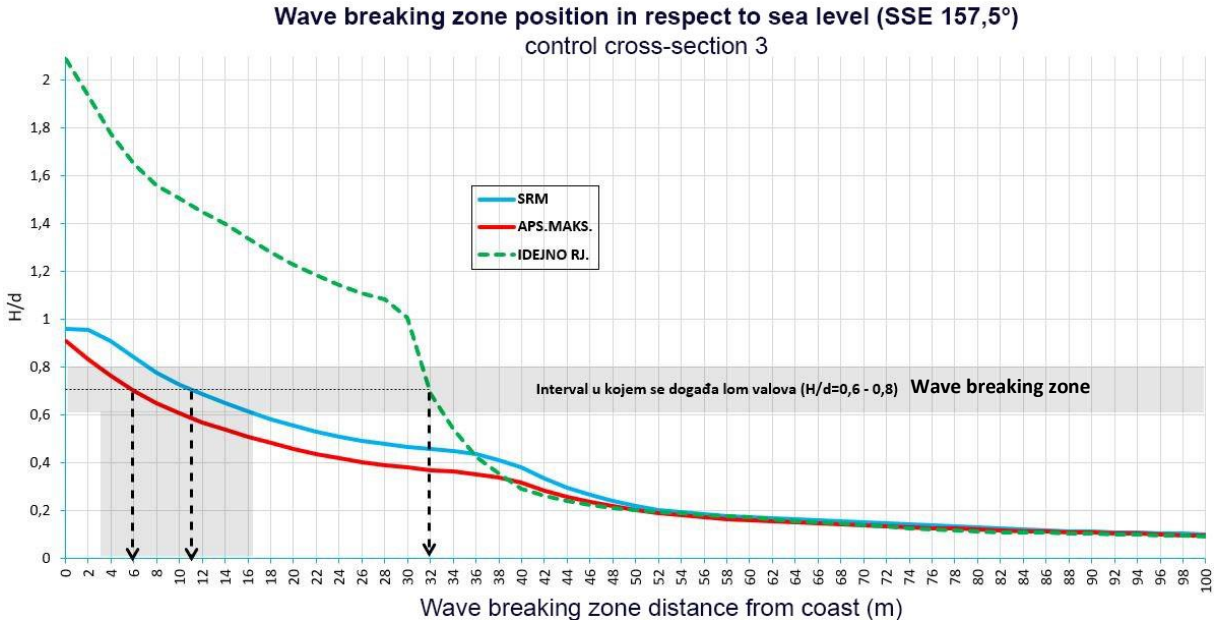

Figure 8.17 – Position of wave breaking zone relative to sea level for wave direction SSE (157.5°) for cross-sectional cross-section 3, Podgora (Makarska Riviera)

As is evident from Figures 6.43 and 6.44 for numerical simulations with wave direction SSE (157.5°), wave breaking zones with both analyzed sea levels, reveal that wave breaking occurs in the immediate vicinity of the coastal line in question and on the coastal line itself. Due to the rotation of the wave fronts towards the coastline, as can be seen from Figure 6.41, the waves due to the transformations they experience, primarily due to the processes of refraction and diffraction, slightly lose at wave height and bring most of the wave energy to the coast where their breakage occurs. This is best evident from cross-section 3, from which it is observed that for simulations with elevated sea level, i.e., with a level corresponding to the absolute maximum, the wave breaking zone moves towards the shore by approximately 5 meters in relation to the simulation with sea level corresponding to the middle sea level (SRM) (Figure 8.17).

The results of the numerical simulation A17 for the proposal of the conceptual design of the Podgora beach with a sea level corresponding to the absolute maximum, show that the zone of wave breaking is moving towards the open sea (Figure 6.45). This is best seen from the control section, from which it is noticed that it is a shift of 26 meters in relation to the numerical simulation for the existing state and the level corresponding to the absolute maximum (8.17).

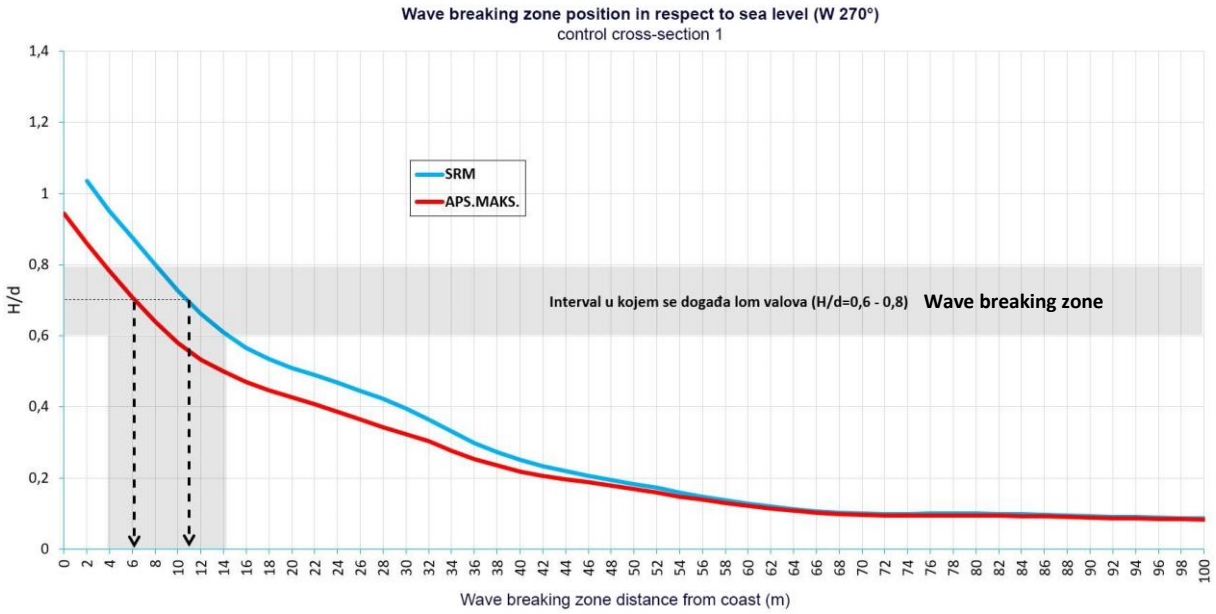

Figure 8.18 – Position of wave breaking zone relative to sea level for wave direction W (270°) for cross-section1, Podgora (Makarska Riviera)

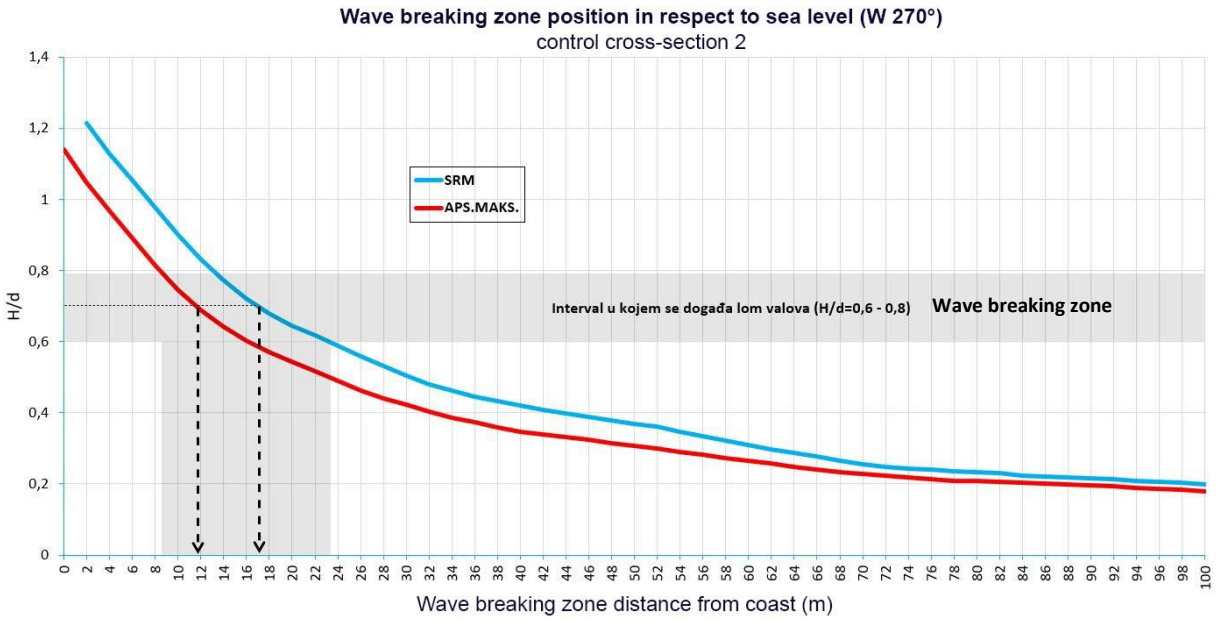

Figure 8.19 – Position of wave breaking zone relative to sea level for wave direction W (270°) for cross-sectional cross-section 2, Podgora (Makarska Riviera)

For numerical simulations for wave direction W (270°), as seen from Figures 6.52 and 6.53, wave breaking occurs in the immediate vicinity of the subject coastal line and on the coastal line itself. The wave fronts are directly directed at the northern coastal line of the respective belt, while in the southern part of the coverage there are wave fronts rotating towards the coastline, which is visible from Figure 6.50. Waves due to the transformations they experience, primarily due to the processes of refraction and diffraction, slightly lose at wave height and bring most of the wave energy where their break occurs in the immediate vicinity of the beach coastline. This is best visible from the control sections (sections 1 and 2), from which it is observed that for simulations with elevated sea level, i.e., with a level corresponding to the absolute maximum, the wave breaking zone moves towards the coast by approximately 5 meters in relation to the simulation with sea level corresponding to the middle sea

level (SRM) (figures 8.18 and 8.19).

In conclusion, regarding the analysis of the appearance of the wave breaking zone for the Podgora beach on the Makarska Riviera, it can be said that Podgora beach is under the considerable influence of the wave breaking process, which is one of the most important erosive processes for grainy beaches. The results of the numerical analysis undoubtedly point to a very high degree of beach vulnerability due to potential sea level rise, as a result of climate change. This is reflected in the drastic shift of wave breaking zones towards the coast for all conducted numerical simulations with a sea level corresponding to the absolute maximum. Therefore, it can be concluded that the beach in the coming period, if the predictions regarding sea level rise are realized, will be under increasing erosive pressure, which could ultimately result in its complete degradation and disappearance if timely activities are not undertaken in terms of the realization of protective construction interventions in the land area and the waters of the beach. On the example of the proposed conceptual design for the control area of Podgora beach, the correct concept of solving detected beach erosion problems is shown, because the wave breaking zones for simulations with the conceptual solution significantly move from the mainland to the sea and thus contribute to increasing the degree of protection of the beach from erosion. This concept represents a quality and coherent basis for the adoption of general guidelines for the protection of beaches from granular materials.

8.3.2. Analysis of the potential transport of beach material calculation results

In order to calculate the potential of sediment transport for a particular point on the considered beach, it is necessary to know the wave height parameter *Hs* at that point, which indicates the potential amount of energy that waves bring to the shore, with the help of which the wave energy flow can be calculated *Pl*, which serves to estimate the size of the potential transport of beach material due to wave-induced currents (Pernat Ž., Vranješ M, 2012).

Based on the analysis given in chapter 7.1.3. of this study, a very high potential for the transport of beach material for the existing state was determined for the Podgora beach on the Makarska Riviera. The analysis considered the dominant direction of the incident waves, and observed variations in the power of the Pl wave along the set control cross-section 100 meters long, whereby increased values for the existing state were detected. Based on the results of numerical modeling, a conclusion was reached about the necessity of undertaking protective construction interventions in the waters in question, and accordingly a proposal for a conceptual design for the control area of the beach in question was made, for which the previously described procedure of observing the variation of the wave Pl along the set control cross-section was also carried out, as well as for the existing situation. Interventions in the land area and the waters of the beach, according to the conceptual design, brought a significant improvement in the situation in terms of the transport of beach material.

In conclusion, regarding the analysis of the calculation of the transport of beach material for Podgora beach on the Makarska Riviera, it can be said that Podgora beach is under a significant hydrodynamic influence that contributes to its high potential of beach material transport from which it is made. On the example of the conceptual design for the control area of Podgora beach, the correct concept of solving detected problems of increased potential transport of beach material, which represents a quality and coherent basis for the adoption of general guidelines for the protection of beaches from granular materials, has been demonstrated.

8.4. Podstrana-Duće area

8.4.1. Analysis of the numerical modeling results

Numerical simulations of waves for beaches on the Podstrana-Duće area were conducted for three

directions of incident waves. These are the following wave directions: SE (135°), SSW (202.5°) and W (270°). Numerical simulations with two sea levels were performed for each of these directions, for the mean sea level (SRM) and the absolute maximum, all in accordance with Table 6.1.

Simulations were carried out for the existing state and the proposal of the conceptual design. Namely, based on the results of numerical simulations and detected problems, a proposal for the control area of Podstrana beach was made in order to eliminate them, and raise the general level of sustainability and resilience of the beach. The conceptual design is conceived by applying basic construction and technical principles (more in Chapter 5), and it is about placing an underwater stone reef at the appropriate distance and depth, and additional plan correction of three existing stone groynes with addition nourishment of the beach with appropriate beach material.

8.4.1.1. Analysis of wave propagation results and wave height fields

In addition to the two-dimensional representation of wave height fields given in Chapter 6 of this study, three control cross-sections of individual lengths of 100 meters (Figure 8.20) were set up in which a detailed observation of wave height variations for simulations with individual directions of incident waves for the mean sea level of SRM was performed (Figures 8.21 to 8.23).

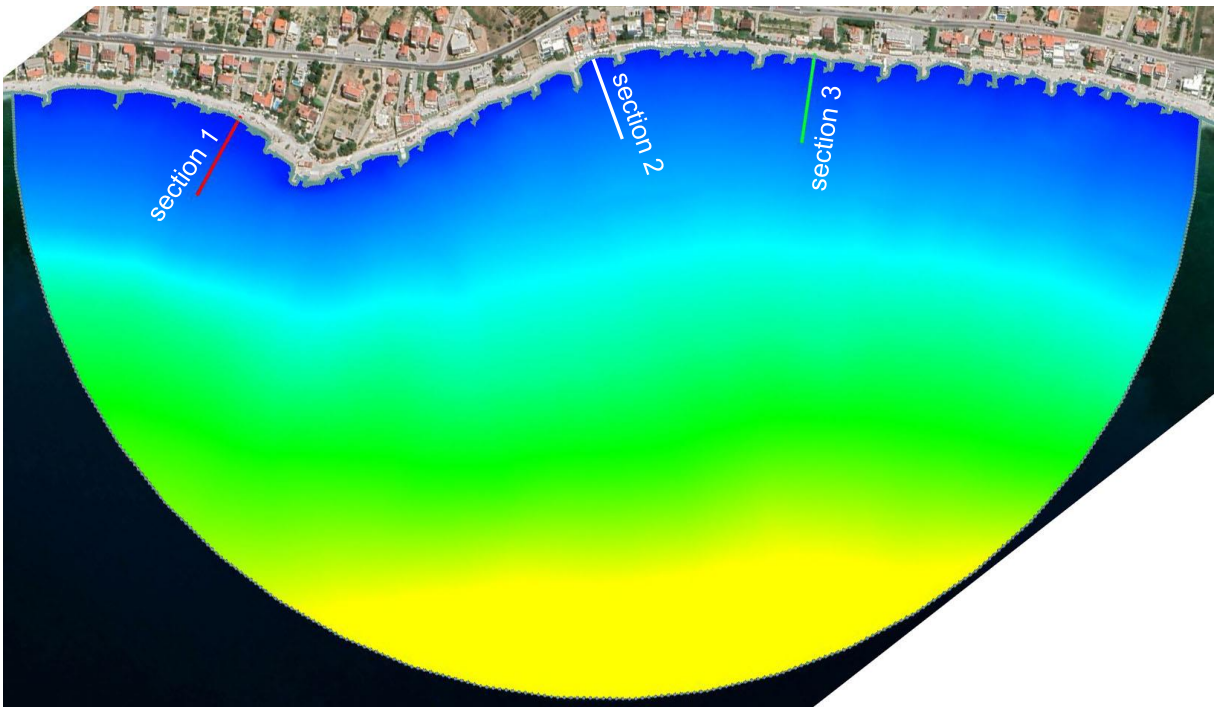

Figure 8.20 – Position of control cross-sections for beaches on the Podstrana-Duće area

The results of numerical modeling for simulation A18 (existing state, direction SE, SRM) show the expected direct exposure of the entire coastal belt of Podstrana beaches to the incident waves. In accordance with the display of fields of significant wave heights (Figure 6.55), it is evident that the highest wave heights appear in the immediate vicinity of the beach line itself. In their encounter towards the shore, the wave fronts tend to rotate towards the shore, due to transformational processes of diffraction and refraction, which is clearly visible from the image of the current wave outline (figure 6.54). In this area, the wave experiences transformations and deformations, simultaneously relaxing wave energy in the form of wave breaking.

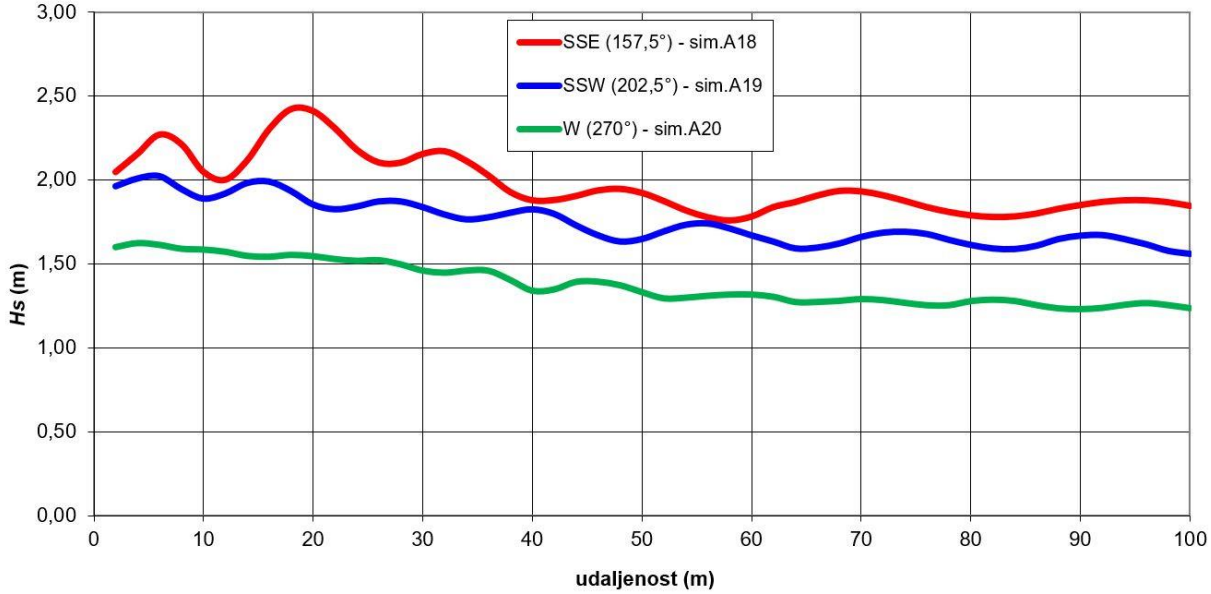

Figure 8.21 – Variation of wave heights *Hs* in control cross-section 1, Podstrana

The results of numerical modeling for simulation A19 (existing state, direction SSW, SRM) show the expected direct exposure of the entire coastal belt of Podstrana beaches to the incoming waves. In accordance with the display of fields of significant wave heights (Figure 6.60), it is evident that the highest wave heights occur in the immediate vicinity of the coastline of the beach. In their encounter towards the shore, the wave fronts directly hit the coastline, with only slight rotations around the capes and groynes, due to the transformational processes of diffraction and refraction, which is clearly visible from the image of the current wave outline (Figure 6.59). This wave direction brings the same level of wave energy throughout the coastal belt, while relaxing it in the form of wave breaking.

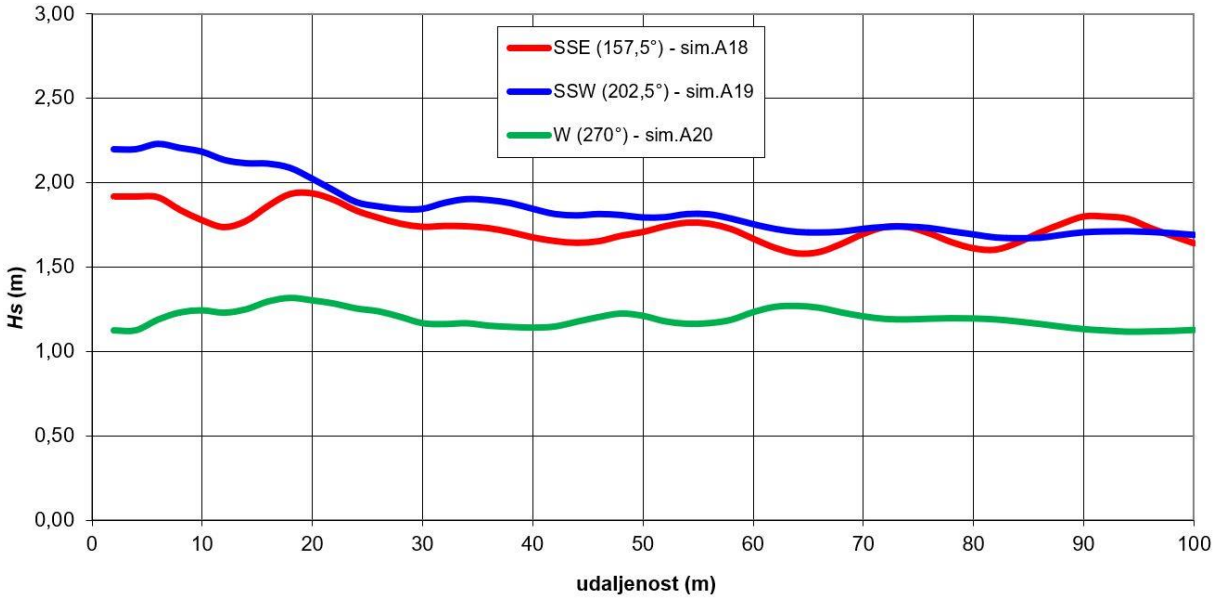

Figure 8.22 – Variation of wave heights *Hs* in control cross-section 2, Podstrana

The results of numerical modeling for simulation A20 (existing state, direction W, SRM) show the expected direct exposure of parts of the coastal belt of Podstrana beaches that are oriented more westwards by incident waves. In accordance with the display of fields of significant wave heights (Figure 6.65), it is evident that the highest wave heights appear in the immediate vicinity of the

coastline precisely in these parts of the beach. In their encounter towards the shore, the wave fronts tend to rotate towards the shore, due to transformational processes of diffraction and refraction, which is clearly visible from the image of the current wave outline (figure 6.64). In this area, the wave experiences transformations and deformations, simultaneously relaxing wave energy in the form of wave breaking.

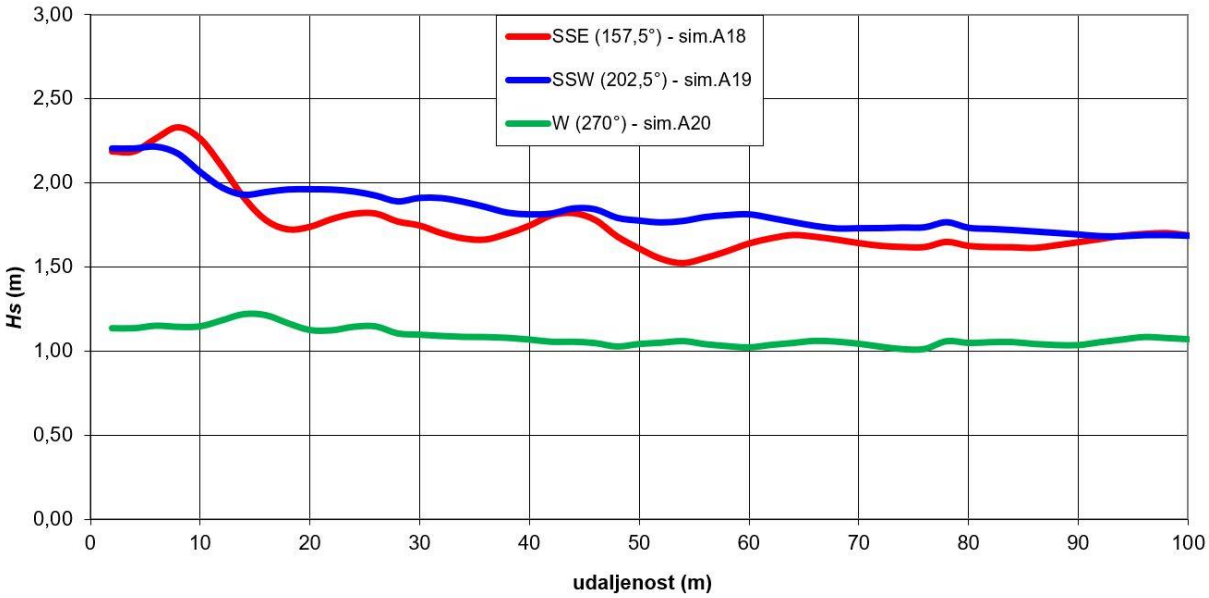

Figure 8.23 – Variation of wave heights *Hs* in control cross-section 3, Podstrana

In conclusion, regarding the analysis of the propagation of waves and wave height fields for beaches on the Podstrana-Duće area, it can be said that the beaches in question are under considerable influence of the incident waves. The results of the numerical analysis undoubtedly indicate a very high degree of exposure of the entire coastal zone, which implies the conclusion that it experiences large hydrodynamic influences, which have a significant impact on its beach material, especially for waves from the directions SE (135°) and SSW (202.5°). This is very well visible in the real state, where the dynamic process of continuous lynching of beach material and simultaneous removal into the deeper sea during the year, precisely during the duration of these waves, is evident.

8.4.1.2. Analysis of wave breaking zone results

For the analysis of the wave breaking zone, as the main cause of beach erosion from granular materials, the results of simulations that were conducted with the same directions of incident waves for different sea levels were compared. The comparison of these results gave an answer to the question of how much potential sea level rise, as a result of climate change, will have an impact on the beach in question.

In addition to the two-dimensional representation of wave breaking zones given in Chapter 6 of this study, three control sections of individual lengths of 100 meters (Figure 8.20) were set up in which a detailed observation and comparison of the position of the wave breaking zone for simulations of one direction and different sea levels was performed (Figures 8.24 to 8.32).

As is evident from Figures 6.56 and 6.57 for numerical simulations with the direction of waves SE (135°), wave breaking zones from both analyzed sea levels, reveal that wave breaking occurs in the immediate vicinity of the coastal line in question and on the coastal line itself. Due to the rotation of the wave fronts towards the coastline, which is evident from Figure 6.54, the waves due to the transformations they experience, primarily due to the processes of refraction and diffraction, slightly

lose at wave height and bring most of the wave energy to the coast where their breakage occurs. This is best evident from all three set control sections, from which it is observed that for simulations with elevated sea level, i.e., with a level corresponding to the absolute maximum, the wave breaking zone moves towards the coast by approximately 25-30 meters in relation to simulations with sea level corresponding to the middle sea level (SRM) (Figures 8.24 to 8.26).

Similar tendencies in the movement of wave breaking zones can be observed for other analyzed wave directions (SSW and W), which is also best observed from the graphics given in Figures 8.27 to 8.29 for the Direction of SSW and in Figures 8.30 to 8.32 for direction W.

The results of numerical simulations A24, A25 and A26, for the proposal of the conceptual design of Podstrana beach with a sea level corresponding to the absolute maximum, show that the zones of wave breaking for all three analyzed wave directions (SE, SSW and W) move towards the open sea (figures 6.58, 6.63 and 6.68). This is best seen from the control sections, from which it is a shift of 10-20 meters in relation to numerical simulations for the existing state and a level corresponding to the absolute maximum (Figures 8.25, 8.28 and 8.32).

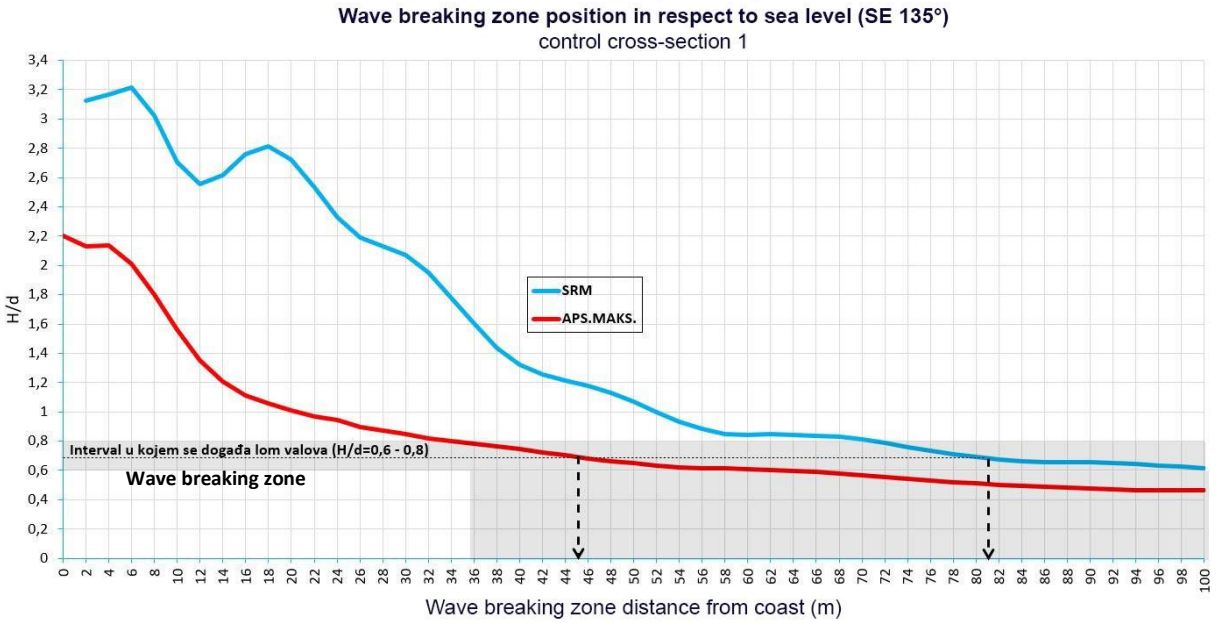

Figure 8.24 – Position of wave breaking zone relative to sea level for wave direction SE (135°) for cross-section 1, Podstrana-Duće area

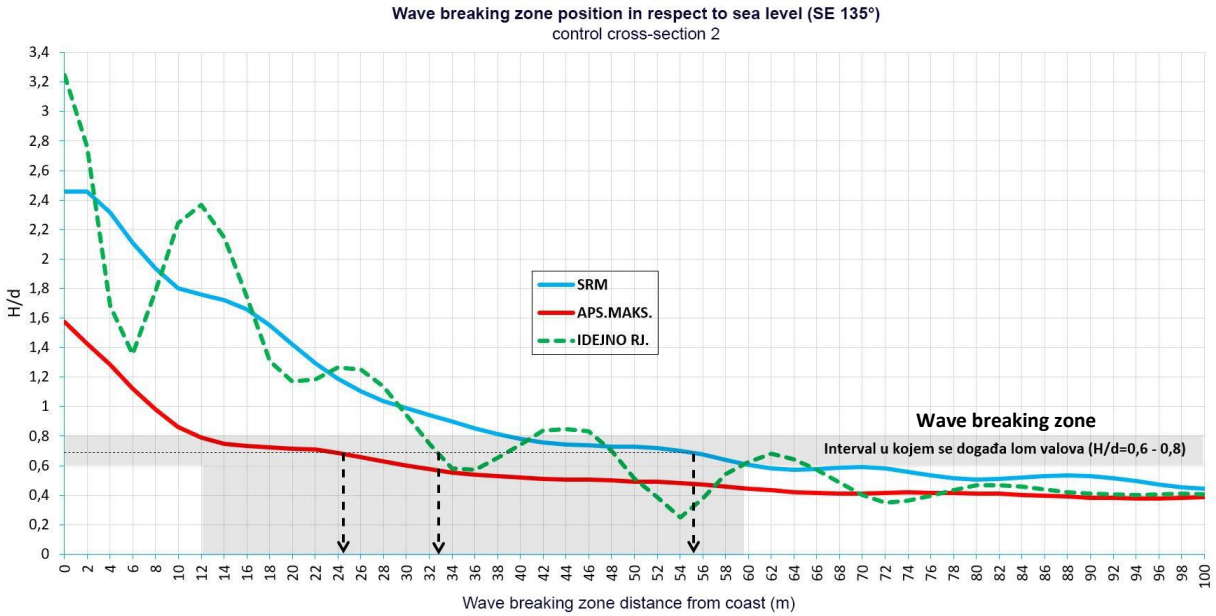

Figure 8.25 – Position of wave breaking zone relative to sea level for wave direction SE (135°) for cross-section 2, Podstrana-Duće stroke

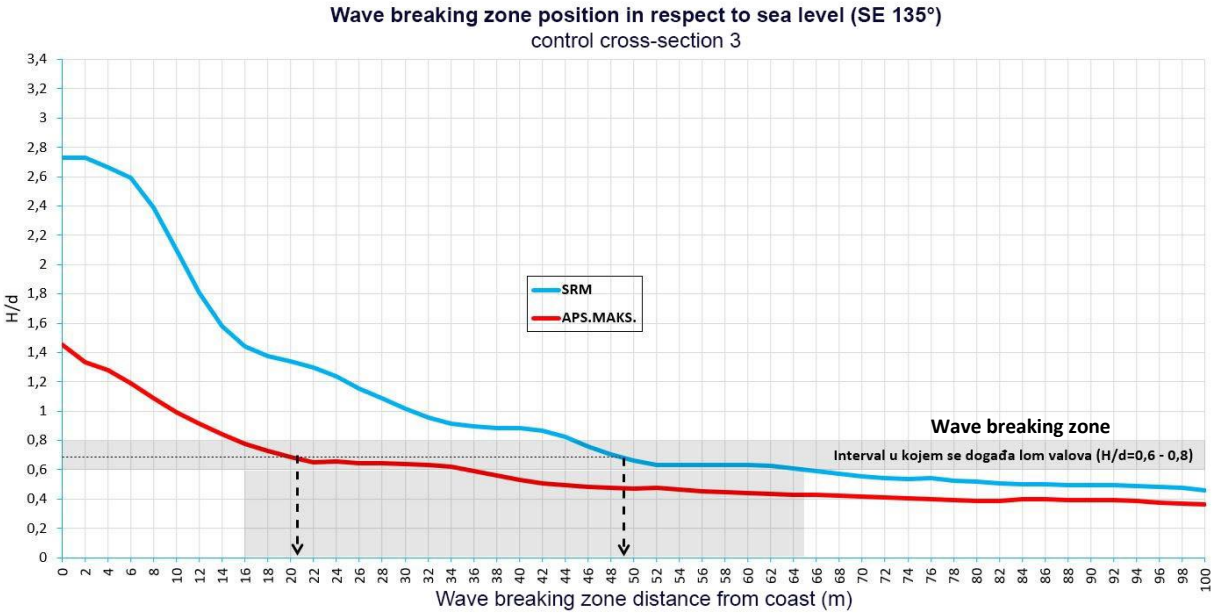

Figure 8.26 – Position of wave breaking zone relative to sea level for wave direction SE (135°) for cross-section 3, Podstrana-Duće stroke

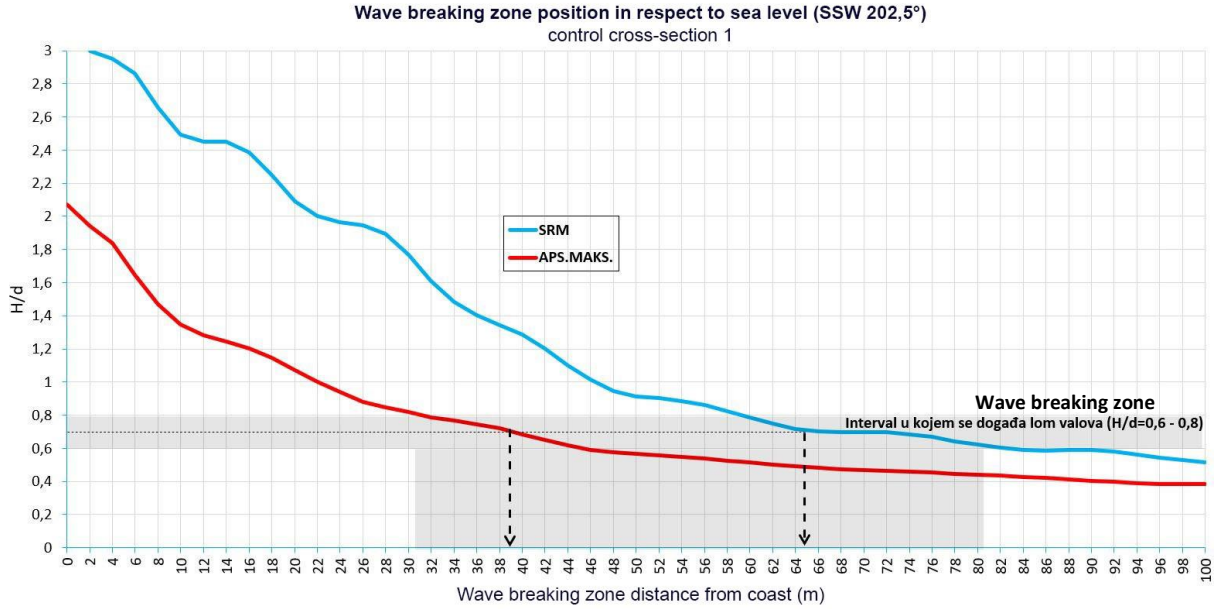

Figure 8.27 – Position of wave breaking zone relative to sea level for wave direction SSW (202.5°) for cross-section 1, Podstrana-Duće

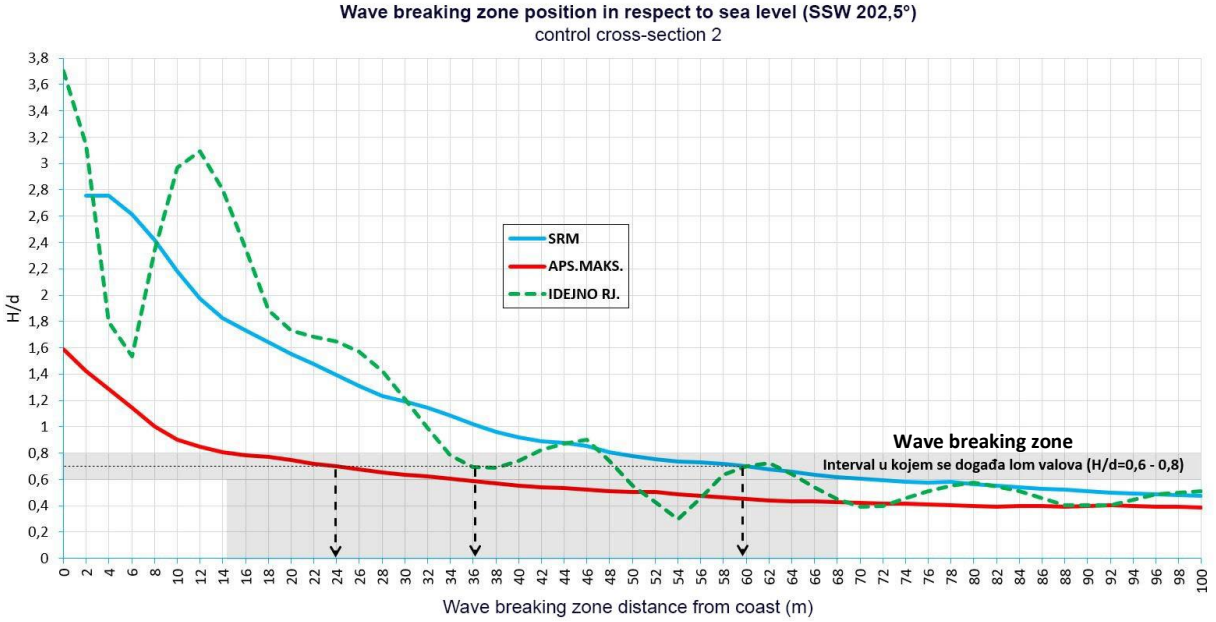

Figure 8.28 – Position of wave breaking zone in relation to sea level for wave direction SSW (202.5°) for cross-section 1, Podstrana-Duće area

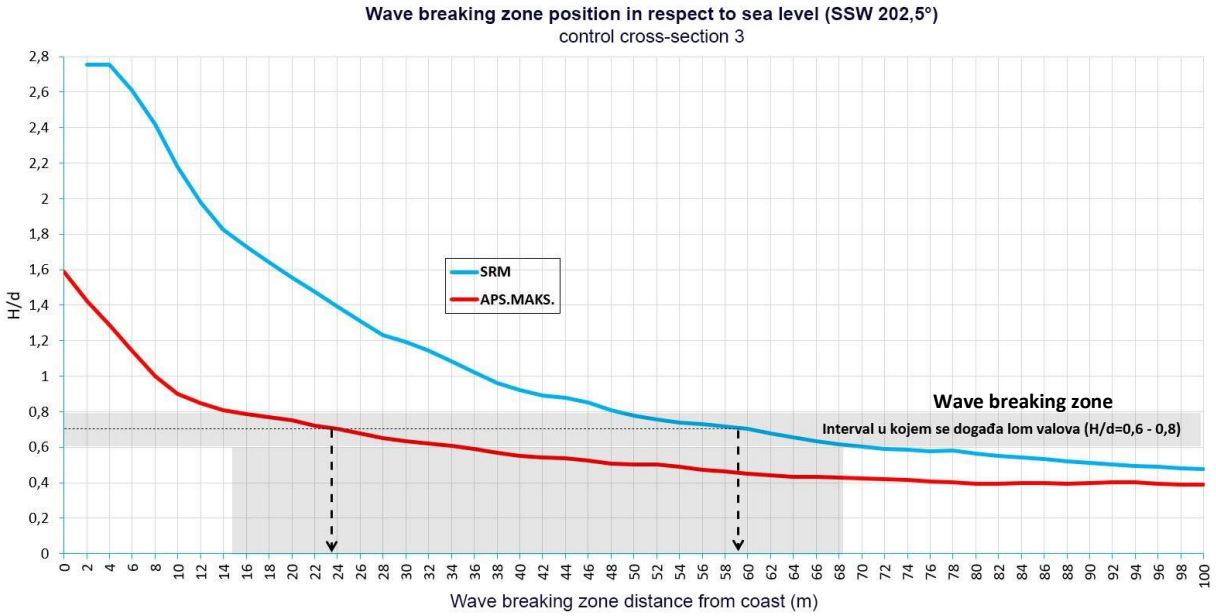

Figure 8.29 – Position of wave breaking zone relative to sea level for wave direction SSW (202.5°) for cross-section 3, Podstrana-Duće area

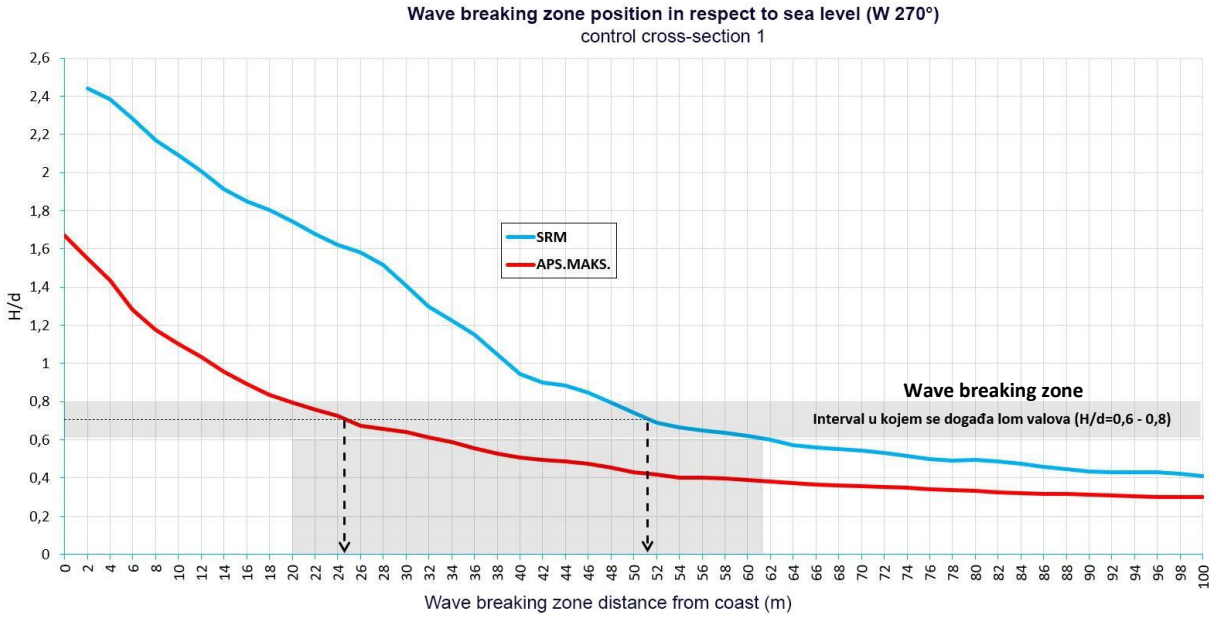

Figure 8.30 – Position of wave breaking zone relative to sea level for wave direction W (270°) for cross-section 1, Podstrana-Duće area

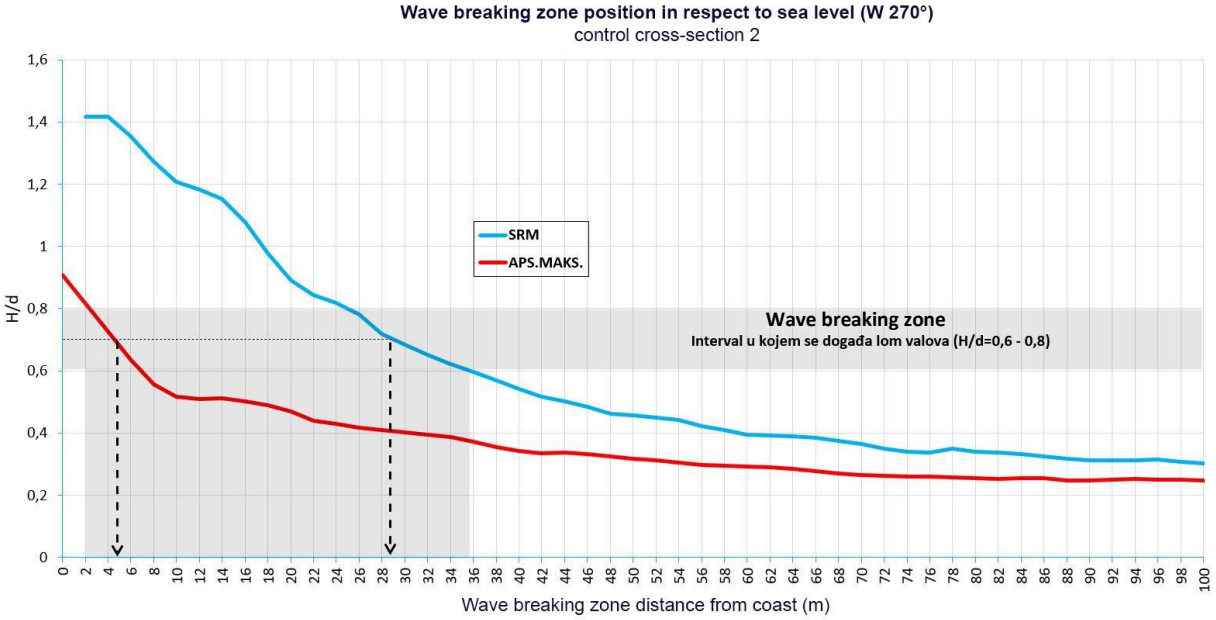

Figure 8.31 – Position of wave breaking zone relative to sea level for wave direction W (270°) for cross-section 2, Podstrana-Duće stroke

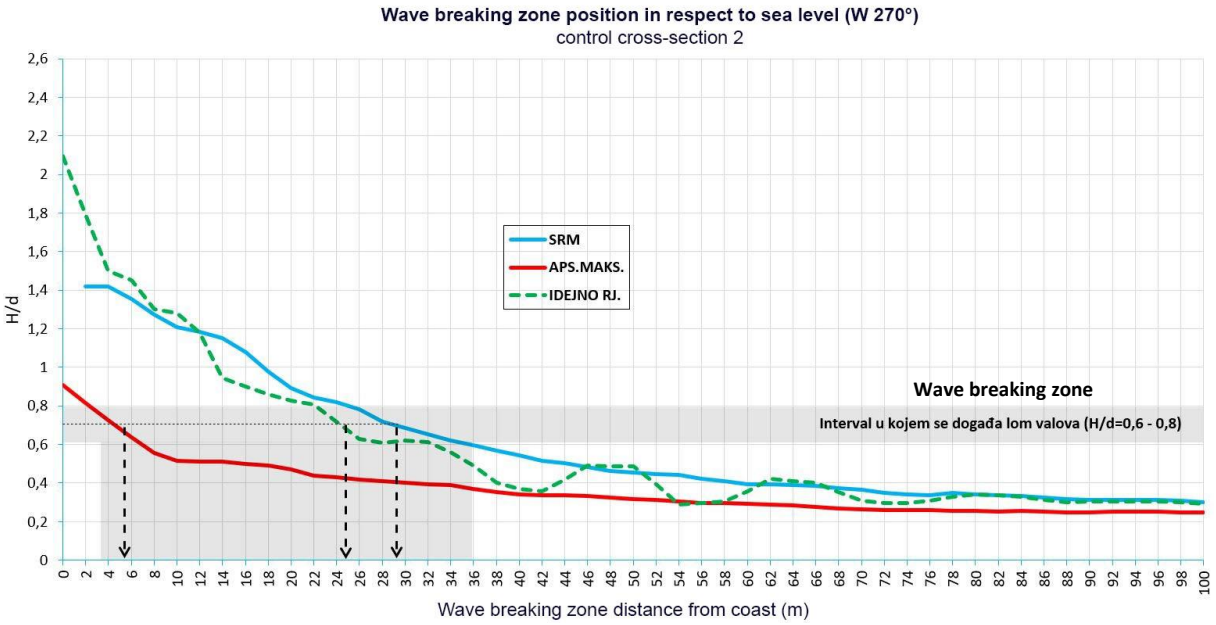

Figure 8.32 – Position of wave breaking zone relative to sea level for wave direction W (270°) for cross-section 3, Podstrana-Duće

In conclusion, as far as the analysis of the wave breaking zone for Podstrana beach is concerned, it can be said that the beaches are significantly influenced by the wave breaking process, which is one of the most important erosive processes for grainy beaches. The results of the conducted numerical analysis undoubtedly point to a very high degree of beach vulnerability due to potential sea level rise, as a result of climate change. This is reflected in the drastic shift of wave breaking zones towards the coast for all conducted numerical simulations with a sea level corresponding to the absolute maximum. Therefore, it can be concluded that the beaches in the coming period, if the predictions regarding rising sea levels are realized, will be under increasing erosive pressure, which could ultimately result in their complete degradation and disappearance if timely activities are not undertaken in terms of the realization of protective construction interventions in the land area and the waters of the beach. On the example of the proposed conceptual design for the control area of Podstrana beach, the correct

concept of solving detected beach erosion problems has been shown, because wave breaking zones for simulations with a conceptual solution significantly move from the mainland to the sea and thus contribute to increasing the degree of protection of the beach from erosion. This concept represents a quality and coherent basis for the adoption of general guidelines for the protection of beaches from granular materials.

8.4.2. Analysis of the potential transport of beach material calculation results

In order to calculate the potential of sediment transport for a particular point on the considered beach, it is necessary to know the wave height parameter *Hs* at that point, which indicates the potential amount of energy that waves bring to the shore, with the help of which the wave energy flow can be calculated *Pl*, which serves to estimate the size of the potential transport of beach material due to wave-induced currents (Pernat Ž., Vranješ M, 2012).

Based on the analysis given in Chapter 7.1.4 of this study, a very high potential for the transport of beach material for the existing state was determined for the beaches on the Podstrana-Duće area. The analysis considered the dominant directions of the incoming waves, and observed variations in the wave power *Pl* along the set control cross-sections, whereby increased values were detected. Based on the results of numerical modeling, a conclusion was reached about the necessity of undertaking protective construction interventions in the waters in question, and accordingly a proposal for a conceptual design for the control area of the beach in question was made, for which the previously described procedure of observing the variation of the wave Pl along the set control cross-section was also carried out, as well as for the existing situation. Interventions in the land area and the waters of the beach, according to the conceptual design, brought a significant improvement in the situation in terms of the transfer (transmission) of beach material.

In conclusion, regarding the analysis of the calculation of the transport of beach material for beaches on the Podstrana-Duće area, it can be said that the beaches on this stretch are under a significant hydrodynamic influence that contributes to their high potential for the transport of sedimentary material from which they are made. On the example of the conceptual design for the control area of Podstrana beach, the correct concept of solving detected problems of increased potential transport of beach material, which represents a quality and coherent basis for the adoption of general guidelines for the protection of beaches from granular materials, has been shown.

8.5. Kašjuni (Split)

8.5.1. Analysis of the numerical modeling results

Numerical simulations of waves for Kašjuni beach in Split were conducted for two directions of incident waves. These are the following wave directions: SSW (202.5°) and W (270°). Numerical simulations with two sea levels were performed for each of these directions, for the mean sea level (SRM) and the absolute maximum, all in accordance with Table 6.1.

Simulations were carried out for the existing state and the proposal of the conceptual design. Namely, based on the results of numerical simulations and detected problems, a proposal for the area of Kašjuni beach was made in order to eliminate them, and raise the general level of sustainability and resilience of the beach. The conceptual design is conceived by applying the basic construction and technical principles (more in chapter 5), and it is about setting the underwater stone reef at the appropriate distance and depth, and the construction of a groyne on the north side of the bay, on its westernmost part with the addition nourishment of the beach with appropriate beach material.

8.5.1.1. Analysis of wave propagation results and wave height fields

In addition to the two-dimensional representation of wave height fields given in Chapter 6 of this study, two control cross-sections of individual lengths of 100 meters (Figure 8.32) were set up in which a detailed observation of wave height variations for simulations with individual directions of incident waves for the mean sea level (SRM) was performed (Figures 8.34 and 8.35).

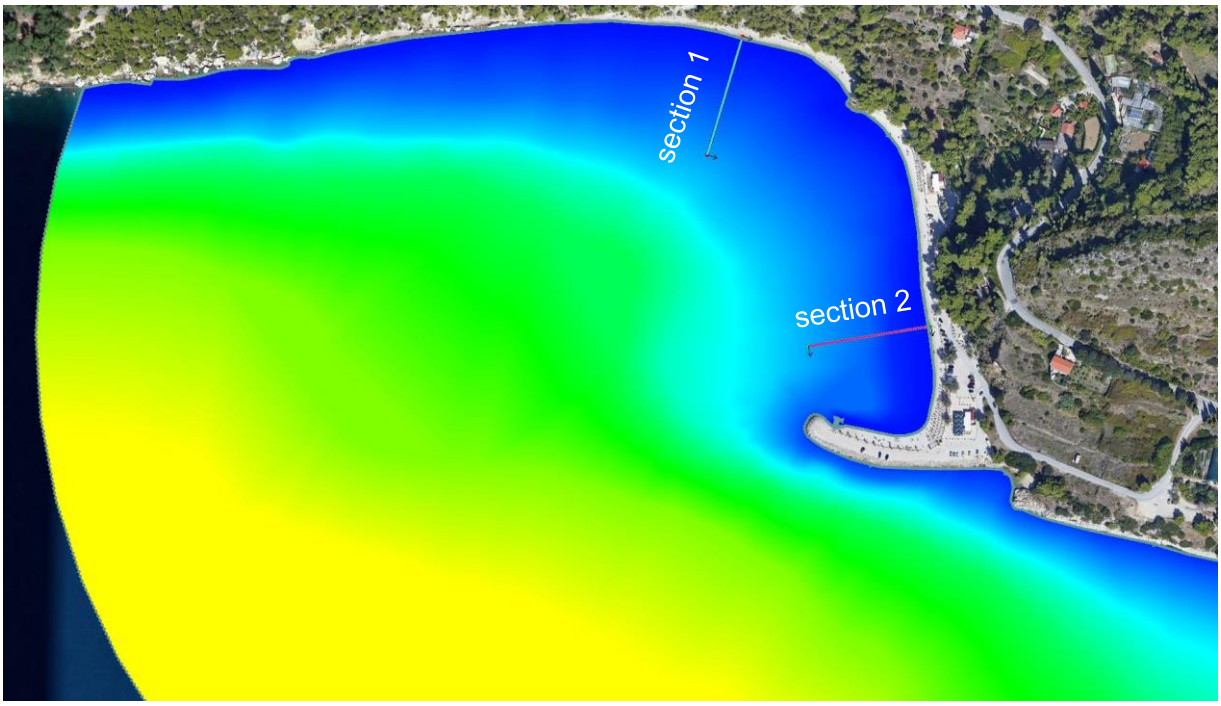

Figure 8.33 – Position of control sections for Kašjuni beach (Split)

The results of numerical modeling for simulation A27 (existing state, direction SSW, SRM) show the way of penetrating incident waves from this direction into the area of the beach itself, after the waves cross the tip of the protective groyne /breakwater. In accordance with the display of fields of significant wave heights (Figure 6.70), it is evident that a significant part of the wave energy is lost precisely on the groyne/breakwater, but some of this energy still reaches the beach line. In their encounter towards the beach, the wave fronts rotate around the tip of the groyne/breakwater, due to transformational processes of diffraction and refraction, which is clearly visible from the image of the current wave outline (figure 6.69).

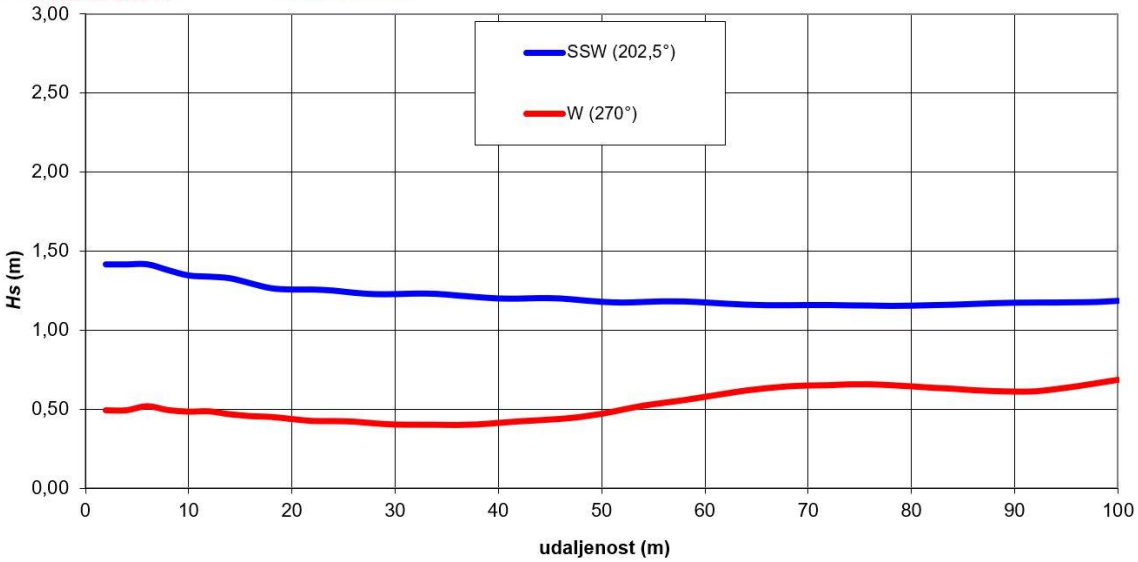

Figure 8.34 – Variation of wave heights *Hs* in control cross-section 1, Kašjuni (Split)

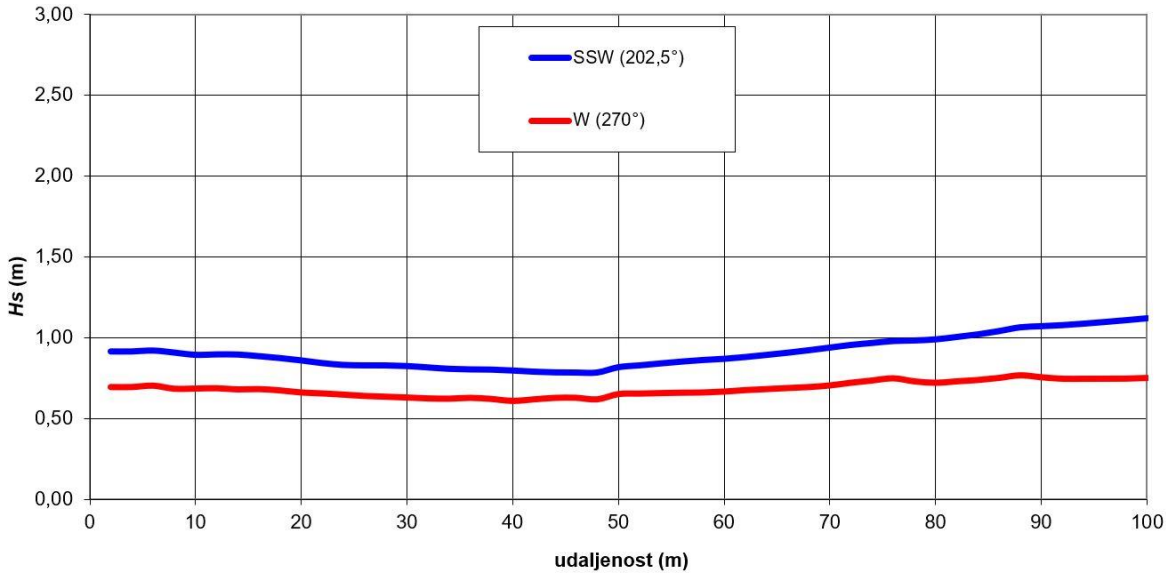

Figure 8.35 – Wave height variation *Hs* in control cross-section 2, Kašjuni (Split)

The results of numerical modeling for simulation A28 (existing state, direction W, SRM) show the expected direct exposure of the entire coastal belt of Kašjuni beach to the incident waves. In accordance with the display of fields of significant wave heights (Figure 6.75), it is evident that the highest wave heights appear shortly before entering the waters of the beach, and in the immediate vicinity of the beach line due to the process of encountering waves in the shallower sea. In their encounter towards the coast, the wave fronts remain directly directed towards the coastline, with only slight rotations around the groyne/breakwater and the northern envelope of the beach, due to transformational processes of diffraction and refraction, which is clearly visible from the image of the current wave outline (figure 6.74).

In conclusion, regarding the analysis of the propagation of waves and wave height fields for the beaches of Kašjuni in Split, it can be said that the beaches in question are under the noticeable influence of the incident waves. The results of the numerical analysis indicate a certain degree of exposure of certain parts of the coastal zone in question, especially the northern part. This implies the conclusion that part of the beach experiences noticeable hydrodynamic influences, which are reflected in the morphology of the beach and the dynamics of beach material. Especially problematic is the

appearance of waves from the direction of SSW (202.5°), which is very well visible in the real state, where during these waves a dynamic process of continuous erosion of the northern part of the coast occurs.

8.5.1.2. Analysis of wave breaking zone results

For the analysis of the wave breaking zone, as the main cause of beach erosion from granular materials, the results of simulations that were conducted with the same directions of incident waves for different sea levels were compared. The comparison of these results gave an answer to the question of how much potential sea level rise, as a result of climate change, will have an impact on the beach in question.

In addition to the two-dimensional representation of wave breaking zones given in Chapter 6 of this study, two control sections of individual lengths of 100 meters (Figure 8.33) were set up in which a detailed observation and comparison of the position of the wave breaking zone for simulations of one direction and different sea levels was performed (Figures 8.36 to 8.38).

As is evident from Figures 6.71 and 6.72 for numerical simulations with wave direction SSW (202.5°), wave breaking zones with both analyzed sea levels, reveal that wave breaking occurs in the immediate vicinity of the coastline in question and on the coastal line itself. Due to the rotation of the wave fronts behind the existing groyne/breakwater, towards the coastline, as can be seen from Figure 6.69, the waves due to the transformations they experience, primarily due to the processes of refraction and diffraction, slightly lose at wave height and bring a fair amount of wave energy to the coast where their breakage occurs. This is observed at both control cross-sections, where it is observed that for simulation with elevated sea level, i.e., with a level corresponding to the absolute maximum, the wave breaking zone moves towards the shore by approximately 20 meters in relation to the simulation with sea level corresponding to the middle sea level (SRM) (figures 8.36 and 8.37).

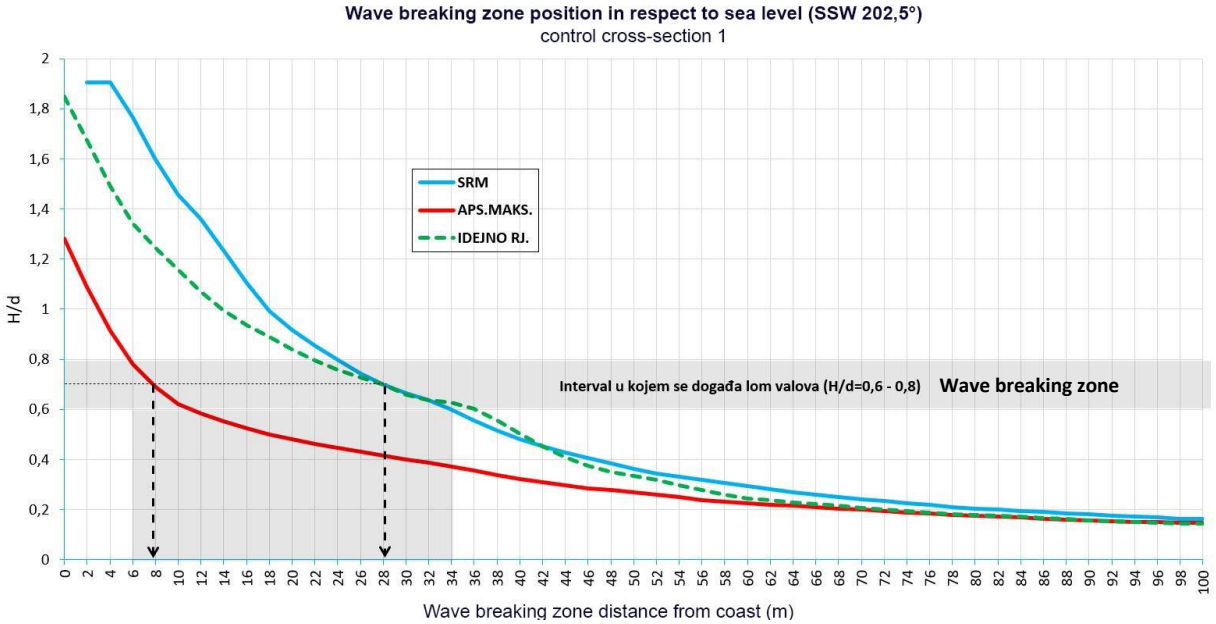

Figure 8.36 – Position of wave breaking zone relative to sea level for wave direction SSW (202.5°) for cross-section 1, Kašjuni beach (Split)

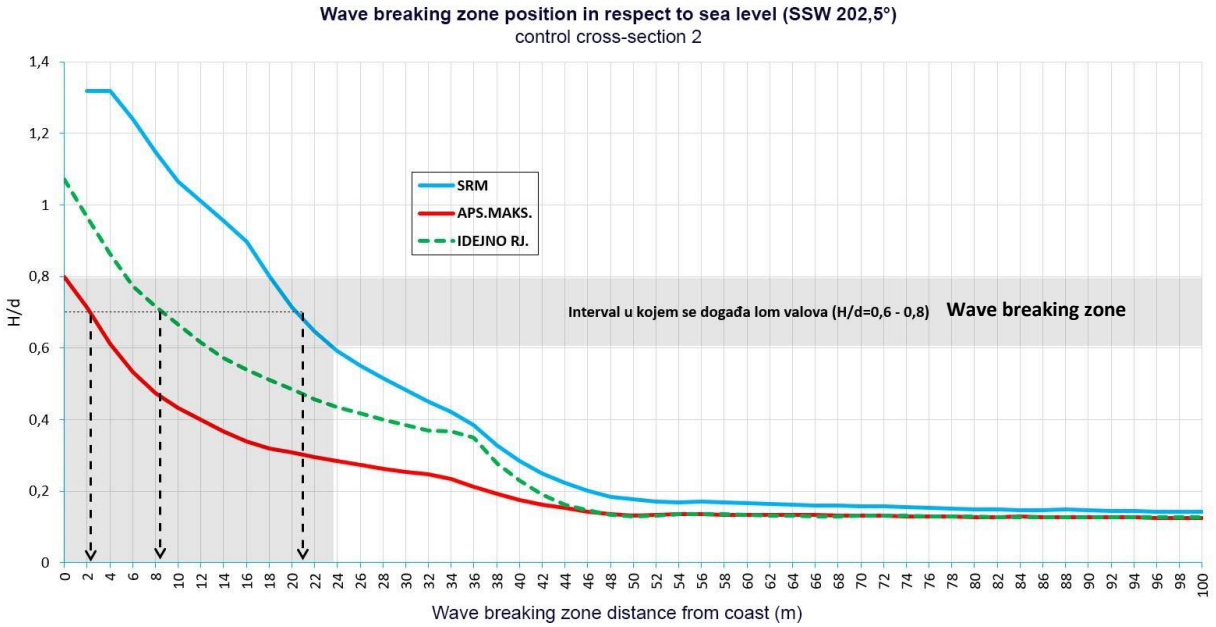

Figure 8.37 – Position of wave breaking zone relative to sea level for wave direction SSW (202.5°) for cross-section 2, Kašjuni beach (Split)

A similar tendency occurs for the second wave direction analyzed – W (270°), where in control cross-section 2 it is observed that for simulation with elevated sea level, i.e., with a level corresponding to the absolute maximum, the wave breaking zone moves towards the coast by approximately 16 meters in relation to the simulation with sea level corresponding to the middle sea level (SRM) (Figure 8.38).

The results of the numerical simulation A31 for the proposal of the conceptual design of Kašjuni beach with a sea level corresponding to the absolute maximum, show that the zone of wave breaking is moving towards the open sea (figure 6.73). This is best evident from the control cross-section 2, from which it is noticed that it is a shift of 14 meters in relation to the numerical simulation for the existing state and the level corresponding to the absolute maximum (8.38).

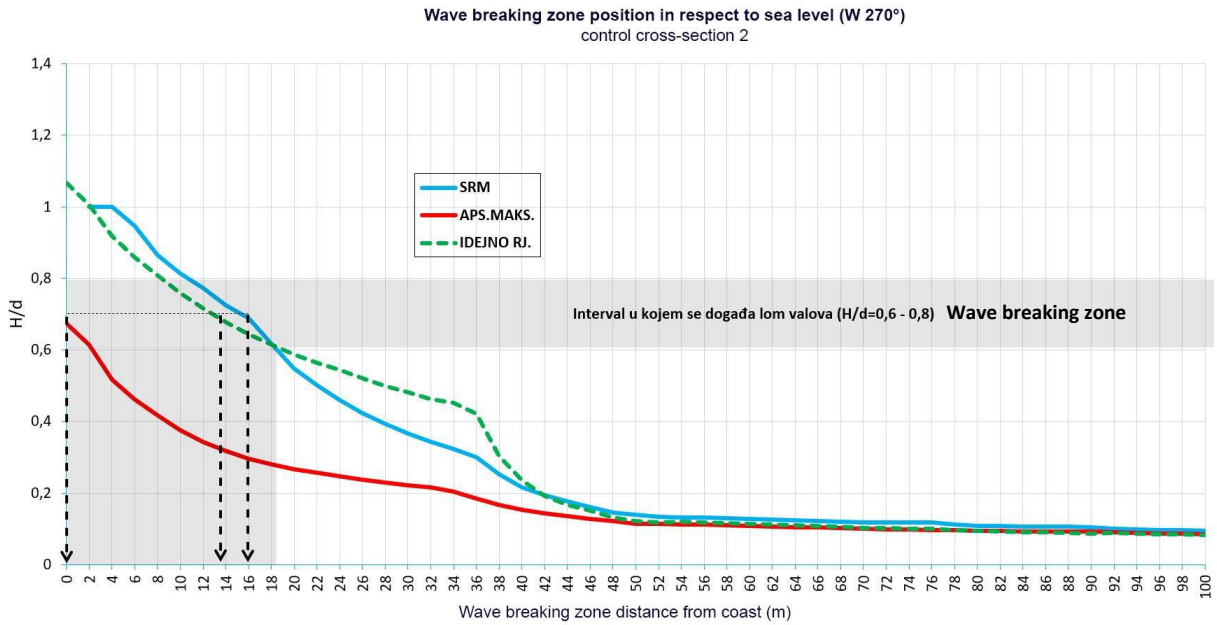

Figure 8.38 – Position of wave breaking zone relative to sea level for wave direction W (270°) for cross-section 2, Kašjuni beach (Split)

In conclusion, regarding the analysis of the occurrence of the wave breaking zone for Kašjuni beach in Split, it can be said that the beach is under the noticeable influence of the wave breaking process, which is one of the most important erosive processes for grainy beaches. The results of the conducted numerical analysis undoubtedly indicate a high degree of beach vulnerability due to potential sea level rise, as a result of climate change. This is reflected in the significant shift of wave breaking zones towards the coast for all conducted numerical simulations with a sea level corresponding to the absolute maximum. Therefore, it can be concluded that the beach in the coming period, if the predictions regarding rising sea levels are realized, will be under increasing erosive pressure, which could ultimately result in its gradual degradation if timely activities are not undertaken in terms of the realization of protective construction interventions in the subject land area and the waters of the beach. On the example of the proposed conceptual design for the control area of Kašjuni beach, the correct concept of solving detected beach erosion problems has been demonstrated, because the wave breaking zones for simulations with the conceptual design significantly move from the mainland to the sea and thus contribute to increasing the degree of protection of the beach from erosion. This concept represents a quality and coherent basis for the adoption of general guidelines for the protection of beaches from granular materials.

8.5.2. Analysis of the potential transport of beach material calculation results

In order to calculate the potential of sediment transport for a particular point on the considered beach, it is necessary to know the wave height parameter *Hs* at that point, which indicates the potential amount of energy that waves bring to the shore, with the help of which the wave energy flow can be calculated *Pl*, which serves to estimate the size of the potential transport of beach material due to wave-induced currents (Pernat Ž., Vranješ M, 2012).

Based on the analysis given in chapter 7.1.5. of this study, for Kašjuni beach in Split, a noticeable potential of transporting beach material for the existing state was determined. In the analysis, the dominant directions of incoming waves were considered, and variations of wave power *Pl* along the set control cross-sections were observed, with increased values detected. Based on the results of numerical modeling, a conclusion was reached about the necessity of undertaking protective construction interventions in the waters in question, and accordingly a proposal for a conceptual design for the control area of the beach in question was made, for which the previously described procedure of observing the variation of the wave Pl along the set control cross-section was also carried out, as well as for the existing situation. Interventions in the land area and the waters of the beach, according to the conceptual design, brought a significant improvement in the situation in terms of the transport of beach material.

In conclusion, regarding the analysis of the calculation of the transport of beach material for Kašjuni beach in Split, it can be said that the beach is under a noticeable hydrodynamic influence that contributes to the potential of transport of sedimentary material from which it is made. On the example of the conceptual design for the control area of Kašjuni beach, the correct concept of solving detected problems of increased potential transport of beach material, which represents a quality and coherent basis for the adoption of general guidelines for the protection of beaches from granular materials, is shown.

9. MEASURES TO ENSURE BEACH SUSTAINABILITY AND ADAPTATION TO CLIMATE CHANGES

9.1. General measures of stabilization and beach nourishment

In accordance with the conducted analysis from the previous chapters, which confirmed the correctness of the proposed methodology for solving the problem of erosion and the sustainability of beaches from granular materials, it is possible to adopt general measures of stabilization of beaches in order to ensure their sustainability in the current conditions and conditions that could bring the consequences of climate changes in the future, as well as measures of their artificial nourishment with new beach material.

As shown by the previous analysis for five selected beach locations in Split-Dalmatia County, this is a very complex problem, solving which should consider the peculiarities that each beach location brings, and a whole range of participating factors of importance for the considered beaches made of granular materials. Given the complex physical background of processes that dominantly affect the erosion and sustainability of beaches ultimately, it is necessary to use some of the numerical wave models when analyzing and solving the problem, which can model all the physical processes that affect beaches made of granular materials.

9.2. Effects of climate change on beach-relevant variables

The negative effects of climate changes, and in particular the impact of sea level rise and the occurrence of stormy weather, will have a significant impact on beaches made of granular materials. In addition to the increased erosion that will intensify due to these influences, it is expected to increase changes in their morphology, geometry and composition, which can consequently lead to their gradual degradation, even complete disappearance.

Therefore, in order to achieve the final goal, which is the stabilization of beaches for current and future conditions, it is important to detect and categorize zones or beaches, given the degree of threat due to potential changes, for which it will be necessary to adopt general plans for their preservation, but also concrete technical solutions that would reduce the potential of their erosion. The principle of categorization of beaches and beach zones shown for five selected locations within Split-Dalmatia County (table 9.1), should be made for the entire county coastal zone, and applied to other counties.

9.2.1. Impact of sea level variability

Given that wind surface waves are the main driving forces of changes in the morphology of beaches made of granular materials, in considering their impact on beach erosion, it is necessary to include, in addition to wave parameters of dominant waves, parameters based on which it is possible to estimate the degree of impact of rising sea levels as a result of climate change. Namely, if the conditions of the main driving forces of sediment transport and changes in the morphology of beaches change, and the increase in sea level is certainly one of the most important factors for this, then in the analysis for the assessment of the degree of vulnerability of beaches from erosion it is necessary to consider the mentioned changes in sea level.

In the analysis given as part of this study, the problem of potential sea rise as a result of climate changes was simulated by choosing an elevated sea level of 1 m, which approximately corresponds to the officially measured absolute maximum (92.3 cm) on the tide gauge set in the City Port of Split (Figure 2.12), whose data are relevant to the area of Split-Dalmatia County in question.

Choosing this increased sea level for analysis can be considered a reasonable assessment of sea level

elevation for the purpose of simulating potential sea level rise as a result of climate change, because it represents an approximate level that has already been detected in the past period and based on which it will be possible to give coherent conclusions about the potential dangers of beach erosion caused by rising seas. Choosing such a relatively significant increase in sea level can be called a "black scenario", because if it is achieved, it is difficult to expect that the problems of beach erosion will be in the foreground, but the population will primarily be preoccupied with some other significant problems and threats that such a rise could cause, such as flooding of wide coastal areas, etc.

However, in terms of the analysis of beach erosion given within this study, this approximation, i.e., the scenario of the consequences of rising sea levels due to climate changes, proved to be a good practice for analysis whose results clearly indicate evident trends of consequential changes on beaches. The obtained results are sufficiently coherent, clear and understandable in relation to the results of the analysis with the current sea level (medium sea level – SRM), which allows their quality extrapolation to the domain of even higher sea level than the analyzed level of 1 meter. Also, the results ensure quality interpolation in domain of raising marine levels lower than 1 meter.

The results of the analysis conducted in this way are sublimated through the conclusions of the analyses performed, and ultimately shaped within the given guidelines.

In general, it can be said that raising the sea level has a detrimental effect on beaches made of granular materials, exponentially increasing the degree of erosion given the size of this elevation.

9.2.2. Influence of precipitation variability

In addition to increasing the intensity and length of dry periods, because of climate changes, the intensity of short-term heavy precipitation is expected to increase, which increases the risk of flash floods characterized by increased water velocities that can cause great damage and additional erosive processes on beaches made of granular materials, and even in locations where they have not been expressed before. Also, a milder increase in the number of days with extreme precipitation is expected, the higher amounts and irregular frequency of which will affect existing beaches in terms of the ability and capacity of stormwater collection and drainage.

In this regard, it is necessary to apply the procedures of integral consideration and proper technical solution in the planning and design of coastal zones and zones of individual beaches, in order to adequately solve the observed and potential problems with torrential and precipitation drainage, which could bring potential problems with beach erosion from granular materials.

In the analysis procedures for finding quality technical solutions of torrential and stormwater drainage of coastal and beach spatial units, it is necessary to consider the impacts of sea level variability as a result of climate changes. Namely, these two processes interact together, superimposing their influences and therefore should not be viewed separately, but exclusively integrally.

9.3. Guidelines for beach planning and design

9.3.1. Assessment of impacts and limitations

The sequence of procedures of the analysis conducted here, i.e., the methodology, applied to five selected beaches in Split-Dalmatia County, has shown how complex a task the process of ensuring the sustainability of beaches made of granular materials, for existing and future conditions, is a complex task. Apart from the fact that each of the analyzed locations of selected beaches brings a separate spatial and influential aspect by which they differ from each other, and thus require different treatments in the analysis, it can be said that the same happens between individual zones within one beach, where on one beach stretch there can be zones that have completely different spatial and

influential specifics from each other.

For this reason, solving the problem of beach erosion and ensuring their sustainability, it is necessary to approach systematically, applying this study given methodological principles of analysis, in order to come to consistent and high-quality conclusions. The study applied procedures for analyzing the coastal areas in question for all selected beach locations, to determine the primary impacts for beaches made of granular materials. After conducting an analysis and assessment of the degree of vulnerability of individual beaches (Table 9.1), it was necessary to assess the possibilities and limitations for ensuring the improvement of the situation in the zones where potential erosion problems were detected (Table 9.2).

On this basis, for individual beaches, i.e., for certain zones within these beaches, for which there are objectively no obstacles to the realization of technical and construction protective interventions, examples of solving these problems are given in the scope of smaller spatial units, i.e., control zones, whose principles are applicable to the entire coastal zone in question with mandatory additional analysis. Namely, the scope of solving the issue of beach erosion for the entire coastal zones in question significantly exceeds the scope of elaboration of this study.

Table 9.1 – Impact rating for the considered beaches

BEACH	UTJECAJI					
	Previous vulnerability assessment[5]	General impact of waves	Impact of wave breaking	Material transport potential	Sea level rise	**Sum**
Zlatni rat	4	4	4	4	4	**20**
Stiniva	5	2	1	1	3	**10**
Podgora	3	4	4	4	4	**19**
Podstrana	3	4	4	3	3	**17**
Kašjuni	2	3	3	2	2	**12**

Rating from 1 to 5 (1 - the lowest impact, 5 - the highest impact)

The only exception in relation to the previously stated in the application of the proposed methodology are the beaches Zlatni rat on Brač and Stiniva on Vis, for which no construction protective interventions have been considered *a priori*, because the coastal areas of these two beaches are in the protected natural landscapes.

As stated, for all beaches, modeling was performed using a numerical model for the existing state with two analyzed sea levels (middle sea level – SRM and absolute maximum), while for the beaches of Podgora, Podstrana and Kašjuni, simulations were additionally carried out with the proposal of conceptual solutions in control zones, with the aim of confirming the correctness of the applied methodology of solving the problem of beach erosion.

Table 9.2 – Assessment of possibilities and limitations for improving the situation of considered beaches

BEACH	CONSTRAINTS			
	Spatial	Organic	Administrative	**Sum**
Zlatni rat	2	5	1	**8**
Stiniva	4	5	1	**10**
Podgora	2	2	1	**5**
Podstrana	2	2	1	**5**
Kašjuni	3	3	1	**7**

Rating from 1 to 5 (1 – minimum limit, 5 - maximum limit)

[5] In accordance with the vulnerability assessment from the Marine Environment and Coastal Management Plan of Split-Dalmatia County (Cooperative Granum Salis, 2021.)

Also, for all the beaches in question, the characteristic granulometric composition of the beach material was determined, by taking samples from the field and analyzing it in an authorized laboratory (Institut IGH d.d. Split).

In addition to numerical modeling and determination of the existing composition of the beaches in question, the beach material transport potential was also calculated based on the results from the numerical wave model, and the calculation of the stable composition of beach material, for each of the five beach locations.

The results of such a detailed analysis are given below for each analyzed beach separately.

9.3.2. Problem analysis and solution proposal

9.3.2.1. Zlatni rat beach (Brač)

For Zlatni rat beach on the island of Brač, a very high degree of wave exposure of certain parts of the beach has been established, especially the very top of the beach and the zones in its immediate vicinity on both sides, which implies that the beach in these zones experiences significant hydrodynamic influences, which have great importance on the morphology of the beach and the dynamics of its beach material. All this is very noticeable in the actual state of the field, where the dynamic process of alternating shifting of the top of the beach due to the waves that occur during the year (section 8.1.1.1) is evident.

Furthermore, Zlatni rat beach on the island of Brač is under considerable influence of the wave breaking process, which is one of the most important erosive processes for grainy beaches. In the analysis with different sea levels, which simulated the scenario of rising the sea as a result of climate changes, it was shown that rising sea levels would contribute to increasing erosive pressures on the beach, due to the shift of the wave breaking zone towards the coast and thus a higher degree of erosion, which could ultimately result in its complete degradation and disappearance unless timely action is taken (chapter 8.1.1.2).

Also, from the analysis of the results of the calculation of the transport of beach material, a very high level of transport potential of beach material was determined, from which the beach Zlatni rat on the island of Brač was made (chapter 7.1.1).

All the above, in addition to the fact that there are objective limitations for the beach in question that do not allow construction interventions in the form of the construction of coastal protective structures (Table 9.2), contributes to the narrowing of the room for maneuver to raise the level of sustainability and resilience of Zlatni rat beach to future impacts and consequences of climate changes.

The solutions that are imposed are primarily based on the establishment of a quality monitoring system for monitoring the situation in the area and waters of the beach in question, which should timely point to clear and unambiguous trends of increasing the vulnerability of the beach in question due to the rise of the sea level and / or the increase of wind wave parameters, and the consequent deterioration of the state of erosion of beach material and the entire beach.

As a logical solution to a potential problem in the future, the technique of beach nourishment with the appropriate granulometric composition of the beach (medium grain rock material D_{50} = 40 mm, chapter 7.2.1) is imposed, with the raising of the altitude level of the flat part of the beach, which would ensure the survival of the beach in conditions of increased sea levels, and the maintenance of approximately the same existing dimensions of the c.

9.3.2.2. Stiniva beach (Vis)

For Stiniva beach on the island of Vis, a very high degree of wave exposure of the outer wider waters of Stiniva beach has been established, i.e., the bay within which it is located, while the narrower waters of the beach are excellently protected and completely without the influence of waves. Thus, Stiniva beach does not experience significant hydrodynamic impacts, which could have significance on the morphology of the beach and the dynamics of its beach material. All this is very noticeable in the actual situation on the ground, where it is not possible to detect places that can be safely stated to be under the significant influence of wave action (section 8.2.1.1).

Furthermore, Stiniva beach on the island of Vis is not affected by the wave breaking process, which is one of the most important erosive processes for grainy beaches. In the analysis with different sea levels, which simulated the scenario of rising the sea as a result of climate changes, it was shown that rising sea levels would not bring a greater degree of beach vulnerability from erosion due to wave breaking, so it can be concluded that the beach will remain in approximately the same state of load due to wave breaking (chapter 8.2.1.2).

Also, from the analysis of the results of the beach material transport potential, a very low level of transport potential of beach material was determined, from which Stiniva beach on the island of Vis was made (chapter 7.1.2).

All the above, in addition to the fact that there are objective limitations for the beach in question that do not allow construction interventions in the form of the construction of coastal protective structures (Table 9.2), contributes to the fact that no special engagement is required to raise the level of sustainability and resilience of Stiniva beach to future impacts and consequences of climate changes.

Nevertheless, as a reasonable step that is imposed, is the establishment of a quality monitoring system for monitoring the situation in the area and waters of the beach in question, which should timely point to clear and unambiguous trends of increasing the vulnerability of the beach in question due to the rise of the sea level and / or the increase of wind wave parameters, and the consequent deterioration of the state of erosion of beach material and the entire beach.

As a logical solution to the potential problem in the future, the technique of nourishment the beach with the appropriate granulometric composition of the beach is imposed, which in principle represents the existing material at the beach location (medium grain stone material D_{50} = 22.3 mm, chapter 4.1.2), with the raising of the height of the flat part of the beach, which would ensure the survival of the beach in conditions of increased sea levels, and the maintenance of the approximate dimensions of the above sea level part of the beach.

9.3.2.3. Podgora beach (Makarska Riviera)

For the Podgora beach on the Makarska Riviera, a very high degree of wave exposure of certain parts of the beach has been determined, depending on the directions of the incident waves. When waves from the southern directions appear, quite expectedly, the southern part of the beach is dominantly exposed, while when waves from western directions appear, the northern belt of the coast in question is most exposed. All this implies that Podgora beach experiences significant hydrodynamic influences, which have great significance on the morphology of the beach and the dynamics of its beach material, which is very noticeable in the actual situation on the ground, where zones are noticed that are under the evident influence of the dynamic process of pushing beach material to the shore and at the same time taking it to the deeper sea during the year (chapter 8.3.1.1).

Furthermore, Podgora beach on the Makarska Riviera is under considerable influence of the wave breaking process, which is one of the most important erosive processes for grainy beaches. In the analysis with different sea levels, which simulated the scenario of rising the sea as a result of climate

changes, it was shown that rising sea levels would contribute to increasing erosive pressures on the beach, due to the shift of the wave breaking zone towards the coast and thus a higher degree of erosion, which could ultimately result in its complete degradation and disappearance if timely activities are not taken in terms of the realization of protective construction interventions in the beach area (section 8.3.1.2).

Also, from the analysis of the results of the calculation of the transport of beach material, a very high level of transport potential of beach material was determined, from which the Beach Podgora on the Makarska Riviera was made (chapter 7.1.3).

Considering the fact that there are no major spatial, ecological and administrative restrictions for the beach in question to improve the detected state of erosion, the construction of protective coastal structures (Table 9.2), a proposal for a conceptual design for the control area has been developed for the coastal belt of Podgora beach, which raises the level of sustainability and resilience of the beach to future impacts and consequences of climate changes, and whose concepts are applicable to the entire coastal zone, with the necessary additional analysis.

On the example of the proposed conceptual design for the control area of Podgora beach, the correct concept of solving detected beach erosion problems is shown, because the wave breaking zones for simulations with the conceptual solution significantly move from the mainland to the sea and thus contribute to increasing the degree of protection of the beach from erosion. At the same time, the conceptual design reduced the general impact of waves in the zone in question and the transport of beach material.

The applied methodology represents a quality and coherent basis for the adoption of general guidelines for the protection of beaches from granular materials. In addition to concrete solutions for the construction of protective coastal structures, the overall solution of the problem of raising the level of sustainability and resilience of Podgora beach to future impacts and consequences of climate changes, should include the establishment of a quality monitoring system for monitoring the situation in the area and waters of the beach in question. It would ensure timely detection of clear and unambiguous trends of increasing the vulnerability of the beach in question due to the rise of the sea level and / or the increase of wind wave parameters, and the consequent deterioration of the state of erosion of beach material and the entire beach.

Also, as a logical complement to the given solutions, the technique of beach nourishment with the appropriate granulometric composition of the beach (medium-sized stone material D_{50} = 30 mm, chapter 7.2.3.) is imposed, with the raising of the height of the flat part of the beach, which would ensure the survival of the beach in conditions of increased sea levels, and the maintenance of approximately the same existing dimension of the above sea level part of the beach.

9.3.2.4. Beaches on the Podstrana-Duće area

A very high degree of wave exposure of certain parts of the beach was determined for Podstrana beach on the Podstrana-Duće area, depending on the directions of the incident waves. The dominant waves that most affect beach erosion are the waves of the south (SE) and SW (SSW). Therefore, it can be said that the beaches on the Podstrana-Duće area experience significant hydrodynamic influences, which have great significance on the morphology of beaches and the dynamics of their beach material, which is very noticeable in the real situation on the ground, where zones are noticed that are under the evident influence of the dynamic process of pushing beach material to the shore and at the same time taking them to the deeper sea during the year (chapter 8.4.1.1).

Furthermore, the beaches on the Podstrana-Duće area are under considerable influence of the wave breaking process, which is one of the most important erosive processes for grainy beaches. In the analysis with different sea levels, which simulated the scenario of rising the sea as a result of climate

changes, it was shown that rising sea levels would contribute to increasing erosive pressures on the beach, due to the shift of the wave breaking zone towards the coast and thus a higher degree of erosion, which could ultimately result in its complete degradation and disappearance if timely activities are not taken in terms of the realization of protective construction interventions in the land area in question the area and waters of the beach (section 8.4.1.2).

Also, from the analysis of the results of the calculation of the transport of beach material, a very high degree of potential of transport of beach material was determined, from which the beaches on the Podstrana-Duće area are made (chapter 7.1.4.).

Due to the fact that there are no major spatial, ecological and administrative restrictions for the beaches on the area in question to improve the detected state of erosion, by building protective coastal structures (Table 9.2), a proposal for a conceptual design for the control area has been developed for the coastal belt of The Podstrana Beach, which raises the level of sustainability and resilience of the beach to future impacts and consequences of climate changes, and whose concepts are also applicable to the entire coastal zone concerned, with the necessary additional analysis.

On the example of the proposed conceptual design for the control area of Podstrana beach, the correct concept of solving detected beach erosion problems has been shown, because wave breaking zones for simulations with a conceptual solution significantly move from the mainland to the sea and thus contribute to increasing the degree of protection of the beach from erosion. At the same time, the conceptual design reduced the general impact of waves in the zone in question and the transfer (transmission) of beach material.

The applied methodology represents a quality and coherent basis for the adoption of general guidelines for the protection of beaches from granular materials. In addition to concrete solutions for the construction of protective coastal buildings, the overall solution of the problem of raising the level of sustainability and resilience of Podstrana beach to future impacts and consequences of climate changes, should include the establishment of a quality monitoring system for monitoring the situation in the area and waters of the beach in question. It would ensure timely detection of clear and unambiguous trends of increasing the vulnerability of the beach in question due to the rise of the sea level and / or the increase of wind wave parameters, and the consequent deterioration of the state of erosion of beach material and the entire beach.

Also, as a logical addition to the given solutions, the technique of beach nourishment with the appropriate granulometric composition of the beach (medium grain rock material D_{50} = 30 mm, chapter 7.2.4.) is imposed, with the raising of the altitude level of the flat part of the beach, which would ensure the survival of the beach in conditions of increased sea levels, and the maintenance of approximately the same existing dimension of the above sea level part of the beach.

9.3.2.5. Kašjuni beach in Split

For Kašjuni beach in Split, a high degree of wave exposure of certain parts of the beach has been determined, depending on the directions of the incident waves. The dominant waves that most affect beach erosion are SW waves (SSW). Therefore, it can be said that Kašjuni beach experiences noticeable hydrodynamic influences, which are reflected in the morphology of the beach and the dynamics of beach material, which is noticeable in the real situation on the ground, where the zones (northern part of the beach) are observed that are under the evident influence of the dynamic process of erosion at the appearance of the previously mentioned direction of the incident waves of lebić (chapter 8.5.1.1).

Furthermore, Kašjuni beach is under the noticeable influence of wave breaking processes, which is one of the most important erosive processes for grainy beaches. In the analysis with different sea levels, which simulated the scenario of rising the sea as a result of climate changes, it was shown that rising sea levels would contribute to increasing erosive pressures on the beach, due to the shifting of the

wave breaking zone towards the coast and thus a higher degree of erosion, which could ultimately result in its complete degradation if timely activities are not taken in terms of the realization of protective construction interventions in the land area concerned and waters of the beach (section 8.5.1.2).

Also, from the analysis of the results of the calculation of the transport of beach material, a noticeable degree of transport potential of beach material was determined, from which Kašjuni beach in Split was made (chapter 7.1.5.).

Since there are only ecological limitations for Kašjuni beach to improve the detected state of erosion by building protective coastal structures (Table 9.2), an integral proposal for the conceptual design for the entire beach has been developed for the coastal belt of Kašjuni beach, which raises the level of sustainability and resilience of the beach to future impacts and consequences of climate changes.

On the example of the proposed conceptual design for Kašjuni beach, the correct concept of solving detected beach erosion problems is shown, because wave breaking zones for simulations with a conceptual solution significantly move from land to the sea and thus contribute to increasing the degree of protection of the beach from erosion. At the same time, the conceptual design reduced the general impact of waves in the zone in question and the transport of beach material.

The applied methodology represents a quality and coherent basis for the adoption of general guidelines for the protection of beaches from granular materials. In addition to concrete solutions for the construction of protective coastal structures, the overall solution of the problem of raising the level of sustainability and resilience of Kašjuni beach to future impacts and consequences of climate changes, should also include the establishment of a quality monitoring system for monitoring the situation in the area and waters of the beach in question. It would ensure timely identification of clear and unambiguous trends of increasing the vulnerability of the beach in question due to the rise of the sea level and / or increase in the parameters of wind waves, and the consequent deterioration of the erosion of beach material and the entire beach.

Also, as a logical addition to the given solutions, the technique of beach nourishment is imposed with the appropriate granulometric composition of the beach (rock material medium grain D_{50} = 22.5 mm, chapter 7.2.5.) with the raising of the altitude level of the flat part of the beach, which would ensure the survival of the beach in conditions of increased sea levels, and the maintenance of the approximate existing dimension of the above sea level part of the beach.

9.3.3. General guidelines

Based on the given analysis and proposals for solving problems for each of the analyzed pilot locations of beaches in Split-Dalmatia County, it is possible to adopt general guidelines in order to ensure the sustainability of beaches in the current conditions, and adapt to the future conditions as a result of climate changes. The guidelines, in general form, apply to all beaches made of granular materials in Split-Dalmatia County.

Given that the proposed methodology has been proven by the analysis in question as the correct procedure in ensuring the set objectives of ensuring the sustainability of beaches made of granular materials, the sequence of procedures given by it constitutes the backbone of these guidelines (Figure 9.1).

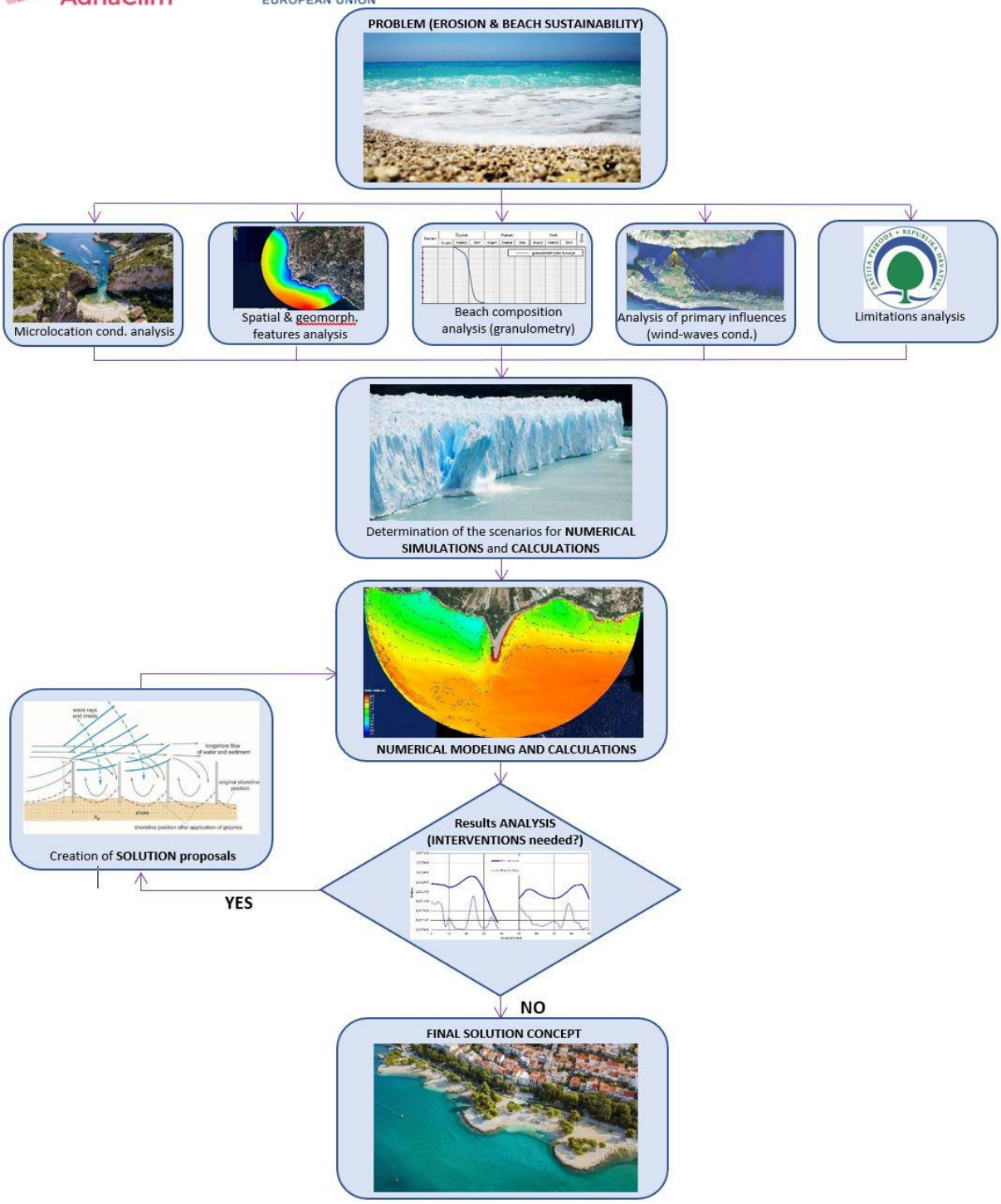

Figure 9.1 – Sequence of procedures (methodologies) for tackling beach erosion and sustainability

Speaking at the general level, beaches made of granular materials are predominantly under hydrodynamic influence of wind waves and fluctuations in sea levels, and consequently all possible combinations of basic physical processes that these influences cause. So-called extreme events, such as the occurrence of extreme wave impacts (storm events) and/or extreme sea levels, are of particular importance. Furthermore, other influences, such as the possibility of torrential coastal flows, and the unavoidable impacts due to human activities, primarily related to construction in the protected coastal zone and activities such as tourism, should not be ignored. Apart from the fact that these influences in their significance and magnitude are not nearly as much of an impact on beach erosion as hydrodynamic, except in exceptional cases, their consideration goes beyond the scope of the study in

question.

What is most important to point out as a key determinant of the guidelines, is the necessity of applying an individual approach for each analyzed beach. In doing so, one should not limit oneself to the spatial definition of the term beach, as a separate unit for analysis, but primarily to the coastal belt of approximately similar or equal spatial, geomorphological, and structural characteristics and influences. In this case, a situation may occur when, as part of one analysis, it is possible to observe several beaches (regardless of the length of the coastal belt), while on the other hand, there is a possibility of the need to perform separate analyses for individual zones within one beach. There is no rule, but the approach can be modified on a case-by-case basis, i.e., from beach to beach, which ensures the applicability of the proposed methodology, and the adoption of consistent conclusions and quality solutions.

As a first step, it is necessary to conduct an analysis of the existing states of microlocation, its spatial and geomorphological features, granulometric composition, and quality analysis of primary wind wave influences and analysis of objective constraints for interventions in space.

Also, it cannot be strongly enough to emphasize the need for the necessity of applying sophisticated numerical models in the execution of the analysis in question. As already emphasized, the complexity of the interaction of hydrodynamic physical wave processes in the coastal area prevents a sufficient level of reliability in judgment and conclusions based solely on the intuition and / or experience of planners or designers. Leonardo da Vinci once said*, "When dealing with water, first experiment then use judgement!"* (Hughes S.A., 1993).

Therefore, only after conducting a numerical analysis of the selected location, according to the procedure presented here, it is possible to draw quality conclusions about how to solve the detected problems in terms of erosion and sustainability of beaches. In doing so, special emphasis should be given to the analysis of general wave impacts, the impact of wave breaking zones and the transport potential of materials, with mandatory considering the potential increase in sea level as a result of climate changes.

Technical solutions with the aim of reducing the potential of beach erosion, for the current and future situation, must be well selected, and precisely determined in terms of consistent selection of all project parameters. Particular attention should be focused on the geometric determinants of certain parts of selected protective coastal structures, such as the correct disposition of protective groynes, underwater reefs or tombolos, and appropriate plan dimensions and heights. As an example, where it is especially necessary to consider the height project parameters are the underwater reefs, because the wrong selection of berm height, necessarily leads to its inefficiency, because in that case the necessary breakdown of waves will not occur on it, necessary for the protection of beach zones from erosion in its hinterland.

As a complement to these technical solutions, and for beaches with significant restrictions on the construction of protective buildings - one of the most important protection measures, the need to establish a quality monitoring system of the situation is imposed given the impact of the consequences of climate changes. The key determinants of monitoring should be systematic measurements of rising sea levels and measurements of the occurrence of extreme waves, and measurements of granulometric changes in the composition of beaches during the year. In addition to these basic determinants, it is necessary to perform systematic monitoring of spatial behavior of the beach during the year, in terms of creating new or losing existing beach areas and detection of other potential problems important for beach erosion. The aim and purpose of the monitoring is to point out the trends of processes that have a significant impact on beach erosion.

Although the basic beach protection procedures presented in section 5.6 of this study ensure a significant degree of protection of beaches from granular materials, complete protection can never be achieved. Therefore, in addition to the already mentioned monitoring, it is necessary to ensure

professionally based beach nourishment with appropriate quality material. Namely, in practice, it has been shown on numerous examples that unprofessionally conducted backfilling of inadequate material only further worsens the existing situation regarding erosion and increasing the negative environmental impact. The methodology and method of determining the granulometric composition of beaches, which should ensure a high degree of stability and sustainability of beach material in the relevant conditions of a particular beach, is shown in chapter 7 of this study, while the need for nourishment should arise from quality monitoring.

When considering material for beach nourishment, in addition to the appropriate granulation of the material itself, it is necessary to consider the possibility of supplying materials. If the stone material for beach nourishment is purchased from separations in quarries, the grains of the material thus obtained usually have relatively sharp edges, which contributes to the beach surfaces covered with such material have a significant reduced comfort of use. Therefore, if the stone is obtained from this source, it is possible to think about the formation of certain coastal zones in which such material would be temporarily imported and left for several seasons for the sea to naturally process and round it, after which it would then be transported to certain locations.

9.4. Establishment of monitoring system on the beaches

As already mentioned, the establishment of a quality monitoring system on beaches for observing consequences brought by climate changes, is one of the complementary, and for beaches with significant restrictions on the construction of protective buildings - one of the most important protection measures.

As an example, for defining technical solutions for systematic monitoring of beach zones, we cite the scientific project *Beachex* 2019-2023, implemented by the Faculty of Civil Engineering of the University of Zagreb and Lancaster Environment Centre – Lancaster University. Namely, as part of this project, the technique of establishing artificial neural networks was applied to predict the needs for the volume of nourishment on beaches and determine morphodynamical changes on beaches, based on the technology of video monitoring, smart pebbles, and hydrographic buoys in combination with geodetic measurements, and systematic diving research to assess the impact of nourishment beaches on plant and animal communities (Bogovac T. et al. 2023).

Furthermore, we also provide a proposal for a monitoring system for erosion management of pebble beaches in Croatia, which is based on relatively cheap methods of SfM (Structure-from-Motion) photogrammetric imaging and multilayer stereo display (MVS) for obtaining a 3D model of a high-resolution beach in order to detect morphological changes and erosion (Kordić B. et al., 2018).

These projects and research, i.e., the technologies used in them, can serve as a good example for defining the technical framework of systematic monitoring of the situation on beaches.

In addition, within the framework of the introduction of quality monitoring, it is proposed to systematically sampling beach material at certain locations of the coastal beach belt, twice a year, where it is necessary to include sampling of materials in the spring and autumn period, with the examination of the granulometric composition of the material proposed here by the methodology, with the aim of obtaining the best possible insight into the behavior of beach material during the year.

9.5. Environmental aspect of the guidelines

One of the declared objectives of these guidelines is the protection and preservation of the coastal zone, as well as ensuring its sustainable and resilient development. In achieving this goal, it should be considered that the given concepts of protection and preservation do not refer only to ensuring the spatial survival of the coastal zone, i.e., beach zones, as exploitation areas (recreational, tourist, etc.),

but to ensuring its overall integrity, where by the ecological aspect is certainly one of the most important factors.

9.5.1. General influence of guidelines application

It is quite clear that any intervention in the area or waters of the beach necessarily brings a certain degree of change in its terrestrial and/or submarine ecological microsystem. Aware of the fact that the consequences of climate changes could have significant impacts on these ecological microsystems, the proposed methodology and adopted guidelines aim to qualitatively contribute to the coastal zone, using the concept of "optimal design", which guarantees that interventions in space (land and / or sea) are minimal in relation to the degree of protection against beach erosion that is to be achieved and which will ensure their sustainability.

No one can argue that the construction of protective groynes of the beach or underwater reefs does not bring a relatively large degree of changes in the natural state of the beach environment. But once built, in accordance with the given guidelines, these protective structures become effective and stable carriers of the resilience and sustainability of the entire belt in question. There are numerous examples of research that speak in favor of how new underwater reefs and groynes of stone blocks represent new habitats for underwater animal and plant life. Although this is a relatively short-lived but sudden impact on the environment during the construction of these protective structures, such an impact can ultimately be far more favorable and overall, less than the impact of an unprofessionally backfilled beach that continuously erodes for many years and covers wide underwater expanses with eroded and smaller material from the beach (section 5.5.4).

If the "black scenarios" of rising sea levels as a result of climate changes are realized, then there is no reasonable alternative to the protection procedures given here, which will not require some kind of "extreme" engineering to achieve the protection of the coastal belts and beaches.

9.5.2. Supplementary solutions in reducing the impact of beach erosion

In addition to the procedures that form the basis of the general guidelines for ensuring beach sustainability and adaptation to climate changes, it is also necessary to think about alternative solutions that could complement the underlying procedures, but not separately, contribute to the achievement of the set goals. This primarily refers to the integral spatial-urban planning and organization of coastal zones, adaptation of the way of using the coastal zone and horticultural breeding that directly contributes to the reduction of erosion of the coastal part right next to the coastline, especially beaches.

As shown in the example of the Coast Plan of Šibenik-Knin County (UNEP/MAP/PAP, 2016), four groups of key management policies were detected in the implementation of the plan: building coastal area resilience, sustainable spatial development, water resources management and sustainable economic development. The proposed space measures aim to preserve the complete landscape values of the coastal zone and improve the quality of the landscape built. In addition to improving the environment, both measures contribute to creating the conditions for improving social cohesion, as well as strengthening the foundations for sustainable tourism. Measures aimed at improving the quality of the built landscape are aimed at facilitating water runoff during storms and flash floods (trees in strategic locations, removal of sealed areas and other measures of green infrastructure). Green infrastructure measures provide conditions for raising the quality of life by increasing the enjoyable areas of local people and tourists. Finally, an integrated approach ensures that all adaptation measures will consider the creation of incentive conditions for climate change mitigation.

9.5.2.1. 'Green solutions' in the spatial organization of coastal zones and the concept of 'coastal setback'

Like the previously described for the example of the Coast Plan of Šibenik-Knin County, for the specific problem that this study deals with, which is beach erosion, for the existing and future situation, it is possible to implement measures to improve the quality of the built landscape in spatial strategies and plans, which would simultaneously improve the condition of beach erosion. These measures would include defining coastal zones, right next to the coastline, which require horticultural landscaping with indigenous plant material resistant to wind and sea action, which, in addition to the basic protection procedures, would contribute to additional protection of beaches from erosion, but also to the protection of property in the immediate vicinity of the coast.

Namely, in addition to the fact that the roots of plants retain submissive material, which helps stabilize the coastal area where they are planted, their water absorption reduces erosion due to stormwater runoff. Also, plants, especially trees, alleviate the dispersion of seawater that occurs due to waves and wind, thus protecting the coastal vegetation, but also the entire hinterland. Furthermore, their beneficial effect on reducing the impact of wind is not negligible either.

As already mentioned, for the horticultural landscaping of coastal zones, which is primarily in the function of protecting beaches from erosion due to the consequences of climate changes, it is necessary to choose plant material that is resistant to the effects of wind and sea. When choosing, care should be taken that the selected plant species are autochthonous and do not stand out visually from the environment in which they are placed. As a good example of horticultural landscaping of the coastal belt, i.e., the beach, we cite the example of beach decoration in Crikvenica (Figure 9.2), on which all the above principles were applied.

Figure 9.2 – Example of horticultural landscaping of the beach in the function of reducing erosion, Crikvenica beach

The concept of "coastal setback", adopted by Adriapt in its Adaptation Options, consists in defining a protective area in which some or all types of construction are prohibited or significantly limited, and is most often defined by a specific distance from the coastline (figure 9.3). The main functions of coastal detachment are coastal protection through the protection of population and human settlements from

coastal floods and erosion, support to the coastal economy (economic use of beaches for tourism and recreation) and preservation of biodiversity, and maintenance of natural beach functions.

Although the concept of "coastal setback" is an integral part of legislation in several countries of the world, with a different definition of distance from the coastline (Table 9.3), it is very often not implemented in practice. However, by adopting a new EU strategy for adaptation to climate change, which calls for 'the principle of ensuring that disaster risk is taken into account in regulations and funding in order to avoid creating new exposure...', further construction on a narrow coastal area should be kept to a minimum.

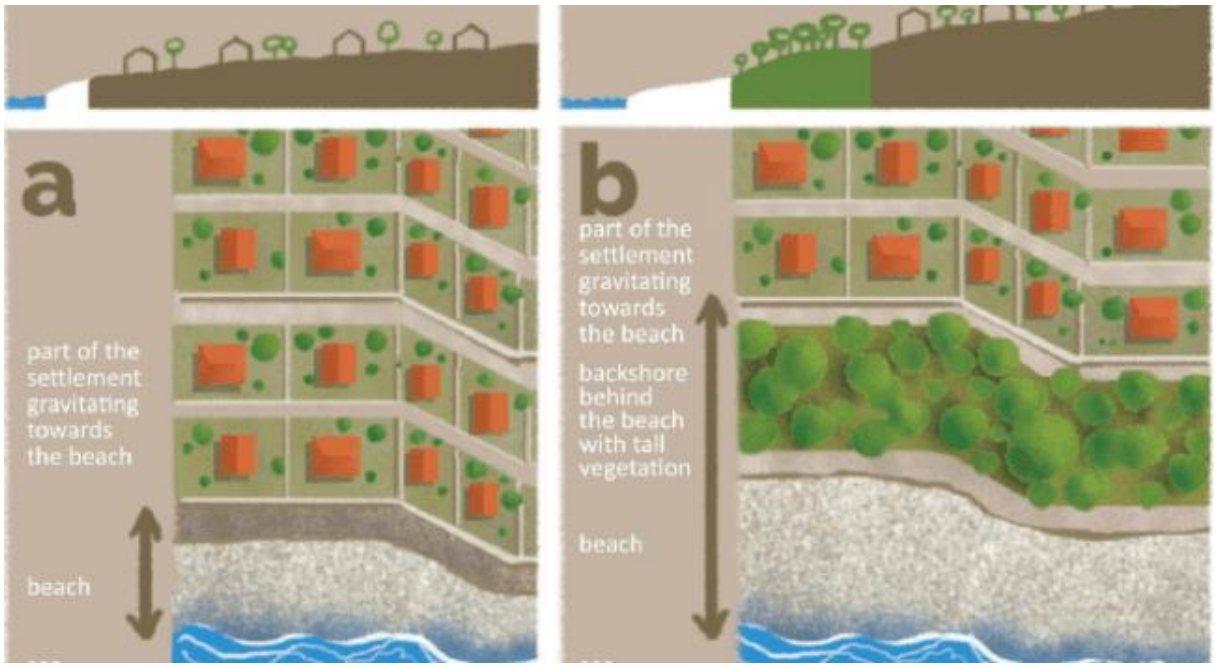

Figure 9.3 – The concept of 'coastal setback' (Adriadapt)

In Croatia, since 2004, various restrictions on construction within the coastal zone have been prescribed by a special Regulation on the Arrangement and Protection of the Protected Coastal Area of the Sea (ZOP), and today the protected coastal area is defined by the Spatial Planning Act, including all prescribed construction restrictions.

Table 9.3 – Definition of distance from the coastline for different countries applying the “coastal setback” concept (Coastalwiki)

Country	Setback from the shoreline [m]	Country	Setback from the shoreline [m]
Bahamas	5 to 15	EU Mediterranean	100
Barbados	30	Germany	100 to 200
Belize	20	Norway	100
Brazil	50 to 200	Poland	200
Chile	80	Turkey	50
Colombia	50	Spain	100
Costa Rica	50 (+150)	Sweden	100
Cuba	40 to 80	Denmark	300
Dominican Republic	60	Australia NSW	1000
Jamaica	30	Australia Victora	200
Mexico	20	New Zealand	20
Nicaragua	50	Canada NB	30
Panama	20	Canada BC	15
Urugay	200	India	200 to 500
Vezuela	15		

The realization of the concept of "coastal setback" can become a contentious issue, because municipalities are very reluctant to change their plans, and coastal setback is often considered a "loss" of potential for building on attractive lands. In addition, conflicts over land ownership can also complicate the realization of the concept of "coastal setback".

As for the costs of implementing the concept of "coastal setback", the work of existing local authorities in charge of planning is crucial. Given that in most cases it is necessary to consider the payments of compensation to privately owned land owners in the coastal setback zone, the implementation of the coastal setback policy will have the lowest costs if it is carried out proactively, before significant, inappropriate construction occurs.

A relatively recently produced study (Lincke D. et al., 2020), confirms that "coastal setback" zones are an effective measure of adaptation of the Croatian coast, based on the modelling performed for two variants of the coastal setback zones. The first variant limits future construction, while the second variant extends construction restrictions to already built areas that are not protected by embankments and coastal walls. The conclusion of the study is that the financial impacts of sea level rise can be significantly reduced by integrating coastal setback zones into an adaptation strategy. If protection and construction restrictions in coastal setback zones are combined, future costs incurred as a result of flooding coastal areas can be reduced by up to 39%. The combination of protection and organized withdrawal through coastal setback zones can reduce future costs incurred as a result of flooding coastal areas by up to 93%. The study considered only the benefits that coastal setback zones bring in terms of exposure to coastal floods, while benefits in the fields of biodiversity protection, maintenance of ecosystem services, coastal erosion or benefits for tourism and recreation were not considered.

9.5.2.2. Protection and restoration of Posidonia seagrass meadows

Also, when considering and resolving the issue of beach erosion, one should not ignore the favorable impact of underwater vegetation, such as the flowering meadows of Posidonia, on reducing the potential of erosion of grainy beaches, especially in the underwater parts of beaches, but also on the mitigation of wave action (Adriadapt).

Namely, by retaining sediment in seagrasses, the bottom becomes shallower, and the waves move

away from the shore, which mitigates coastal erosion during stormy weather (Figure 9.4). Seagrasses also slow down the movement of sea currents between the seabed and their own leaves. Recent studies have shown that the height of waves in areas covered with dense seagrass meadows is 10-20% lower compared to bare seabed (phys.org, 2016).

Posidonia meadows are endangered in areas directly exposed to human activities such as unregulated anchoring, congestion and increased turbidity from inadequate material for backfilling and/or nourishment beaches, eutrophication and other types of pollution, improper fishing with nets "winks", trawls and other equipment that is pulled along the seabed, and the spread of invasive species.

Once tiny material swept away from an inexpertly nourished beach begins to cover the areas where *Posidonia* grows, these areas begin to fragment, and sedimentary material becomes increasingly affected by erosion, gradually increasing wear and take away rates, thus preventing its further growth (Evans S.M., 2019).

The importance of protecting seagrass has been recognized on several levels: Posidonia has been included in priority habitats by the Natura 2000 Protection of Natural Habitats Directive and natura 2000 protected areas. In Croatia, areas of special importance for nature protection (ASCI) have been established (based on the Berne Convention) covering all types of seagrasses, as part of the "Emerald Network". In addition, all species of seagrass at the national level in Croatia are protected by the Nature Protection Act as a strictly protected species.

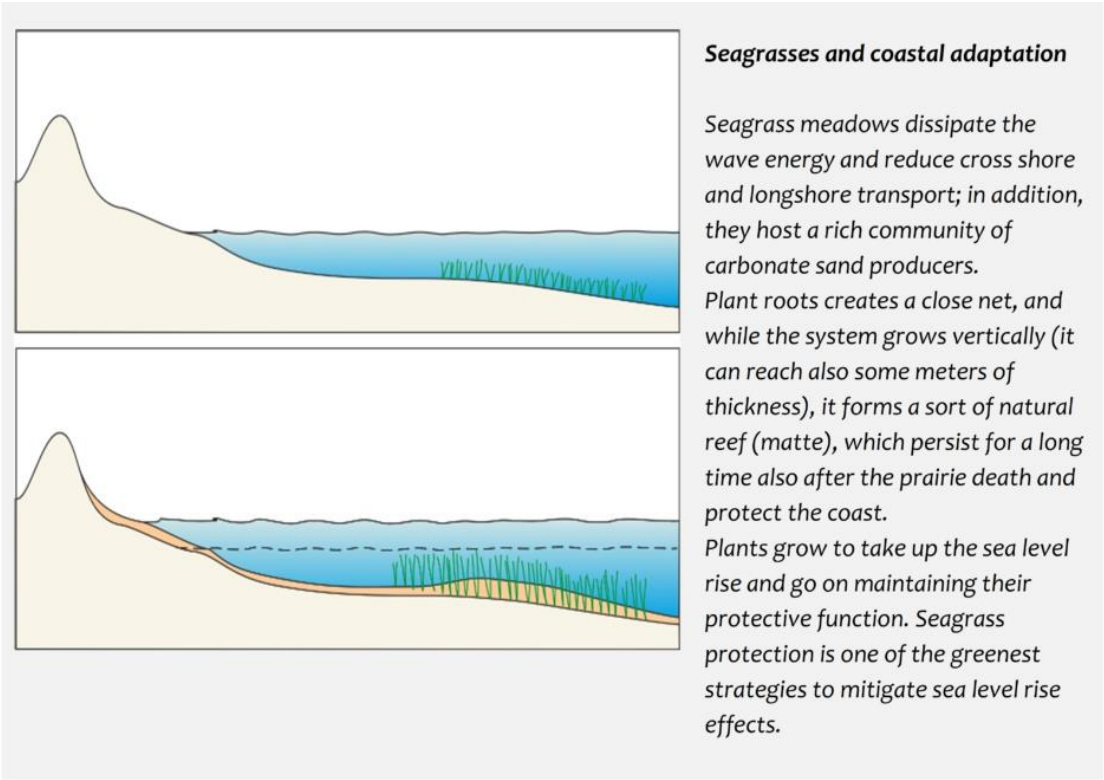

Figure 9.4 – Seagrasses and coastal adaptation (Adriadapt)

In addition to protecting against erosion, the preservation of seagrass meadows offers many other advantages, such as the supply of marine species with food, shelter and breeding area, carbon sequestration, oxygen production and coastal protection by absorbing sediments.

Several projects of planting Posidonia have been carried out in the Mediterranean so far, with varying success. Transplantation can require considerable costs and a lot of effort made; therefore, it can be said that the protection of seagrass is a far more cost-effective measure.

Transplanting Posidonia can be a relatively fast process, but since it grows rather slowly (only 1 cm per year in height), it will take a relatively long period to observe the results, that is, the level of success of such activities.

10. LITERATURE

[1] AdriAdapt, Interreg V-A Italy-Croatia Programm (https://adriadapt.eu)

[2] Berkhoff J.C.W., Computation of combined refraction-diffraction, Proceedings 13th Int. Conf. Coastal Eng., ASCE, Vancouver, 471-490, 1972.

[3] Berkhoff J.C.W., Mathematical model for simple harmonic linear water waves. Wave breaking and diffraction, Publication no.163, Delft Hydraulics Laboratory, the Netherlands, 1976.

[4] Bogovac T. et al., Analiza dohranjivanja i nasipavanja plaža u Hrvatskoj, Građevinar 4, 2023.

[5] Booij N., Gravity Waves on Water with Non-uniform Depth & Current, Ph.D.thesis, Technical Univ of Delft, the Netherands, 1981.

[6] Bruun P., Sea-Level Rise as a Cause of Shore Erosion, Journal of the Waterways and Harbors Division, 88, 1962.

[7] Carević D. et al., Analiza stanja dohranjivanja i nasipavanja plaža u Hrvatskoj, Građevinar 1/2022, 2022.

[8] CEM (Coastal Engineering Manual), U.S.Army Corps of Engineers, 2003.

[9] Chakrabarti S.K., Hydrodinamics of Offshore Structures, Southhampton: Computational Mechanics Pubs, p. 155-157, 1987.

[10] Chandrasekera C.N., Cheung K.F., Extended linear refraction-diffraction model, *Journal of Waterway, Port, Coastal and Ocean Engineering*, 123(5), 280-286, 1997.

[11] Chhabra N., Application of numerical model CGWAVE for wave prediction at Ponce de Leon inlet, Florida, USA, The University of Maine, 2004.

[12] Climate-ADAPT Strategy 2022-2024, the planning instrument with objectives, governance and priority lines of activities, European Commision, European Environment Agency

[13] Codignotto J.O. et al, Wind-wave climate change and increasing erosion in outer Rio de la Plata, Argentina, Continental Shelf Research, 38, 2012.

[14] Dean R.G., Dalrymple R.A., Water Waves Mechanics for Engineers and Scientists, Advanced Series on Ocean Engineering – Volume 2, World Scientific, 2007.

[15] Demirbilek Z., Panchang V.G., CGWAVE: A Coastal Surface Water Wave Model of the Mild Slope Equation, Technical Report CHL-98-26, US Army Corps of Engineers Waterways Experiment Station, Vicksburg, Mississippi, 39, 180, 1998.

[16] Evans S.M. et al., Correction: Seagrass on the brink: Decline of threatened seagrass Posidonia australis continues following protection, PLOS ONE 14(4), 2019.

[17] Goda Y., Random Seas and Design of Maritime Structures, Advanced Series on Ocean Engineering – Volume 15, World Scientific, 2000.

[18] Gumbel E.J., Statistics of Extremes, Columbia University Press, New, York, 1958.

[19] Hanson H. et al., Beach nourishment projects, practices and objectives – a European overview, Coastal engineering 47, p.81-111, 2002.

[20] Institut IGH d.d., Laboratorijsko ispitivanje žala uzorkovanog s pet morskih plaža u Splitsko-dalmatinskoj županiji, 2023.

[21] Isacson M. de St. Q., MacKenzie N.G., Long Term Distribution of Ocean Waves, Journal of Waterway, Port, Coastal and Ocean Division, A.S.C.E Proceedings Vol.107, p. 93-109, 1986.

[22] Jamal M.H., Modelling Coarse-Grained Beach Profile Evolution, Univesrity of Plymouth, 2011.

[23] Jones N.L., Richards D.R., Mesh Generation for Estuarine Flow Models, Journal of Waterway, Port, Coastal and Ocean Engineering, v118, 6, 3-20, 1992.

[24] Kordić B, et al., Implementing an efficient beach erosion monitoring system for coastal management in Croatia, Ocean & Coastal Management 156, 2018.

[25] Li D., Los Angeles – Long Beach harbor pier 400, harbor resonance study using numerical model, CGWAVE, The University of Maine, 2002.

[26] Lincke D. et al, The effectiveness of setback zones for adapting to sea-level rise in Croatia, Regional Environmental Change 20 (46), Springer, 2020.

[27] Liu S., Sun B., Self-adaptive FEM Numerical Modeling of Mild Slope Equation, Third Chinese-German Joint Symposium on Coastal and Ocean Engineering, National Cheng Kung University, Tainan, 2006.

[28] Panchang V., Chen W., Xu B., Schlenker K., Demirbilek Z., Okihiro M., Exterior Bathymetric Effects in Elliptic Harbor Wave Models, Journal of Waterway, Port, Coastal and Ocean Engineering, v126, 2, 71-78, 2000.

[29] Pernat Ž., Vranješ M., Hidrodinamička valna analiza – osnova za projektiranje održivih plaža, Građevinar 6/2012, 2012.

[30] Phys.org, Seagrass a crucial weapon against coastal erosion, https://phys.org/news/2016-06-seagrass-crucial-weapon-coastal-erosion.html, 2016.

[31] Pilarczyk K.W., Zeidler R.B., Offshore breakwaters and shore evolution control, A.A. Balkema, Rotterdam, 1996.

[32] Pršić M., Vodnogospodarske građevine – Pomorske gradnje, Tehničko Veleučilište Zagreb, 2008.

[33] Reeve D, Chadwick A. & Fleming C., Coastal engineering: processes, theory and practice, Spon Press, 2004.

[34] Sawaragi T., Coastal Engineering-waves, beaches, wave-structure interactions, Elsevier, 1995.

[35] Schwartz M.L., The Bruun Theory of Sea-Level Rise as a Cause of Shore Erosion, The Journal of Geology, 75, 1967.

[36] Shore Protection Manual – 4th edition, Coastal Engineering Research Center, U.S. Government Printing Office: Washington, DC, USA, 1984.

[37] Sorensen R.M., Basic Coastal Engineering, Department of Civil and Environmental Engineering Leigh University, Betlehem, Pennsylvania, Springer, 2006.

[38] Soulsby R., Marine Sands, Thomas Telford, 1997.

[39] Thompson E.F., Chen H.S., Hadley L.L., Validation of Numerical Model for Wind Waves and Swell in Harbors, Journal of Waterway, Port, Coastal and Ocean Engineering, v122, 5, 245-257, 1996.

[40] UNEP/MAP/PAP: Integrated Coastal Zone Management Plan of the Šibenik-Knin County, Split, Priority Action Programme, 2016.

[41] WMO, Handbook on Wave Analysis and Forecasting, WMO, 2006.

[42] Zadruga Granum Salis, Plan upravljanja morskim okolišem i obalnim područjem Splitsko-dalmatinske županije, 2021.

[43] Zhang J., Incorporating Rubble Mound Jetties in Elliptic Harbor Wave Models, Graduate Studies of Texas A&M University, 2007.

[44] Zubier K., Panchang V., Demirbilek Z., Simulation of Waves at Duck (North Carolina) using Two Numerical Models, Coastal Engineering Journal, v45, 3, 439-469, 2003.